

9

*[Handwritten signature]*



AFATL-TR-76-85

**INVESTIGATION OF POSSIBLE FIN FAILURES  
OF GBU-10 AND GBU-12 BOMBS CARRIED  
ON THE INBOARD WING STATION  
OF AN F-4 AIRCRAFT**

**AIRCRAFT COMPATIBILITY BRANCH  
MUNITIONS DIVISION**

**AUGUST 1976**

DDC  
RECEIVED  
DEC 15 1976  
D

Approved for public release; distribution unlimited

**AIR FORCE ARMAMENT LABORATORY**

AIR FORCE SYSTEMS COMMAND • UNITED STATES AIR FORCE

**EGLIN AIR FORCE BASE, FLORIDA**



ADA033340

UNCLASSIFIED

SECURITY CLASSIFICATION OF THIS PAGE (When Data Entered)

## REPORT DOCUMENTATION PAGE

READ INSTRUCTIONS  
BEFORE COMPLETING FORM

1. REPORT NUMBER

AFATL-TR-76-85

2. GOVT ACCESSION NO.

3. RECIPIENT'S CATALOG NUMBER

4. TITLE (and Subtitle)

INVESTIGATION OF POSSIBLE FIN FAILURES OF  
GBU-10 AND GBU-12 BOMBS CARRIED ON THE INBOARD  
WING STATION OF AN F-4 AIRCRAFT.

5. TYPE OF REPORT &amp; PERIOD COVERED

6. PERFORMING ORG. REPORT NUMBER

7. AUTHOR(s)

Alfred V. Marrin

8. CONTRACT OR GRANT NUMBER(s)

9. PERFORMING ORGANIZATION NAME AND ADDRESS

Aircraft Compatibility Branch, Munitions Division  
Air Force Armament Laboratory  
Eglin Air Force Base, Florida 3254210. PROGRAM ELEMENT, PROJECT, TASK  
AREA & WORK UNIT NUMBERS

Project No. 2171

Task No. 60

Work Unit No. 003

11. CONTROLLING OFFICE NAME AND ADDRESS

Air Force Armament Laboratory  
Armament Development and Test Center  
Eglin Air Force Base, Florida 32542

12. REPORT DATE

Aug 1976

13. NUMBER OF PAGES

299

14. MONITORING AGENCY NAME &amp; ADDRESS (if different from Controlling Office)

12361 p.

15. SECURITY CLASS. (of this report)

UNCLASSIFIED

15a. DECLASSIFICATION/DOWNGRADING  
SCHEDULE

16. DISTRIBUTION STATEMENT (of this Report)

## DISTRIBUTION STATEMENT A

Approved for public release;  
Distribution Unlimited

17. DISTRIBUTION STATEMENT (of the abstract entered in Block 20, if different from Report)

9 Technical rept.

18. SUPPLEMENTARY NOTES

Available in DDC.

19. KEY WORDS (Continue on reverse side if necessary and identify by block number)

Flow Angularity

F-4 Aircraft

GBU-10 Bomb

GBU-12 Bomb

Aircraft/Weapon Interference

Aircraft/Weapon Separation

20. ABSTRACT (Continue on reverse side if necessary and identify by block number)

This report documents a study performed to isolate the cause of a collision  
between an F-4 aircraft and a GBU-12 bomb. The study was generalized to  
predict the resulting GBU-10 bomb trajectory conditions.

DD FORM 1 JAN 73 1473

EDITION OF 1 NOV 65 IS OBSOLETE

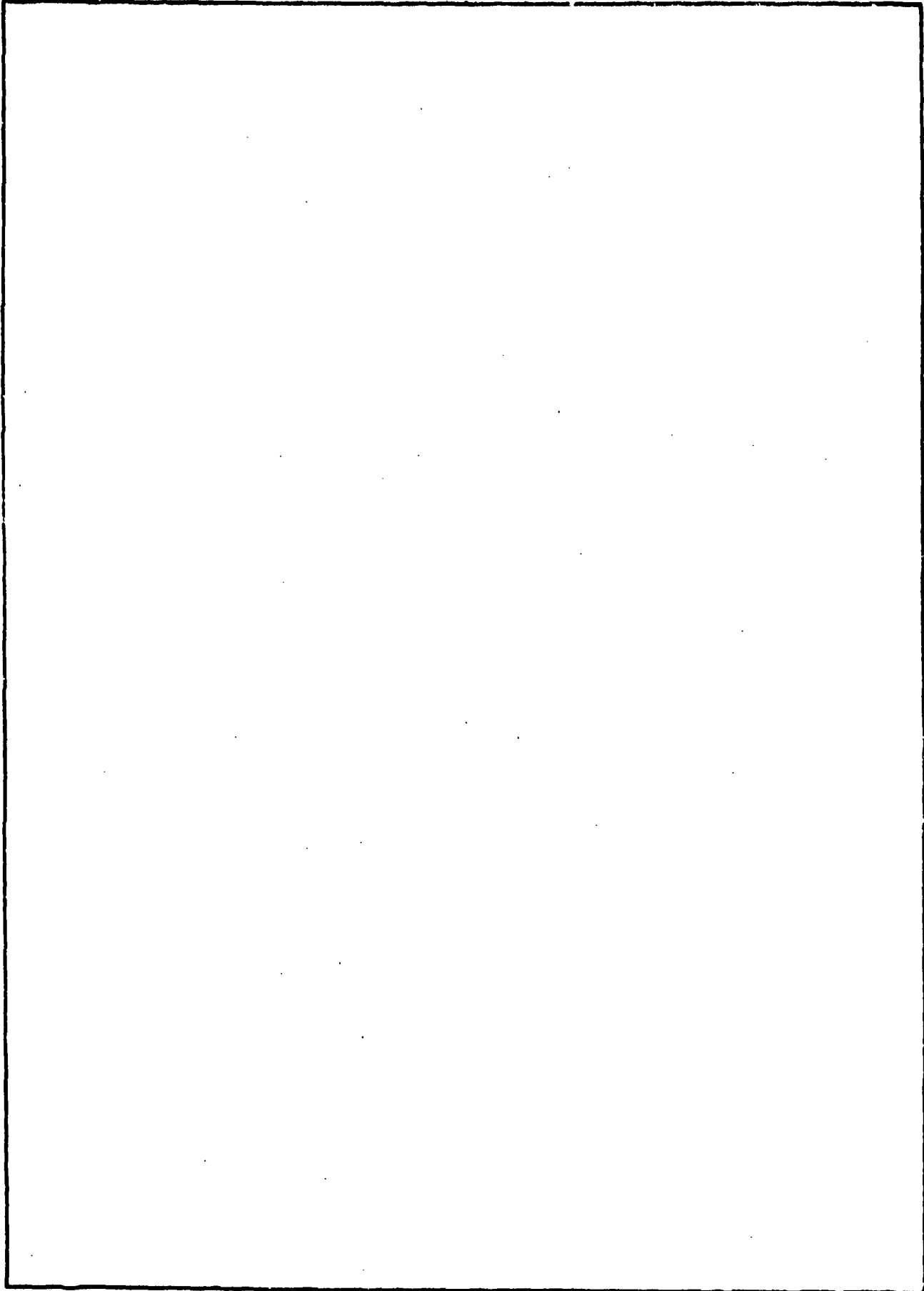
UNCLASSIFIED

SECURITY CLASSIFICATION OF THIS PAGE (When Data Entered)

400 936

UNCLASSIFIED

SECURITY CLASSIFICATION OF THIS PAGE(When Data Entered)



UNCLASSIFIED

SECURITY CLASSIFICATION OF THIS PAGE(When Data Entered)

## PREFACE

This report is based on a study performed by the Aircraft Compatibility Branch of the Munitions Division of the Air Force Armament Laboratory to determine the cause of a GBU-12 bomb collision with the delivery aircraft, an F-4. This effort was conducted under Project 2171C003.

**This technical report has been reviewed and is approved for publication.**

FOR THE COMMANDER

*William F. Brockman*  
WILLIAM F. BROCKMAN, Colonel, USAF  
Chief, Munitions Division

107

WATER TIGHTENING ☒

BALANCE ☐

☐

NO.

IDENTIFICATION CODES

ALL OTHER SPECIAL

A

DDC  
RECEIVED  
DEC 15 1976  
RECEIVED  
D



# TABLE OF CONTENTS

Section	Title	Page
I	INTRODUCTION . . . . .	1
II	ANALYSIS PROCEDURES. . . . .	2
III	DISCUSSION OF RESULTS. . . . .	4
IV	CONCLUSIONS. . . . .	5
Appendix		
A	GBU-12 BOMB TRAJECTORIES RESULTING FROM A (-5/-3) ORIFICE COMBINATION AT MACH 0.7. . . . .	7
B	GBU-12 BOMB TRAJECTORIES RESULTING FROM A (-5/-3) ORIFICE COMBINATION AT MACH 0.85 . . . . .	16
C	GBU-12 BOMB TRAJECTORIES RESULTING FROM A (-5/-3) ORIFICE COMBINATION AT MACH 0.95 . . . . .	25
D	GBU-12 BOMB TRAJECTORIES RESULTING FROM A (-5/-3) ORIFICE COMBINATION AT MACH 1.2. . . . .	34
E	GBU-12 BOMB TRAJECTORIES RESULTING FROM A (-3/-3) ORIFICE COMBINATION AT MACH 0.7. . . . .	43
F	GBU-12 BOMB TRAJECTORIES RESULTING FROM A (-3/-3) ORIFICE COMBINATION AT MACH 0.85 . . . . .	52
G	GBU-12 BOMB TRAJECTORIES RESULTING FROM A (-3/-3) ORIFICE COMBINATION AT MACH 0.95 . . . . .	61
H	GBU-12 BOMB TRAJECTORIES RESULTING FROM A (-3/-3) ORIFICE COMBINATION AT MACH 1.2. . . . .	70
I	GBU-12 BOMB TRAJECTORIES RESULTING FROM A (-3/-5) ORIFICE COMBINATION AT MACH 0.7. . . . .	79
J	GBU-12 BOMB TRAJECTORIES RESULTING FROM A (-3/-5) ORIFICE COMBINATION AT MACH 0.85 . . . . .	88
K	GBU-12 BOMB TRAJECTORIES RESULTING FROM A (-3/-5) ORIFICE COMBINATION AT MACH 0.95 . . . . .	97

# TABLE OF CONTENTS (CONTINUED)

Appendix	Title	Page
L	GBU-12 BOMB TRAJECTORIES RESULTING FROM A (-3/-5) ORIFICE COMBINATION AT MACH 1.2. . . . .	106
M	GBU-10 BOMB TRAJECTORIES RESULTING FROM A (-5/-3) ORIFICE COMBINATION AT MACH 0.7. . . . .	115
N	GBU-10 BOMB TRAJECTORIES RESULTING FROM A (-5/-3) ORIFICE COMBINATION AT MACH 0.85 . . . . .	124
O	GBU-10 BOMB TRAJECTORIES RESULTING FROM A (-5/-3) ORIFICE COMBINATION AT MACH 0.95 . . . . .	133
P	GBU-10 BOMB TRAJECTORIES RESULTING FROM A (-5/-3) ORIFICE COMBINATION AT MACH 1.2. . . . .	142
Q	GBU-10 BOMB TRAJECTORIES RESULTING FROM A (-3/-3) ORIFICE COMBINATION AT MACH 0.7. . . . .	151
R	GBU-10 BOMB TRAJECTORIES RESULTING FROM A (-3/-3) ORIFICE COMBINATION AT MACH 0.85 . . . . .	160
S	GBU-10 BOMB TRAJECTORIES RESULTING FROM A (-3/-3) ORIFICE COMBINATION AT MACH 0.95 . . . . .	169
T	GBU-10 BOMB TRAJECTORIES RESULTING FROM A (-3/-3) ORIFICE COMBINATION AT MACH 1.2. . . . .	178
U	GBU-10 BOMB TRAJECTORIES RESULTING FROM A (-3/-5) ORIFICE COMBINATION AT MACH 0.7. . . . .	187
V	GBU-10 BOMB TRAJECTORIES RESULTING FROM A (-3/-5) ORIFICE COMBINATION AT MACH 0.85 . . . . .	196
W	GBU-10 BOMB TRAJECTORIES RESULTING FROM A (-3/-5) ORIFICE COMBINATION AT MACH 0.95 . . . . .	205
X	GBU-10 BOMB TRAJECTORIES RESULTING FROM A (-3/-5) ORIFICE COMBINATION AT MACH 1.2. . . . .	214
AA	GBU-12 BOMB TRAJECTORIES RESULTING FROM A PARTIAL FIN OPENING AT MACH 0.7. . . . .	223
BB	GBU-12 BOMB TRAJECTORIES RESULTING FROM A PARTIAL FIN OPENING AT MACH 0.85 . . . . .	232

# TABLE OF CONTENTS (CONCLUDED)

Appendix	Title	Page
CC	GBU-12 BOMB TRAJECTORIES RESULTING FROM A PARTIAL FIN OPENING AT MACH 0.95 . . . . .	241
DD	GBU-12 BOMB TRAJECTORIES RESULTING FROM A PARTIAL FIN OPENING AT MACH 1.2. . . . .	250
EE	GBU-10 BOMB TRAJECTORIES RESULTING FROM A PARTIAL FIN OPENING AT MACH 0.7. . . . .	259
FF	GBU-10 BOMB TRAJECTORIES RESULTING FROM A PARTIAL FIN OPENING AT MACH 0.85 . . . . .	268
GG	GBU-10 BOMB TRAJECTORIES RESULTING FROM A PARTIAL FIN OPENING AT MACH 0.95 . . . . .	277
HH	GBU-10 BOMB TRAJECTORIES RESULTING FROM A PARTIAL FIN OPENING AT MACH 1.2. . . . .	286
	REFERENCES . . . . .	295

## LIST OF SYMBOLS, SIGN CONVENTIONS, AND AXIS NOTATION

x - positive forward, measured from the installed location of the cg  
y - positive outboard, measured from the installed location of the cg  
z - positive down, measured from the installed location of the cg

$\phi$ , roll angle - positive clockwise about the x-axis

$\theta$ , pitch angle - positive nose-up about the y-axis

$\psi$ , yaw angle - positive nose-outboard about the z-axis

$\alpha$  - angle-of-attack

cg - center of gravity of the store

## SECTION I

### INTRODUCTION

A GBU-12 bomb, on separating from the delivery aircraft, an F-4, was observed to pitch up as the ejectors kicked it away from the parent aircraft. The store continued to rotate nose-up until the resulting angle-of-attack was sufficiently large to generate a lift force greater than the weight and consequently the munition "flew" back into the F-4, impacting the wing and the externally carried fuel tank. Over 160 missions of GBU-10 and GBU-12 bombs had been flown previously, and fin failures on approximately 5 percent of those missions had not evinced an aircraft safety problem. Since there had been no flight safety problem in the past, it was hypothesized that the failure of the fins to open had actually compounded a problem due to (1) an unprecedented adverse interference flow field, (2) out-of-tolerance mass properties, or (3) a rack malfunction. The orifices removed from the dismantled rack were compared. It was found that even though they were stamped identically, the bore sizes were different. The consequence of unequal orifices in the rack would be an ejector force imbalance, and there would be a resulting moment applied to the store. Validation of the premise that the ejector force mismatch had coupled with the fin failure to cause the aircraft/weapon collision was undertaken by means of computer simulations of the separation event. Since no onboard camera coverage was available, the computer simulations were compared qualitatively with chase film with the hope that the simulated separation trajectories would be relatively insensitive to variations in those parameters which were hypothesized as potential candidates but were not, in fact, causative of the collision.

It should be noted that the approach employed was the flow angularity technique originally developed by Captain Stephen C. Korn, USAF (Reference 1). The assumption was made that it is valid to generalize interference effects, with constraints, as was demonstrated by Captain Korn in Reference 2.

## SECTION II

### ANALYSIS PROCEDURES

The recorded flight conditions when the collision occurred were 450 KTAS at 2000 feet altitude. Simulated flight conditions were Mach 0.7 at 2000 feet, which is within 10 knots of the actual flight. To identify effects due to dynamic pressure variations, the launches were also simulated at Mach 0.85, 0.95, and 1.2, with the added benefit that all follow-on flight testing was bracketed by the above simulations.

To determine if an unusually severe flow field existing about the inboard wing station had caused the weapon/aircraft collision, the interference effects collected in the four-foot transonic wind tunnel in the Propulsion Wind Tunnel (PWT) facility at Arnold Engineering Development Center (AEDC) (see Reference 3) were used as measured, then were halved, doubled, and inverted and halved. Computer simulations were also run with the measured interference effects inverted and scaled by a factor of five, but the results showed that the munitions' trajectories could not be corrected from impacting the parent aircraft, which is in no way representative of previous testing and, as such, were discarded.

The 0.081-inch-diameter orifices (-3) are standard forward and aft for the F-4 rack, but with the findings that one of the orifices was stamped (-3) but was actually 0.110 inch in diameter and therefore should have been marked (-5), and the observed motion of the store, it was assumed that the larger orifice was in the rearward slot. Since the rack was dismantled when the orifices were inspected, the assumed position of the larger orifice needed validation. Simulating the ejector force combinations which would result from a (-5) aft and comparing the resulting trajectories with chase film provided the necessary correlation.

To show that the collision was the result of multiple failures and not due solely to either a rack malfunction or the fin failure, trajectory simulations were run with the fins opening partially. The stability accrued from even the partial fin opening was sufficient to damp out the most severe oscillations and led to the decision not to model the complete fin opening event as it would provide no new or useful information on the problem of the aircraft/weapon collision. Similarly, the autopilot was not modeled because of the 1.5-second time delay to activate, and by this time either a collision has occurred or cannot occur. Fully active canards are not of concern until the autopilot is enabled, but prior to the autopilot assuming control, the canards are damped. The variations in free-stream aerodynamics due to damped canards are properly defined as higher-order terms, and it was felt that a catastrophic failure such as the collision under investigation did not lend itself to extensive modeling initially. This decision was further substantiated by the urgency of determining primary causes.

Free-stream aerodynamics were obtained for both the GBU-10 and GBU-12 bombs from Reference 4. Typical mass properties were obtained from Reference 5 and were then corroborated for the specific munition that impacted the F-4 aircraft from the Bomb C/G Facility Test Report (ADTC Form 693).

## SECTION III

### DISCUSSION OF RESULTS

The important output parameters in this investigation were the attitude and position of the munition when the PEP fins had failed to open. Appendices A through L present plots of the GBU-12 bomb trajectories generated by the simulation, and Appendices M through X present plots of the GBU-10 bomb trajectories for the fin failure condition. A separate appendix for each Mach number/ejector force combination was chosen to facilitate comparison of results. In each appendix, X, Y, and Z position of the store cg relative to the installed position on the pylon and roll, pitch, and yaw rotations about the cg are for each value of flow field intensity. The time scale for all simulations is constant to facilitate cross-correlation, but where the equations of motion have passed through a single point, i.e.,  $90^\circ$  for any one of the Euler angles, the mathematics breakdown and the predicted trajectories are no longer valid. The rationale behind simulating to 3 seconds was based on studying the damping from the fin opening event which occurs at a fixed distance from the launch aircraft (the length of the lanyard) and at some finite time after launch. The results from the simulations which treat the partial opening of the fins are presented in Appendices AA through DD for the GBU-12 bomb and in Appendices EE through HH for the GBU-10 bomb.

In each appendix, it can be seen that as flow field intensity is increased the translational motion correspondingly increases, and the period of the rotational motion is shortened without significantly affecting the amplitude. In some of the figures presenting rotational motion, the apparent change in amplitude is actually due to a change in scaling. Figures -7 and -8 in each appendix present trajectories for an inverted and halved flow field for which the translational motion is markedly reduced, and, as expected, the rotational motions are the mirror image of motions from the unaltered flow field. Comparison of the data presented in the flow appendices for which the ejector force combination remains unchanged (e.g., Appendices A, B, C, and D, or Appendices Q, R, S, and T) shows that increasing Mach number has the same effect as increasing flow field intensity, but the resulting variances are more marked. For a one-to-one comparison of fin failure to partial fin opening, Appendices E through H correspond to Appendices AA through DD and Appendices Q through T correspond to Appendices EE through HH, respectively.

As can be seen from the figures, there is very little change in roll angle. The change in the frequency of response is particularly noticeable while the total amplitudes do not change significantly, but the yaw angle is reduced by an order of magnitude.



## SECTION IV

### CONCLUSIONS

As was hypothesized, the overriding parameter in the simulated aircraft/GBU-12 bomb separation problem was the mismatched orifice combination, and Appendices I through L show that a collision occurs with that ejector force combination, regardless of Mach number or flow field effects. Appendices U through X show that the increased inertia and gravity effects accruing from the sheer mass of the GBU-10 bomb are sufficiently large that no aircraft safety problem exists.

APPENDIX A

GBU-12 BOMB TRAJECTORIES RESULTING FROM A  
(-5/-3) ORIFICE COMBINATION AT MACH 0.7

17710-25  
0

5-1-55

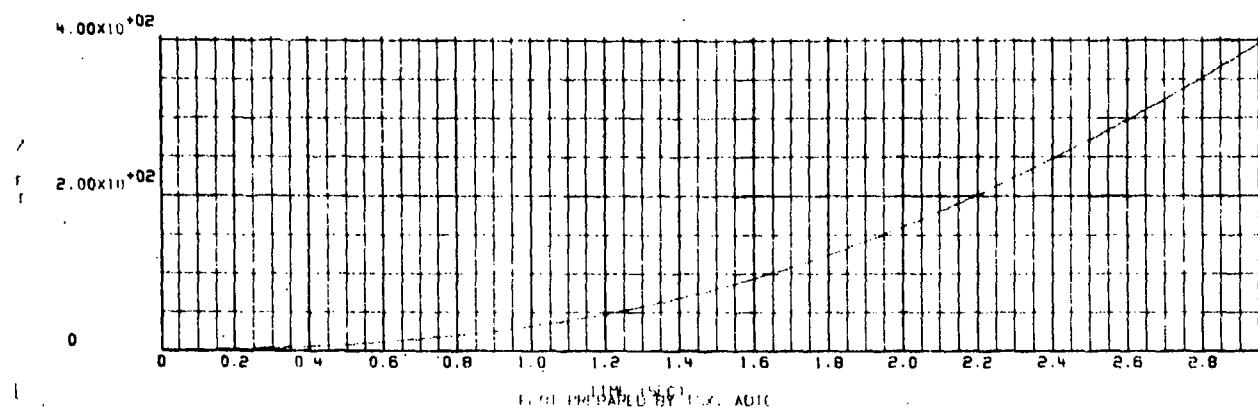
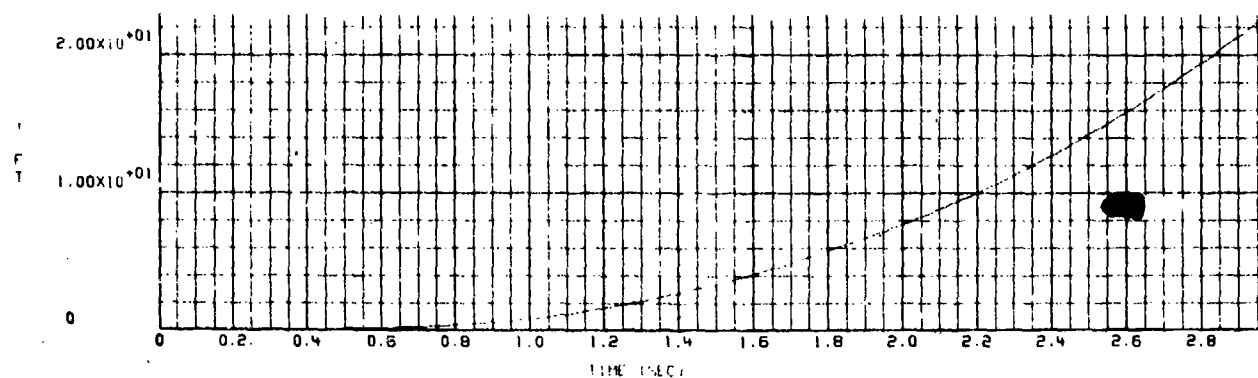
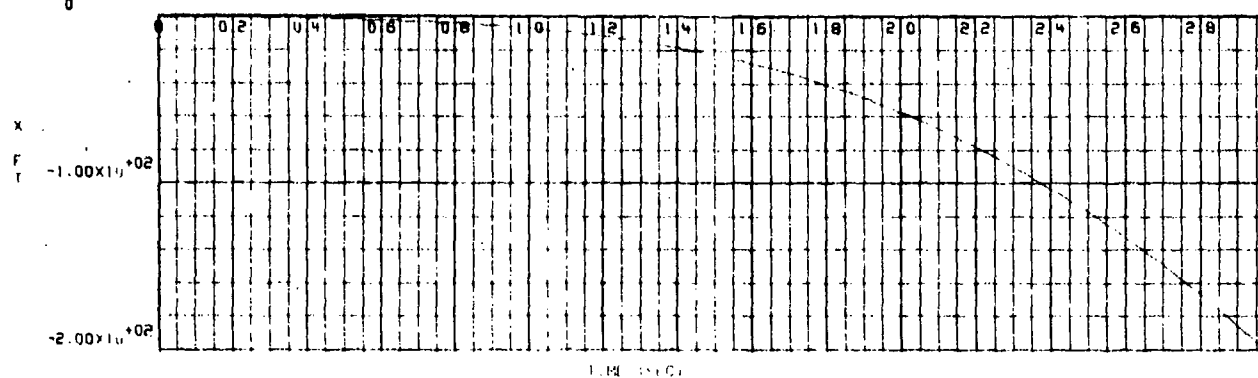


Figure A-1. X, Y, and Z Position Versus Time for a Flow Field Intensity of 1/2

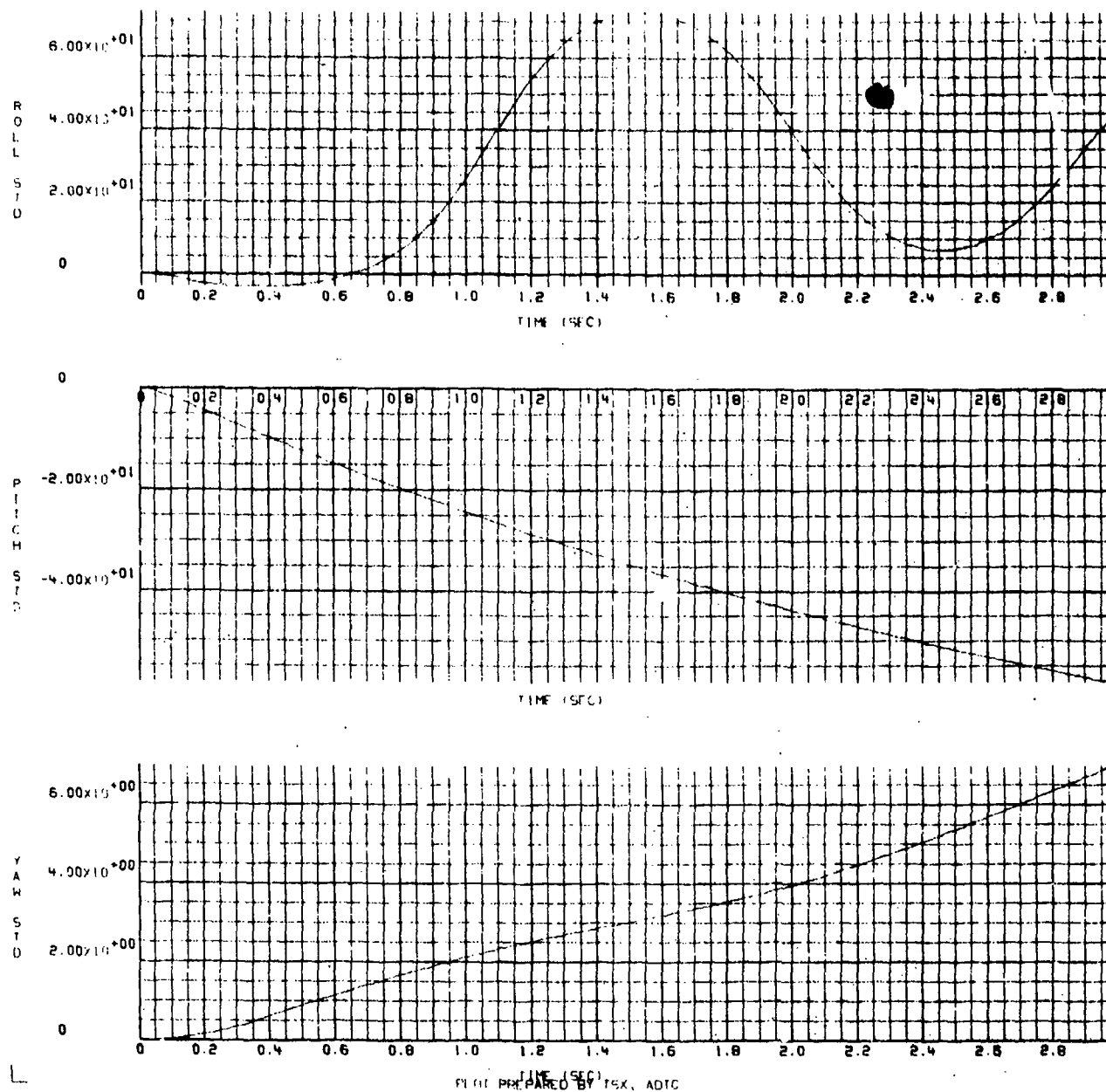


Figure A-2.  $\phi$ ,  $\theta$ , and  $\psi$  Rotation Versus Time for a Flow Field Intensity of  $1/2$

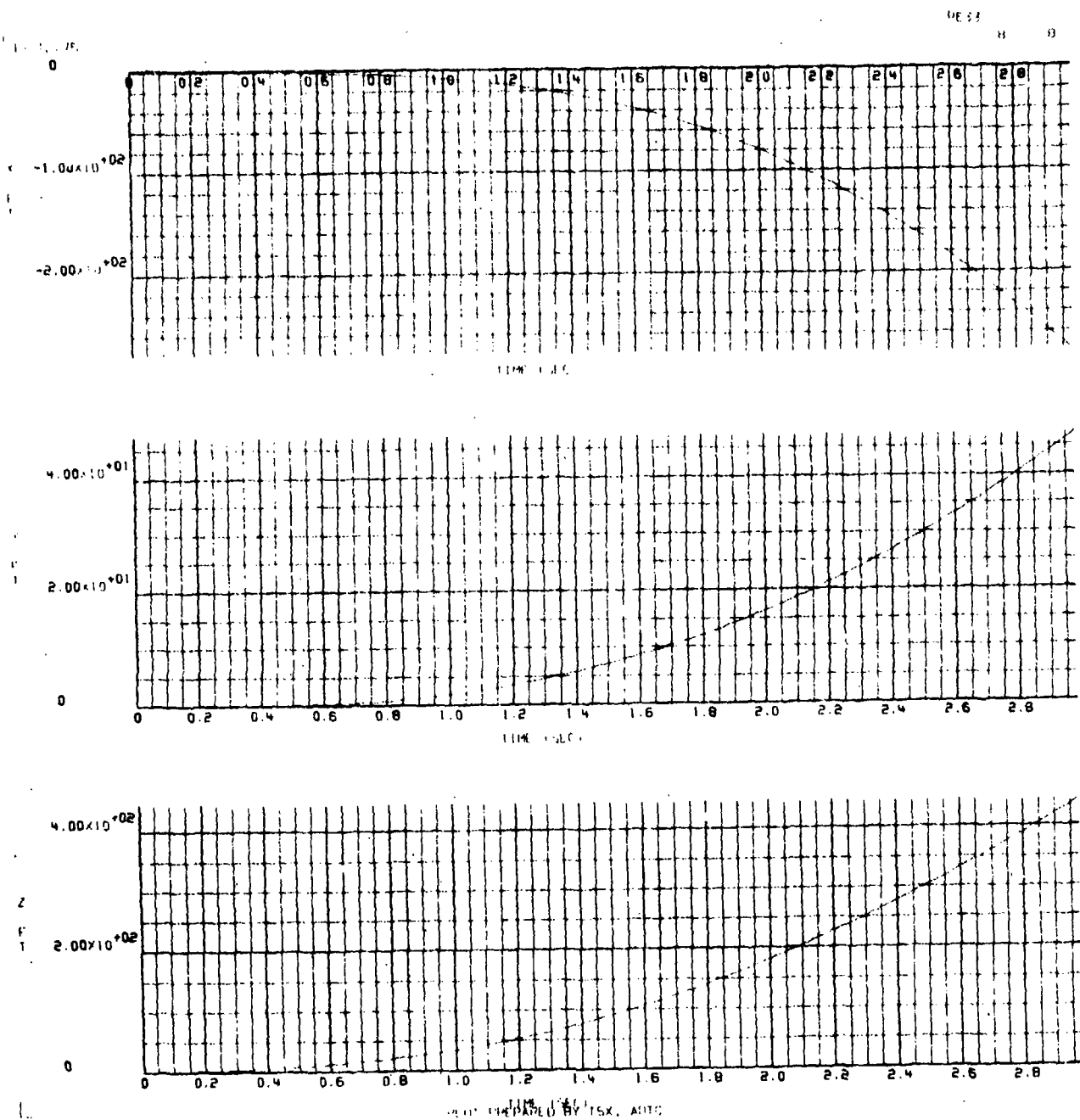


Figure A-3. X, Y, and Z Position Versus Time for a Flow Field Intensity of 1 (as measured in the wind tunnel)

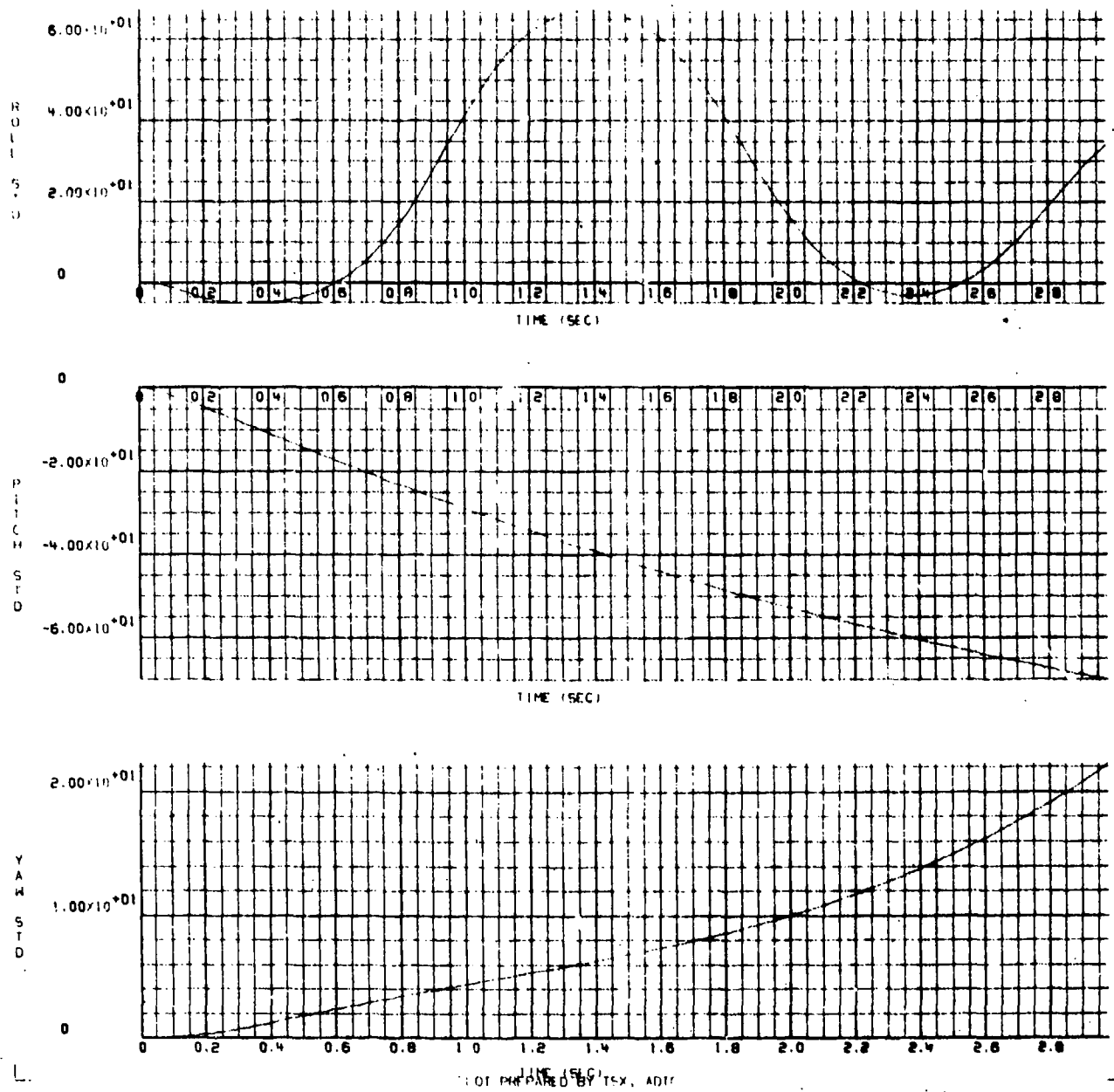


Figure A-4.  $\phi$ ,  $\theta$ , and  $\psi$  Rotation Versus Time for a Flow Field Intensity of 1 (unchanged from the wind tunnel measured values)

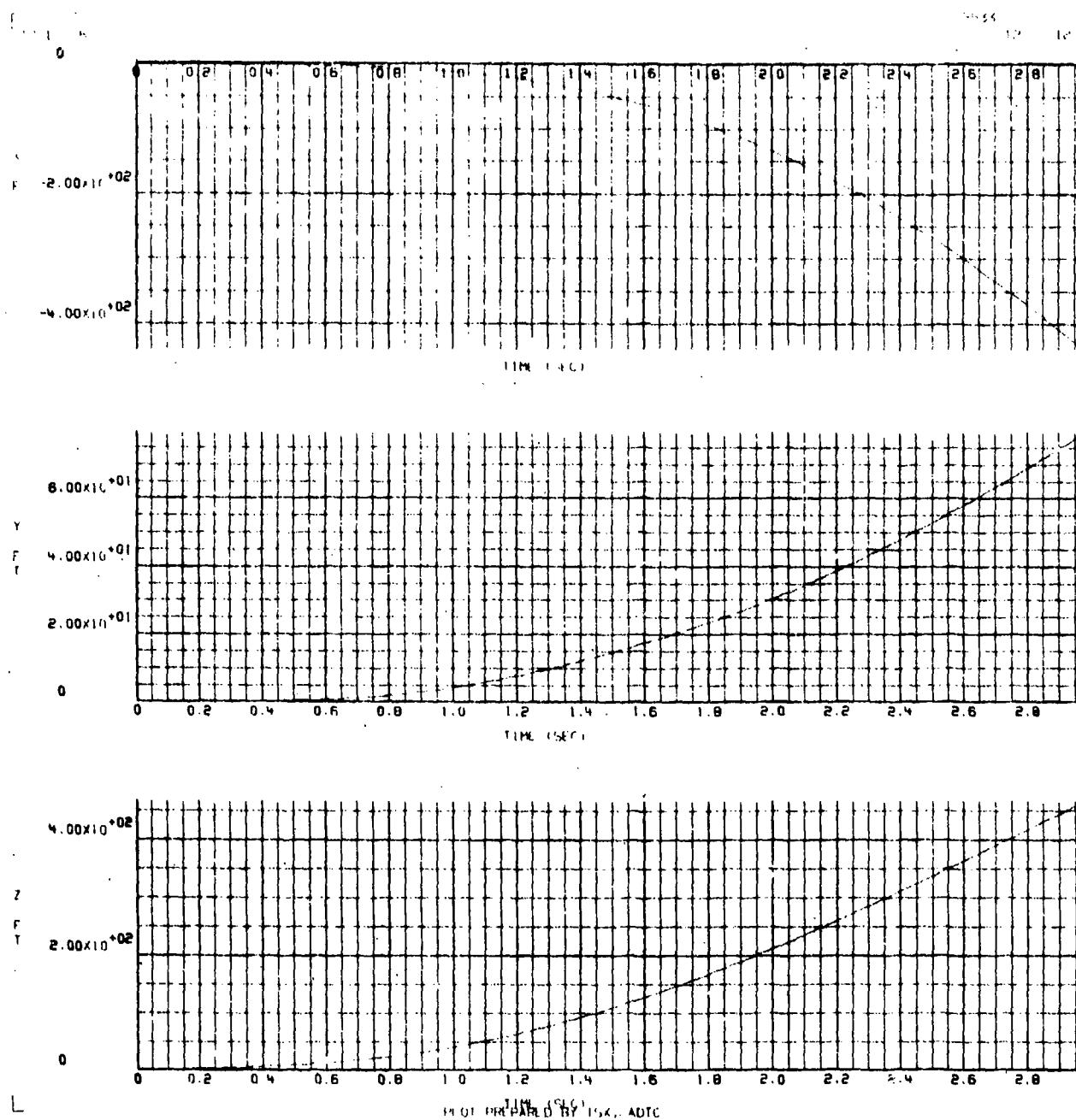


Figure A-5. X, Y, and Z Position Versus Time for a Flow Field Intensity of 2

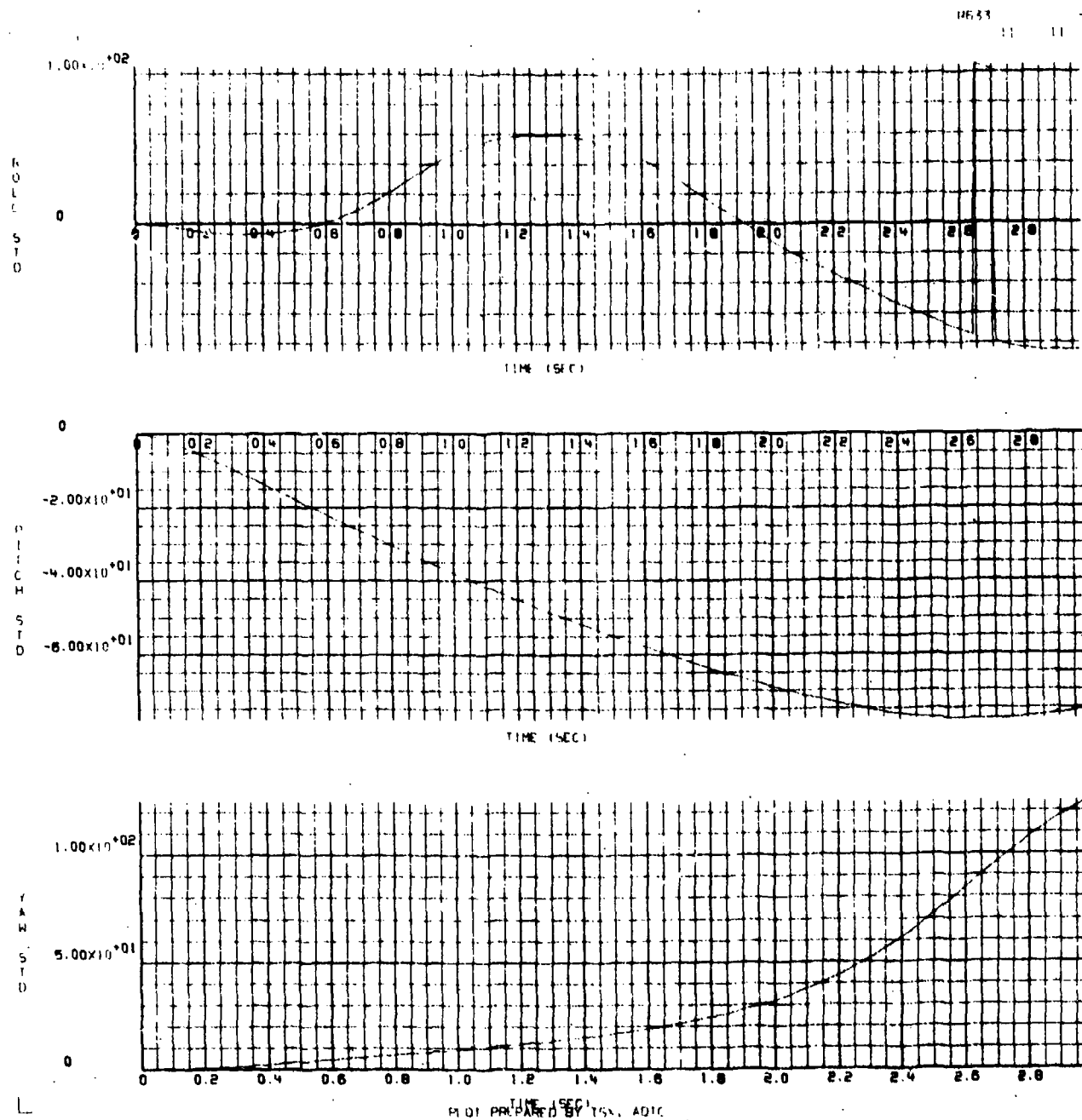
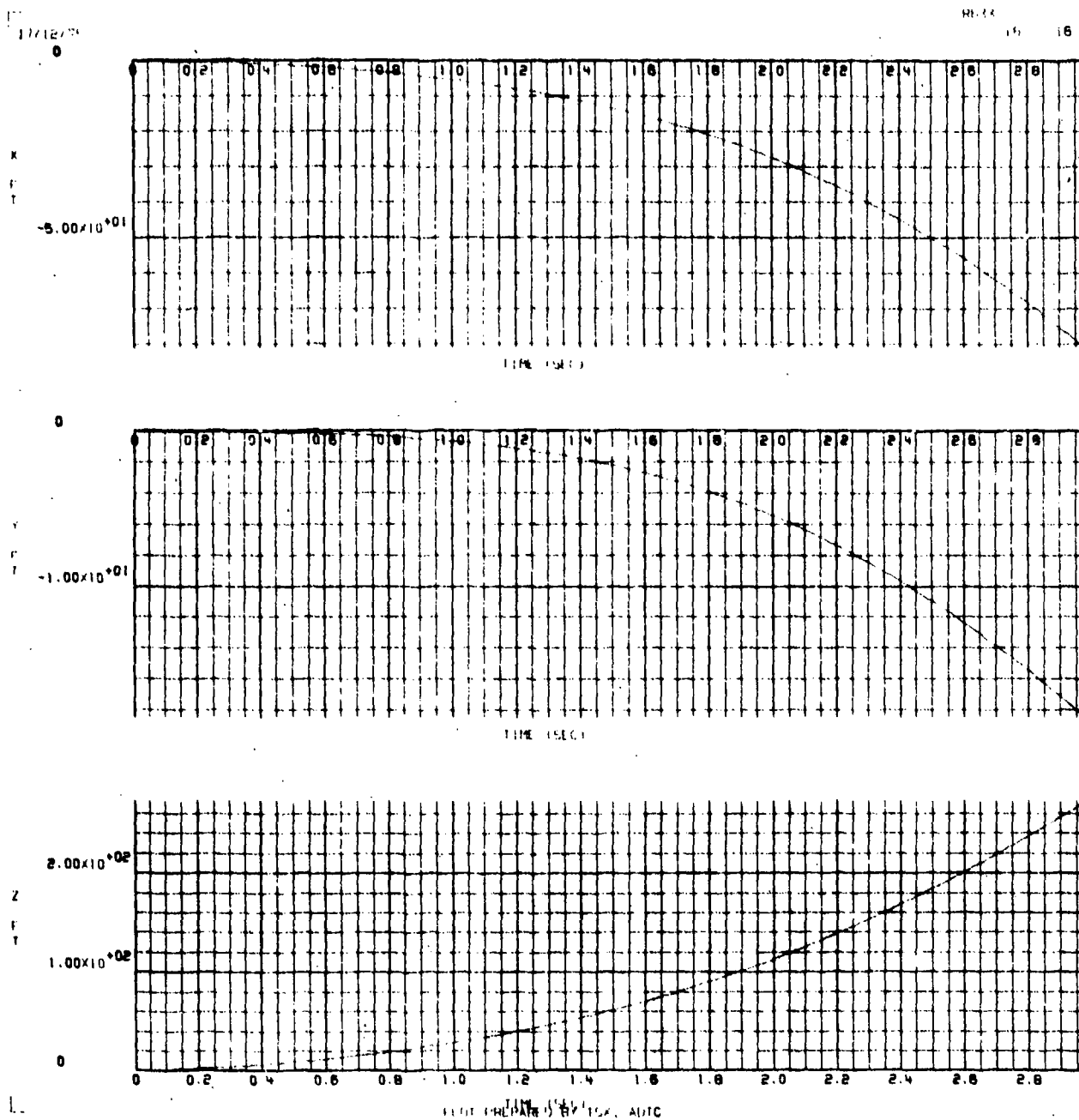


Figure A-6.  $\phi$ ,  $\theta$ , and  $\psi$  Rotation Versus Time for a Flow Field Intensity of 2





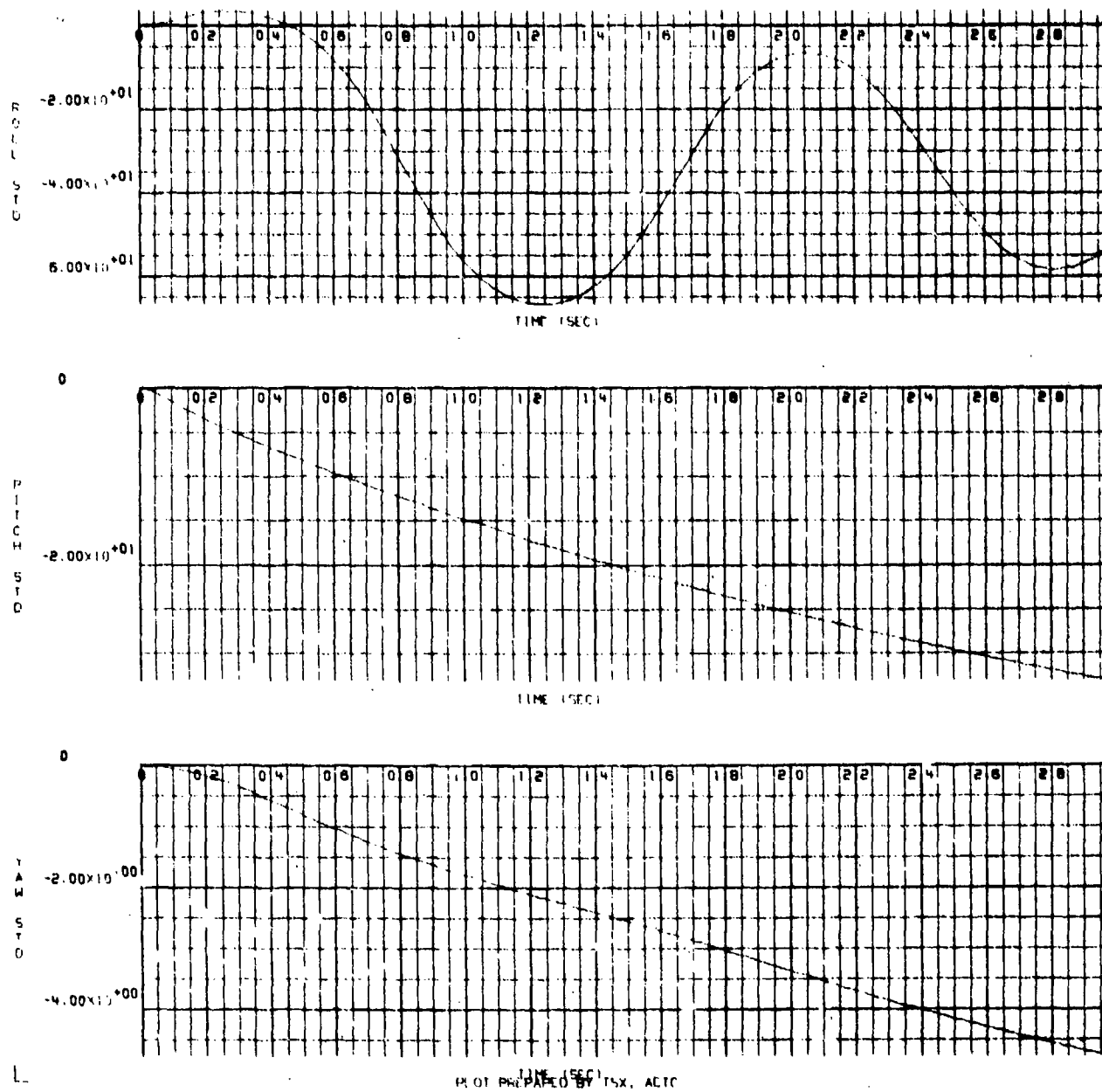


Figure A-8.  $\phi$ ,  $\theta$ , and  $\psi$  Rotation Versus Time for a Flow Field intensity of  $-1/2$

**APPENDIX B**

**GBU-12 BOMB TRAJECTORIES RESULTING FROM A  
(-5/-3) ORIFICE COMBINATION AT MACH 0.85**

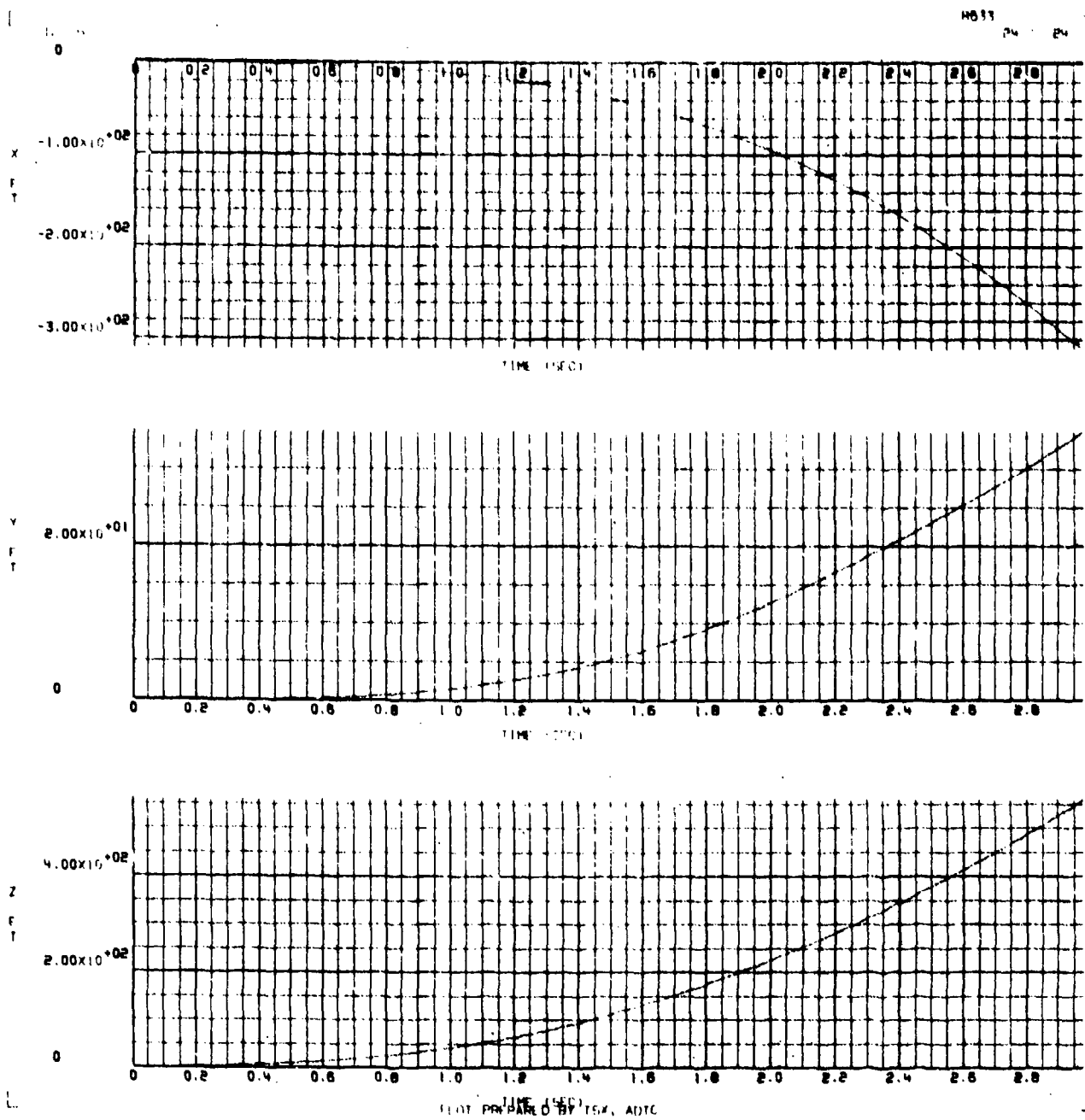


Figure B-1. X, Y, and Z Position Versus Time for a Flow Field Intensity of 1/2

12-15

0543

23 23

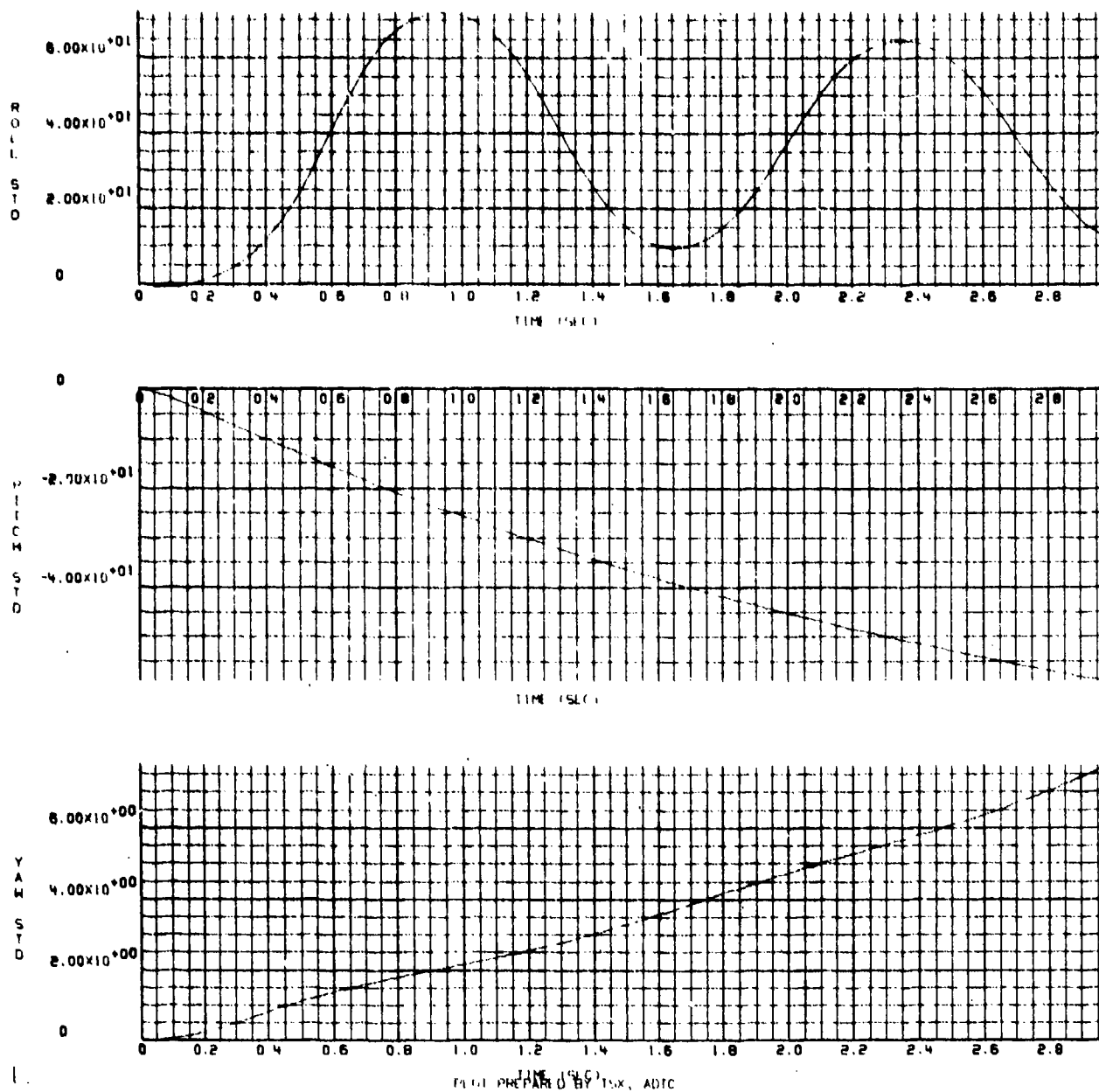


Figure B-2.  $\phi$ ,  $\theta$ , and  $\psi$  Rotation Versus Time for a Flow Field Intensity of  $1/2$

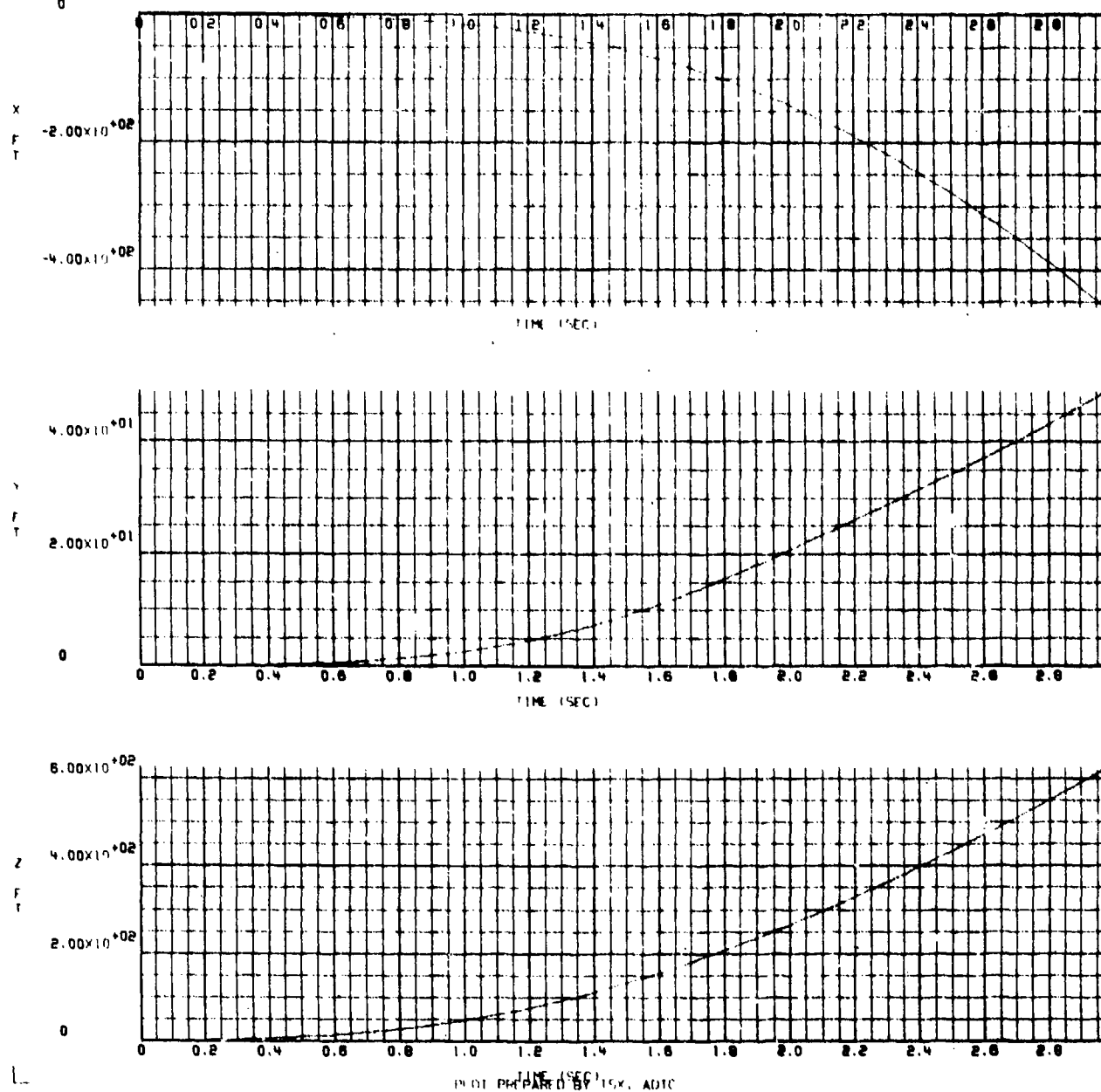


Figure B-3. X, Y, and Z Position Versus Time for a Flow Field Intensity of 1 (as measured in the wind tunnel)

17/12/75

RG33

27

27

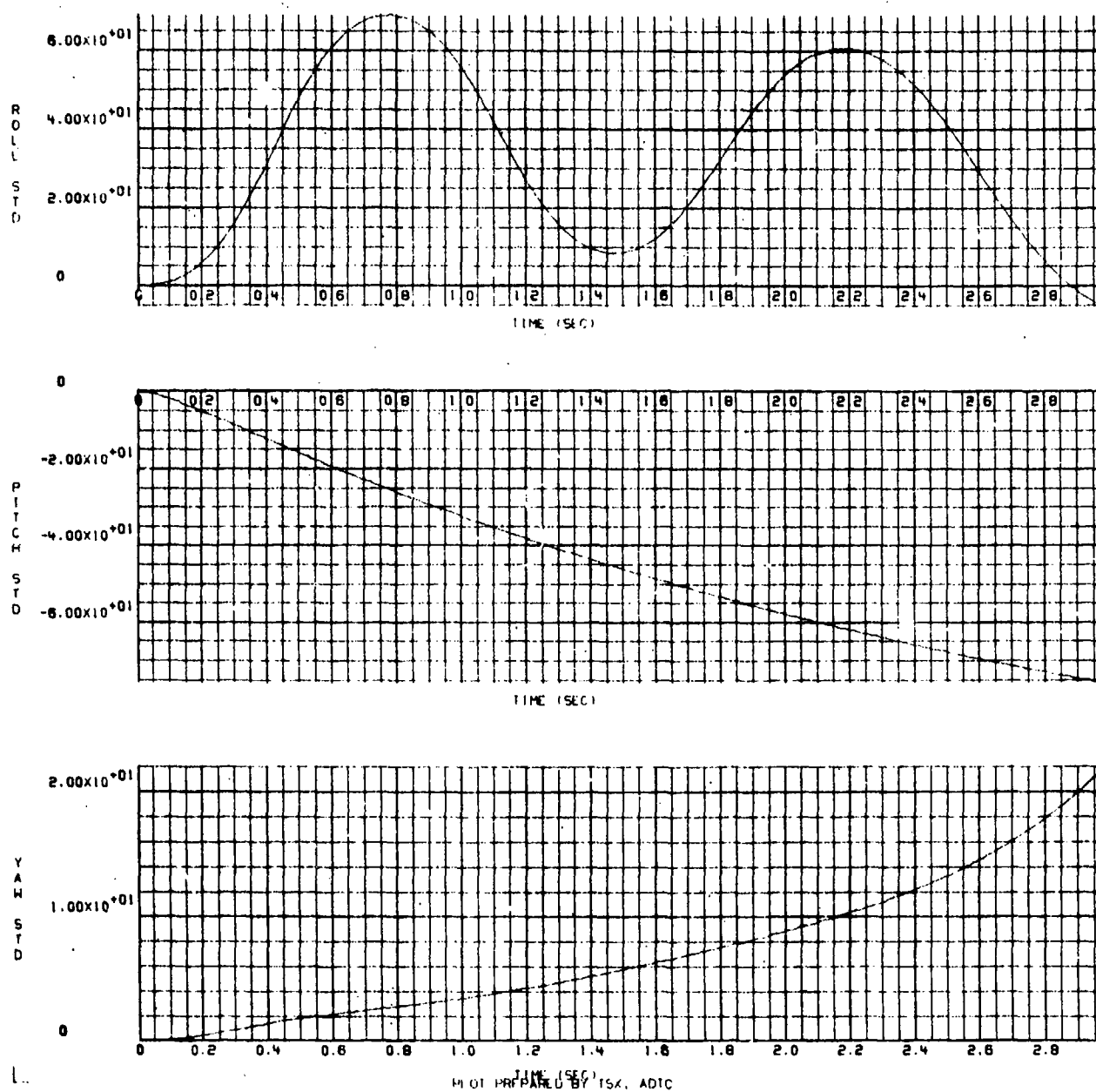


Figure B-4.  $\phi$ ,  $\theta$ , and  $\psi$  Rotation Versus Time for a Flow Field Intensity of 1 (unchanged from the wind tunnel measured values)

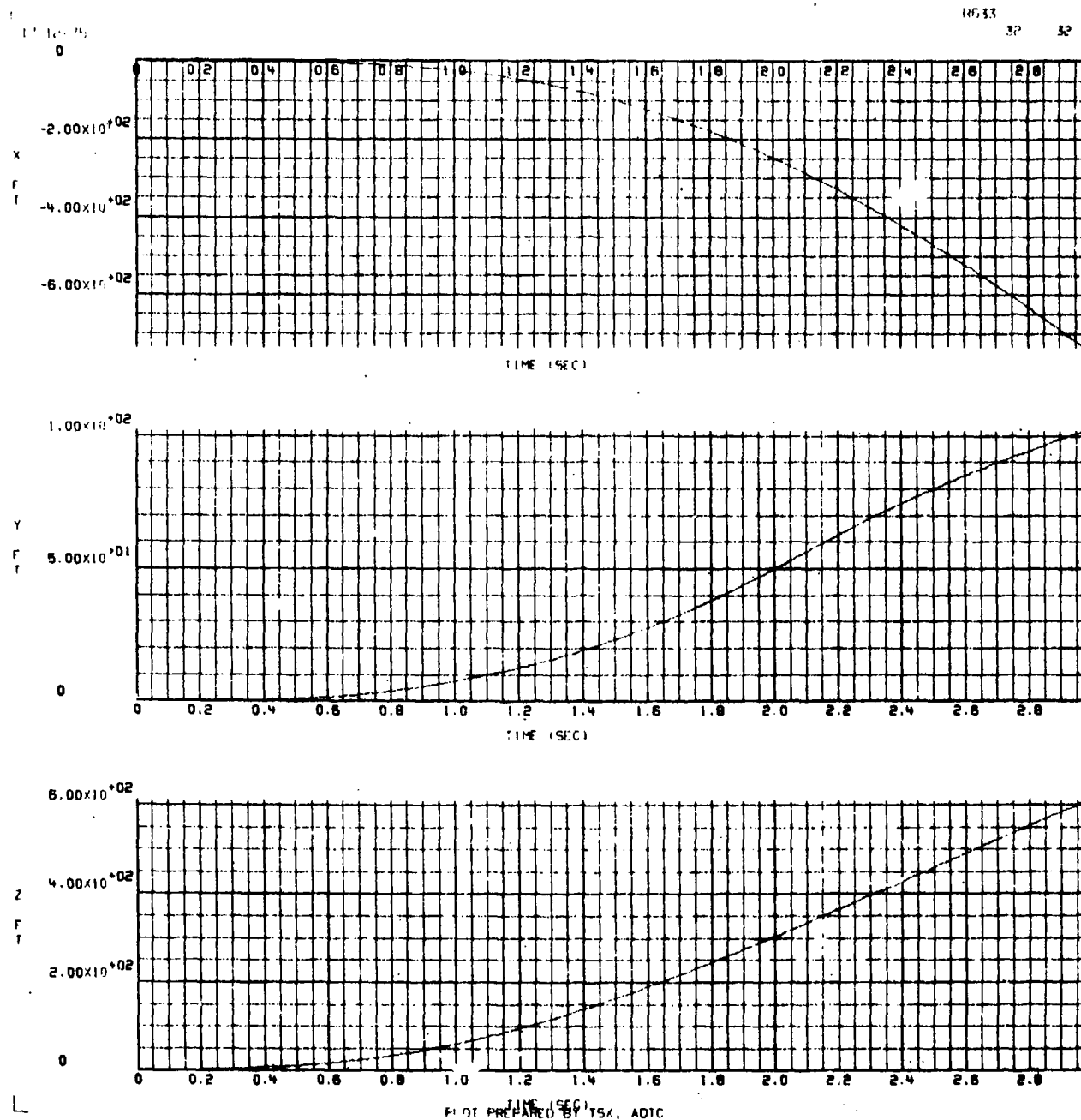
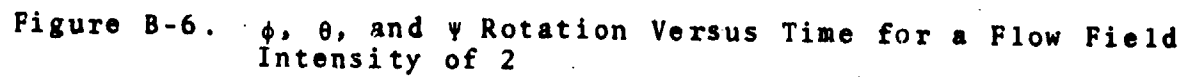
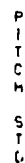


Figure B-5. X, Y, and Z Position Versus Time for a Flow Field Intensity of 2



ROLL  
STO

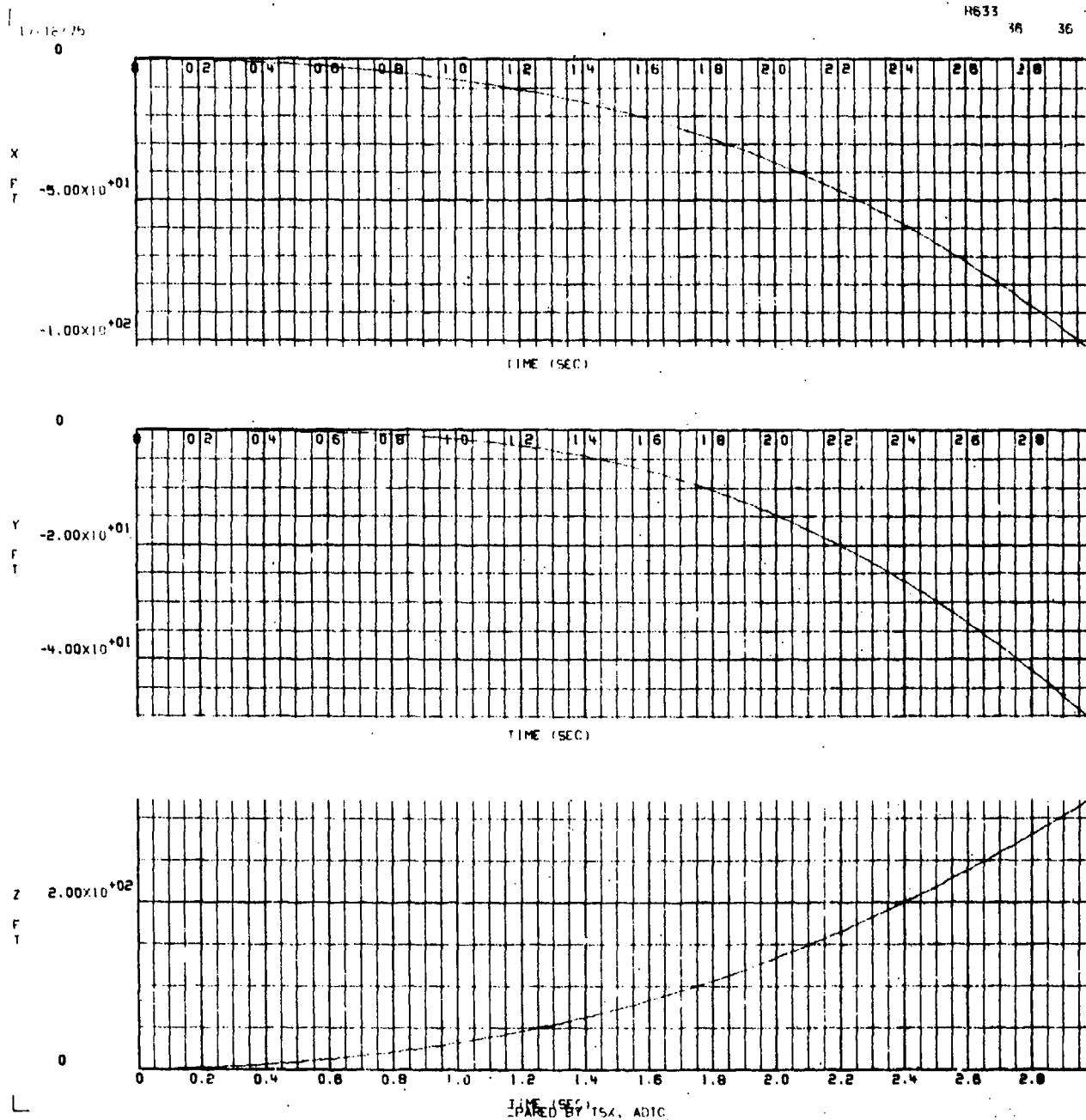


Figure B-7. X, Y, and Z Position Versus Time for a Flow Field Intensity of  $-1/2$

17/12/75

#633

35 35

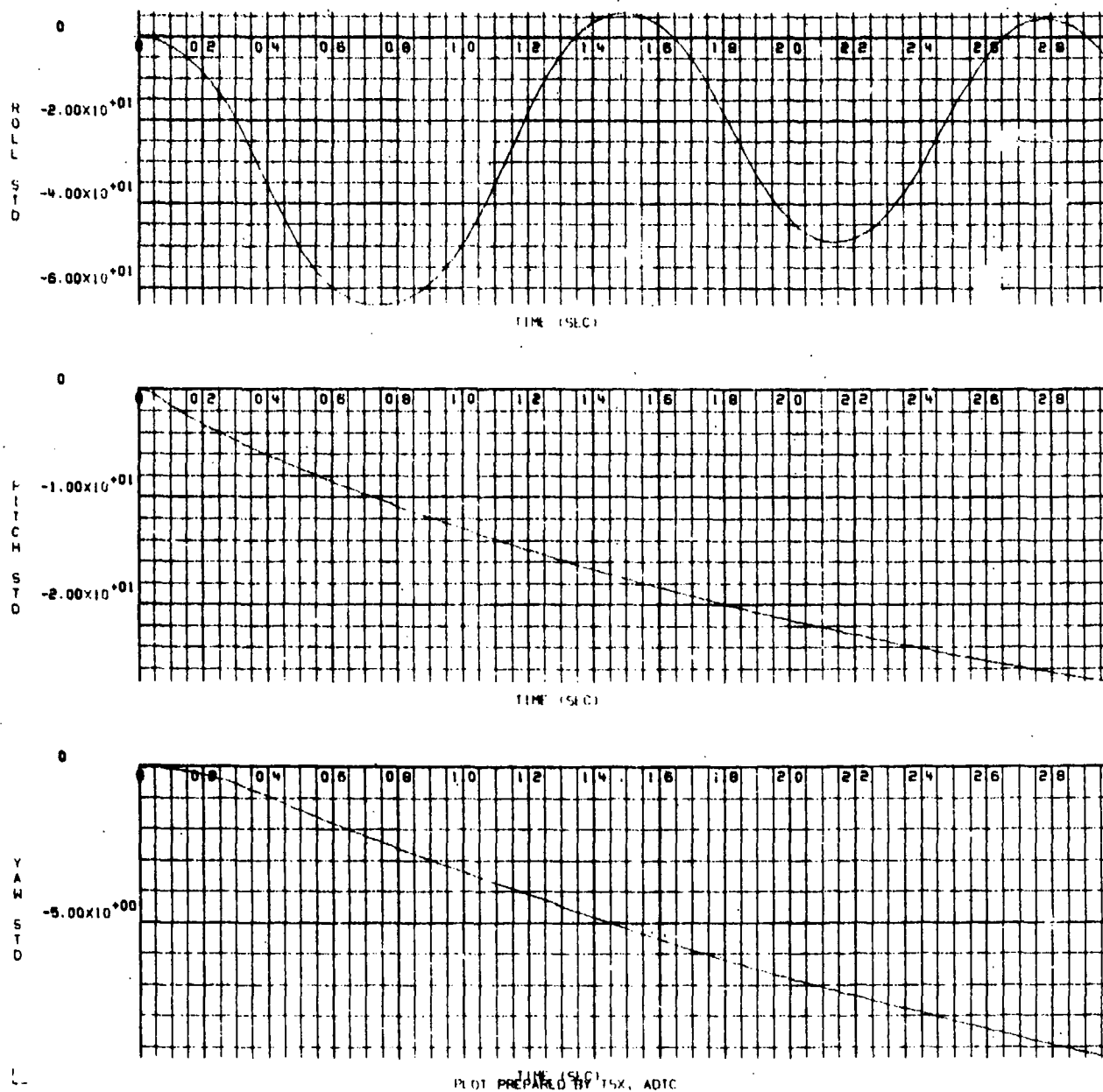


Figure B-8.  $\phi$ ,  $\theta$ , and  $\psi$  Rotation Versus Time for a Flow Field Intensity of  $-1/2$

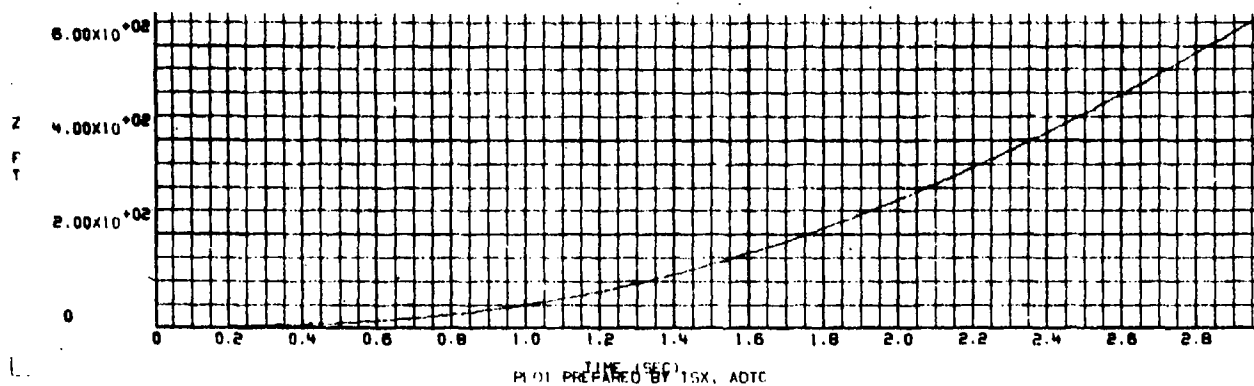
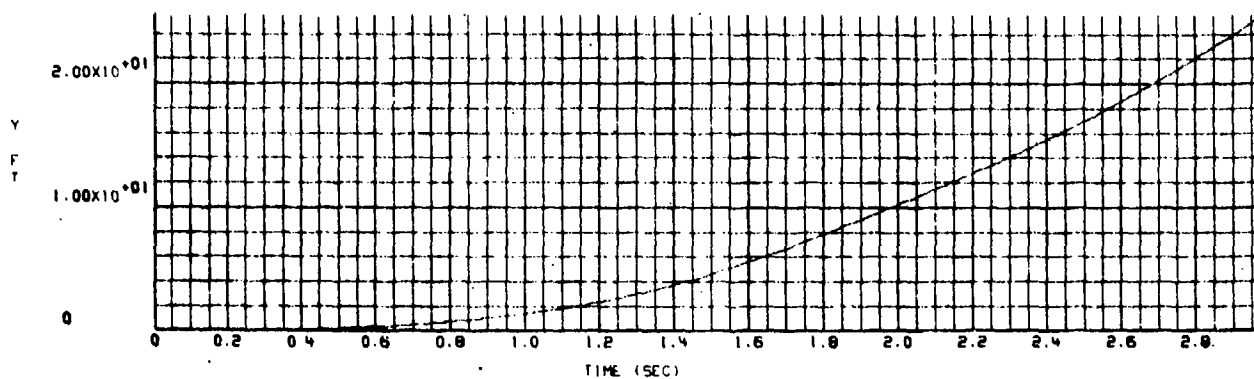
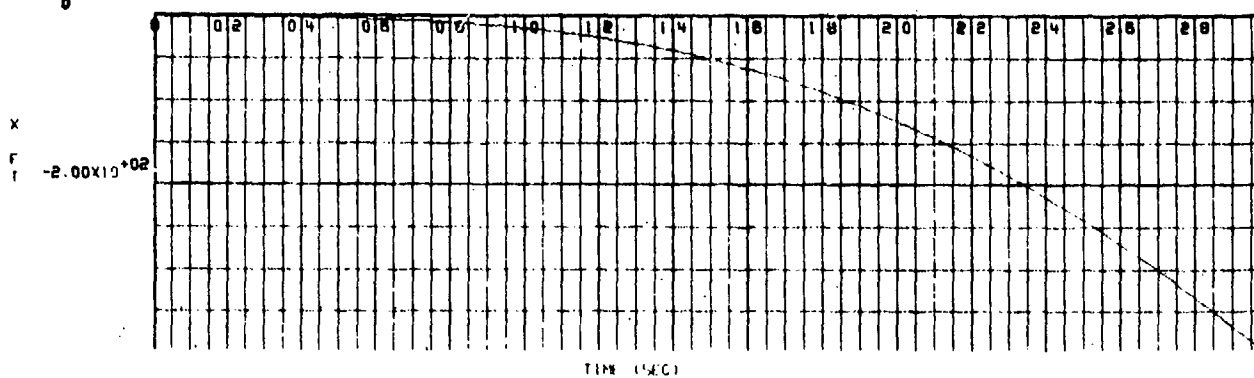
APPENDIX C

GBU-12 BOMB TRAJECTORIES RESULTING FROM A  
(-5/-3) ORIFICE COMBINATION AT MACH 0.95

17/12/75  
0

R833

44 44



PI 01 PREPARED BY ISX, ADTC

Figure C-1. X, Y, and Z Position Versus Time for a Flow Field Intensity of 1/2

12/12/75

R633 43 43

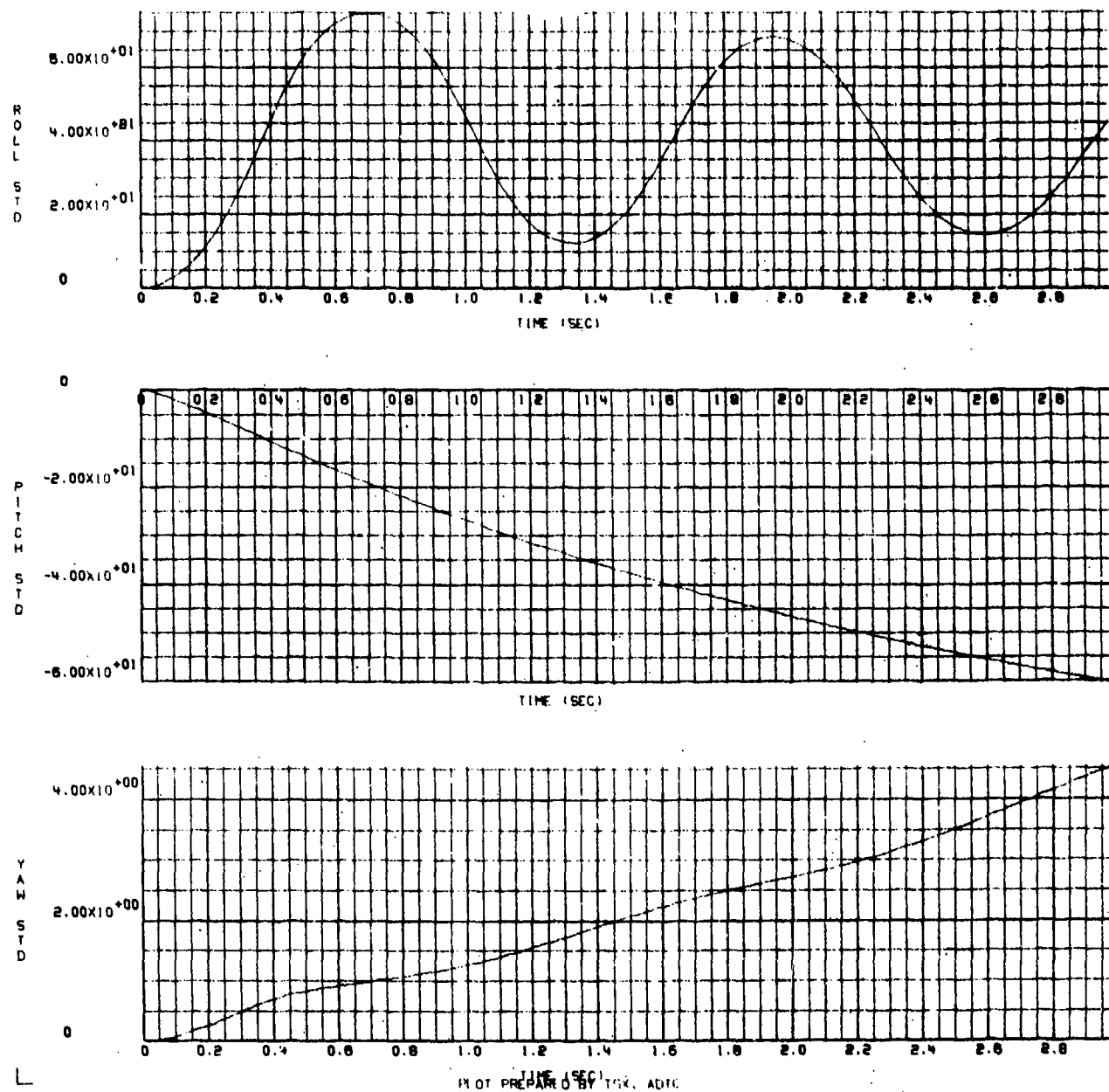
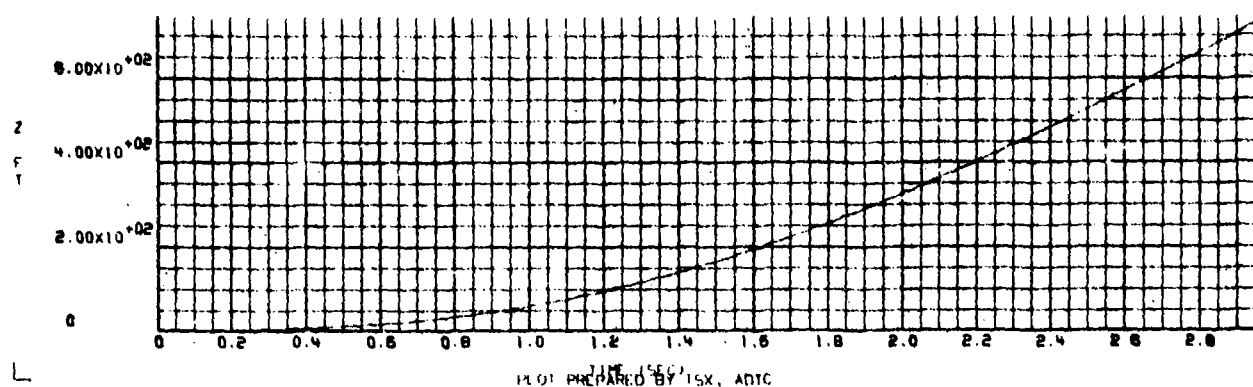
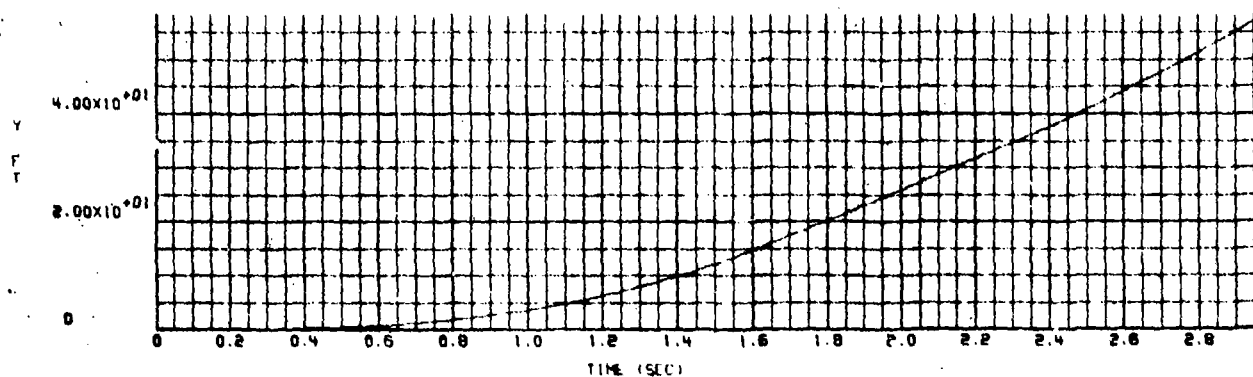
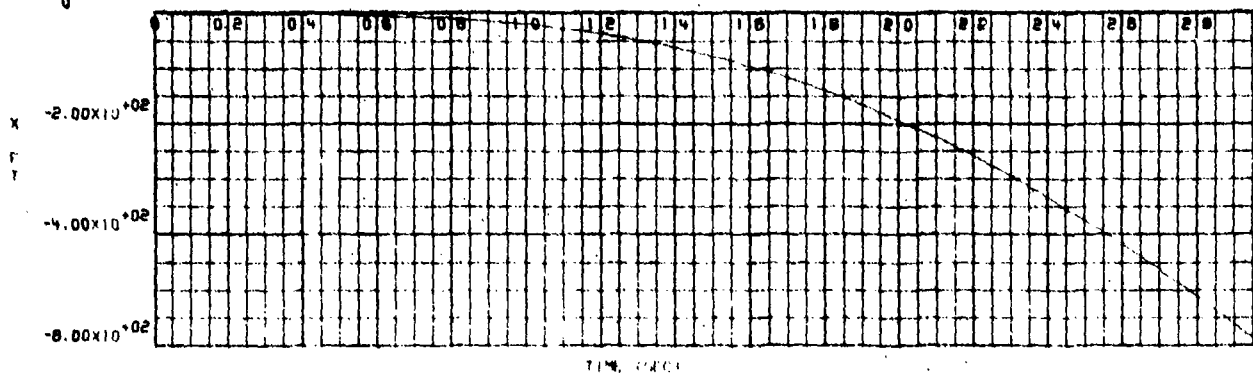


Figure C-2.  $\phi$ ,  $\theta$ , and  $\psi$  Rotation Versus Time for a Flow Field Intensity of  $1/2$

17-12/75  
0

R613

48 48



DATE 1-5-67  
PLOT PREPARED BY ISX, ARDC

Figure C-3. X, Y, and Z Position Versus Time for a Flow Field Intensity of 1 (as measured in the wind tunnel)

1/12/75

R633

47 47

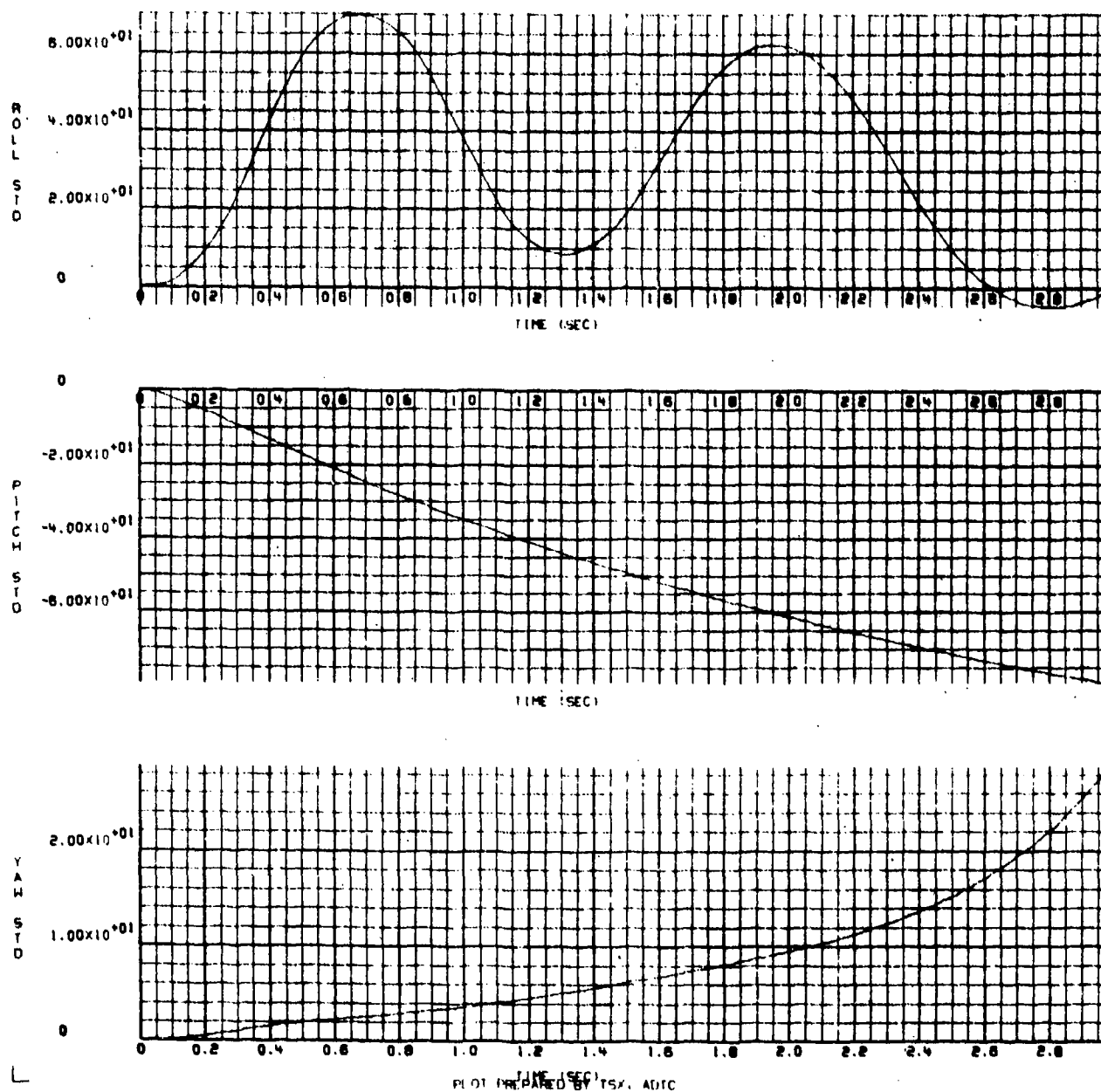


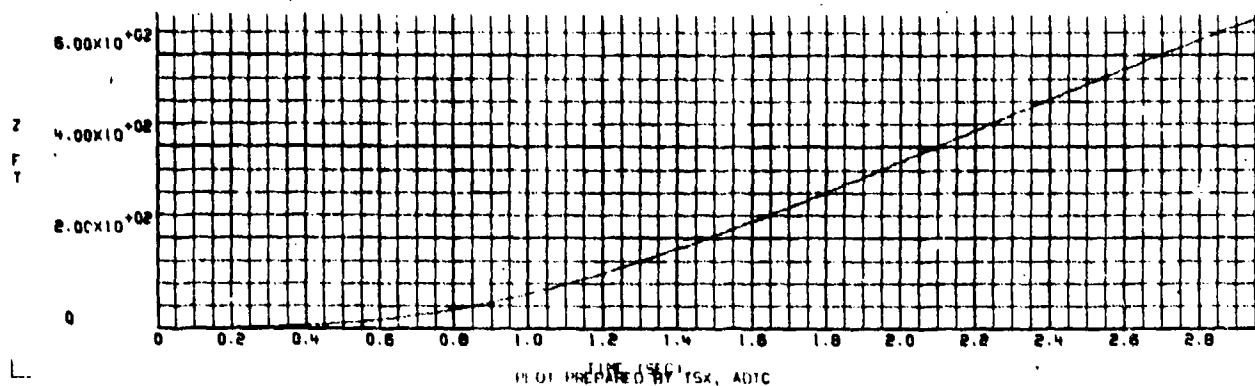
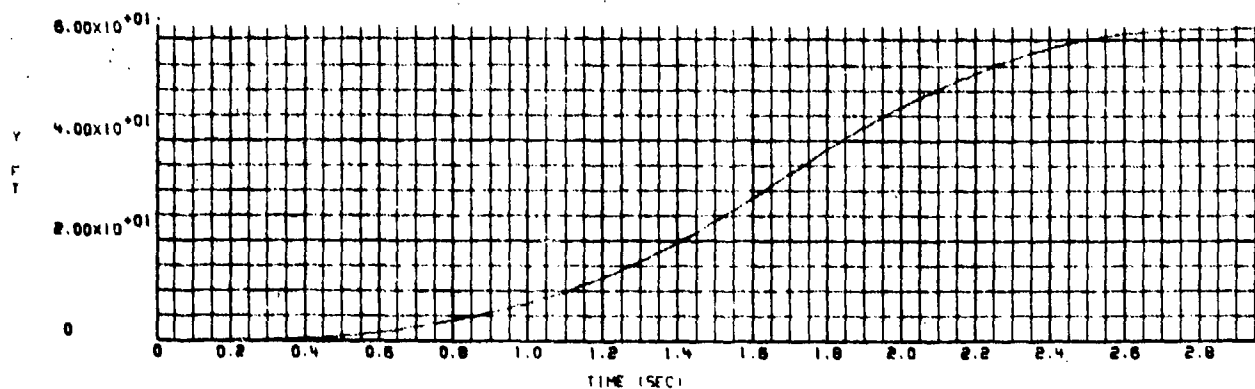
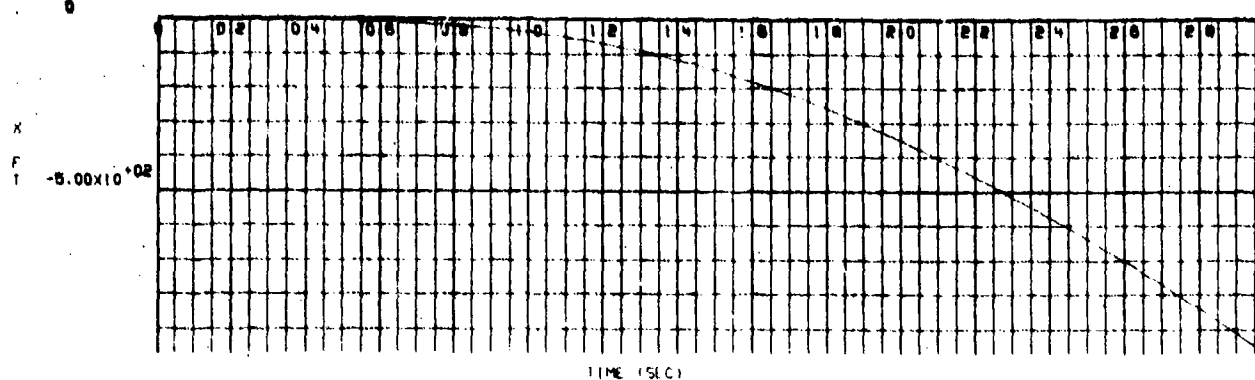
Figure C-4.  $\phi$ ,  $\theta$ , and  $\psi$  Rotation Versus Time for a Flow Field Intensity of 1 (unchanged from the wind tunnel measured values)



17/12/75  
0

R633

52 52



PLT PREPARED BY TSX, ADTC

Figure C-5. X, Y, and Z Position Versus Time for a Flow Field Intensity of 2

12/75

R633 51 81

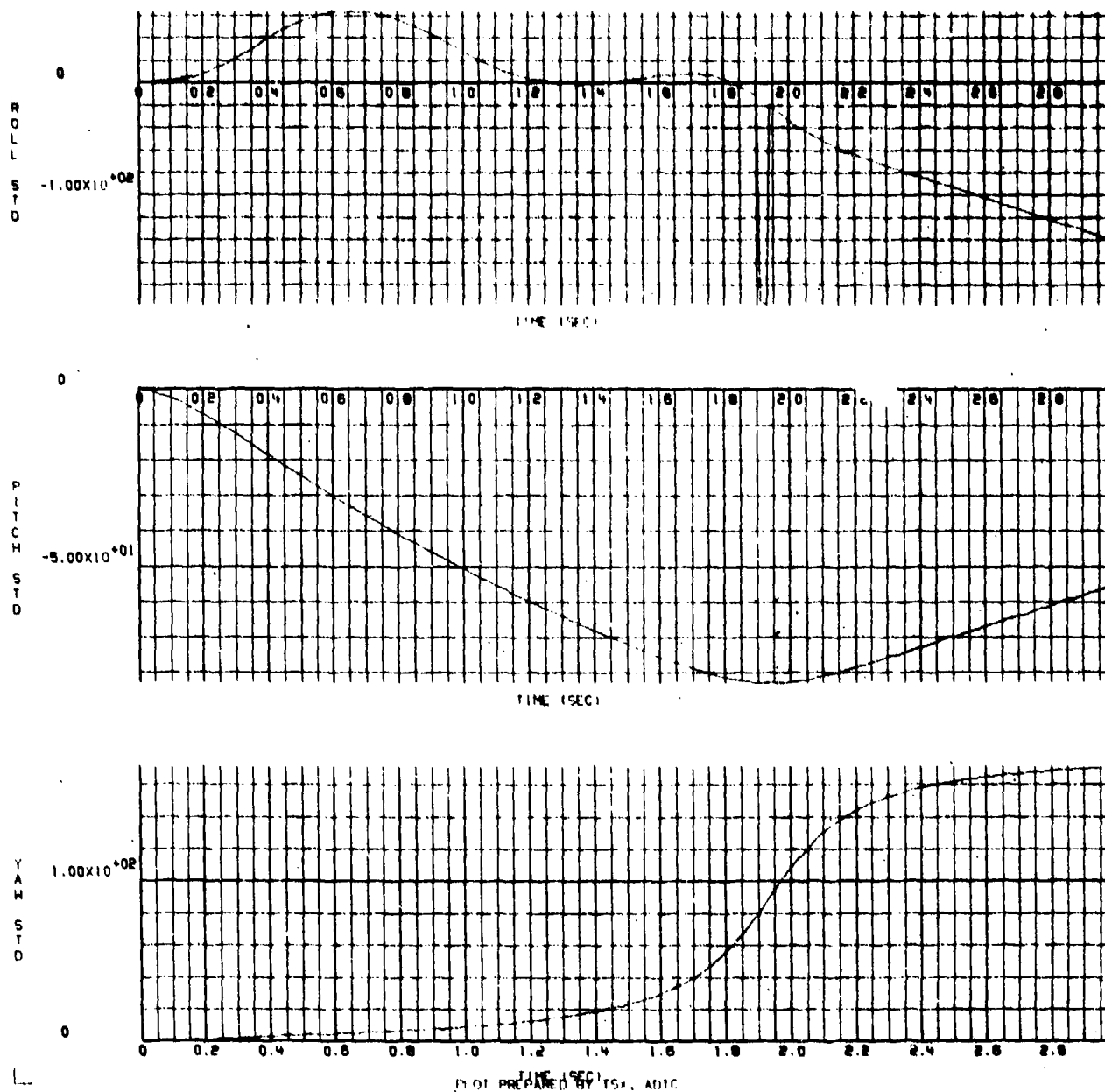


Figure C-6.  $\phi$ ,  $\theta$ , and  $\psi$  Rotation Versus Time for a Flow Field Intensity of 2

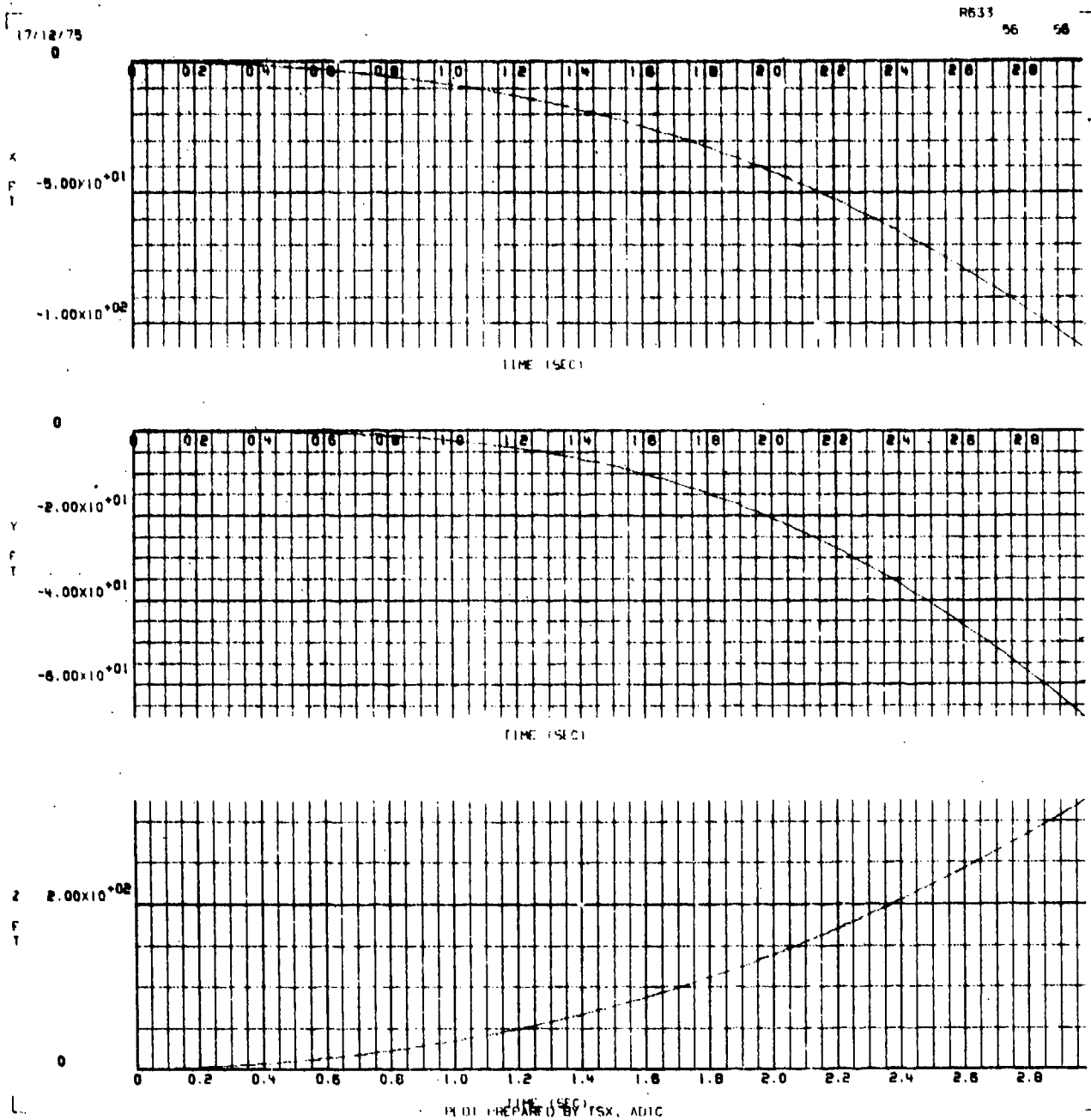


Figure C-7. X, Y, and Z Position Versus Time for a Flow Field Intensity of  $-1/2$

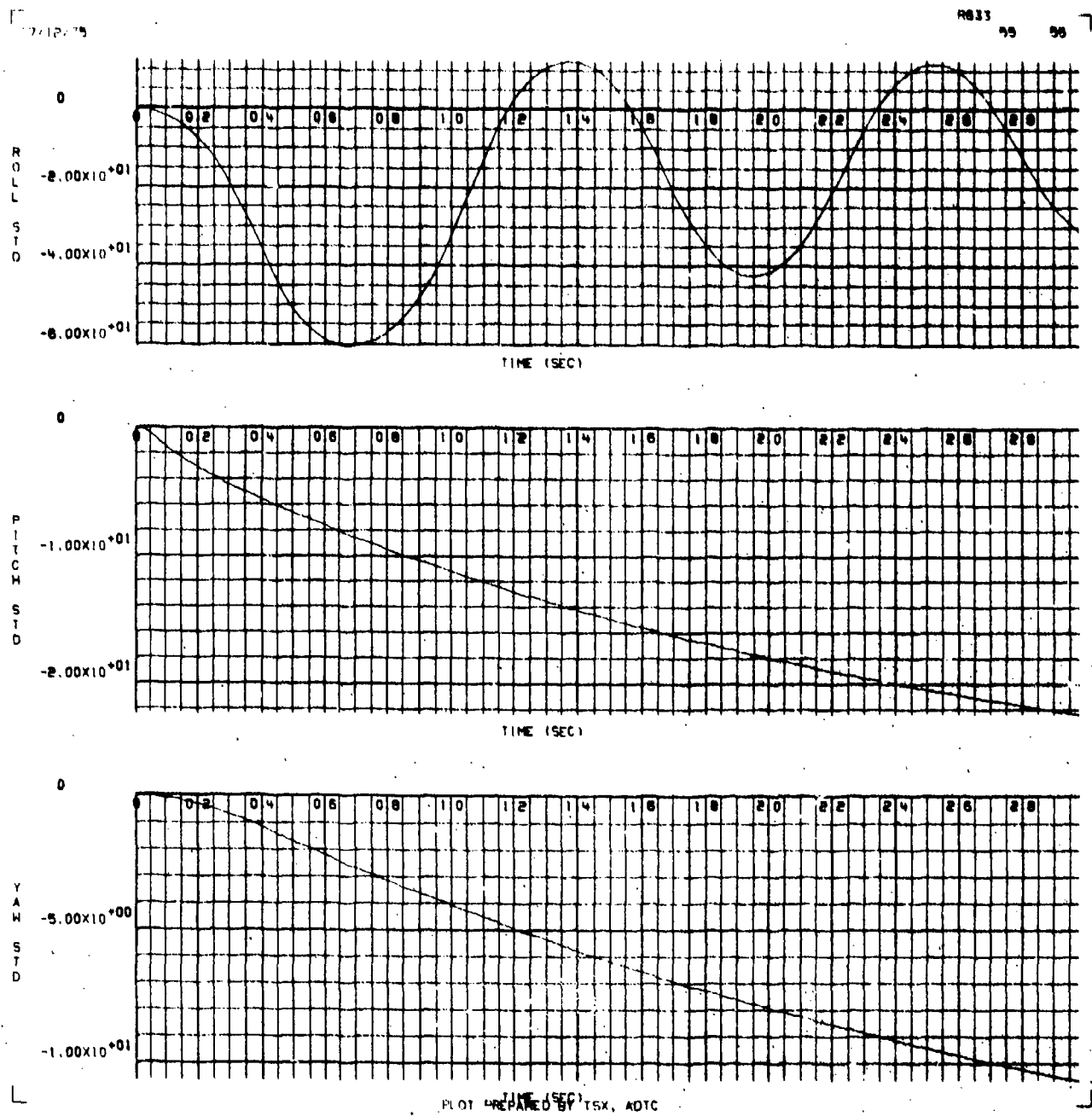


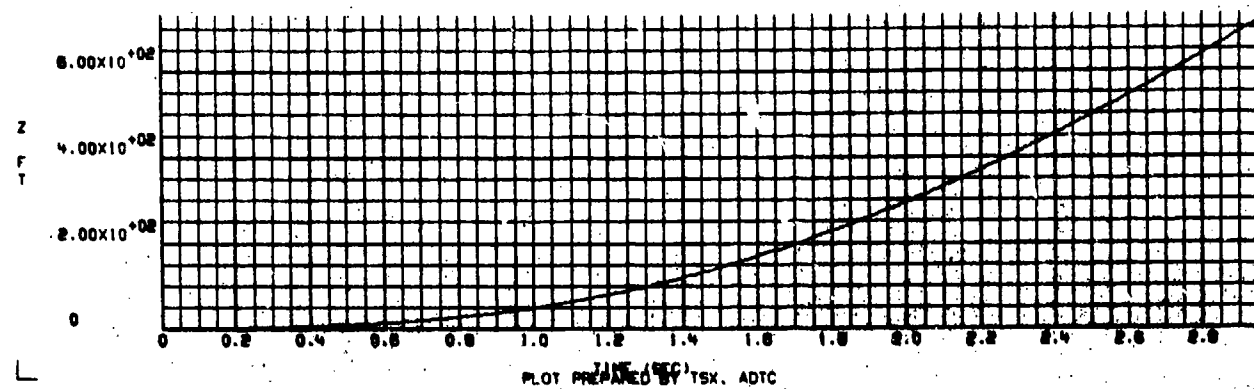
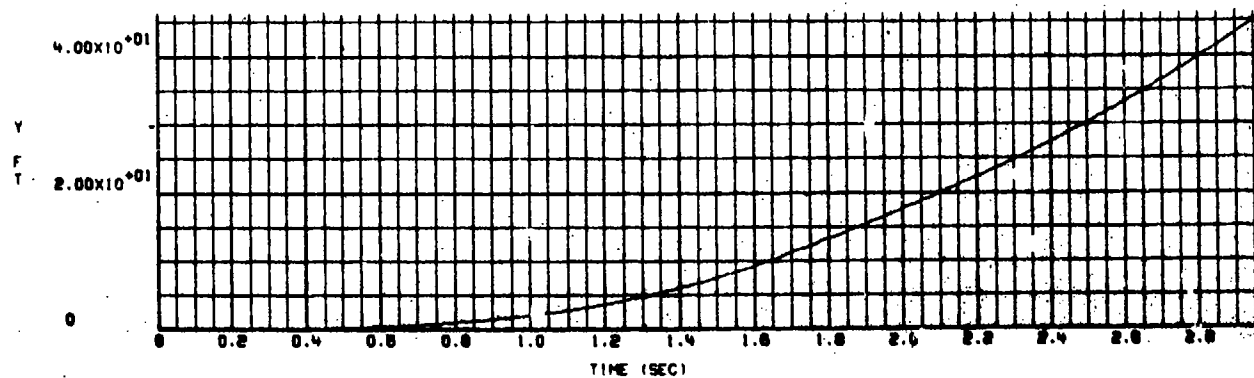
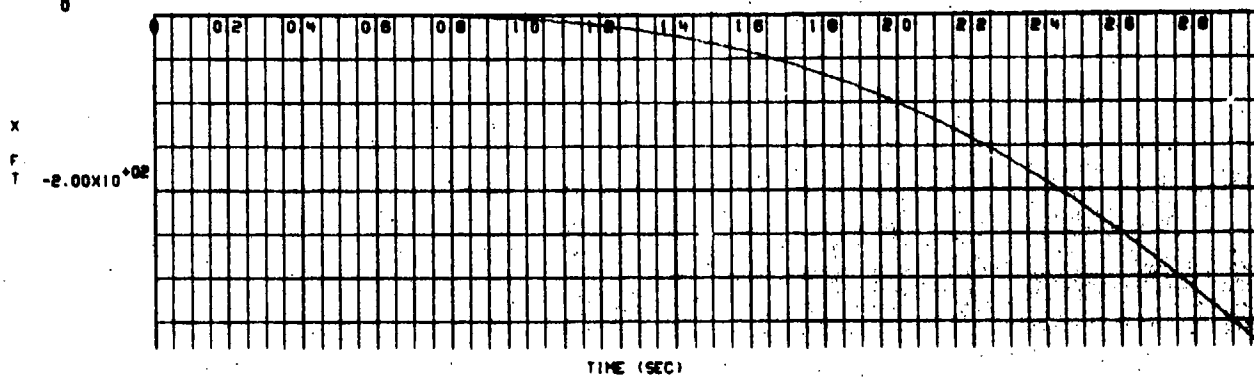
Figure C-8.  $\phi$ ,  $\theta$ , and  $\psi$  Rotation Versus Time for a Flow Field Intensity of  $-1/2$

APPENDIX D

GBU-12 BOMB TRAJECTORIES RESULTING FROM A  
(-5/-3) ORIFICE COMBINATION AT MACH 1.2

17/12/75  
0

R033 04 04

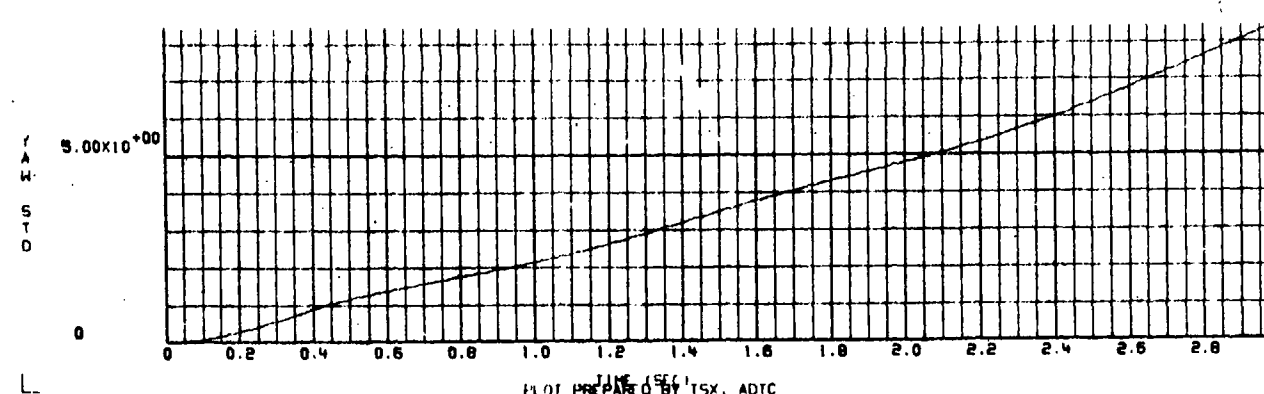
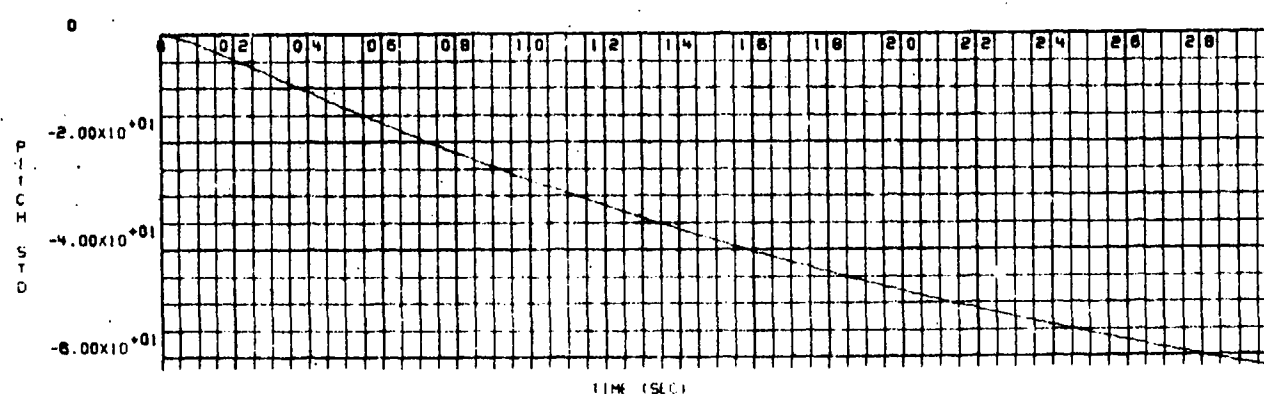
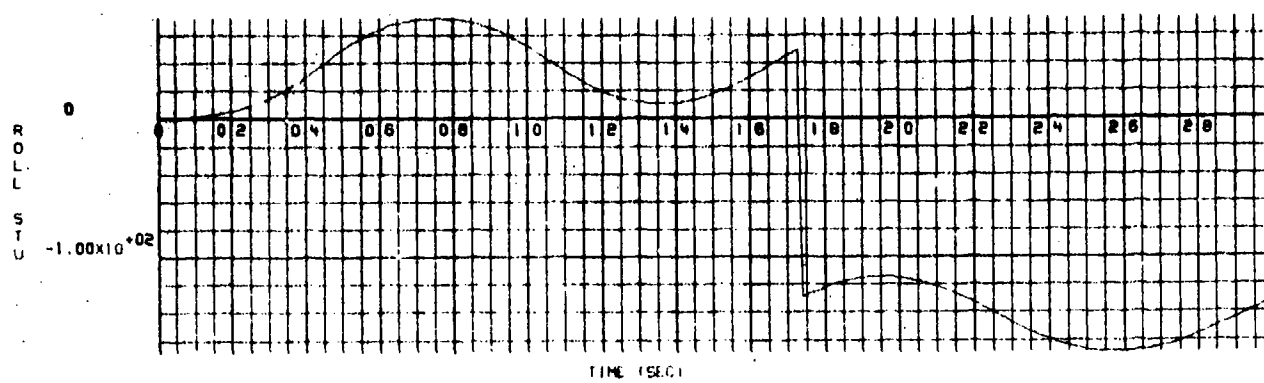


PLOT PREPARED BY TSX, ADTC

Figure D-1. X, Y, and Z Position Versus Time for a Flow Field Intensity of 1/2

17/12/75

R633 63 63

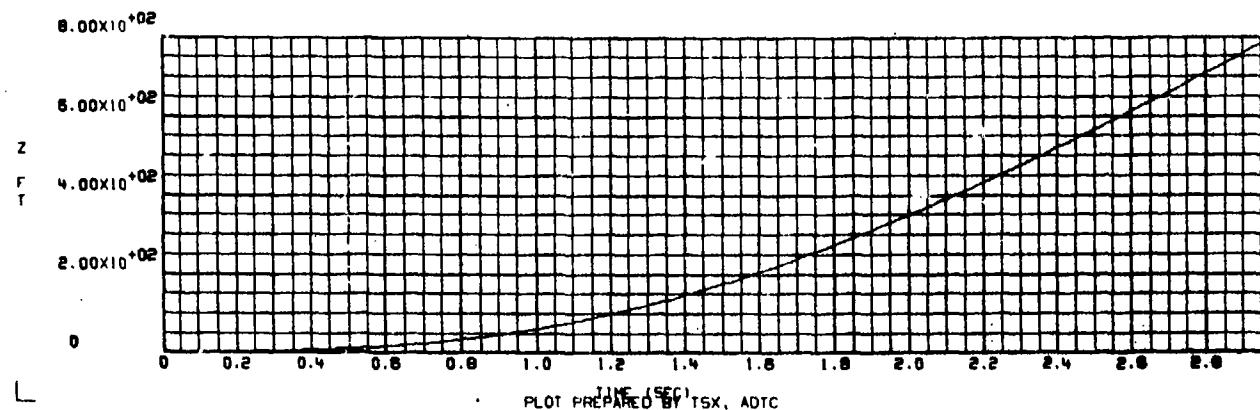
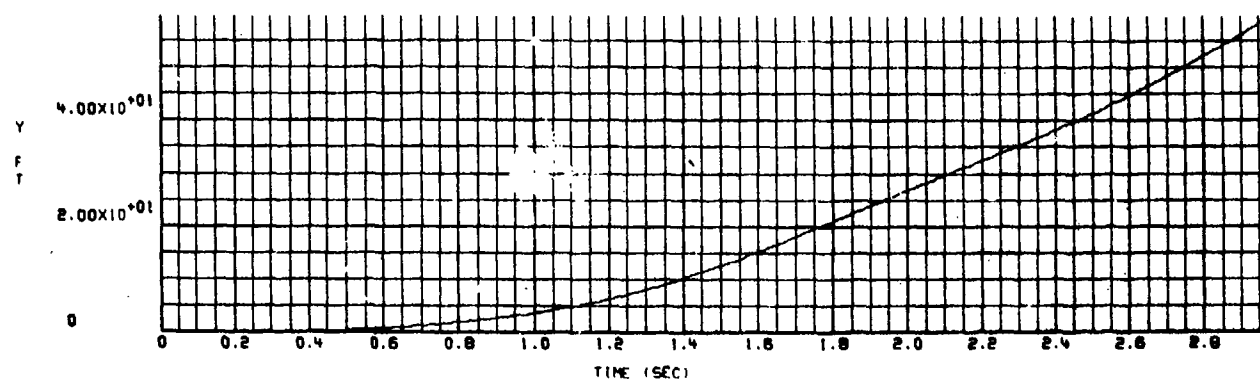
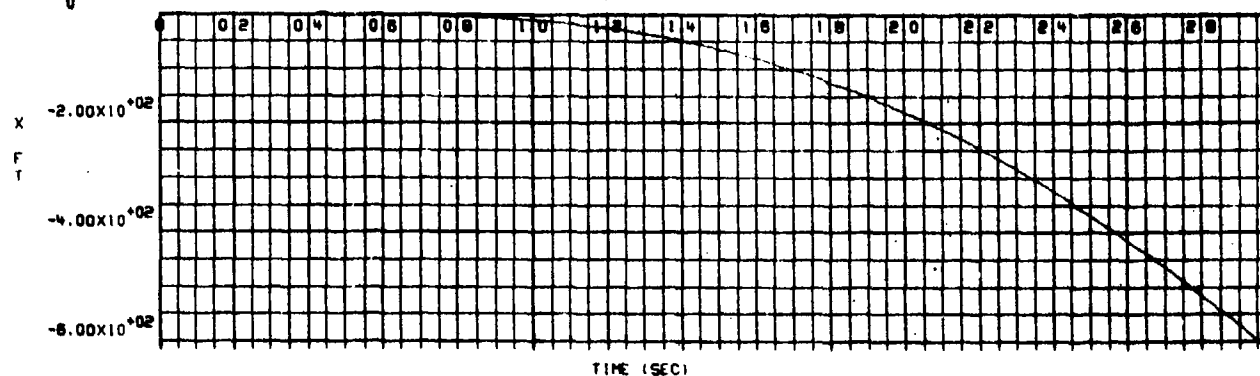


TIME (SEC)  
PLOT PREPARED BY TSX, ADTC

Figure D-2.  $\phi$ ,  $\theta$ , and  $\psi$  Rotation Versus Time for a Flow Field Intensity of 1/2

17/12/75  
0

R633 66 66



PLOT PREPARED BY TSX, ADTC

Figure D-3. X, Y, and Z Position Versus Time for a Flow Field Intensity of 1 (as measured in the wind tunnel)



17/12/75

R633

67

67

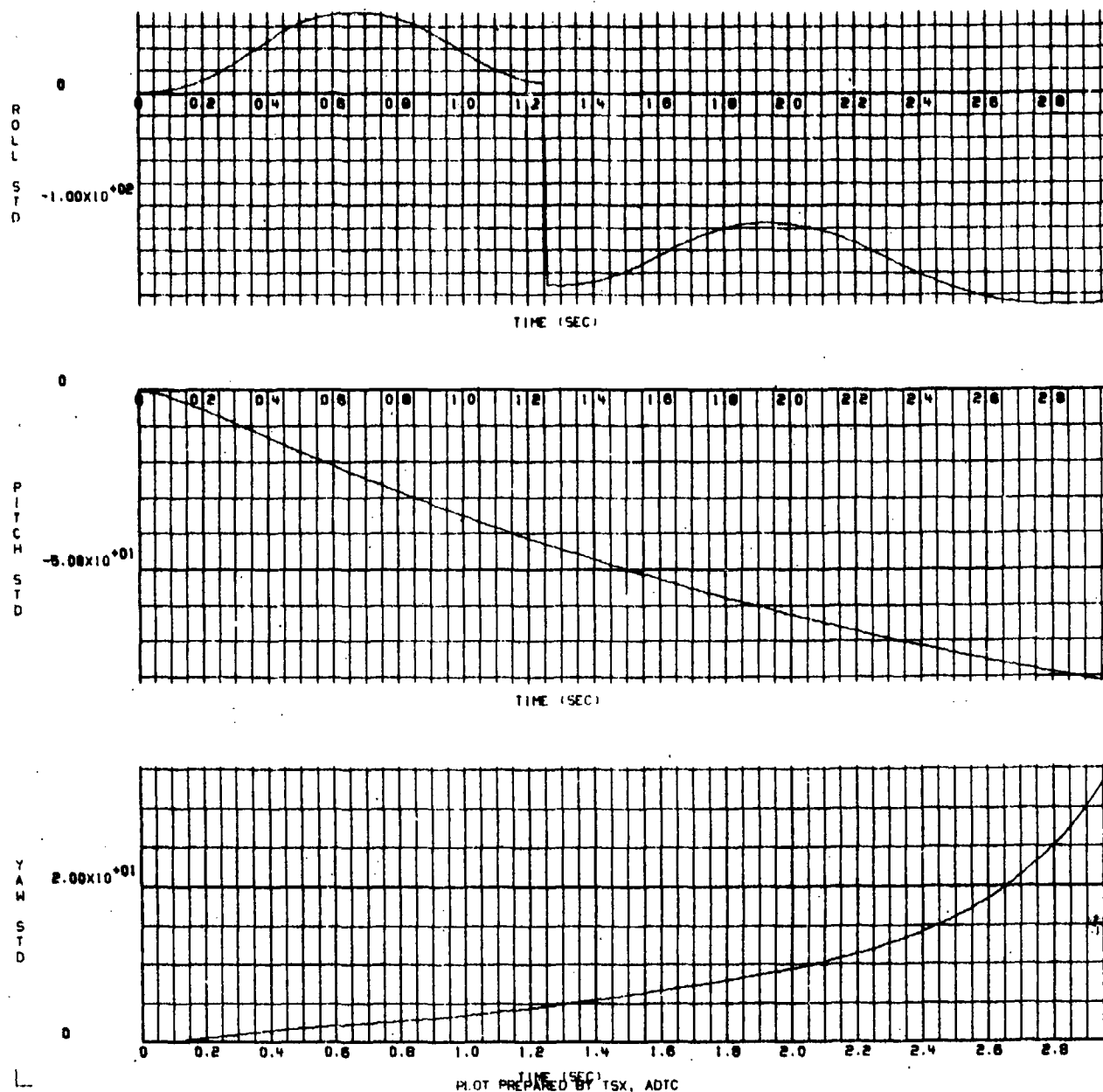


Figure D-4.  $\phi$ ,  $\theta$ , and  $\psi$  Rotation Versus Time for a Flow Field Intensity of 1 (unchanged from the wind tunnel measured values)

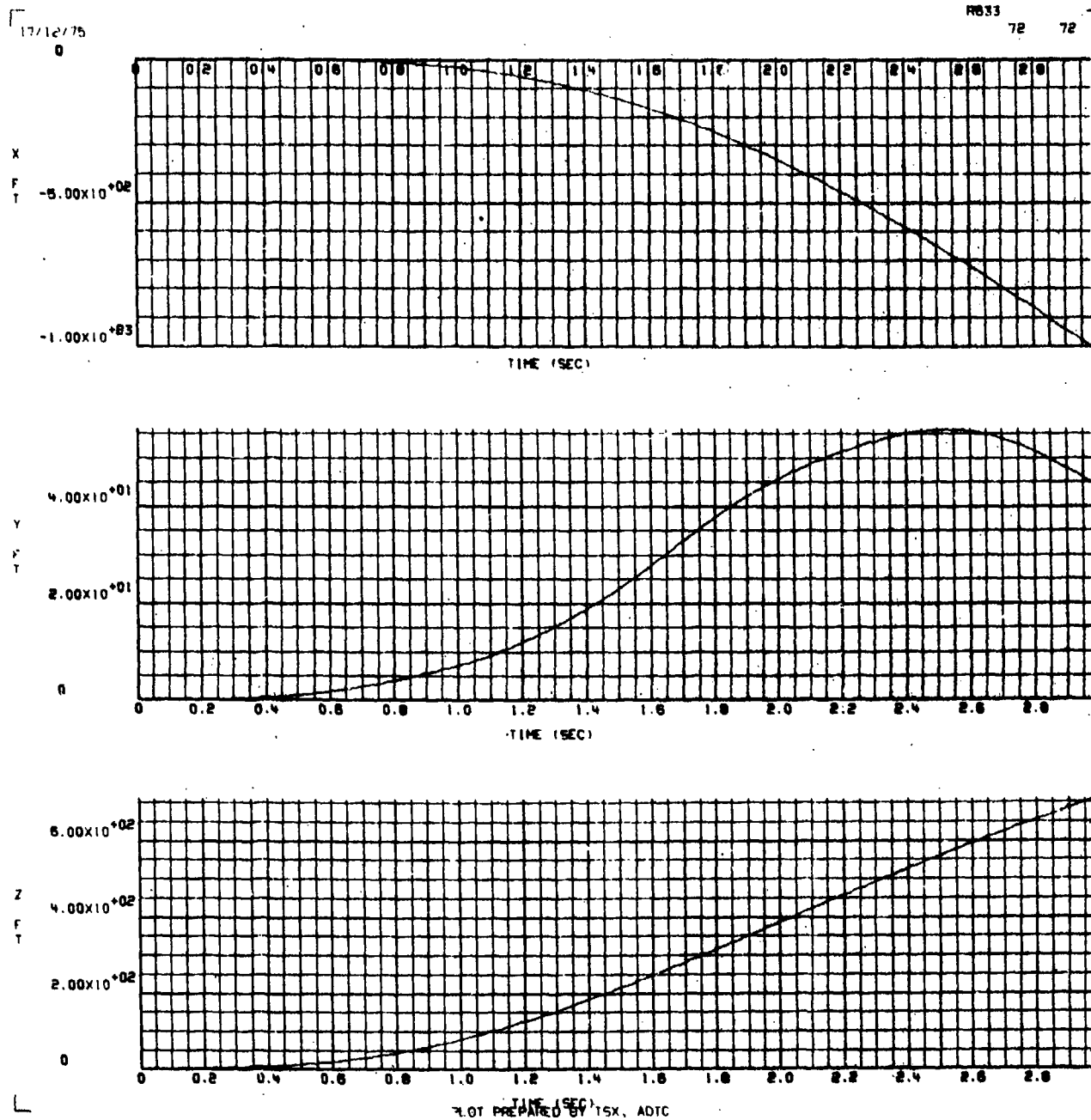


Figure D-5. X, Y, and Z Position Versus Time for a Flow Field Intensity of 2

17/12/75

R633

71

71

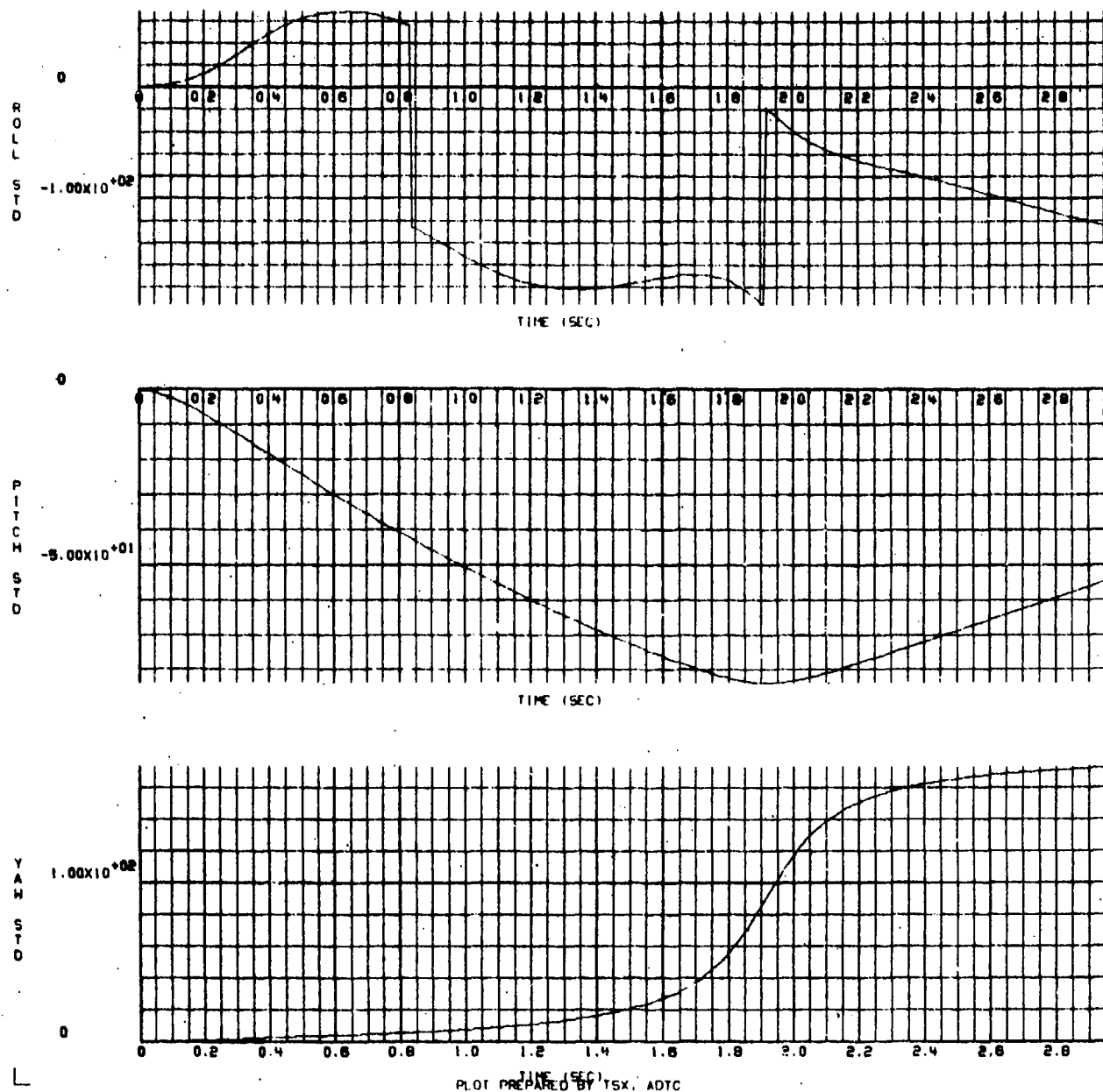
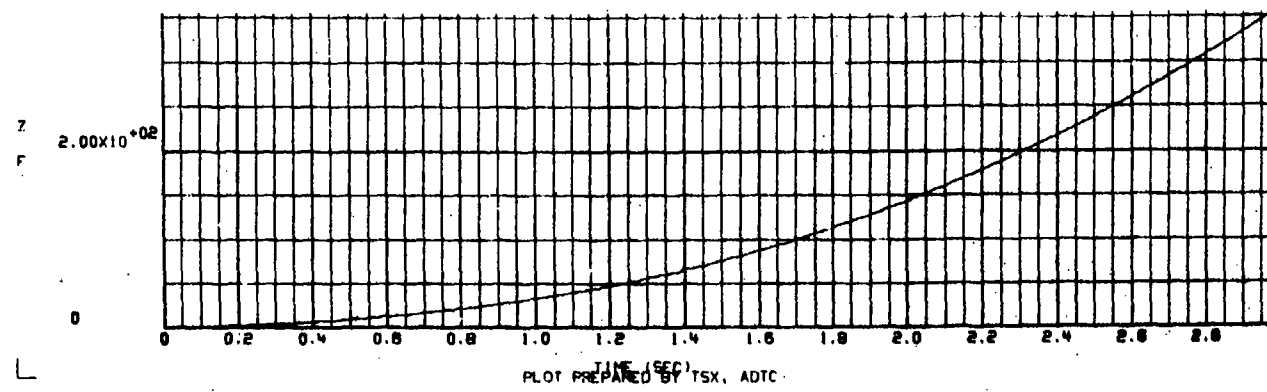
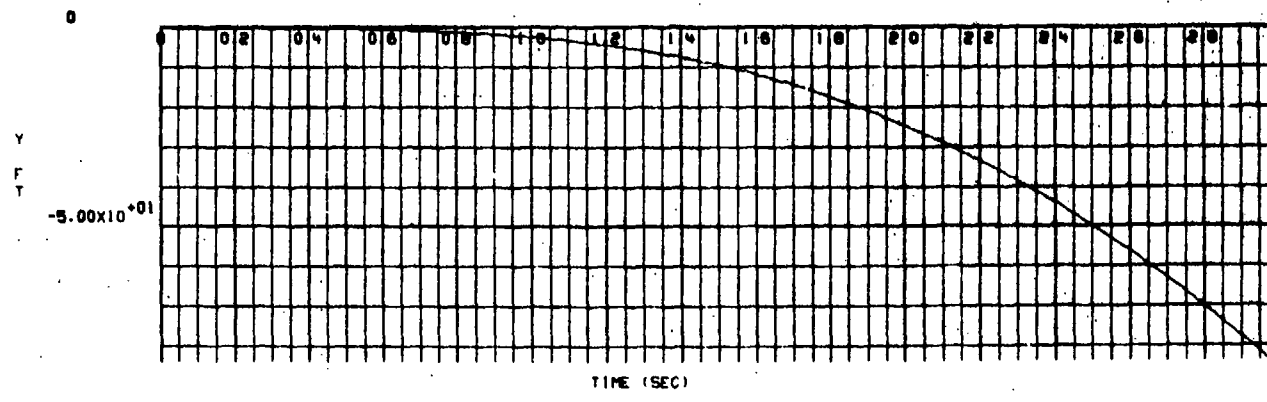
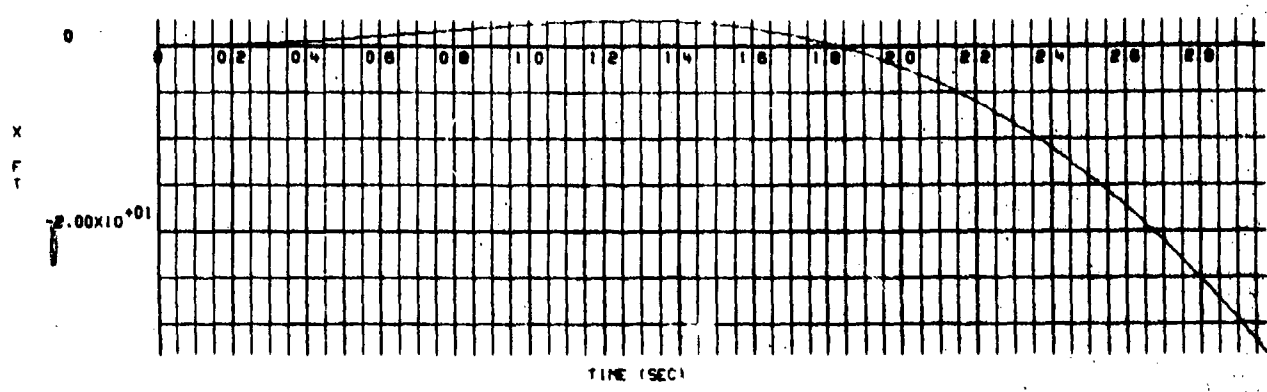


Figure D-6.  $\phi$ ,  $\theta$ , and  $\psi$  Rotation Versus Time for a Flow Field Intensity of 2

17/12/75

R633 76 76



PLOT PREPARED BY TSX, ADTC

Figure D-7. X, Y, and Z Position Versus Time for a Flow Field Intensity of  $-1/2$

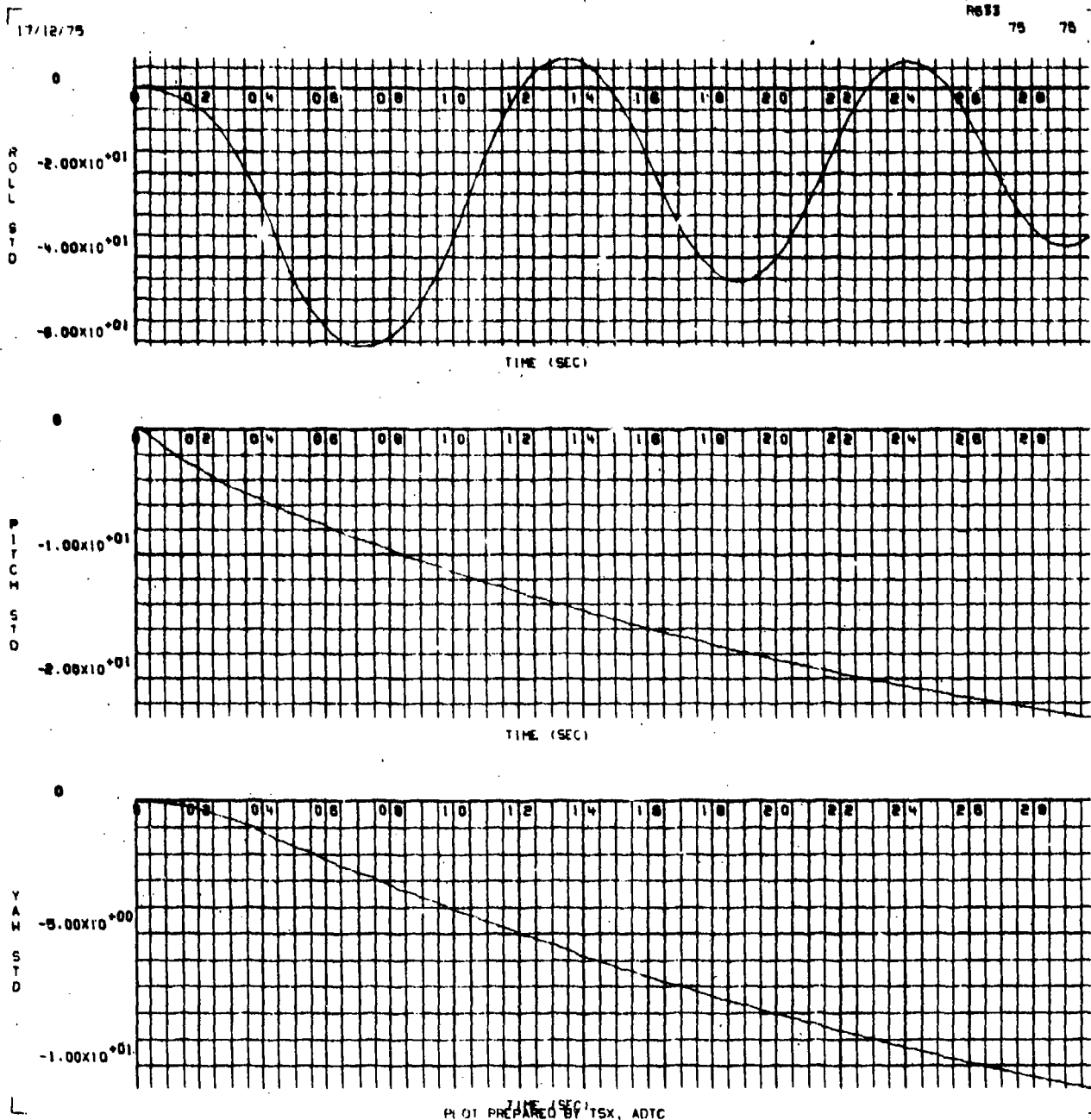


Figure D-8.  $\phi$ ,  $\theta$ , and  $\psi$  Rotation Versus Time for a Flow Field Intensity of  $-1/2$

APPENDIX E

GBU-12 BOMB TRAJECTORIES RESULTING FROM A  
(-3/-3) ORIFICE COMBINATION AT MACH 0.7



45,31

44





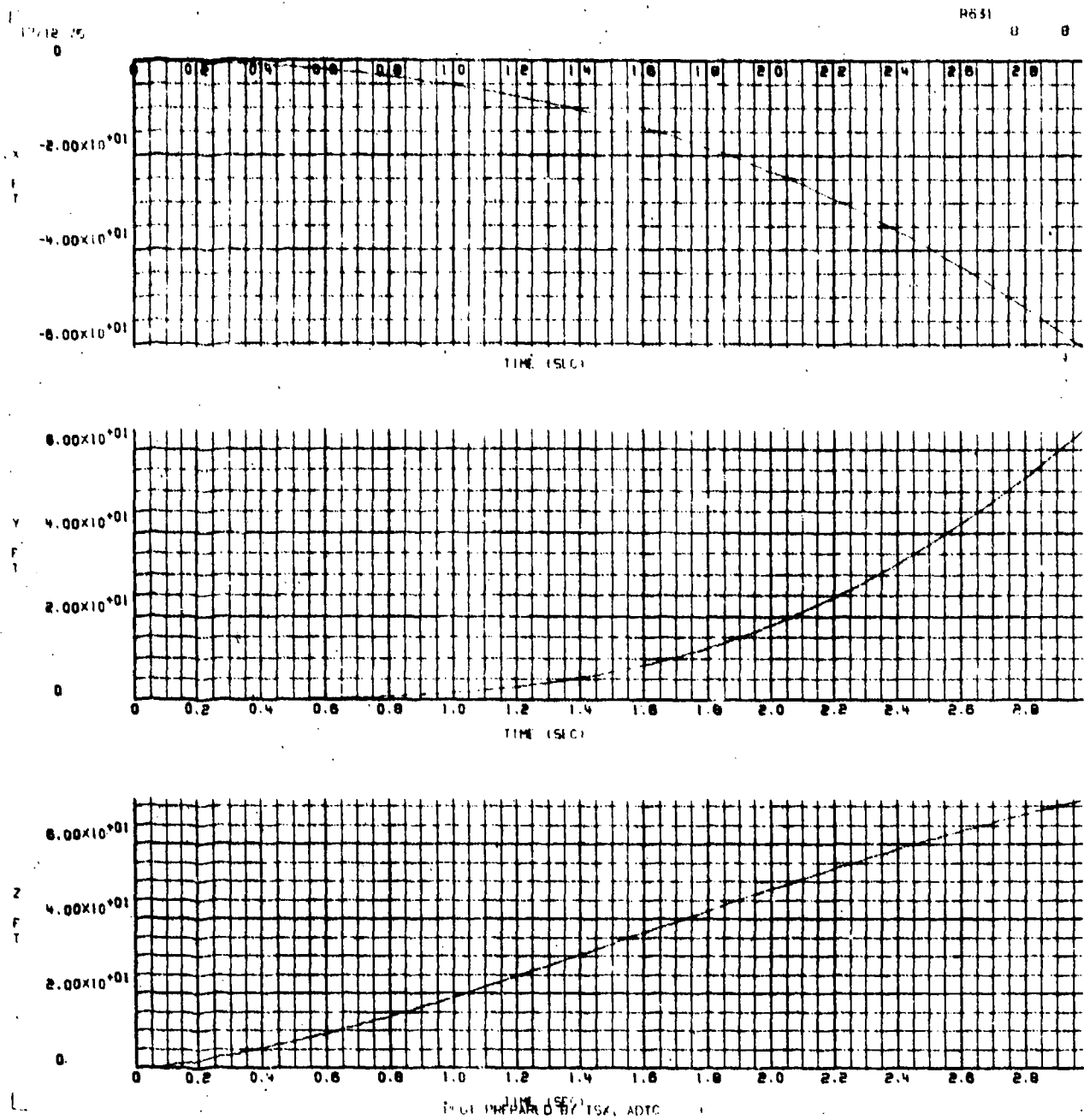


Figure E-3. X, Y, and Z Position Versus Time for a Flow Field Intensity of 1 (as measured in the wind tunnel)

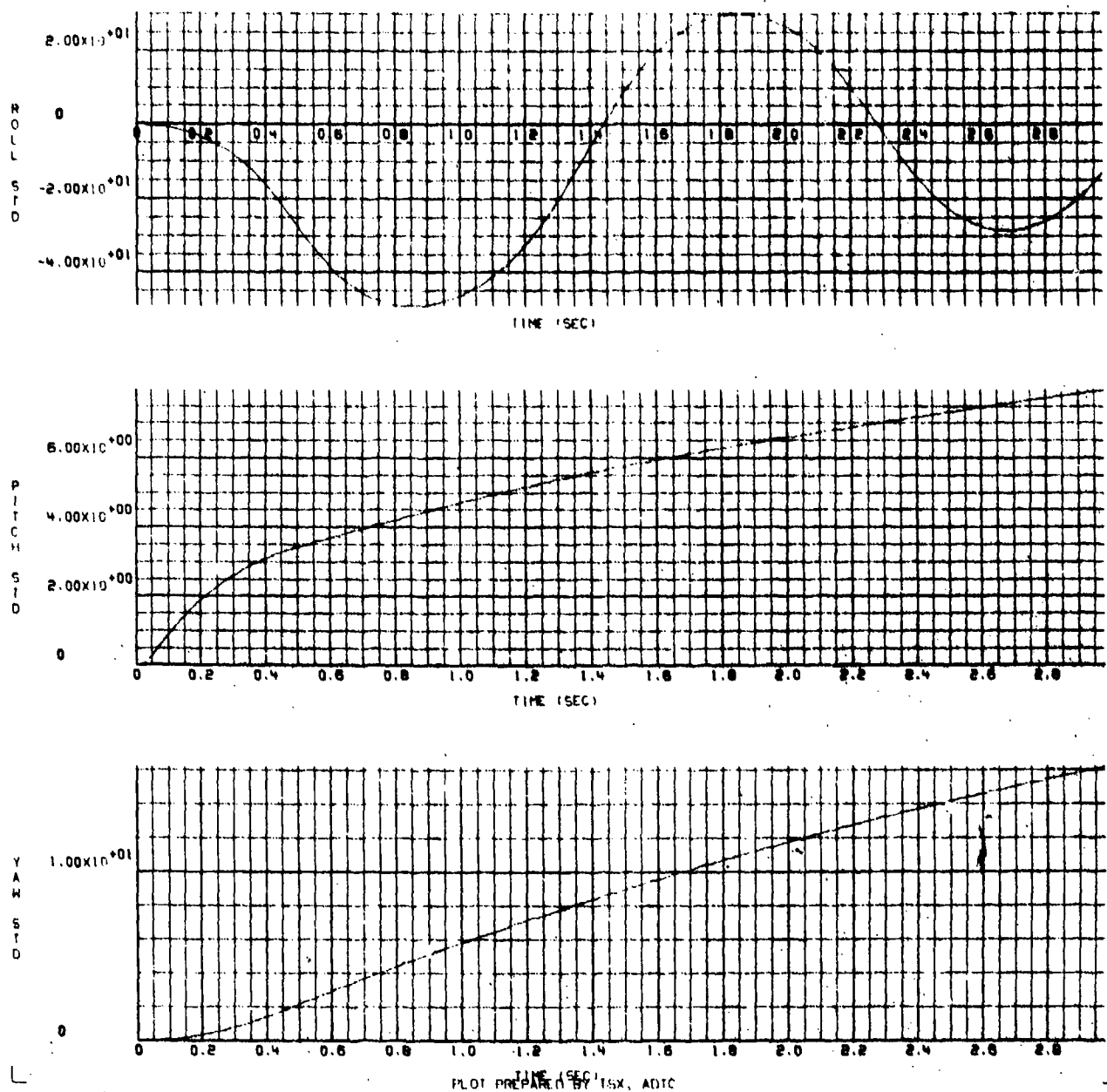
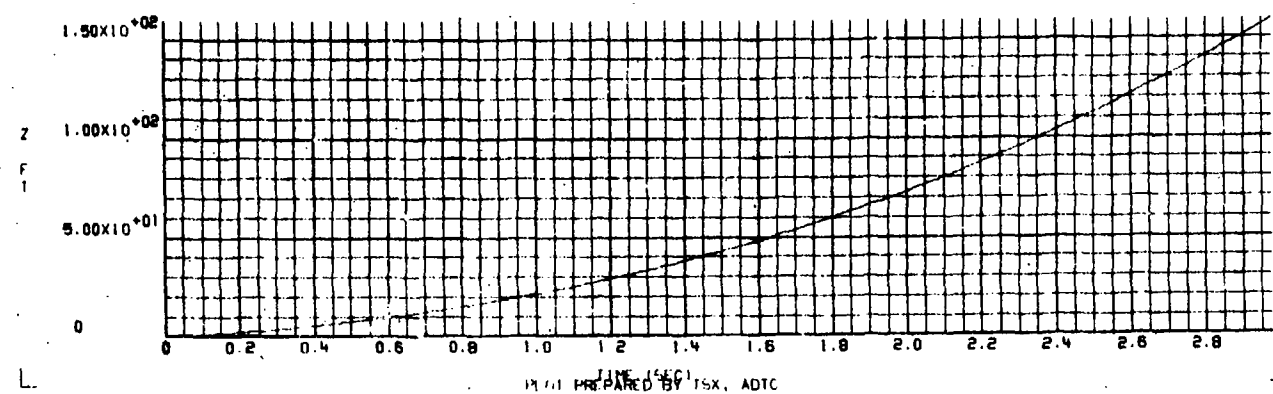
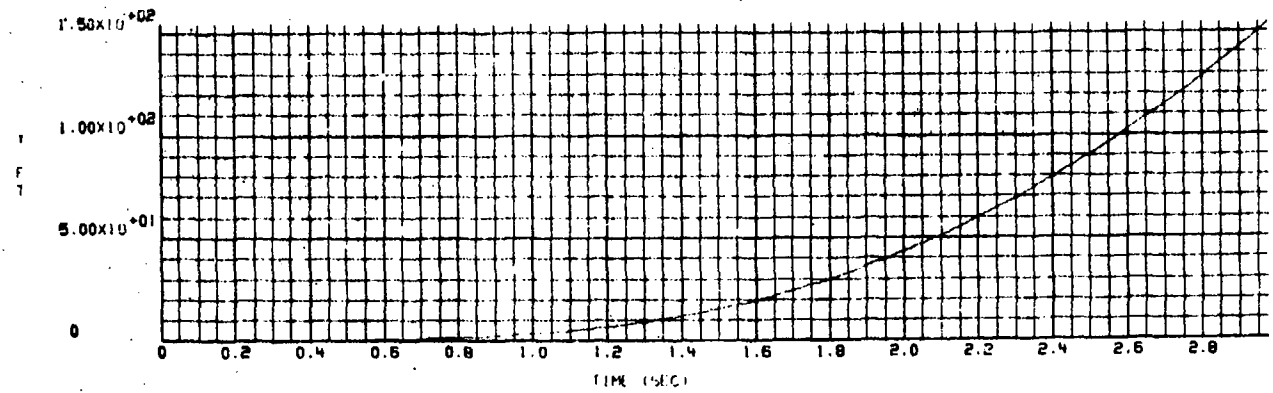
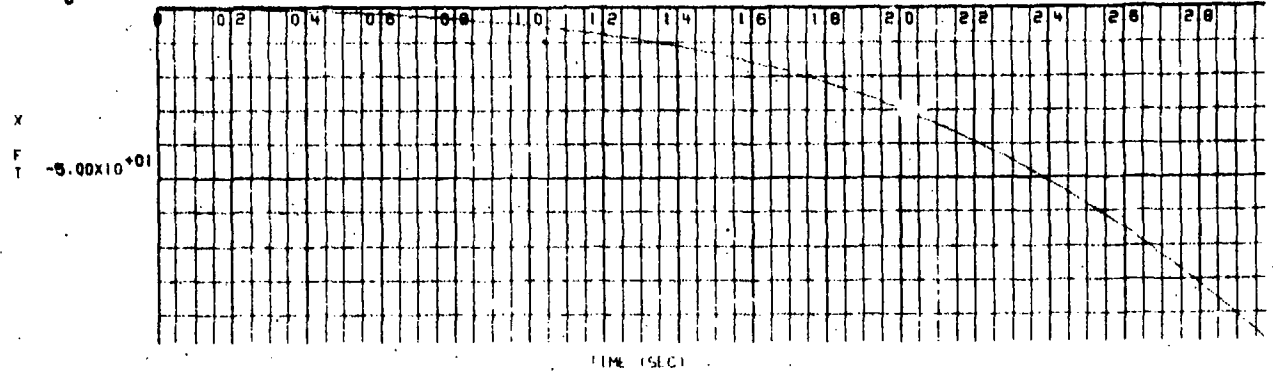


Figure E-4.  $\phi$ ,  $\theta$ , and  $\psi$  Rotation Versus Time for a Flow Field Intensity of 1 (unchanged from the wind tunnel measured values)

12/12/75  
0

R631 12 12 1



PLT PREPARED BY TSX, ADTC

Figure E-5. X, Y, and Z Position Versus Time for a Flow Field Intensity of 2

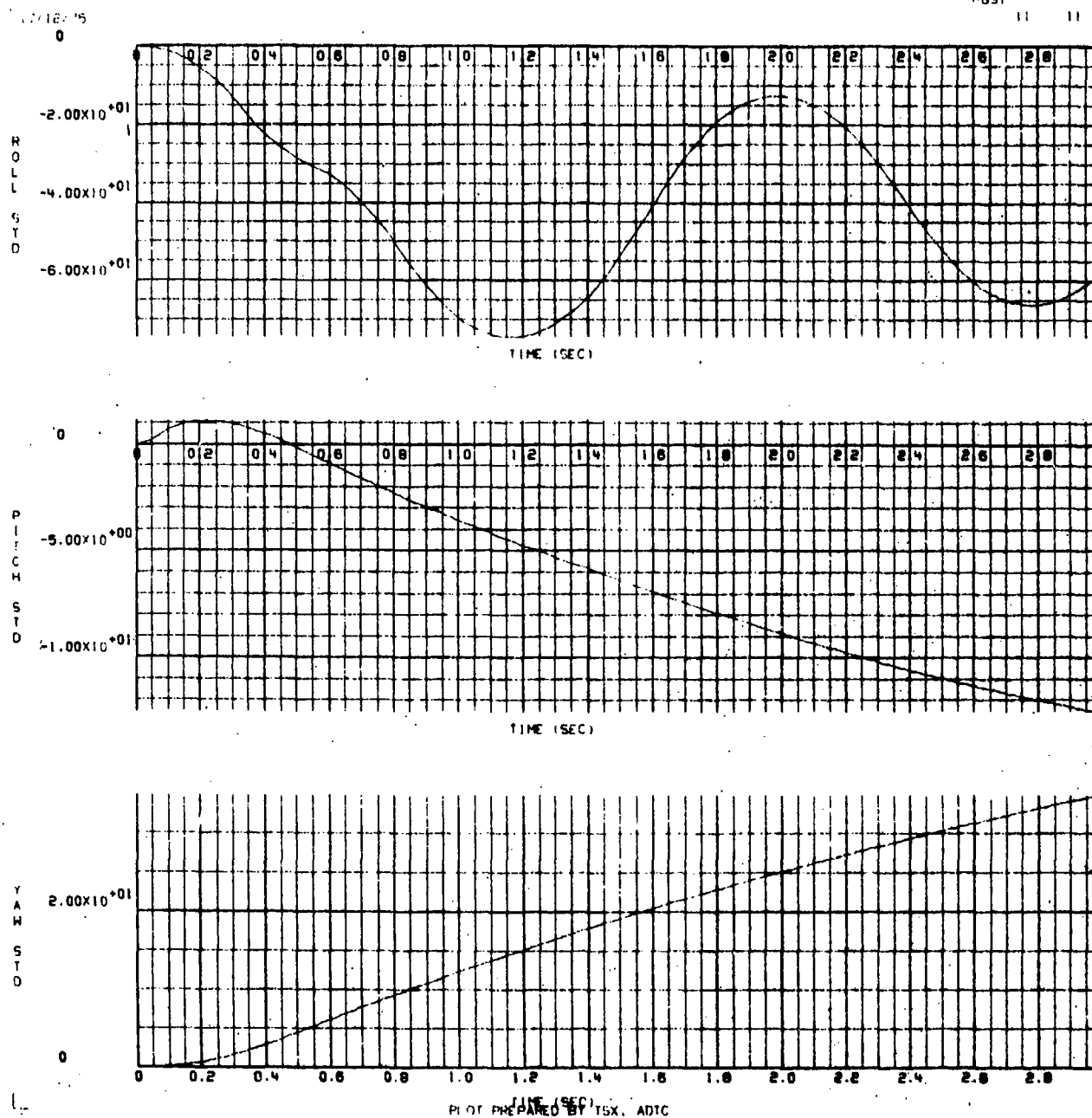
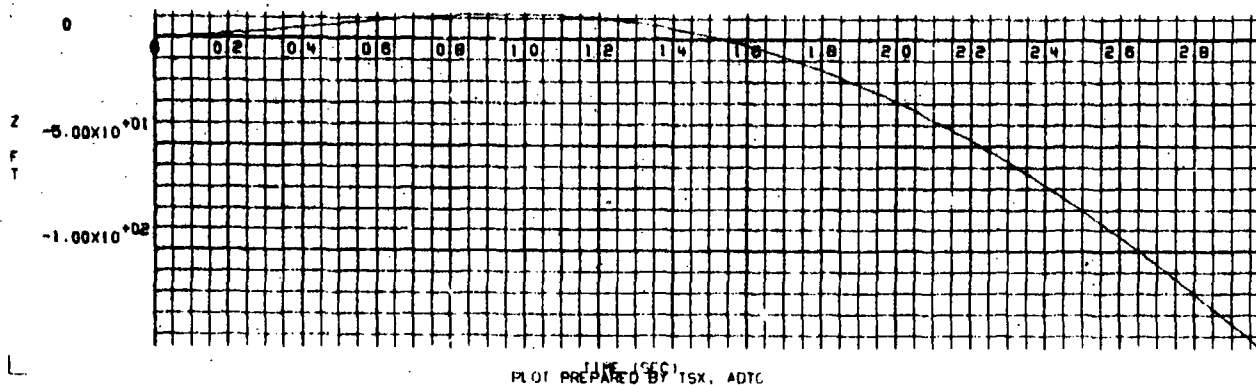
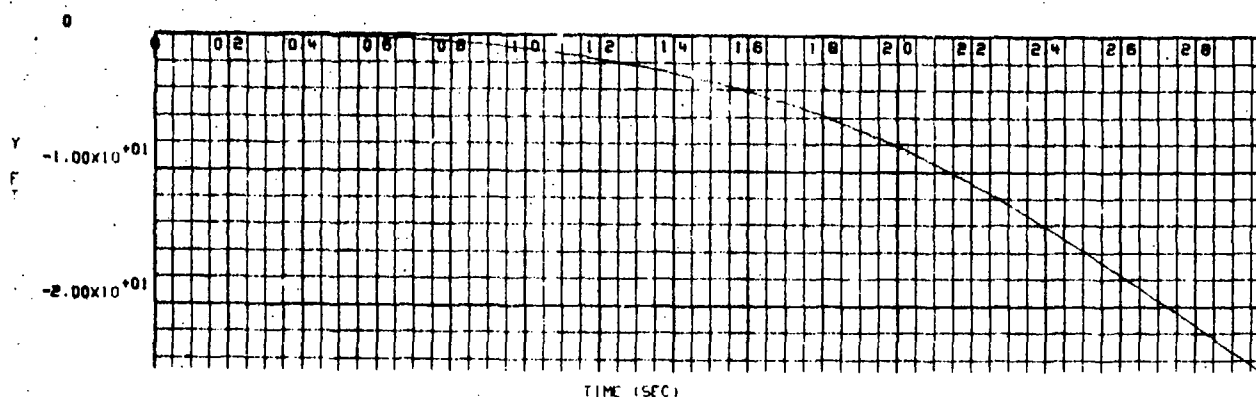
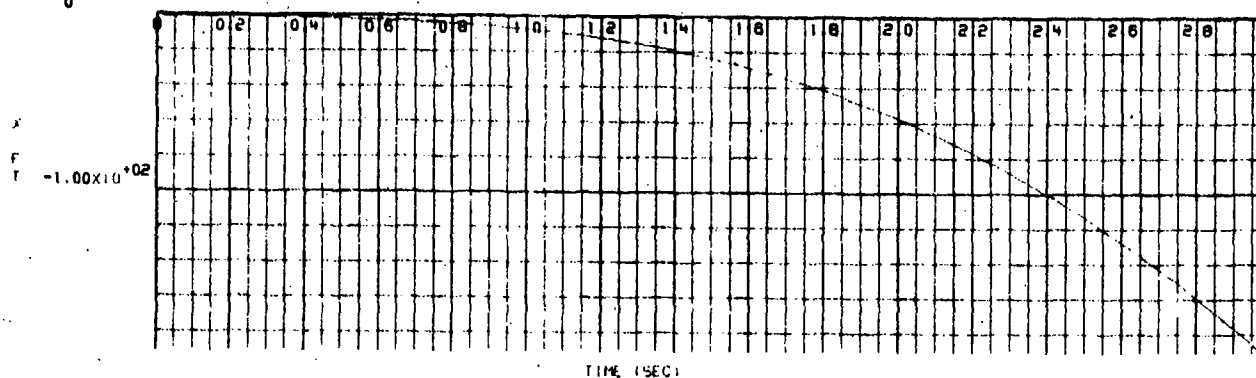


Figure E-6.  $\phi$ ,  $\theta$ , and  $\psi$  Rotation Versus Time for a Flow Field Intensity of 2

17/12/75  
0

H531

10 1F



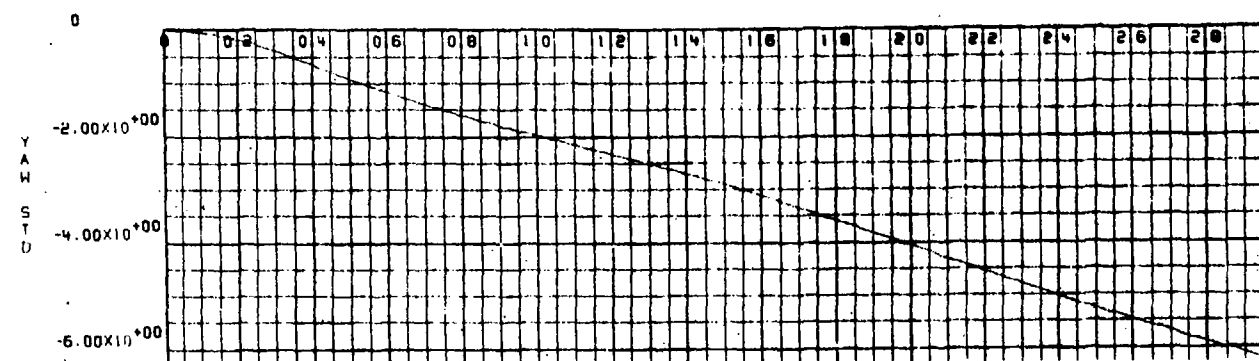
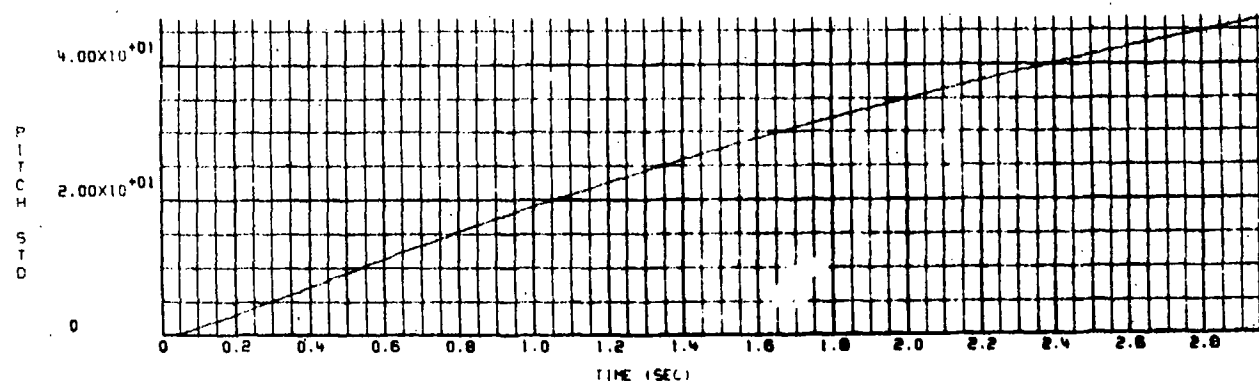
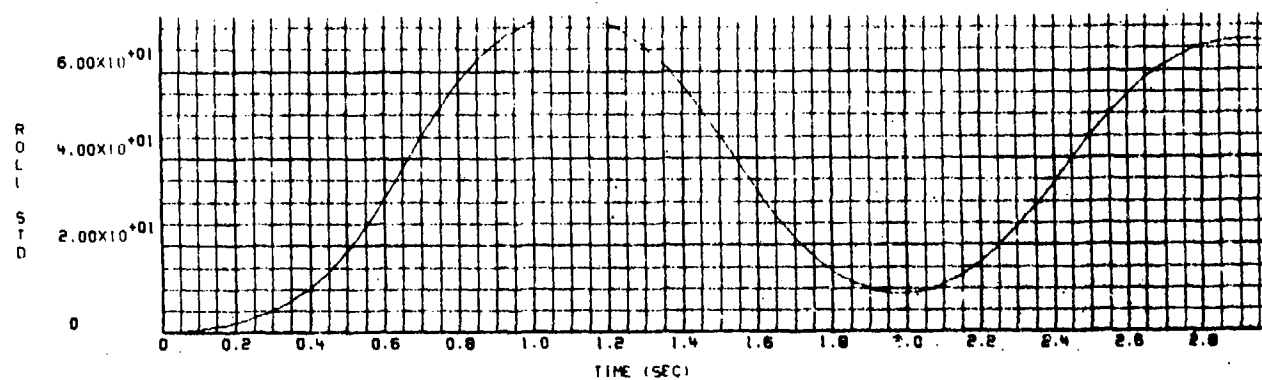
PLOT PREPARED BY TSX, ADTG

Figure E-7. X, Y, and Z Position Versus Time for a Flow Field Intensity of  $-1/2$

17/12/75

R831

15 15



TIME (SEC)  
PLOT PREPARED BY TSX, ADIC

Figure E-8.  $\phi$ ,  $\theta$ , and  $\psi$  Rotation Versus Time for a Flow Field Intensity of  $-1/2$

**APPENDIX F**

**GBU-12 BOMB TRAJECTORIES RESULTING FROM A  
(-3/-3) ORIFICE COMBINATION AT MACH 0.85**

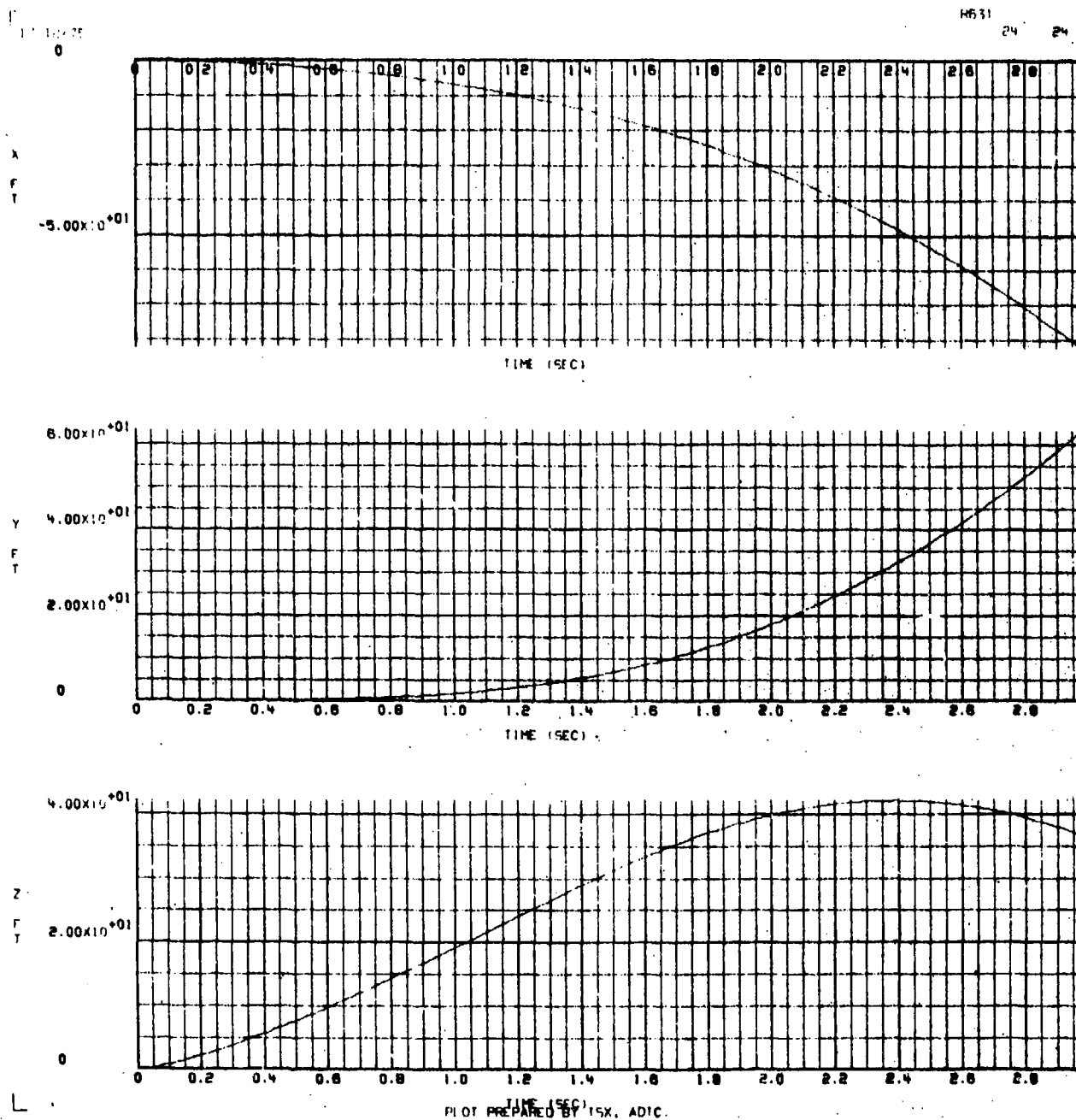


Figure P-1. X, Y, and Z Position Versus Time for a Flow Field Intensity of  $1/2$



17/12/75

R631

23 23

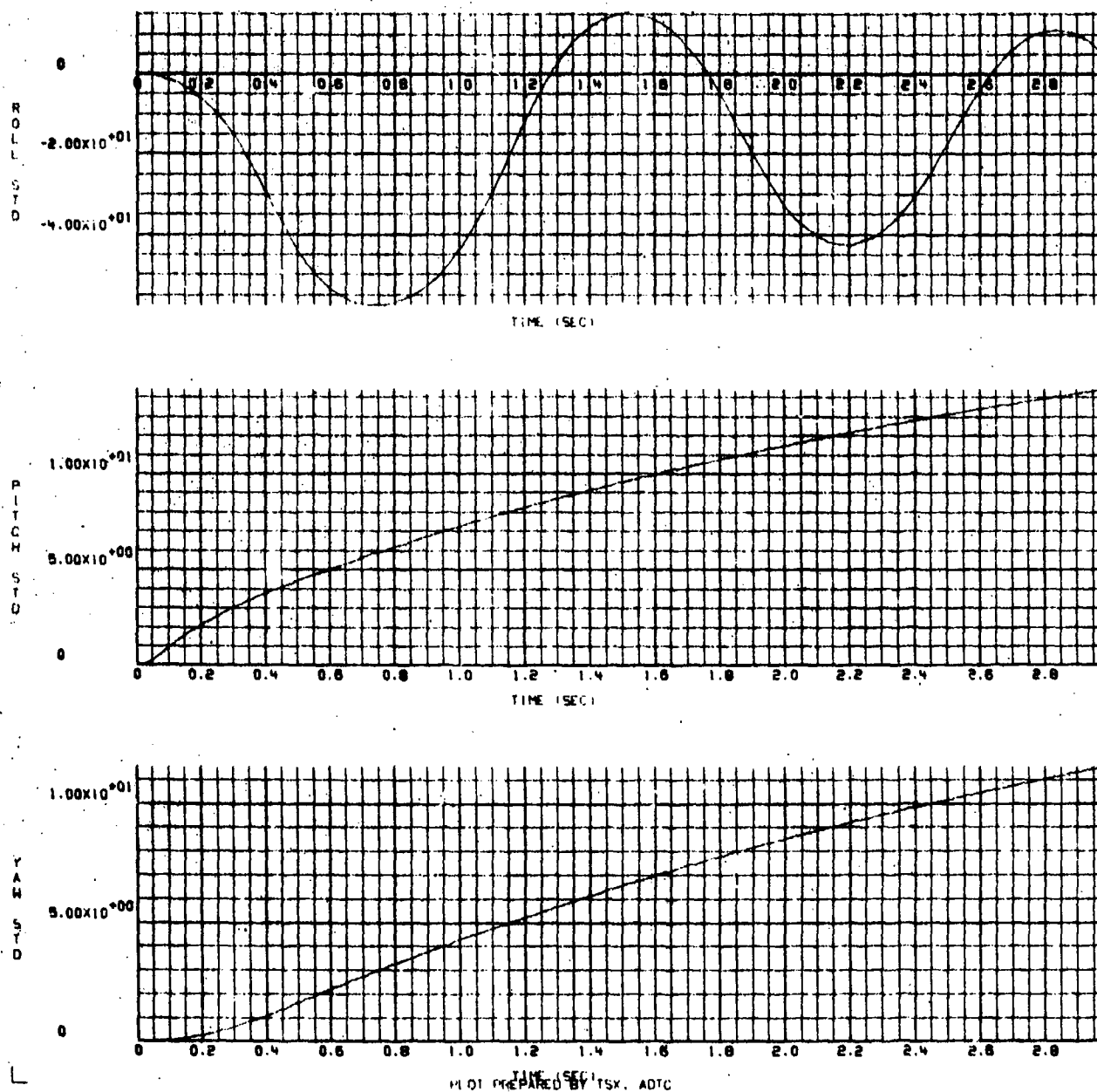
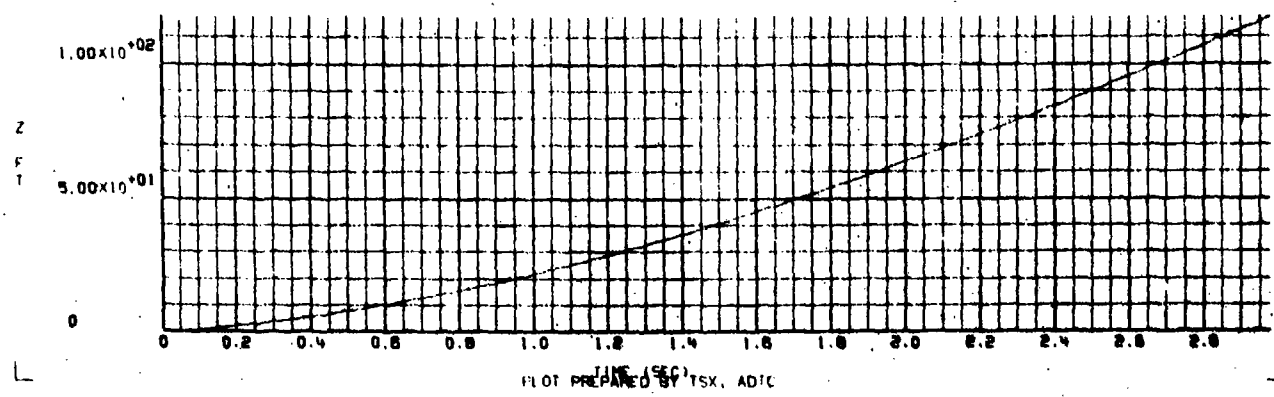
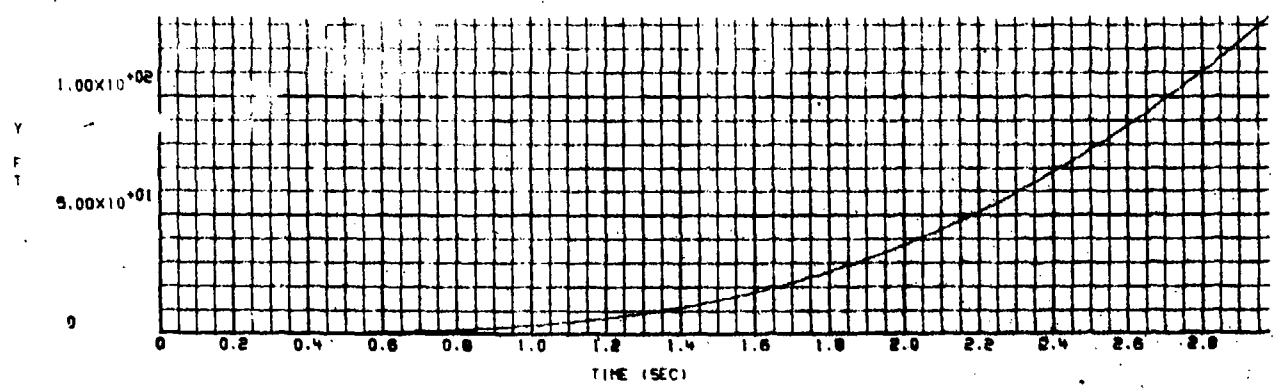
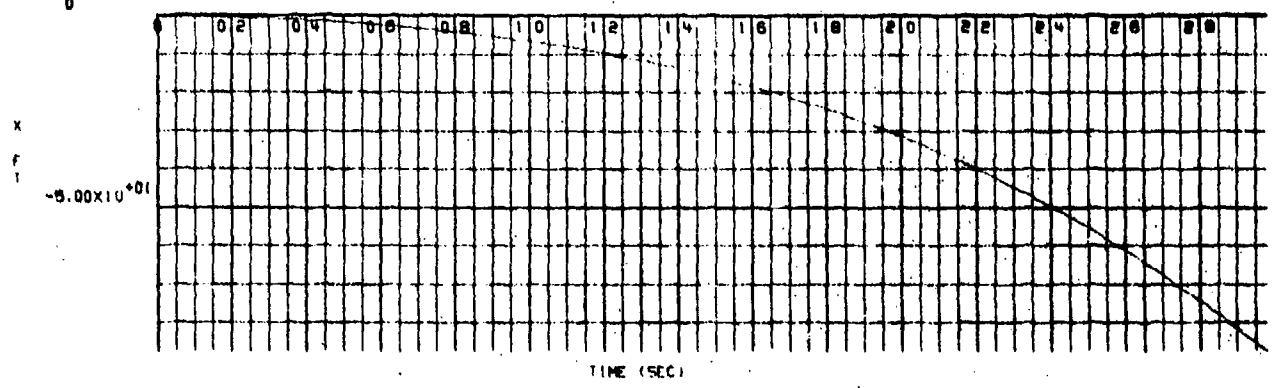


Figure F-2.  $\phi$ ,  $\theta$ , and  $\psi$  Rotation Versus Time for a Flow Field Intensity of  $1/2$

17-10-75  
0

R831 28 28

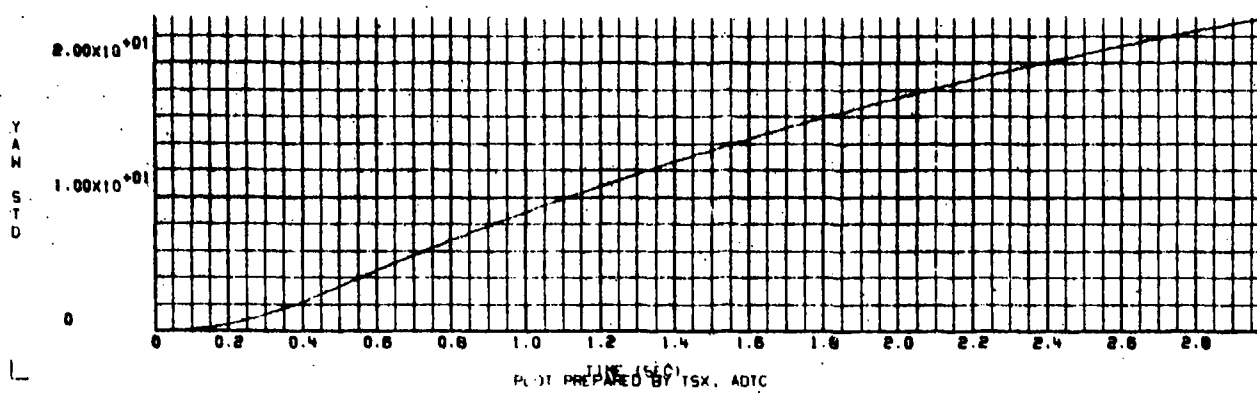
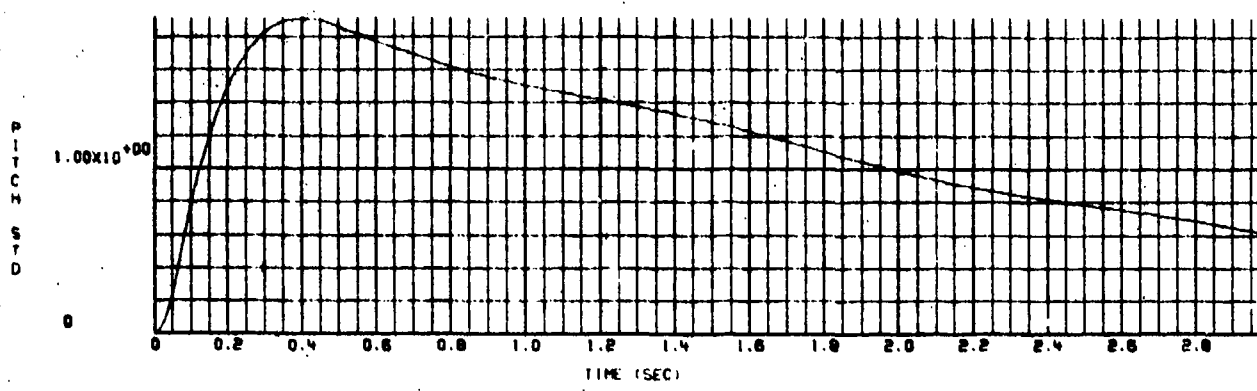
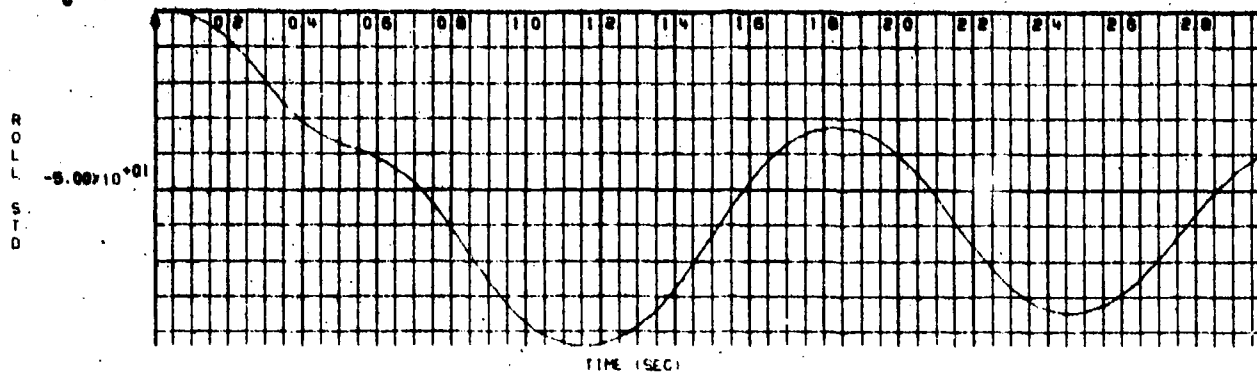


PLOT PREPARED BY TSX, ADIC

Figure F-3. X, Y, and Z Position Versus Time for a Flow Field Intensity of 1 (as measured in the wind tunnel)

17/12/75  
0

R631 27 27



PLT PREPARED BY TSX, ADTC

Figure P-4.  $\phi$ ,  $\theta$ , and  $\gamma$  Rotation Versus Time for a Flow Field Intensity of 1 (unchanged from the wind tunnel measured values)

17/12/75  
0

R631

32 32

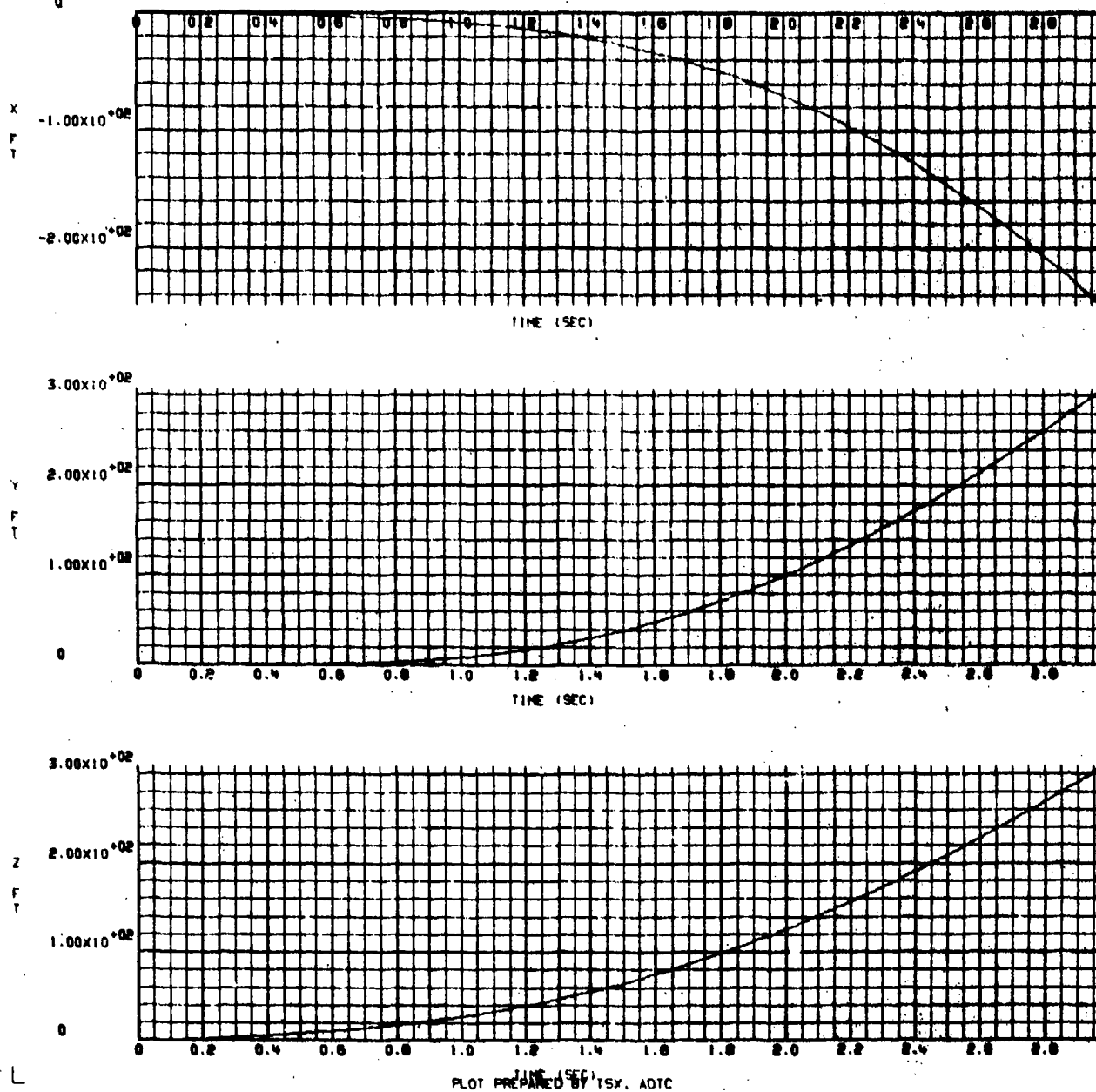
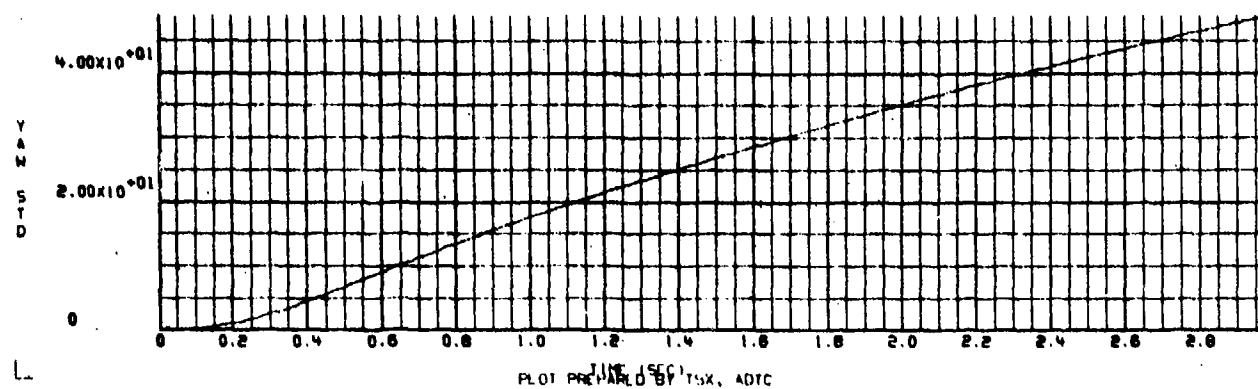
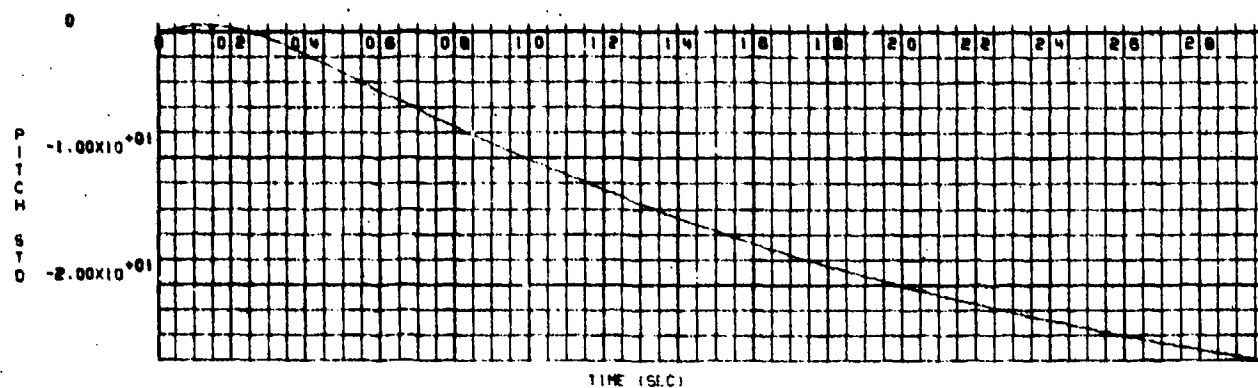
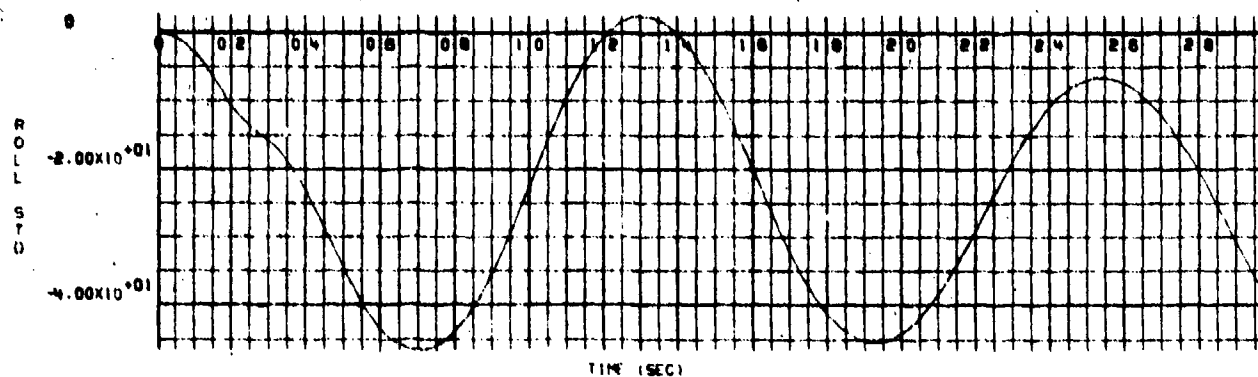


Figure F-5. X, Y, and Z Position Versus Time for a Flow Field Intensity of 2

17-12-75

8631

31 31



TIME (SEC) TSX, ADTC  
PLOT PREPARED BY

Figure F-6.  $\phi$ ,  $\theta$ , and  $\psi$  Rotation Versus Time for a Flow Field Intensity of 2

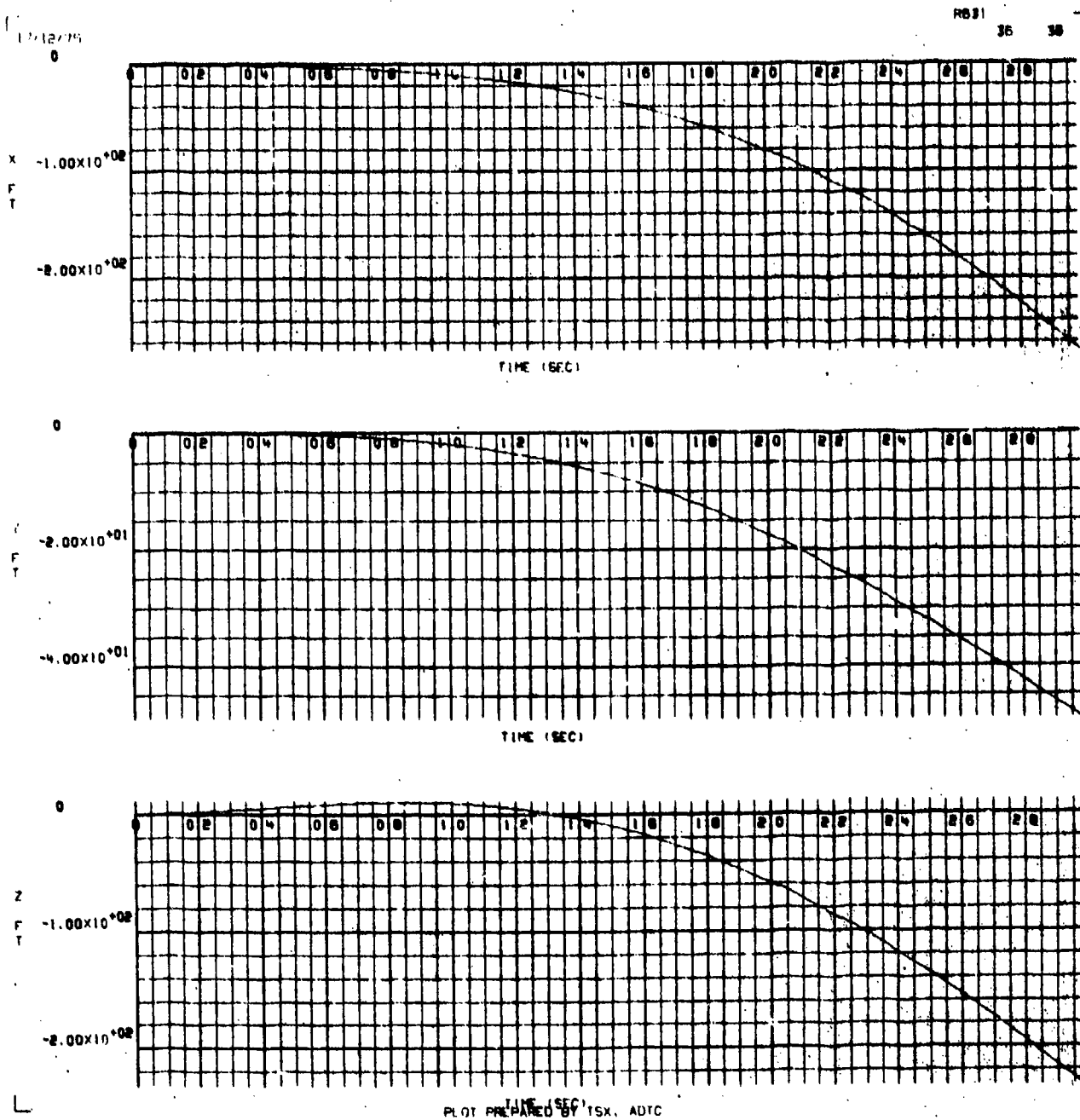
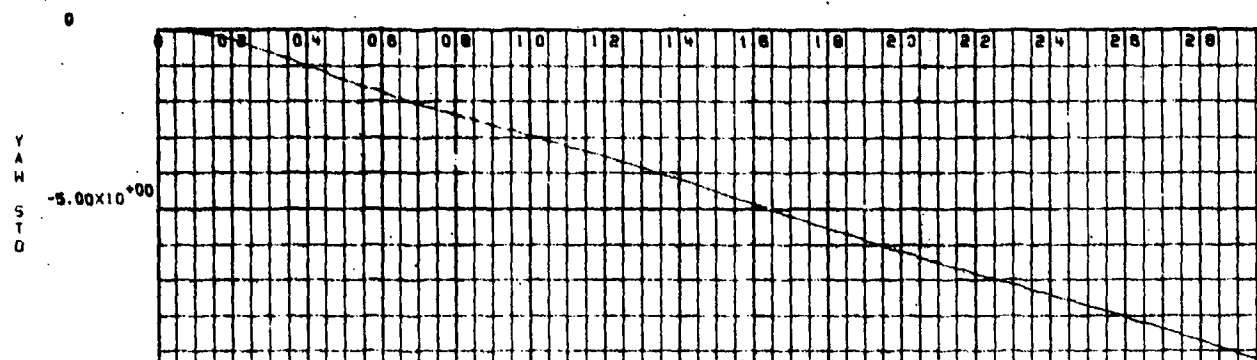
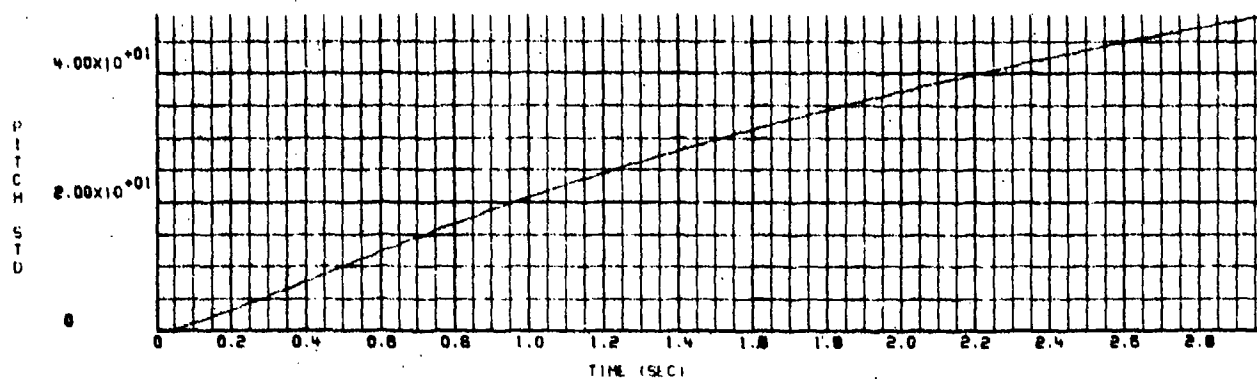
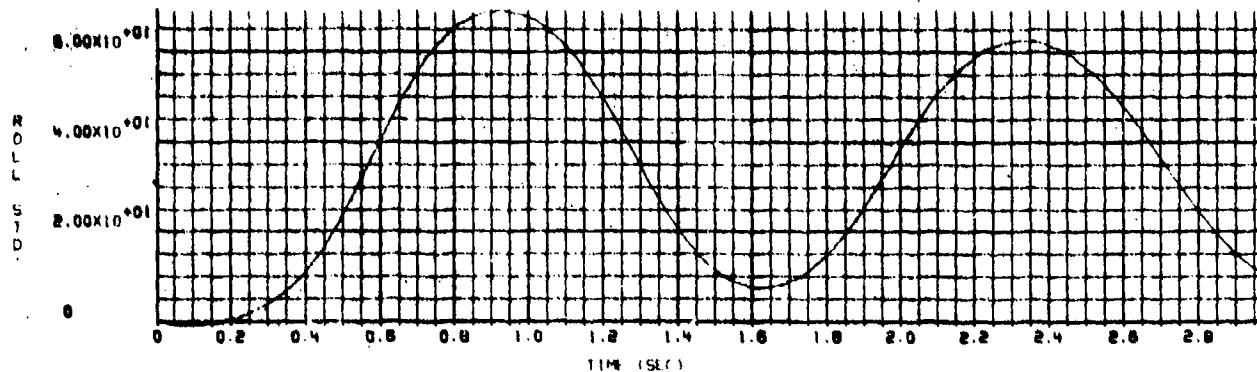


Figure F-7. X, Y, and Z Position Versus Time for a Flow Field Intensity of  $-1/2$ .

17/12/79

R631

35 30



TIME (SEC)  
PLOT PREPARED BY TSX, ADTC

Figure F-8.  $\phi$ ,  $\theta$ , and  $\psi$  Rotation Versus Time for a Flow Field Intensity of  $-1/2$

APPENDIX G

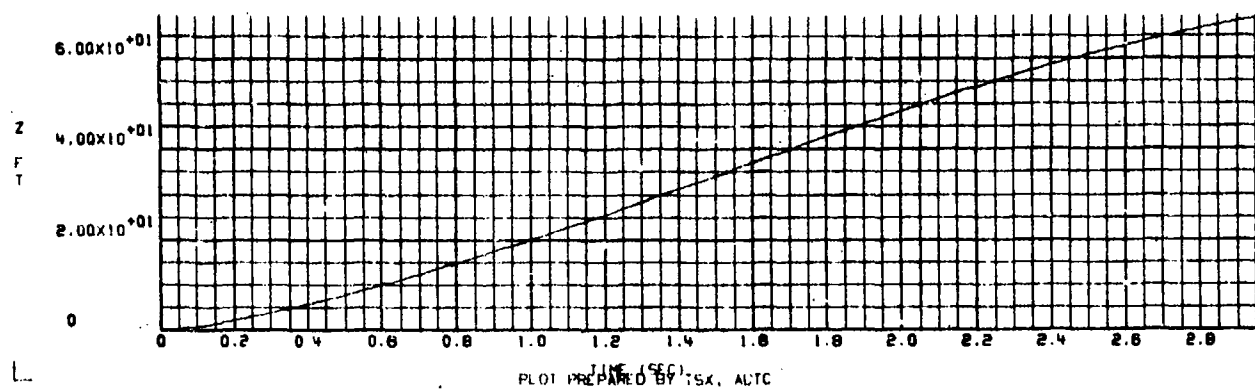
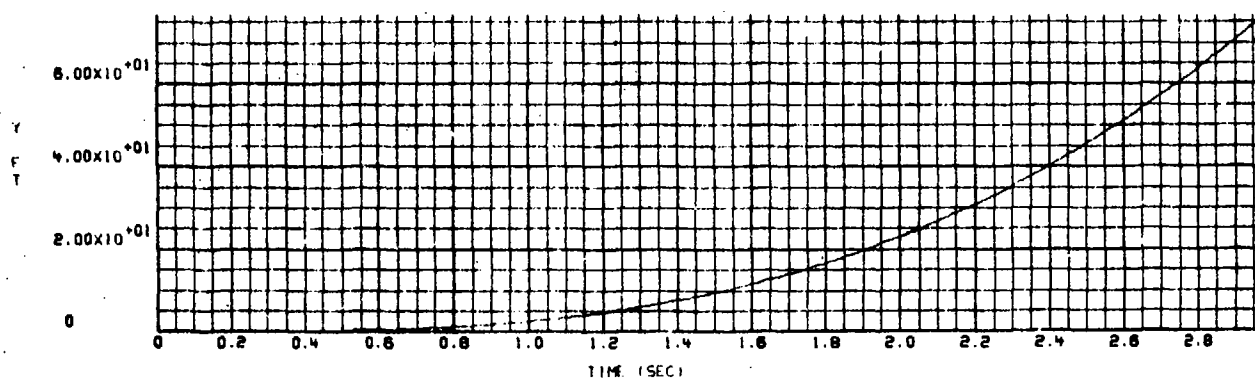
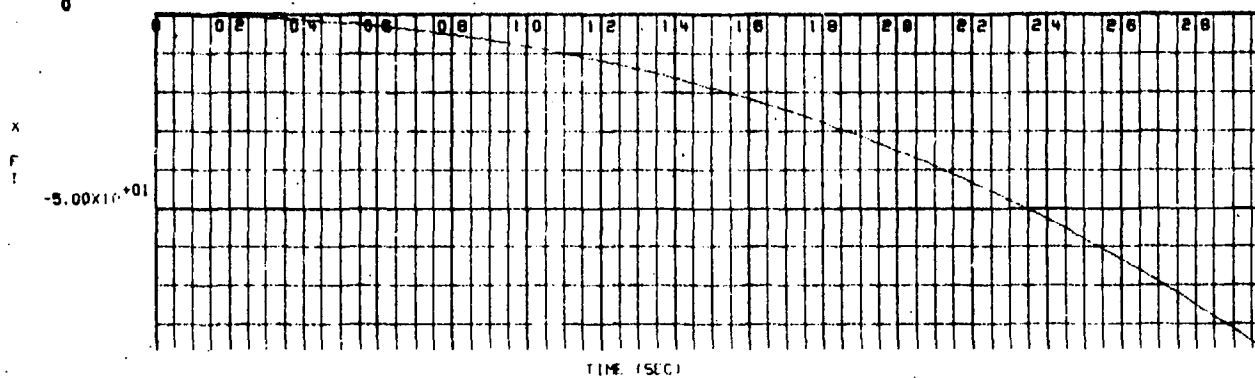
GBU-12 BOMB TRAJECTORIES RESULTING FROM A  
(-3/-3) ORIFICE COMBINATION AT MACH 0.95



17/12/75  
0

R631

44 44

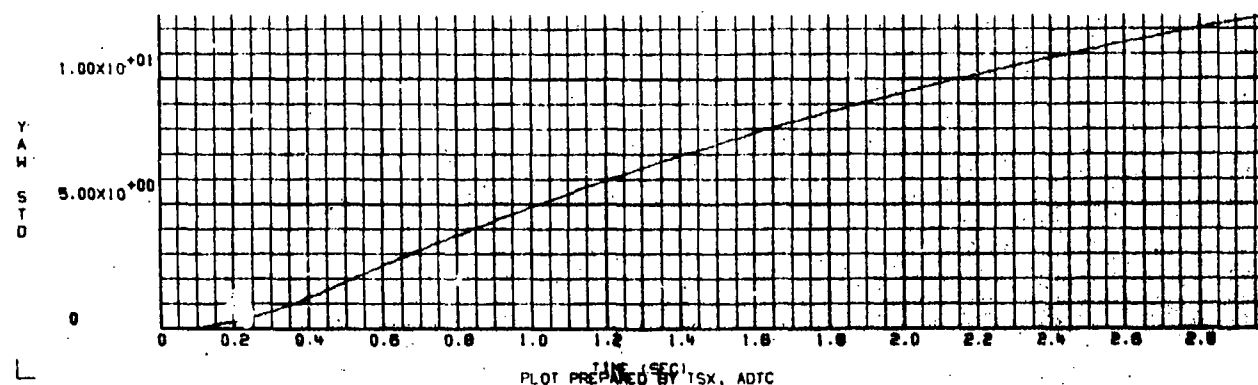
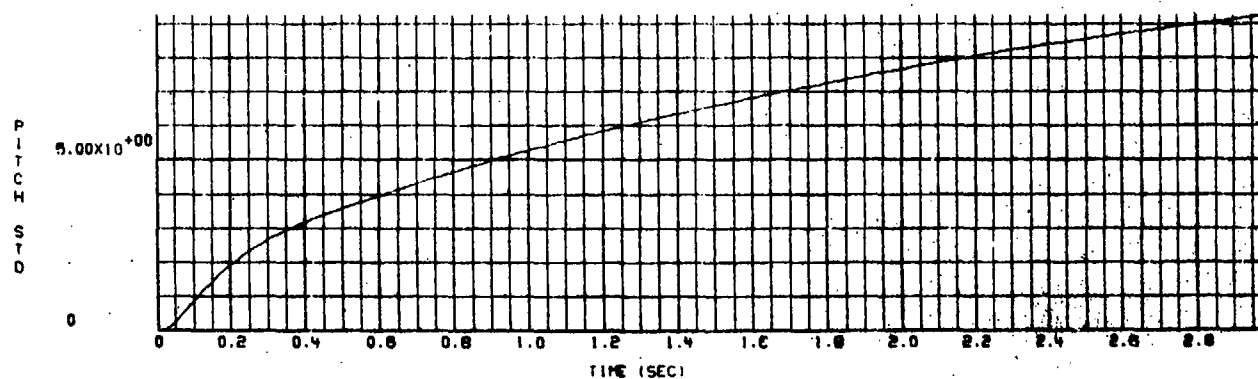
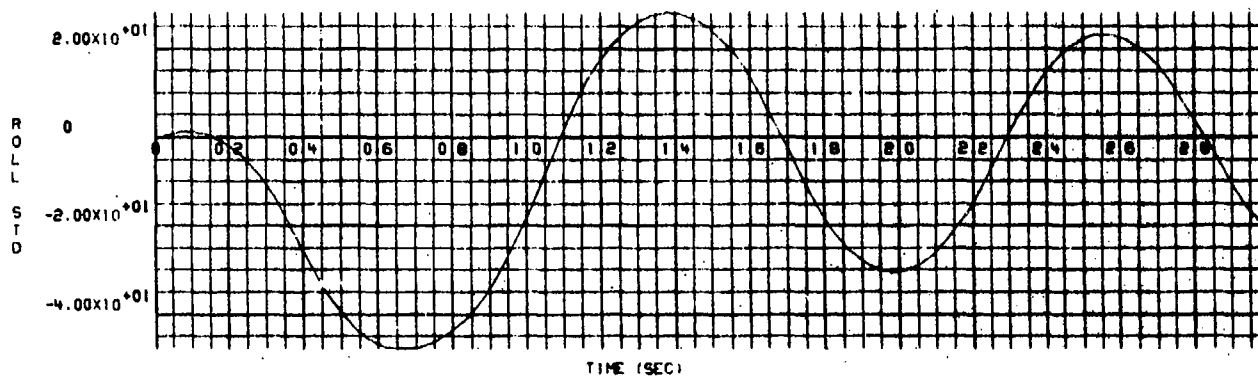


PLOT PREPARED BY: TSX, ALTC

Figure G-1. X, Y, and Z Position Versus Time for a Flow Field Intensity of 1/2

17/12/75

R631 43 43



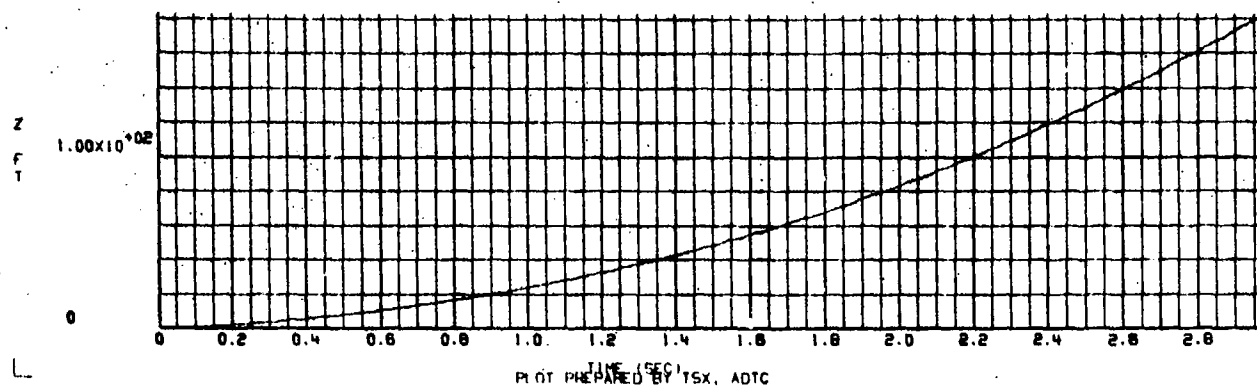
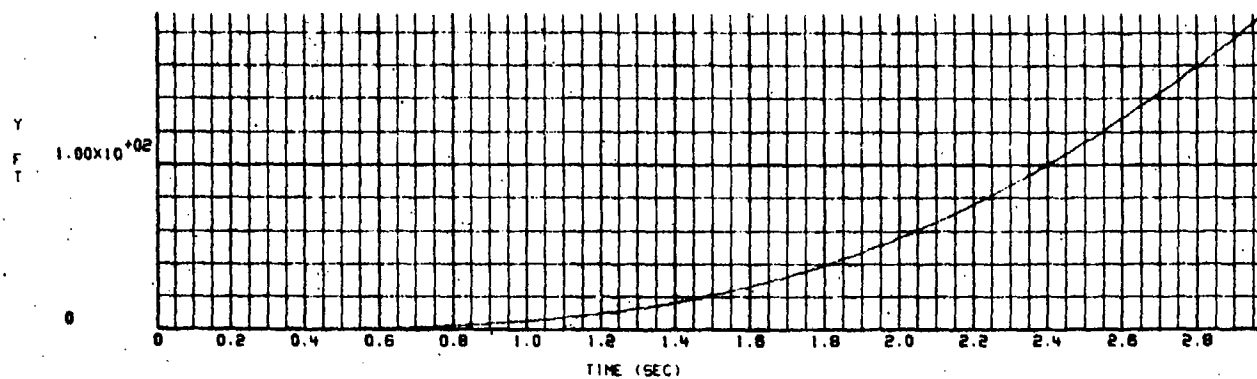
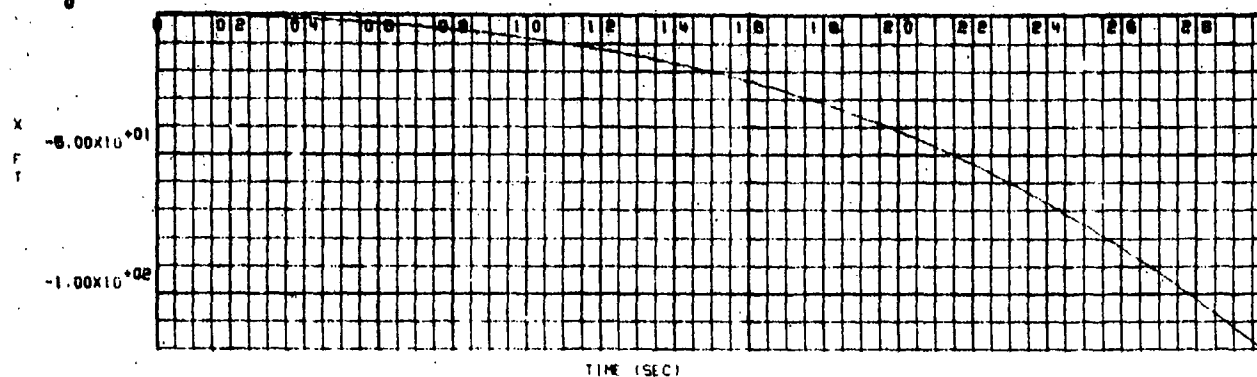
PLOT PREPARED BY TSX, ADTC

Figure G-2.  $\phi$ ,  $\theta$ , and  $\psi$  Rotation Versus Time for a Flow Field Intensity of  $1/2$

17/12/75  
0

R631

48 48



PI OT PREPARED BY TSX, ADTC

Figure G-3. X, Y, and Z Position Versus Time for a Flow Field Intensity of 1 (as measured in the wind tunnel)

17:13:75  
0

R631 47 47

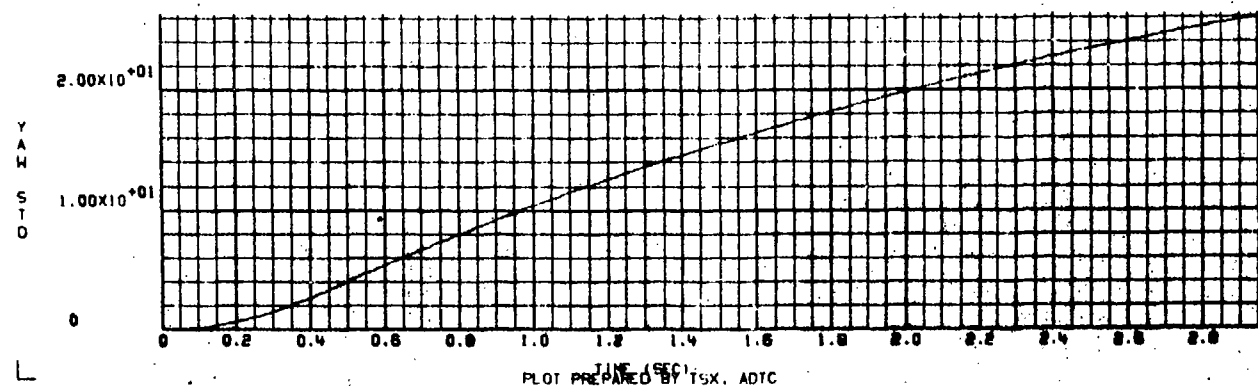
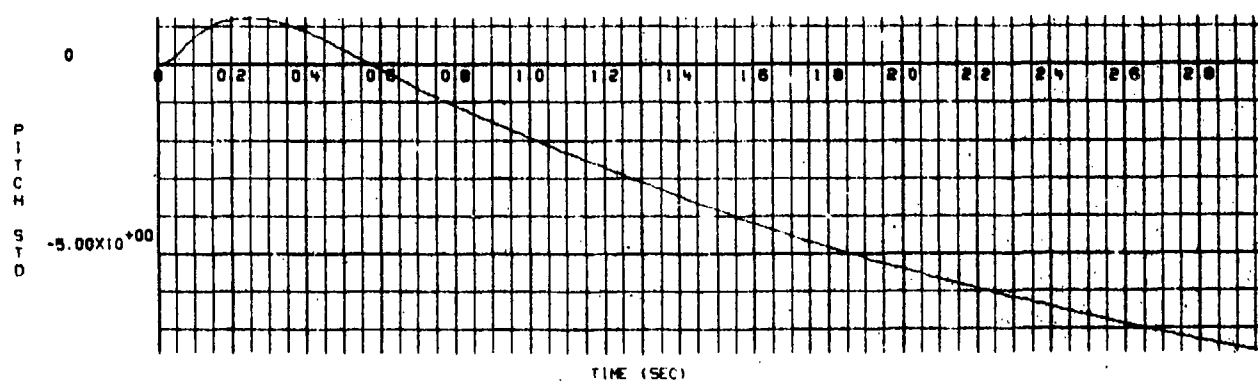
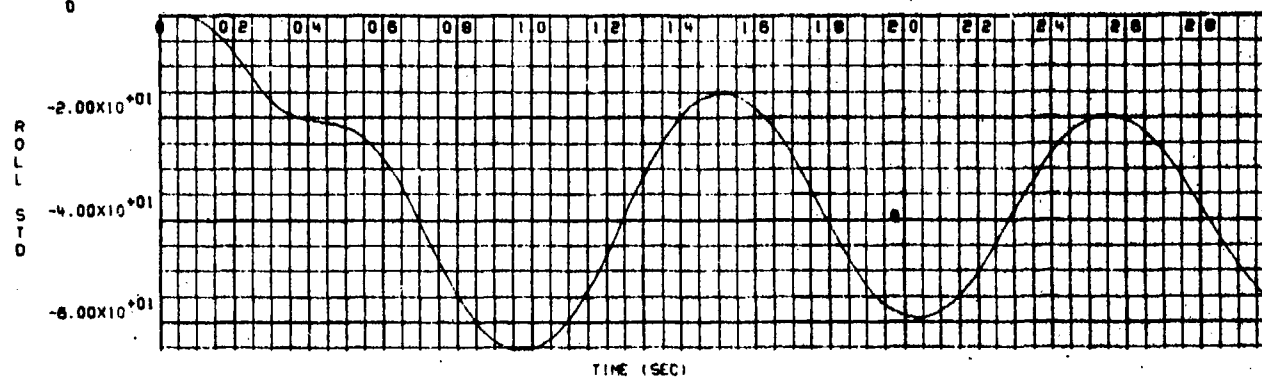
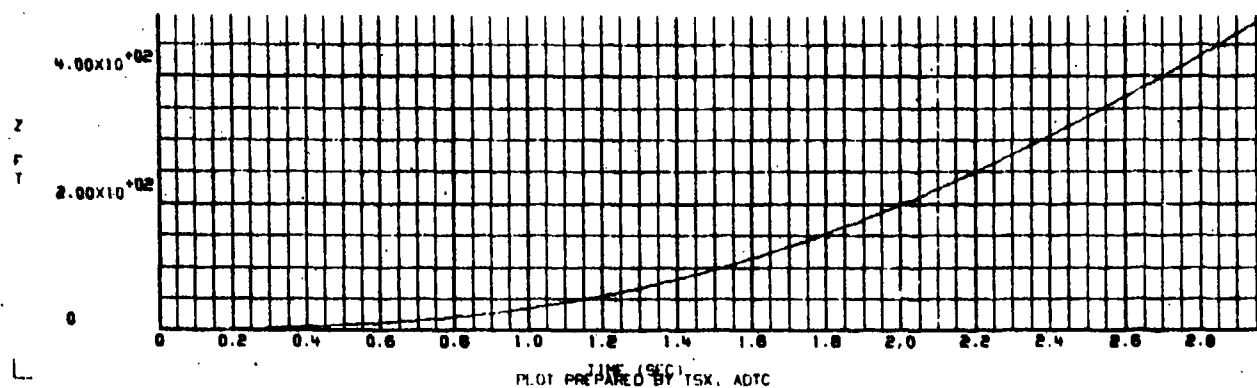
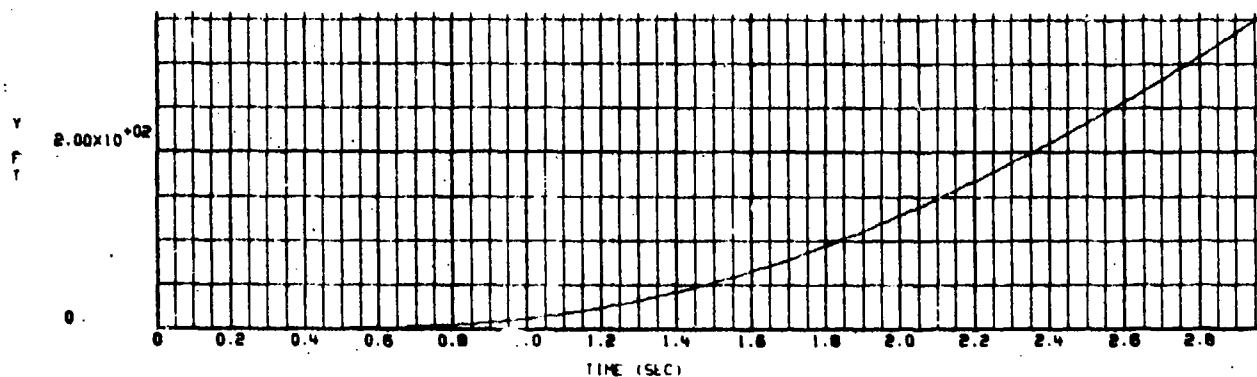
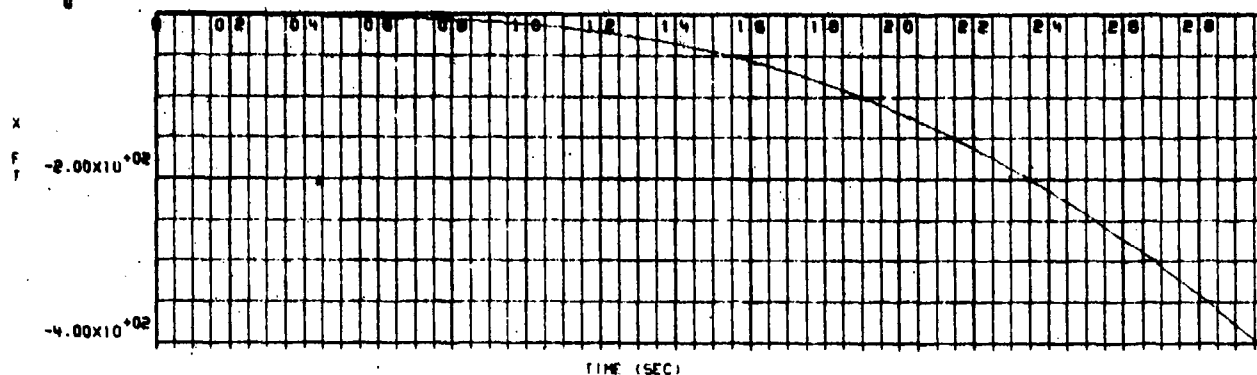


Figure G-4.  $\phi$ ,  $\theta$ , and  $\psi$  Rotation Versus Time for a Flow Field Intensity of 1 (unchanged from the wind tunnel measured values)

17/12/75  
0

R631 52 52



PLOT PREPARED BY TSX, ADTC

Figure G-5. X, Y, and Z Position Versus Time for a Flow Field Intensity of 2

17/12/75

R631

51 51

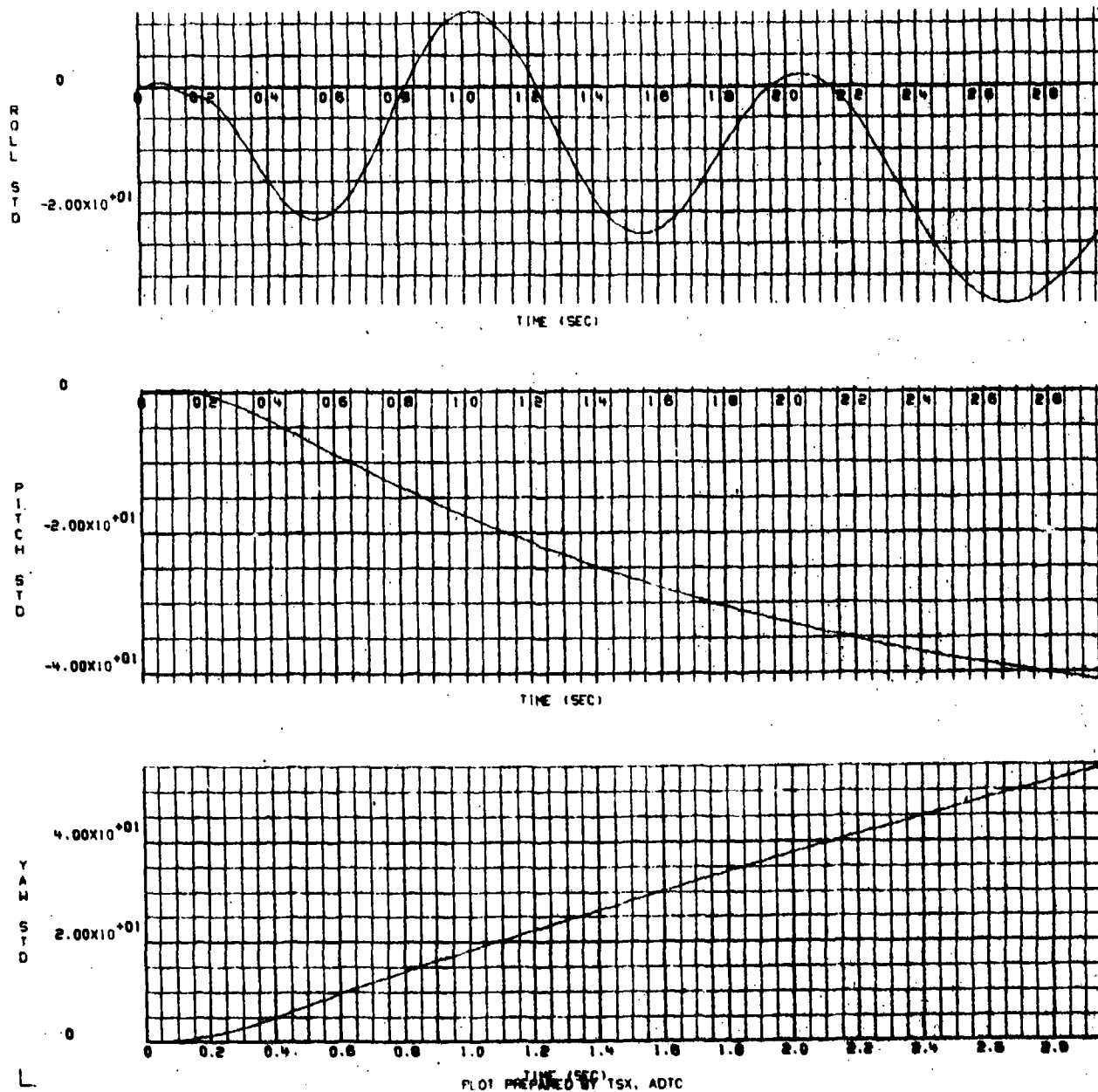


Figure G-6.  $\phi$ ,  $\theta$ , and  $\gamma$  Rotation Versus Time for a Flow Field Intensity of 2

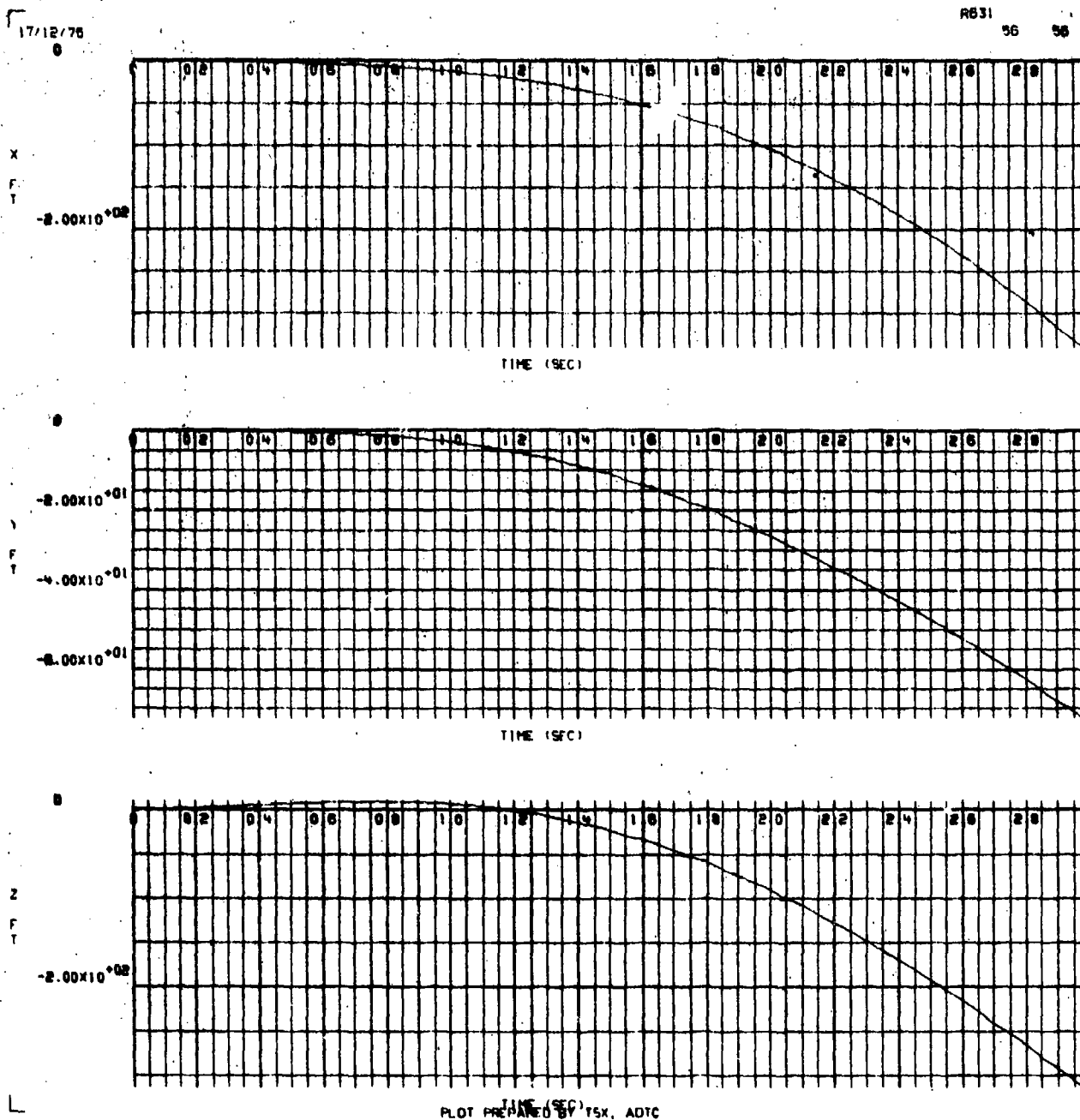


Figure G-7. X, Y, and Z Position Versus Time for a Flow Field Intensity of  $-1/2$

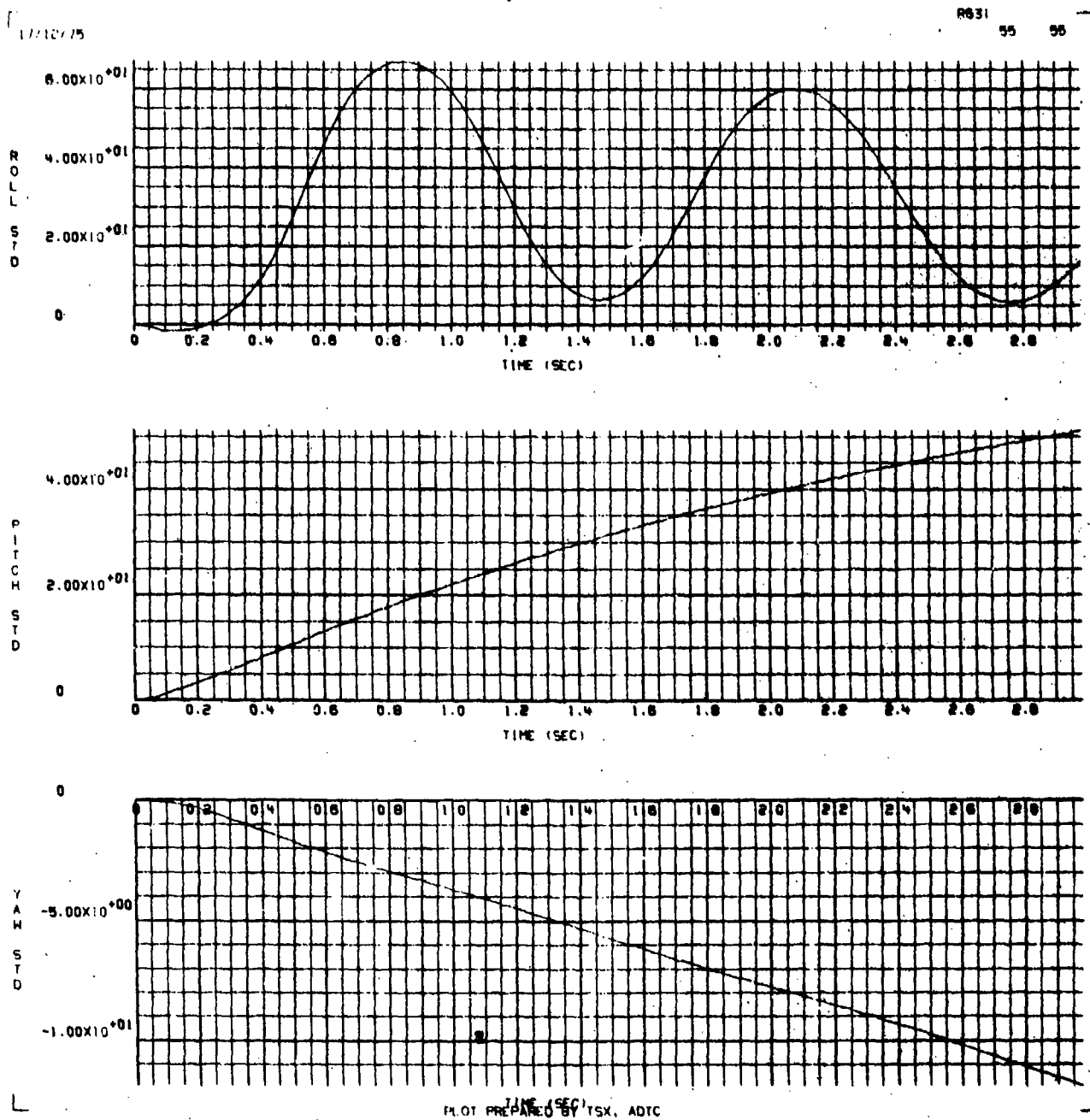


Figure G-8.  $\psi$ ,  $\theta$ , and  $\gamma$  Rotation Versus Time for a Flow Field Intensity of  $-1/2$



**APPENDIX H**

**GBU-12 BOMB TRAJECTORIES RESULTING FROM A  
(-3/-3) ORIFICE COMBINATION AT MACH 1.2**

11-12-75

0631 54 64

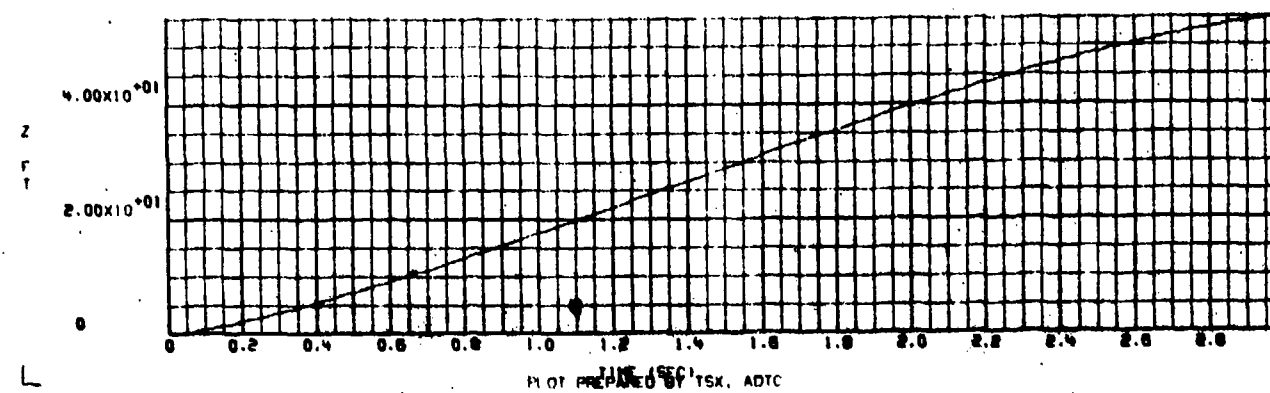
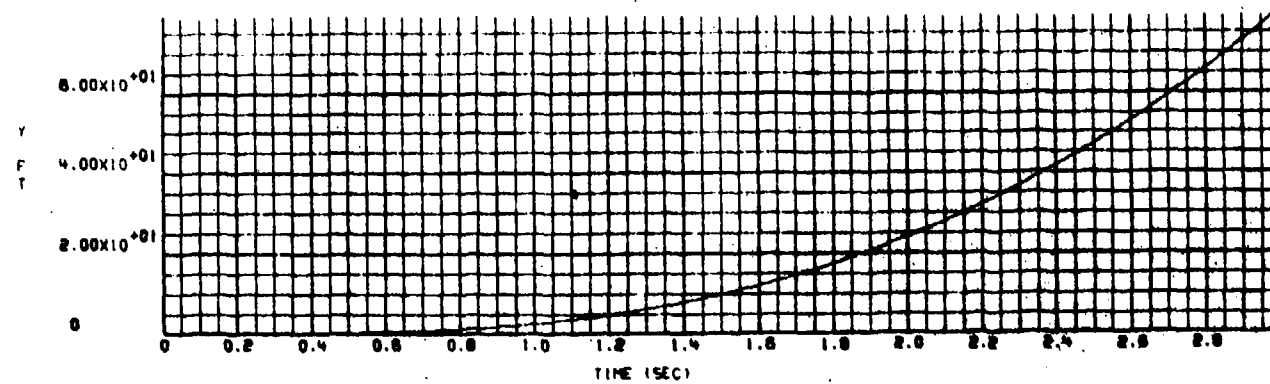
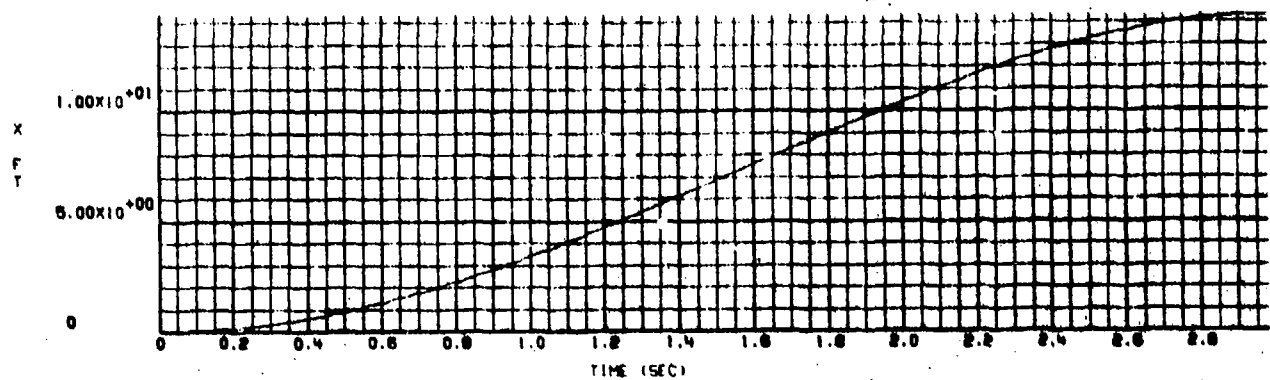


Figure H-1. X, Y, and Z Position Versus Time for a Flow Field Intensity of  $1/2$

17/12/75

#651

63 63

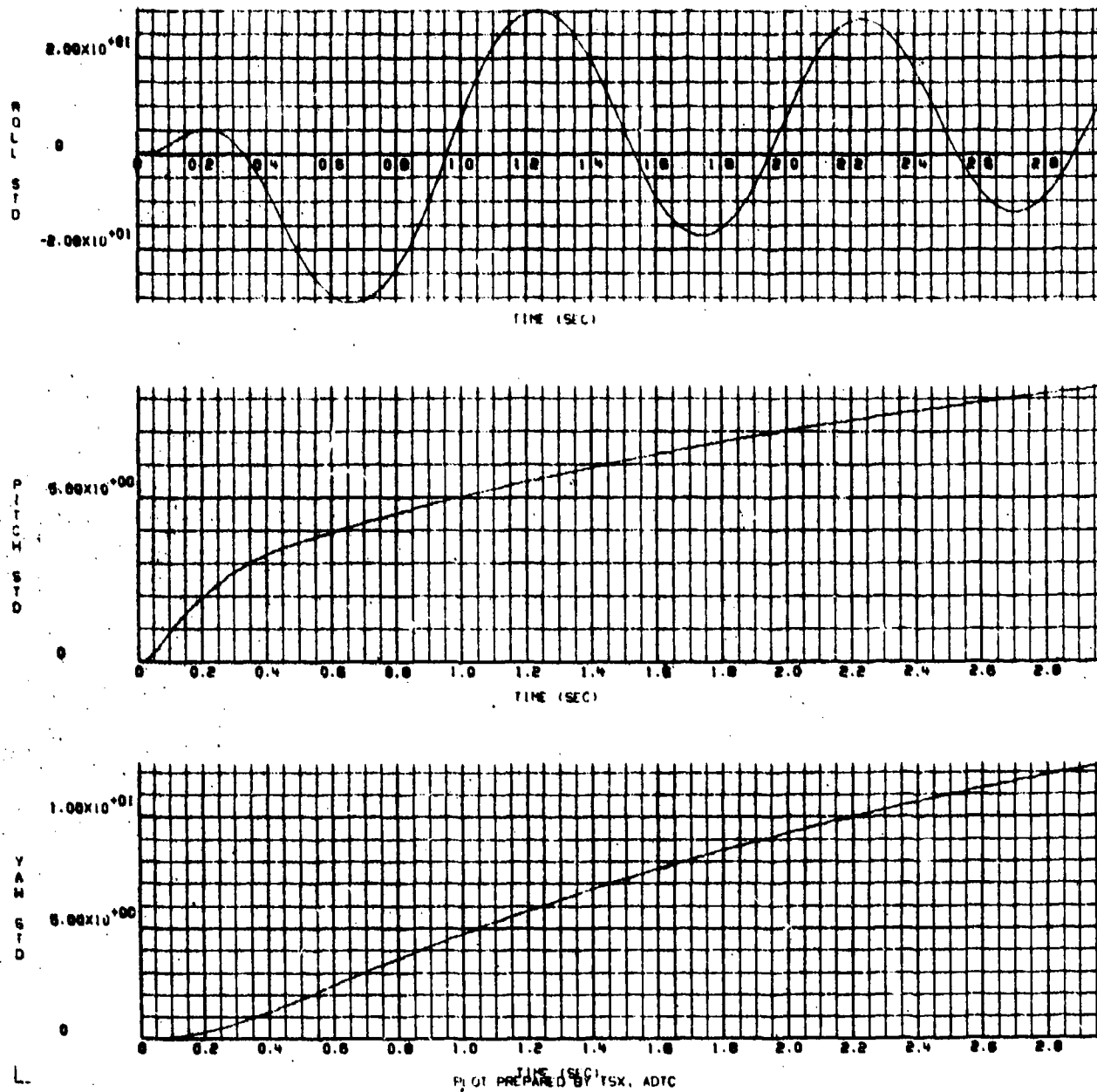
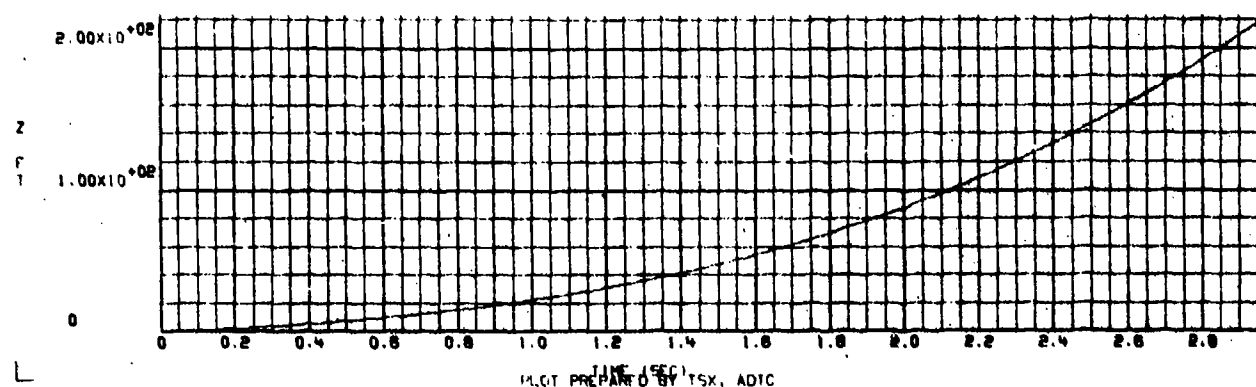
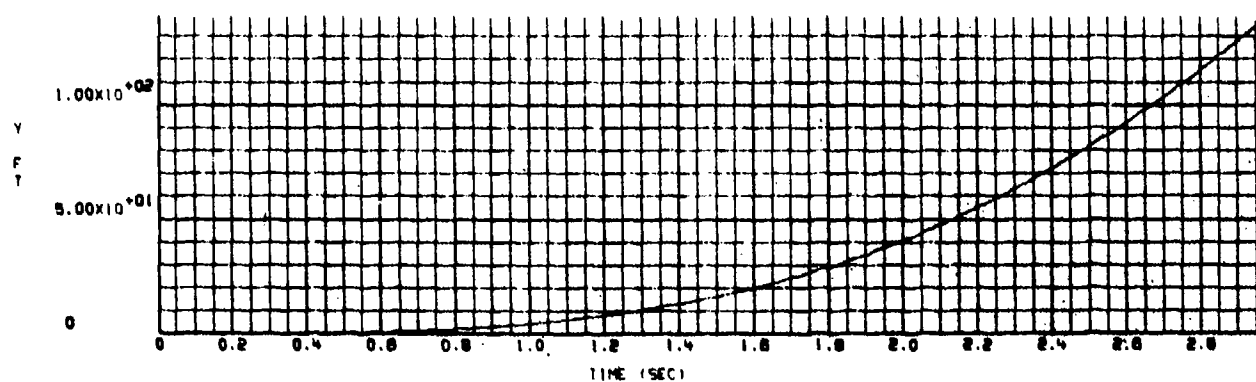
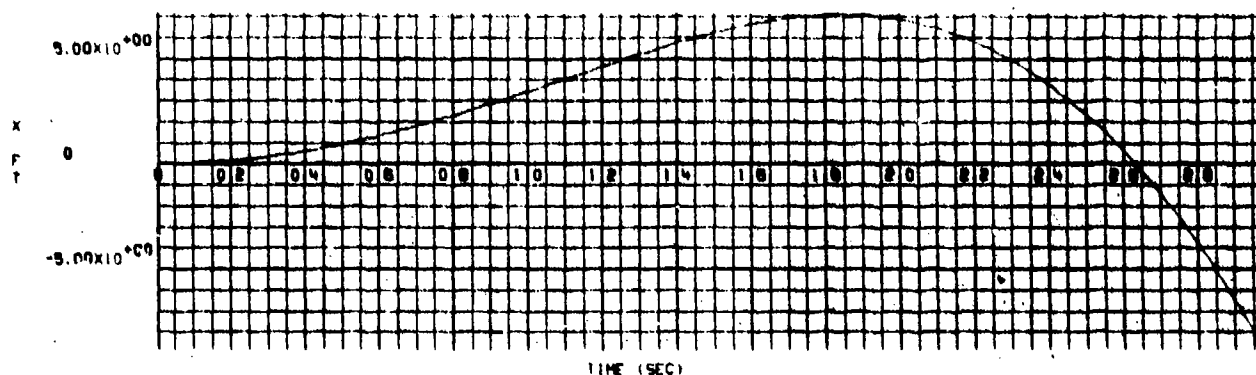


Figure H-2.  $\phi$ ,  $\theta$ , and  $\psi$  Rotation Versus Time for a Flow Field Intensity of  $1/2$

12/12/75

R631 68 68



TIME (SEC)  
PLOT PREPARED BY TSX, ADIC

Figure H-3. X, Y, and Z Position Versus Time for a Flow Field Intensity of 1 (as measured in the wind tunnel)

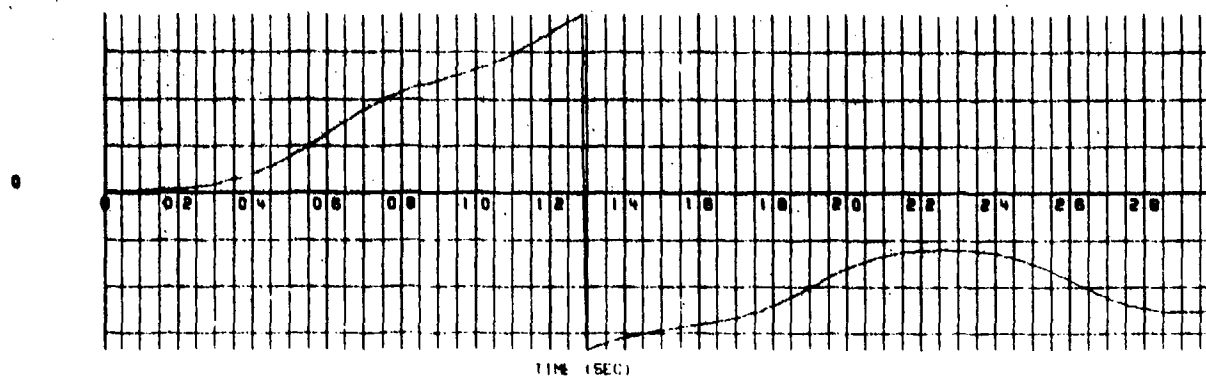
17/12/75

R631

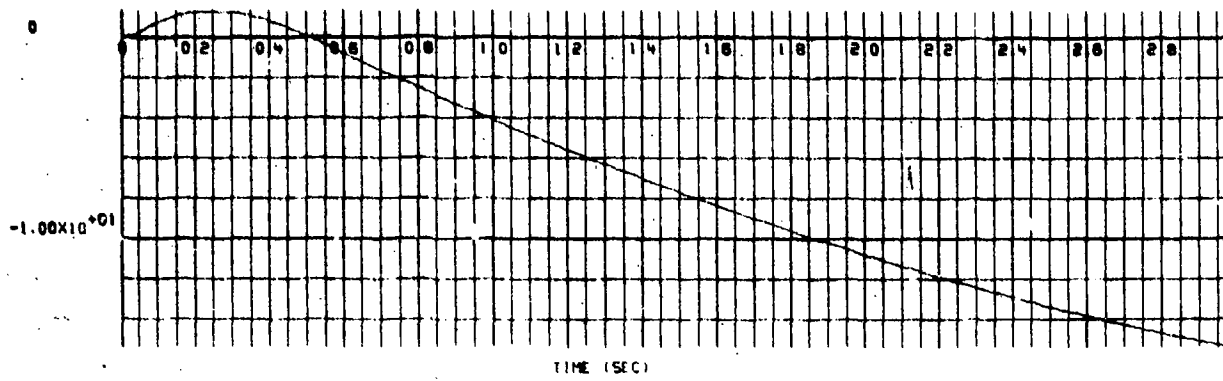
67

67

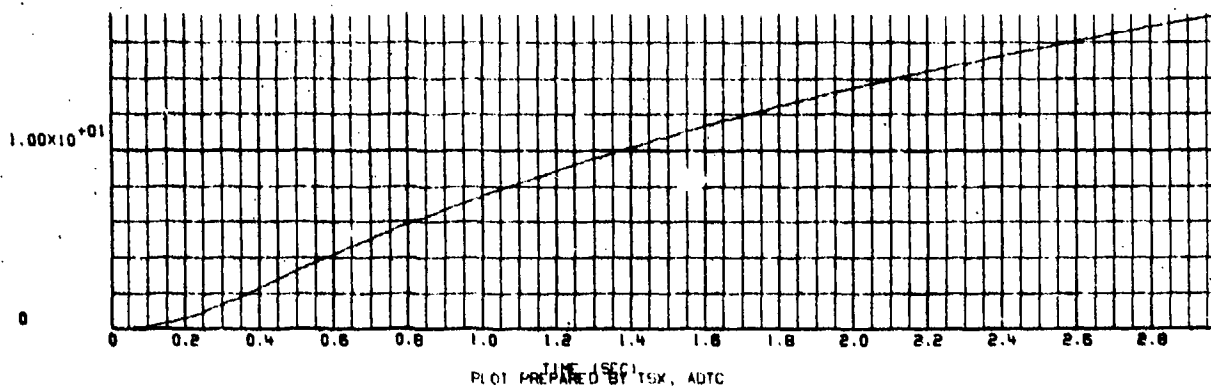
ROLL  
STU



PITCH  
STD



YAW  
STD



TIME (SEC)  
PLOT PREPARED BY TSK, ADTC

Figure H-4.  $\phi$ ,  $\theta$ , and  $\psi$  Rotation Versus Time for a Flow Field Intensity of 1 (unchanged from the wind tunnel measured values)

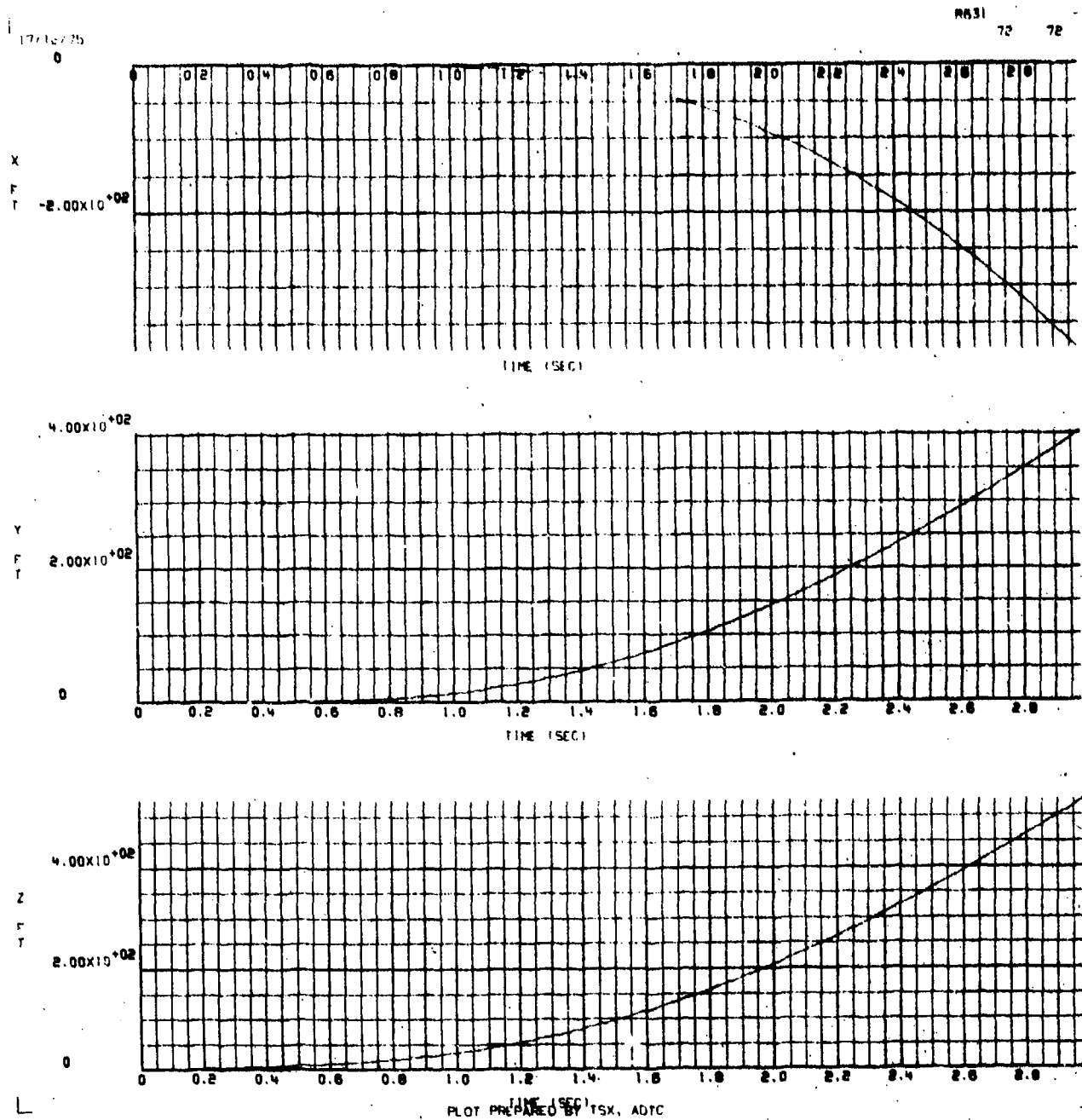
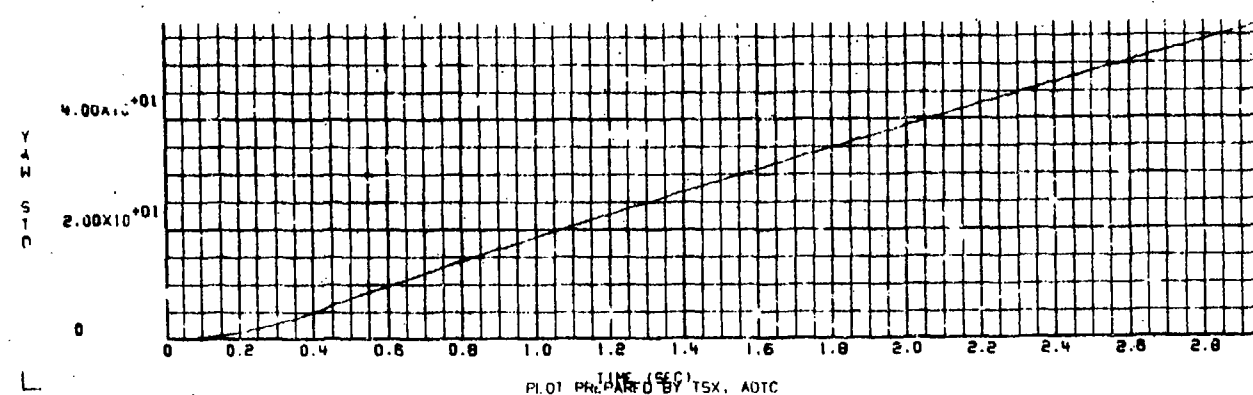
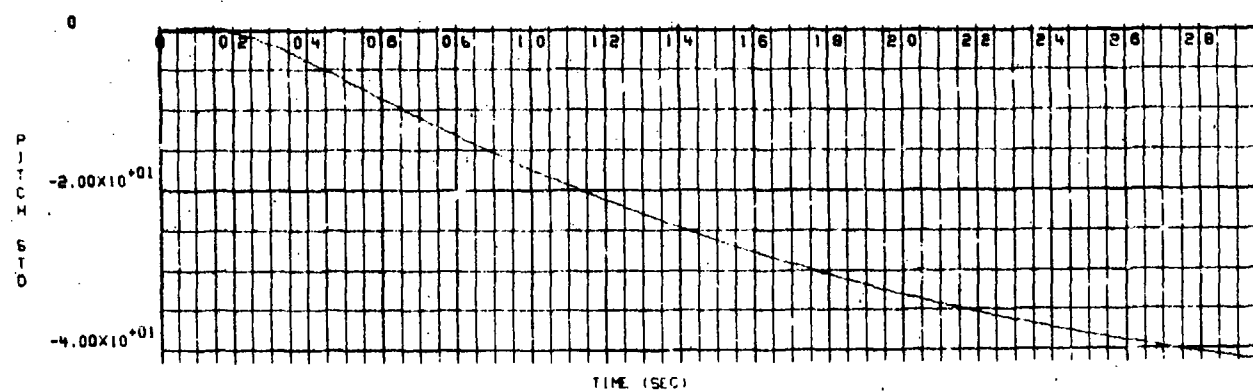
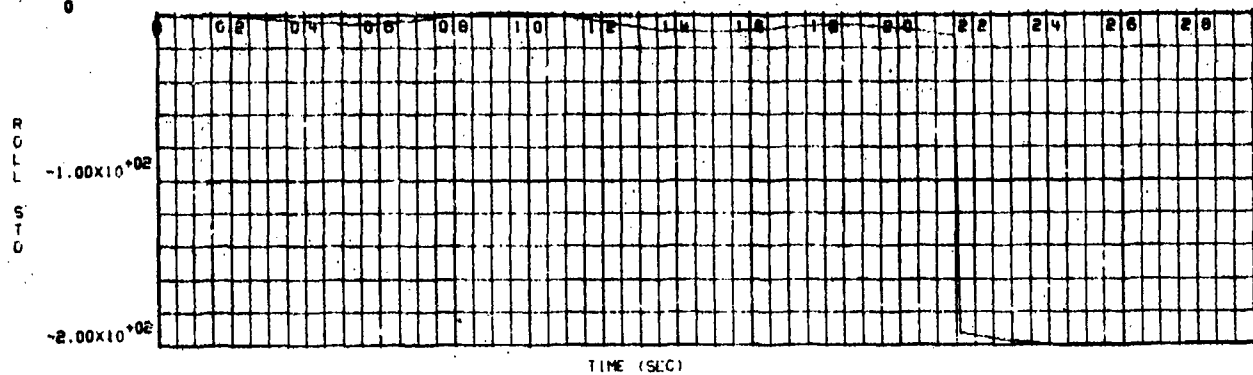


Figure H-5. X, Y, and Z Position Versus Time for a Flow Field Intensity of 2

17/12/75  
0

R631 71 71



PILOT PREPARED BY TSX, ADTC

Figure H-6.  $\phi$ ,  $\theta$ , and  $\psi$  Rotation Versus Time for a Flow Field Intensity of 2

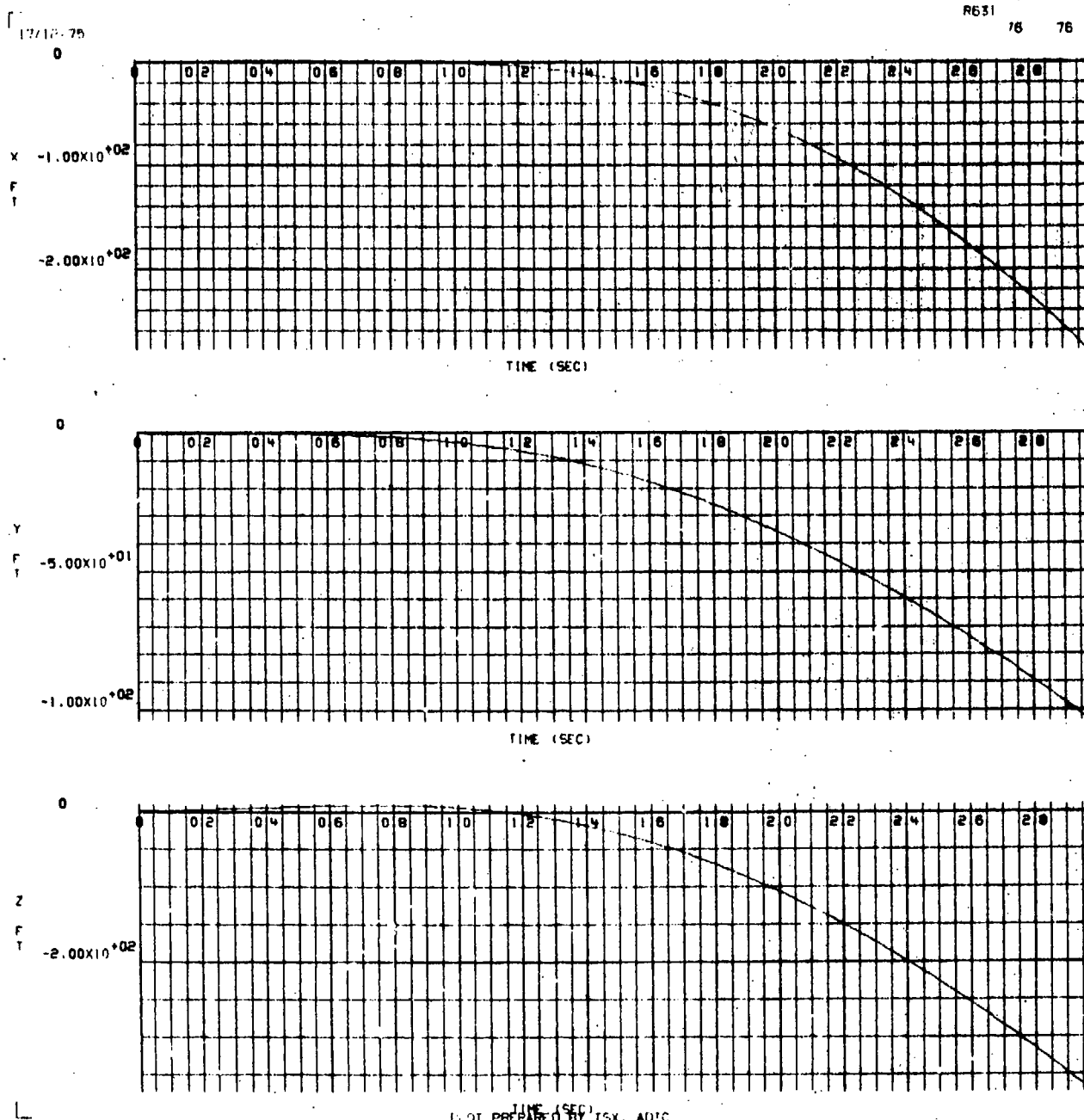


Figure H-7. X, Y, and Z Position Versus Time for a Flow Field Intensity of  $-1/2$



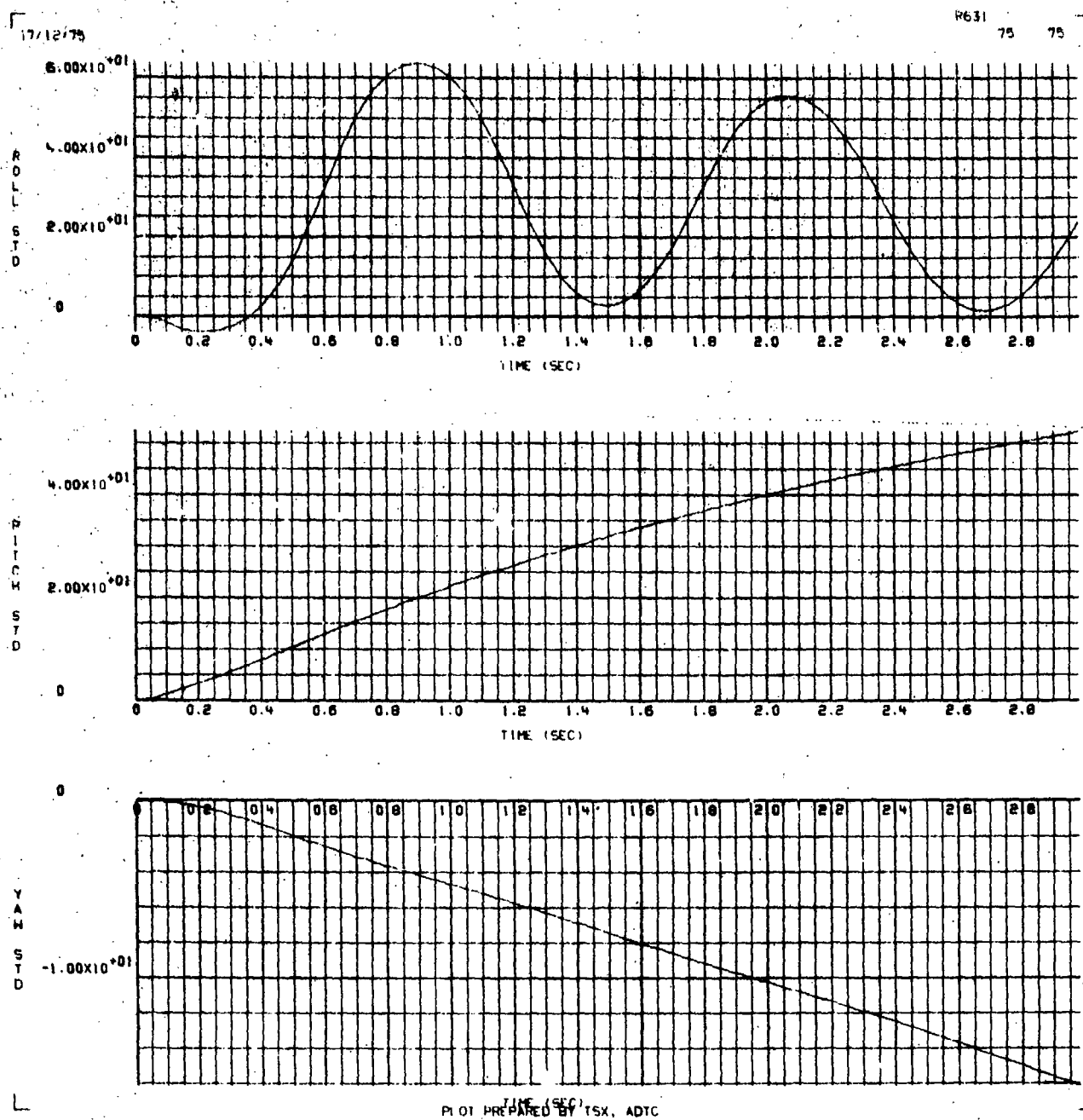


Figure H-8.  $\phi$ ,  $\theta$ , and  $\psi$  Rotation Versus Time for a Flow Field Intensity of  $-1/2$

APPENDIX I

GBU-12 BOMB TRAJECTORIES RESULTING FROM A  
(-3/-5) ORIFICE COMBINATION AT MACH 0.7

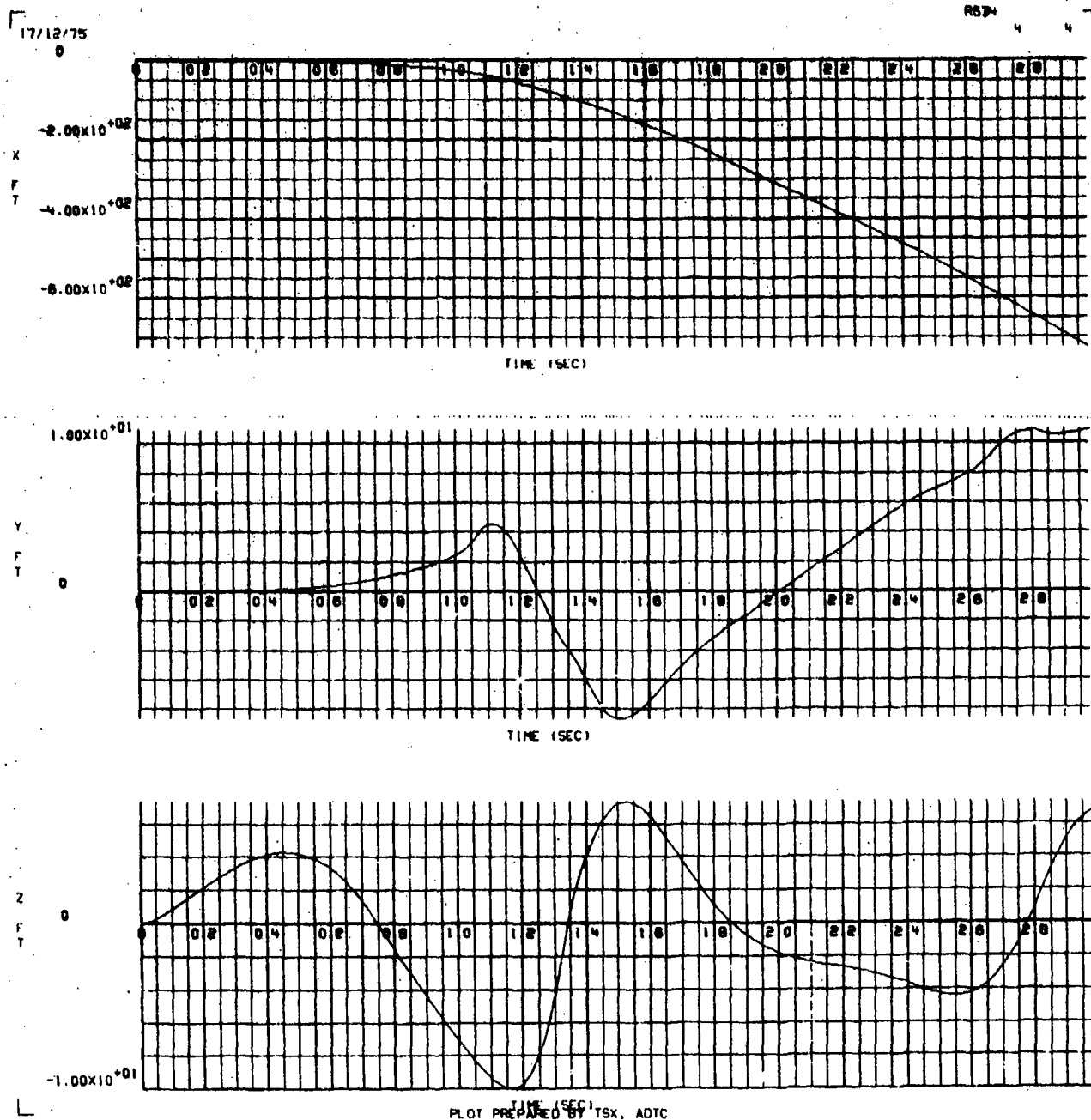
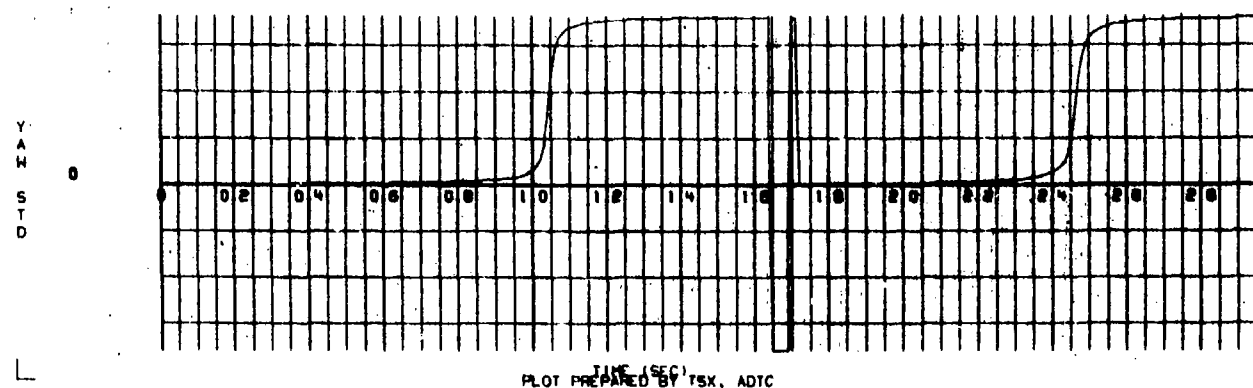
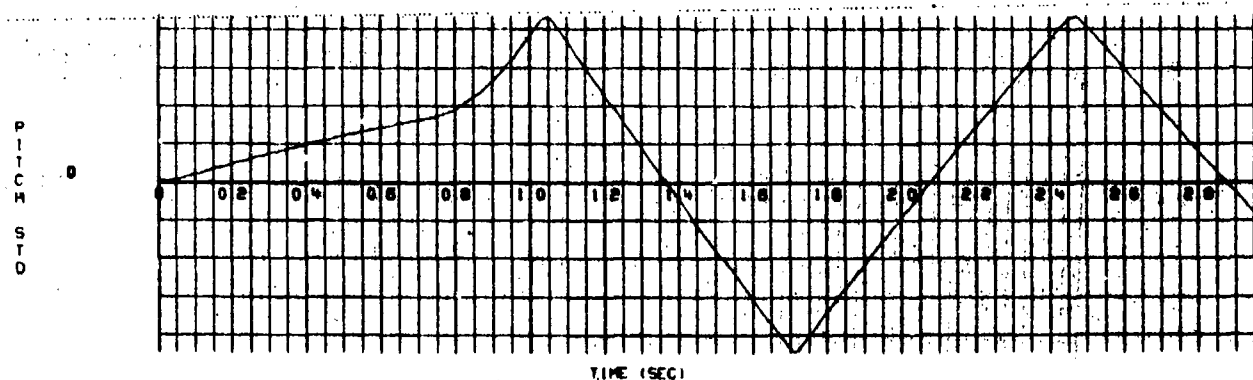
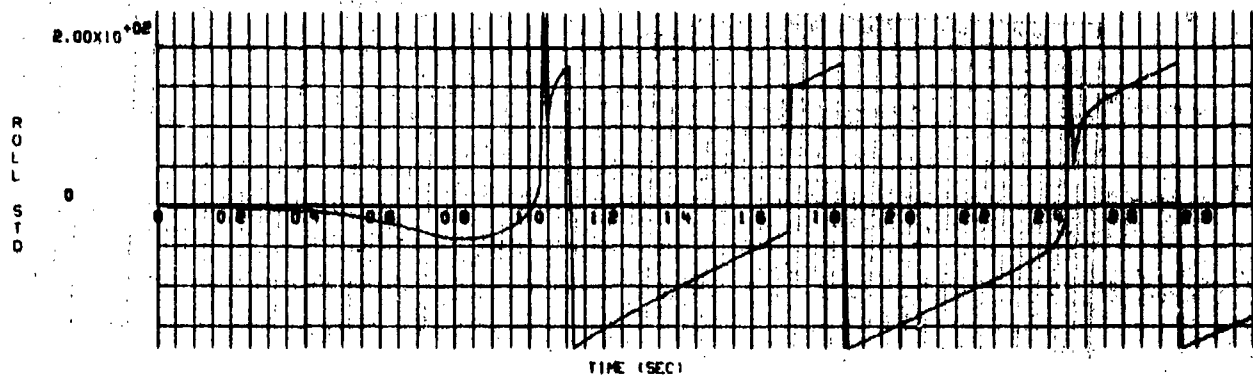


Figure I-1. X, Y, and Z Position Versus Time for a Flow Field Intensity of 1/2

17/12/75

R634



PLOT PREPARED BY TSX, ADTC

Figure I-2.  $\phi$ ,  $\theta$ , and  $\psi$  Rotation Versus Time for a Flow Field Intensity of 1/2

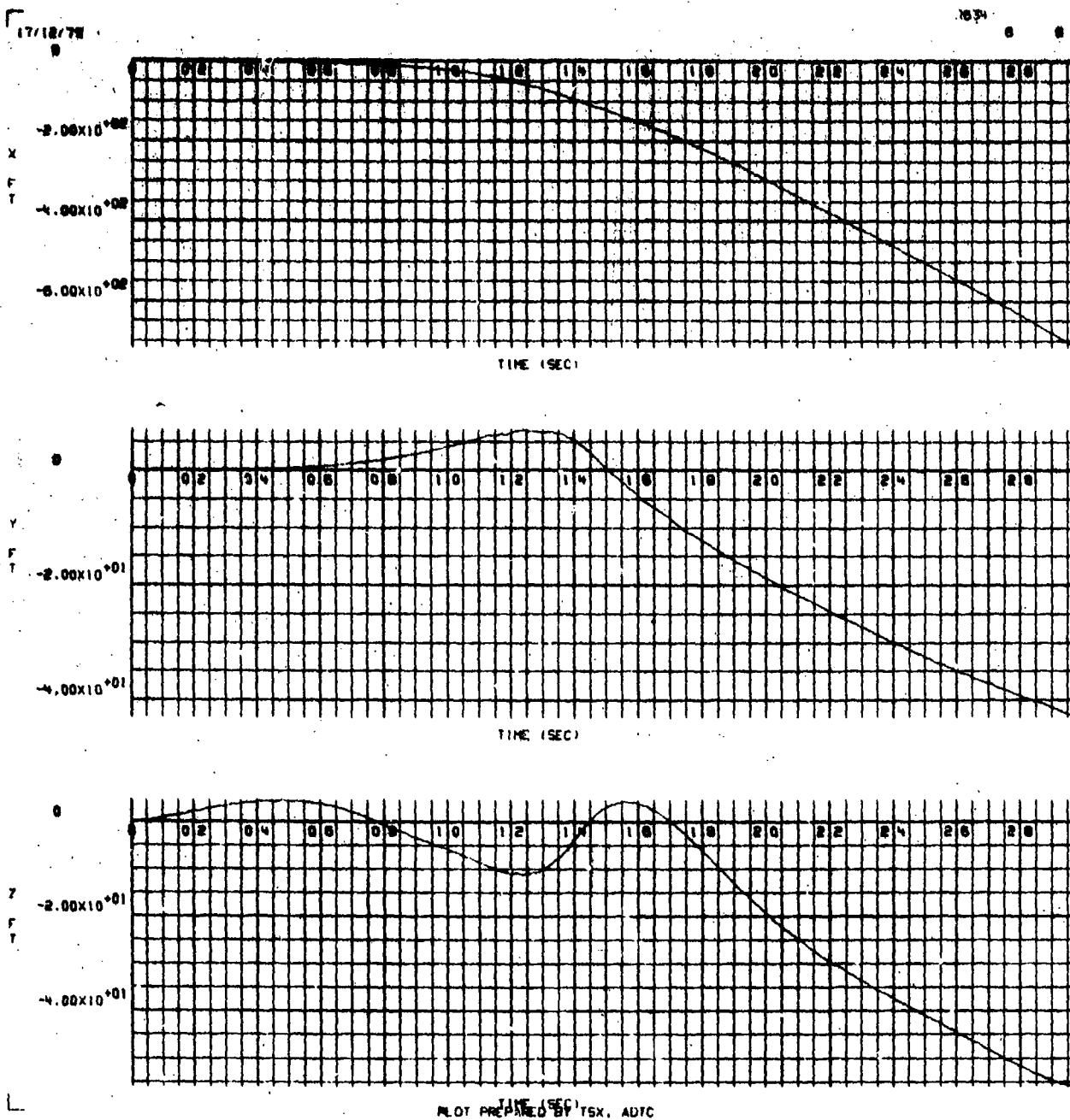


Figure I-3. X, Y, and Z Position Versus Time for a Flow Field Intensity of 1 (as measured in the wind tunnel)

17/12/75

7 7

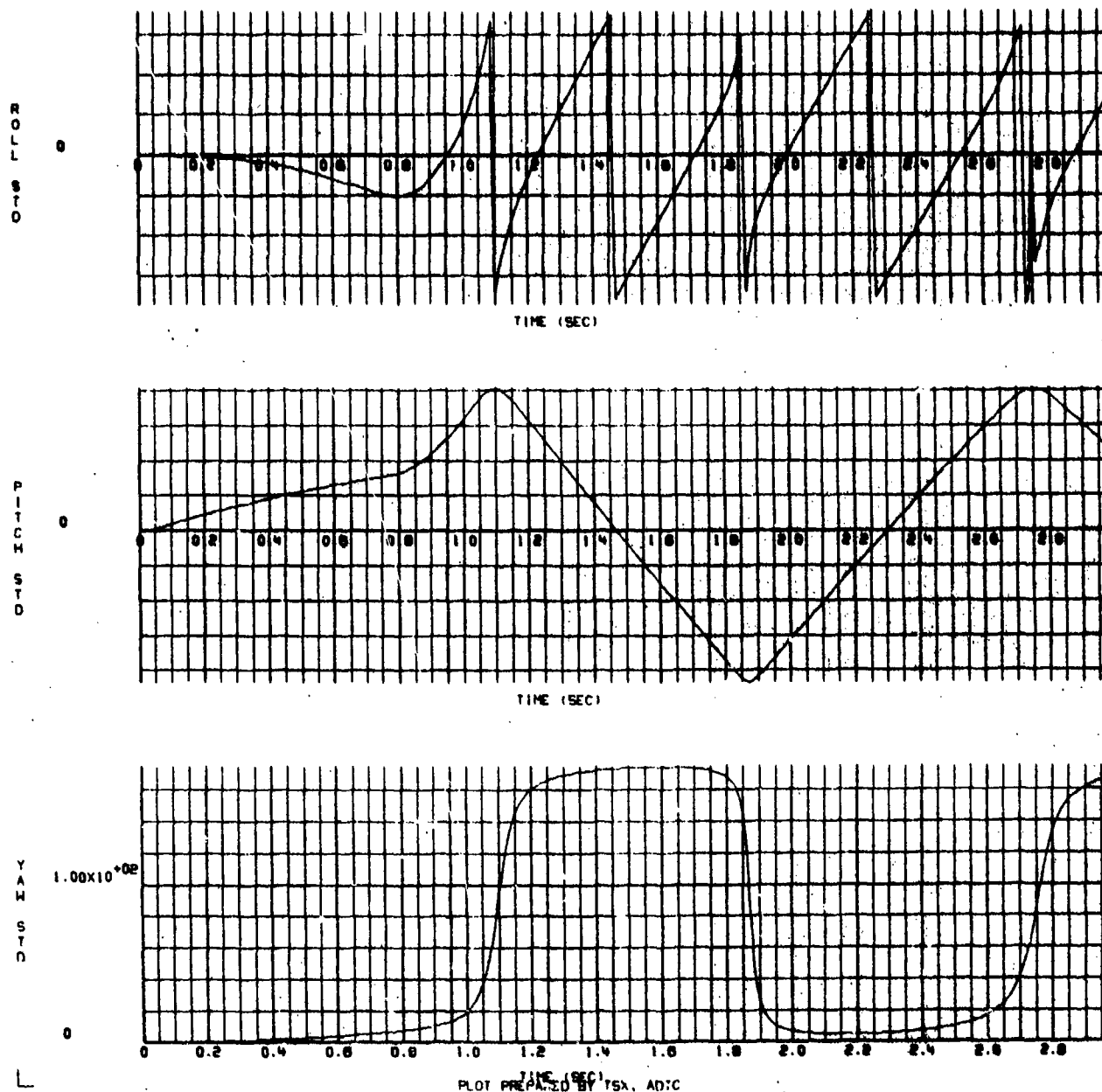


Figure I-4.  $\phi$ ,  $\theta$ , and  $\psi$  Rotation Versus Time for a Flow Field Intensity of 1 (unchanged from the wind tunnel measured values)

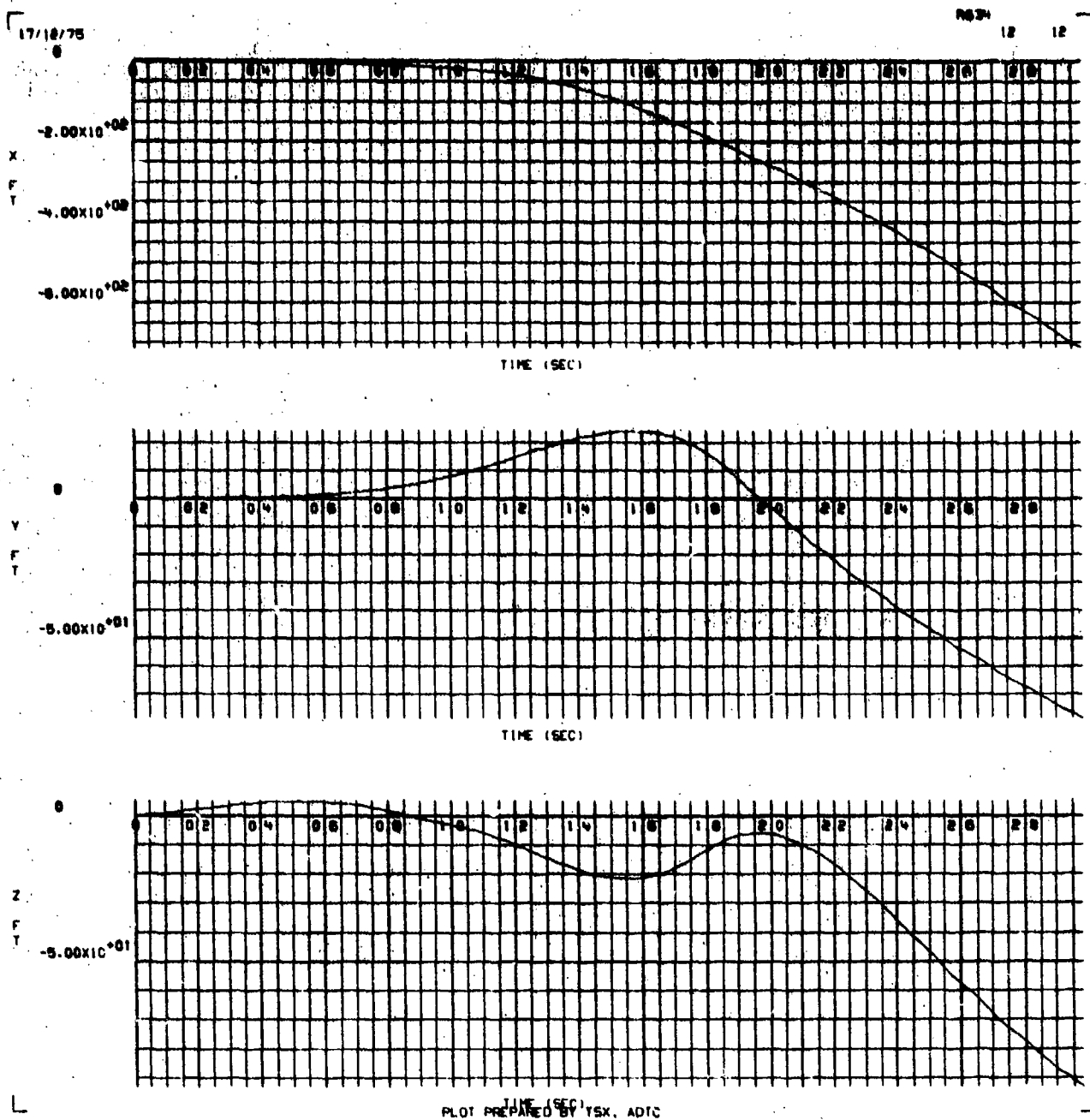


Figure I-5. X, Y, and Z Position Versus Time for a Flow Field Intensity of 2

17/12/75

1034

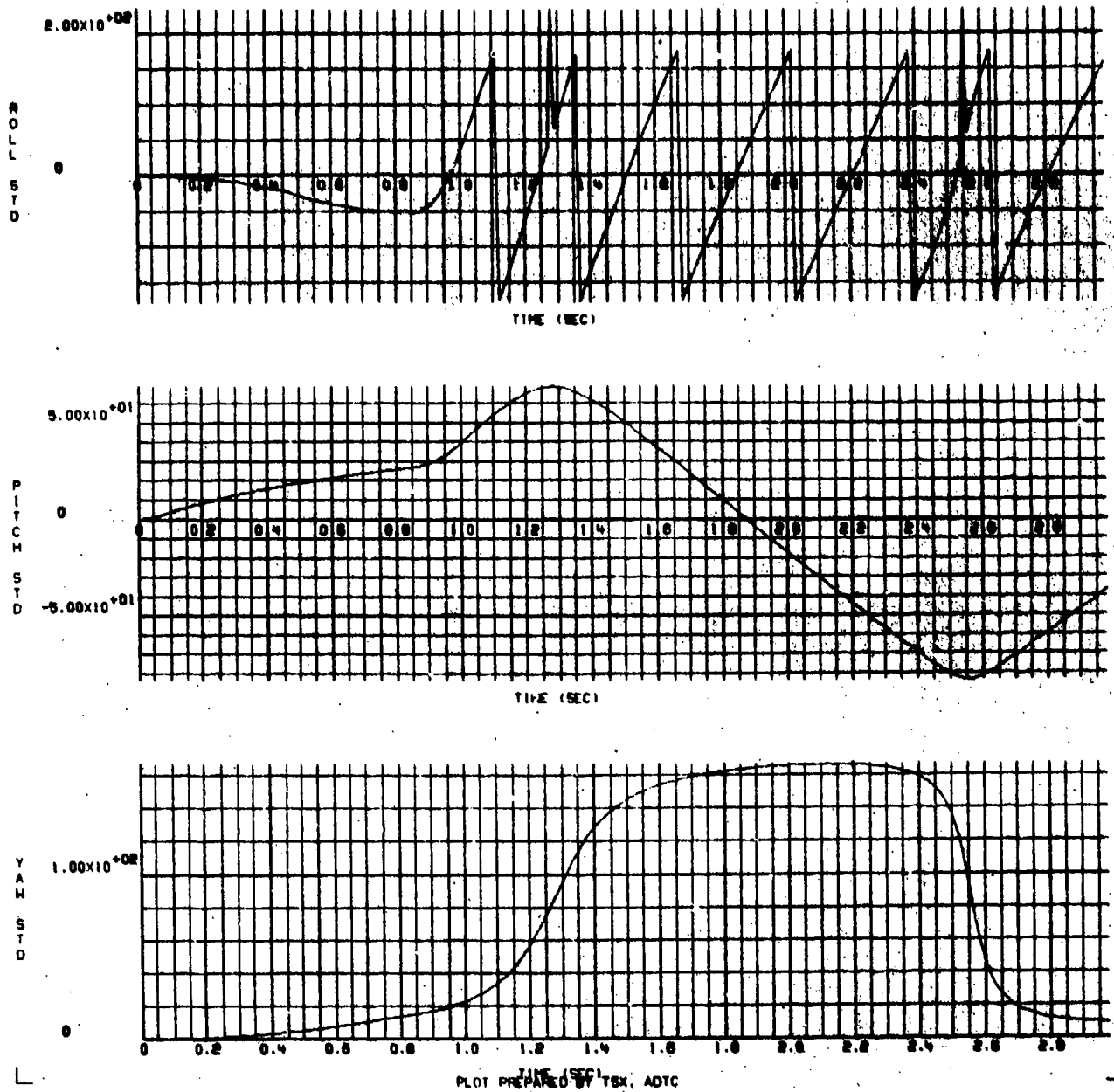


Figure I-6.  $\phi$ ,  $\theta$ , and  $\psi$  Rotation Versus Time for a Flow Field Intensity of 2



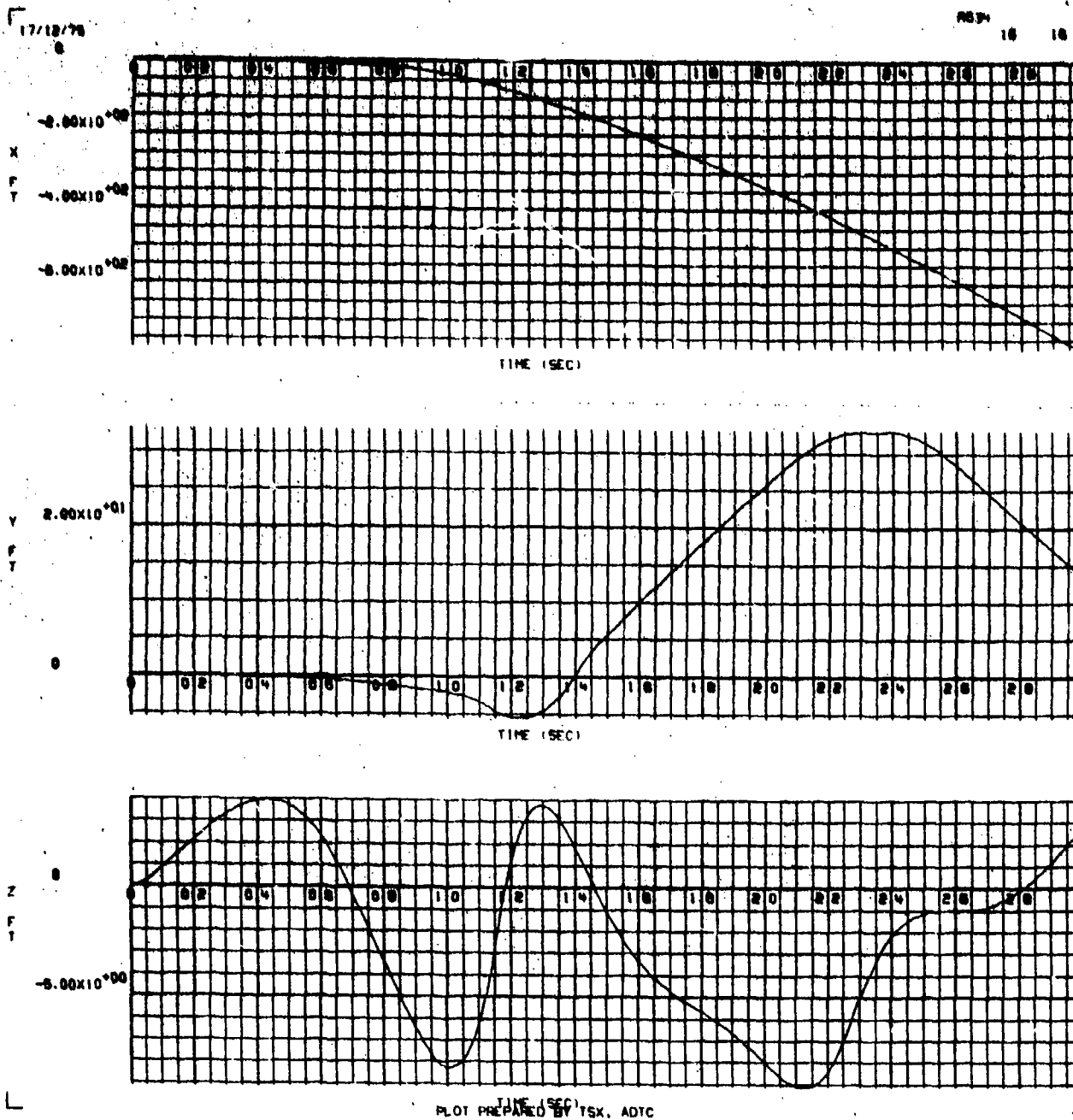
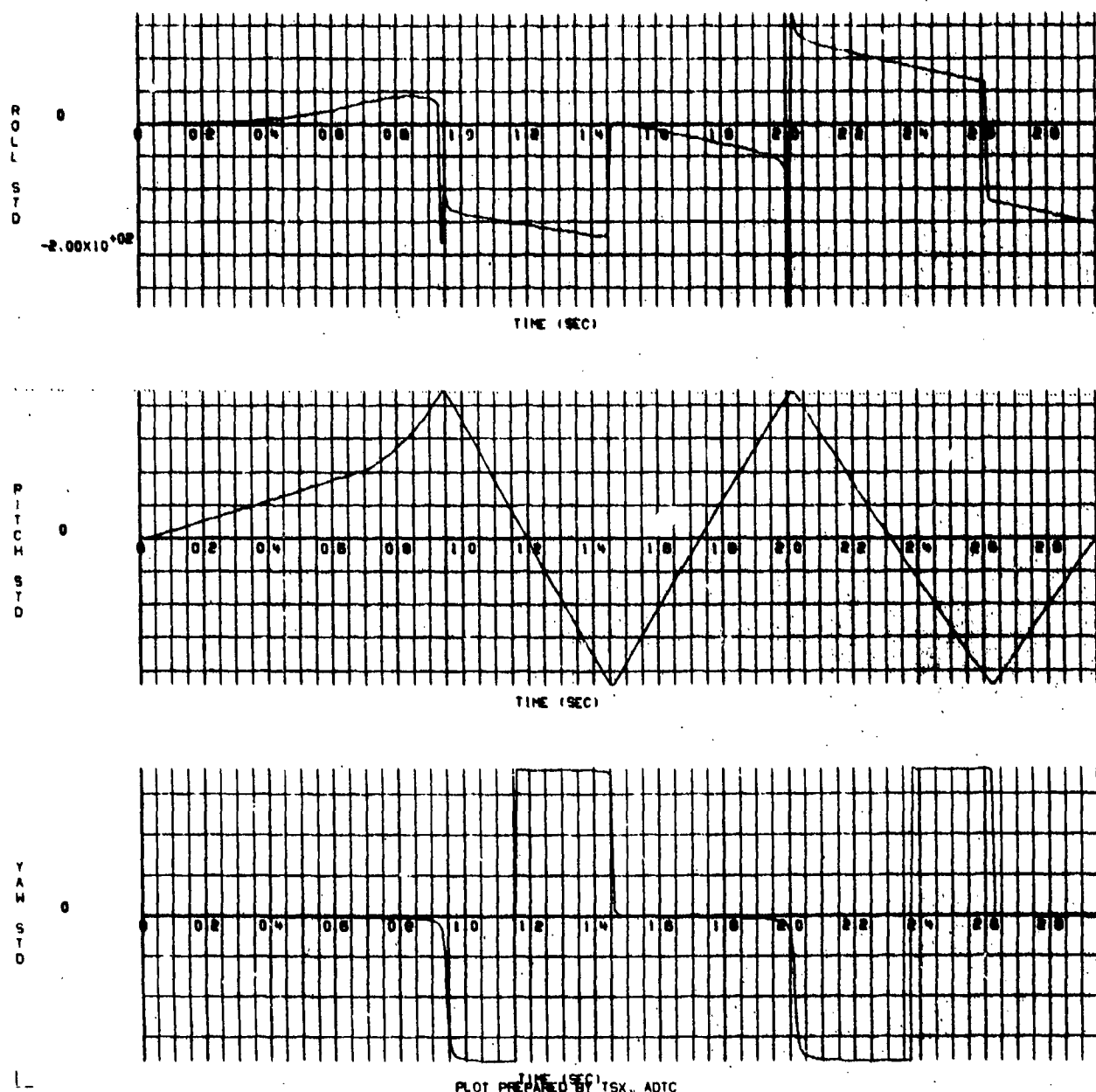


Figure I-7. X, Y, and Z Position Versus Time for a Flow Field Intensity of  $-1/2$

17/12/75

RG34

15 15



PLOT PREPARED BY TSX, ADTC

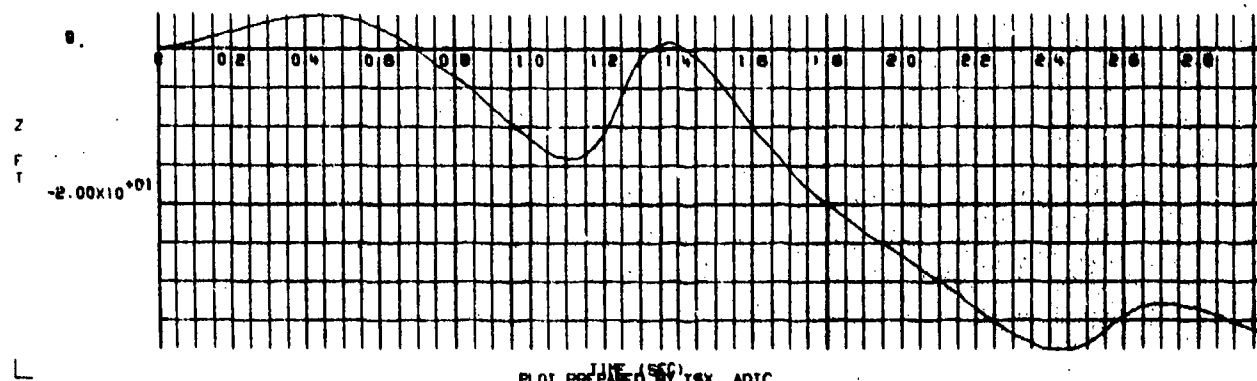
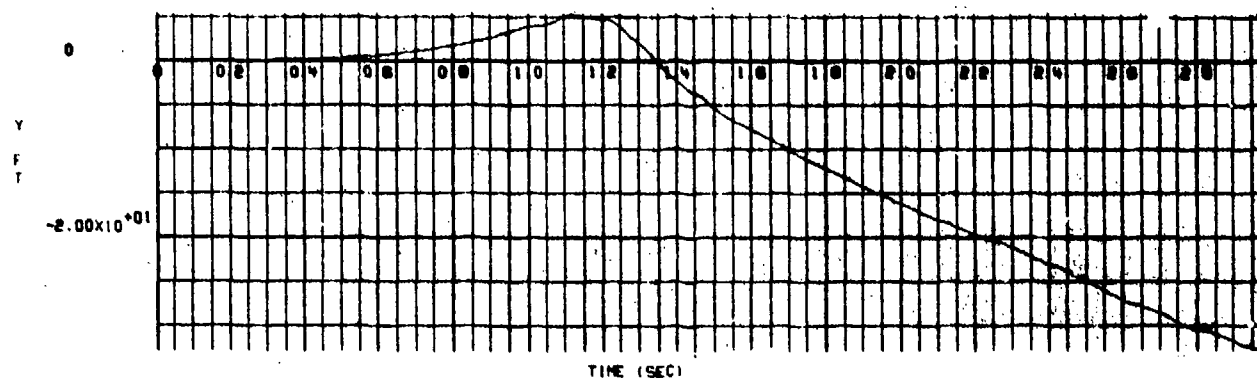
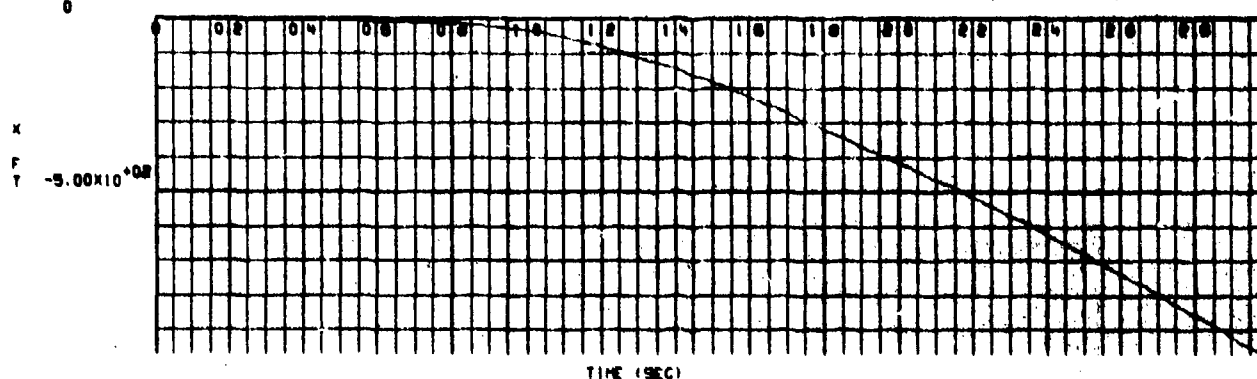
Figure I-8.  $\phi$ ,  $\theta$ , and  $\psi$  Rotation Versus Time for a Flow Field Intensity of  $-1/2$

**APPENDIX J**

**GBU-12 BOMB TRAJECTORIES RESULTING FROM A  
(-3/-5) ORIFICE COMBINATION AT MACH 0.85**

17/12/75  
0

NO. 34



JUL 1975  
PLOT PREPARED BY TSX, ADTC

Figure J-1. X, Y, and Z Position Versus Time for a Flow Field Intensity of 1/2

17/12/75

R634

23

23

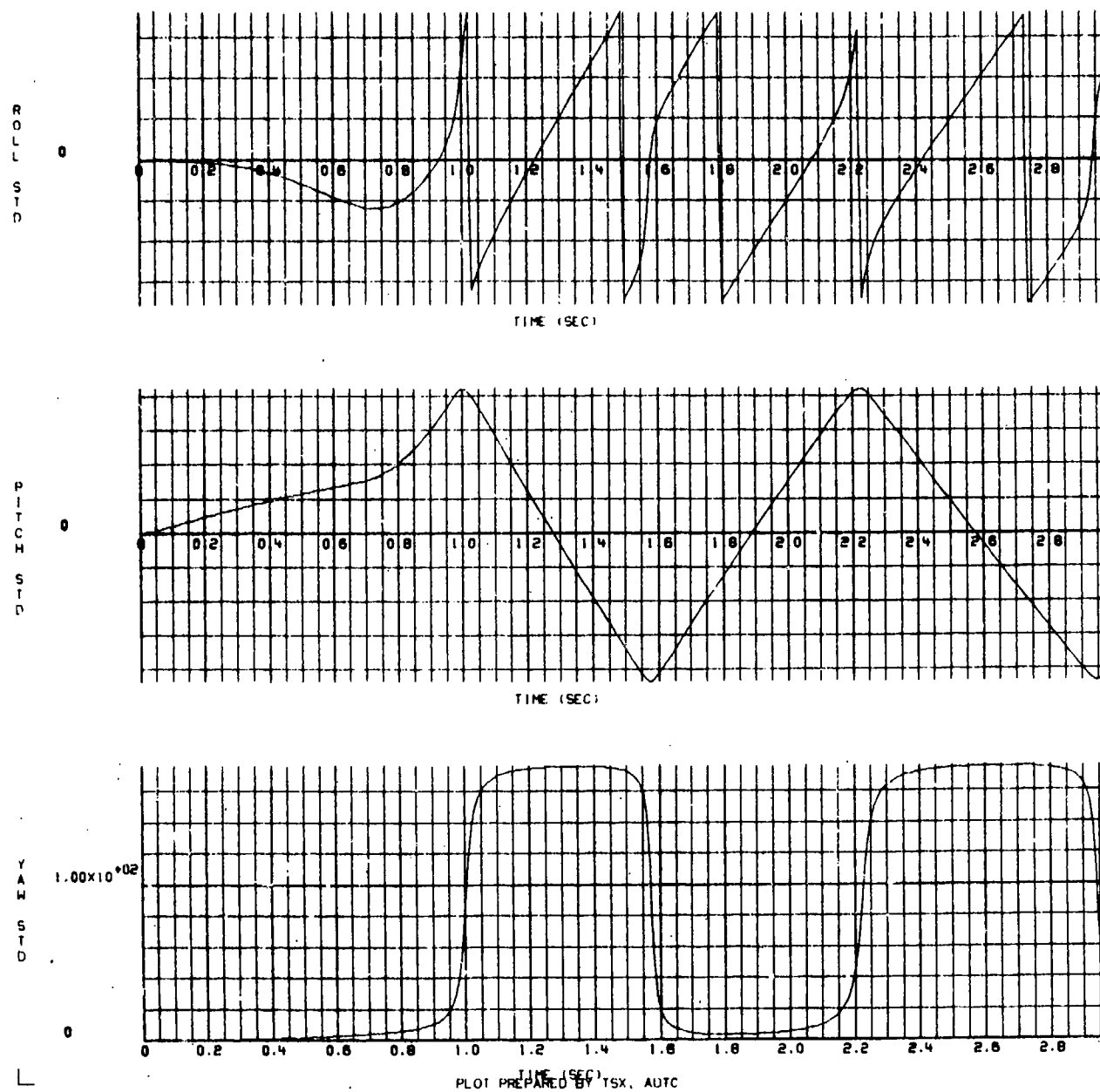


Figure J-2.  $\phi$ ,  $\theta$ , and  $\psi$  Rotation Versus Time for a Flow Field Intensity of 1/2

17/12/75  
0

R634 2R 20

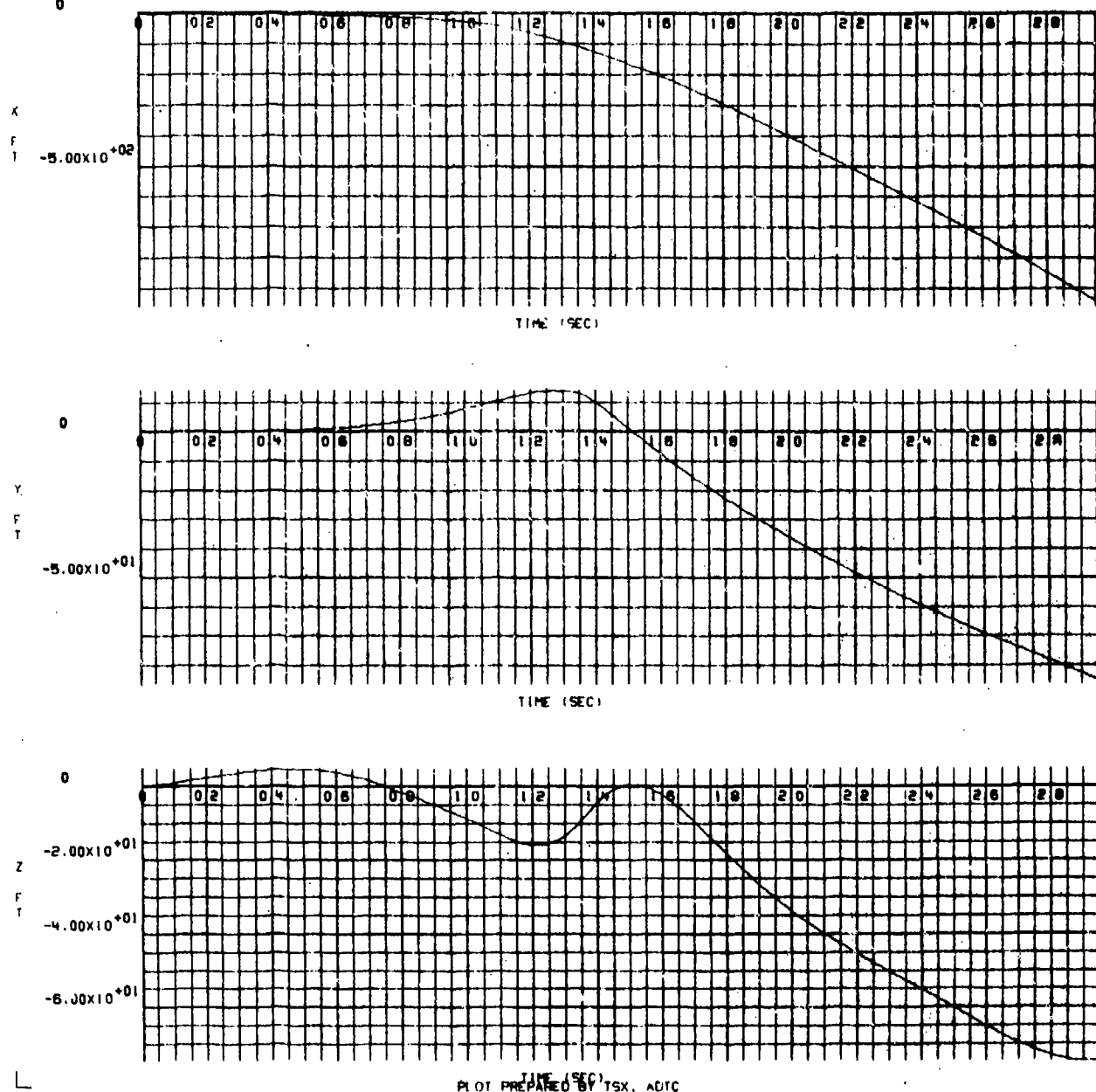


Figure J-3. X, Y, and Z Position Versus Time for a Flow Field Intensity of 1 (as measured in the wind tunnel)

17-12-75

RF-34 27 27

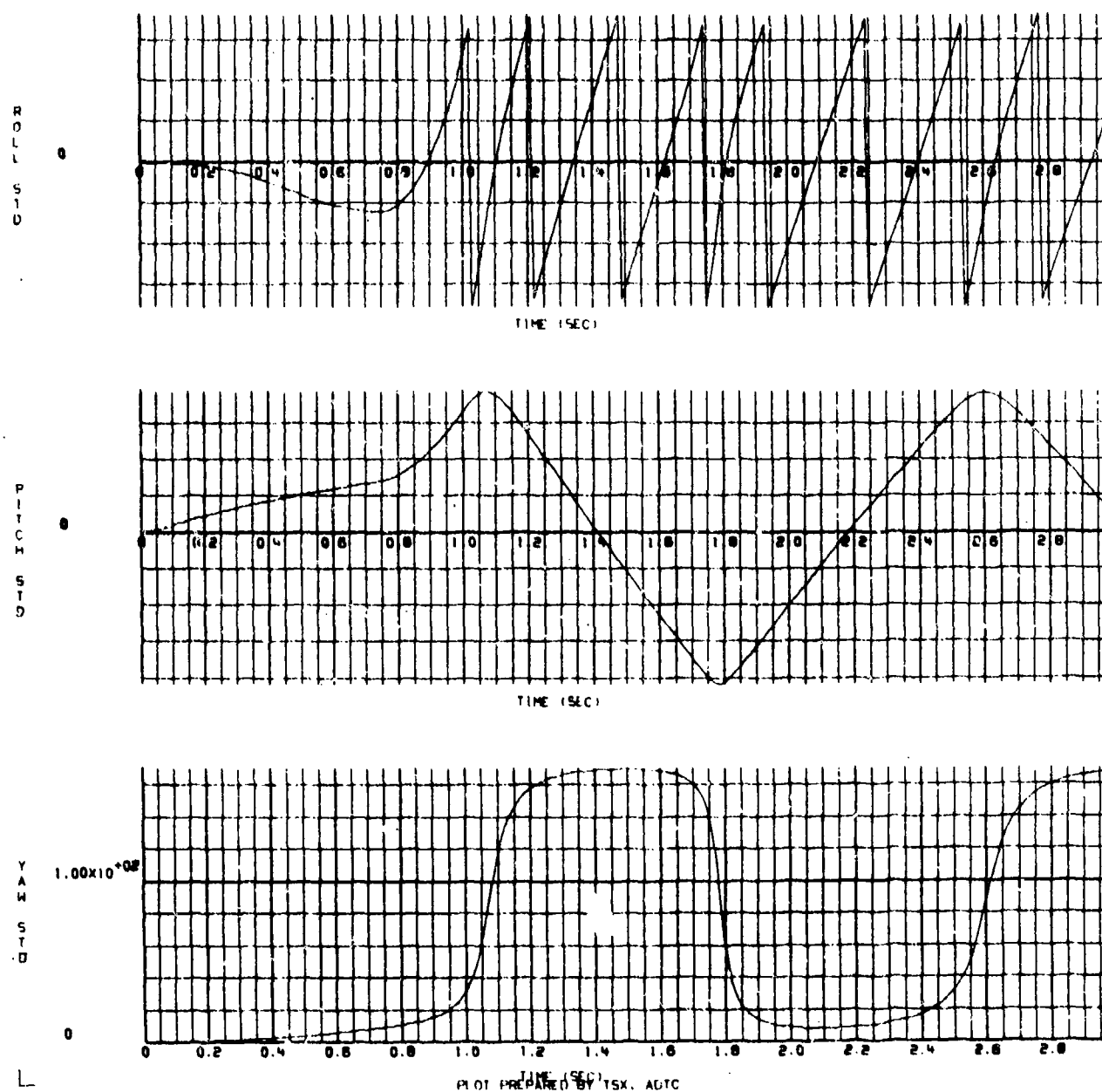


Figure J-4.  $\phi$ ,  $\theta$ , and  $\psi$  Rotation Versus Time for a Flow Field Intensity of 1 (unchanged from the wind tunnel measured values)

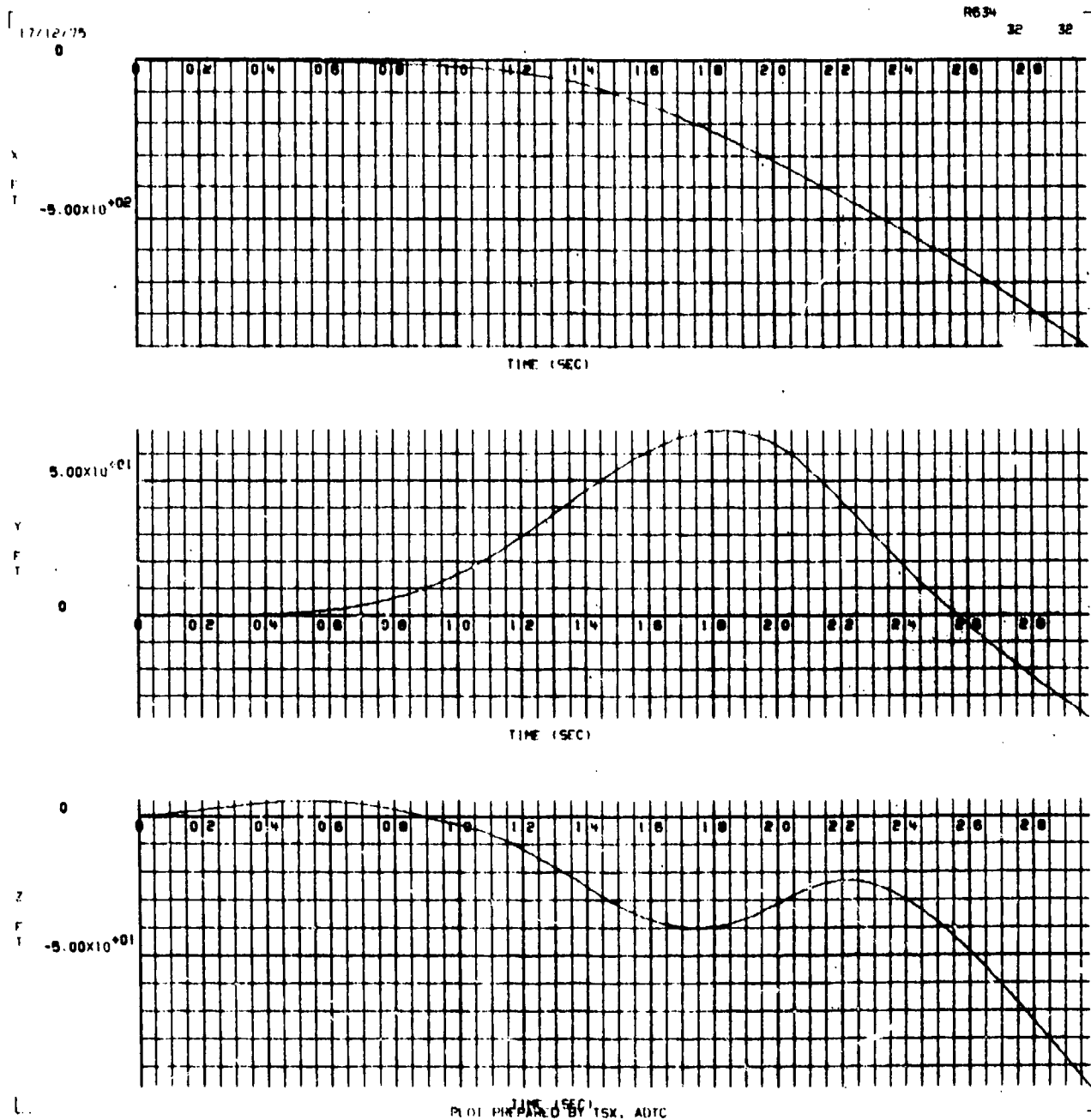
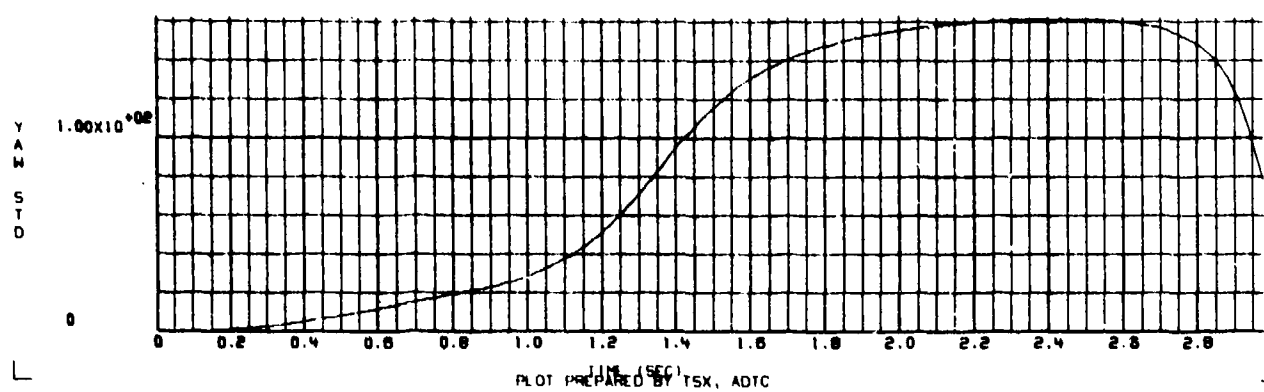
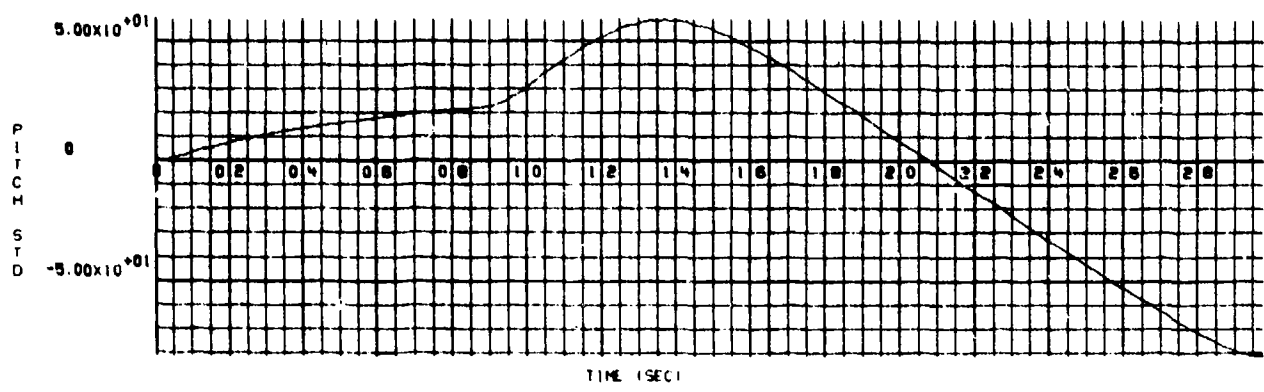
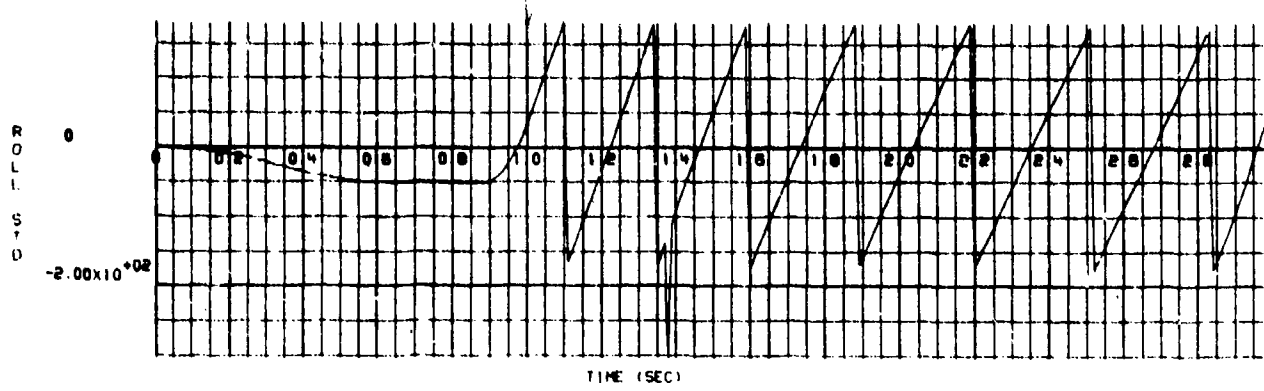


Figure J-5. X, Y, and Z Position Versus Time for a Flow Field Intensity of 2



17/12/75

R634 31 31



TIME (SEC)  
PLOT PREPARED BY TSX, ADTC

Figure 3-6.  $\phi$ ,  $\theta$ , and  $\psi$  Rotation Versus Time for a Flow Field Intensity of 2

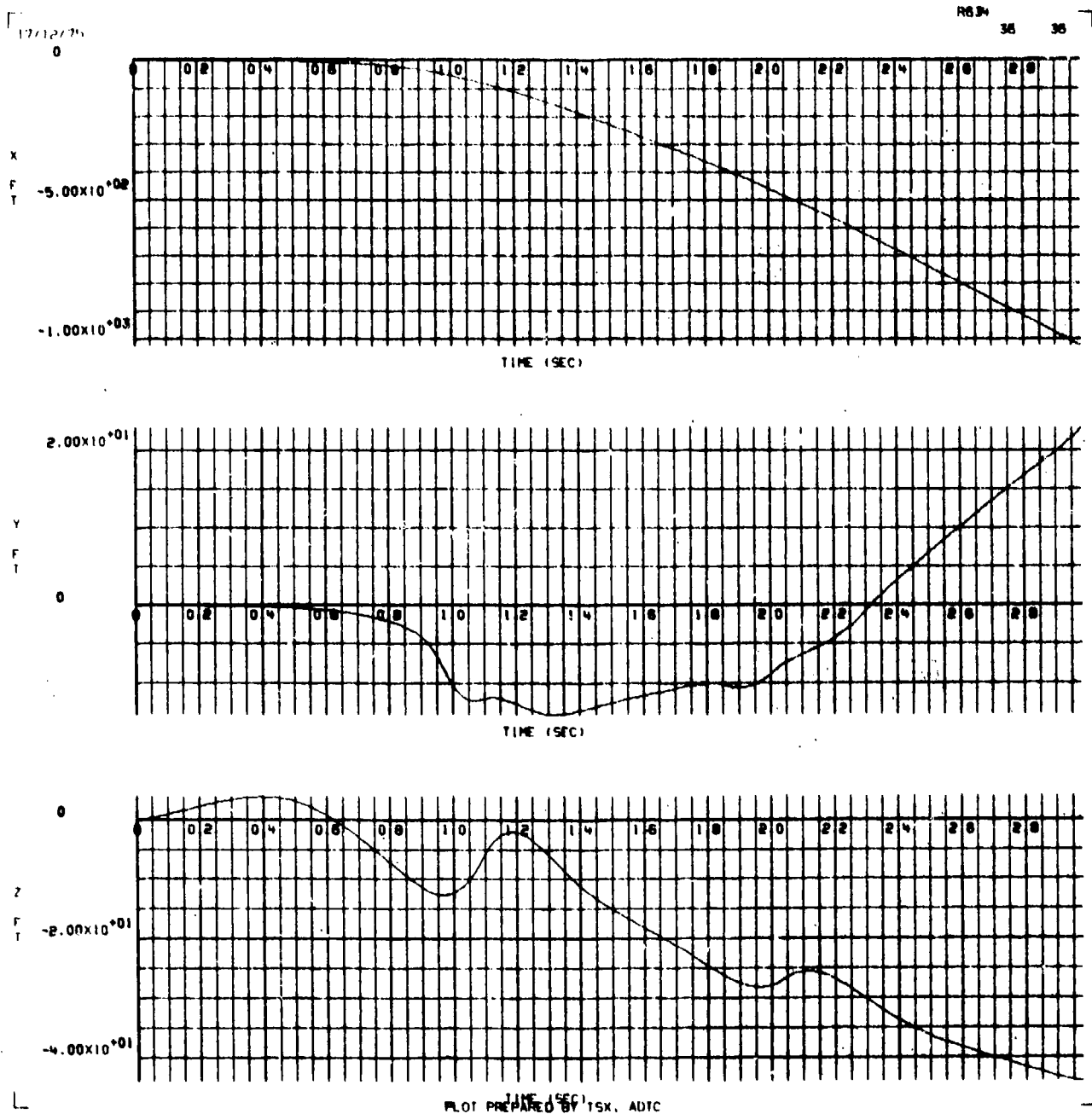


Figure J-7. X, Y, and Z Position Versus Time for a Flow Field Intensity of  $-1/2$

17/12/75

AS34

35

35

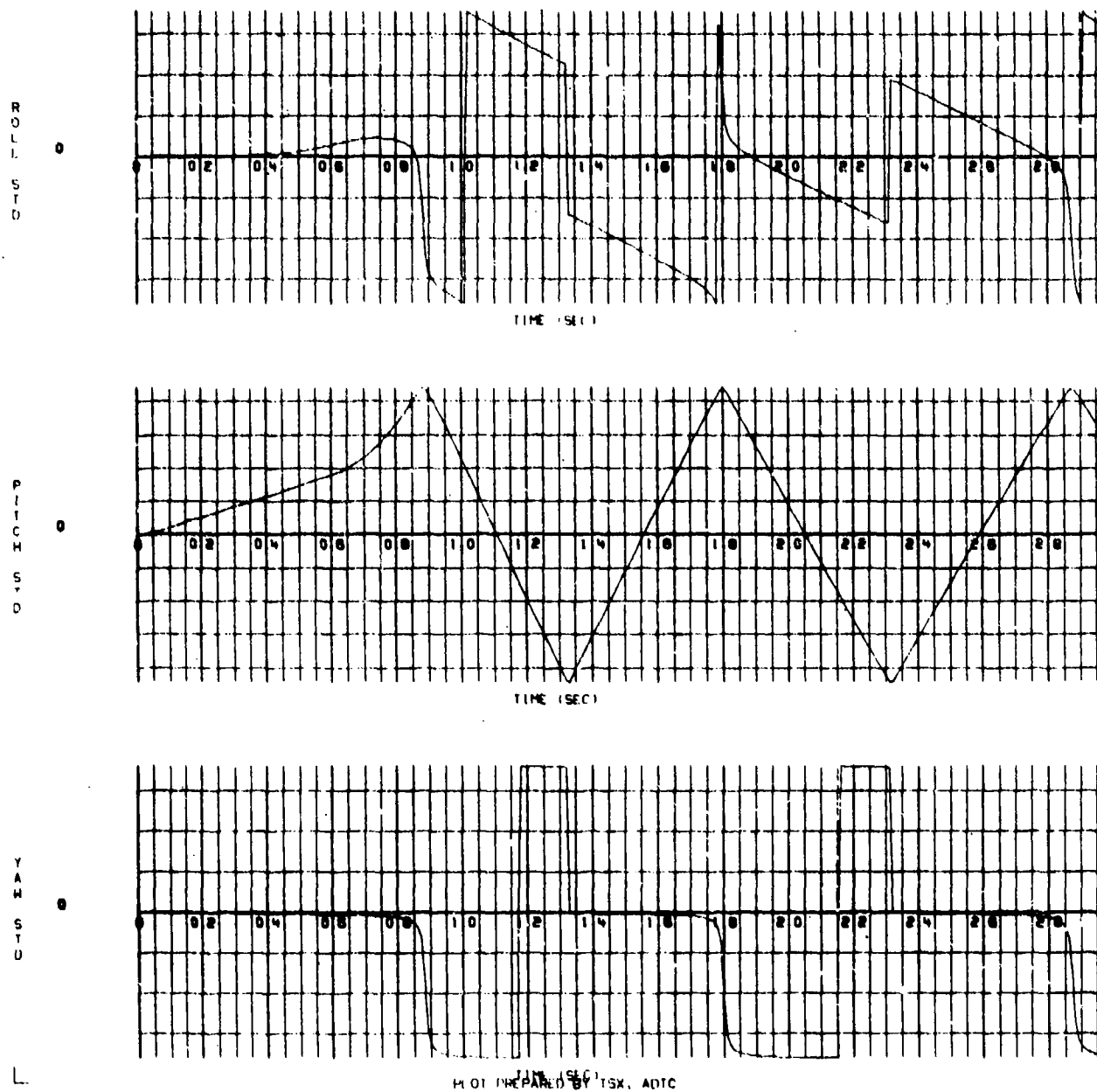


PHOTO PREPARED BY TSX, ADTC

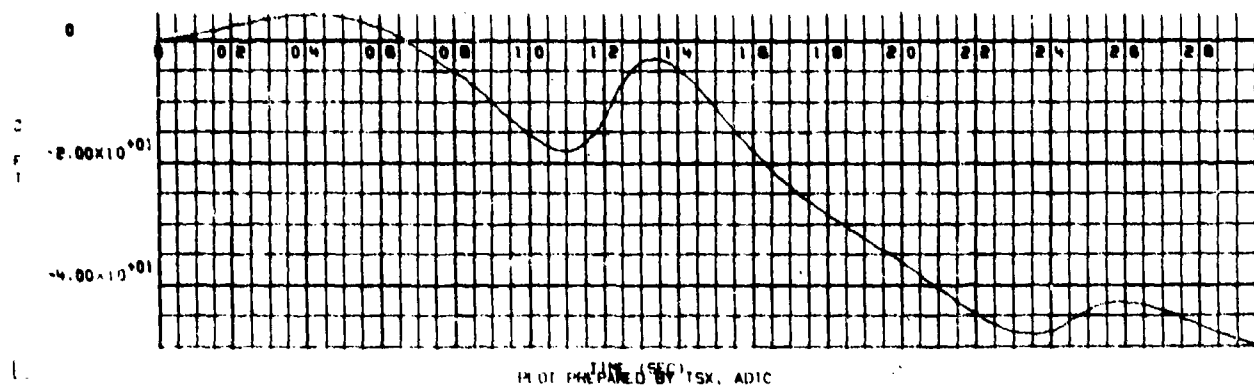
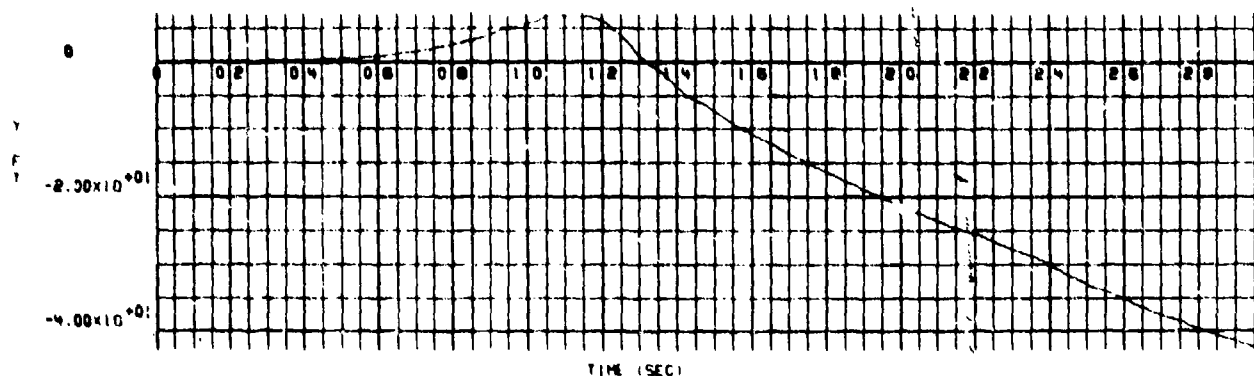
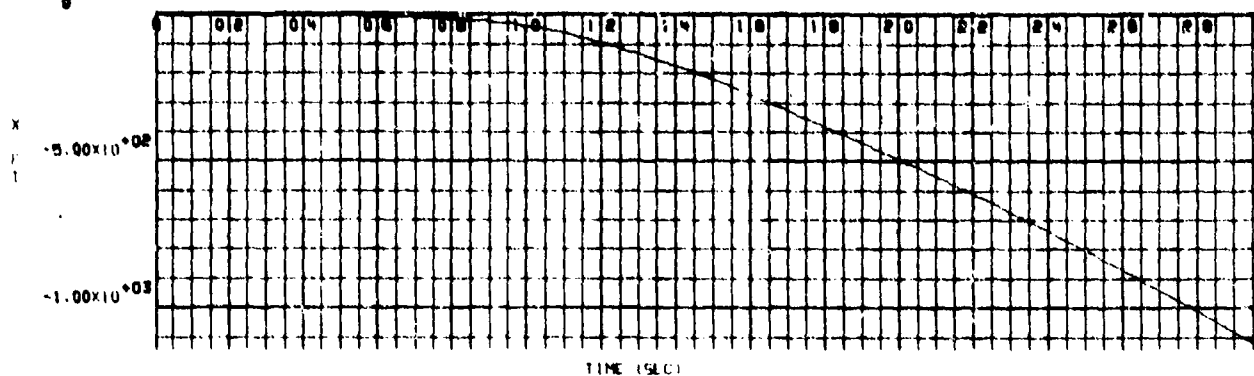
Figure J-8.  $\phi$ ,  $\theta$ , and  $\psi$  Rotation Versus Time for a Flow Field Intensity of  $-1/2$

**APPENDIX K**

**GBU-12 BOMB TRAJECTORIES RESULTING FROM A  
(-3/-5) ORIFICE COMBINATION AT MACH 0.95**

17/12/76  
0

R634  
44 44



Plot prepared by TSX, ADIC

Figure K-1. X, Y, and Z Position Versus Time for a Flow Field Intensity of 1/2

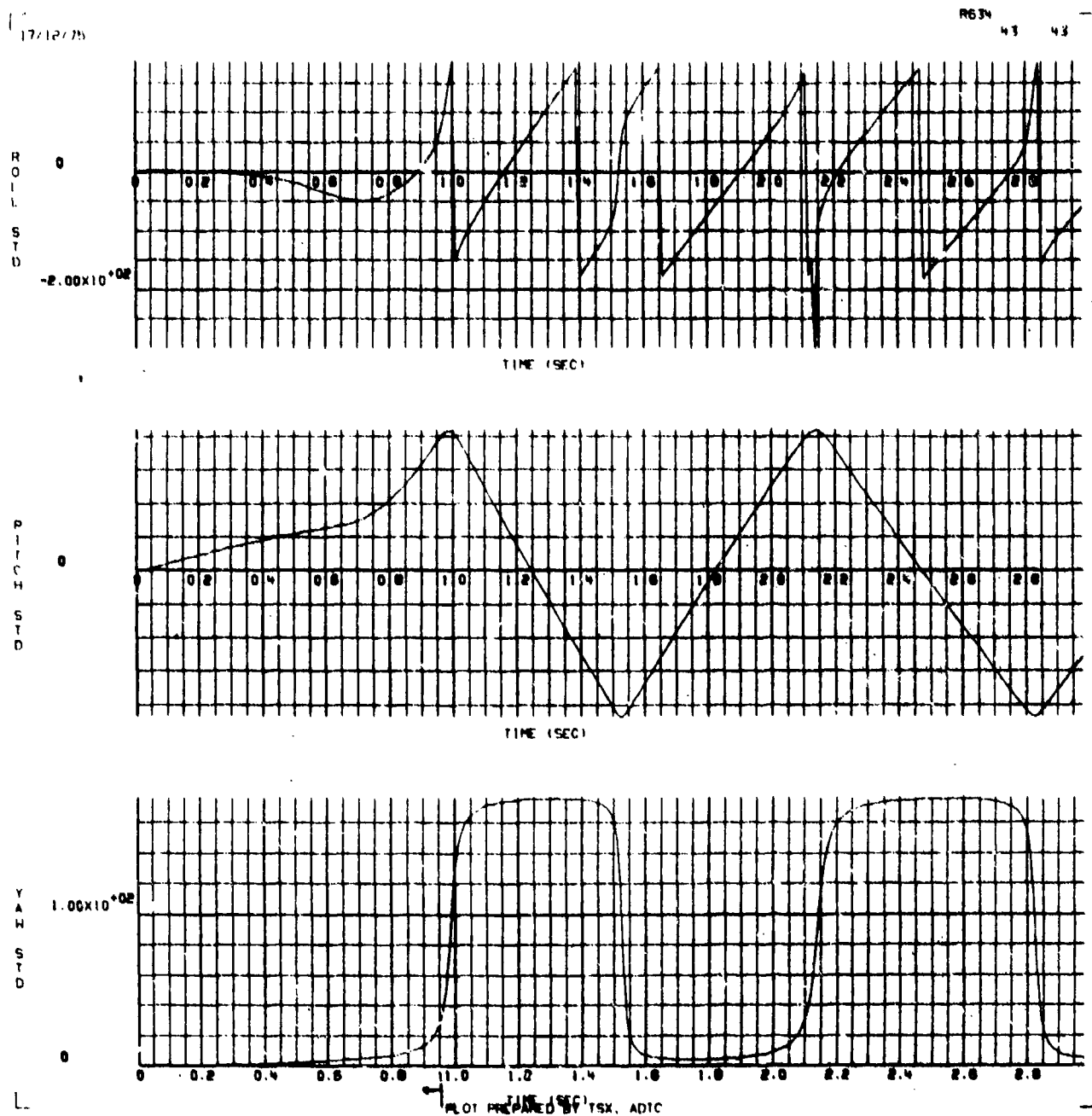


Figure K-2.  $\phi$ ,  $\theta$ , and  $\psi$  Rotation Versus Time for a Flow Field Intensity of  $1/2$

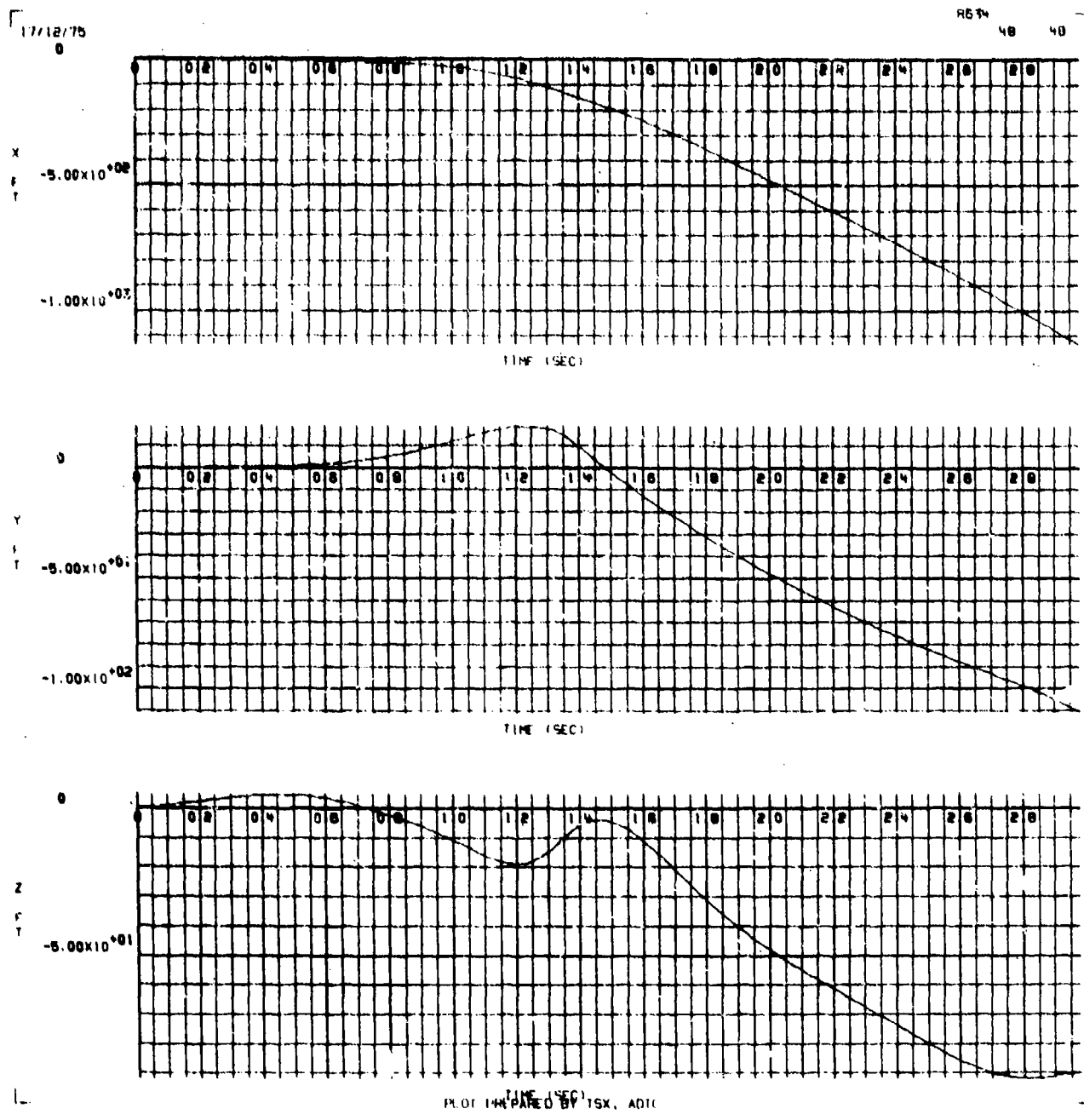


Figure K-3. X, Y, and Z Position Versus Time for a Flow Field Intensity of 1 (as measured in the wind tunnel)

17/12/75

R634 47 47

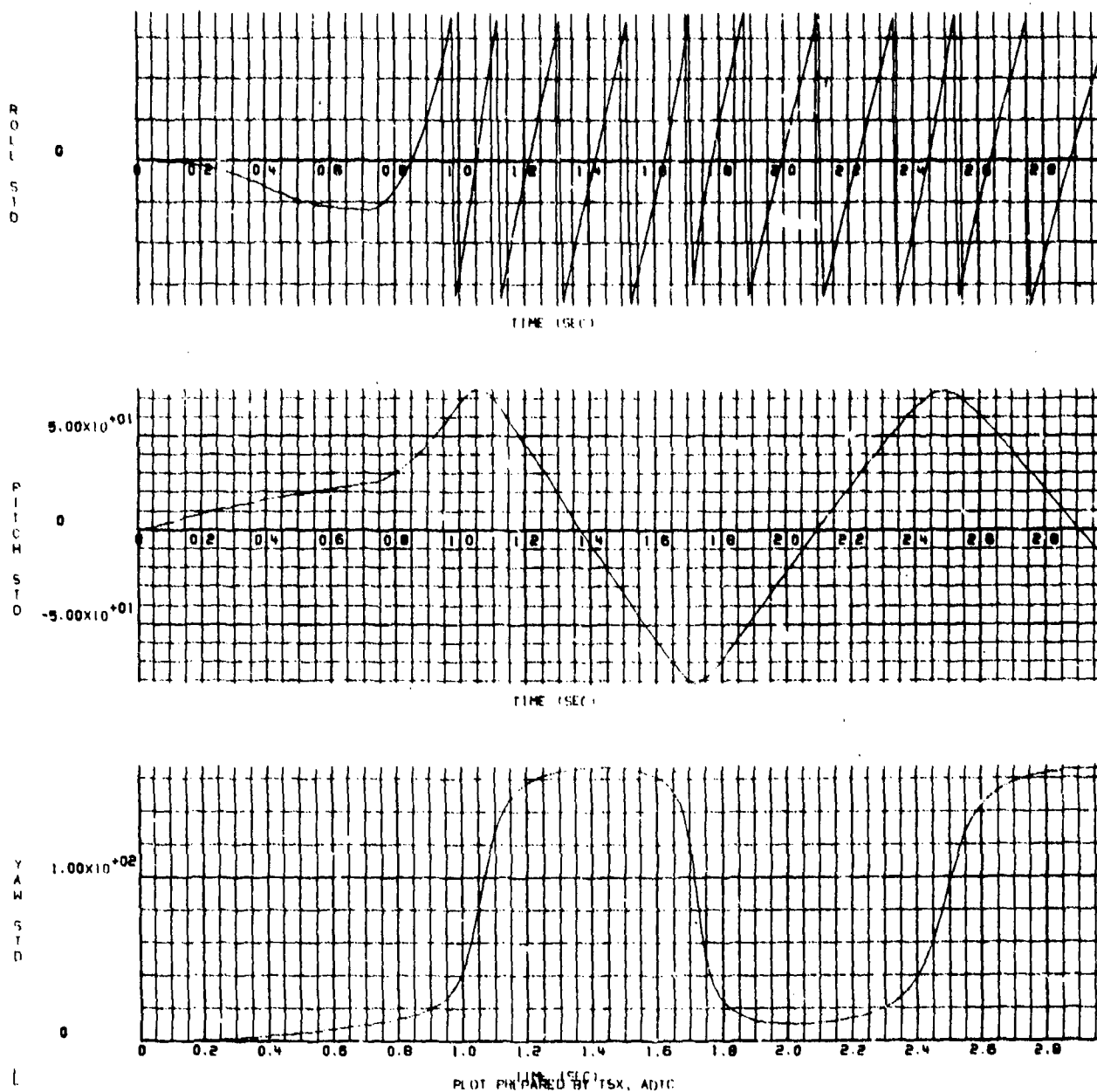


Figure K-4.  $\phi$ ,  $\theta$ , and  $\psi$  Rotation Versus Time for a Flow Field Intensity of 1 (unchanged from the wind tunnel measured values)



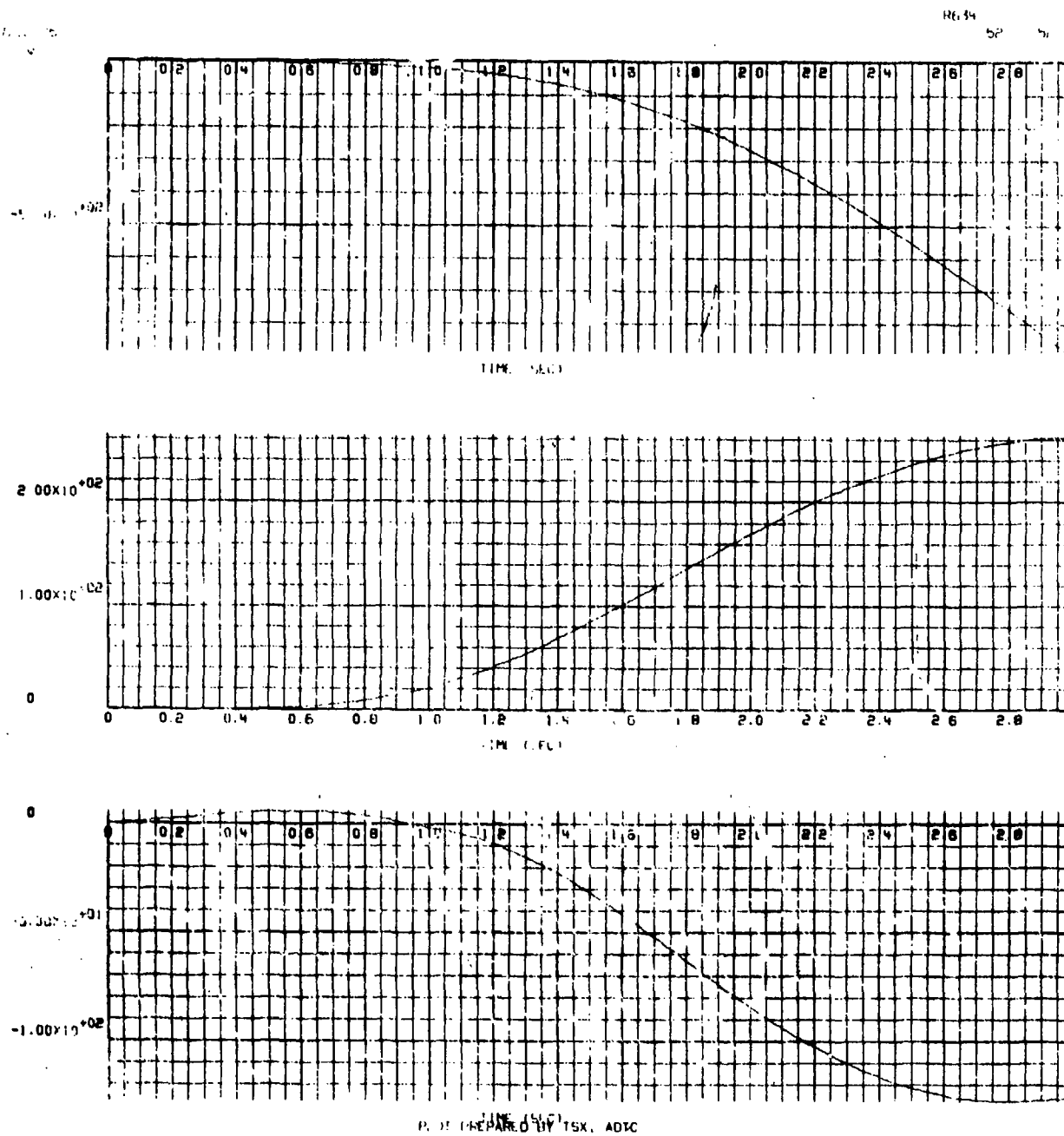


Figure K-5. X, Y, and Z Position Versus Time for a Flow Field Intensity of 2

17/12/75

H634

51 51

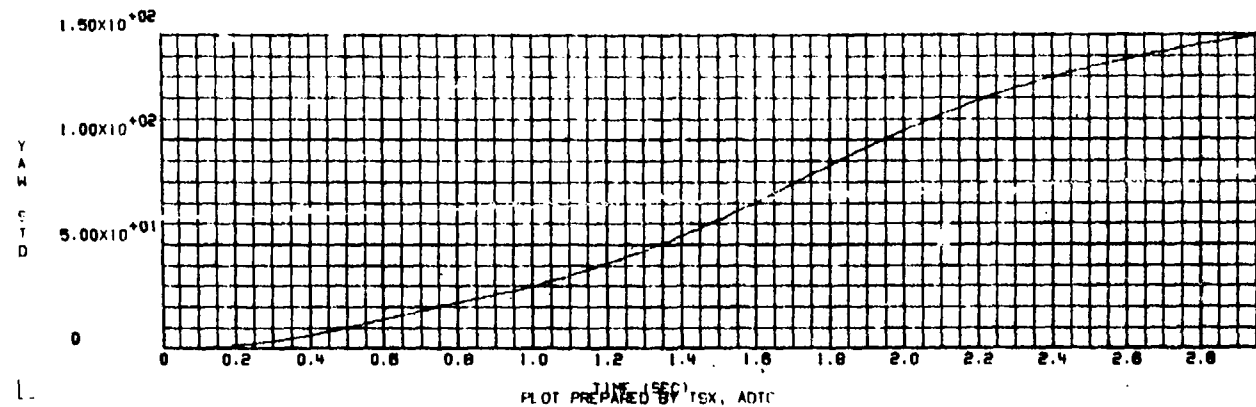
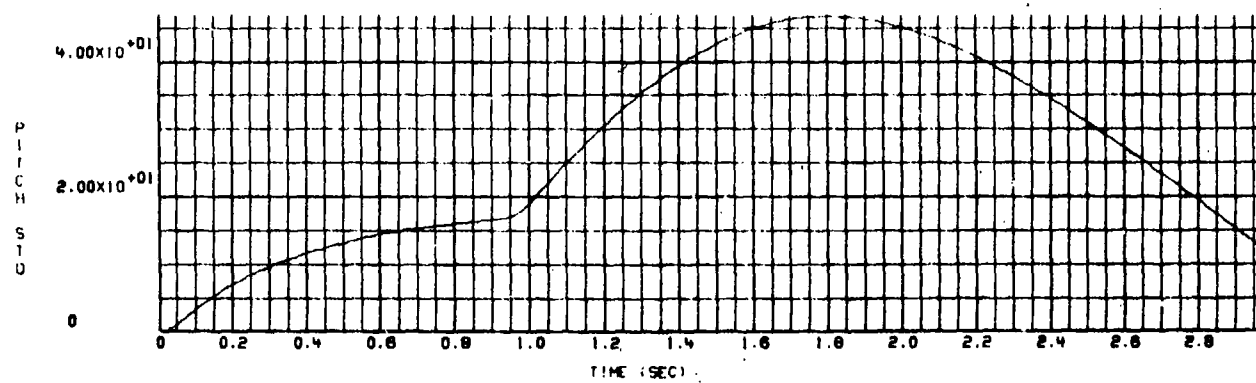
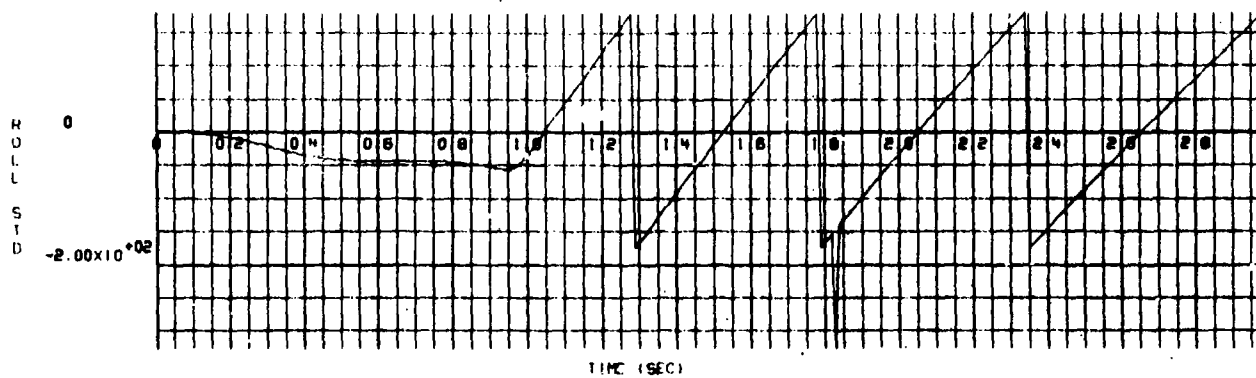
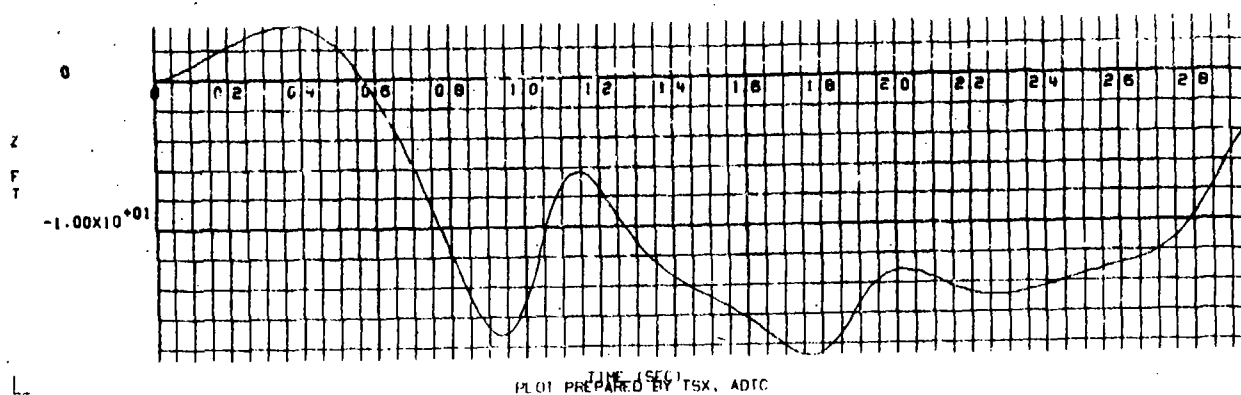
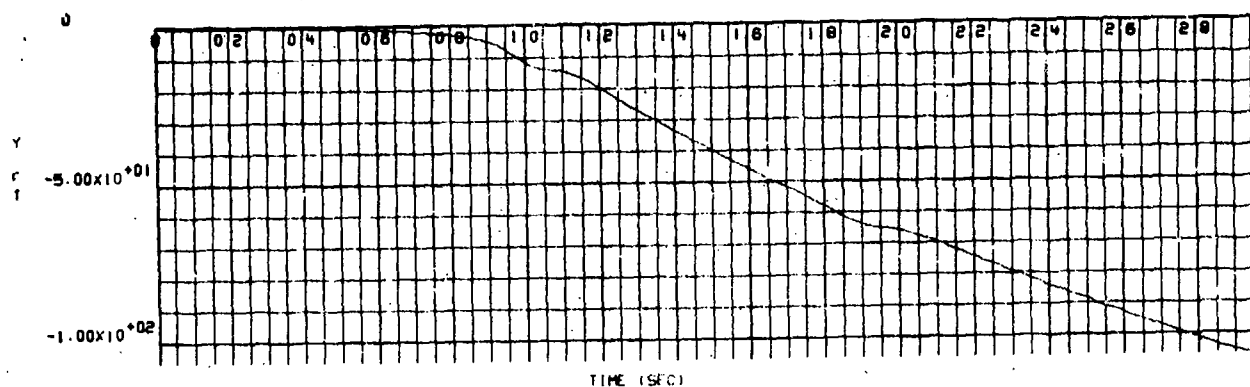
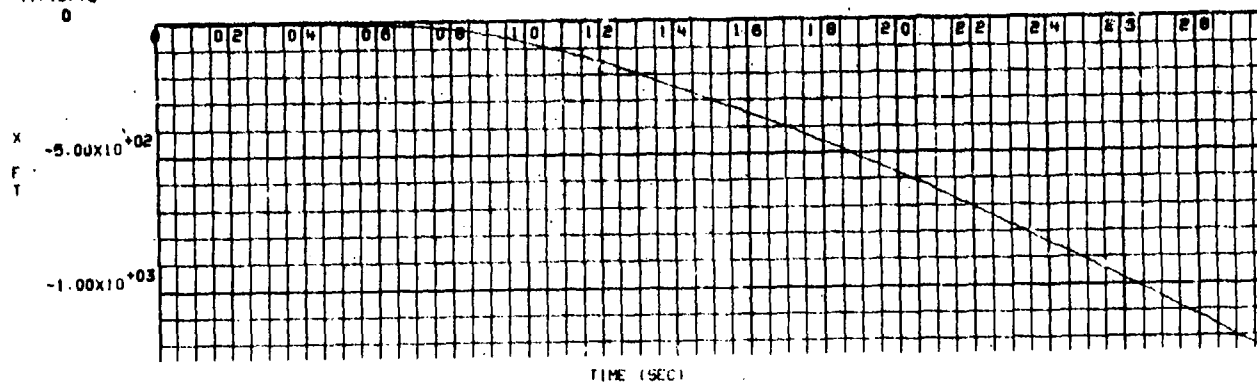


Figure K-6.  $\phi$ ,  $\theta$ , and  $\psi$  Rotation Versus Time for a Flow Field Intensity of 2

17/12/75  
0

R634 56 56



PLOT PREPARED BY TSX, ADTC

Figure K-7. X, Y, and Z Position Versus Time for a Flow Field Intensity of  $-1/2$

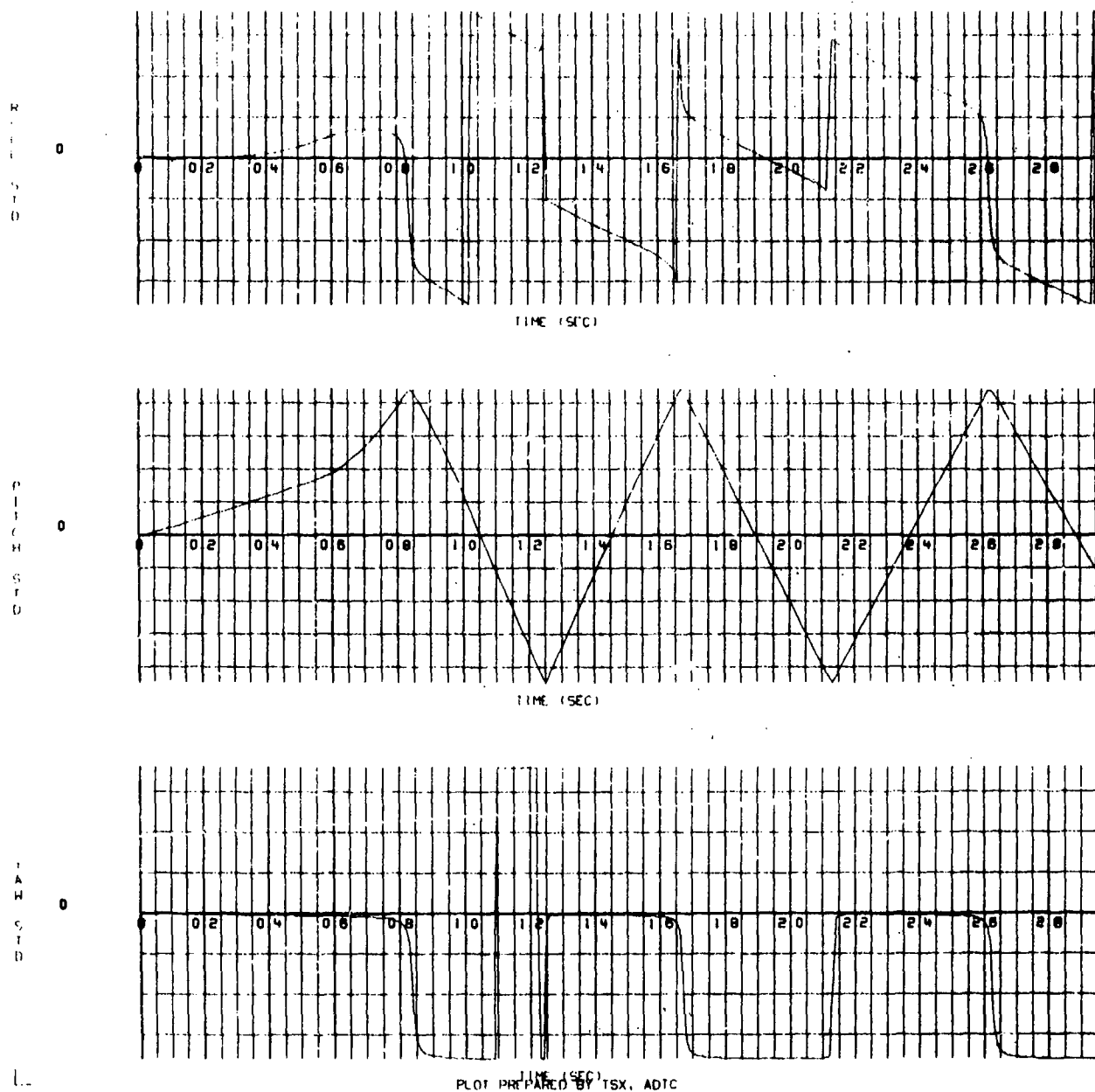


Figure K-8.  $\phi$ ,  $\theta$ , and  $\psi$  Rotation Versus Time for a Flow Field Intensity of  $-1/2$

APPENDIX L

GBU-12 BOMB TRAJECTORIES RESULTING FROM A  
(-3/-5) ORIFICE COMBINATION AT MACH 1.2

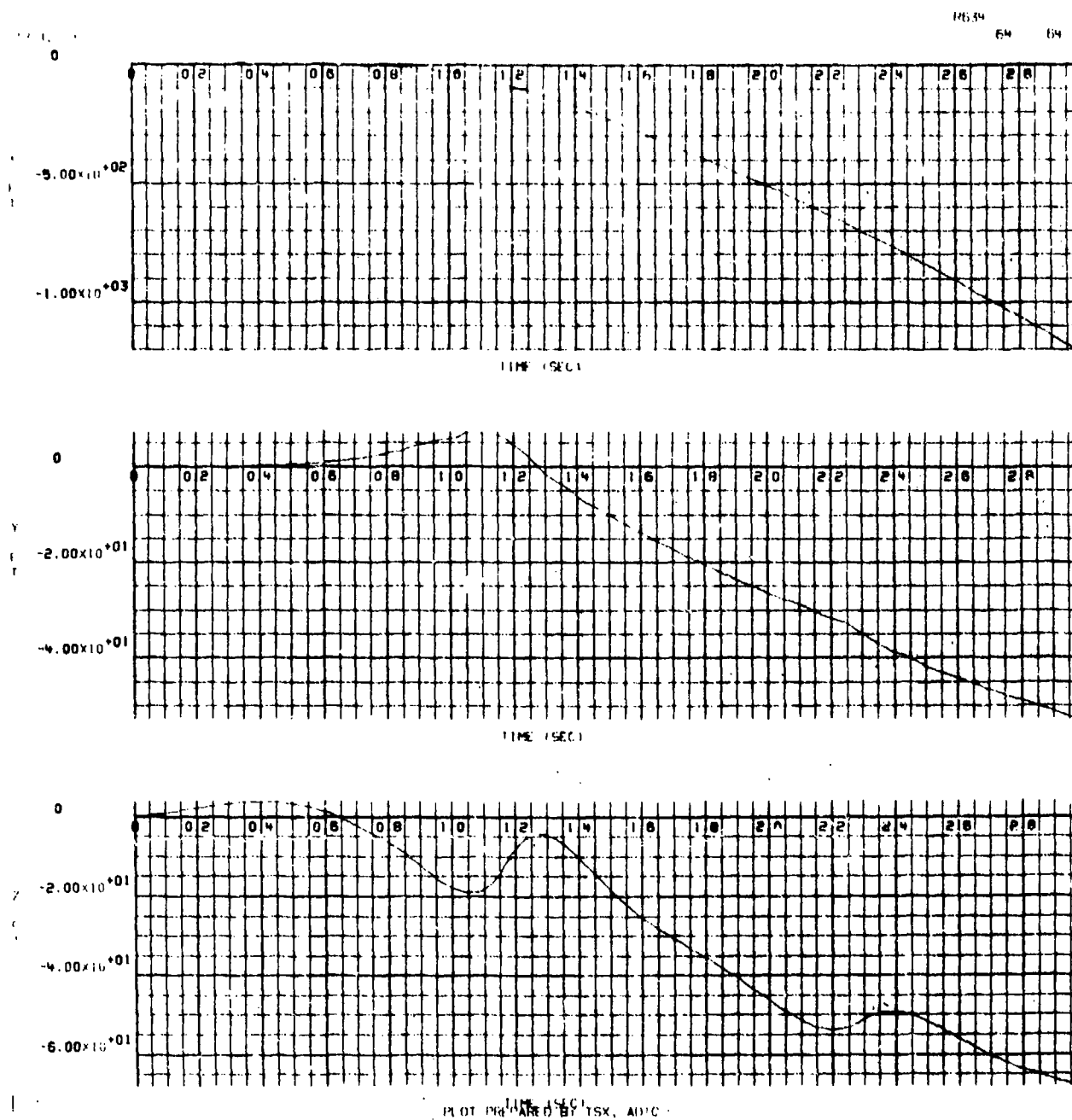


Figure L-1. X, Y, and Z Position Versus Time for a Flow Field Intensity of 1/2

17/12/75

165 94

153

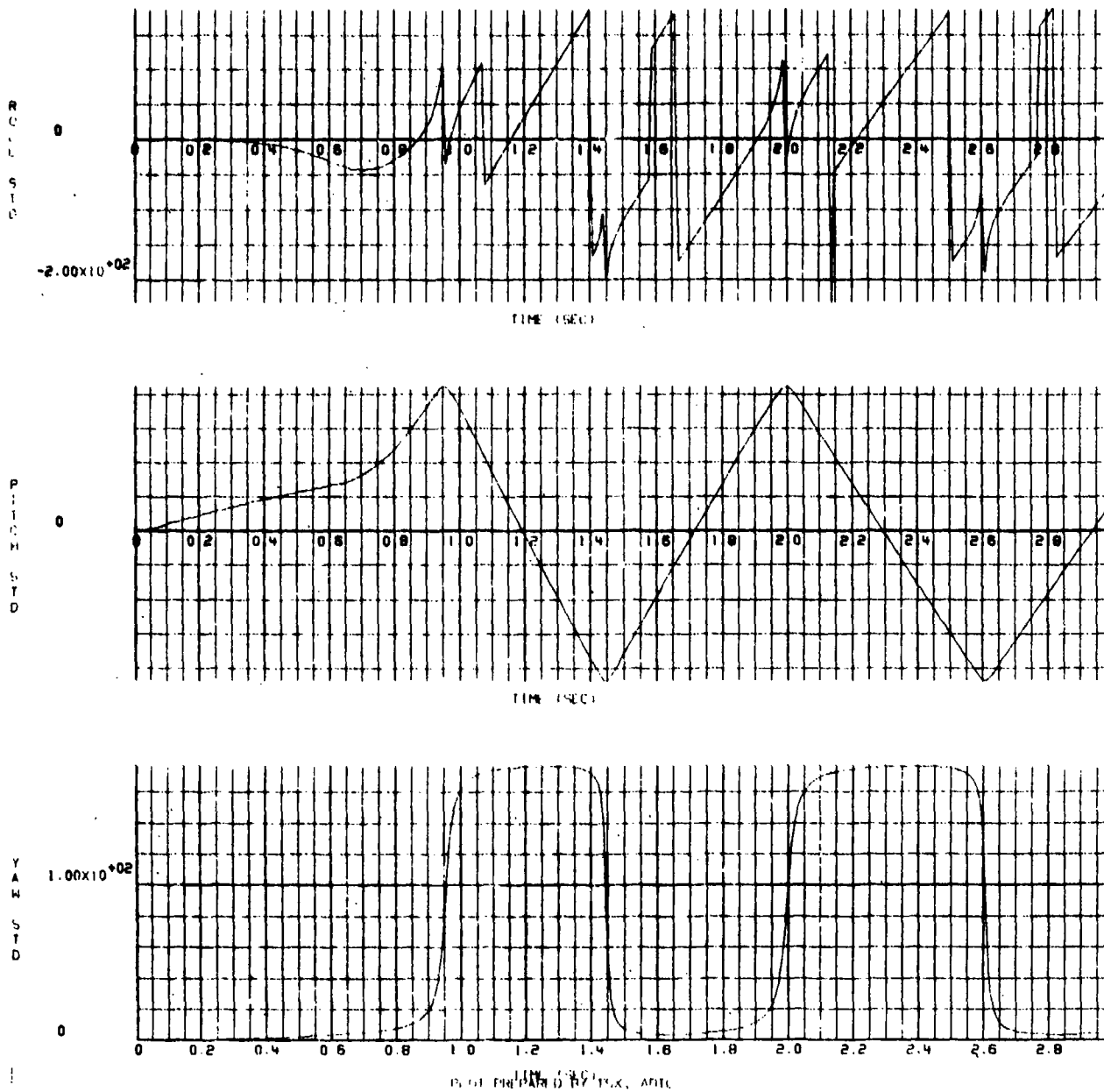


Figure L-2.  $\phi$ ,  $\theta$ , and  $\psi$  Rotation Versus Time for a Flow Field Intensity of 1/2

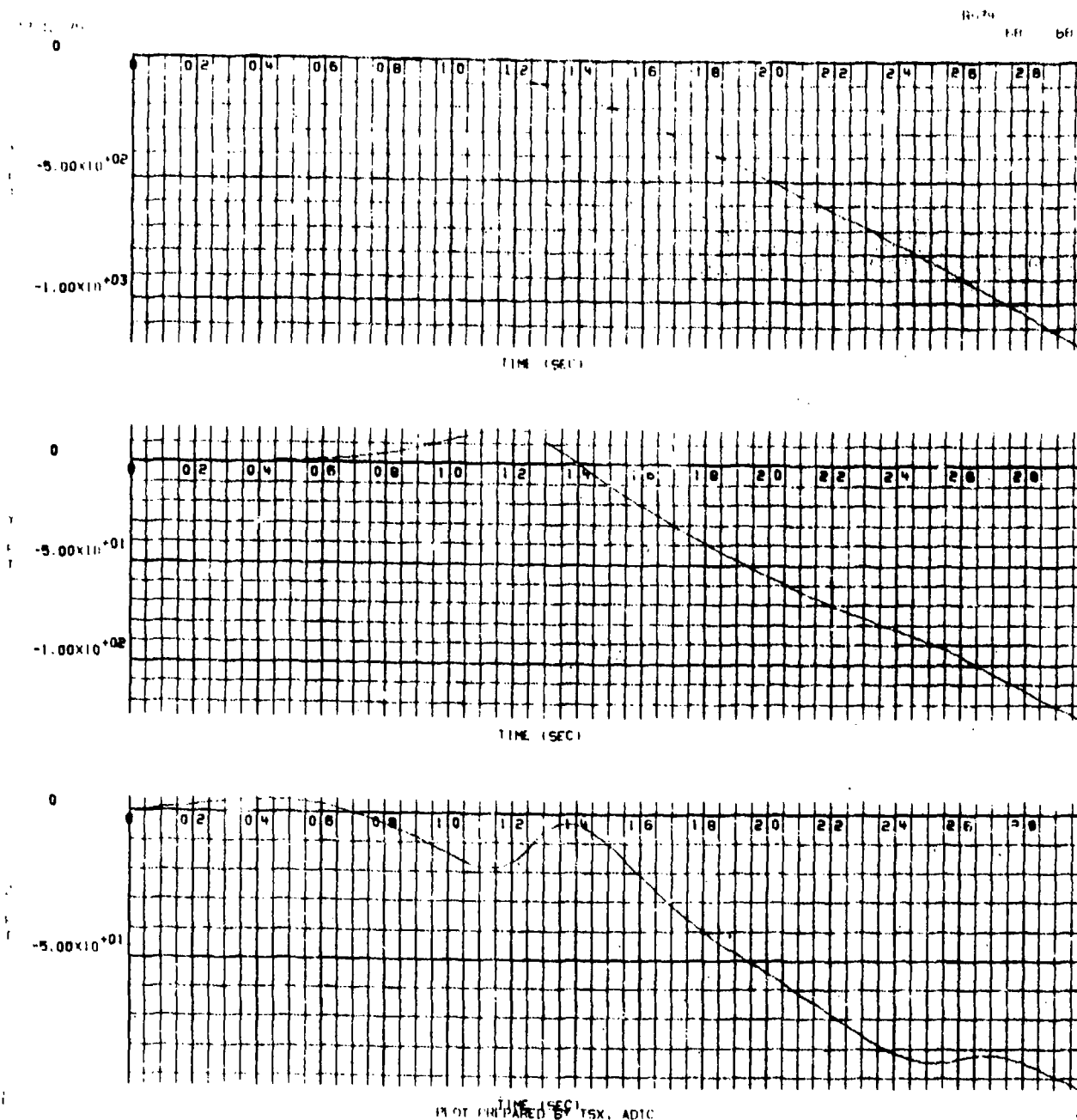


Figure L-3. X, Y, and Z Position Versus Time for a Flow Field Intensity of 1 (as measured in the wind tunnel)



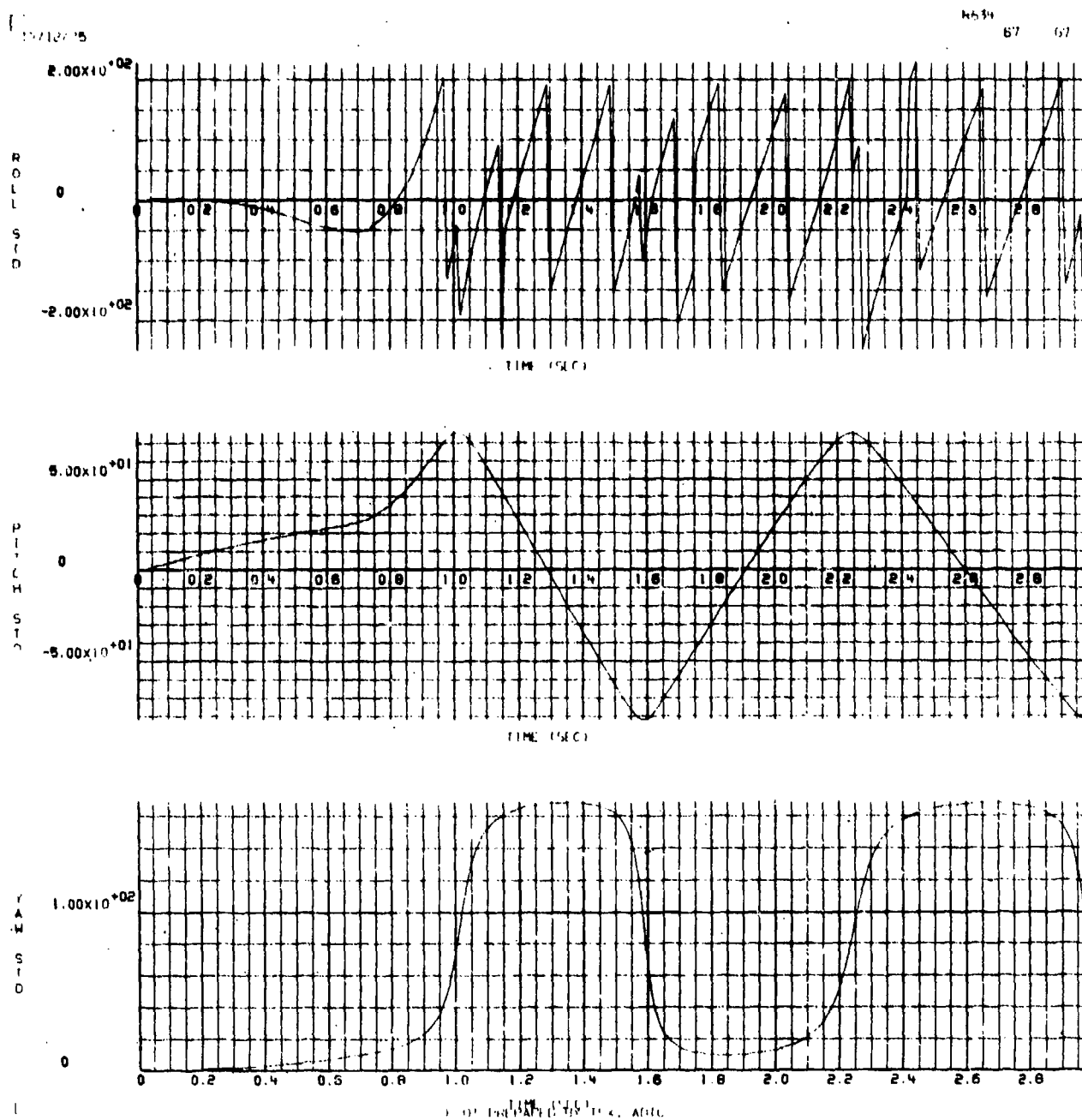


Figure L-4.  $\phi$ ,  $\theta$ , and  $\psi$  Rotation Versus Time for a Flow Field Intensity of 1 (unchanged from the wind tunnel measured values)

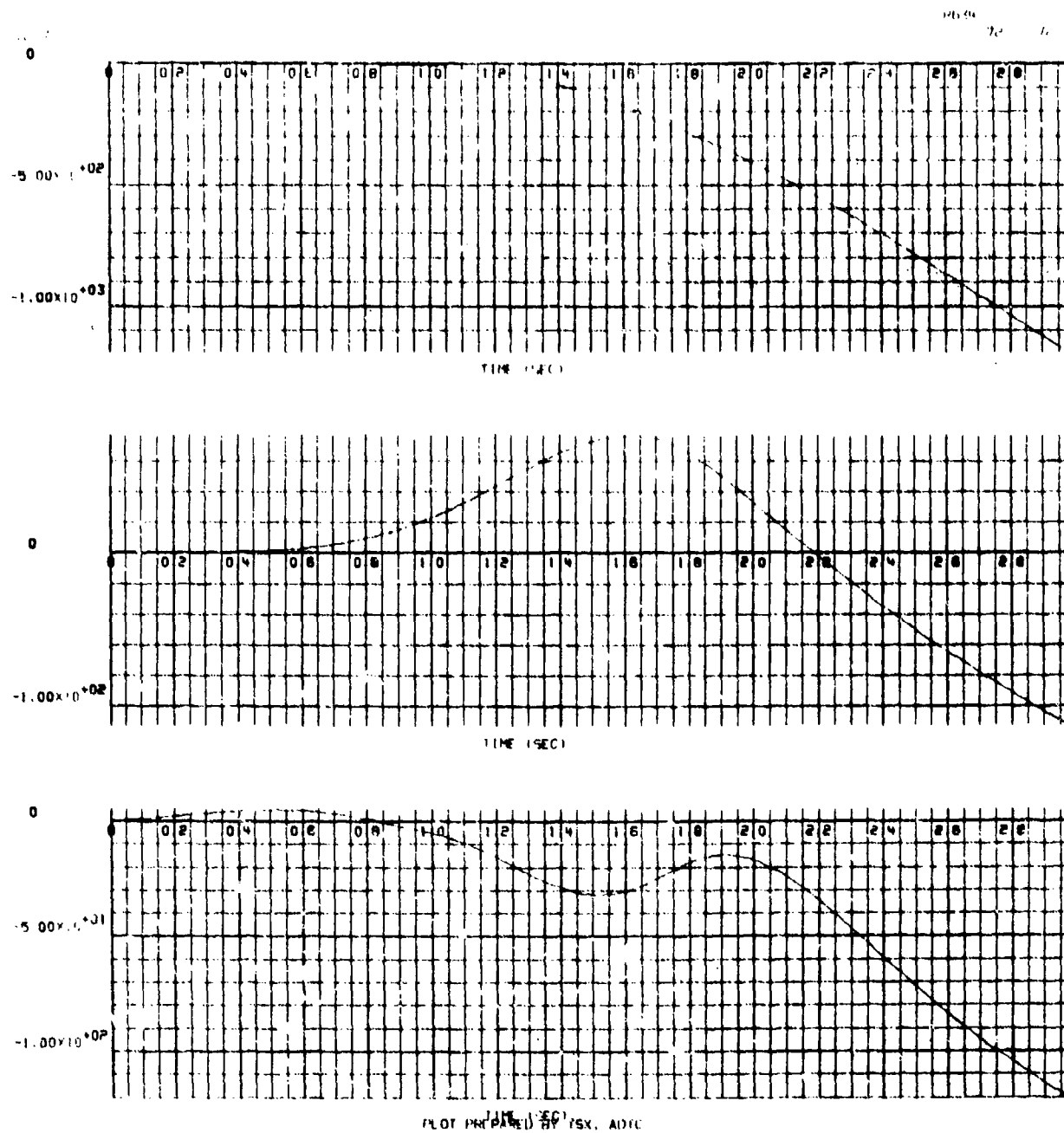
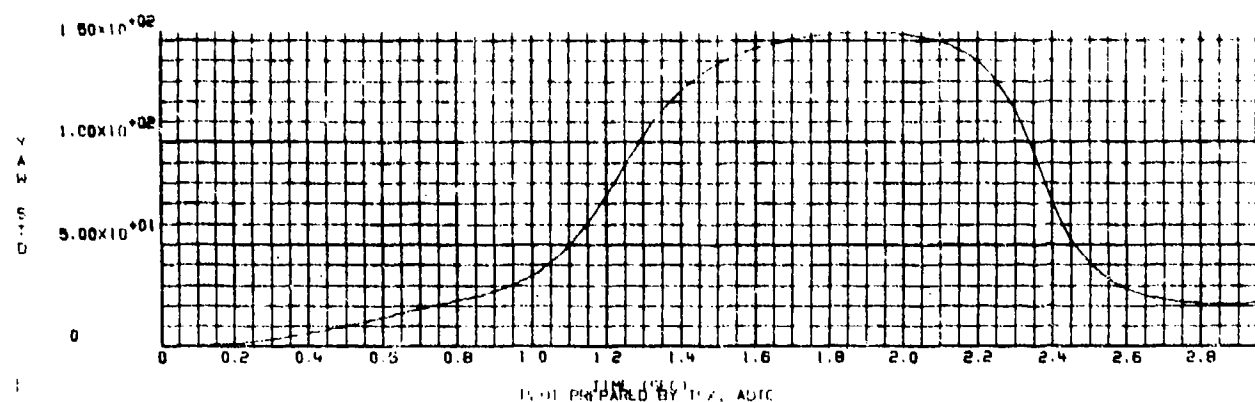
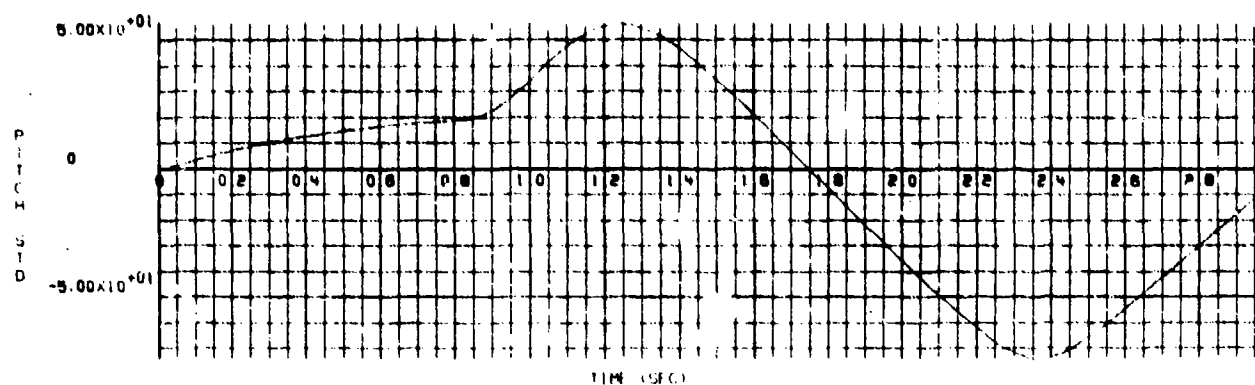
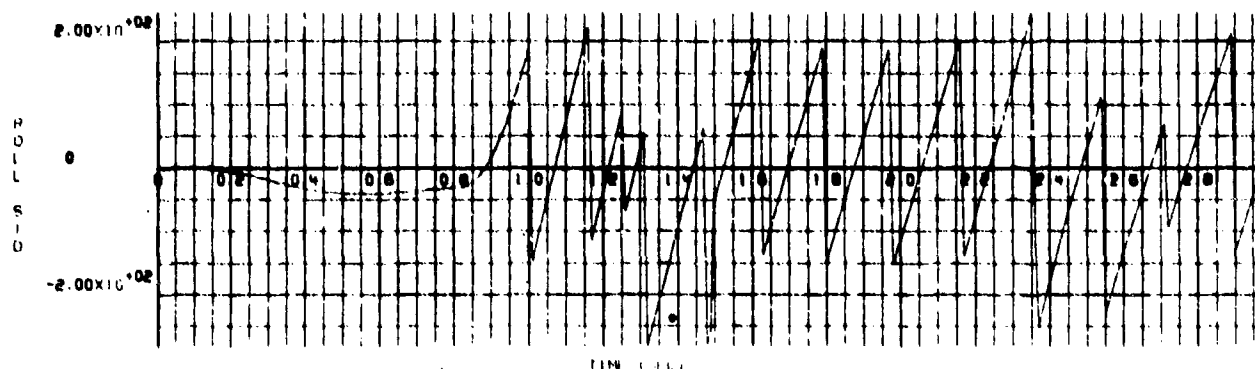


Figure L-5. X, Y, and Z Position Versus Time for a Flow Field Intensity of 2

11/12/75

11674



11-11 PREPARED BY T. A. ADIC

Figure L-6.  $\phi$ ,  $\theta$ , and  $\psi$  Rotation Versus Time for a Flow Field Intensity of 2

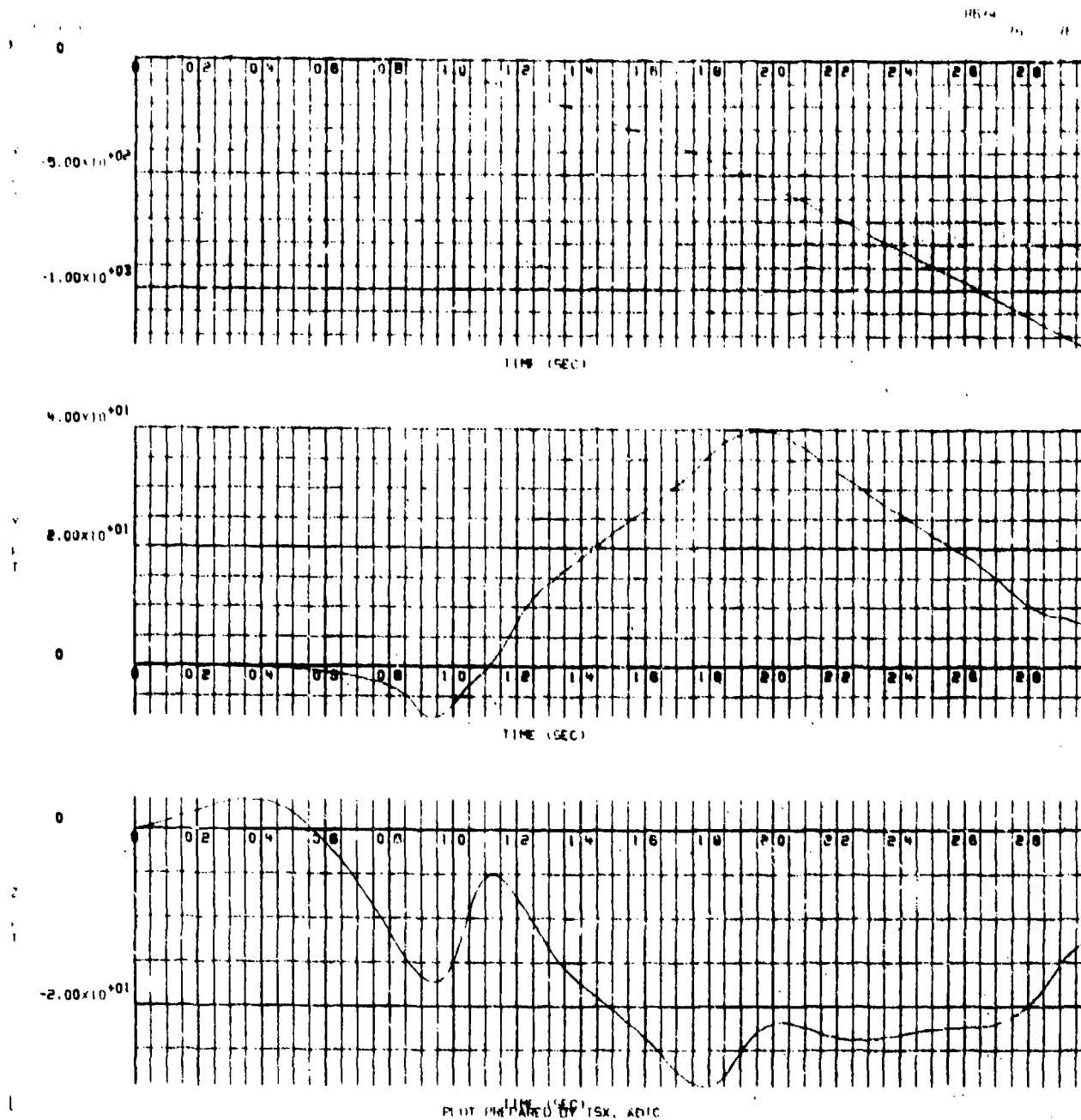


Figure L-7. X, Y, and Z Position Versus Time for a Flow Field Intensity of  $-1/2$

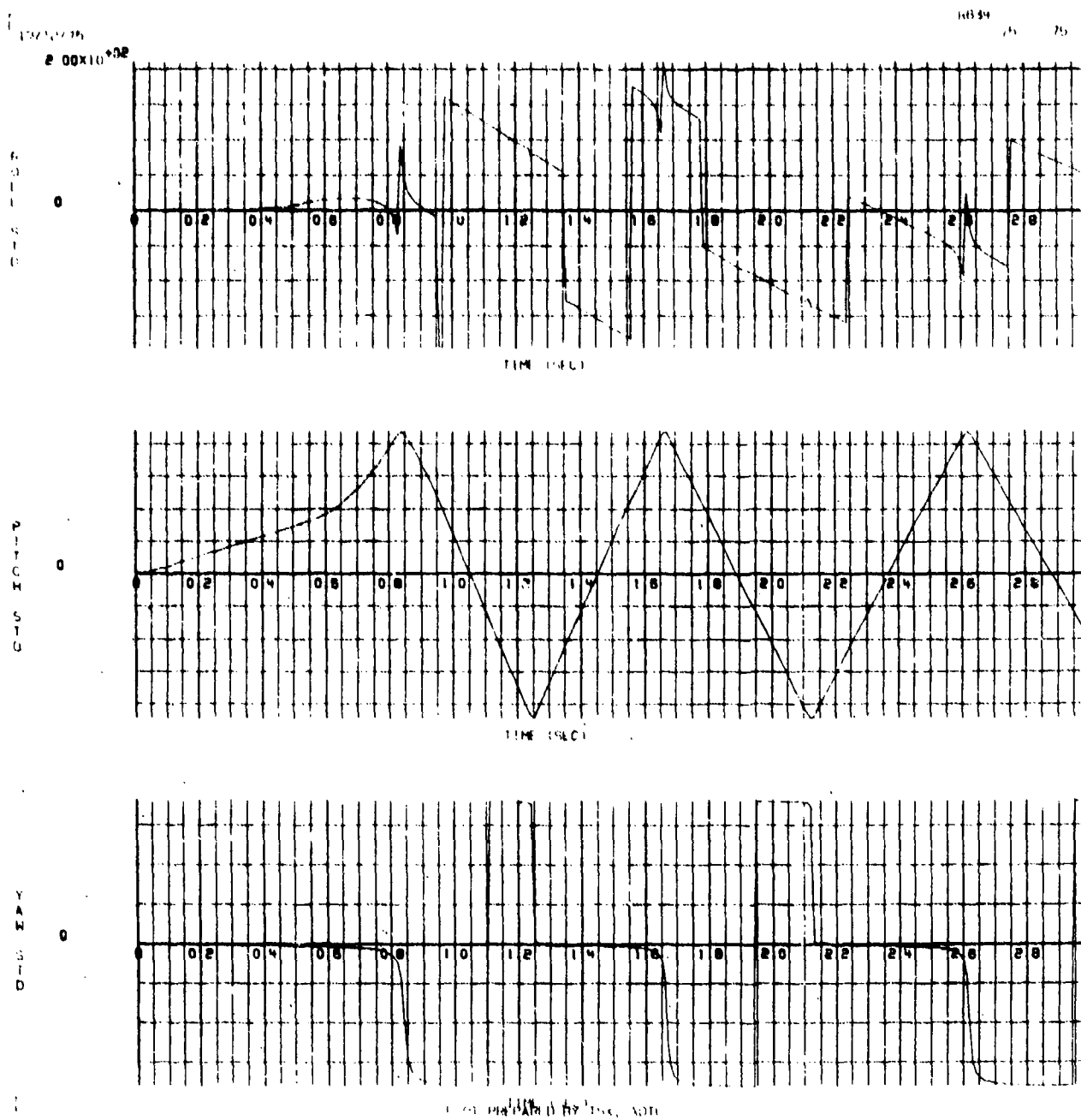


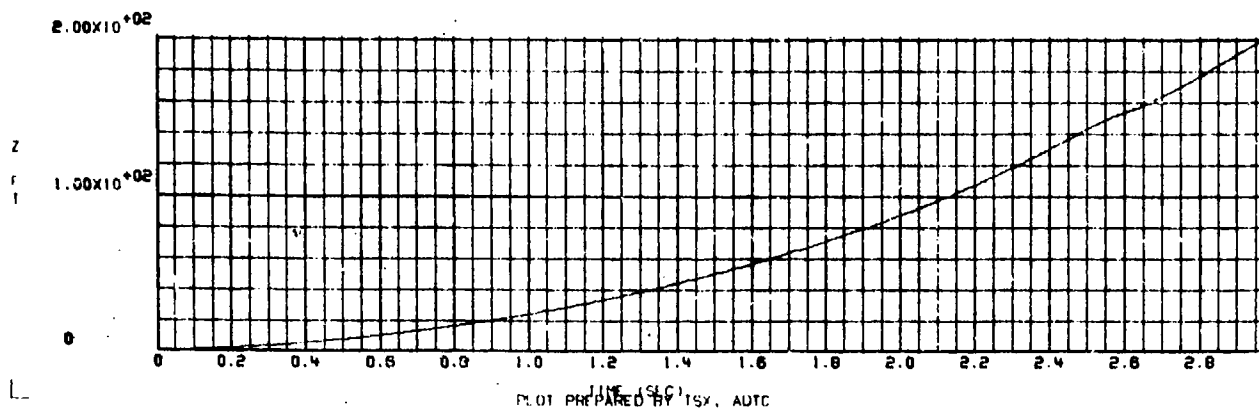
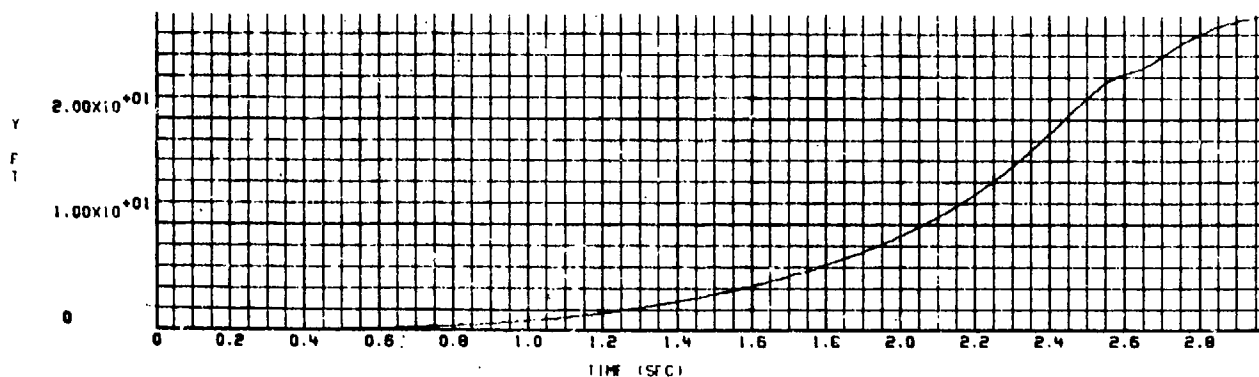
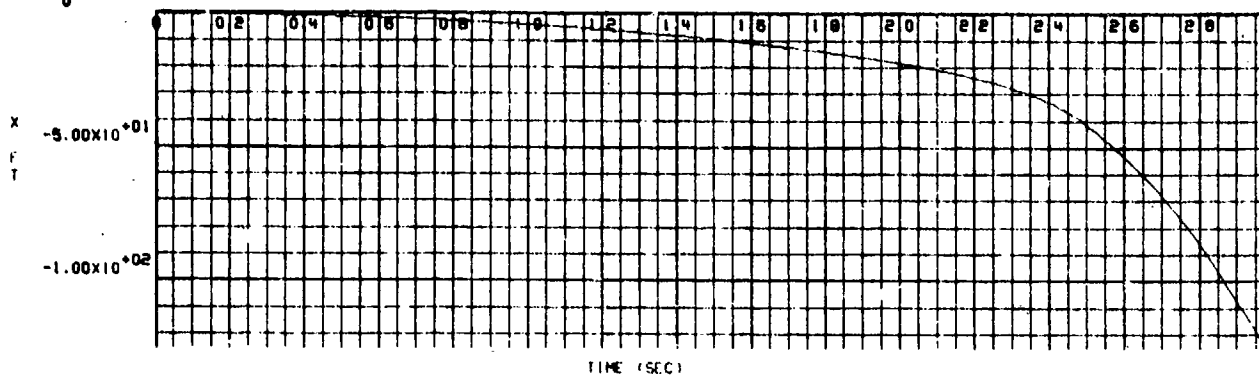
Figure L-8.  $\phi$ ,  $\theta$ , and  $\psi$  Rotation Versus Time for a Flow Field Intensity of  $-1/2$

APPENDIX M

GBU-10 BOMB TRAJECTORIES RESULTING FROM A  
(-5/-3) ORIFICE COMBINATION AT MACH 0.7

16/12/75  
0

P652



PLOT PREPARED BY TSX, AUTC

Figure M-1. X, Y, and Z Position Versus Time for a Flow Field Intensity of 1/2

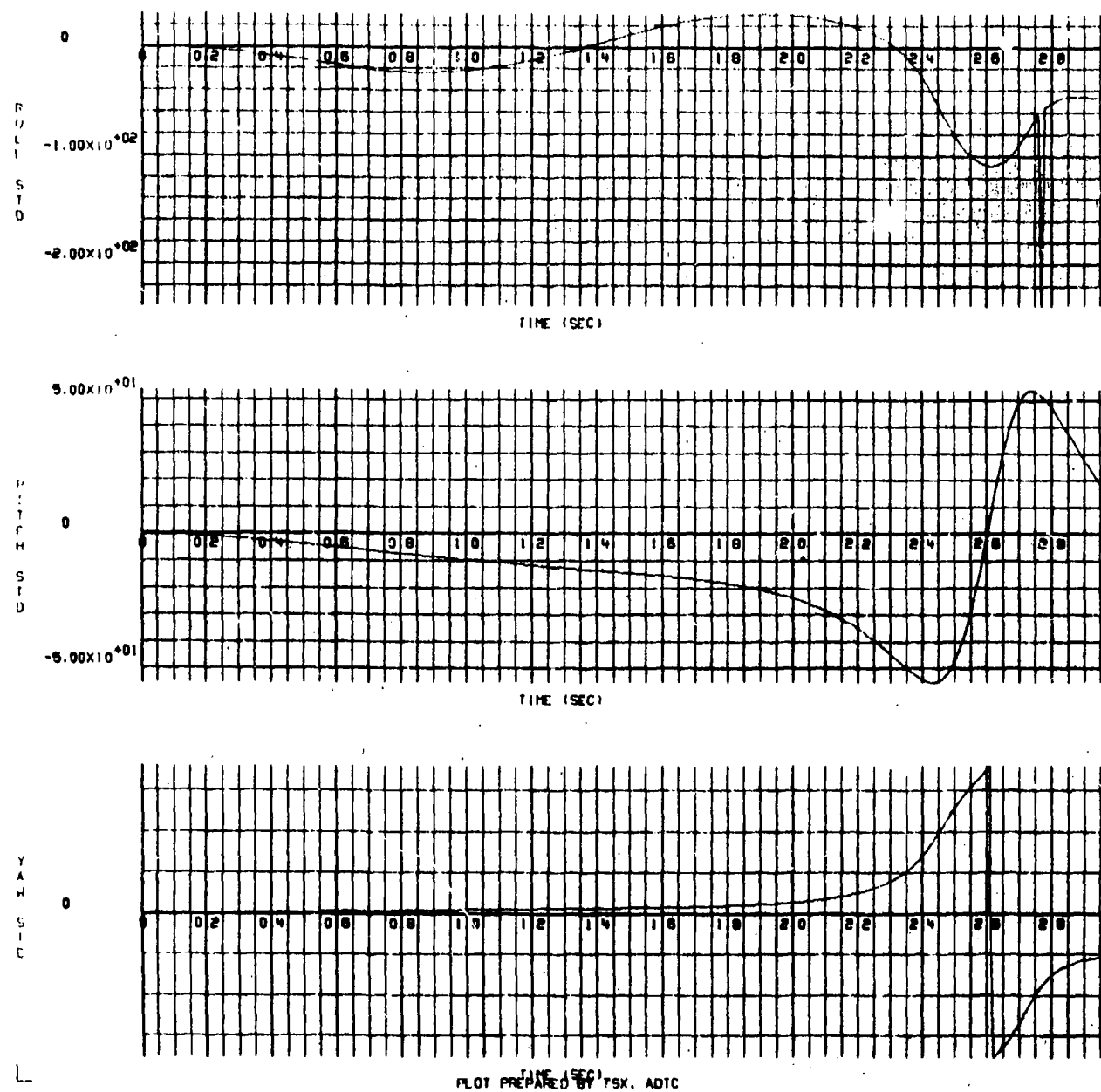


Figure M-2.  $\phi$ ,  $\theta$ , and  $\gamma$  Rotation Versus Time for a Flow Field Intensity of  $1/2$



16/12/75  
0

R652

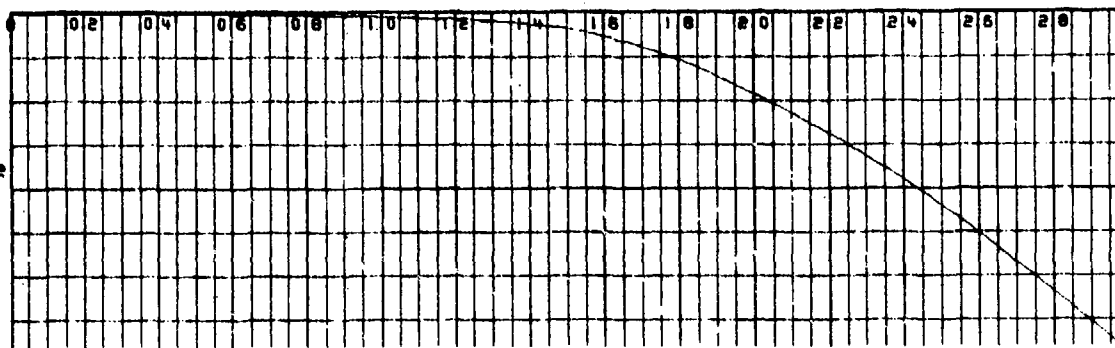
A 9

X

F

T

$-2.00 \times 10^{+02}$



TIME (SEC)

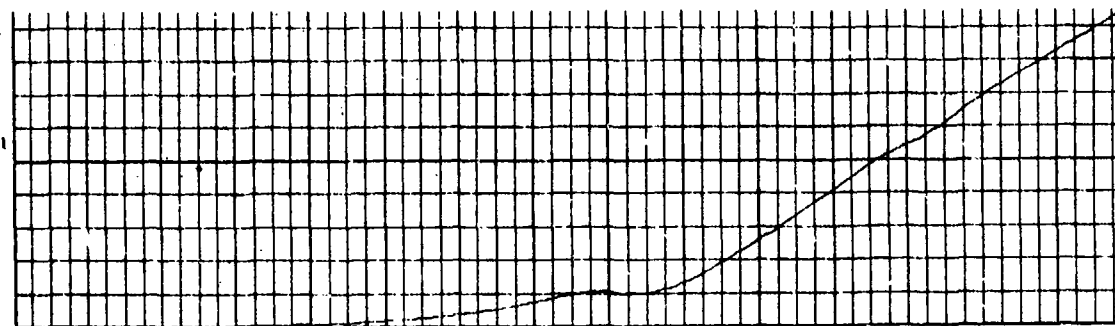
Y

F

T

$5.00 \times 10^{+01}$

0



TIME (SEC)

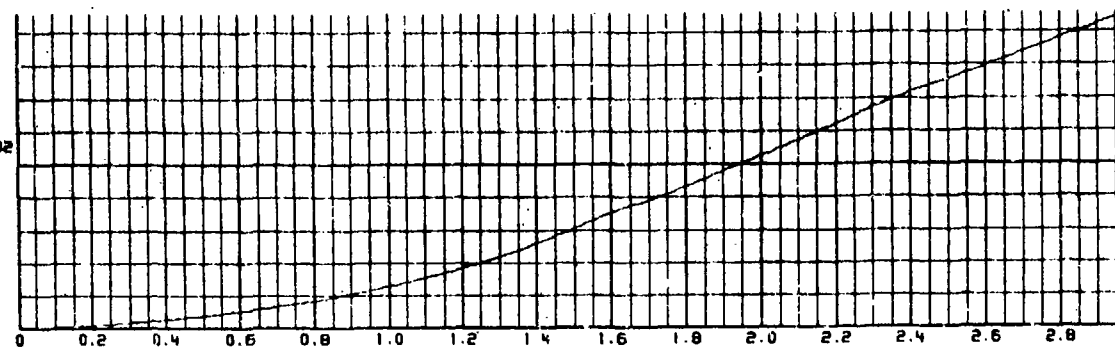
Z

F

T

$1.00 \times 10^{+02}$

0



TIME (SEC)  
PLOT PREPARED BY TSX, ADIC

Figure M-3. X, Y, and Z Position Versus Time for a Flow Field Intensity of 1 (as measured in the wind tunnel)

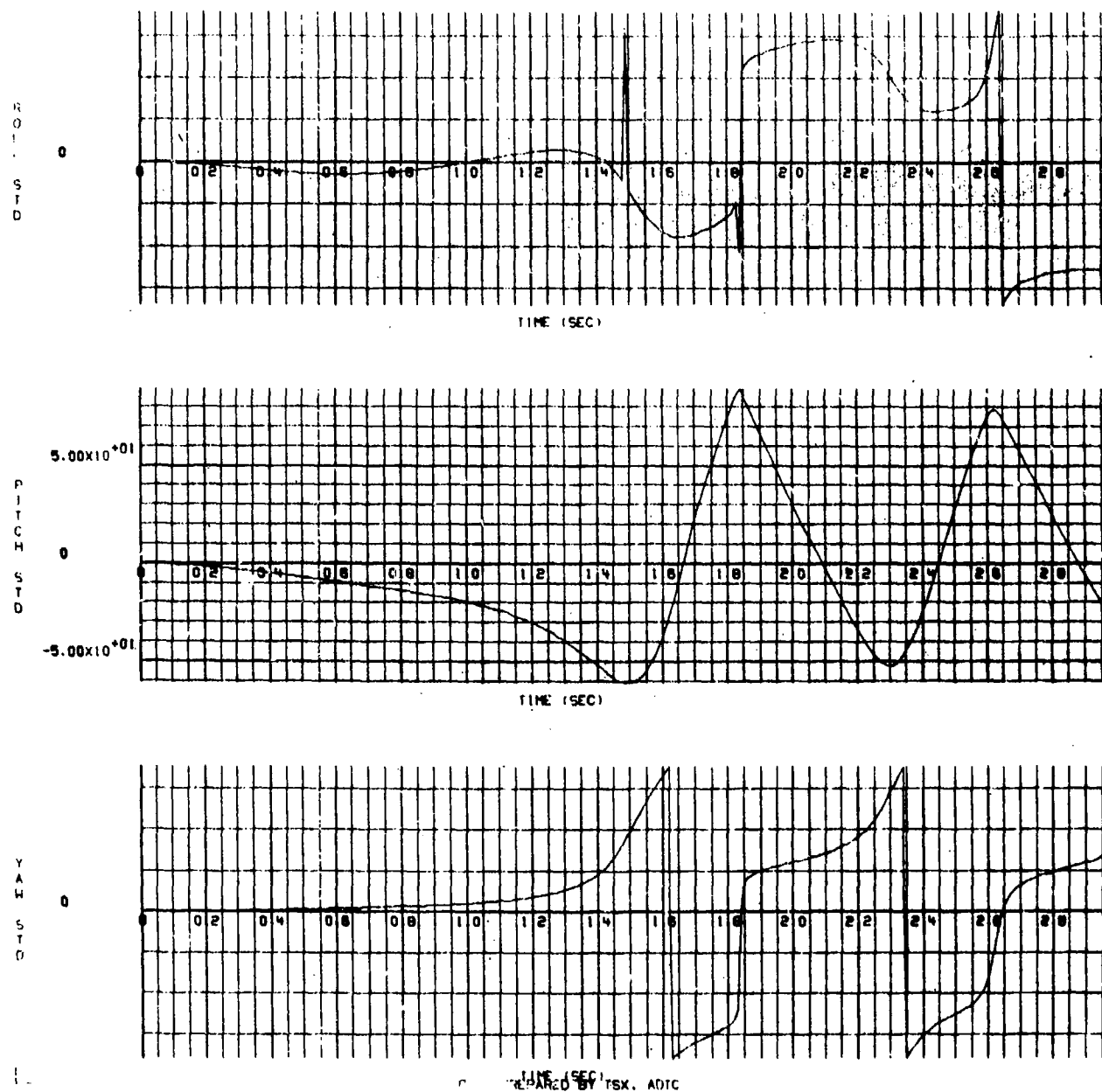
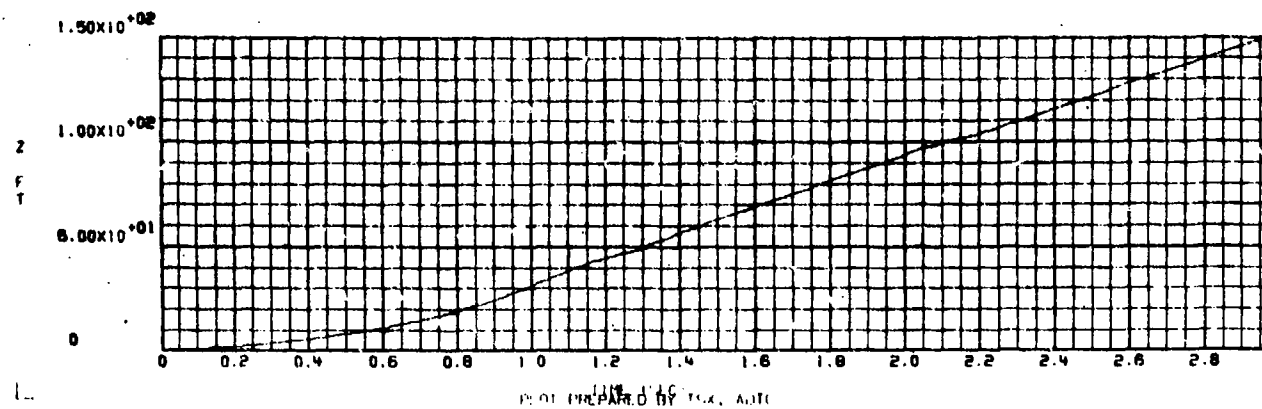
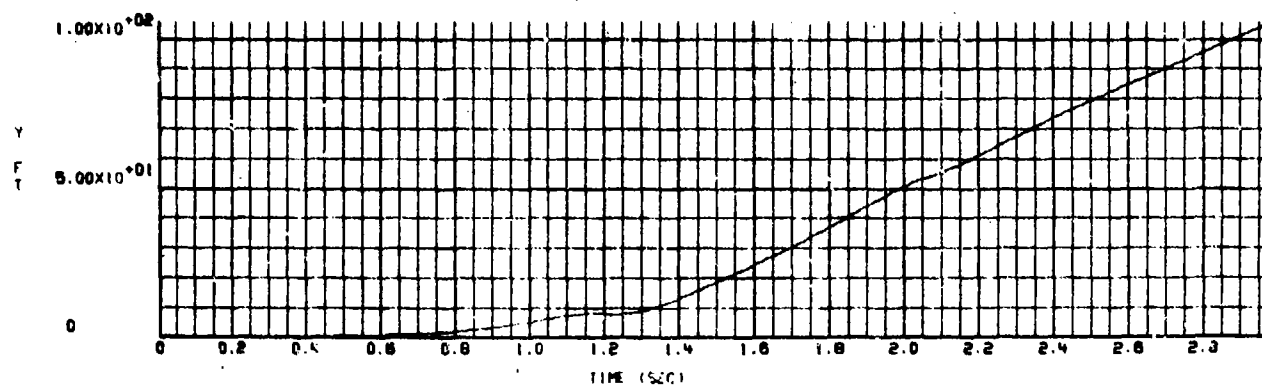
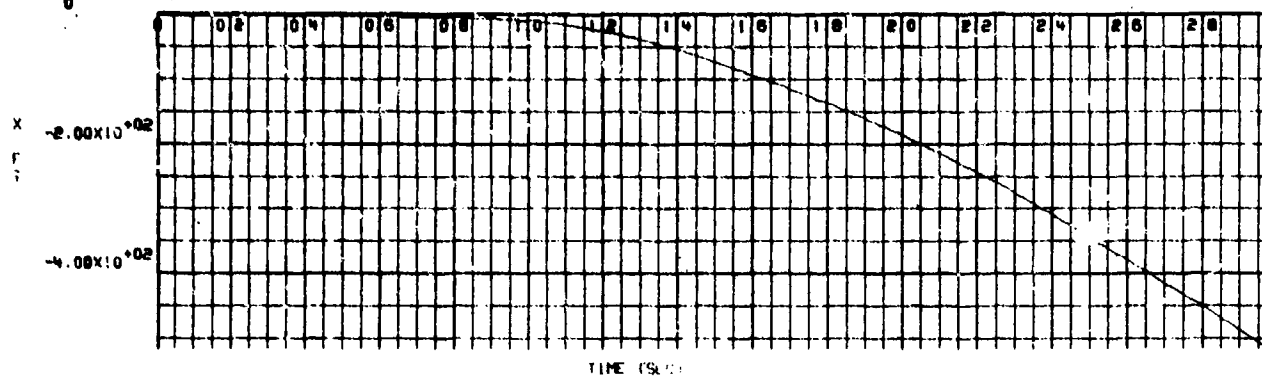


Figure M-4.  $\phi$ ,  $\theta$ , and  $\psi$  Rotation Versus Time for a Flow Field Intensity of 1 (unchanged from the wind tunnel measured values)

15/12/75  
0

R652

12 12

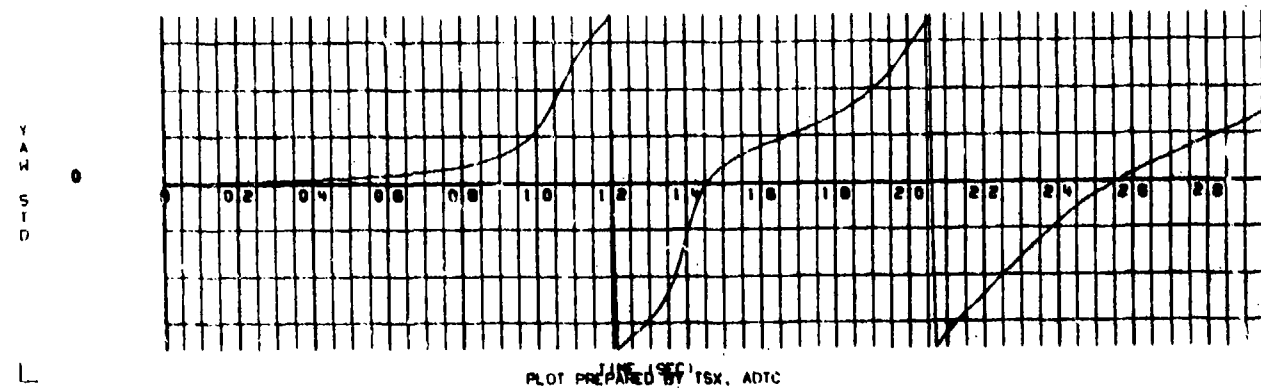
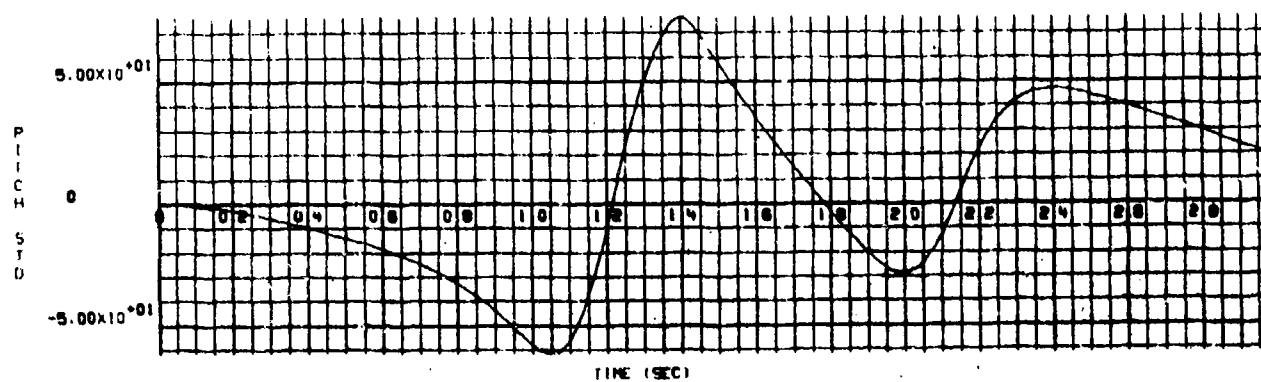
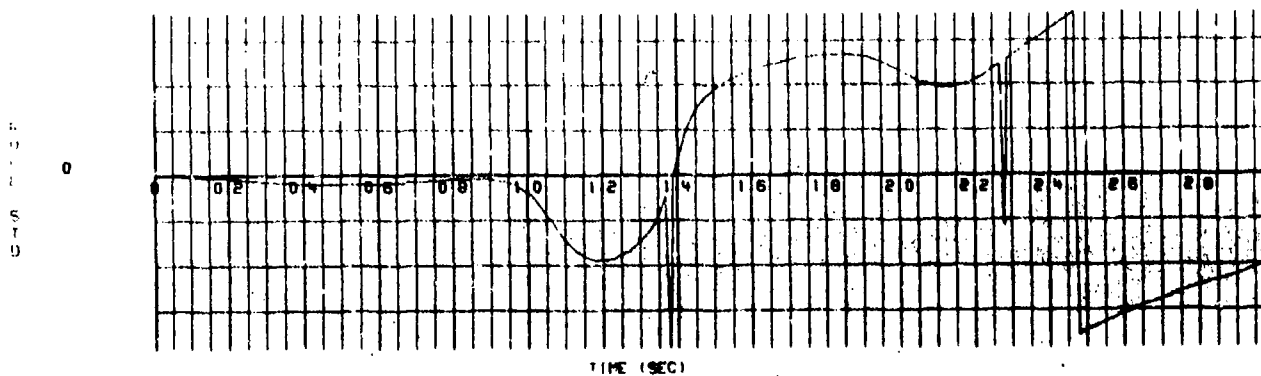


1316 1110  
PLOT PREPARED BY TOL. ADIC

Figure M-5. X, Y, and Z Position Versus Time for a Flow Field Intensity of 2

16 12 75

R652



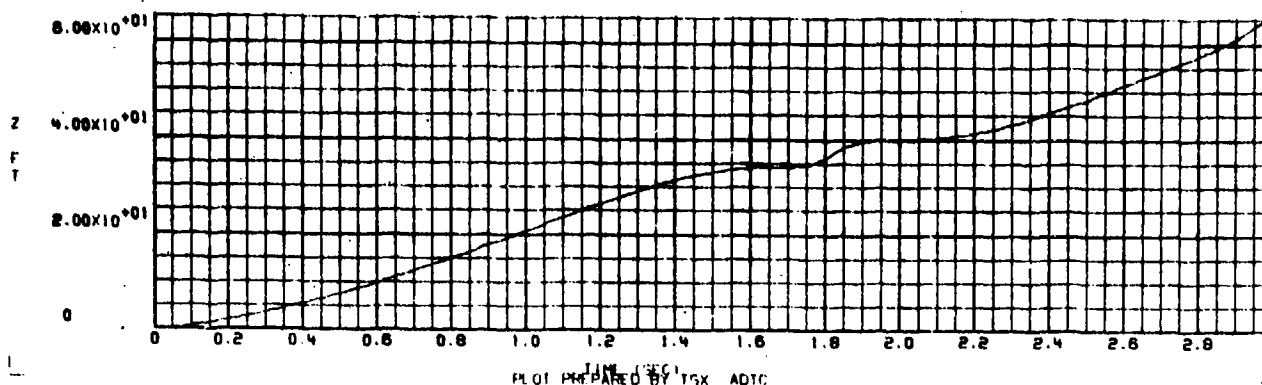
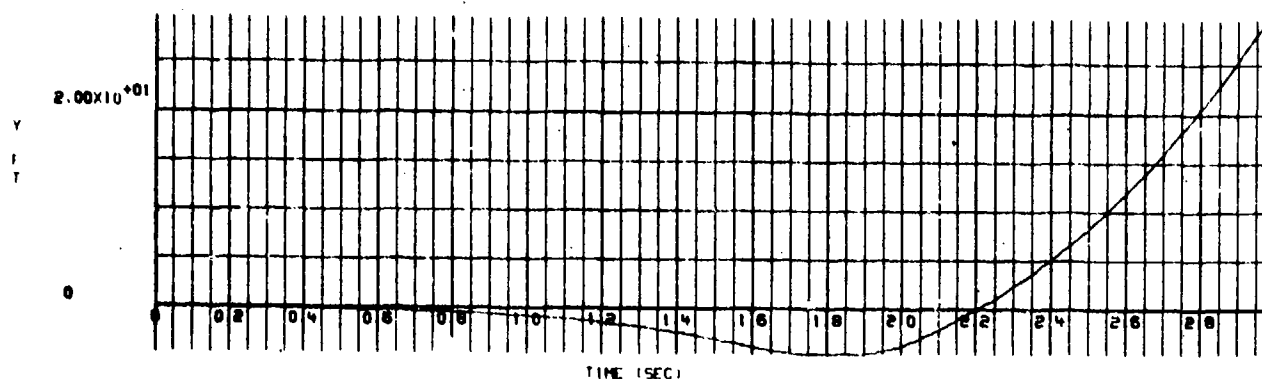
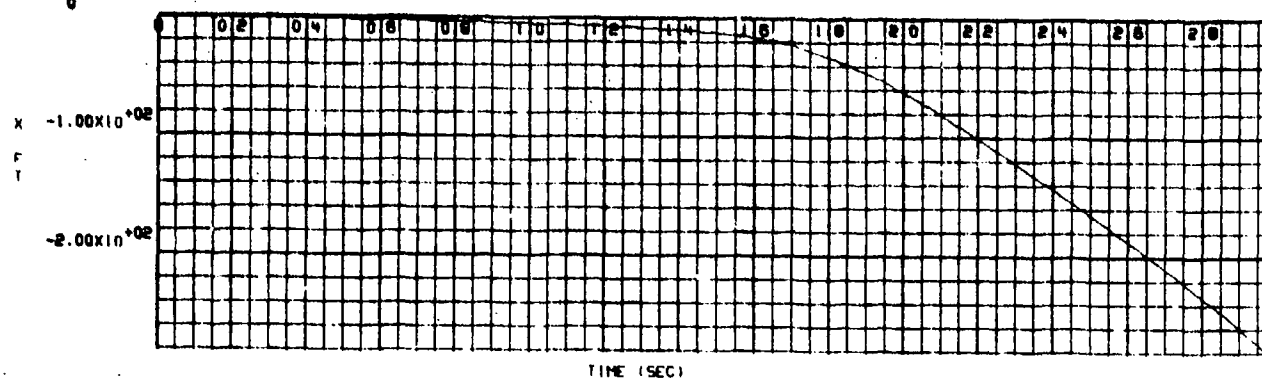
TIME (SEC)  
PLOT PREPARED BY TSX, ADTC

Figure M-6.  $\phi$ ,  $\theta$ , and  $\gamma$  Rotation Versus Time for a Flow Field Intensity of 2

16/12/75  
0

R652

16 16



PLOT PREPARED BY T5X ADTC

Figure M-7. X, Y, and Z Position Versus Time for a Flow Field Intensity of  $-1/2$

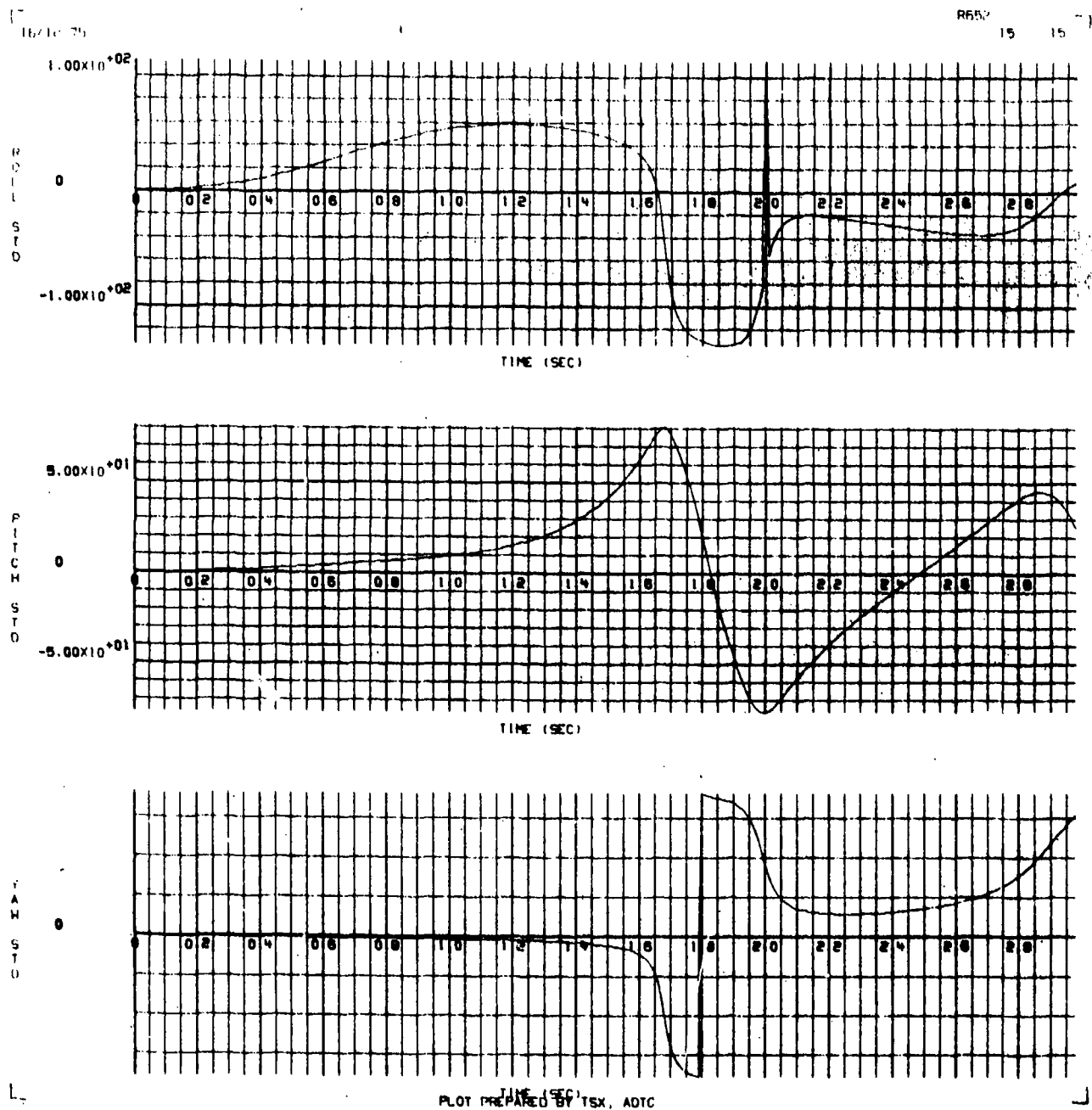


Figure M-8.  $\phi$ ,  $\theta$ , and  $\psi$  Rotation Versus Time for a Flow Field Intensity of  $-1/2$

APPENDIX N

GBU-10 BOMB TRAJECTORIES RESULTING FROM A  
(-5/-3) ORIFICE COMBINATION AT MACH 0.85

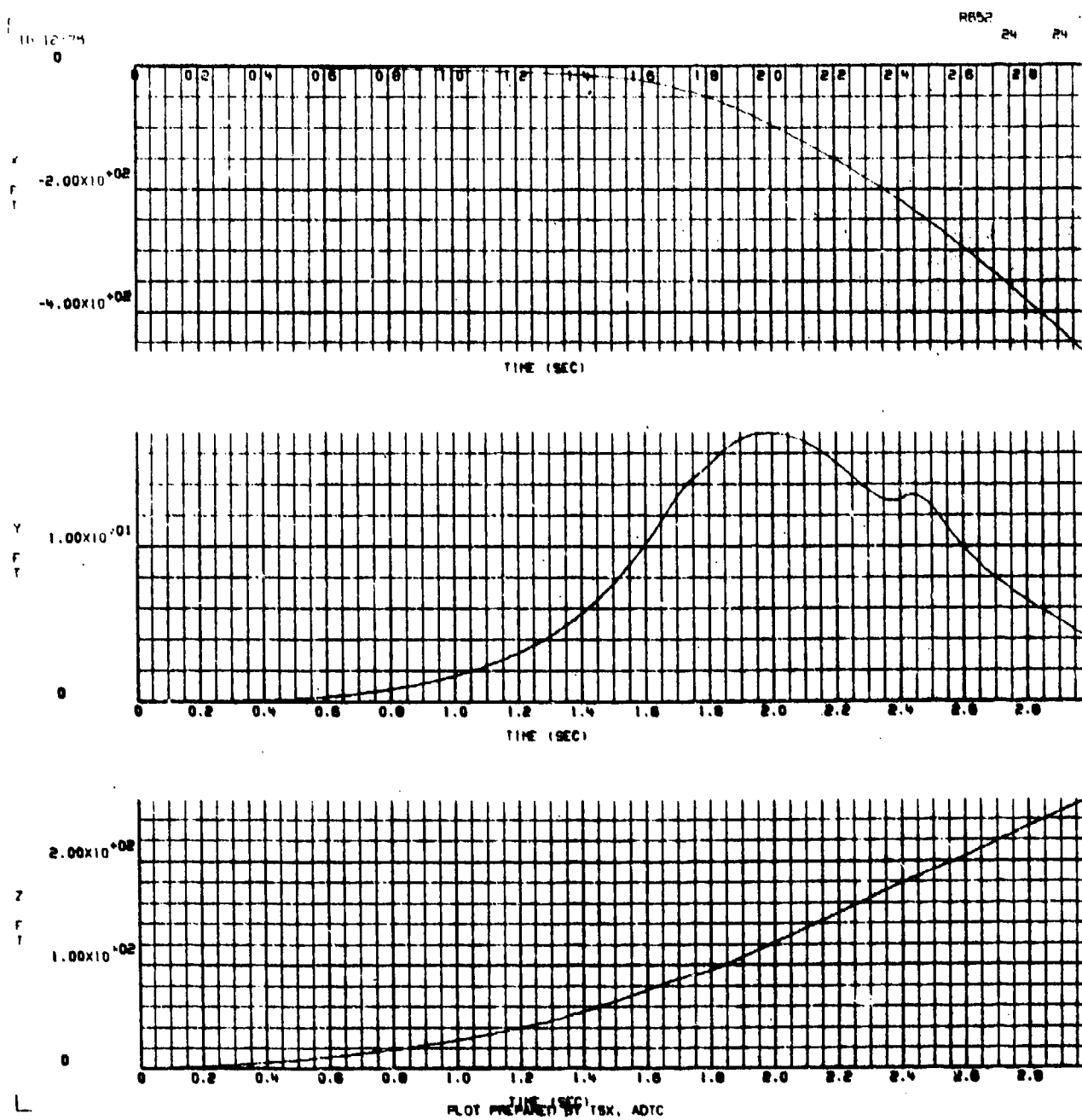


Figure N-1. X, Y, and Z Position Versus Time for a Flow Field Intensity of 1/2



16/12/75

R602

23 23

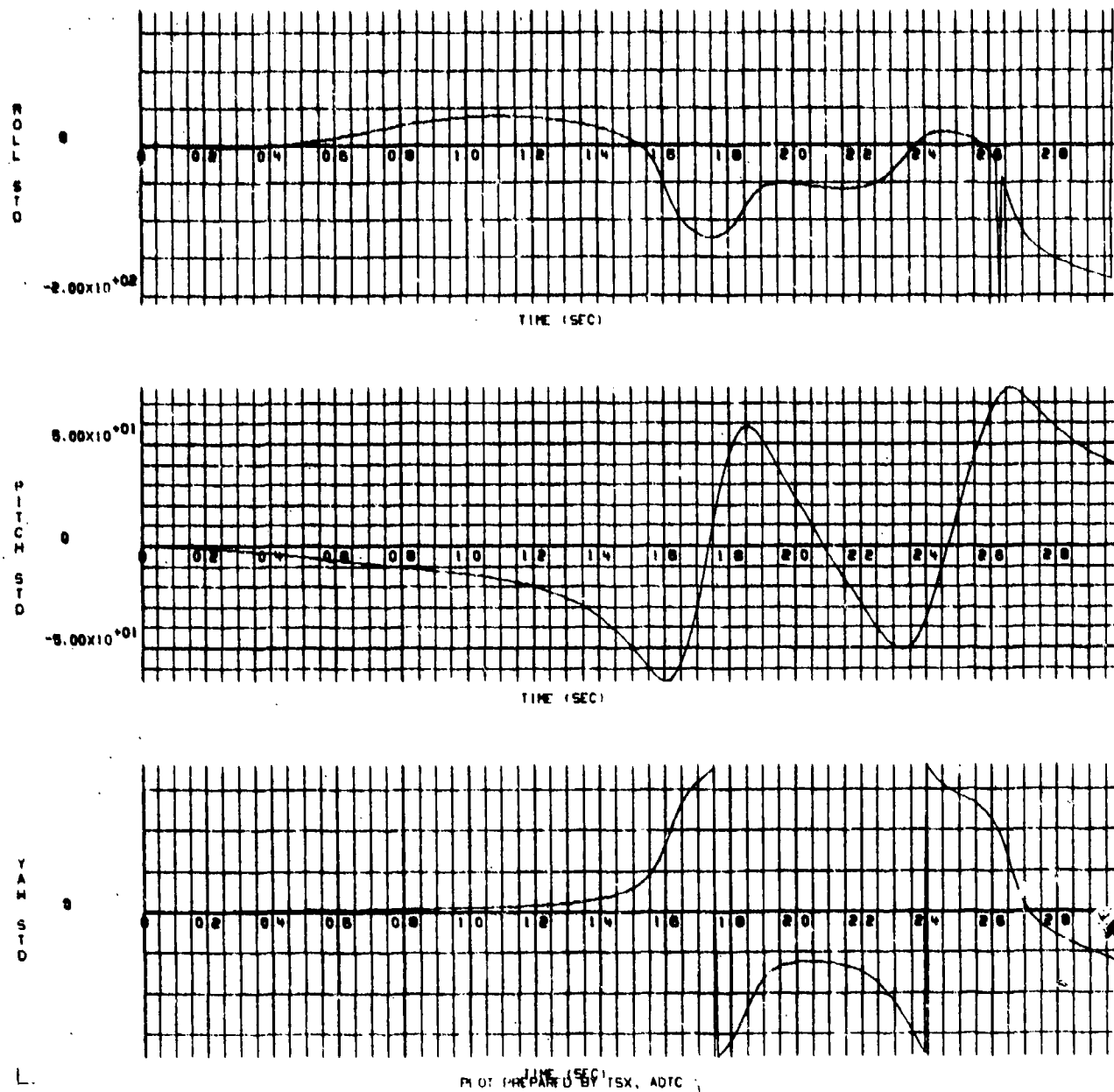


Figure N-2.  $\phi$ ,  $\theta$ , and  $\psi$  Rotation Versus Time for a Flow Field Intensity of  $1/2$

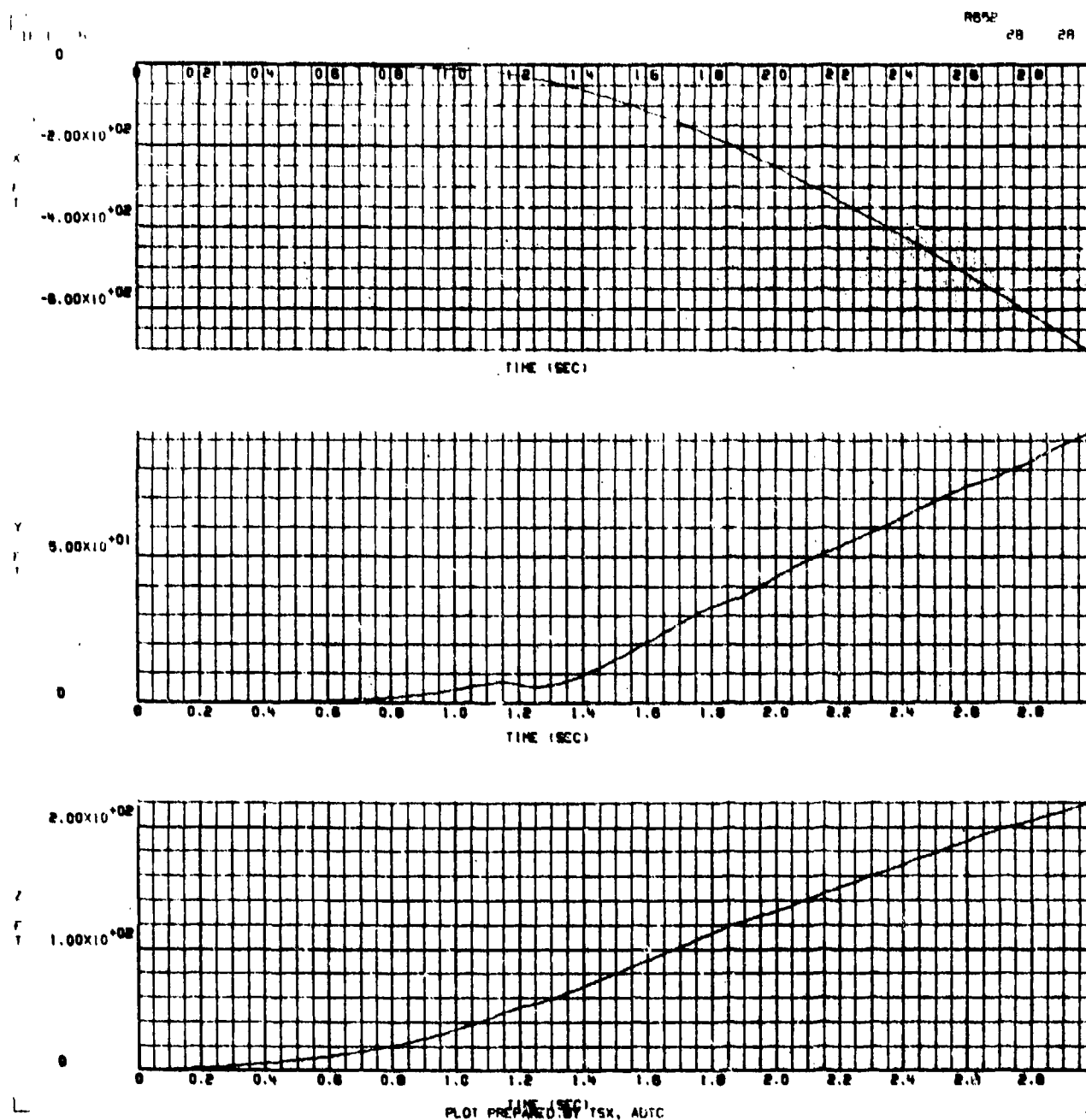


Figure N-3. X, Y, and Z Position Versus Time for a Flow Field Intensity of 1 (as measured in the wind tunnel)

12552 P7 P7



128

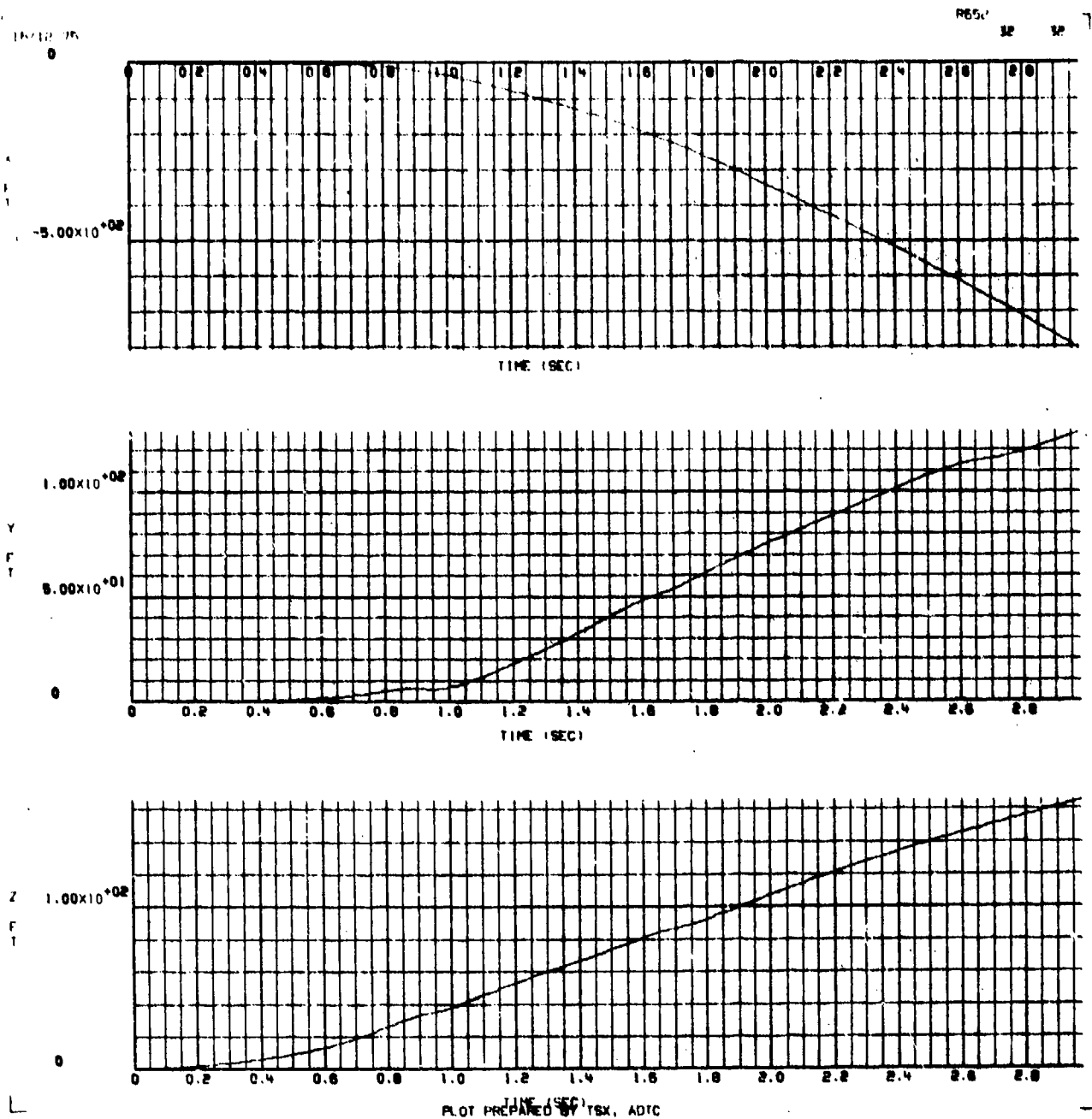
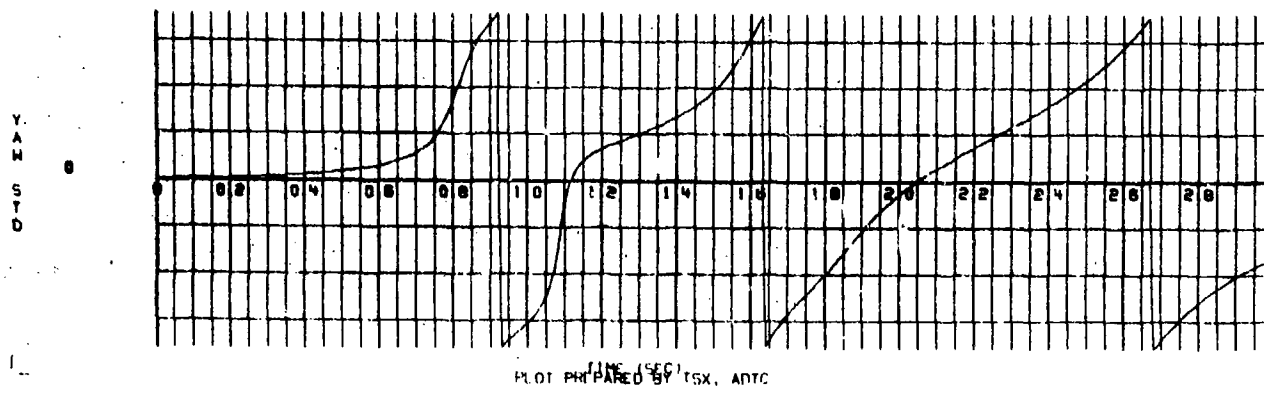
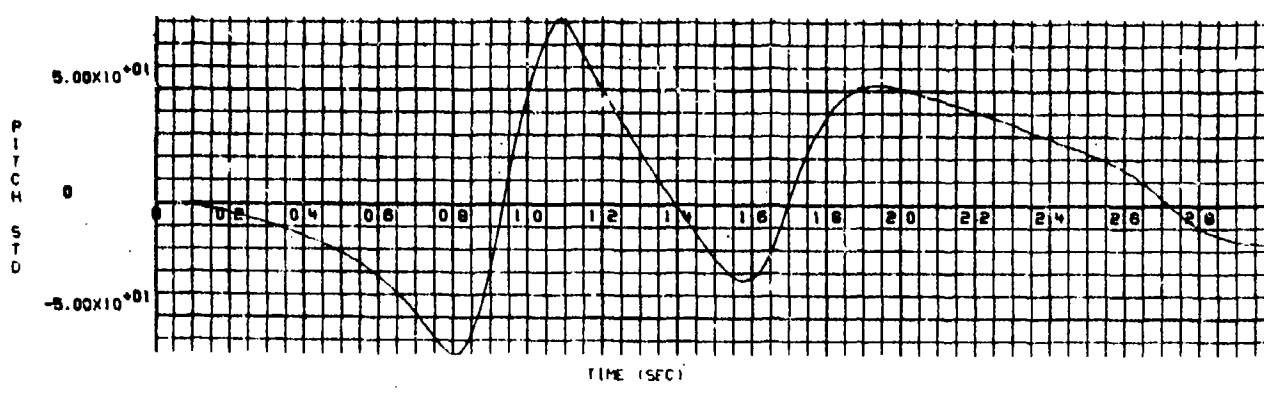
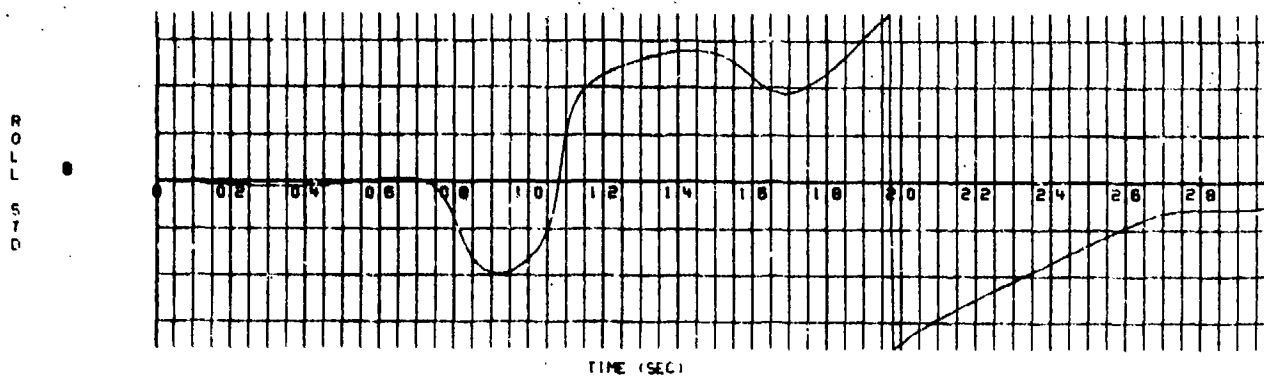


Figure N-5. X, Y, and Z Position Versus Time for a Flow Field Intensity of 2

15/12/75

R662 31 31



PLOT PREPARED BY TSX, ADTC

Figure N-6.  $\phi$ ,  $\theta$ , and  $\psi$  Rotation Versus Time for a Flow Field Intensity of 2

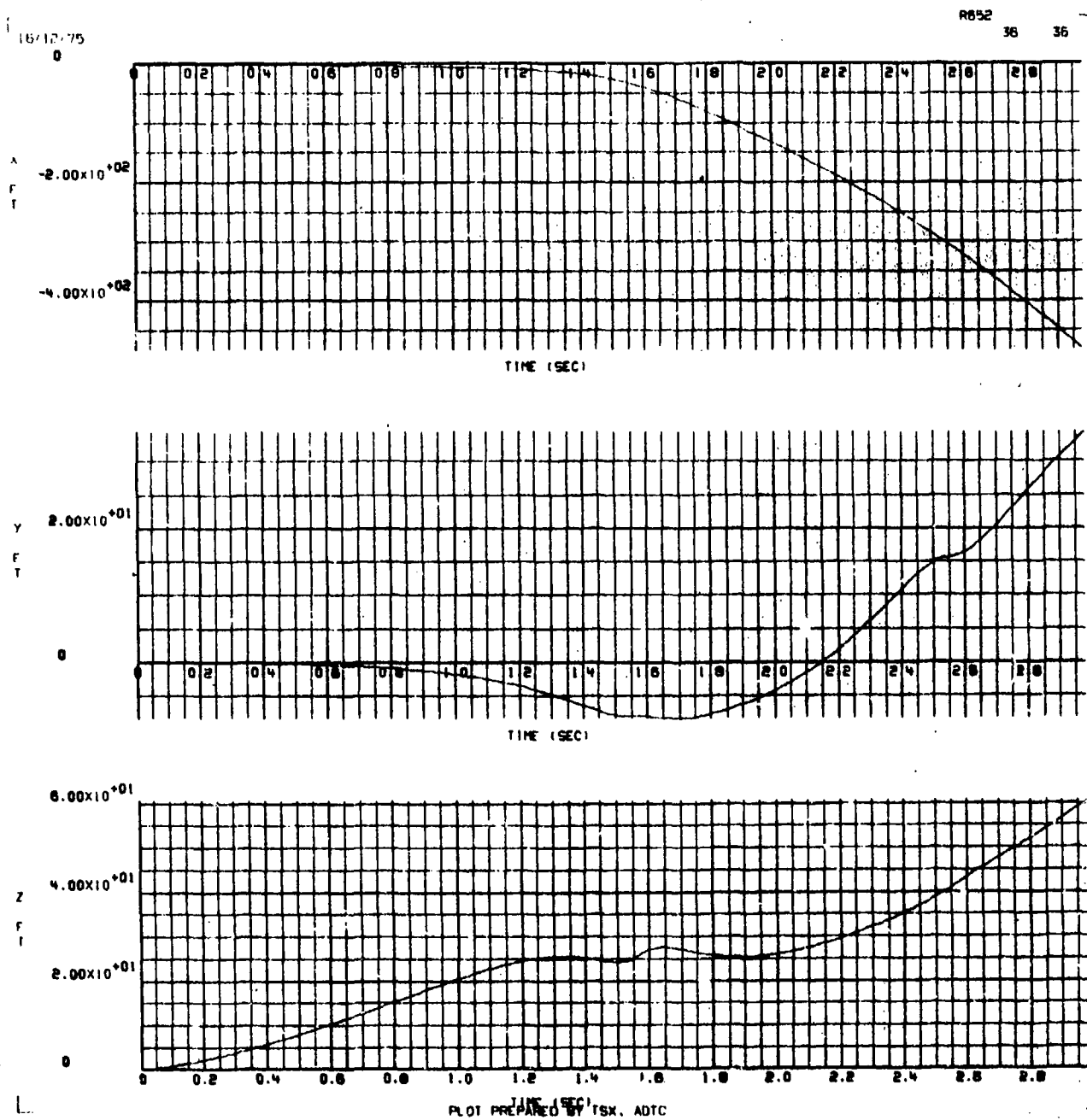


Figure N-7. X, Y, and Z Position Versus Time for a Flow Field Intensity of  $-1/2$

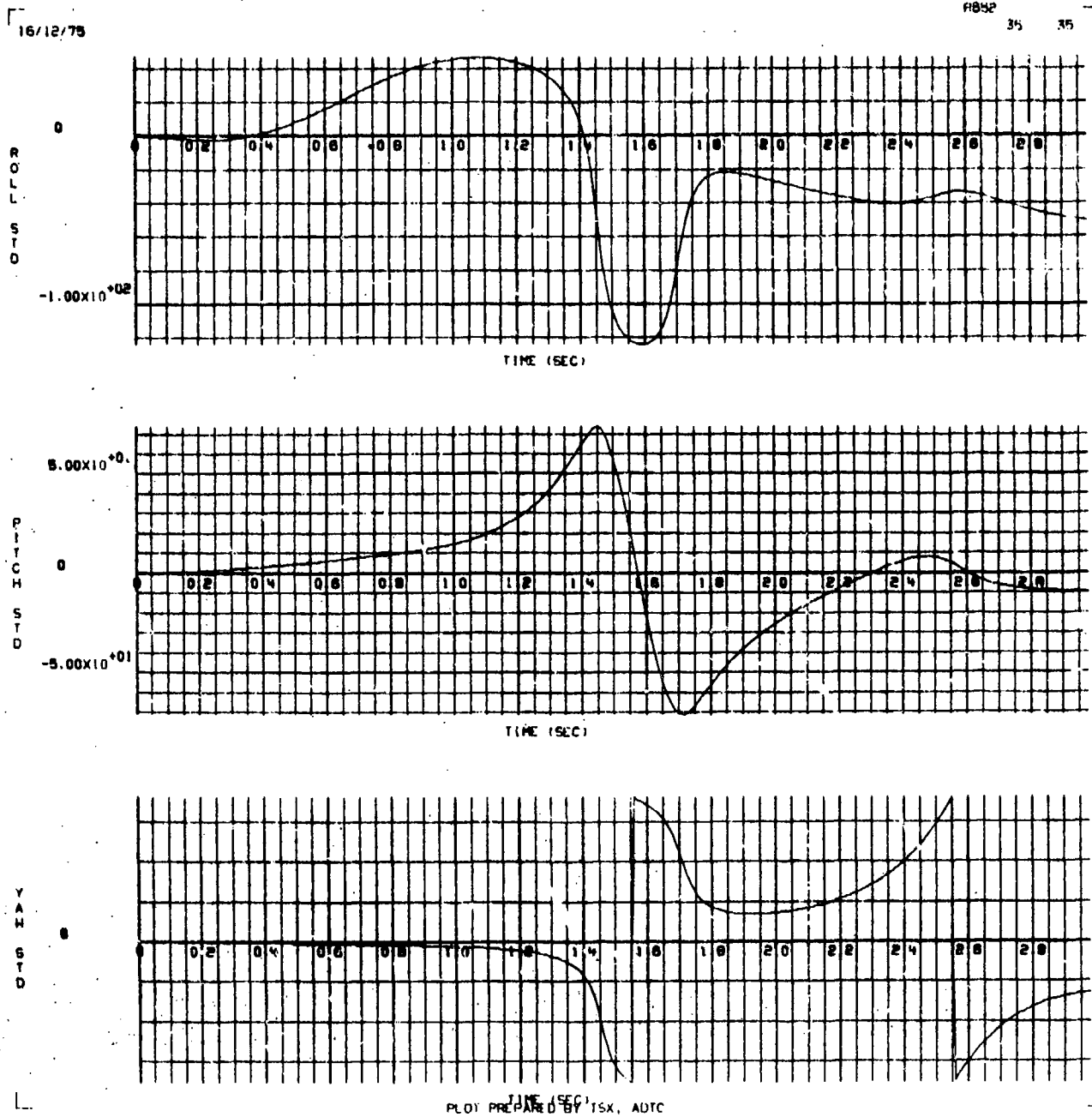


Figure N-8.  $\phi$ ,  $\theta$ , and  $\psi$  Rotation Versus Time for a Flow Field Intensity of  $-1/2$

APPENDIX O

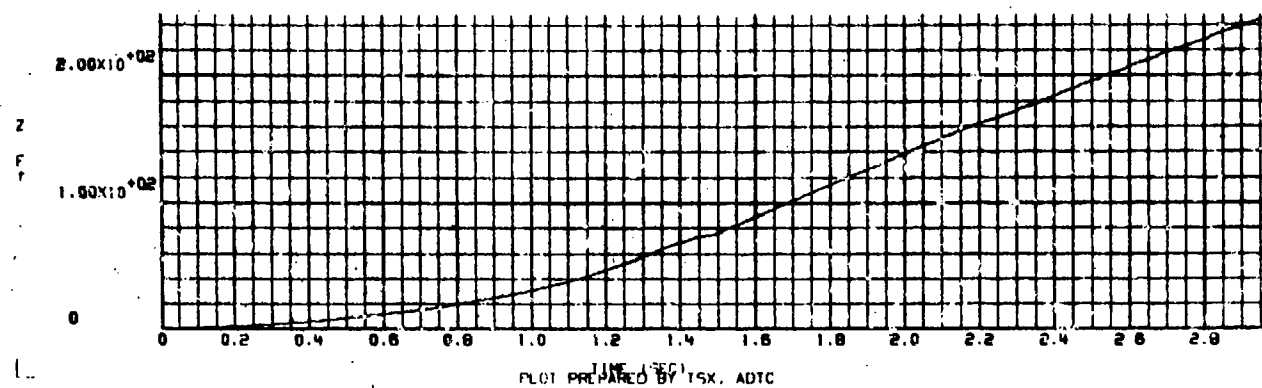
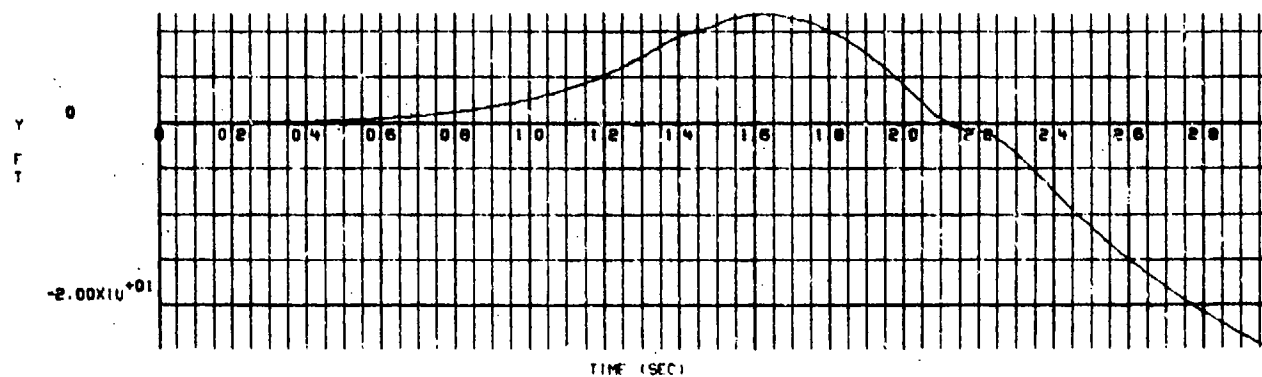
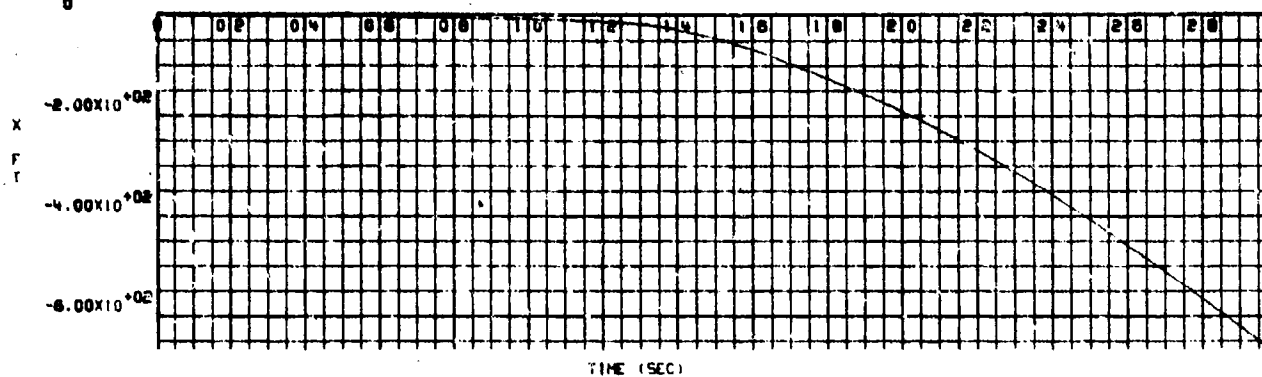
GBU-10 BOMB TRAJECTORIES RESULTING FROM A  
(-5/-3) ORIFICE COMBINATION AT MACH 0.95



16/12/75  
0

R852

44 44



PL01 PREPARED BY TSX, ADIC

Figure 0-1. X, Y, and Z Position Versus Time for a Flow Field Intensity of  $1/2$

16/12/75

R642

43

43

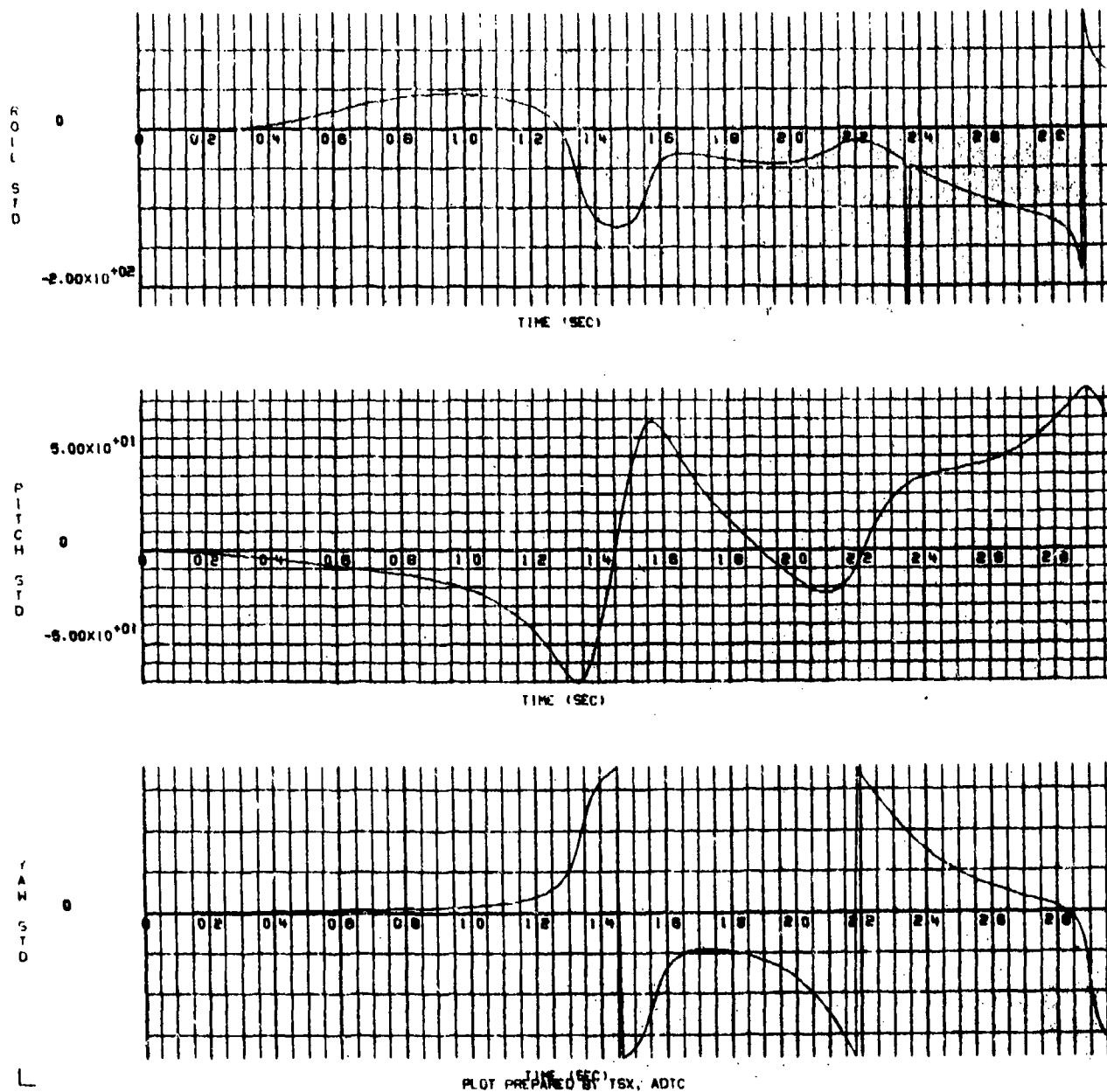
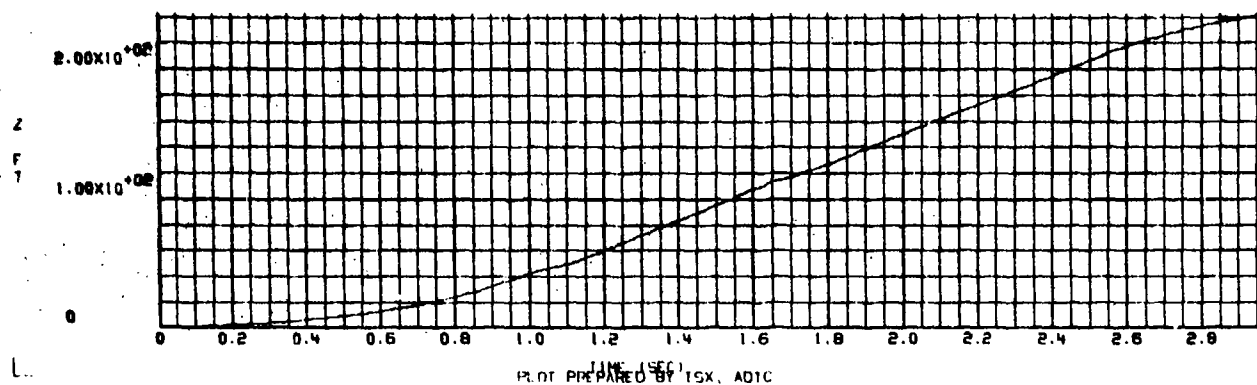
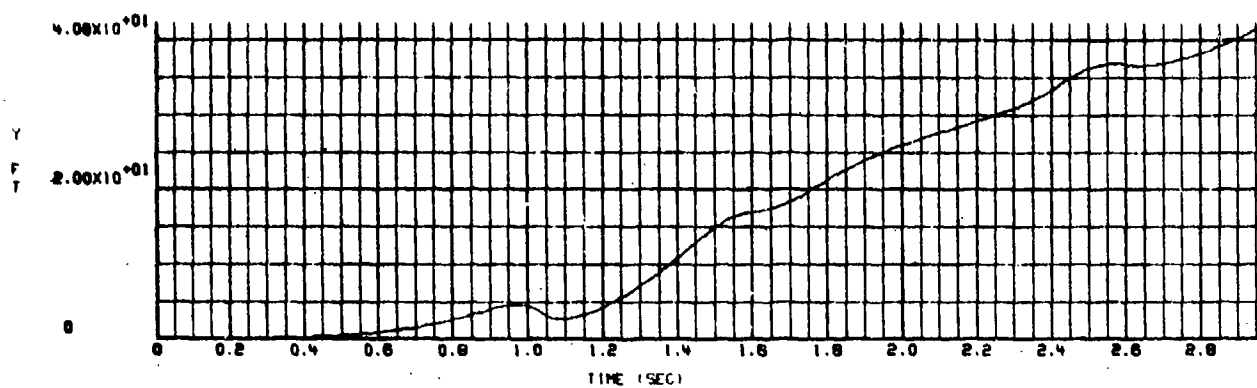
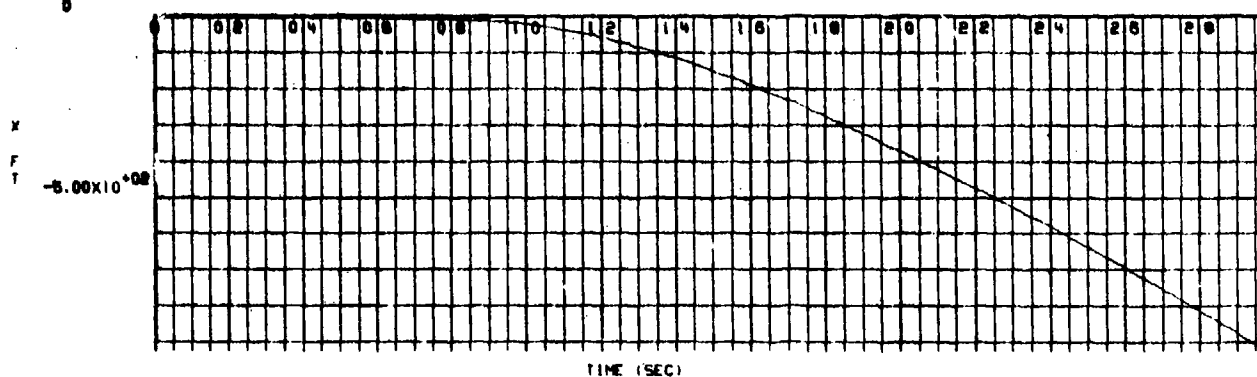


Figure O-2.  $\phi$ ,  $\theta$ , and  $\psi$  Rotation Versus Time for a Flow Field Intensity of 1/2

18/12/75  
0

R652

48 48



PLT PREPARED BY TSX, ADIC

Figure 0-3. X, Y, and Z Position Versus Time for a Flow Field Intensity of 1 (as measured in the wind tunnel)

16/12/75

H652

47

47

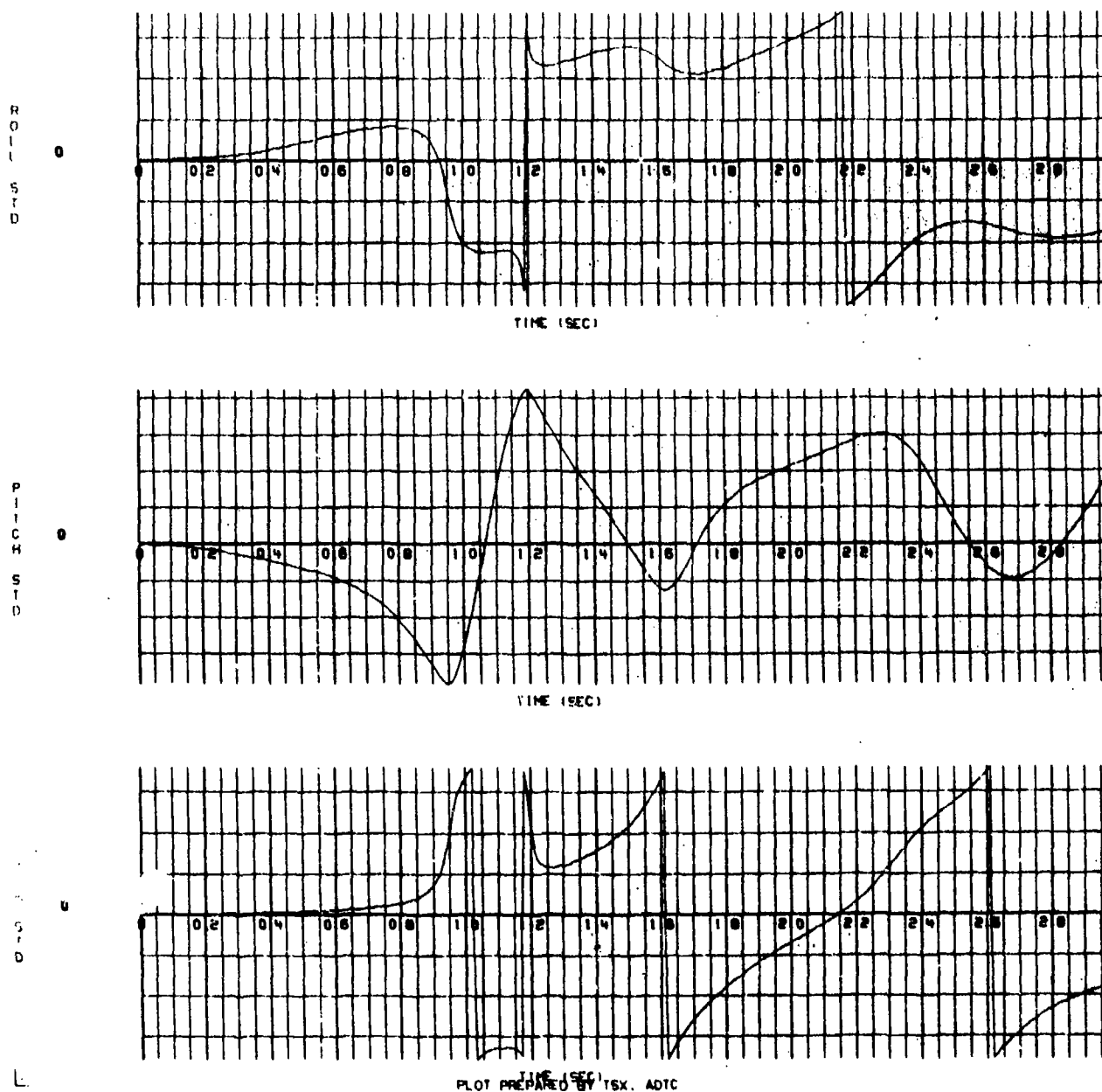
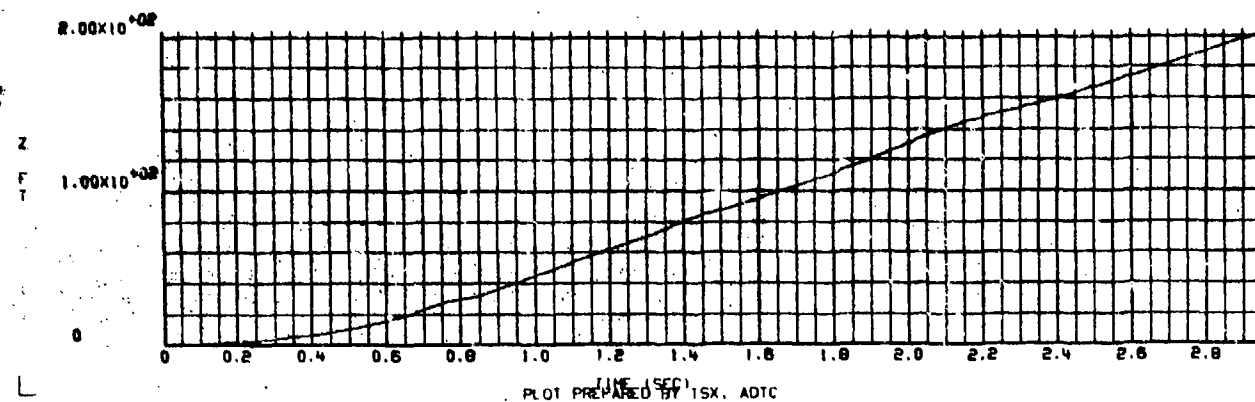
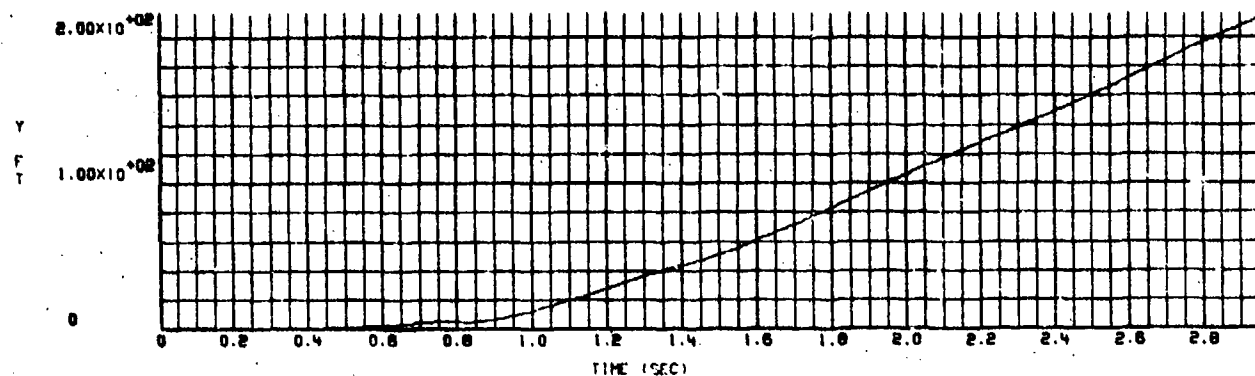
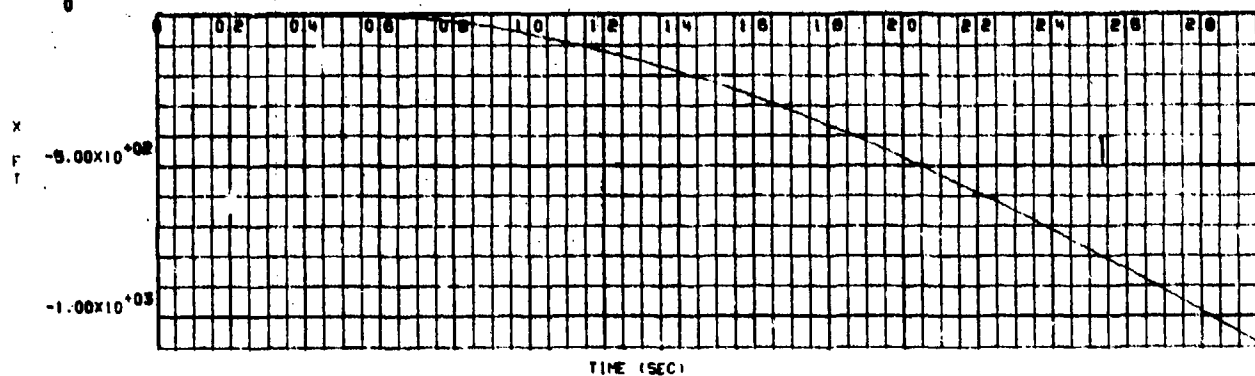


Figure O-1  $\phi$ ,  $\theta$ , and  $\psi$  Rotation Versus Time for a Flow Field Intensity of 1 (unchanged from the wind tunnel measured values)

RB52 52 52



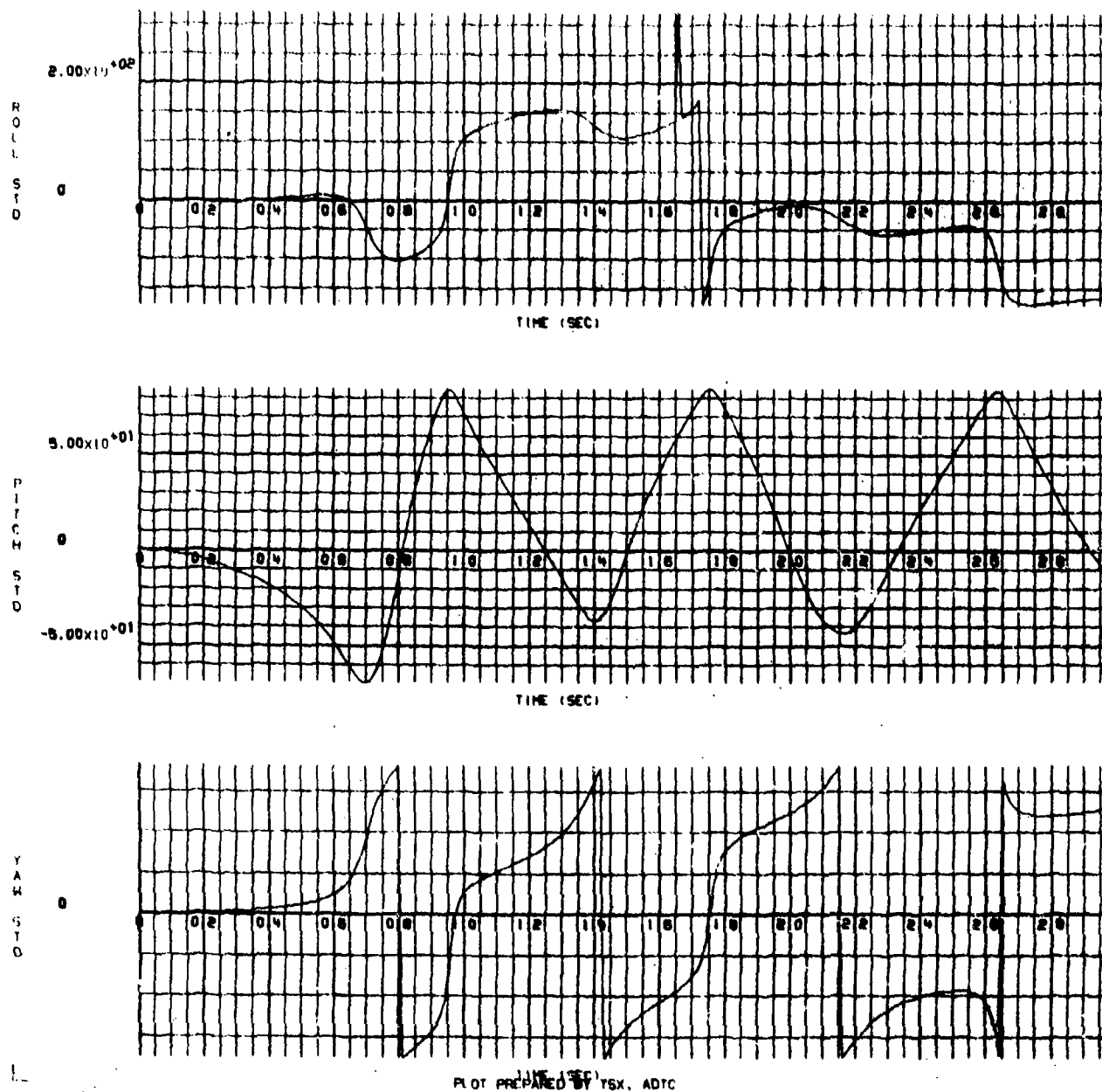
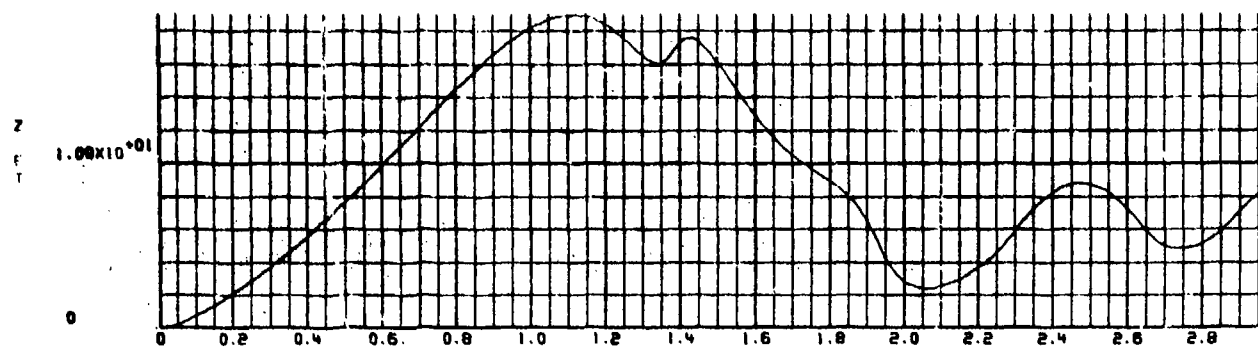
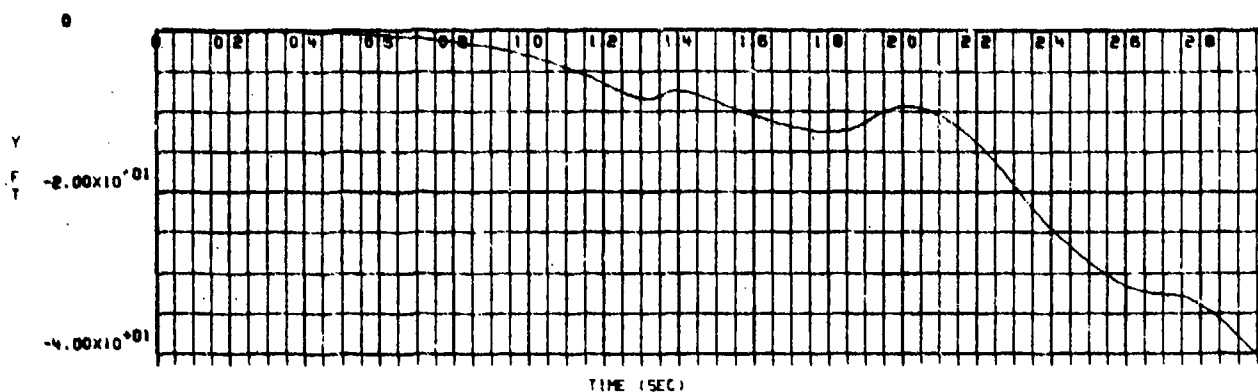
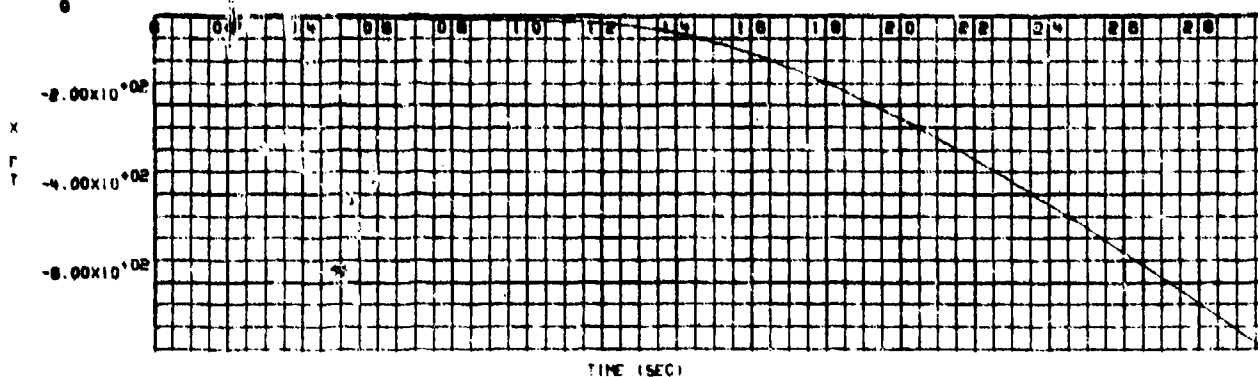


Figure O-6.  $\phi$ ,  $\theta$ , and  $\psi$  Rotation Versus Time for a Flow Field Intensity of 2

18/12/75  
0

4052 56 93



LINE (SEC)  
PLOT PREPARED BY ISX, ADTC

Figure 0-7. X, Y, and Z Position Versus Time for a Flow Field Intensity of  $-1/2$

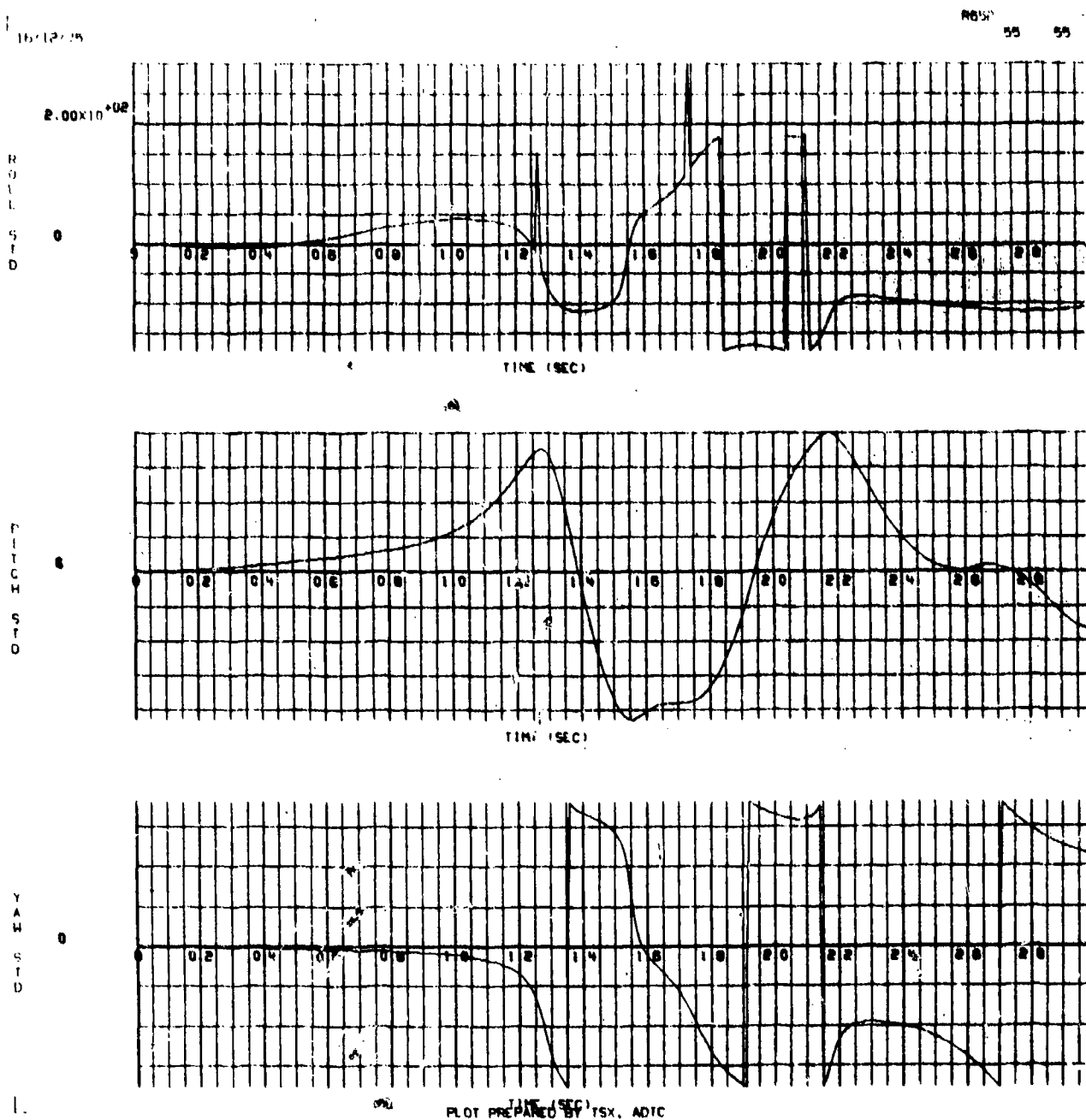


Figure O-8.  $\phi$ ,  $\theta$ , and  $\psi$  Rotation Versus Time for a Flow Field Intensity of  $-1/2$



APPENDIX P

GBU-10 BOMB TRAJECTORIES RESULTING FROM A  
(-5/-3) ORIFICE COMBINATION AT MACH 1.2

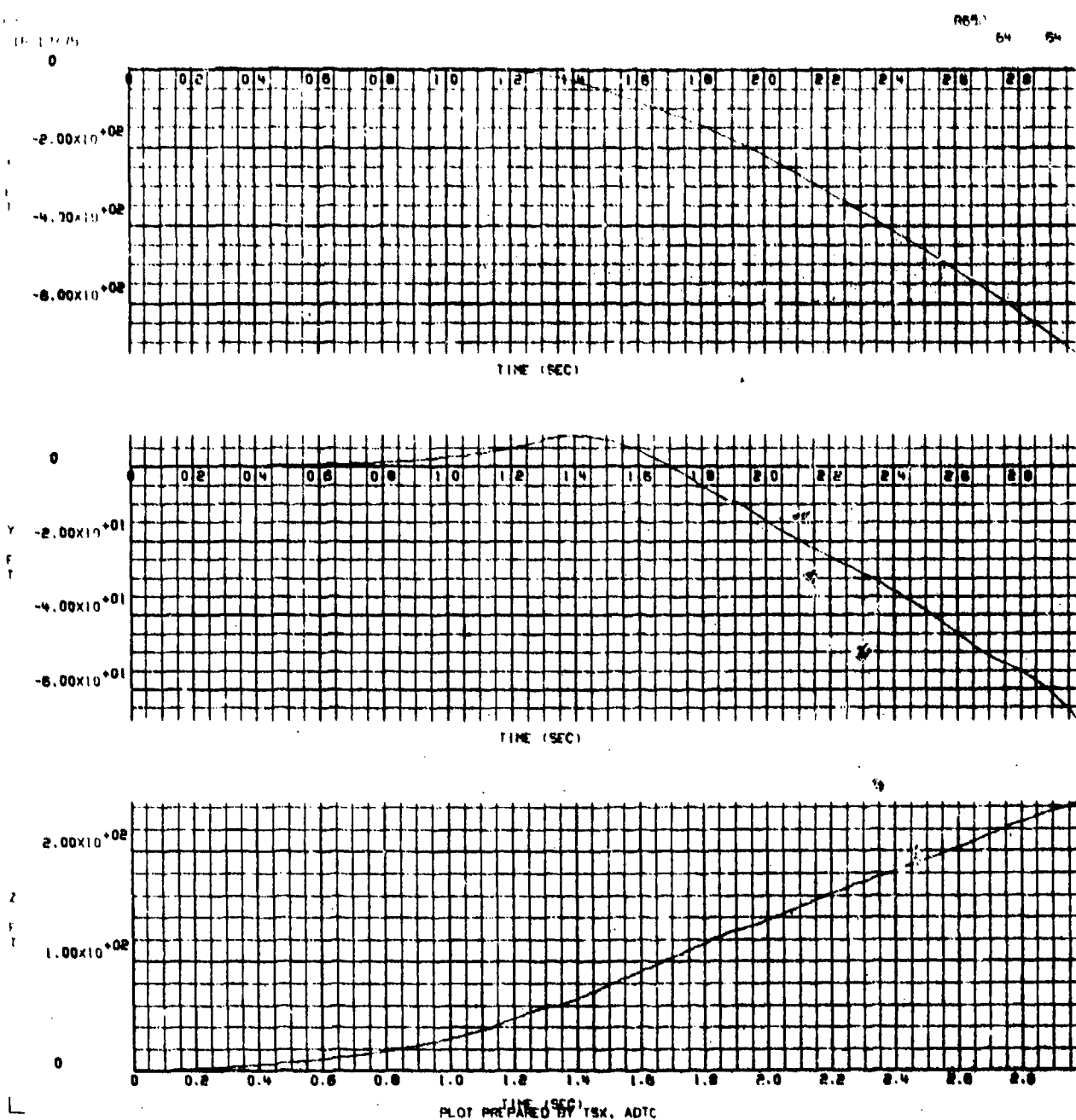


Figure P-1. X, Y, and Z Position Versus Time for a Flow Field Intensity of 1/2

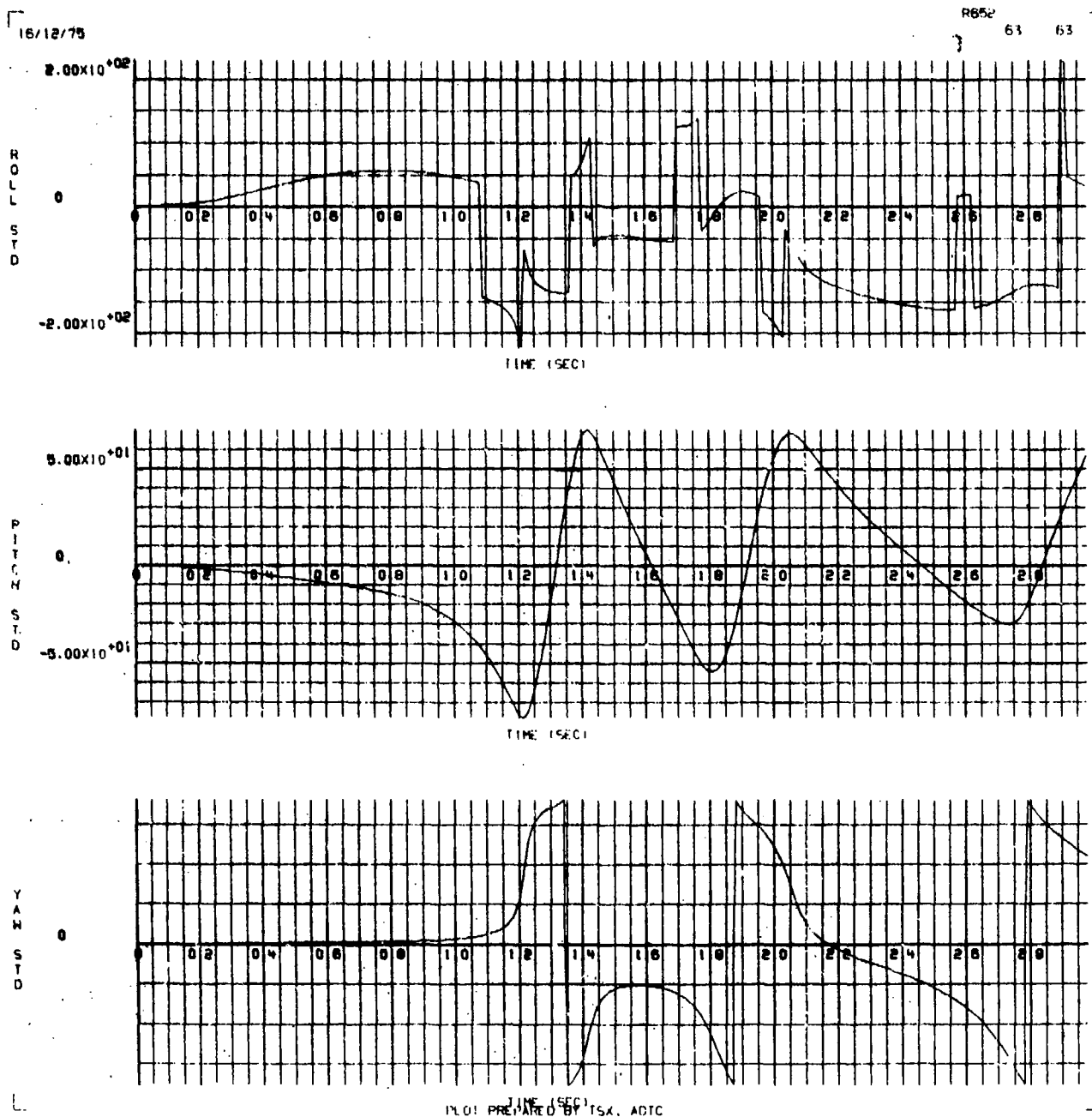


Figure P-2.  $\phi$ ,  $\theta$ , and  $\psi$  Rotation Versus Time for a Flow Field Intensity of 1/2

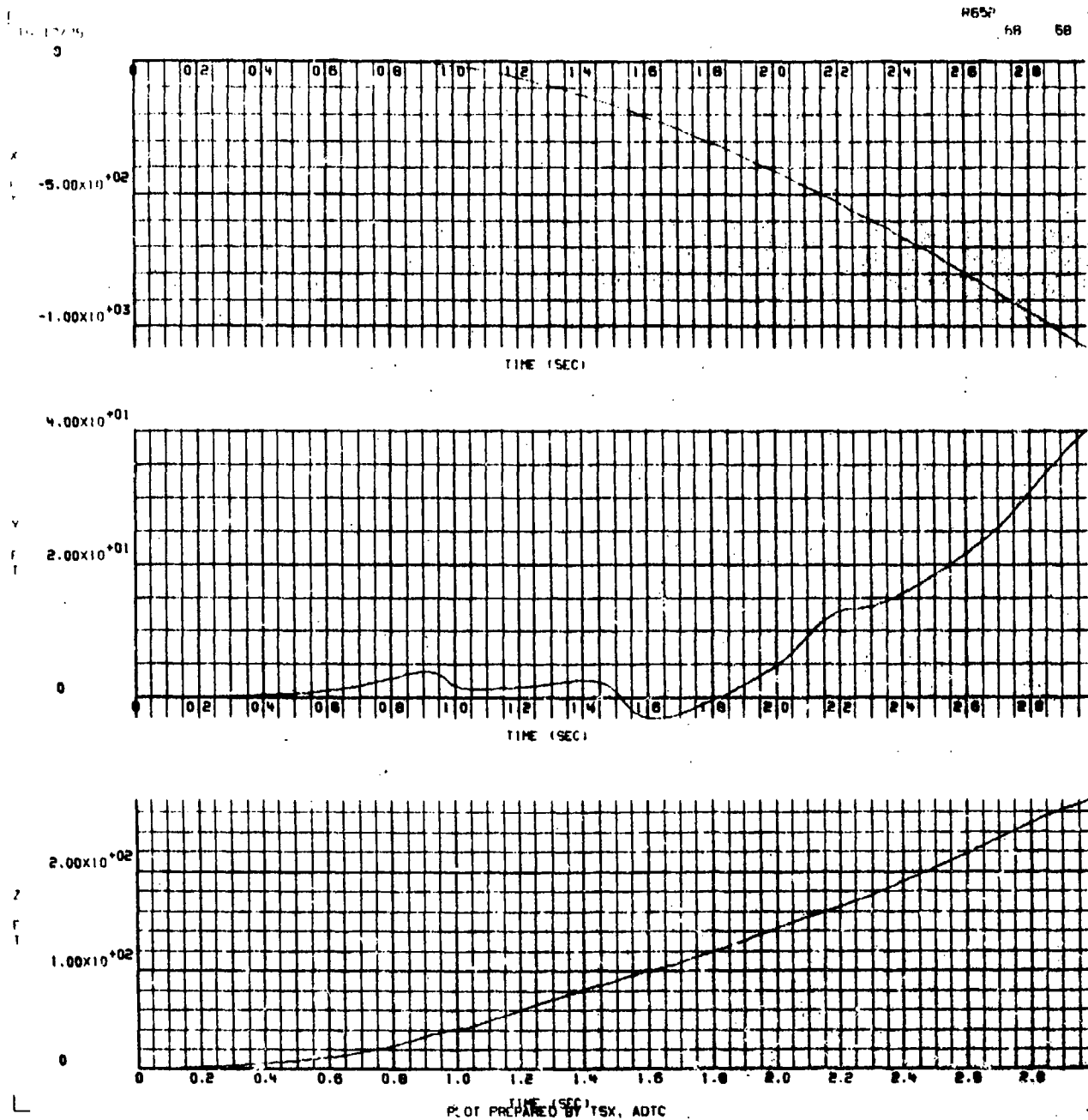


Figure P-3. X, Y, and Z Position Versus Time for a Flow Field Intensity of 1 (as measured in the wind tunnel)

18/12/75

R652

67 67

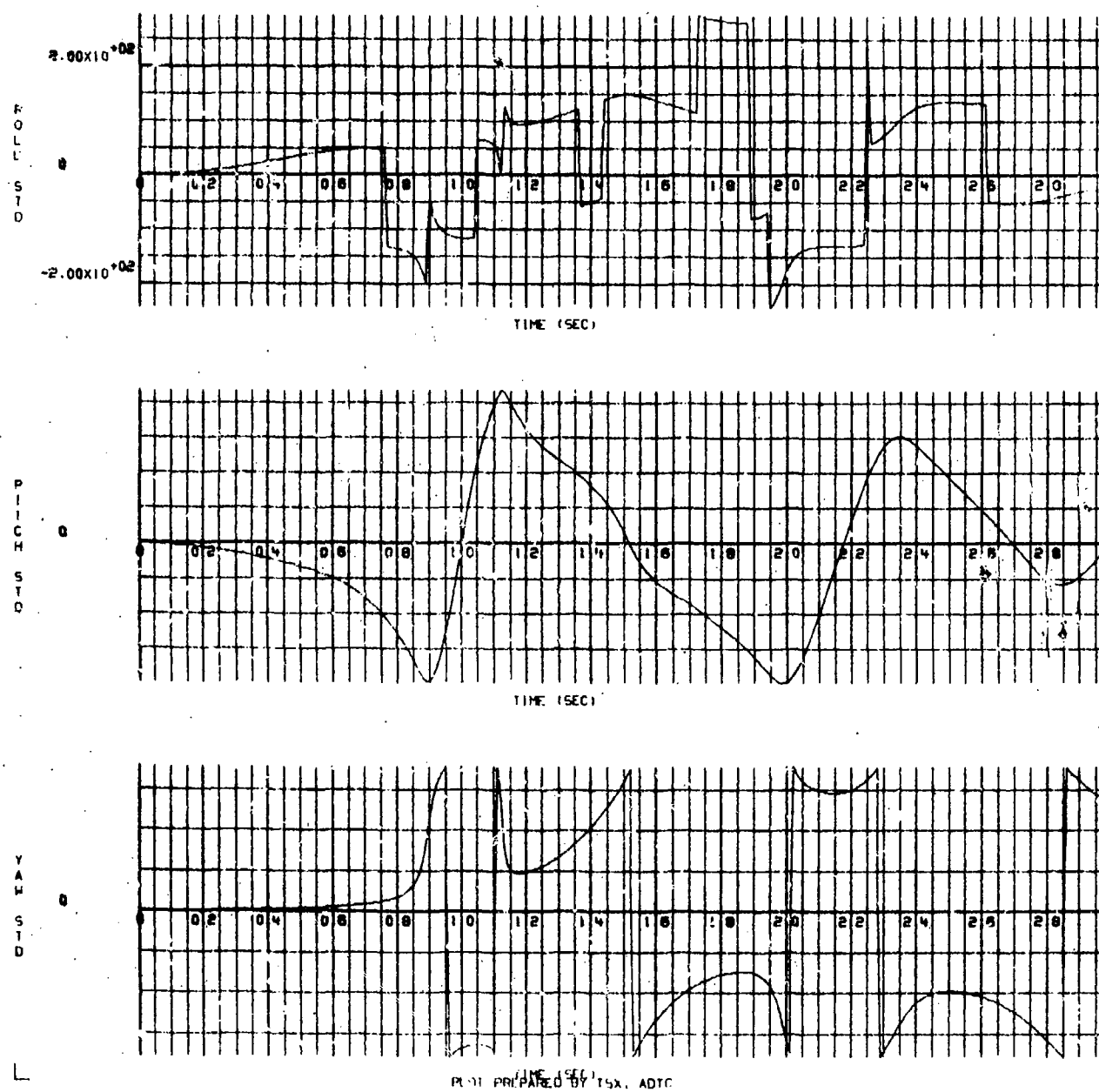
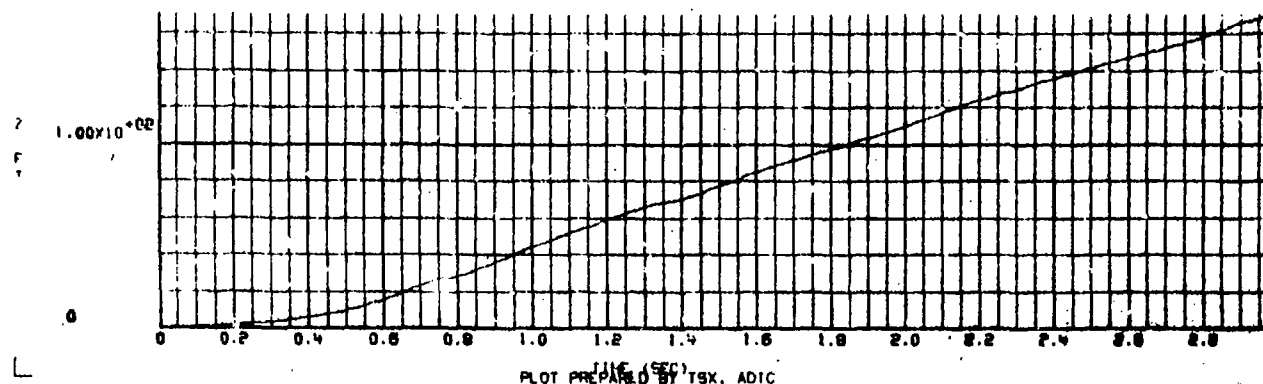
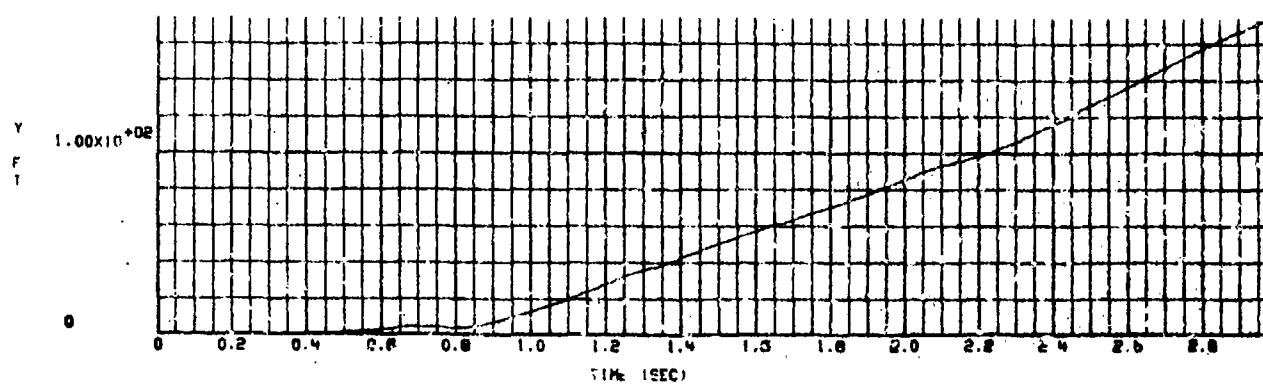
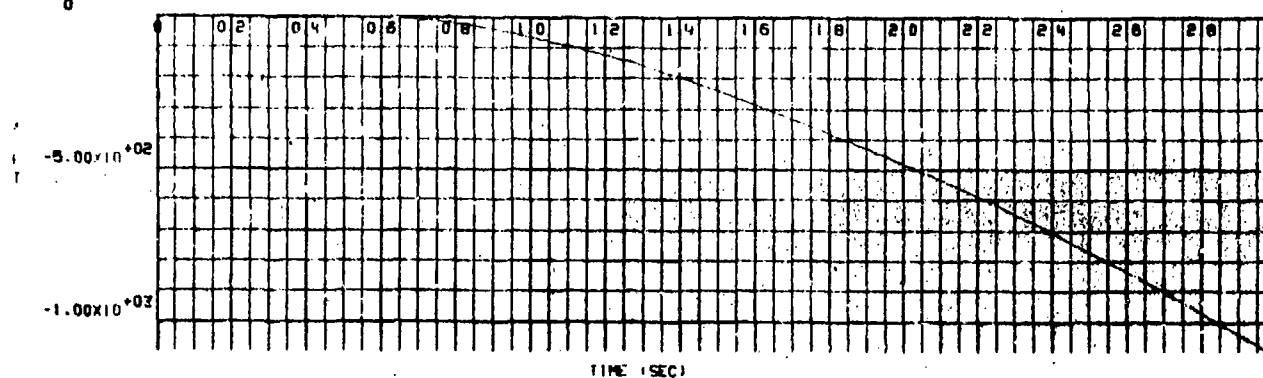


Figure P-4.  $\phi$ ,  $\theta$ , and  $\psi$  Rotation Versus Time for a Flow Field Intensity of 1 (unchanged from the wind tunnel measured values)

16 12 75  
0

R652

72 72



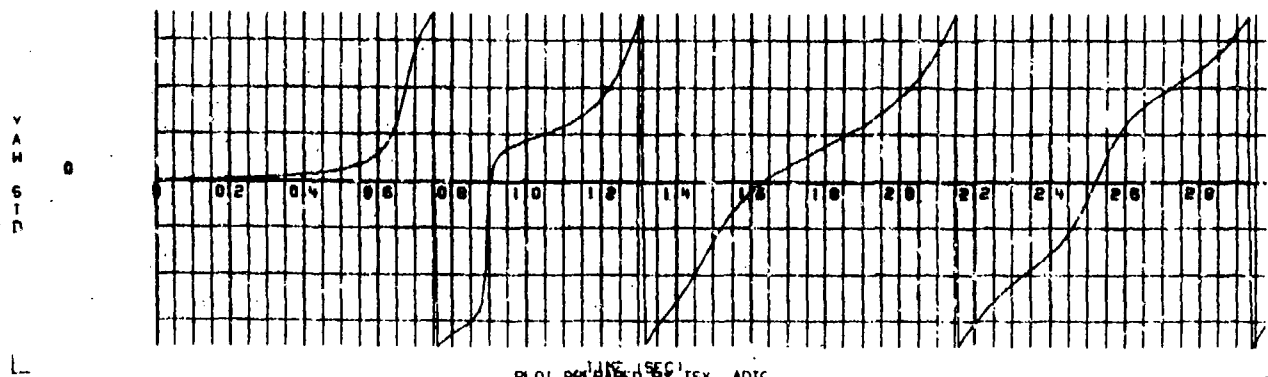
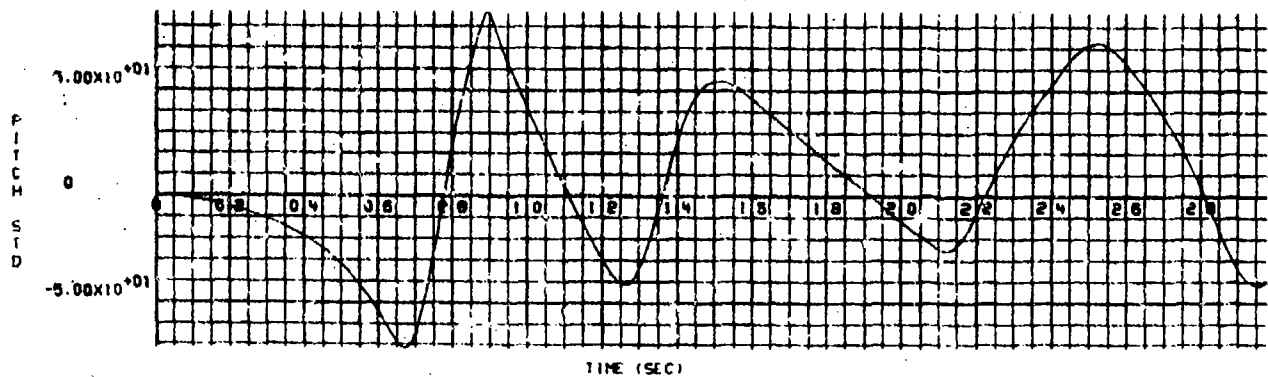
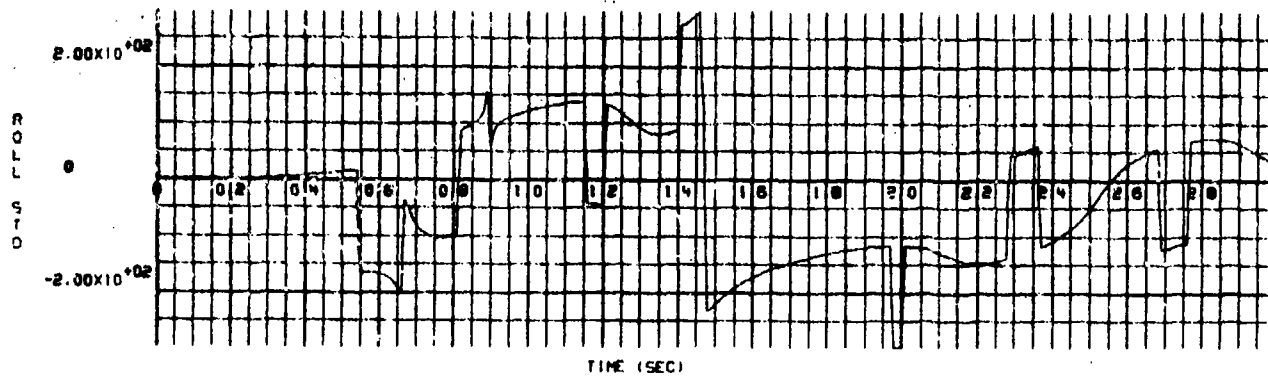
PLOT PREPARED BY TSX, ADIC

Figure P-5. X, Y, and Z Position Versus Time for a Flow Field Intensity of 2

16/12/75

R552

71 71



11/11/75  
PLOT PREPARED BY TSX, ADTC

Figure P-6.  $\phi$ ,  $\theta$ , and  $\psi$  Rotation Versus Time for a Flow Field Intensity of 2

16-12/75  
0

1152  
90 80

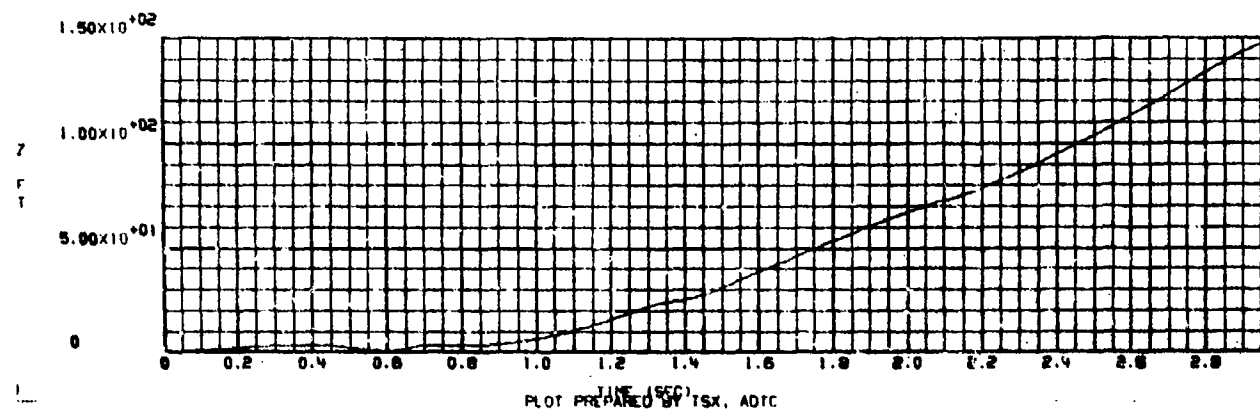
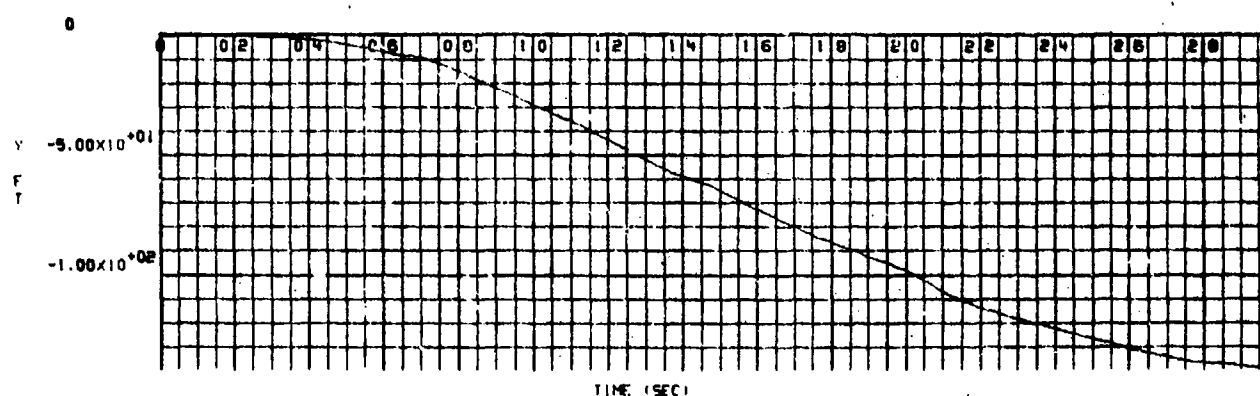
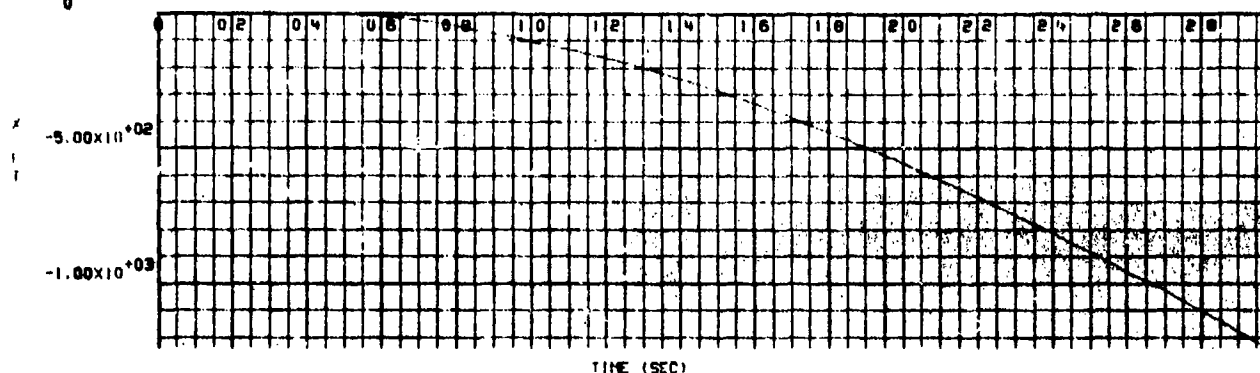


Figure P-7. X, Y, and Z Position Versus Time for a Flow Field Intensity of  $-1/2$



18/12/75

Revised

79

79

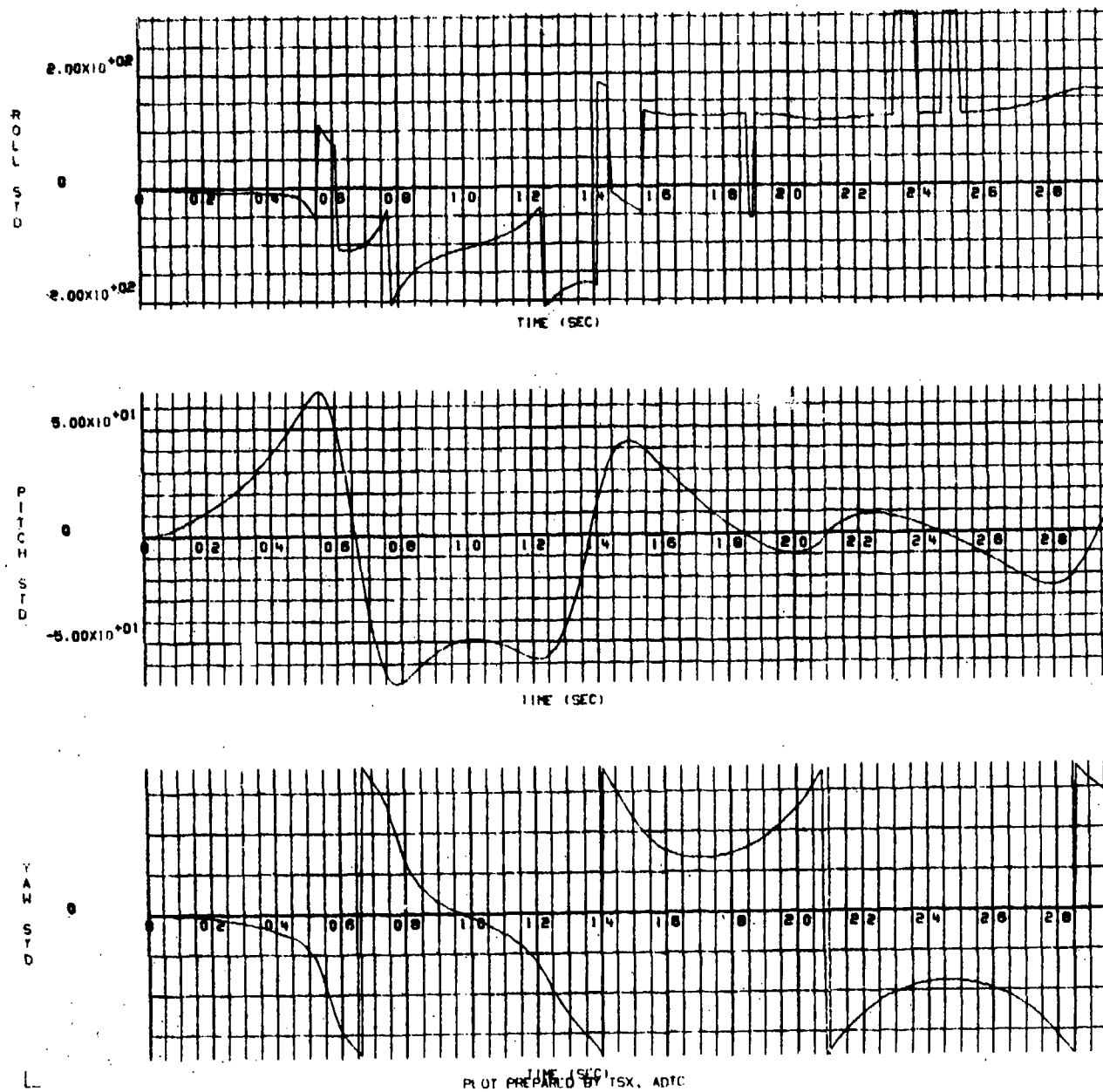


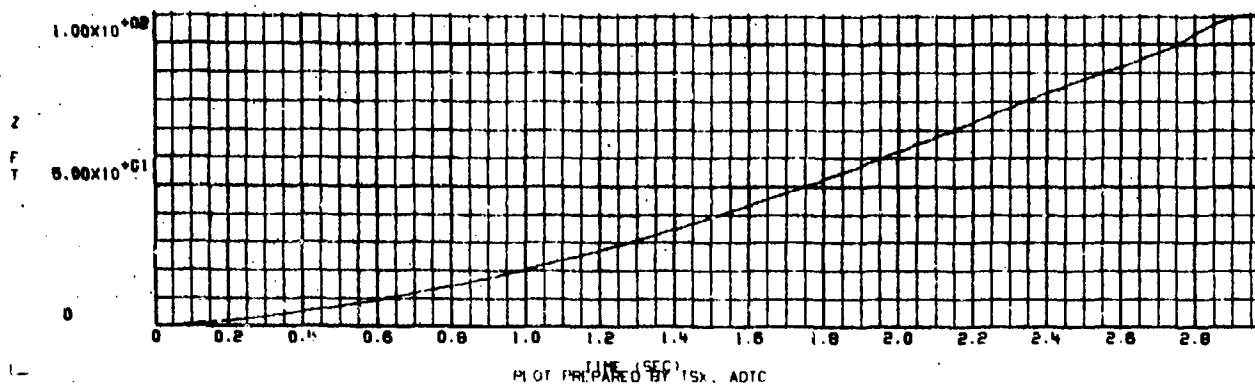
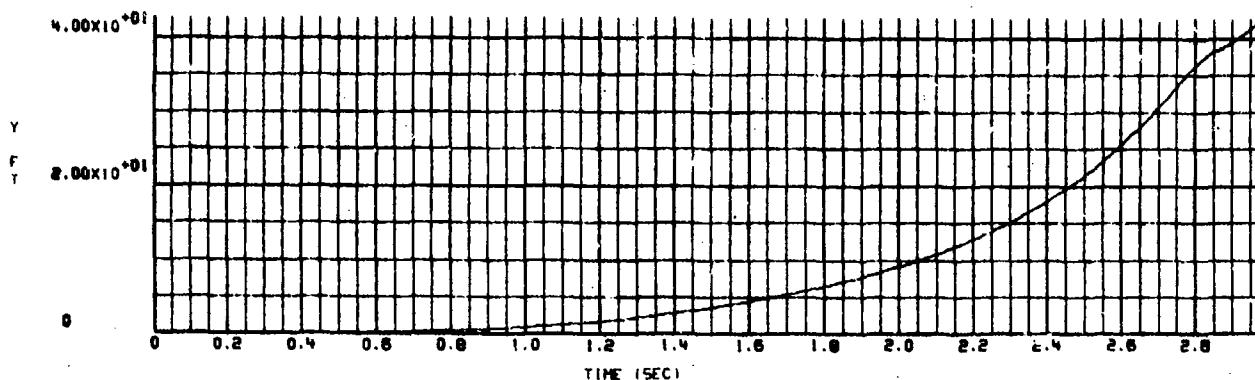
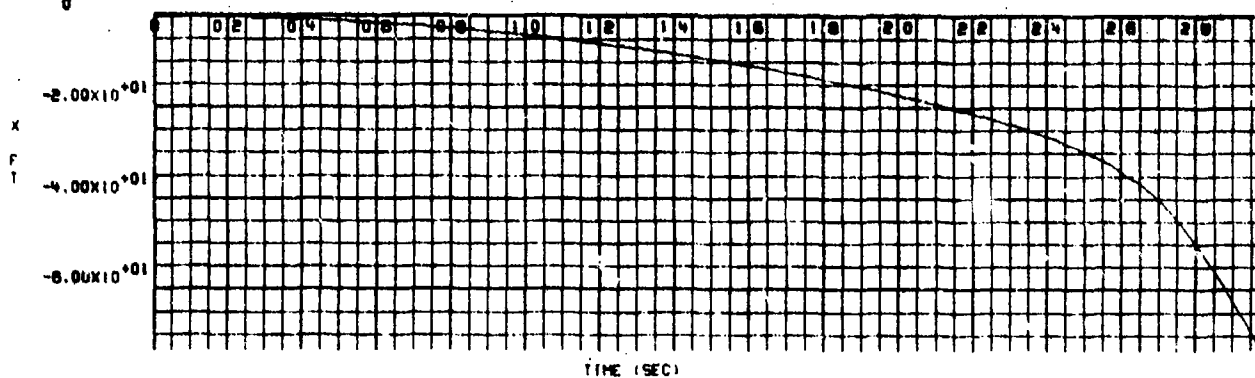
Figure P-8.  $\phi$ ,  $\theta$ , and  $\psi$  Rotation Versus Time for a Flow Field Intensity of  $-1/2$

APPENDIX Q

GBU-10 BOMB TRAJECTORIES RESULTING FROM A  
(-3/-3) ORIFICE COMBINATION AT MACH 0.7

15/12/75  
0

R638



TIME (SEC)  
PLOT PREPARED BY TSX, ADTC

Figure Q-1. X, Y, and Z Position Versus Time for a Flow Field Intensity of 1/2

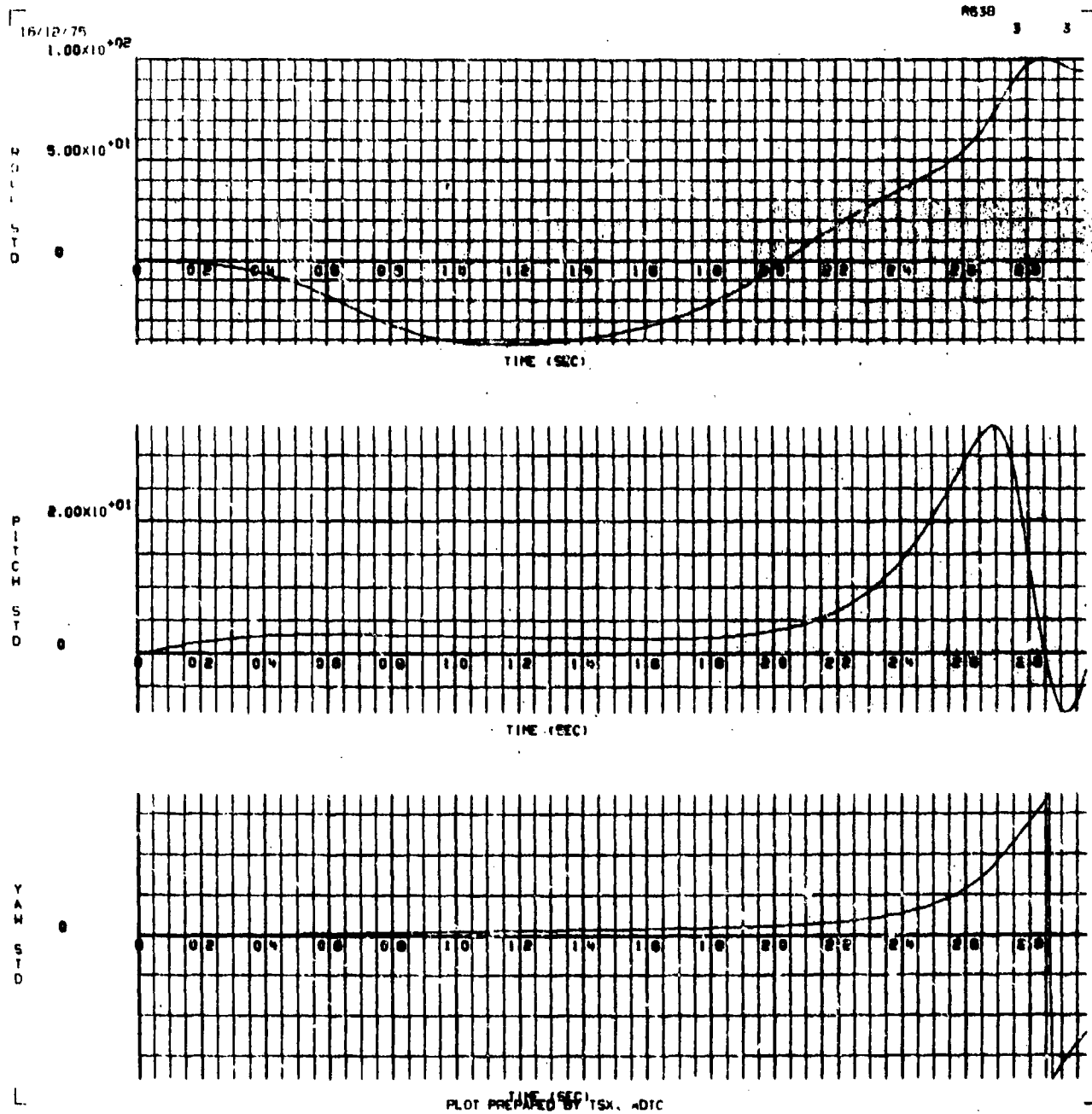


Figure Q-2.  $\phi$ ,  $\theta$ , and  $\psi$  Rotation Versus Time for a Flow Field Intensity of 1/2

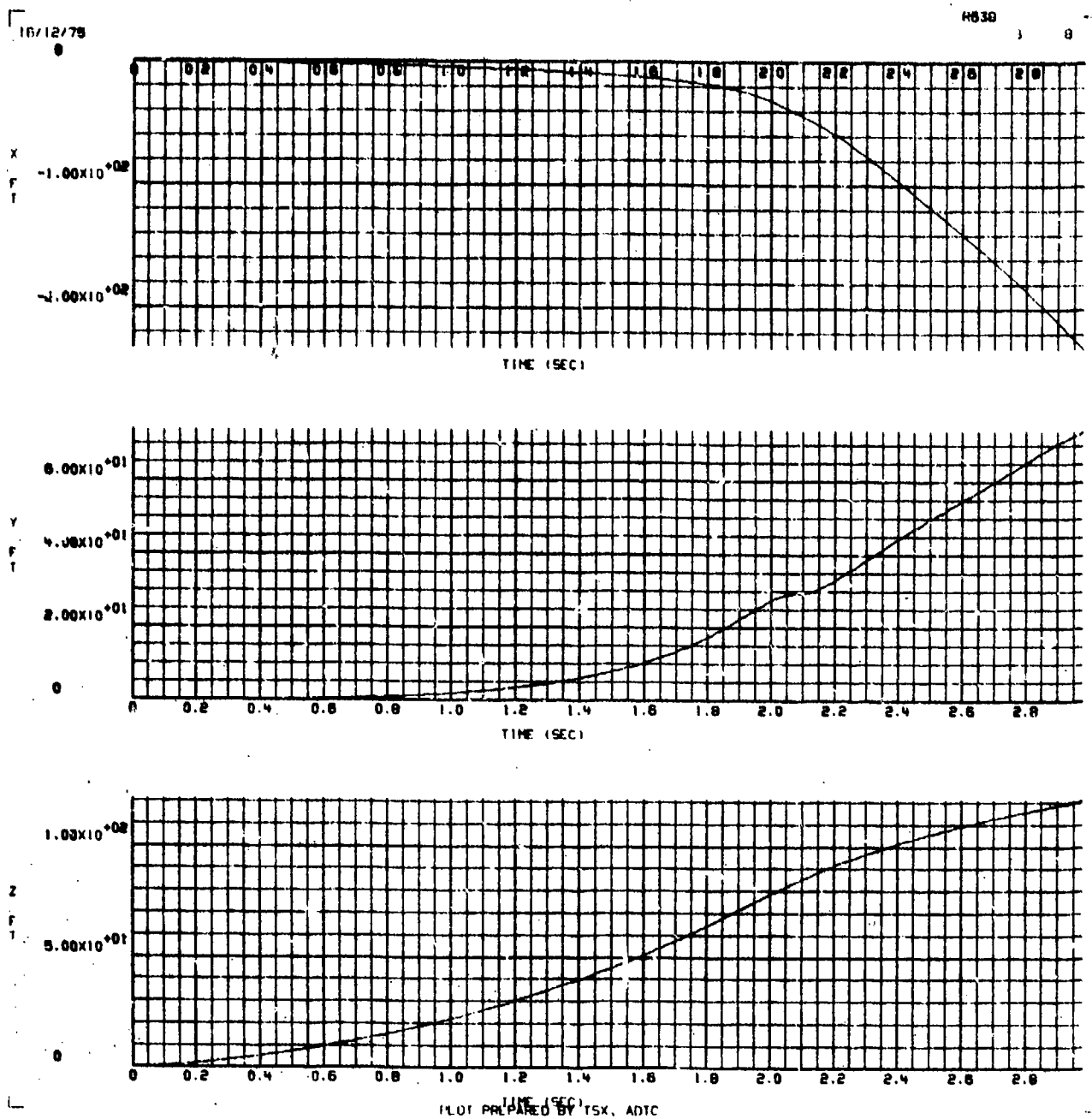


Figure Q-3. X, Y, and Z Position Versus Time for a Flow Field Intensity of 1 (as measured in the wind tunnel)

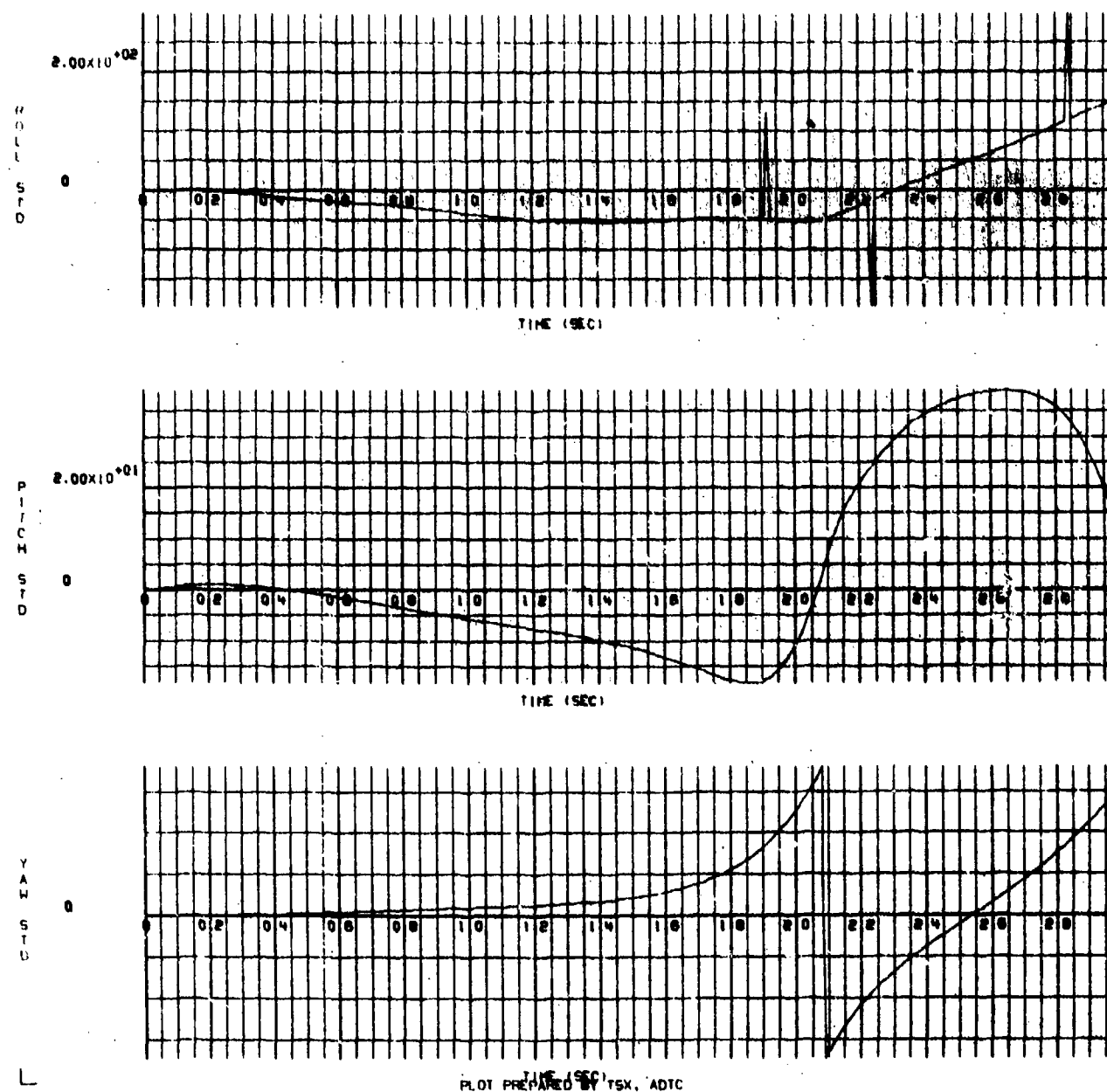
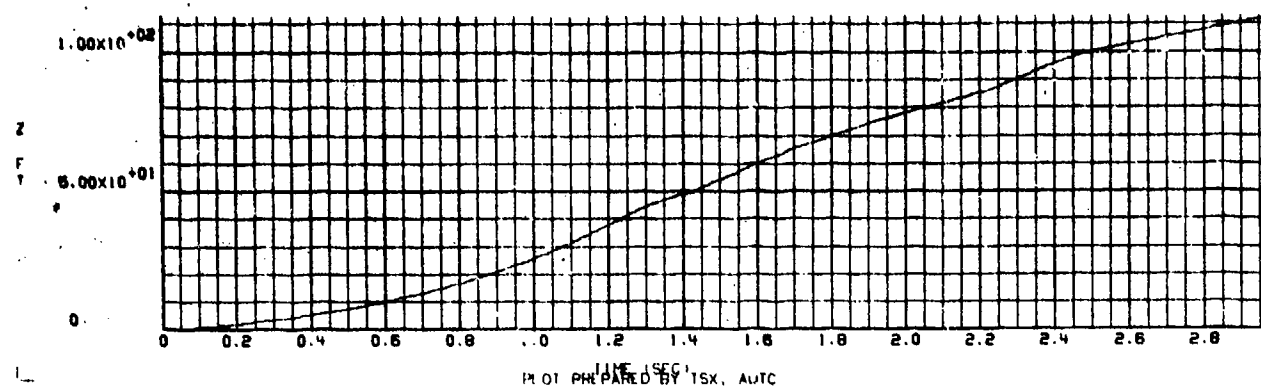
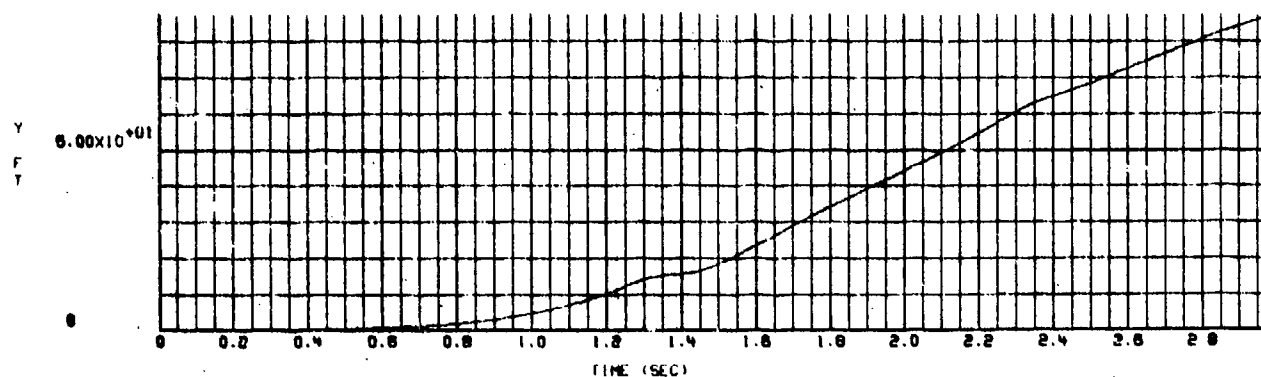
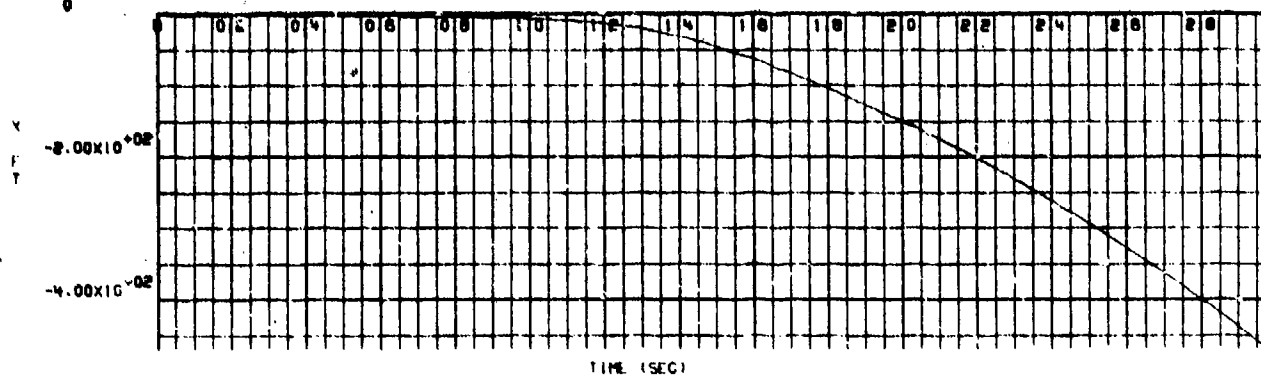


Figure Q-4.  $\phi$ ,  $\theta$ , and  $\psi$  Rotation Versus Time for a Flow Field Intensity of 1 (unchanged from the wind tunnel measured values)

16/12/75  
0

R638

1P 12

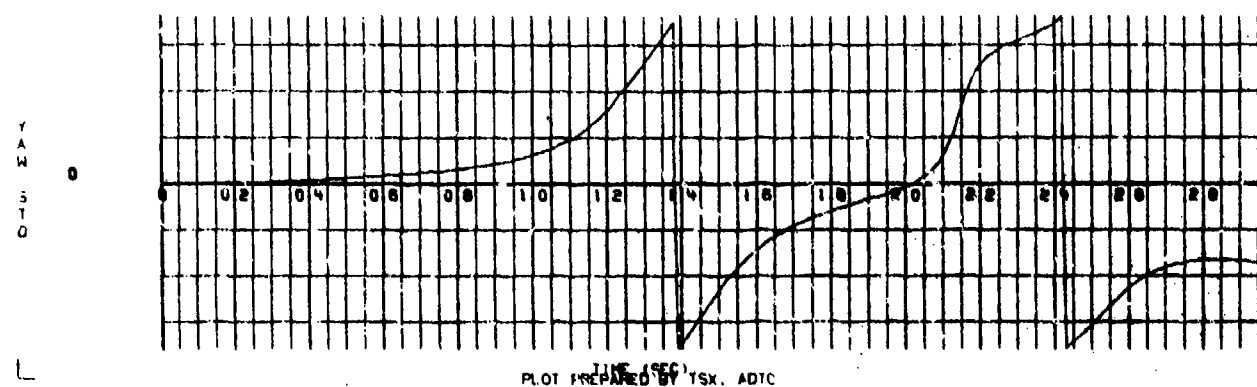
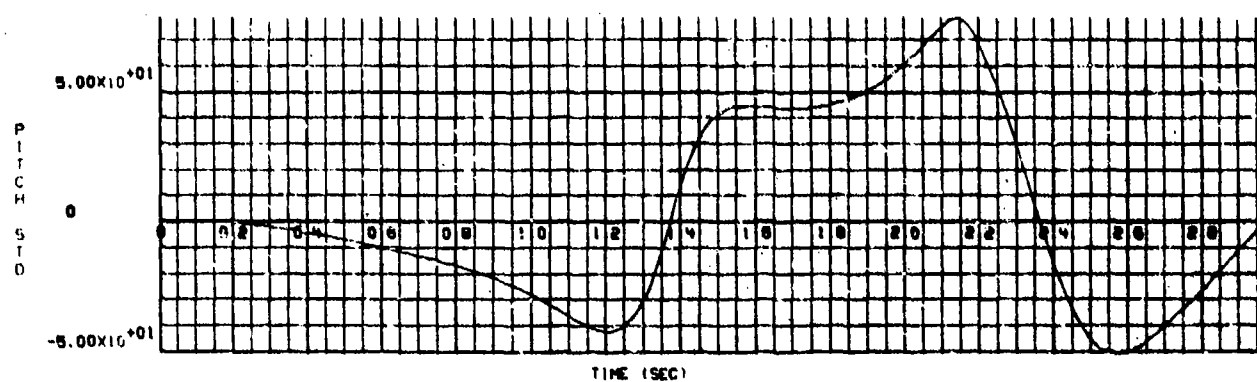
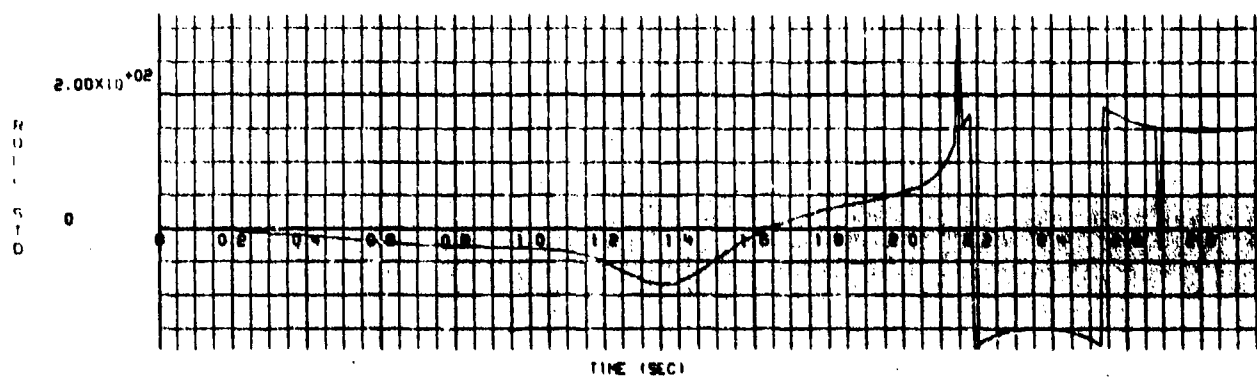


TIME (SEC)  
PLOT PREPARED BY TSX, AUTC

Figure Q-5. X, Y, and Z Position Versus Time for a Flow Field Intensity of 2

16-12-75

R638



PLOT PREPARED BY TSX, ADTC

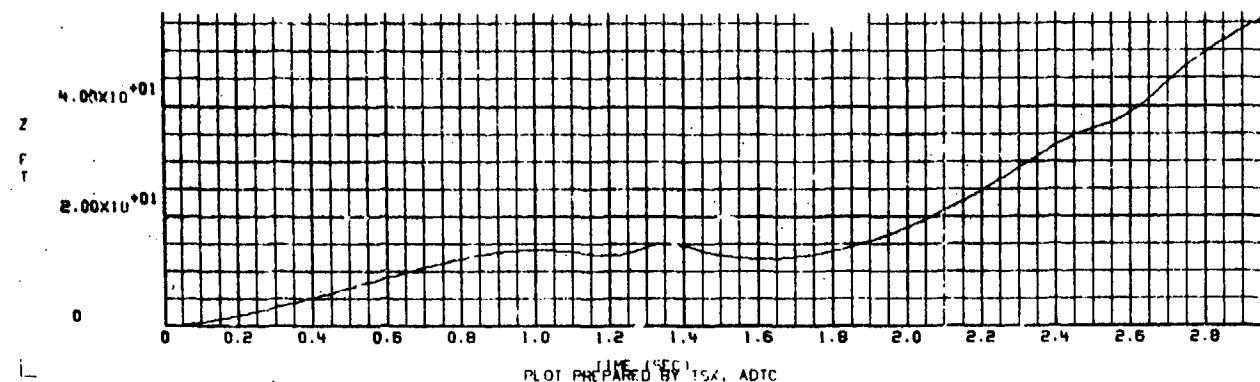
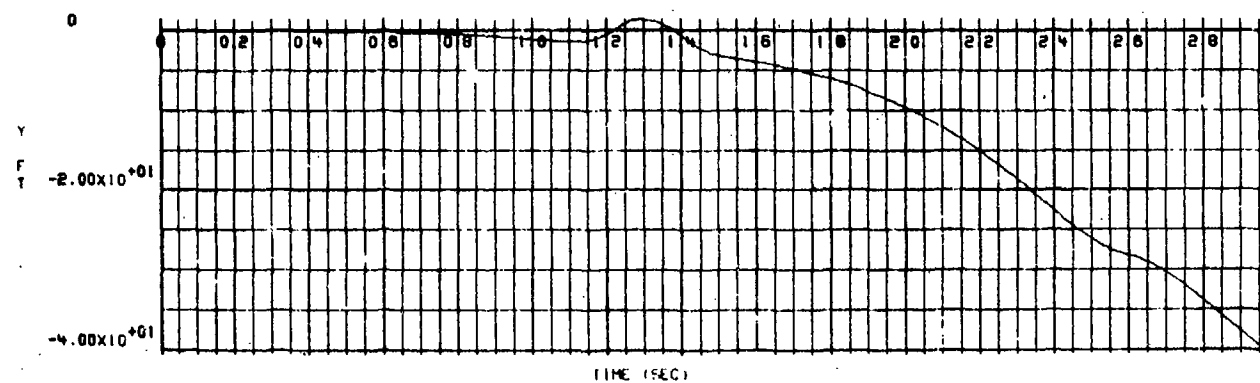
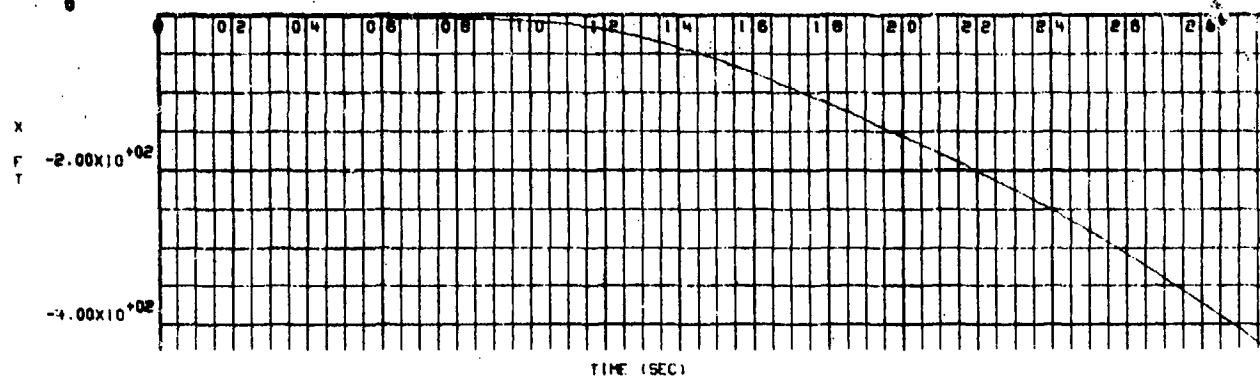
Figure Q-6.  $\phi$ ,  $\theta$ , and  $\psi$  Rotation Versus Time for a Flow Field Intensity of 2



16/12/75

H638

16 15



PLOT PREPARED BY 15A, ADTC

Figure Q-7. X, Y, and Z Position Versus Time for a Flow Field Intensity of  $-1/2$

10/12/75

R638

15 15

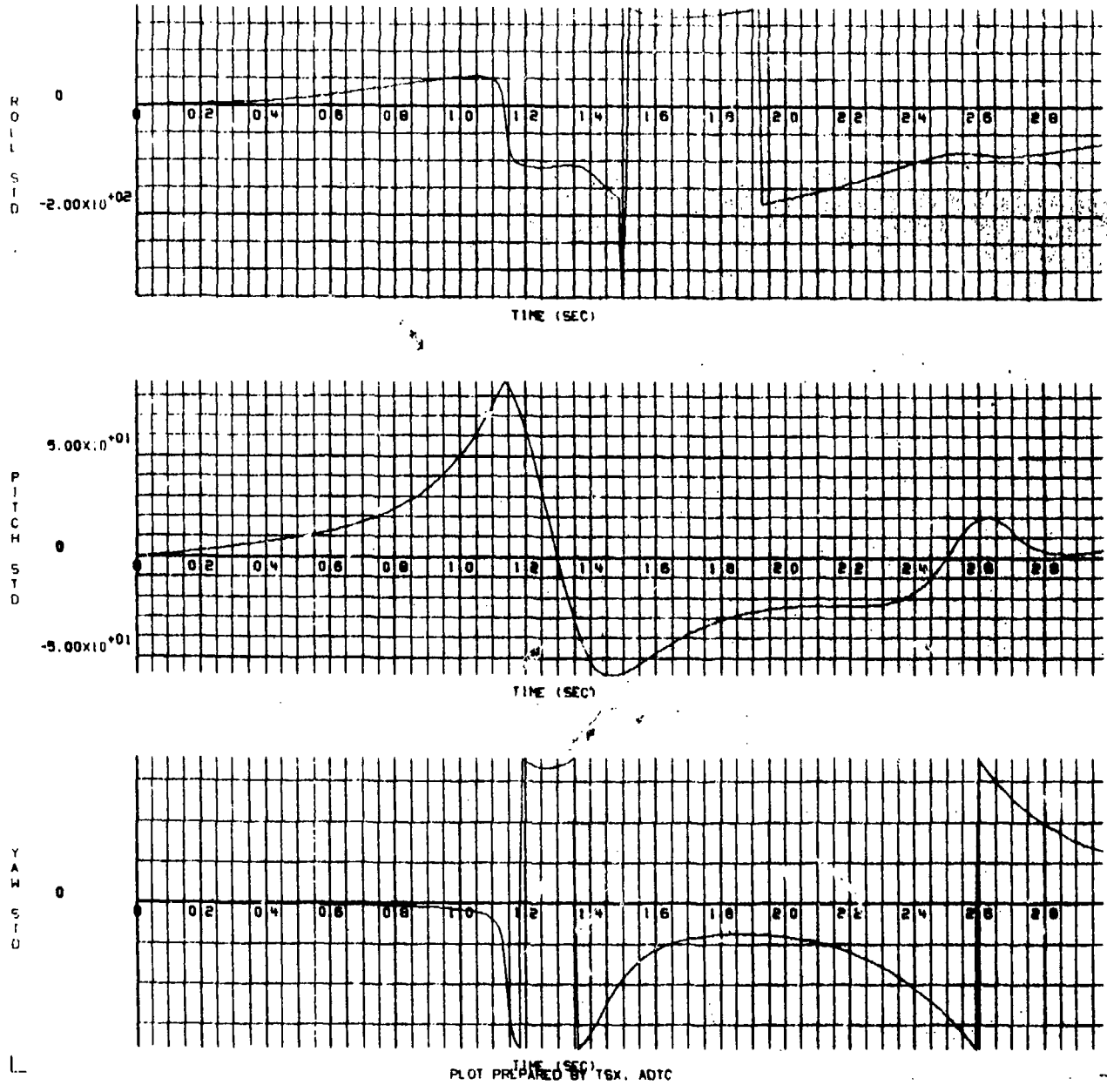


Figure Q-8.  $\phi$ ,  $\theta$ , and  $\psi$  Rotation Versus Time for a Flow Field Intensity of  $-1/2$

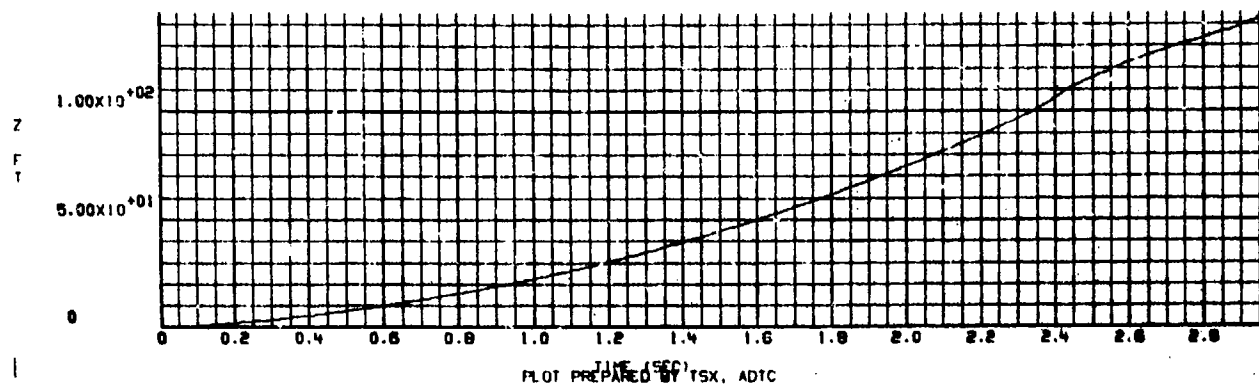
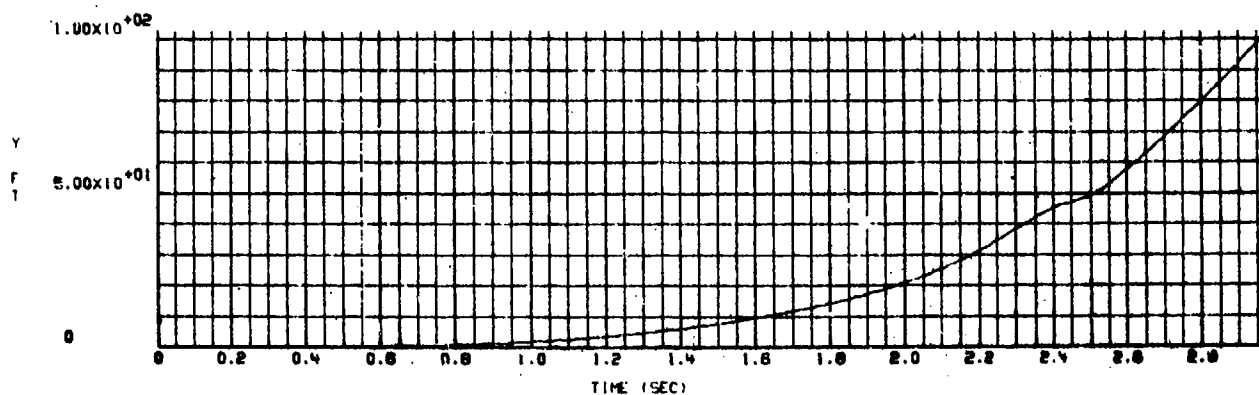
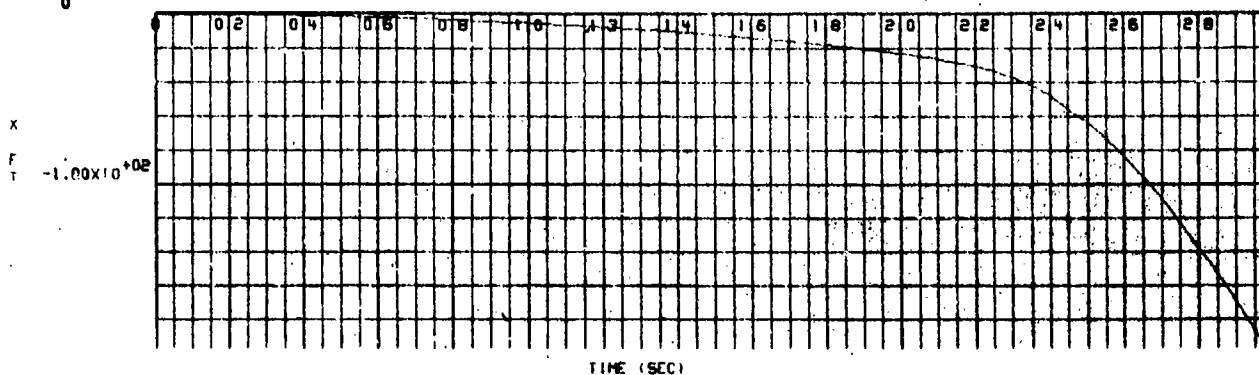
APPENDIX R

GBU-10 BOMB TRAJECTORIES RESULTING FROM A  
(-3/-3) ORIFICE COMBINATION AT MACH 0.85

16/12/75  
0

R638

24 24



PLOT PREPARED BY TSX, ADTC

Figure R-1. X, Y, and Z Position Versus Time for a Flow Field Intensity of 1/2

9638 23 23

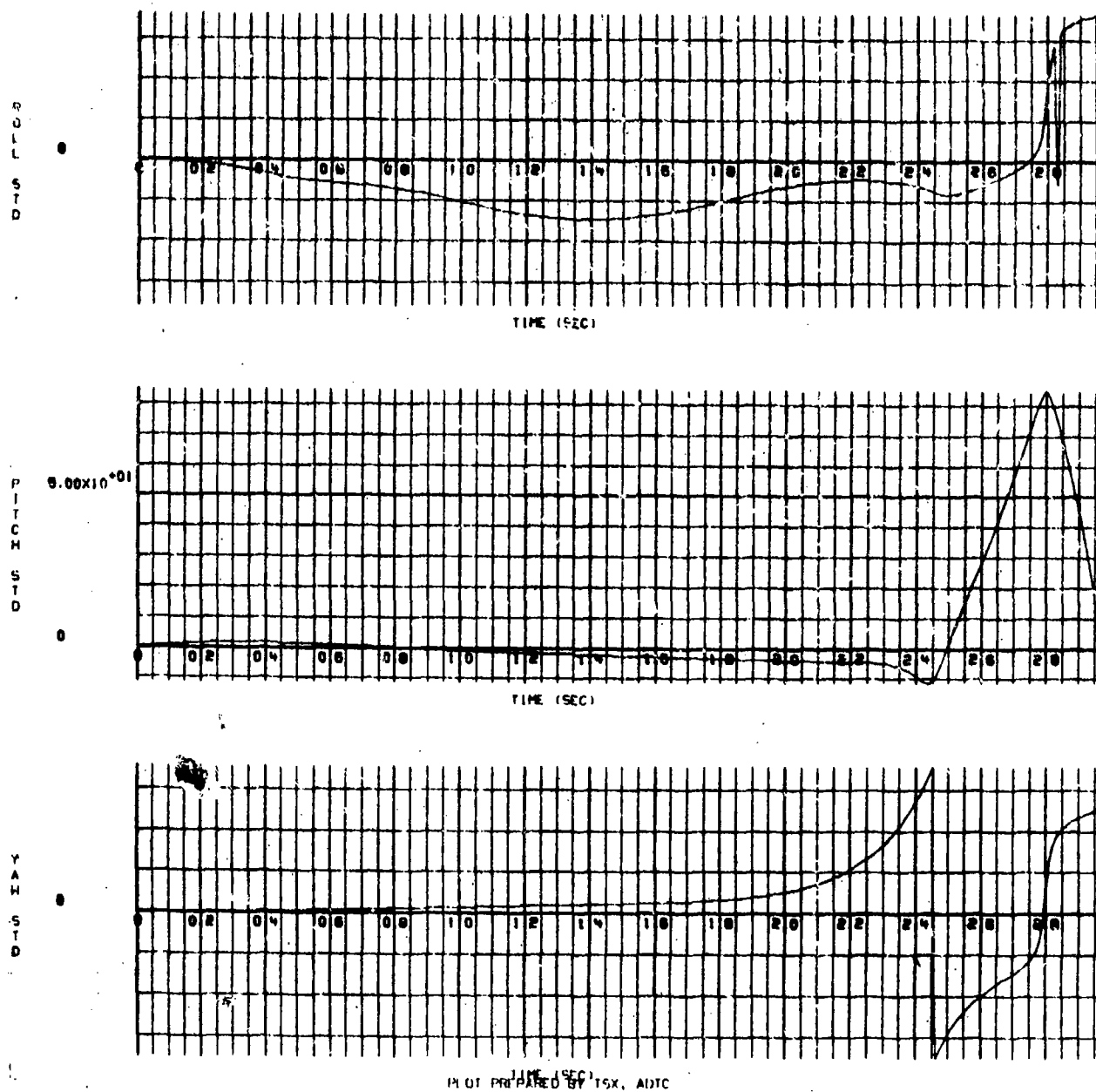
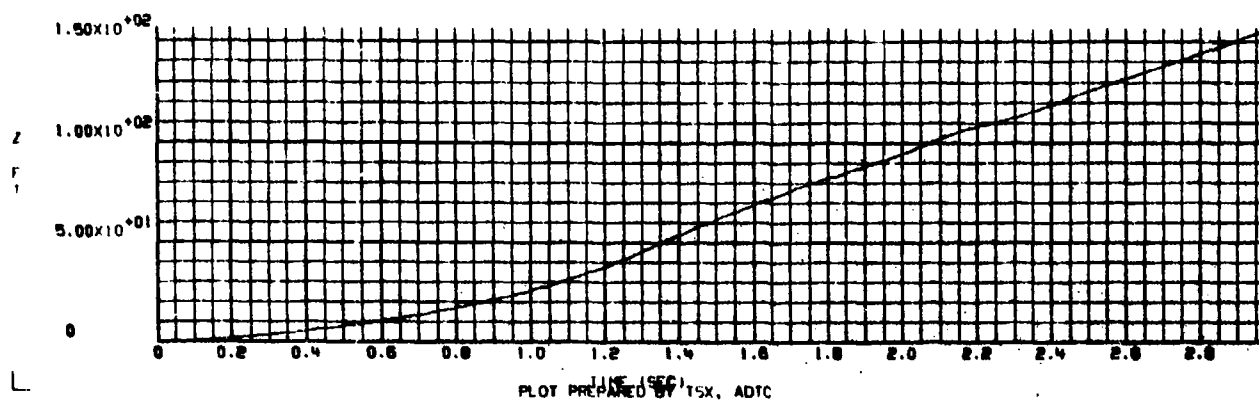
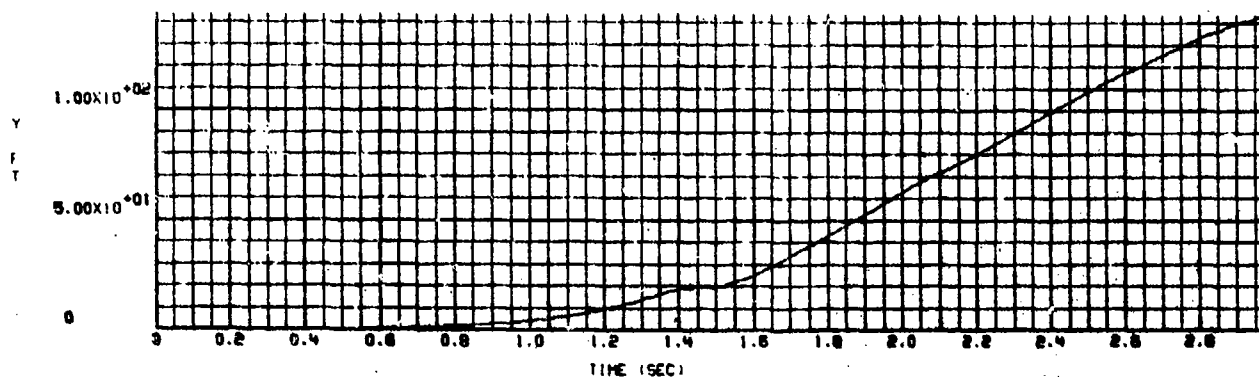
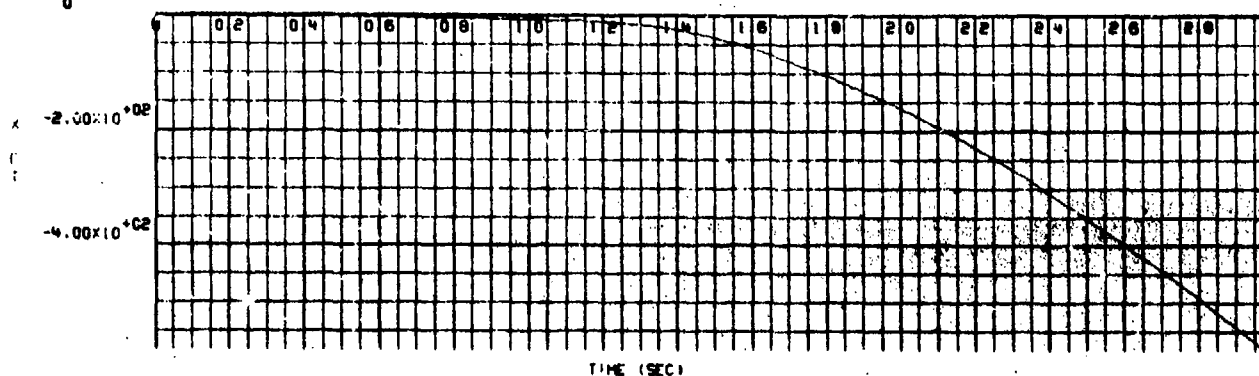


Figure R-2.  $\phi$ ,  $\theta$ , and  $\psi$  Rotation Versus Time for a Flow Field Intensity of  $1/2$

16/12/75  
0

R638  
P8 L8



PLOT PREPARED BY TSX, ADTC

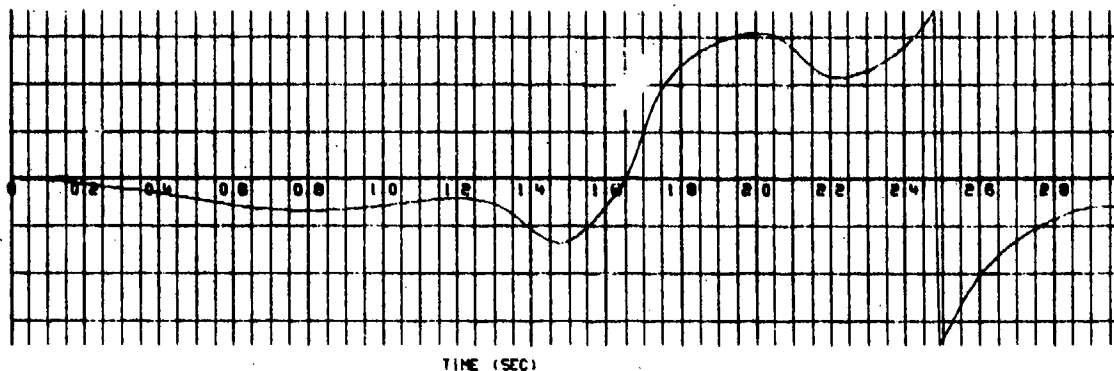
Figure R-3. X, Y, and Z Position Versus Time for a Flow Field Intensity of 1 (as measured in the wind tunnel)

18/12/75

R638

27 27

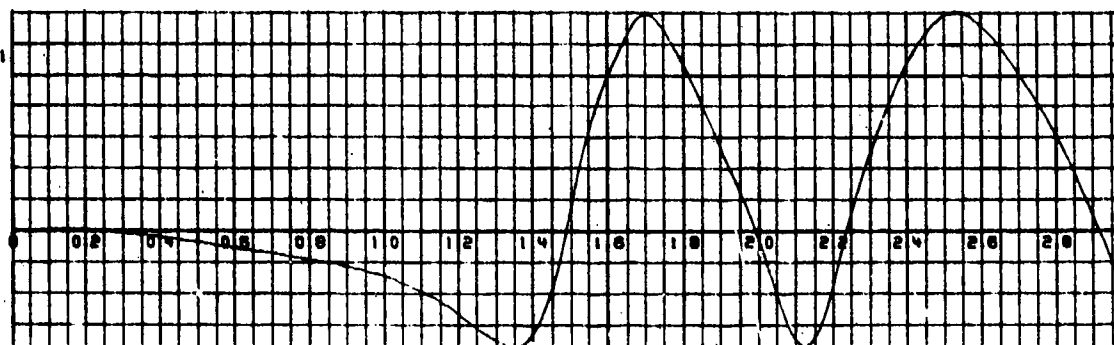
ROLL  
S  
I  
D  
E



TIME (SEC)

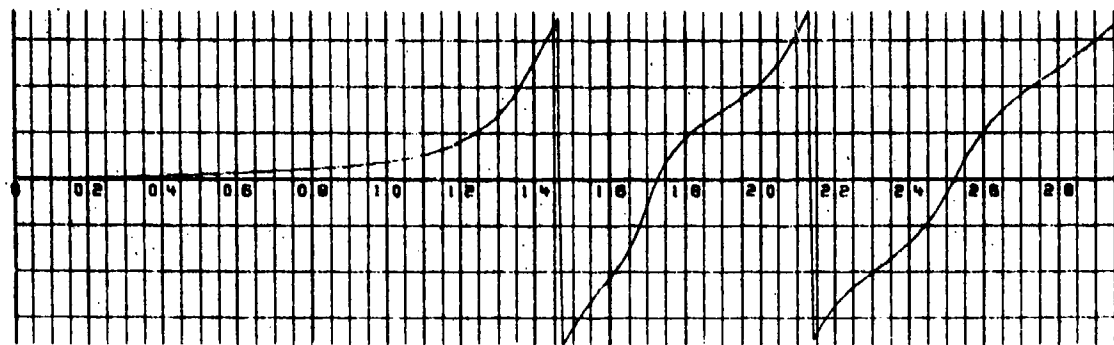
PITCH  
S  
I  
D  
E

$8.00 \times 10^{-01}$



TIME (SEC)

YAW  
S  
I  
D  
E



TIME (SEC)  
PLOT PREPARED BY ISX, ADTC

Figure R-4.  $\phi$ ,  $\theta$ , and  $\psi$  Rotation Versus Time for a Flow Field Intensity of 1 (unchanged from the wind tunnel measured values)

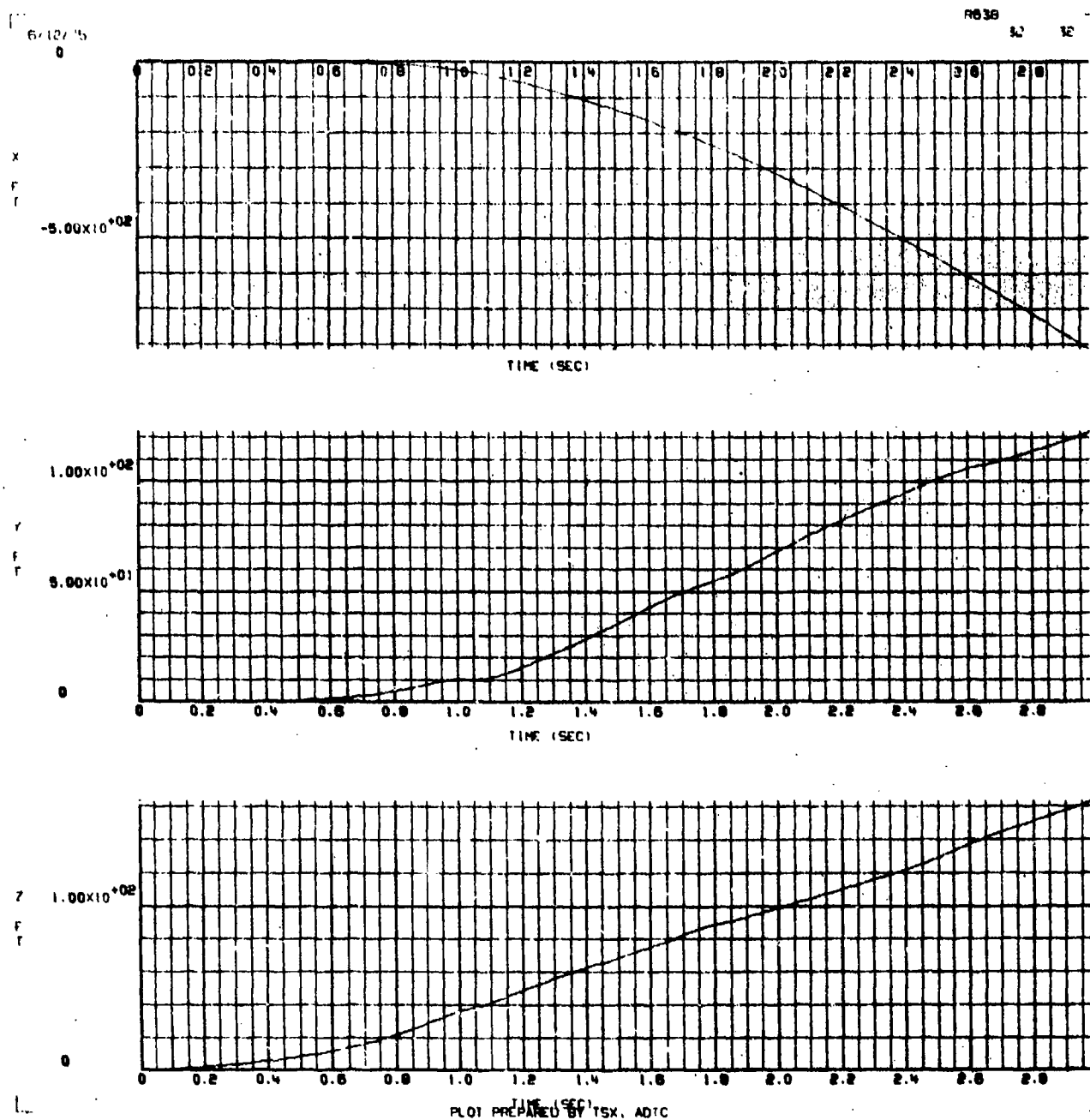


Figure R-5. X, Y, and Z Position Versus Time for a Flow Field Intensity of 2



18/12/73

RE 39

31

31

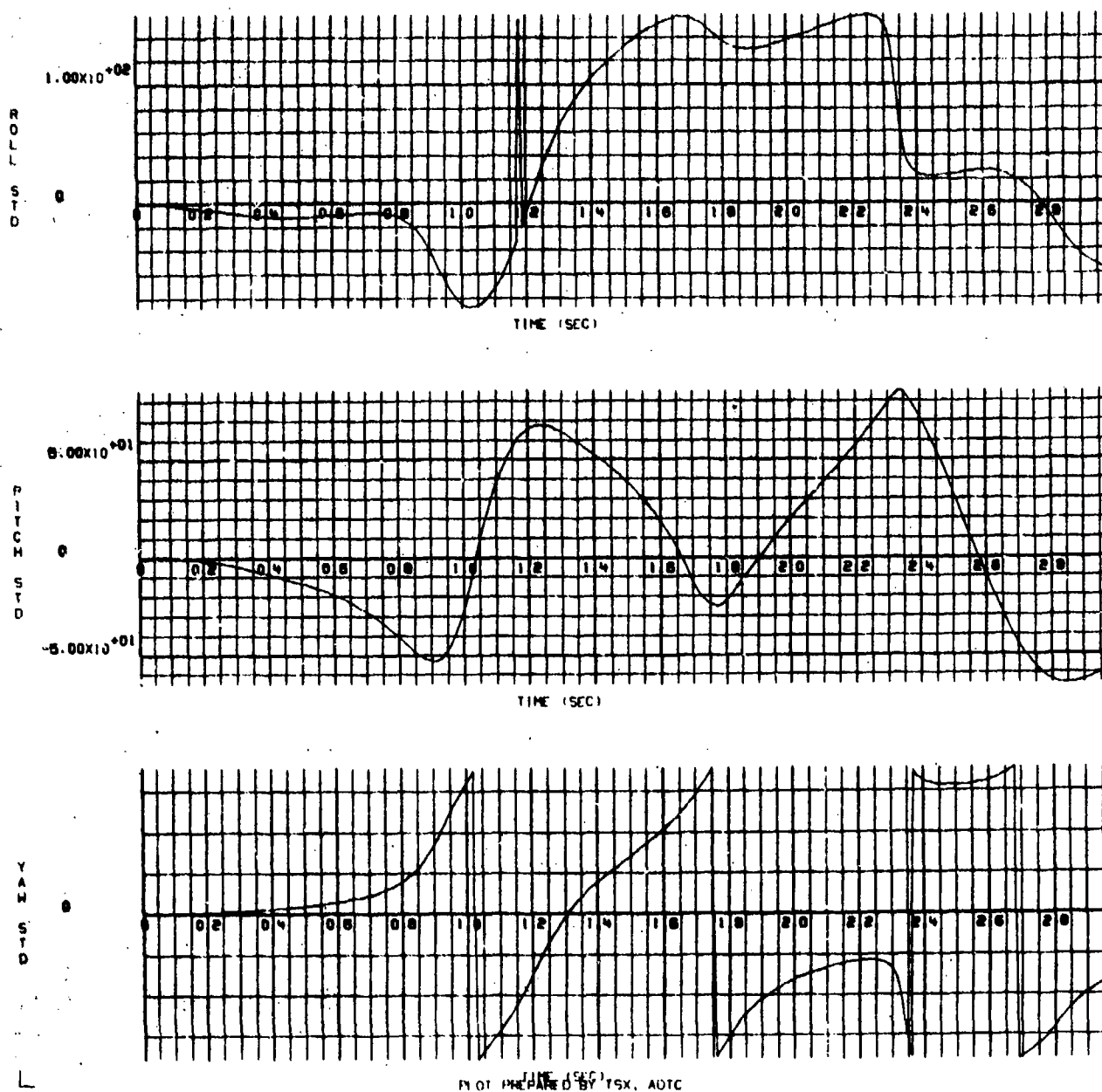


Figure R-6.  $\phi$ ,  $\theta$ , and  $\psi$  Rotation Versus Time for a Flow Field Intensity of 2

16/12/75  
0

8638 35 35

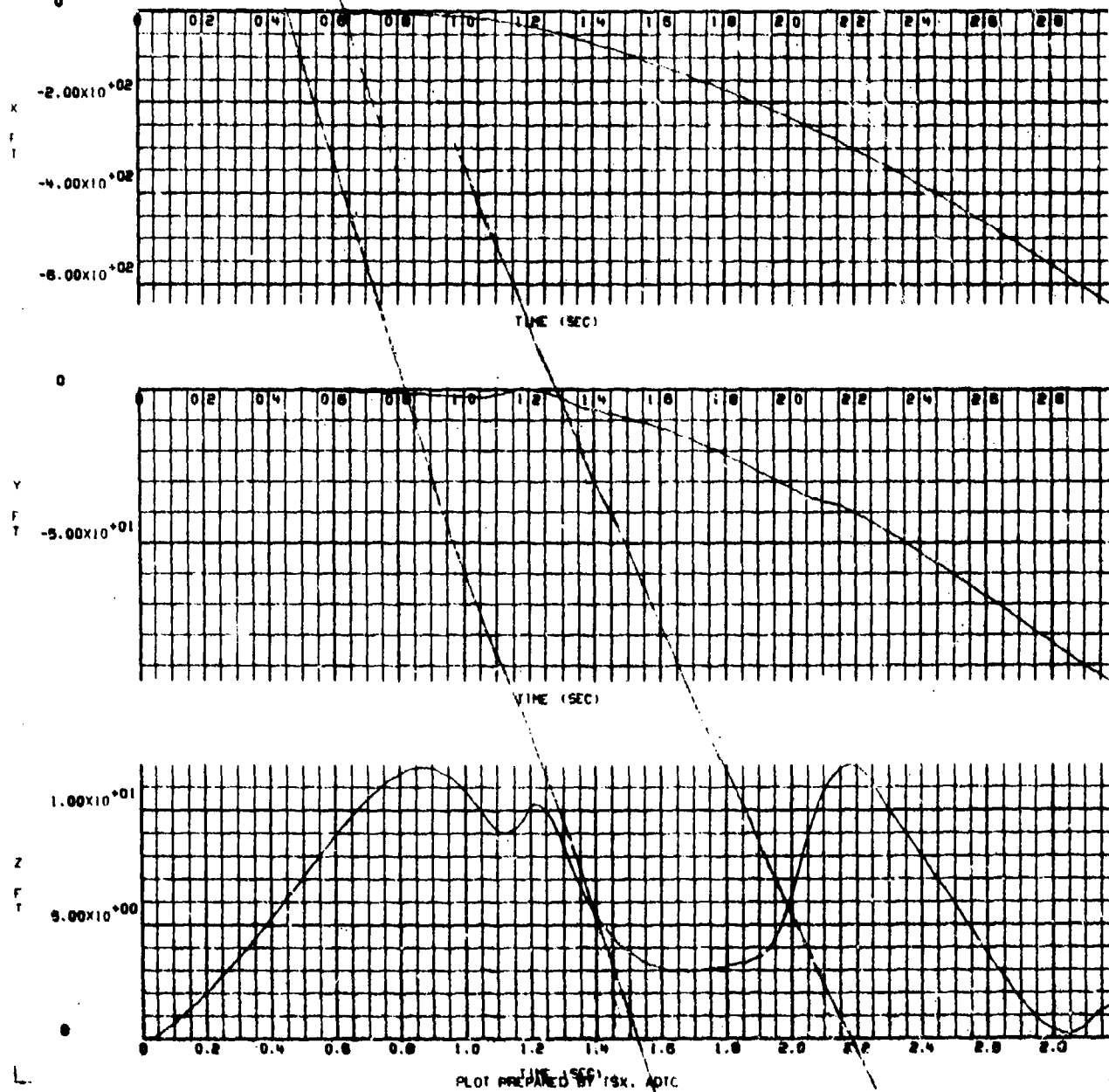


Figure R-7. X, Y, and Z Position Versus Time for a Flow Field Intensity of  $-1/2$

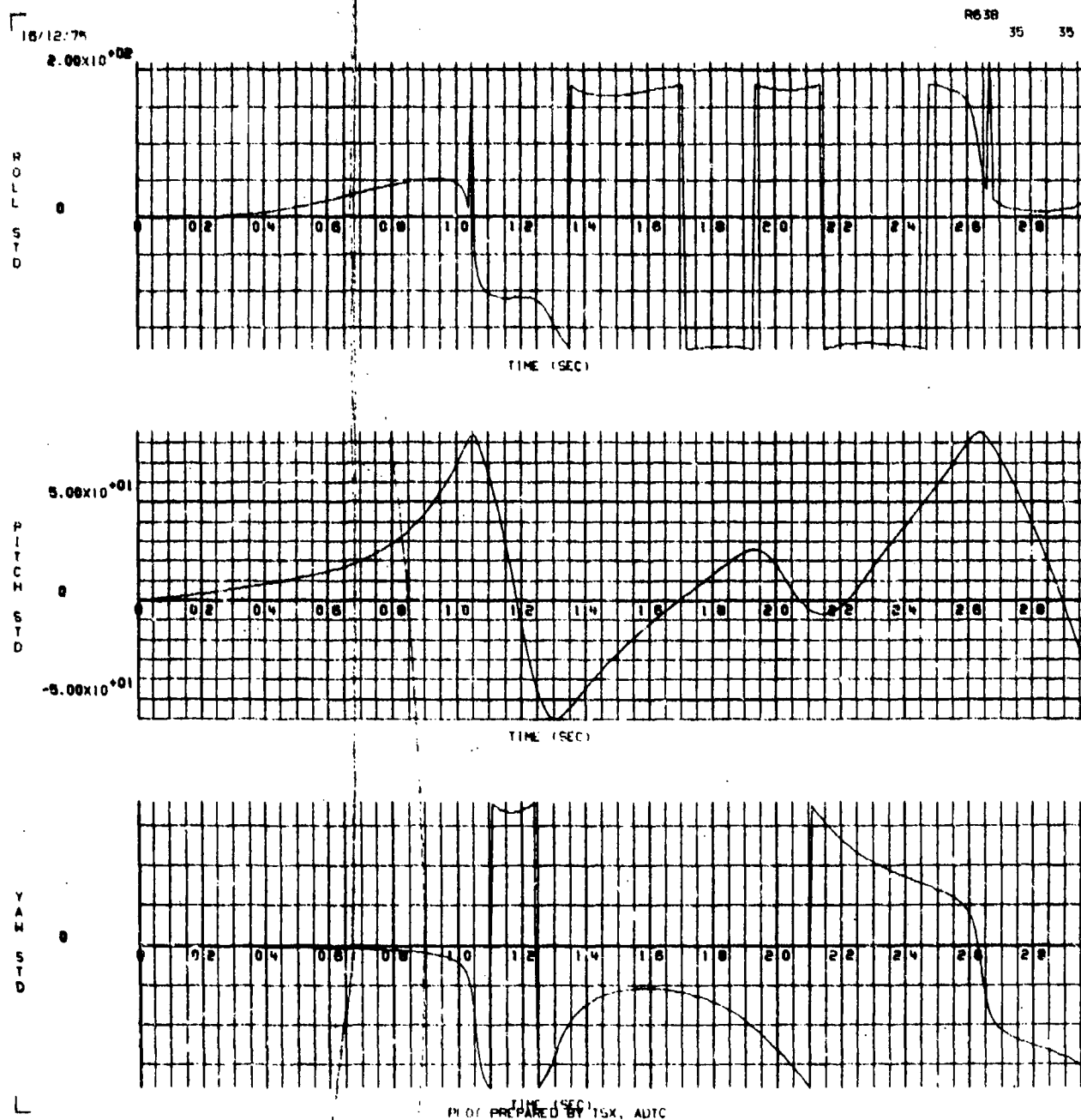


Figure R-8.  $\phi$ ,  $\theta$ , and  $\psi$  Rotation Versus Time for a Flow Field Intensity of  $-1/2$

APPENDIX S

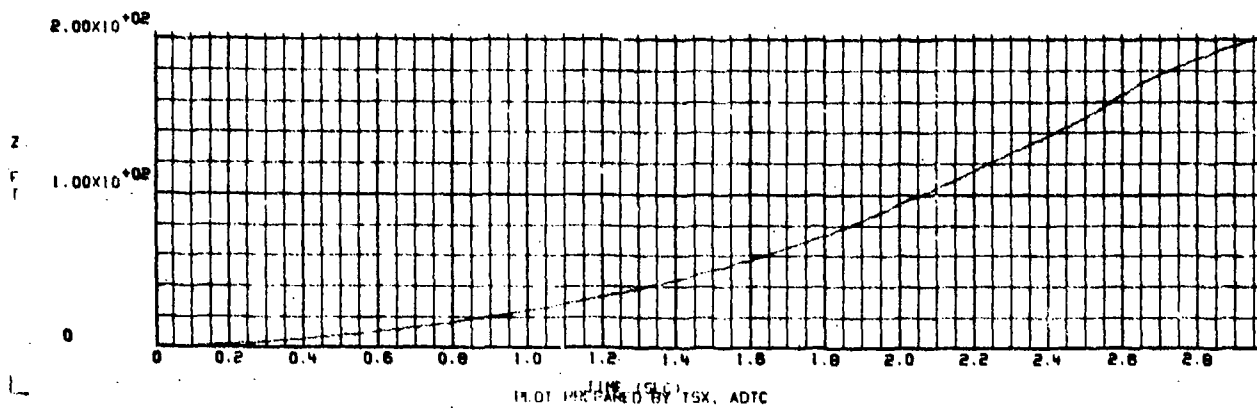
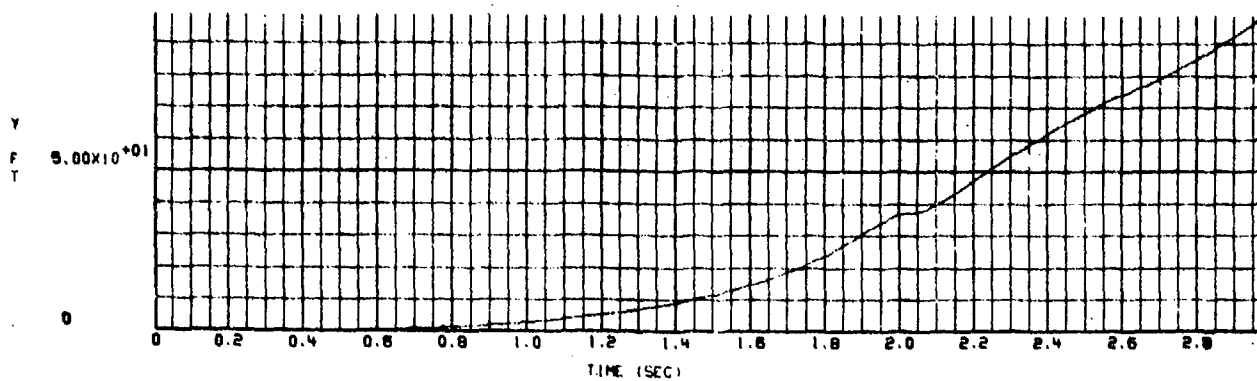
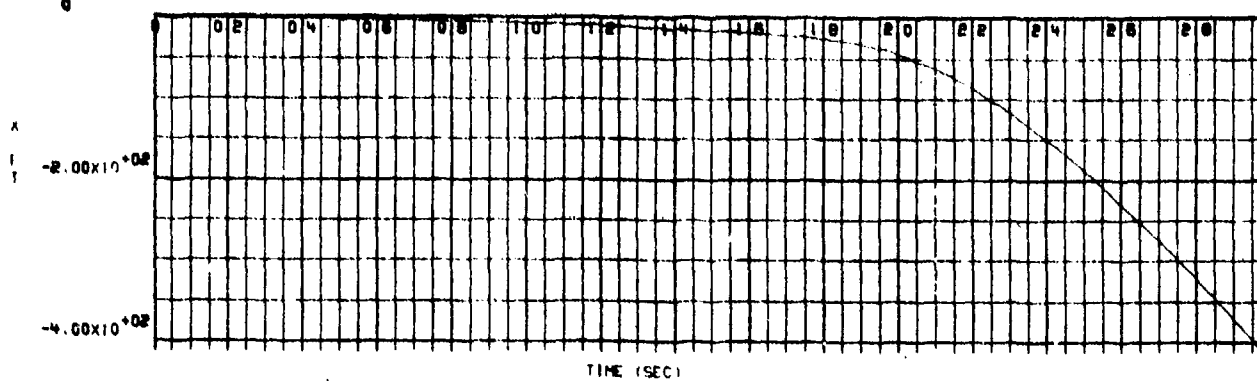
GBU-10 BOMB TRAJECTORIES RESULTING FROM A  
(-3/-3) ORIFICE COMBINATION AT MACH 0.95

18/12/75  
0

R63H

14

44



14.01 PREPARED BY TSX, ADTC

Figure S-1. X, Y, and Z Position Versus Time for a Flow Field Intensity of 1/2

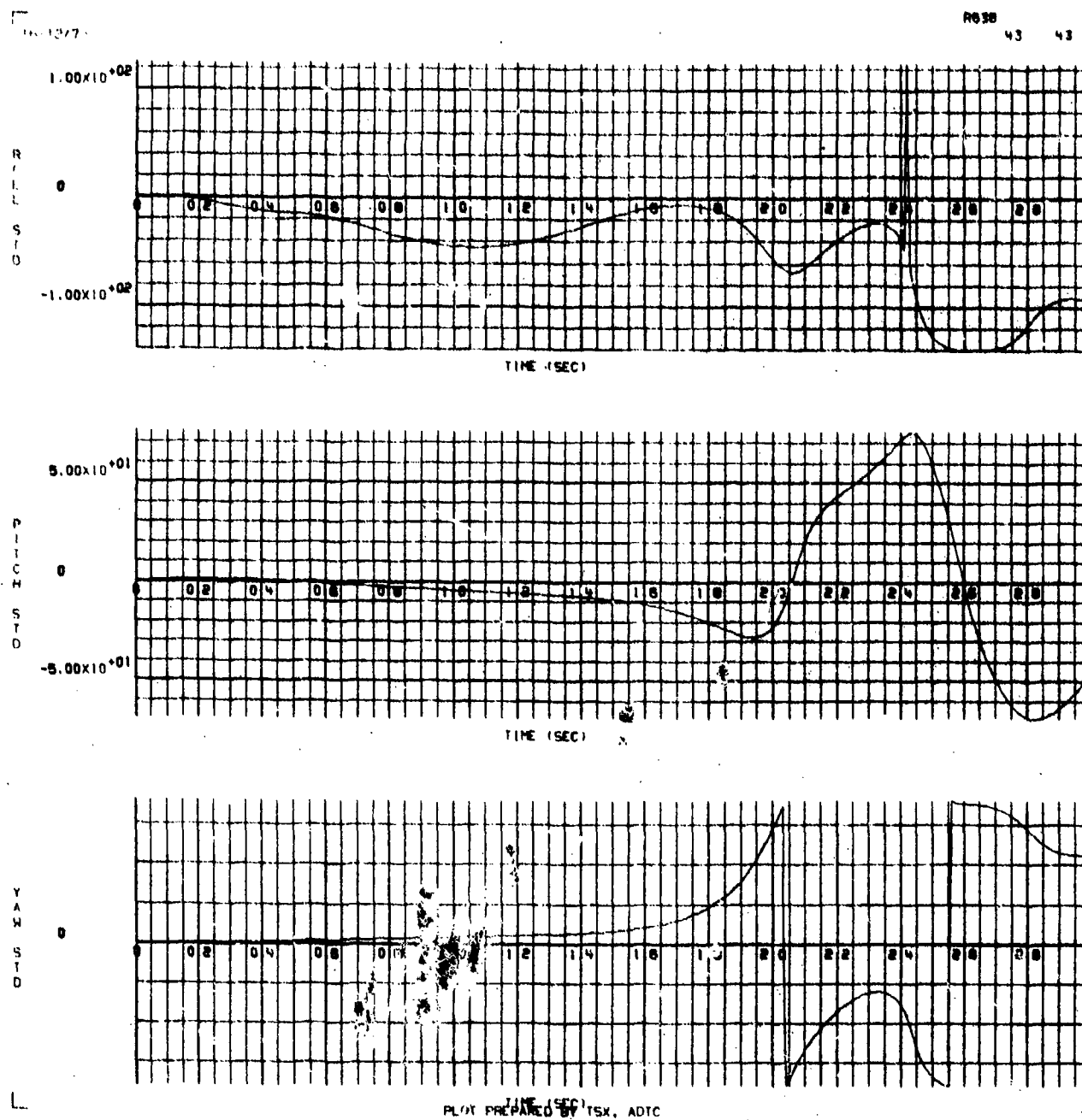


Figure S-2.  $\phi$ ,  $\theta$ , and  $\psi$  Rotation Versus Time for a Flow Field Intensity of  $1/2$

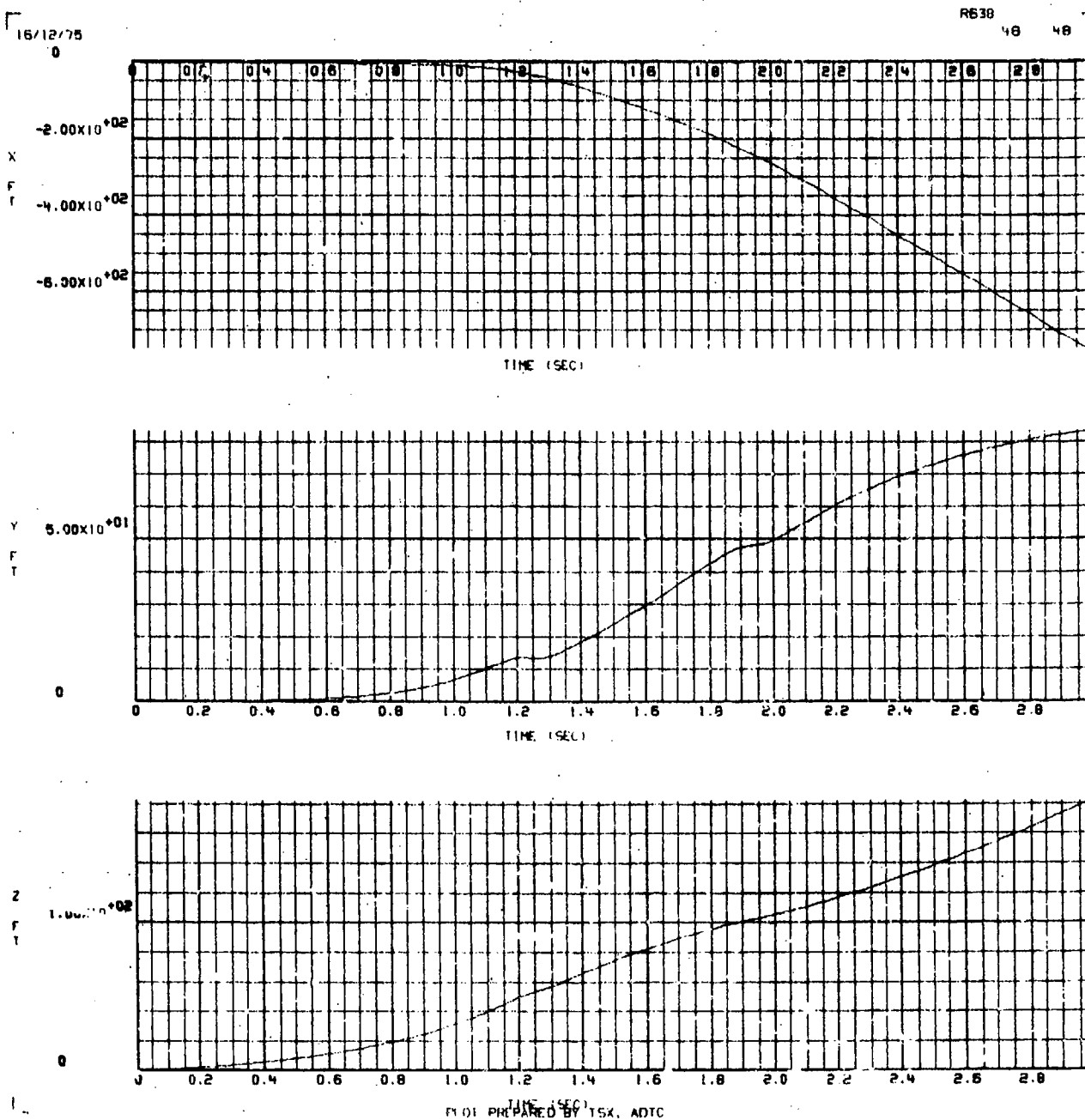


Figure S-3. X, Y, and Z Position Versus Time for a Flow Field Intensity of 1 (as measured in the wind tunnel)

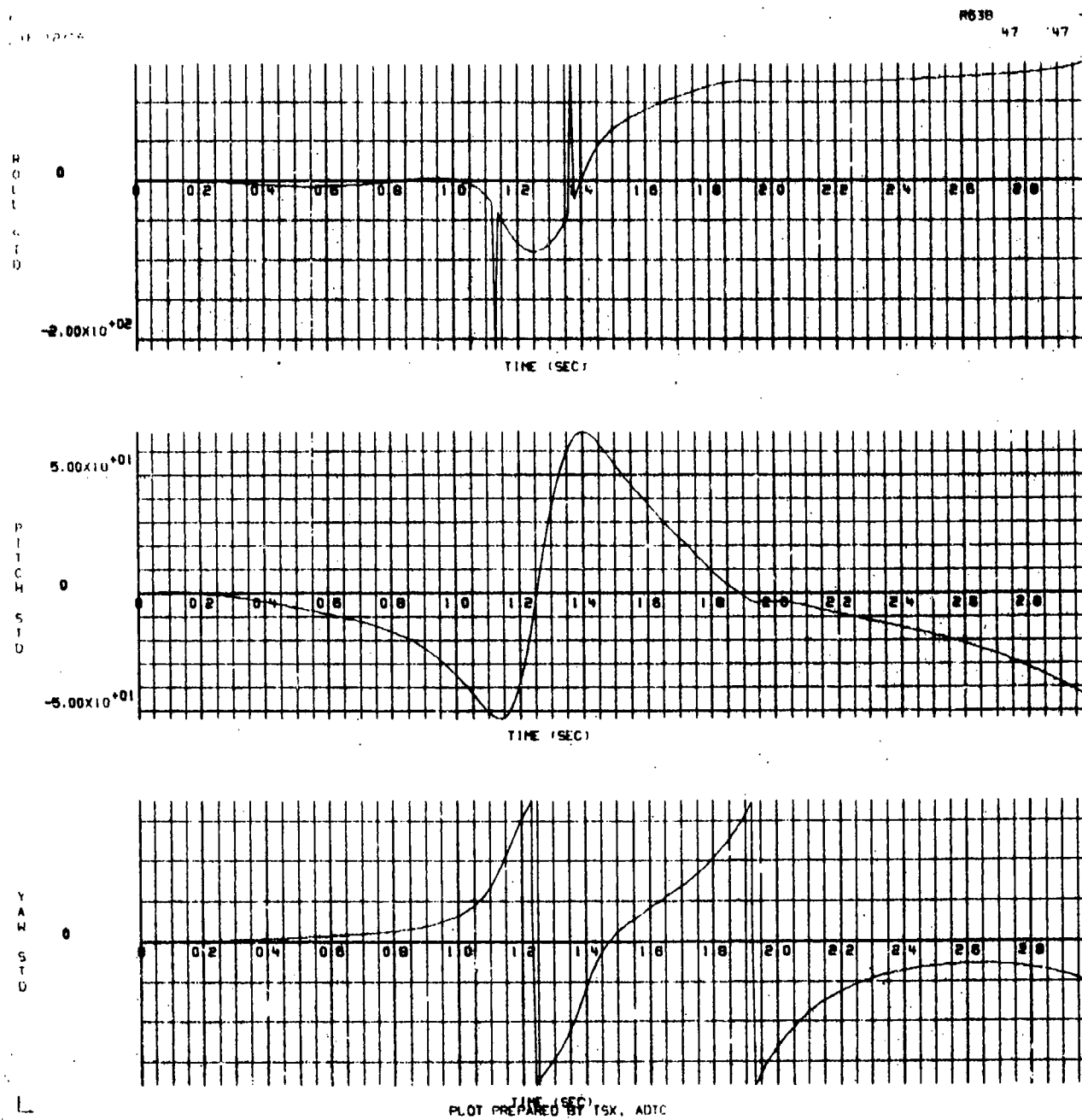


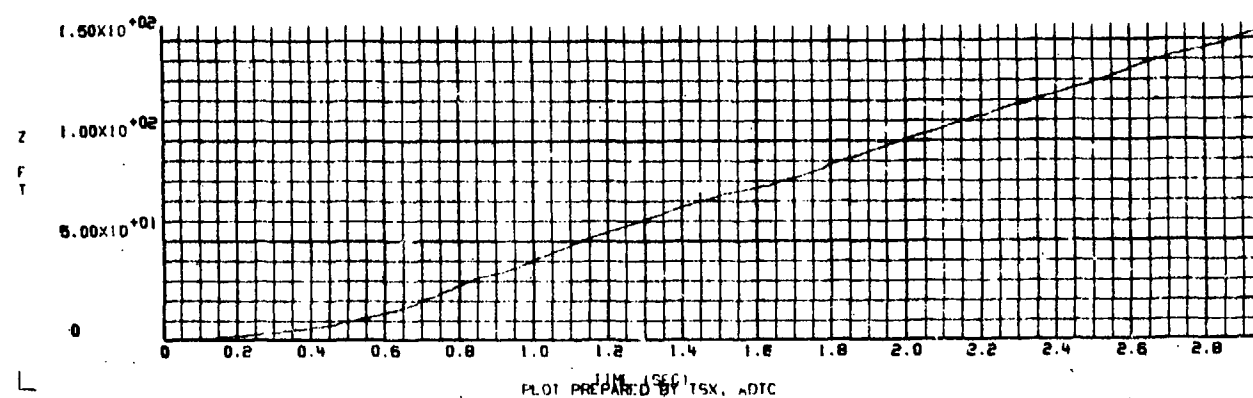
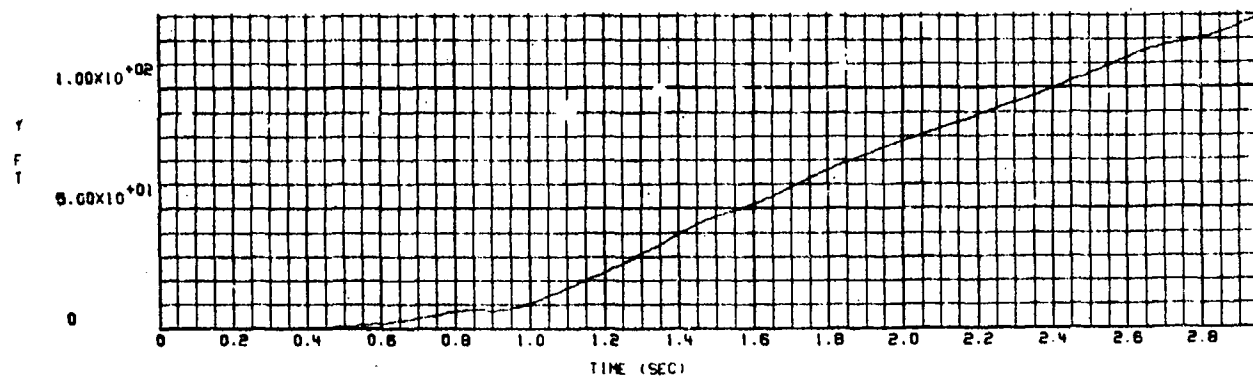
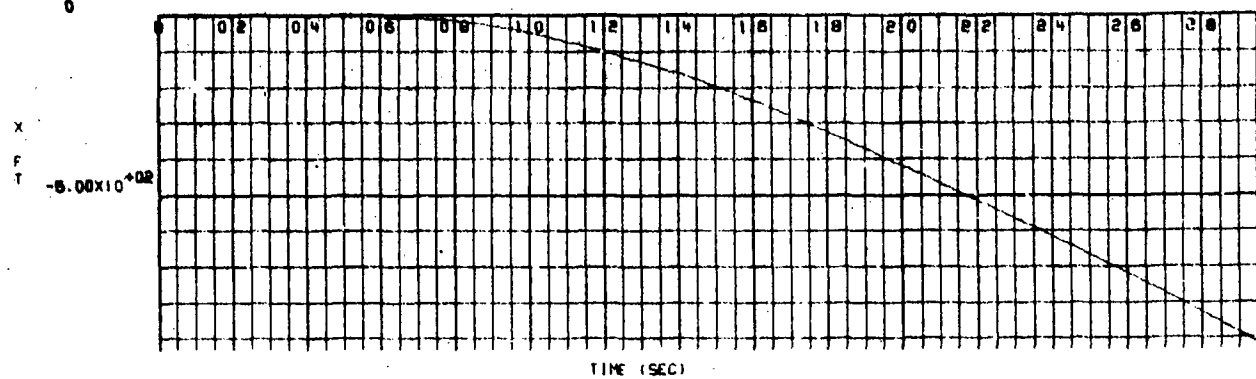
Figure S-4.  $\phi$ ,  $\theta$ , and  $\psi$  Rotation Versus Time for a Flow Field Intensity of 1 (unchanged from the wind tunnel measured values)



16/12/75  
0

R638

52 52



PLOT PREPARED BY TSX, ADIC

Figure S-5. X, Y, and Z Position Versus Time for a Flow Field Intensity of 2

16/12/75

R63A

51 51

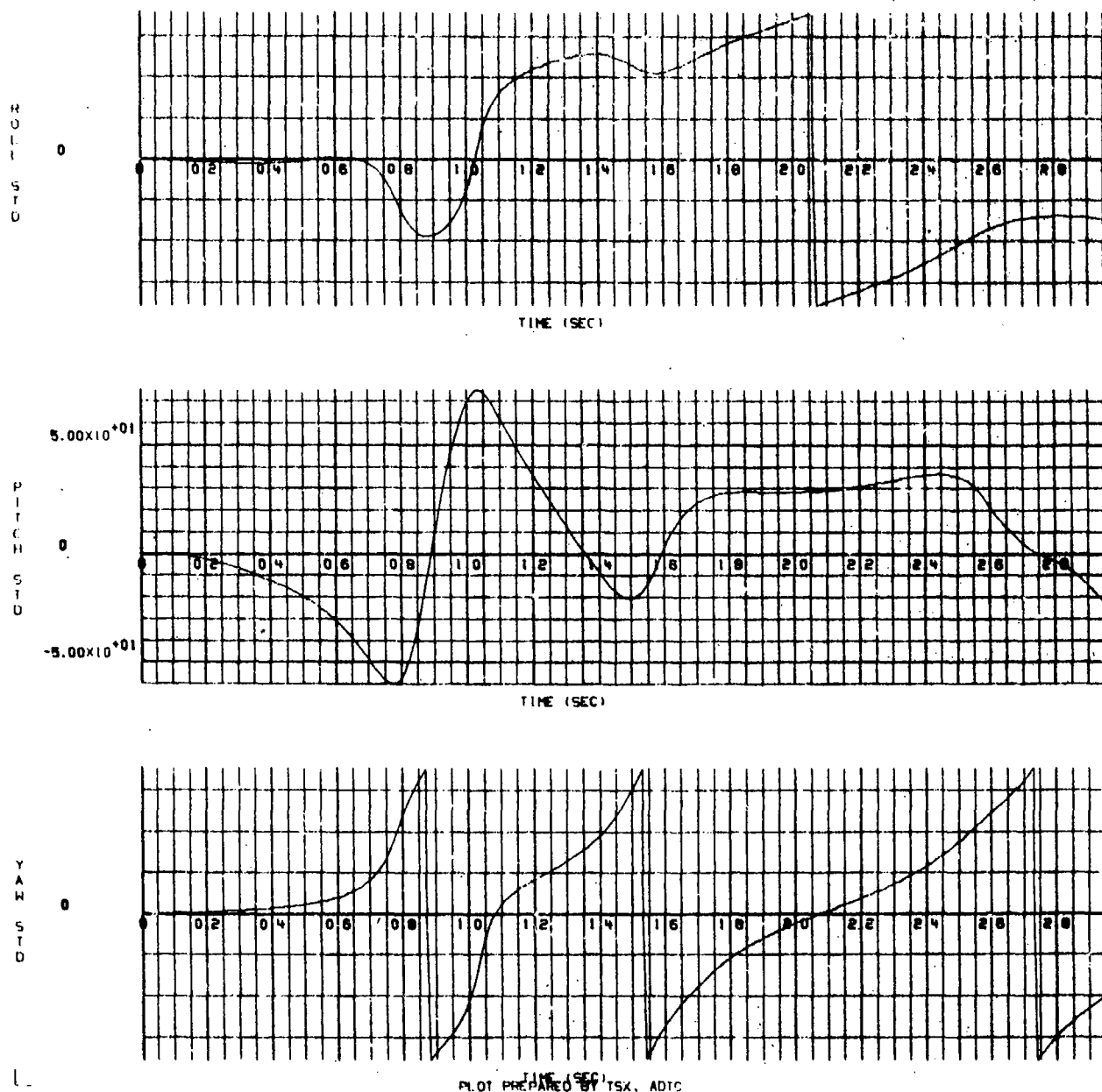
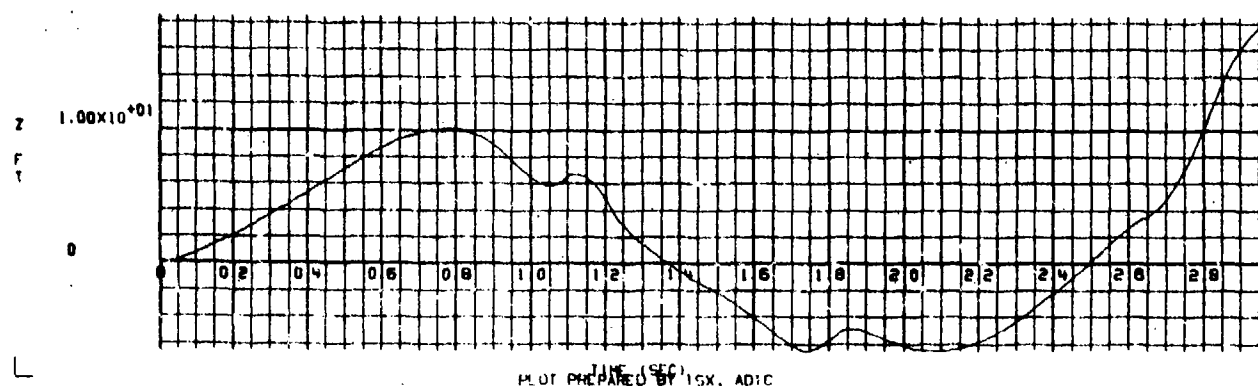
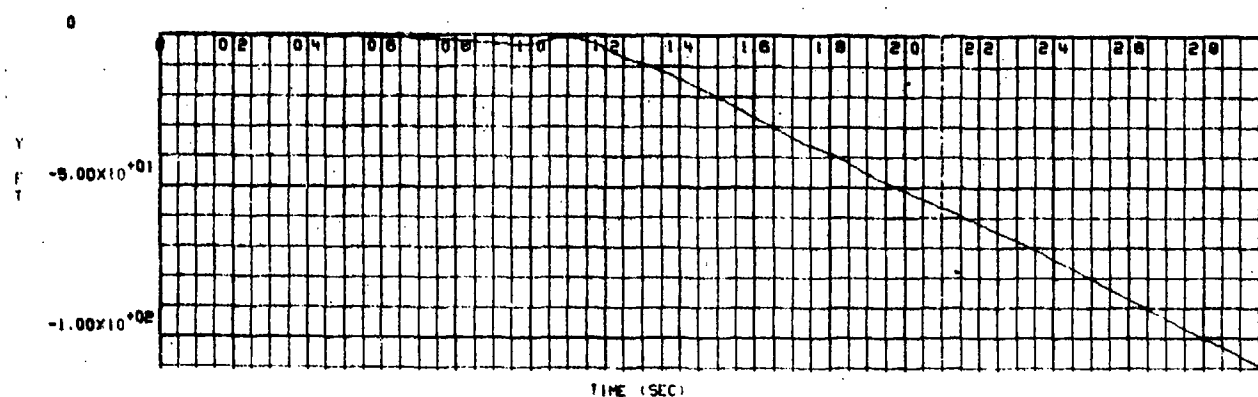
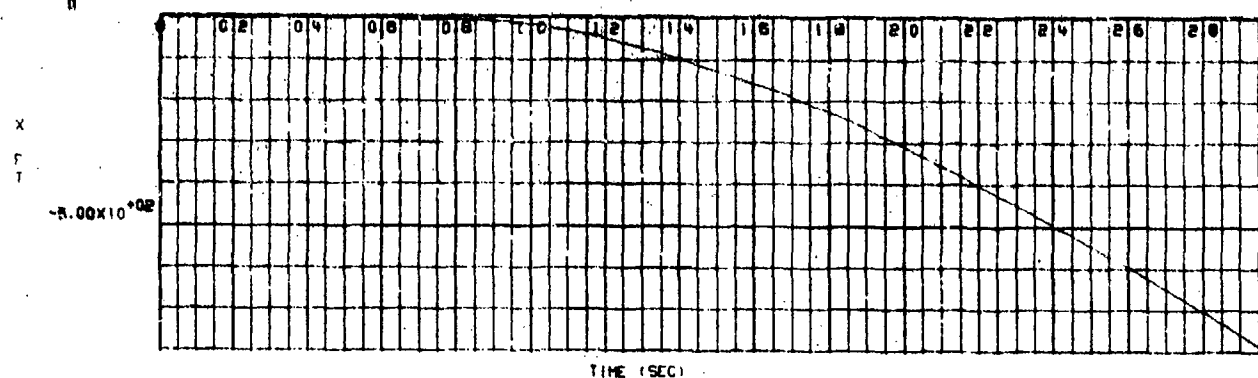


Figure S-6.  $\phi$ ,  $\theta$ , and  $\psi$  Rotation Versus Time for a Flow Field Intensity of 2

16/12/75  
0

0638 56 56



PLOT PREPARED BY 15X, ADIC

Figure 3-7. X, Y, and Z Position Versus Time for a Flow Field Intensity of  $-1/2$

16/12/75

R538

55 55

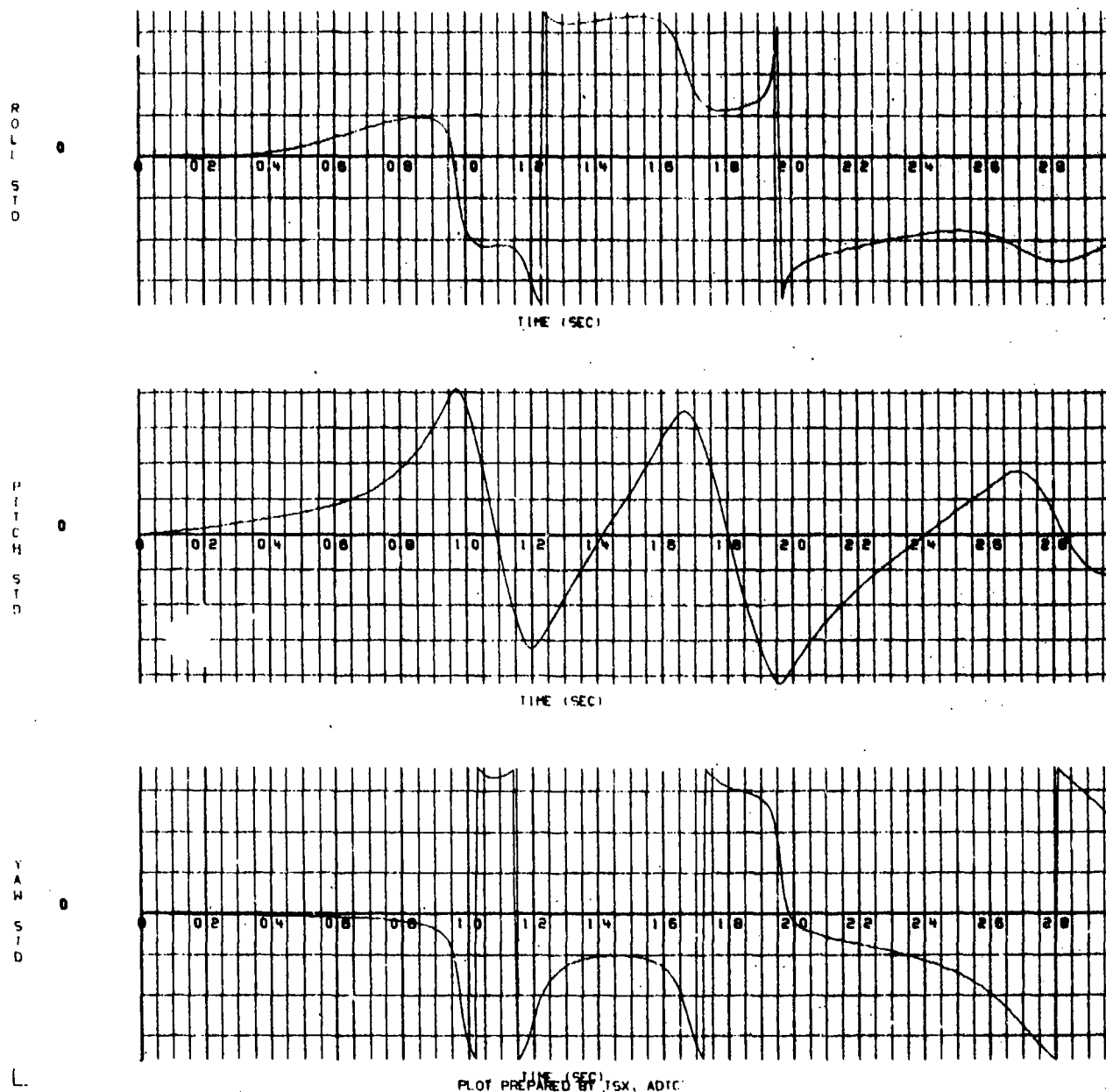


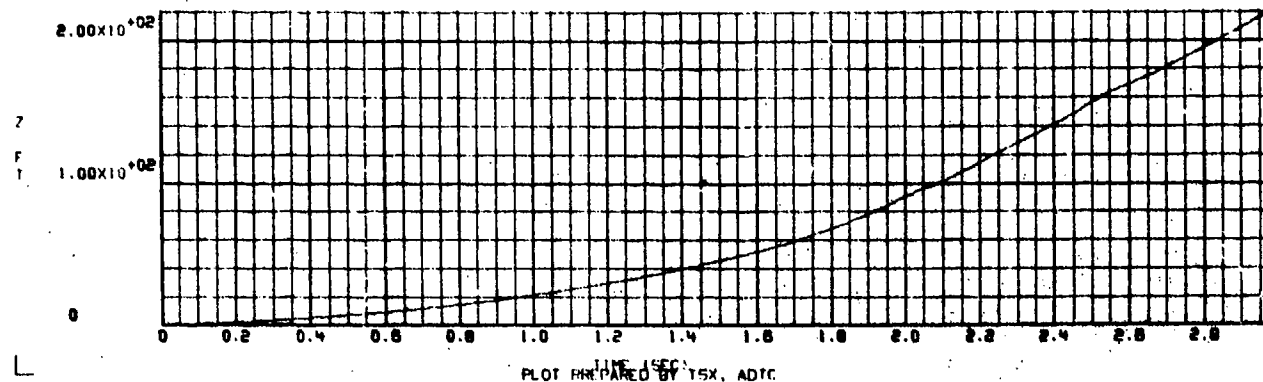
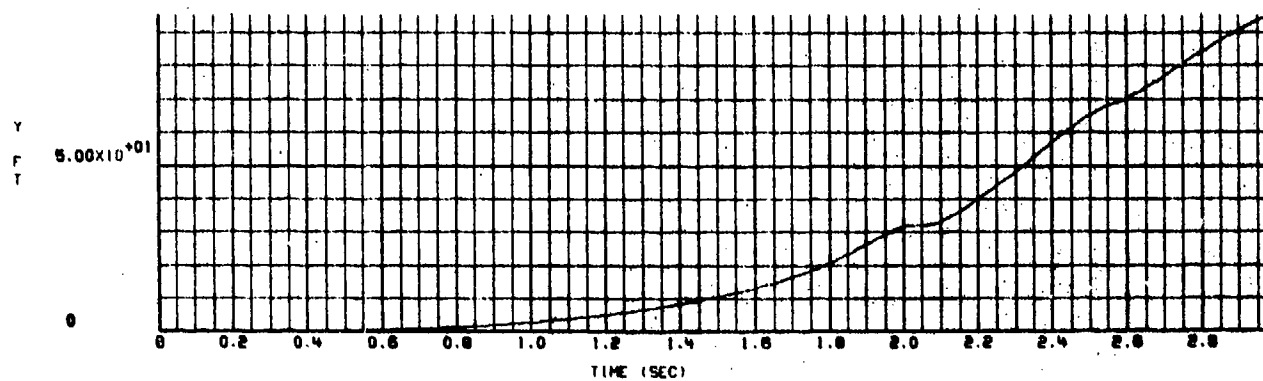
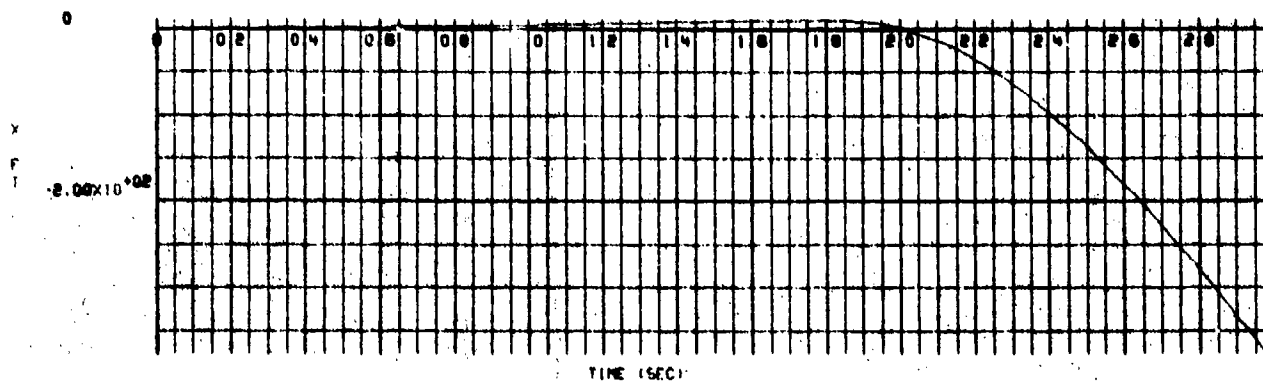
Figure S-8.  $\phi$ ,  $\theta$ , and  $\psi$  Rotation Versus Time for a Flow Field Intensity of  $-1/2$

APPENDIX T

GBU-10 BOMB TRAJECTORIES RESULTING FROM A  
(-3/-3) ORIFICE COMBINATION AT MACH 1.2

16/12/75

RB38 64 64

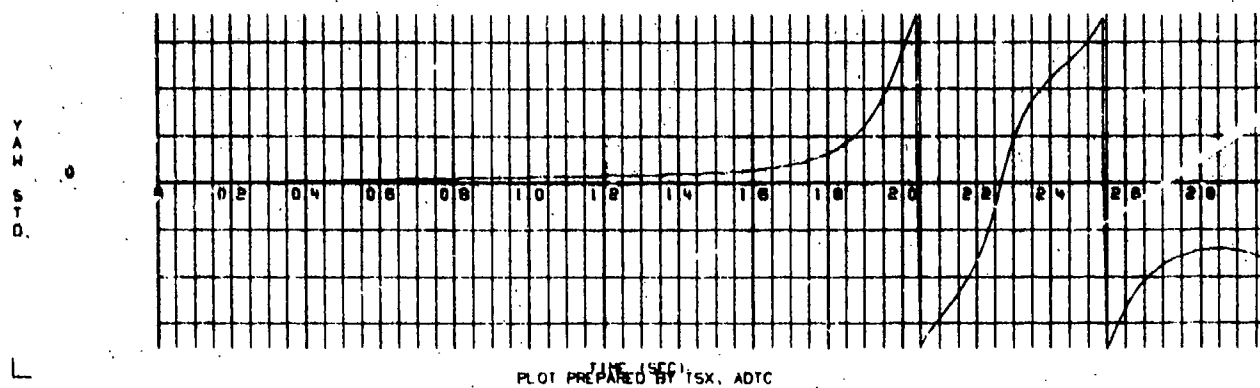
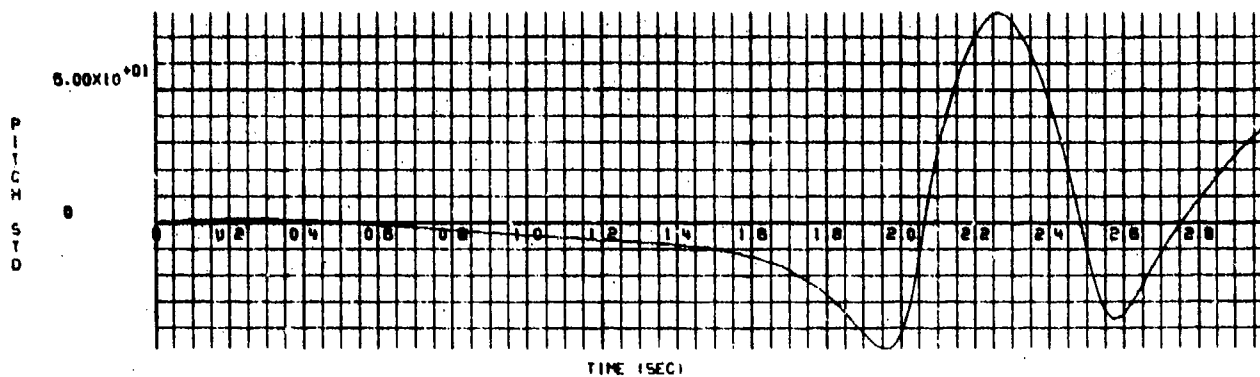
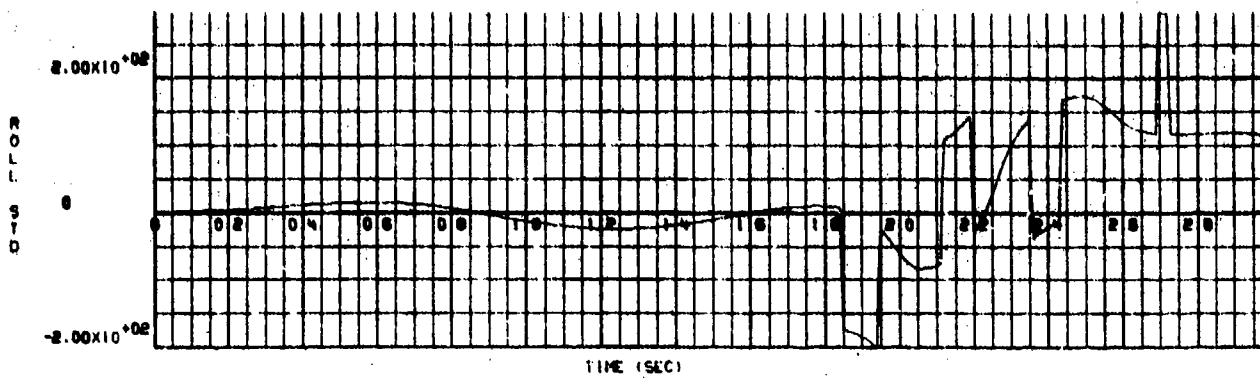


TIME (SEC)  
PLOT PREPARED BY TSX, ADTC

Figure T-1. X, Y, and Z Position Versus Time for a Flow Field Intensity of 1/2

15/12/75

R638 53 63



PLOT PREPARED BY TSX, ADTC

Figure T-2.  $\phi$ ,  $\theta$ , and  $\psi$  Rotation Versus Time for a Flow Field Intensity of  $1/2$

15/12/75

R030

60 00

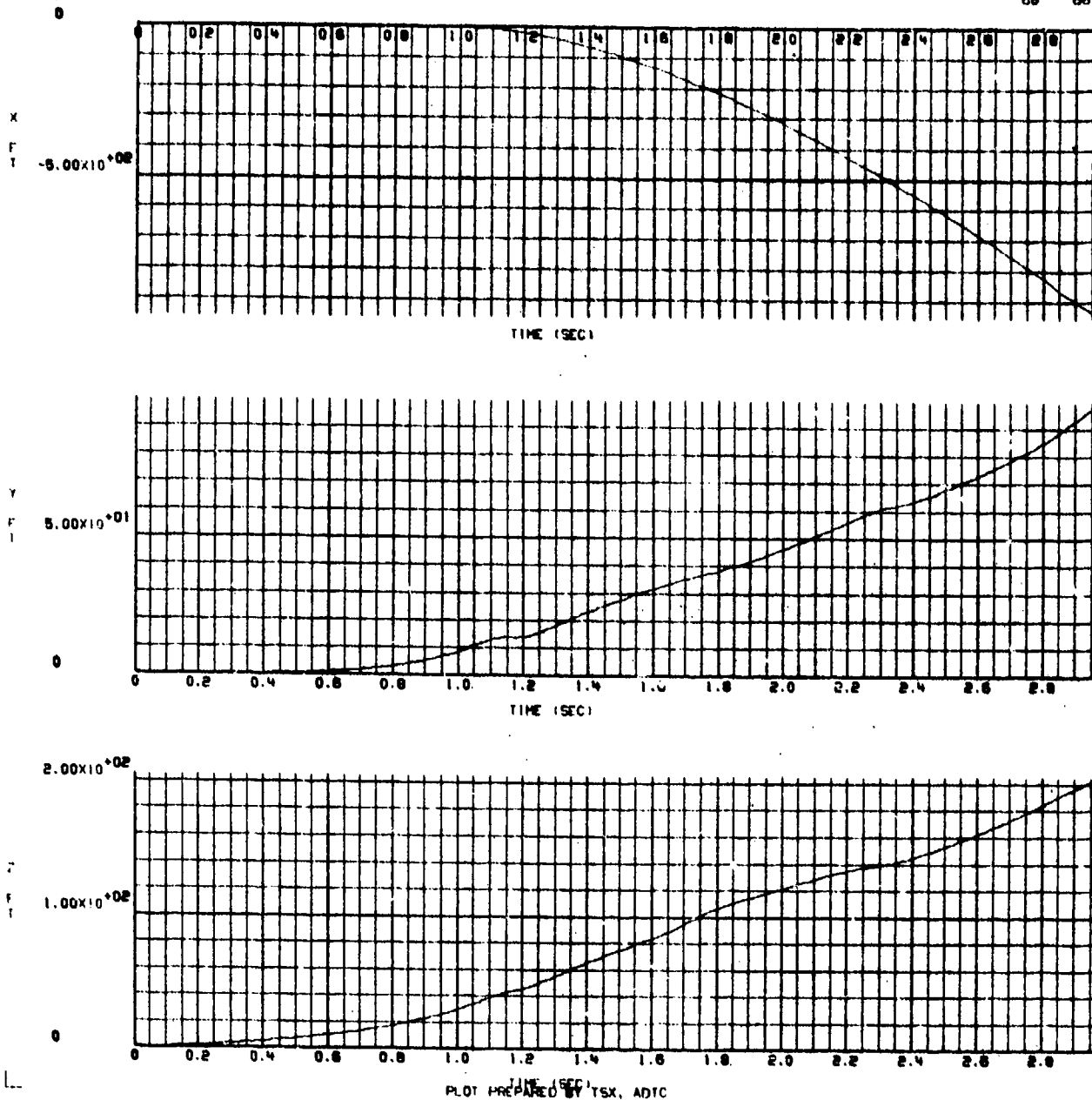


Figure T-3. X, Y, and Z Position Versus Time for a Flow Field Intensity of 1 (as measured in the wind tunnel)



B



182

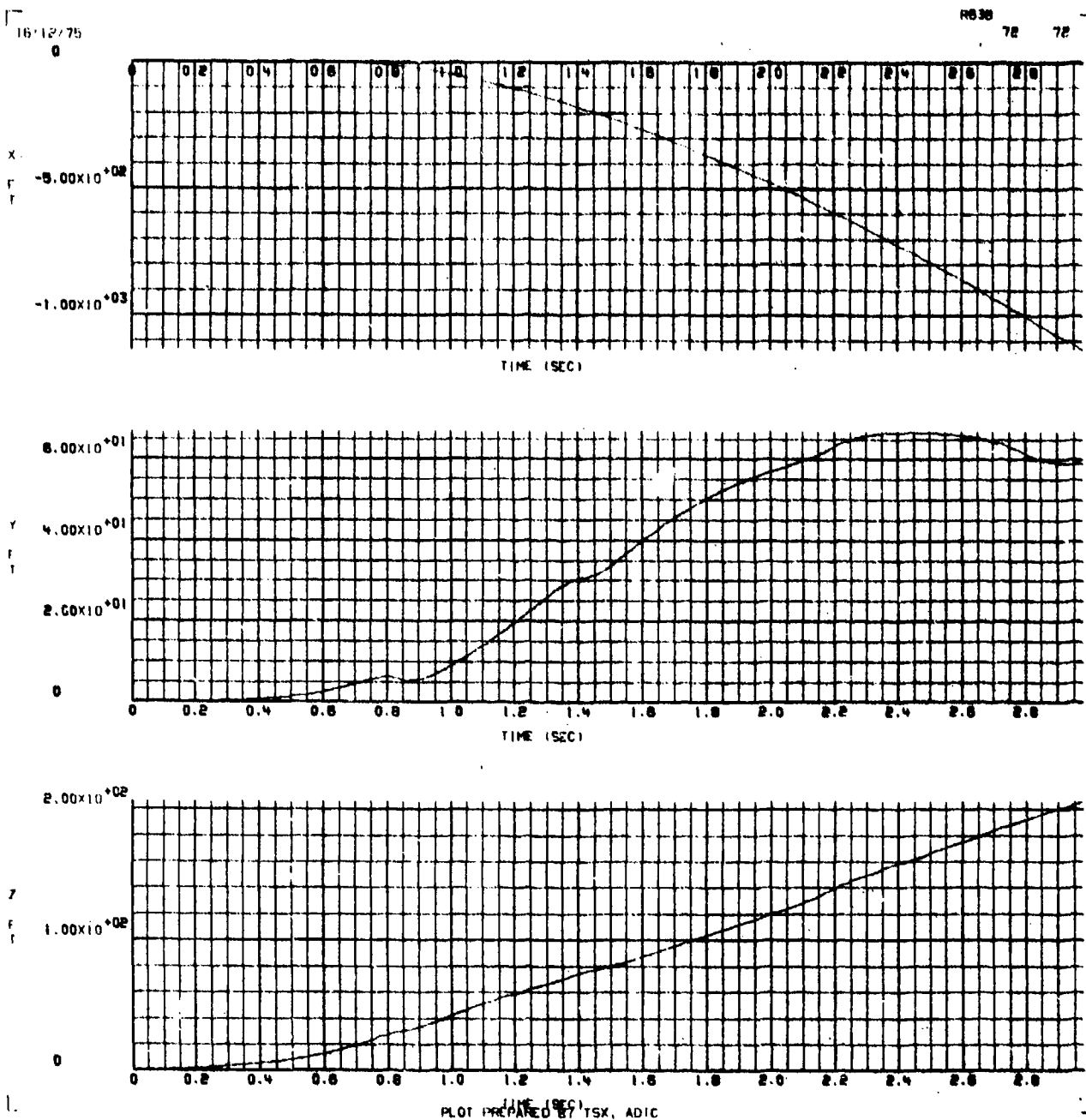


Figure T-5. X, Y, and Z Position Versus Time for a Flow Field Intensity of 2

16/12/75

R030

71

71

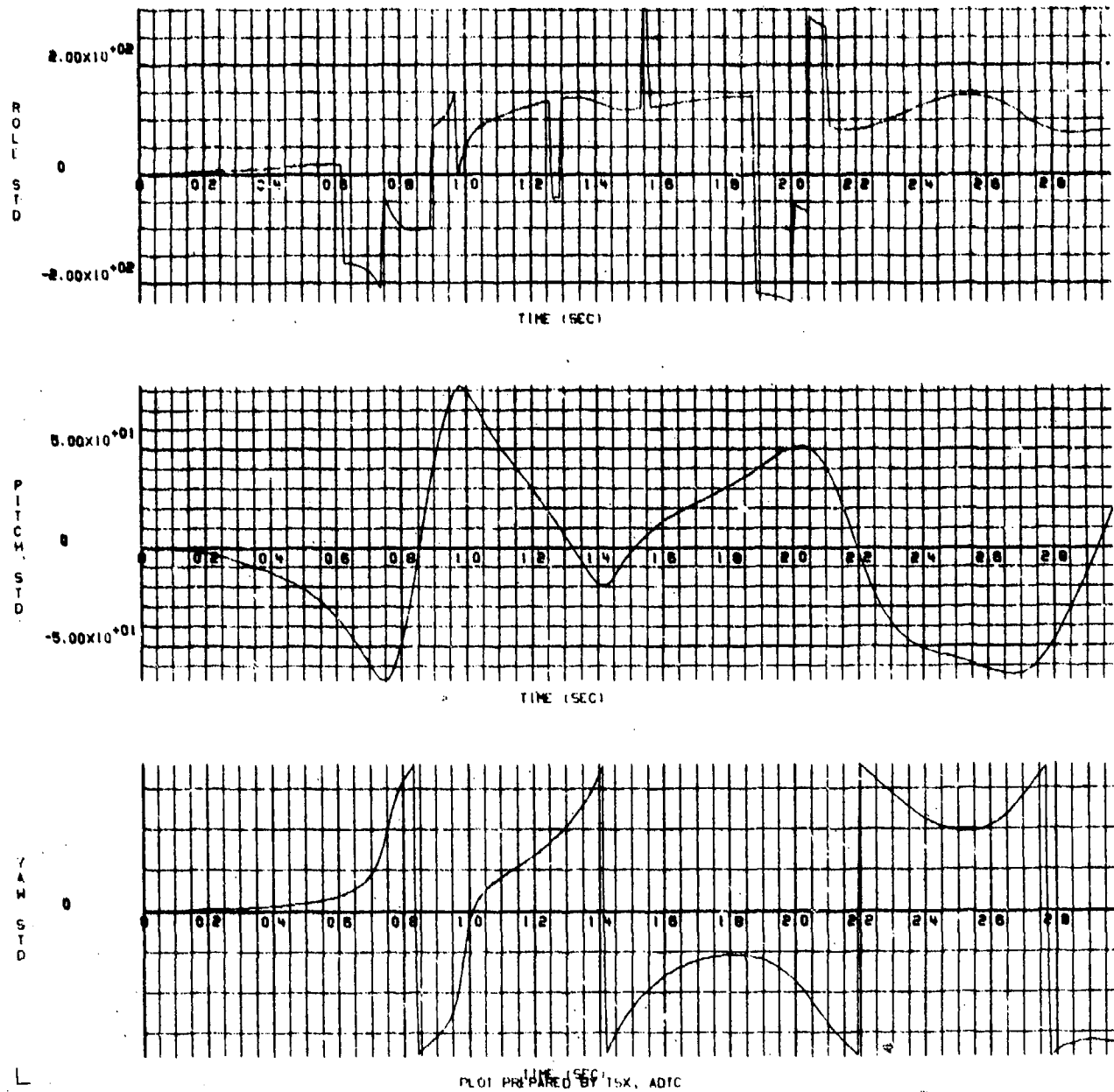


Figure T-6.  $\phi$ ,  $\theta$ , and  $\psi$  Rotation Versus Time for a Flow Field Intensity of 2

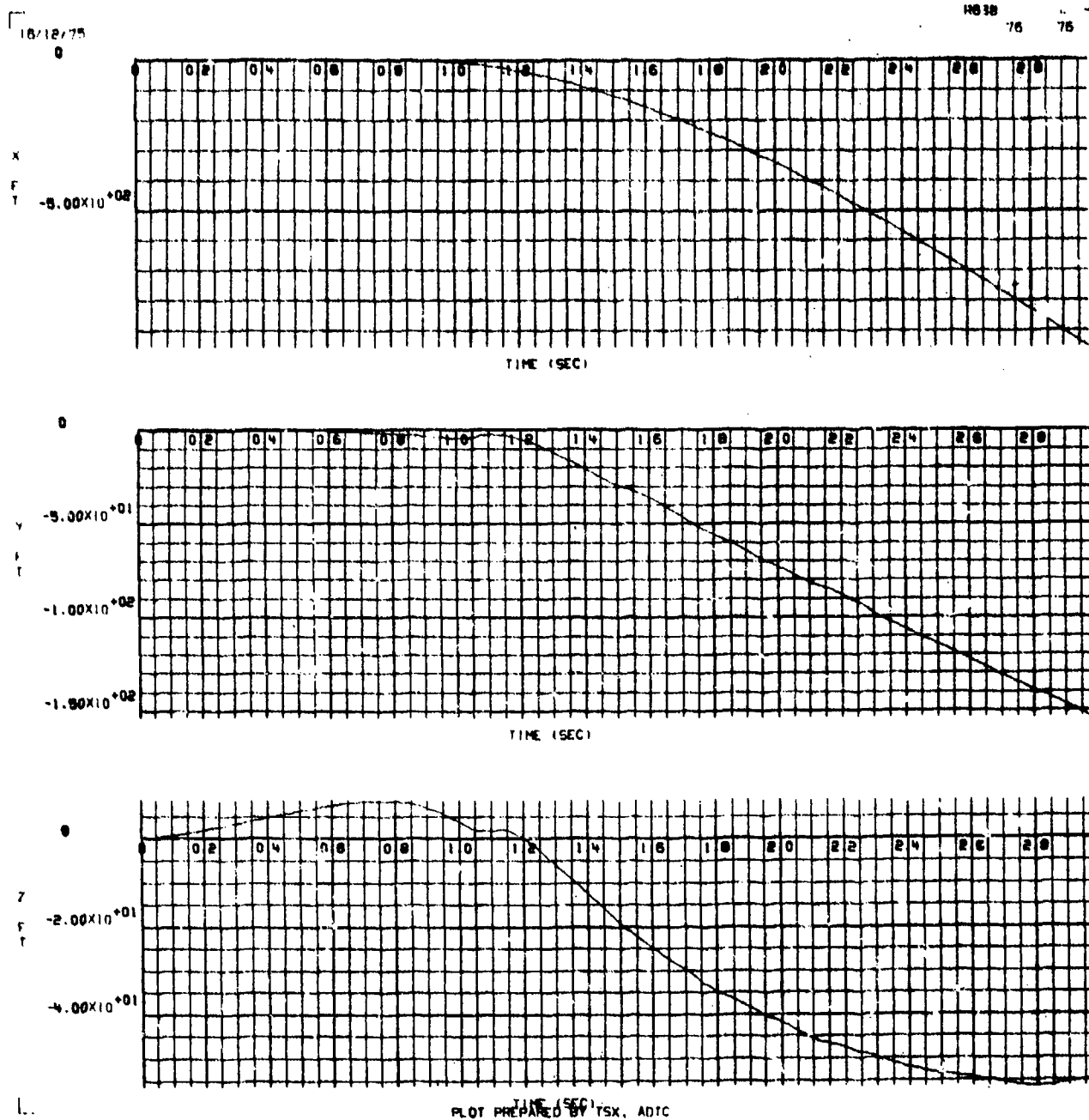
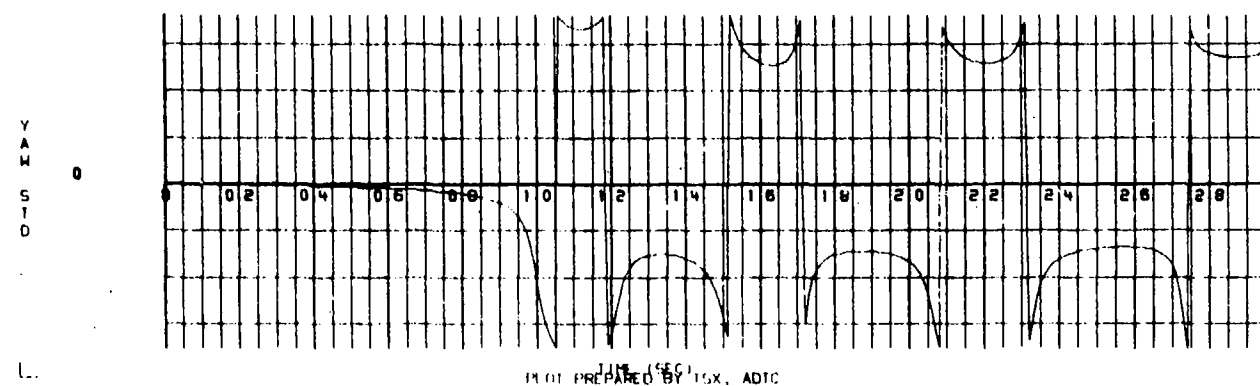
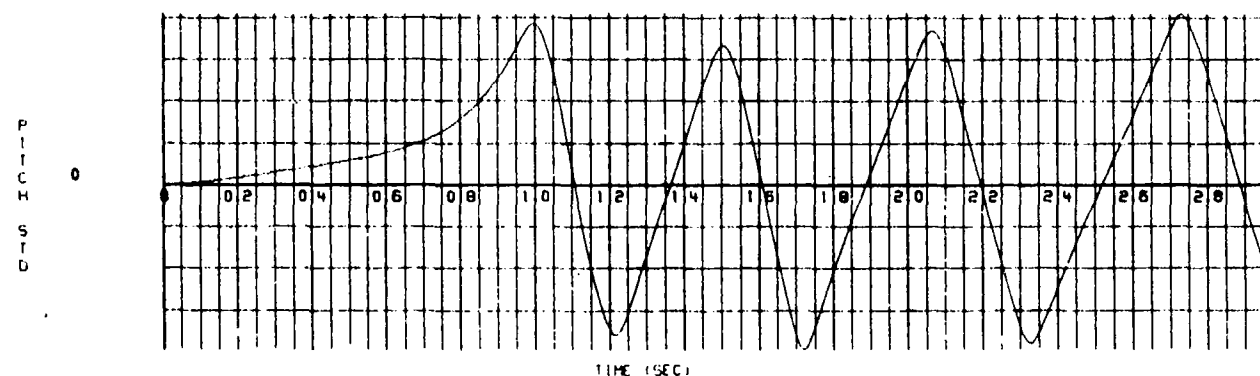
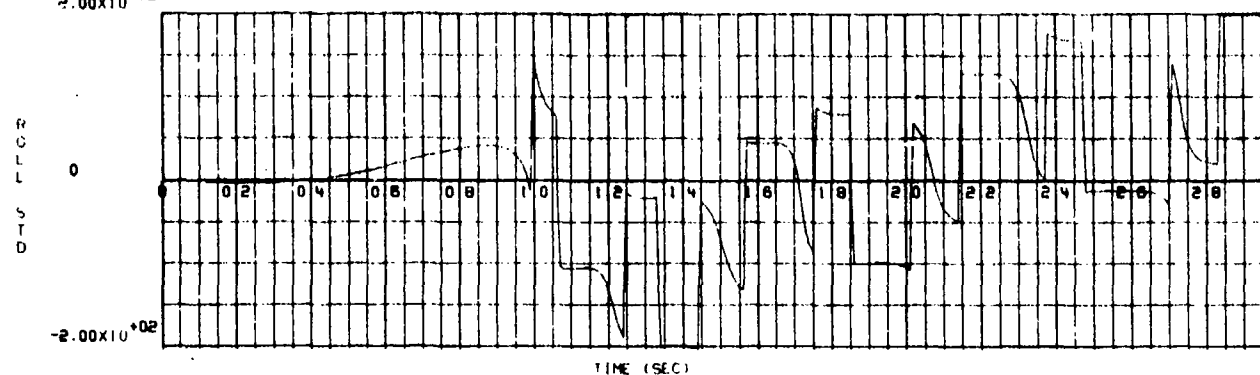


Figure T-7. X, Y, and Z Position Versus Time for a Flow Field Intensity of  $-1/2$

16/12/75  
2.00x10<sup>+02</sup>

R678  
75 75



TIME (SEC)  
PLOT PREPARED BY TSG, ADTC

Figure T-8.  $\phi$ ,  $\theta$ , and  $\psi$  Rotation Versus Time for a Flow Field Intensity of  $-1/2$

APPENDIX U

GBU-10 BOMB TRAJECTORIES RESULTING FROM A  
(-3/-5) ORIFICE COMBINATION AT MACH 0.7

16/12/75  
0

8855

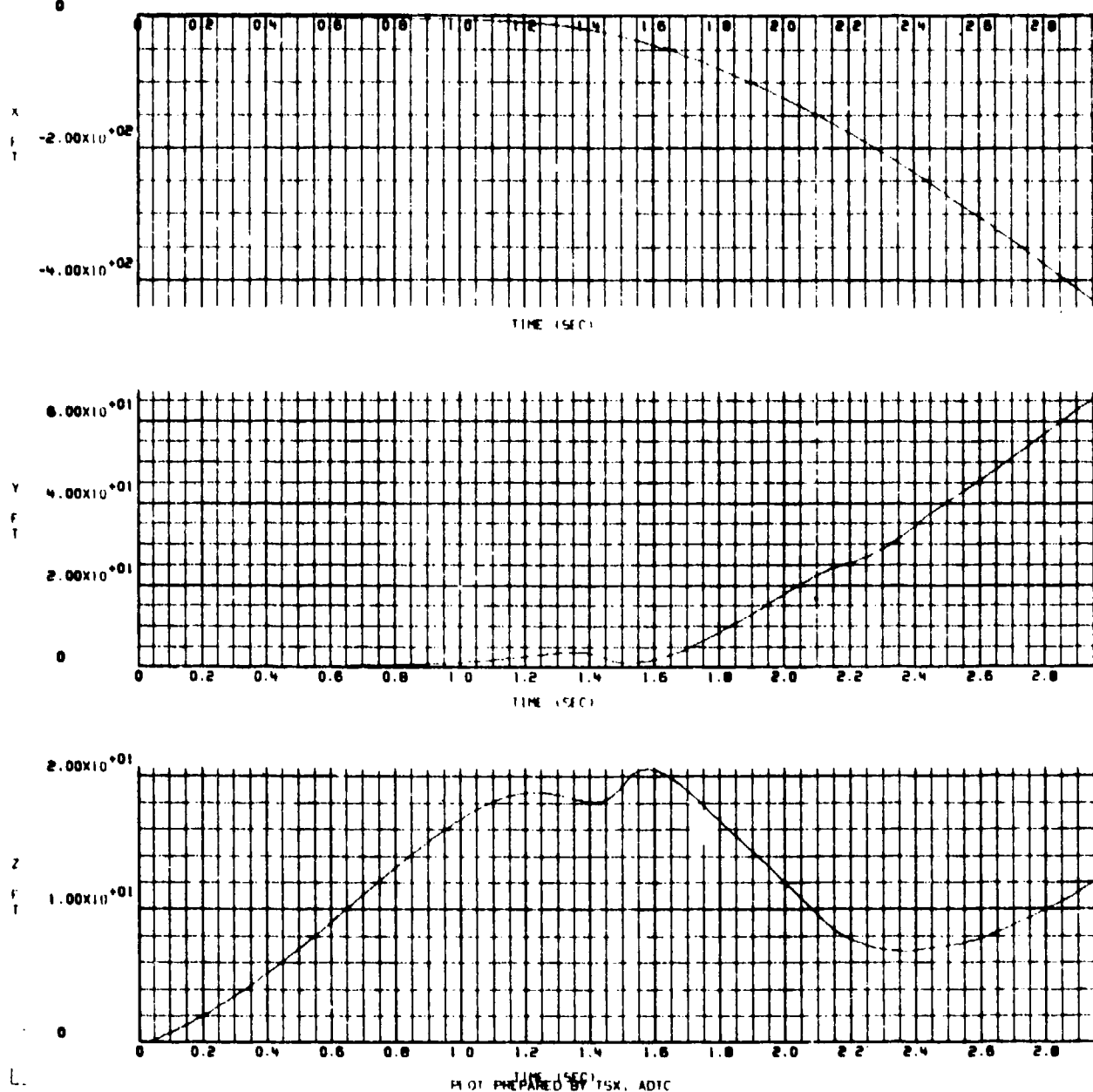
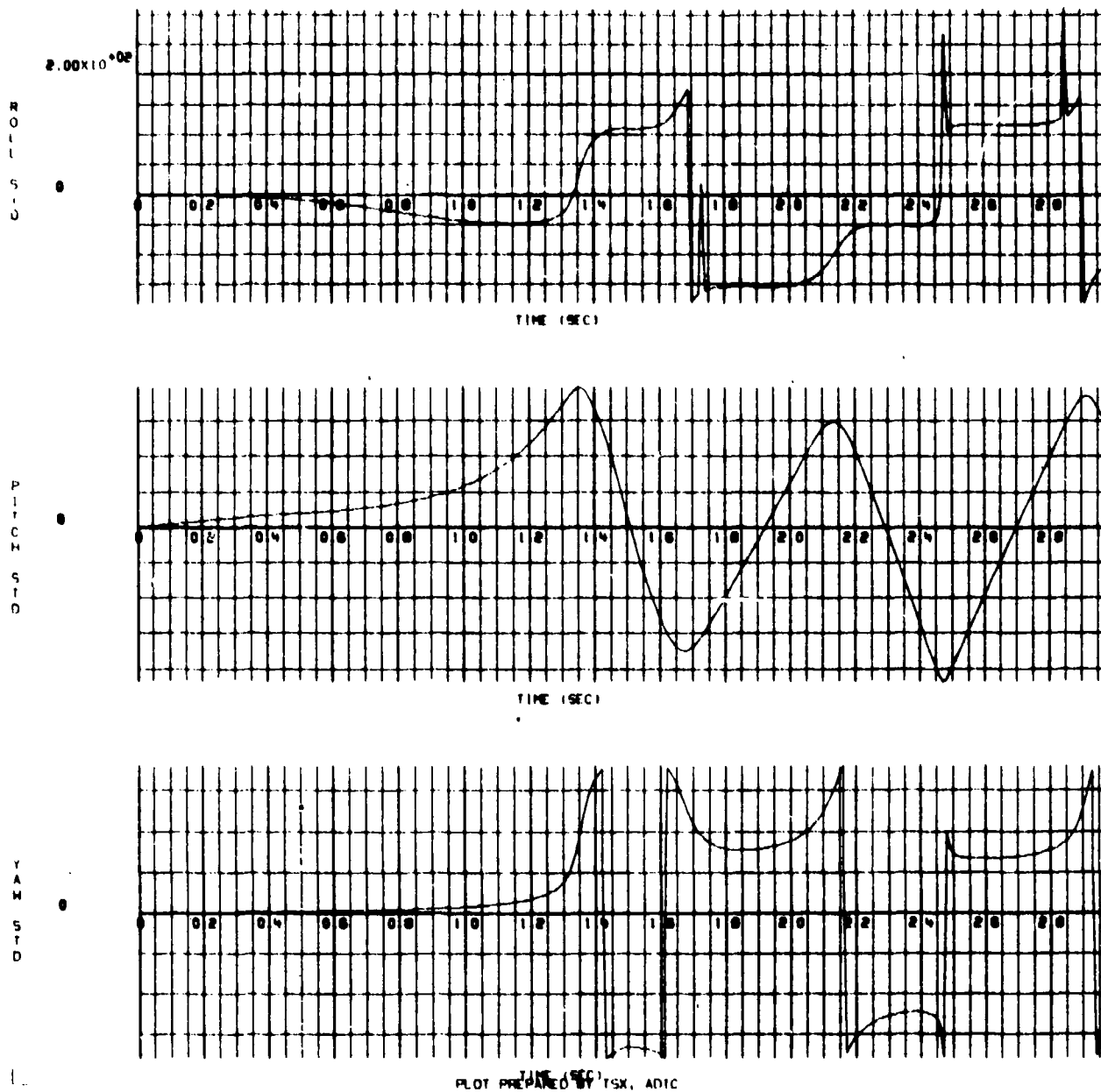


Figure U-1. X, Y, and Z Position Versus Time for a Flow Field Intensity of 1/2

10-10-75

R055



PLOT PREPARED BY TSX, ADIC

Figure U-2.  $\phi$ ,  $\theta$ , and  $\gamma$  Rotation Versus Time for a Flow Field Intensity of  $1/2$



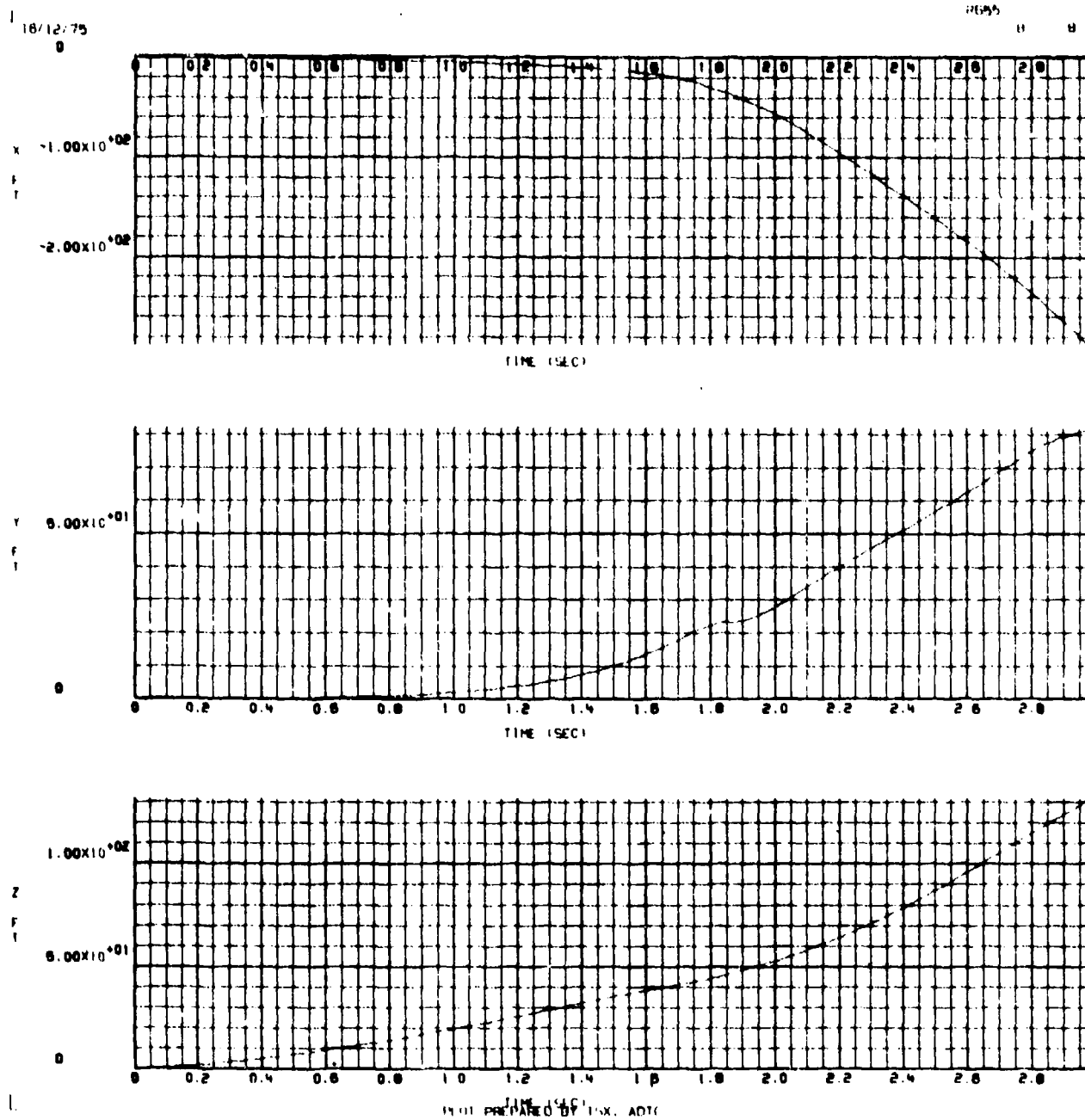


Figure U-3. X, Y, and Z Position Versus Time for a Flow Field Intensity of 1 (as measured in the wind tunnel)

16-12-75

8655

7 7

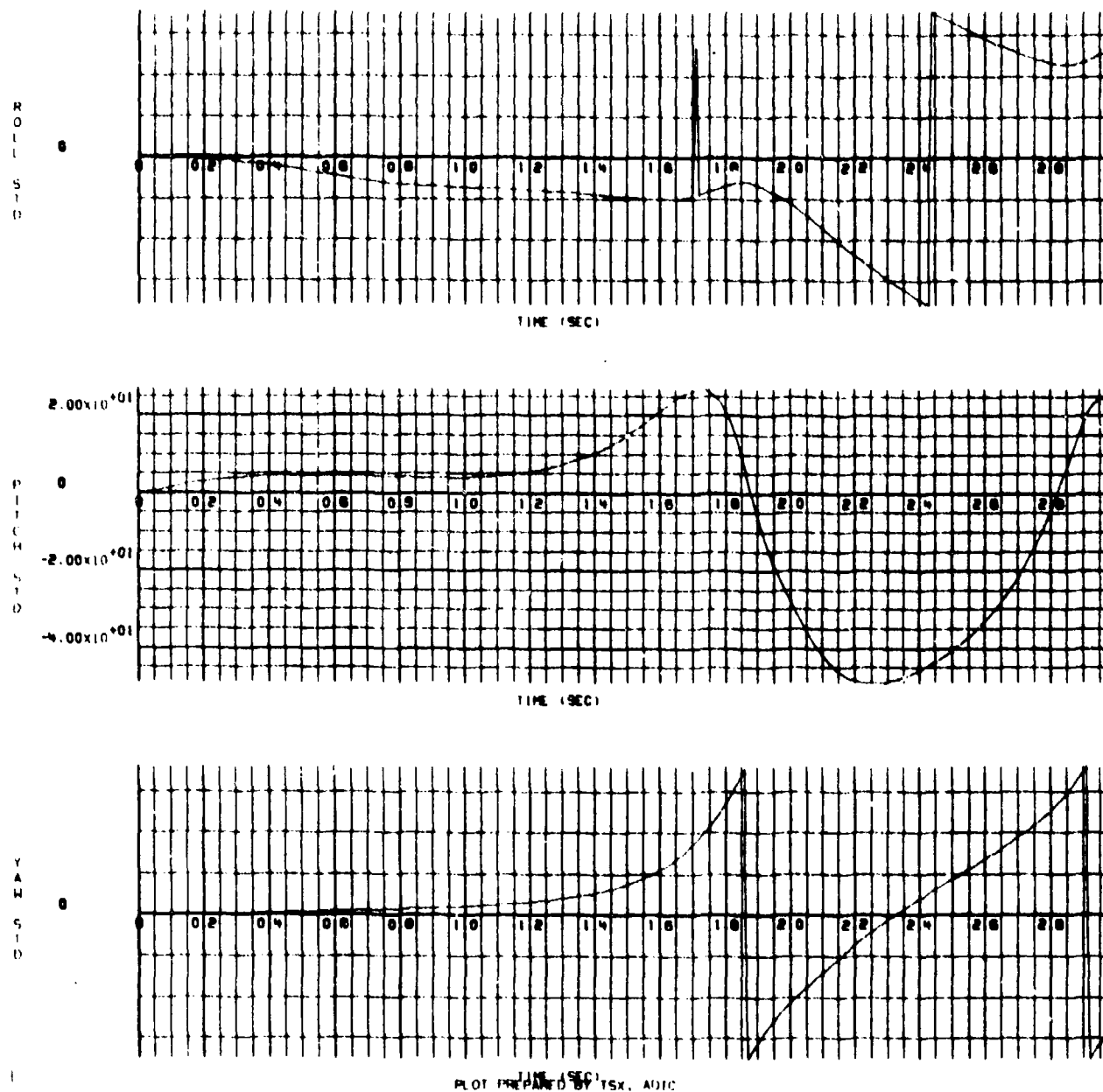


Figure U-4.  $\phi$ ,  $\theta$ , and  $\psi$  Rotation Versus Time for a Plow Field Intensity of 1 (unchanged from the wind tunnel measured values)

16/12/79  
0

RE55

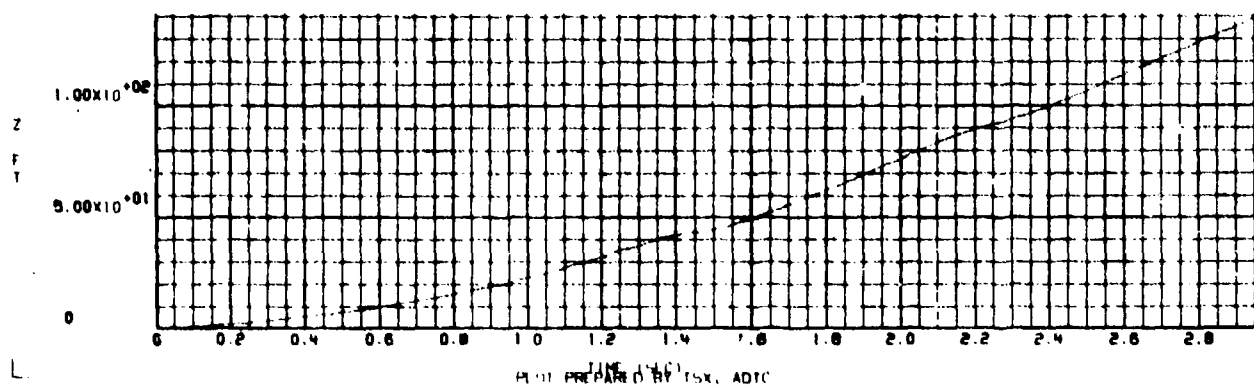
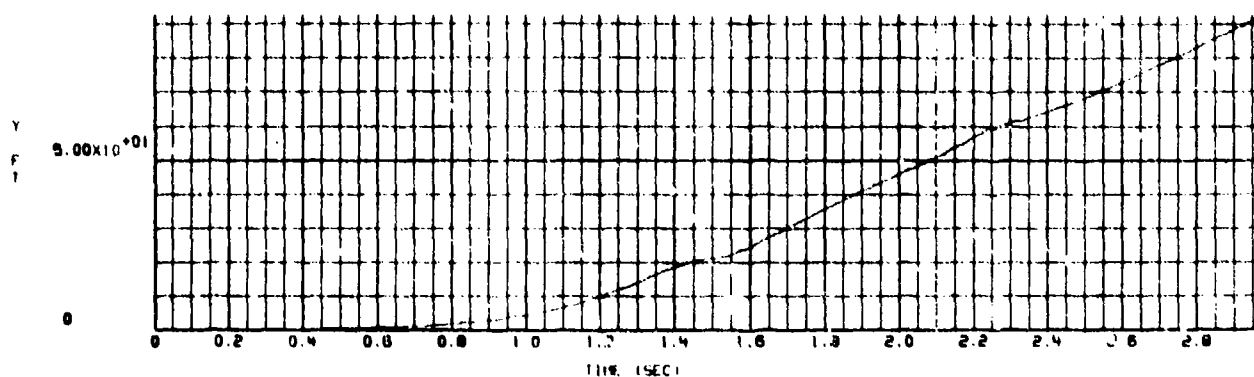
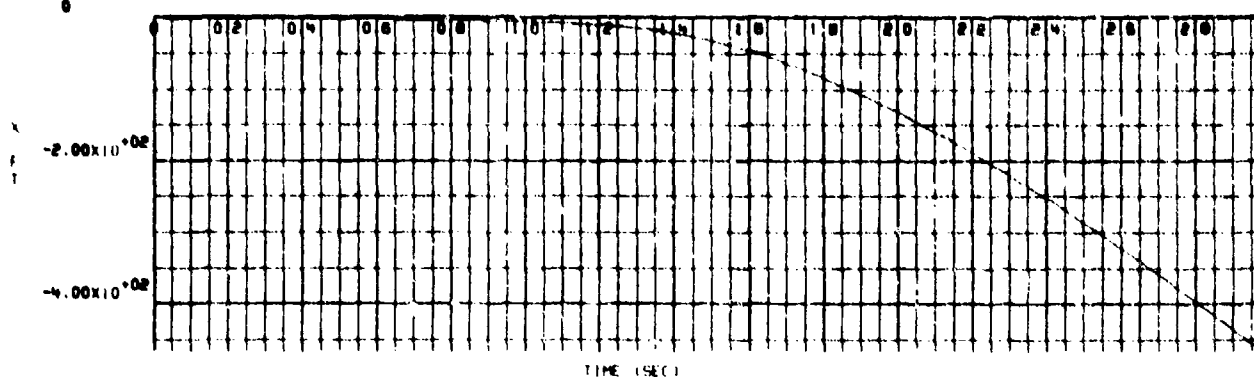
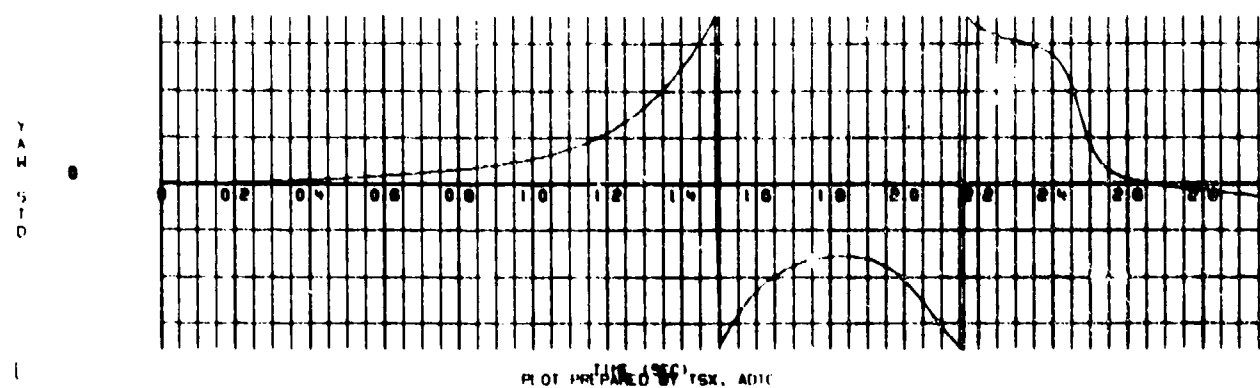
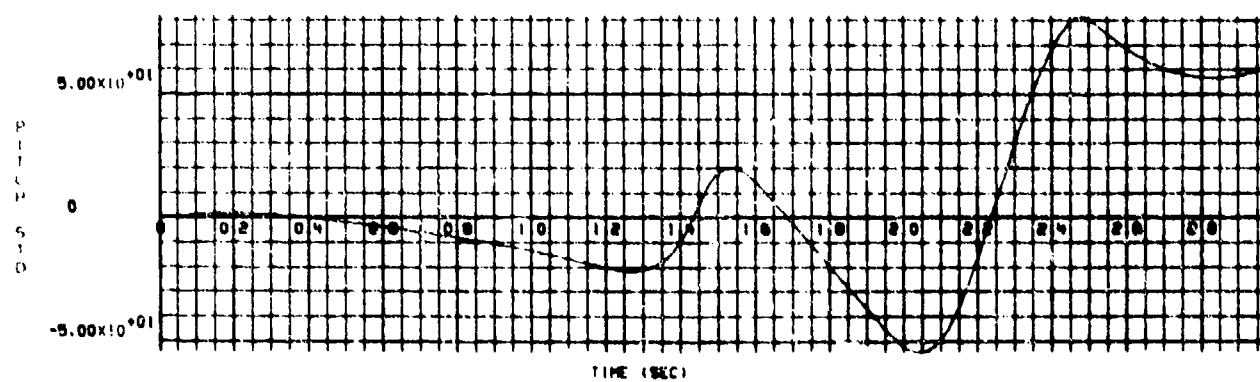
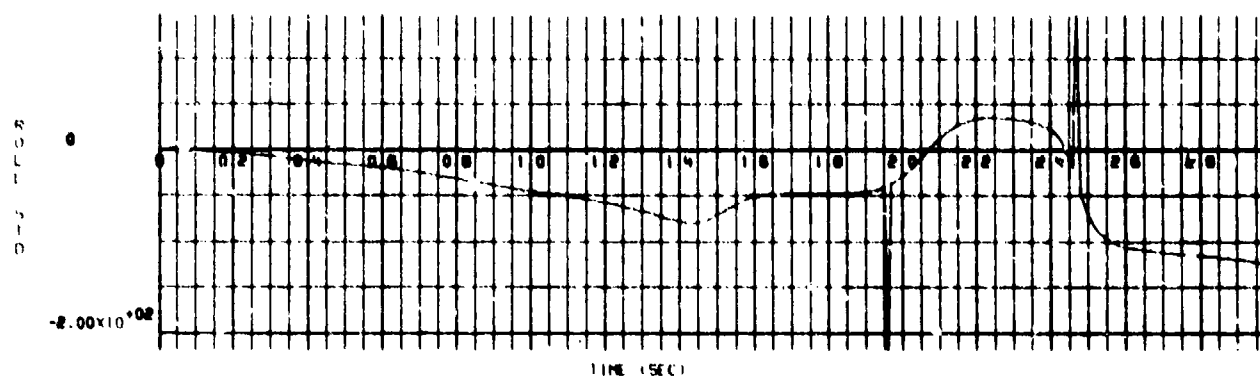


Figure U-5. X, Y, and Z Position Versus Time for a Flow Field Intensity of 2

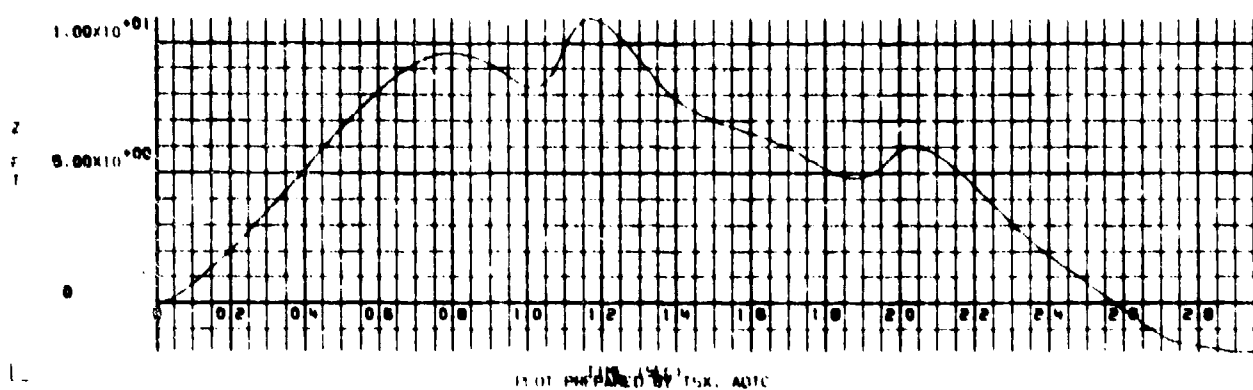
16-10-75

P655



PILOT PREPARED BY TSX, ADIC

Figure U-6.  $\phi$ ,  $\theta$ , and  $\psi$  Rotation Versus Time for a Flow Field Intensity of 2



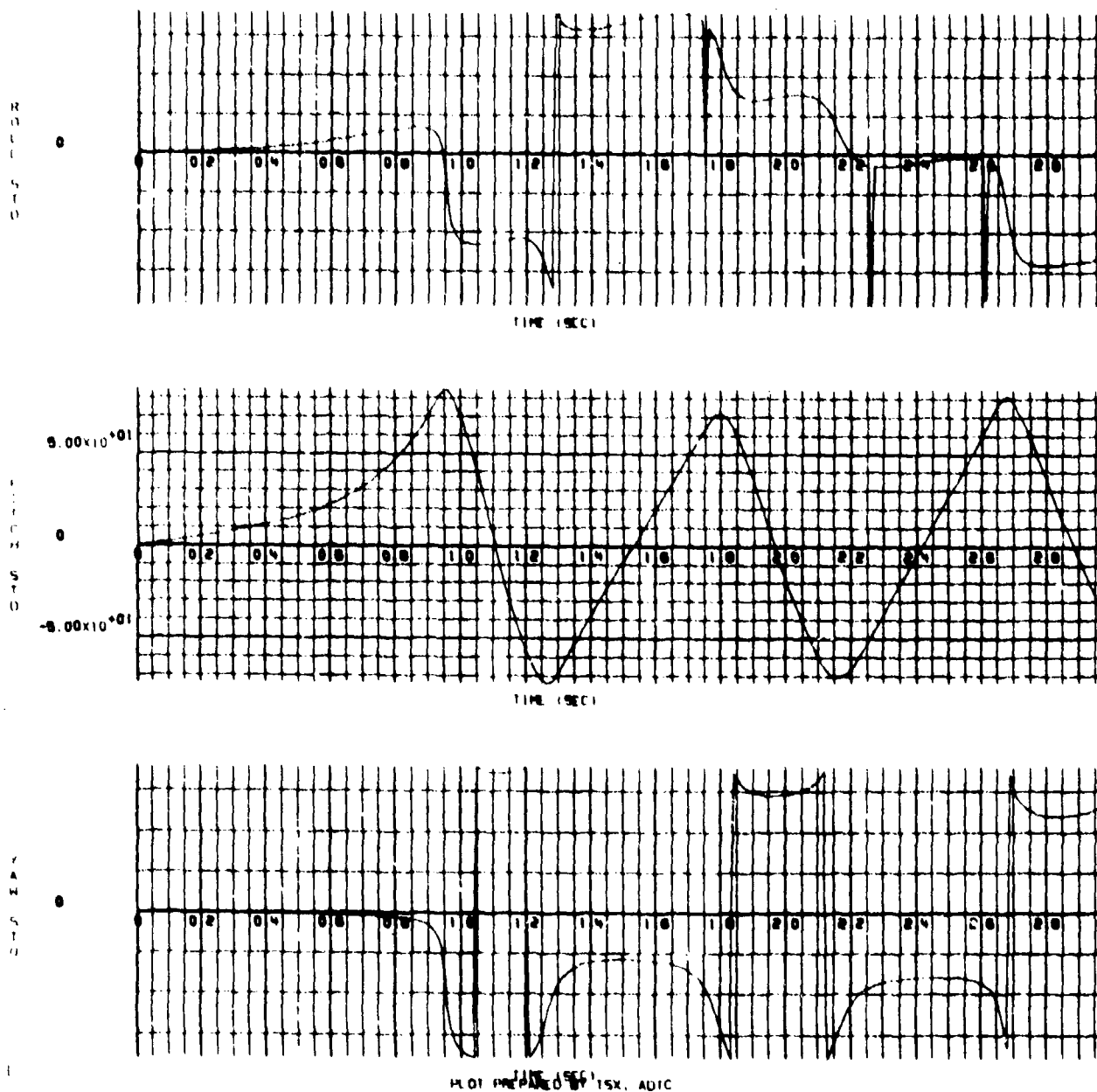


Figure U-8.  $\phi$ ,  $\theta$ , and  $\psi$  Rotation Versus Time for a Flow Field Intensity of  $-1/2$

APPENDIX V

GBU-10 BOMB TRAJECTORIES RESULTING FROM A  
(-3/-5) ORIFICE COMBINATION AT MACH 0.85

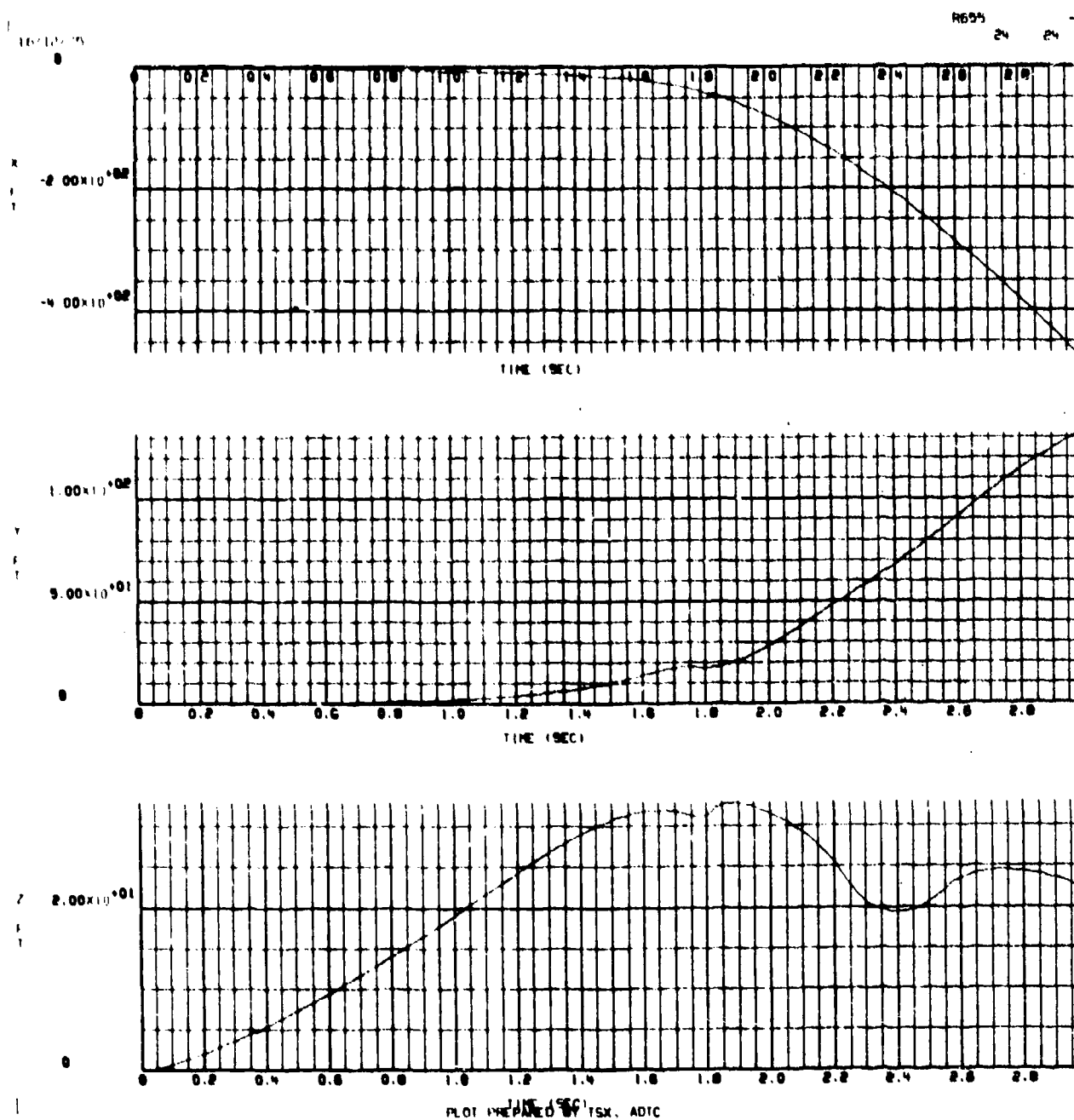
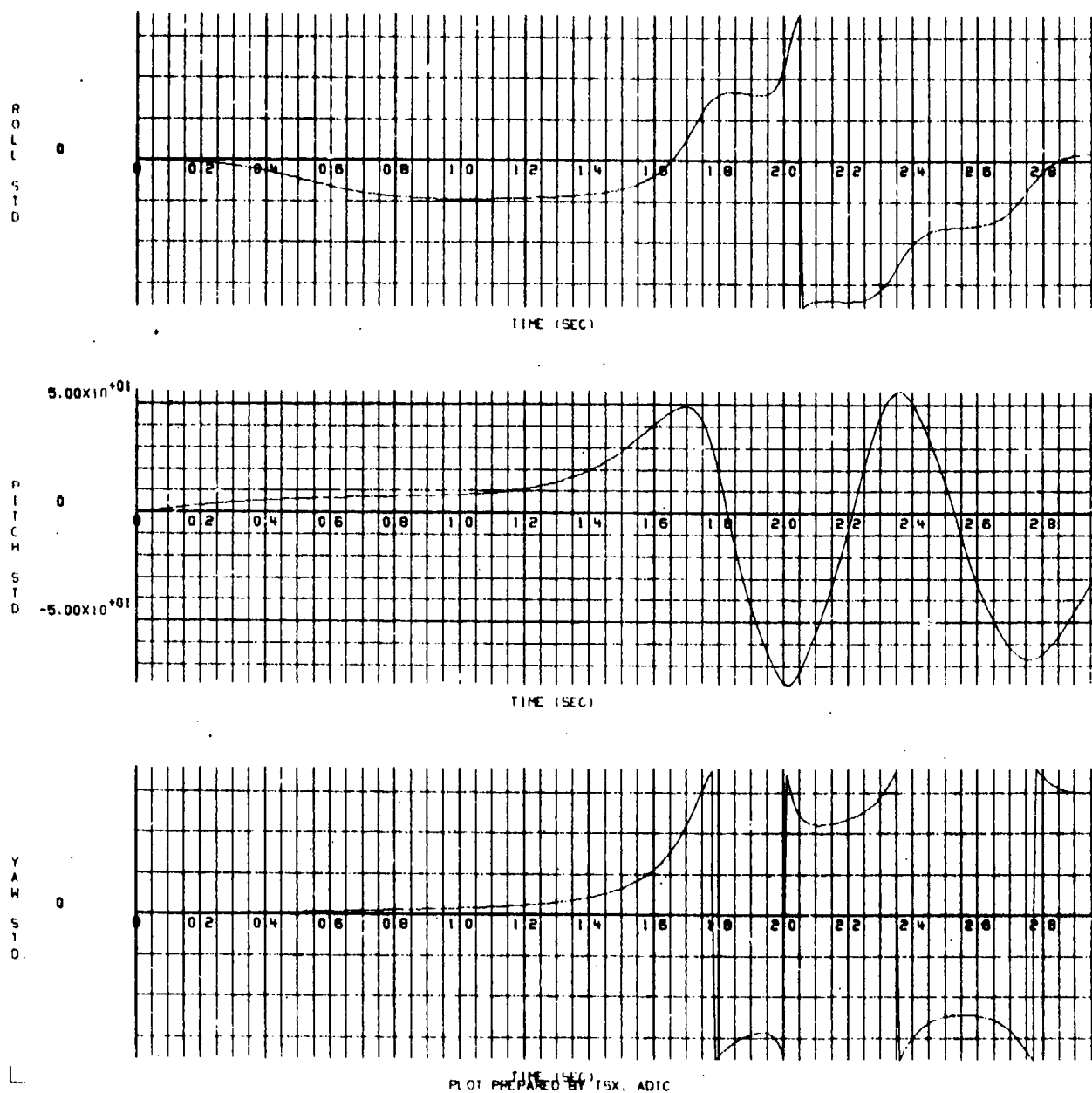


Figure V-1. X, Y, and Z Position Versus Time for a Flow Field Intensity of 1/2



18/12/75

R655 23 23

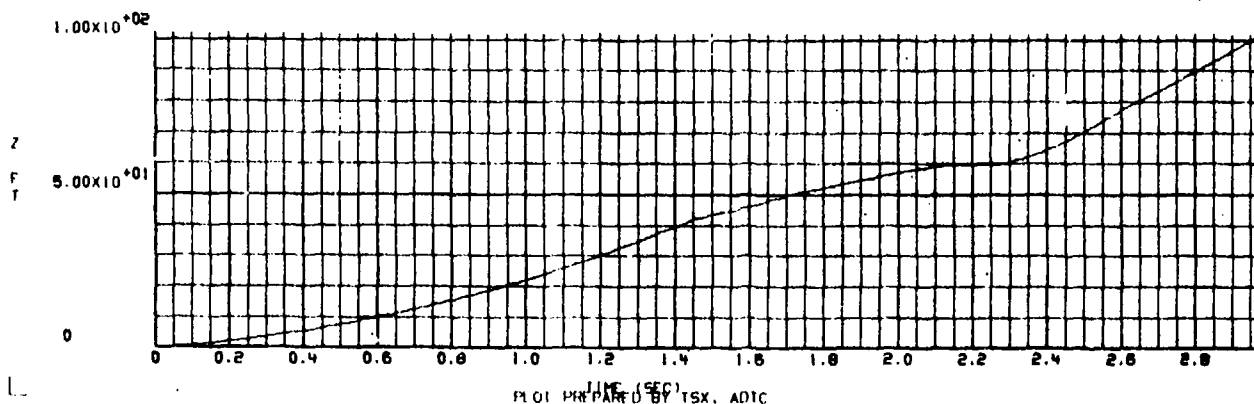
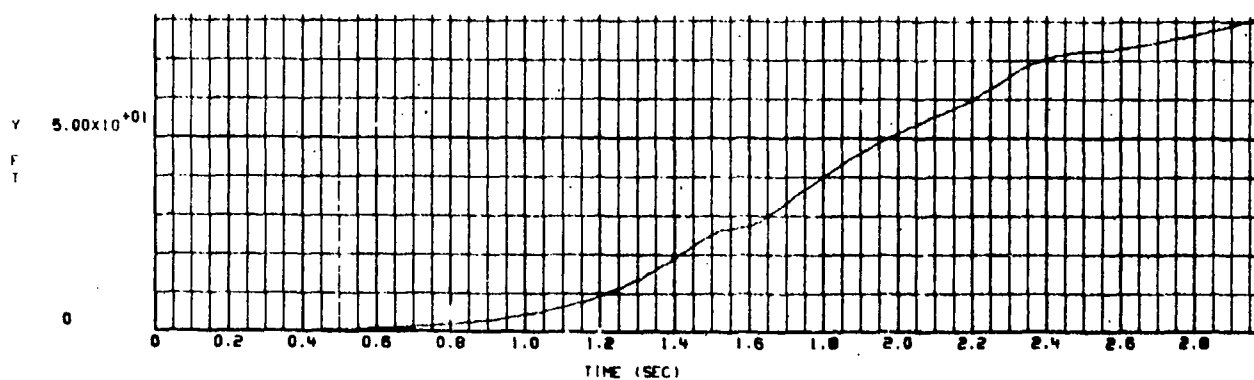
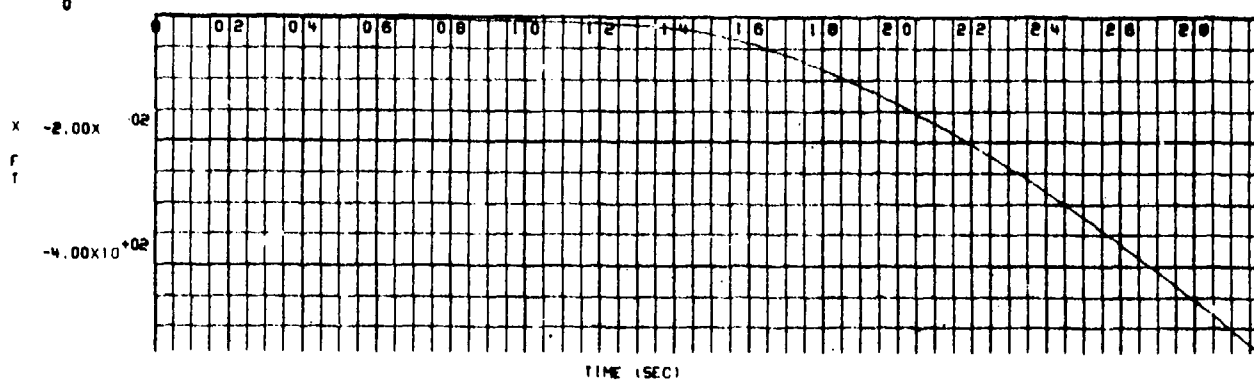


TIME (SEC)  
PLOT PREPARED BY TSX, ADIC

Figure V-2.  $\phi$ ,  $\theta$ , and  $\psi$  Rotation Versus Time for a Flow Field Intensity of 1/2

16/12/75  
0

R055  
20 20



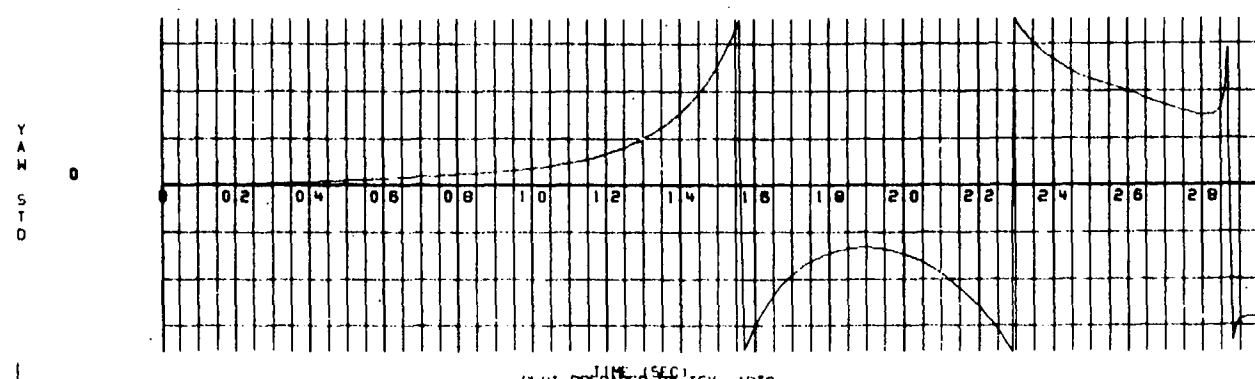
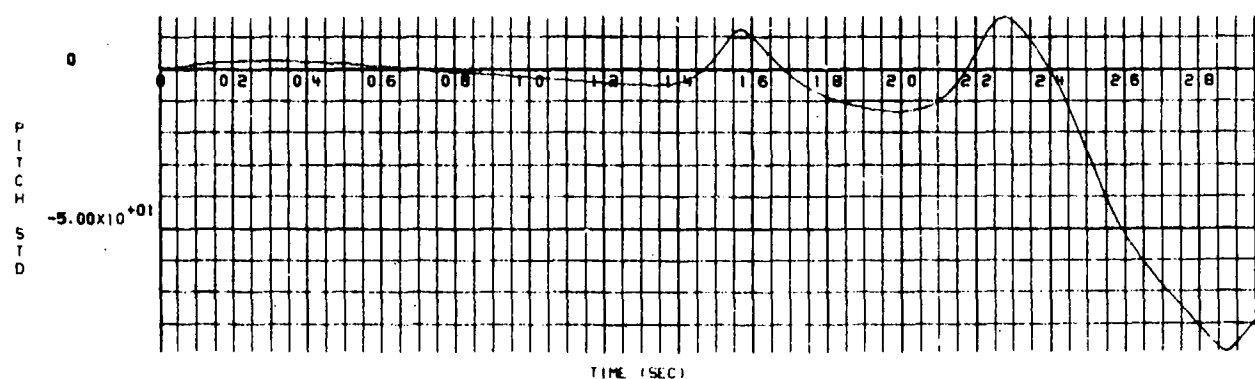
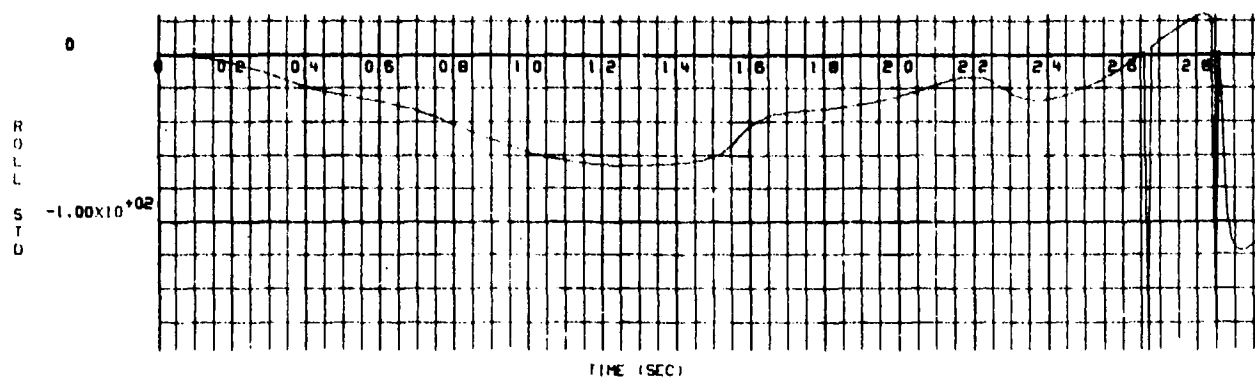
TIME (SEC)  
PLOT PREPARED BY TSX, ADIC

Figure V-3. X, Y, and Z Position Versus Time for a Flow Field Intensity of 1 (as measured in the wind tunnel)

16/12/75

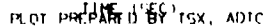
R655

27 27



TIME (SEC)  
PLOT PREPARED BY TSX, ADTC

Figure V-4.  $\phi$ ,  $\theta$ , and  $\psi$  Rotation Versus Time for a Flow Field Intensity of 1 (unchanged from the wind tunnel measured values)



201

16/12/75

R655

31 31

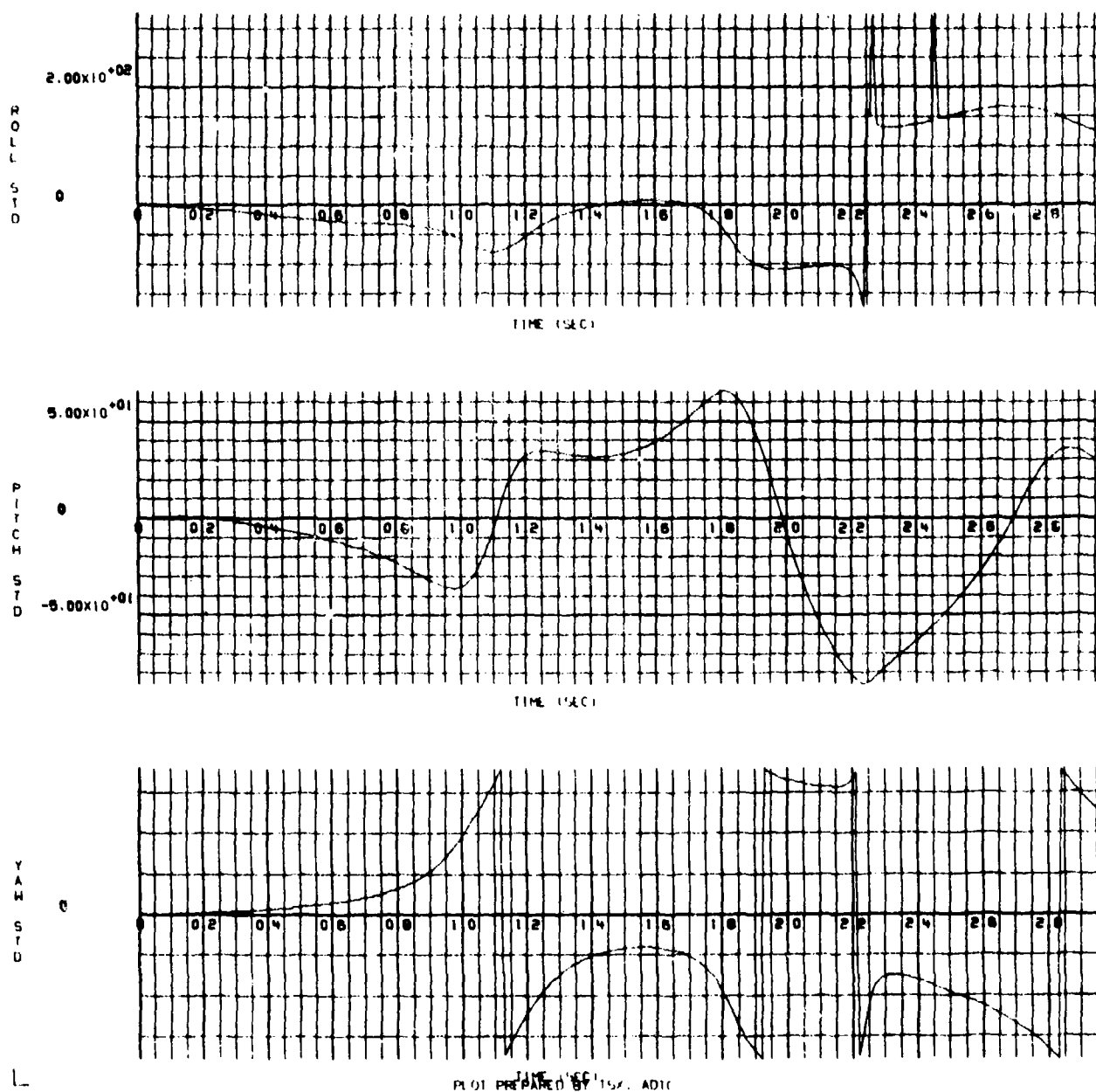


Figure V-6.  $\phi$ ,  $\theta$ , and  $\psi$  Rotation Versus Time for a Flow Field Intensity of 2

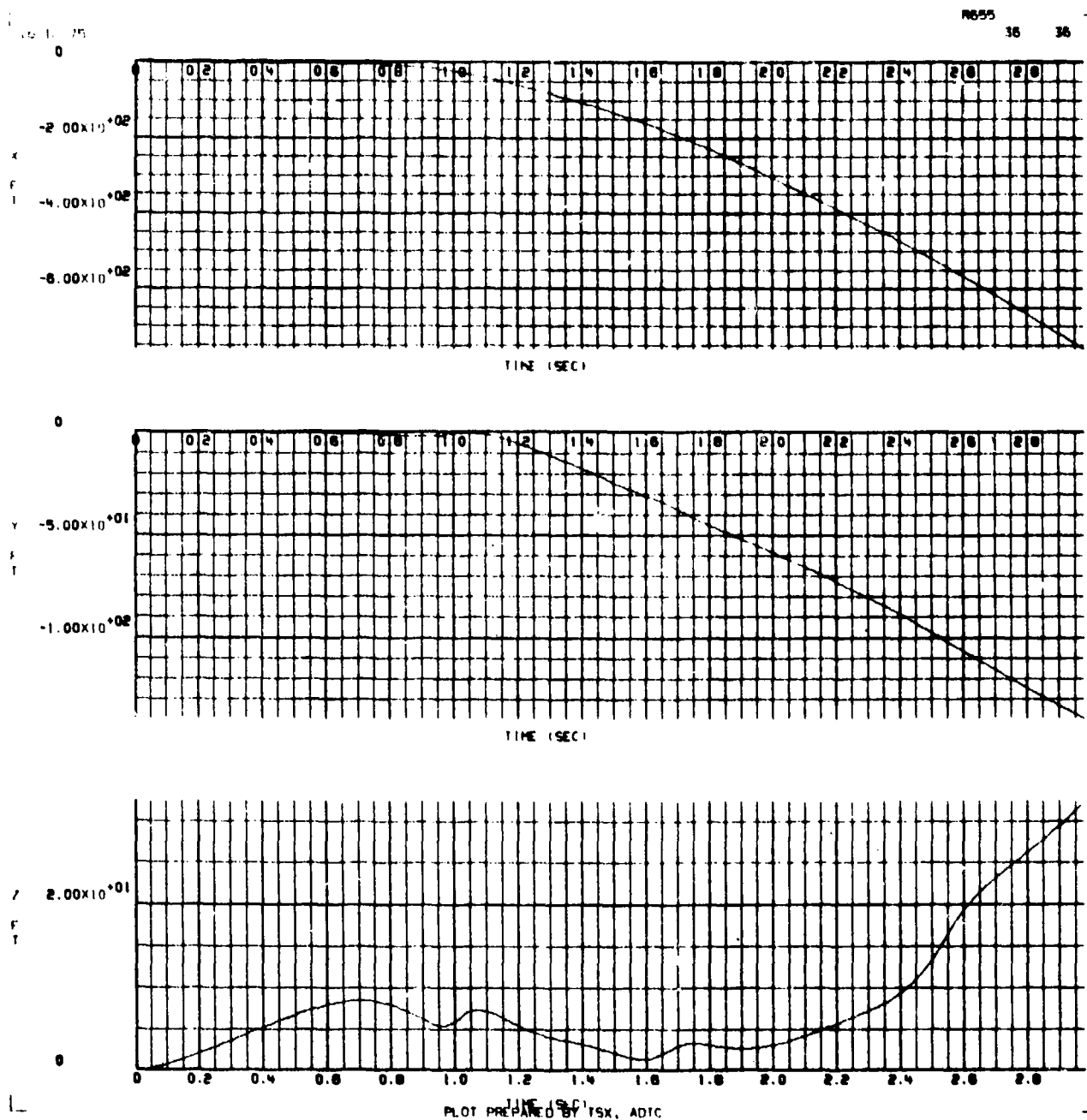
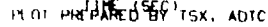


Figure V-7. X, Y, and Z Position Versus Time for a Flow Field Intensity of  $-1/2$

35



204

APPENDIX IV

GBU-10 BOMB TRAJECTORIES RESULTING FROM A  
(-3/-5) ORIFICE COMBINATION AT MACH 0.95



**MS-9**

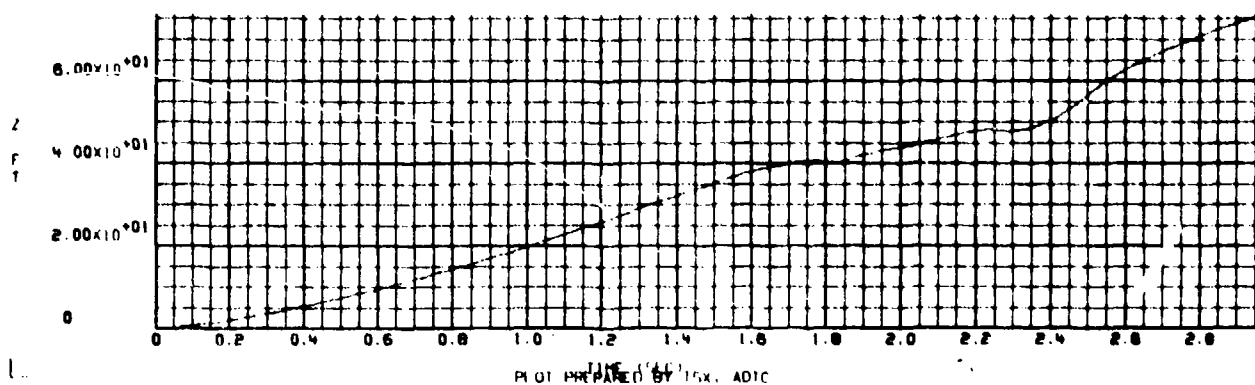
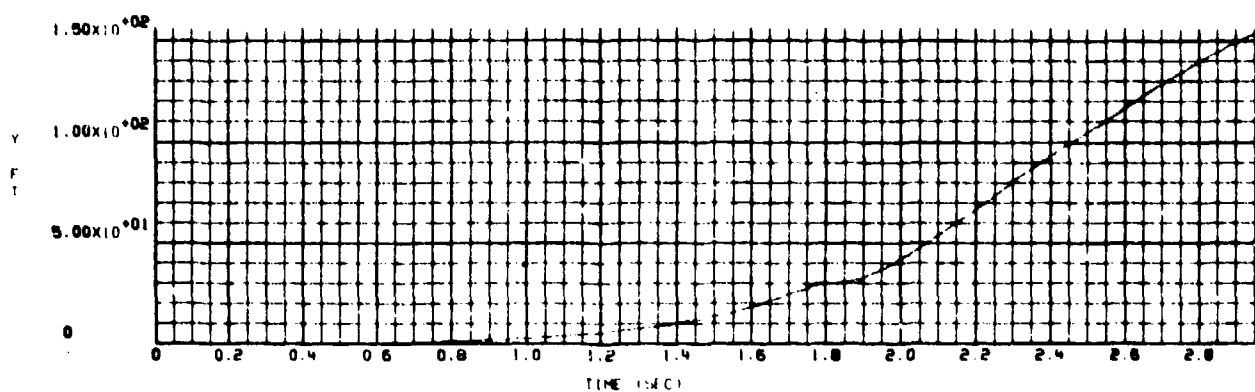
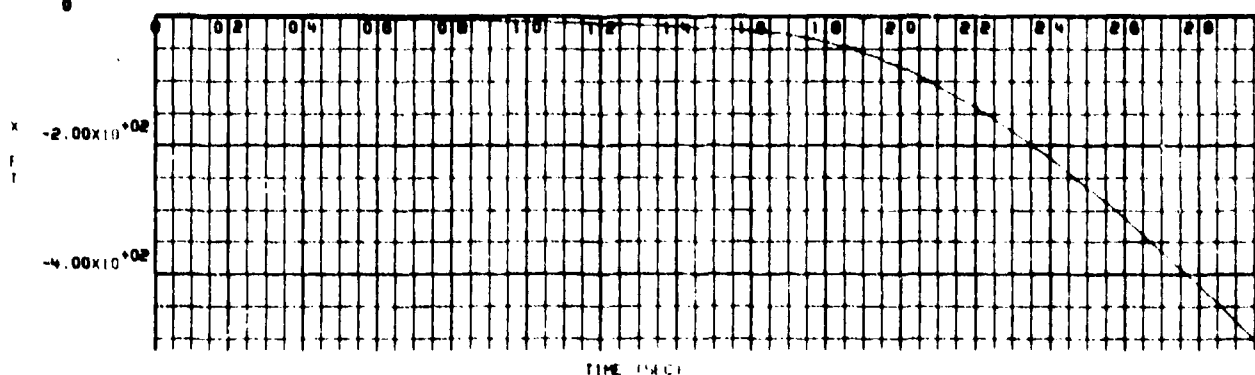


Figure W-1. X, Y, and Z Position Versus Time for a Flow Field Intensity of 1/2

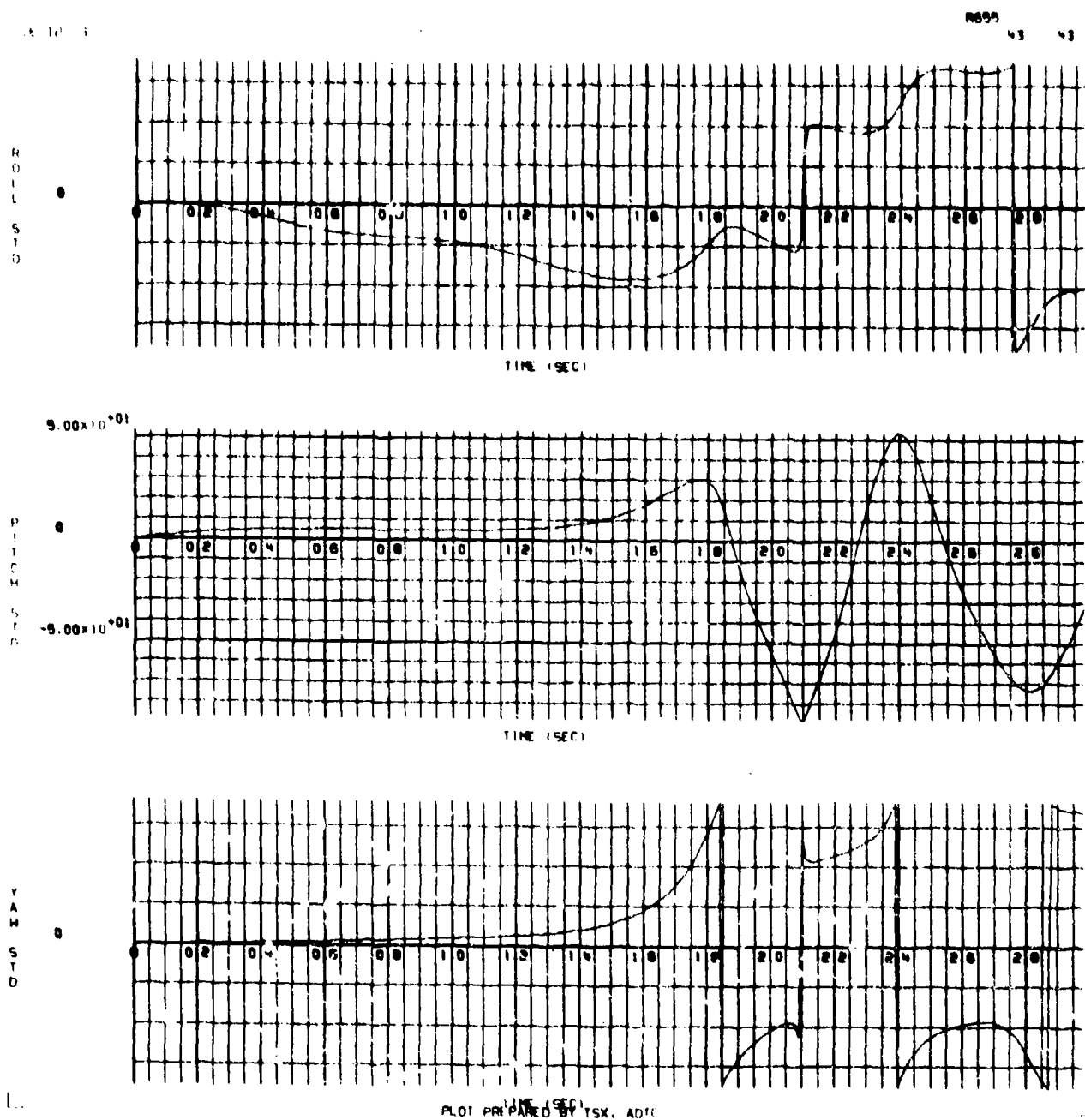
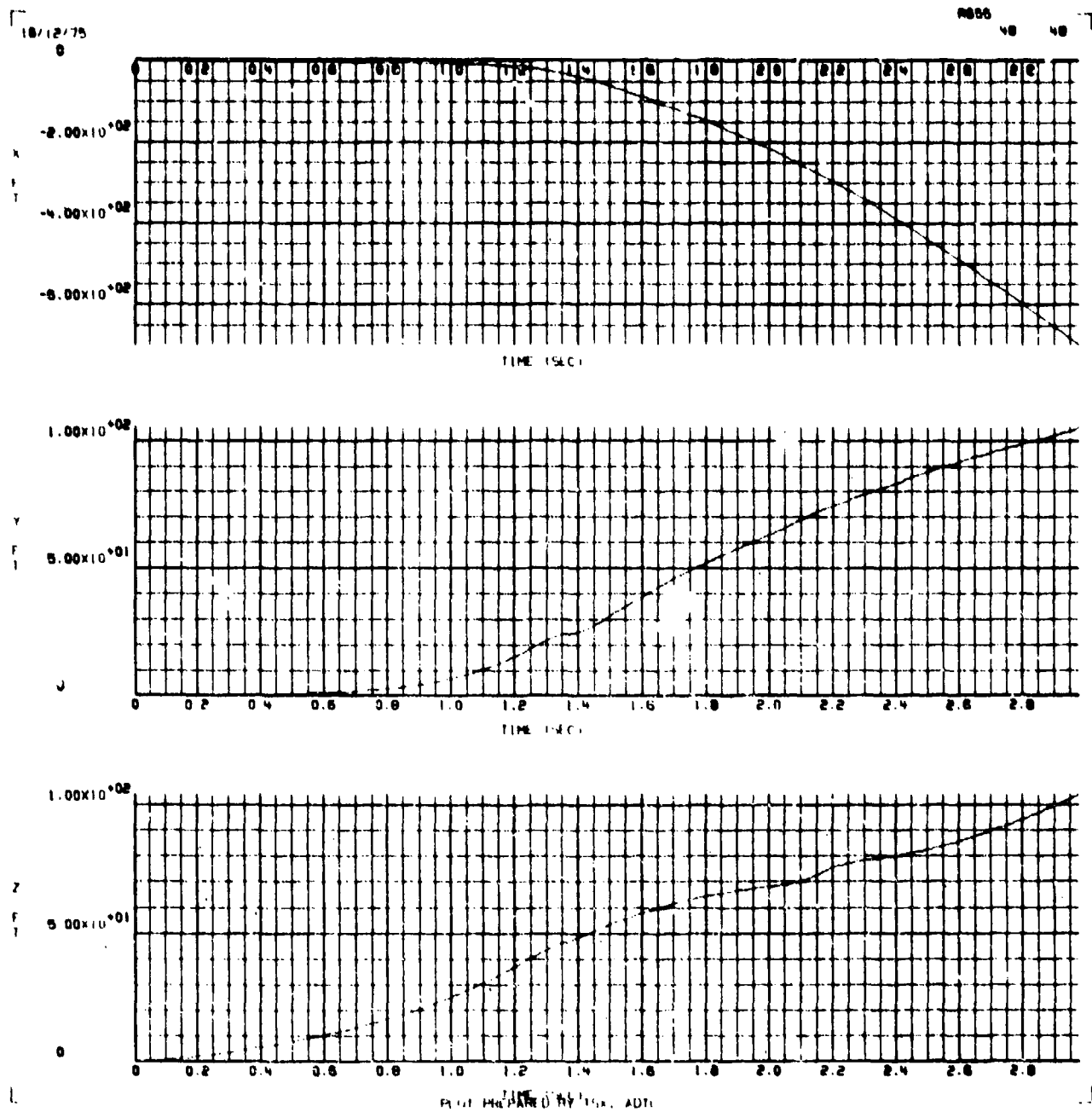


Figure W-2.  $\phi$ ,  $\theta$ , and  $\psi$  Rotation Versus Time for a Flow Field Intensity of  $1/2$



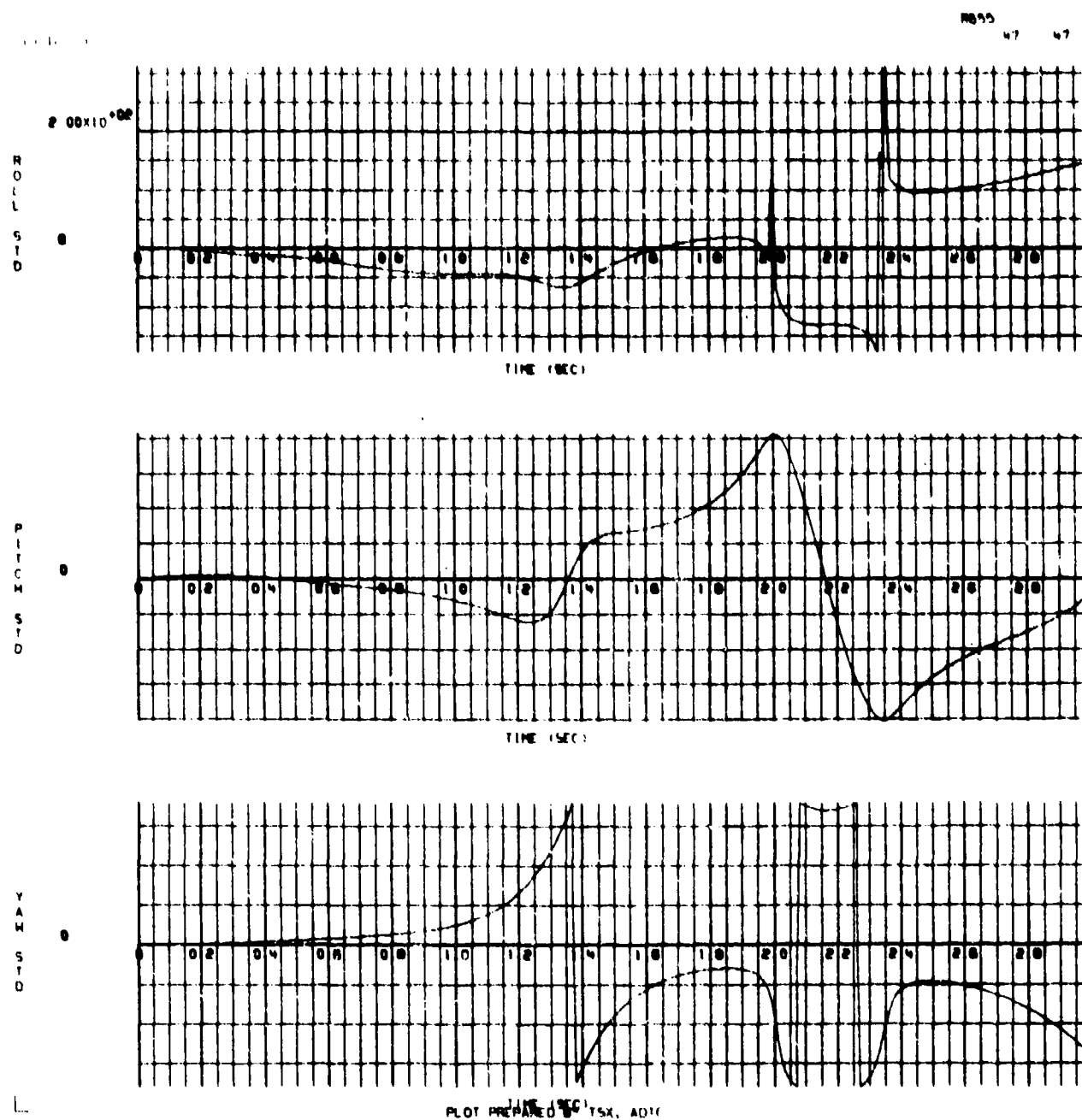


Figure W-4.  $\phi$ ,  $\theta$ , and  $\psi$  Rotation Versus Time for a Flow Field Intensity of 1 (unchanged from the wind tunnel measured values)

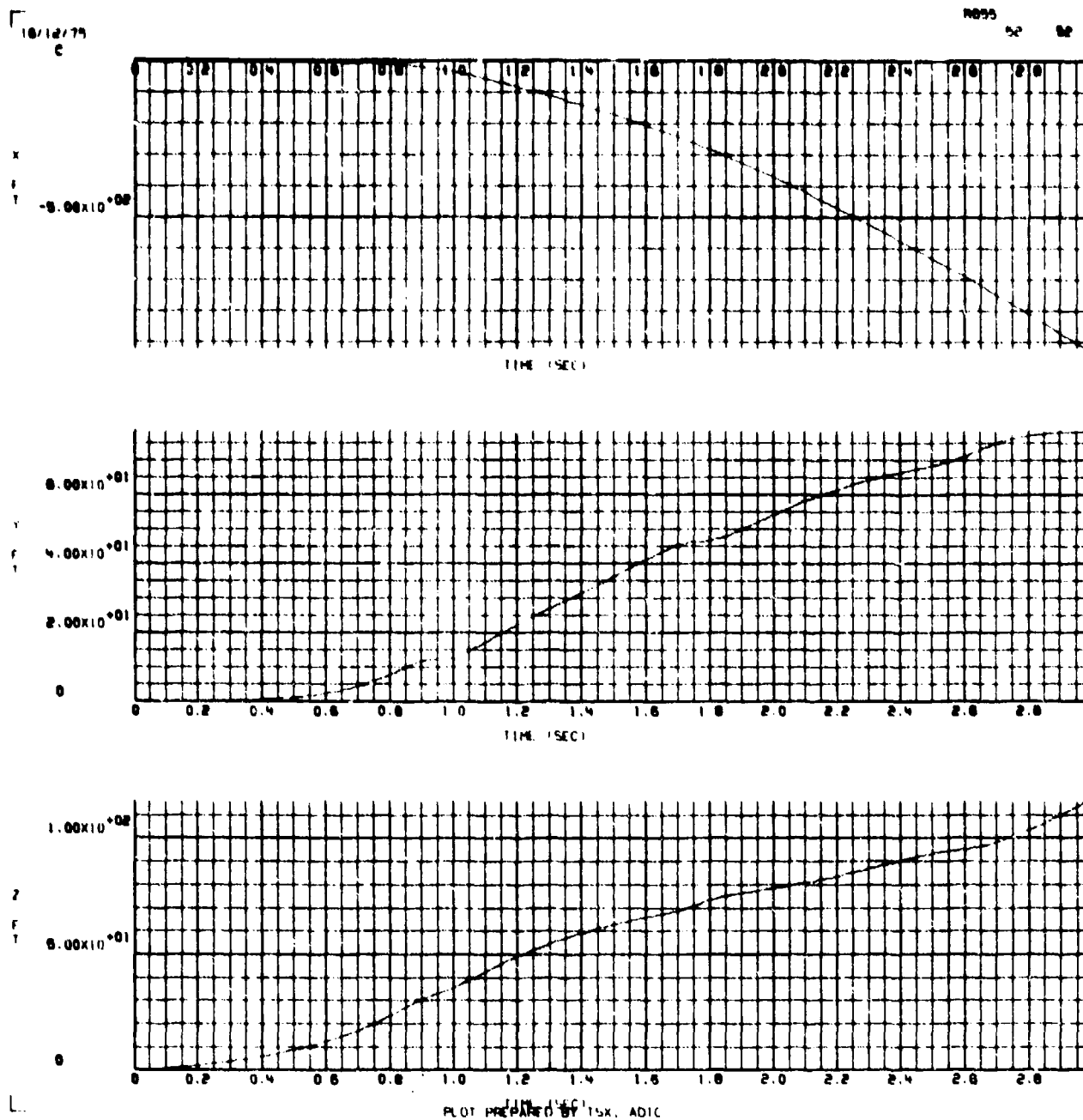


Figure W-5. X, Y, and Z Position Versus Time for a Flow Field Intensity of 2

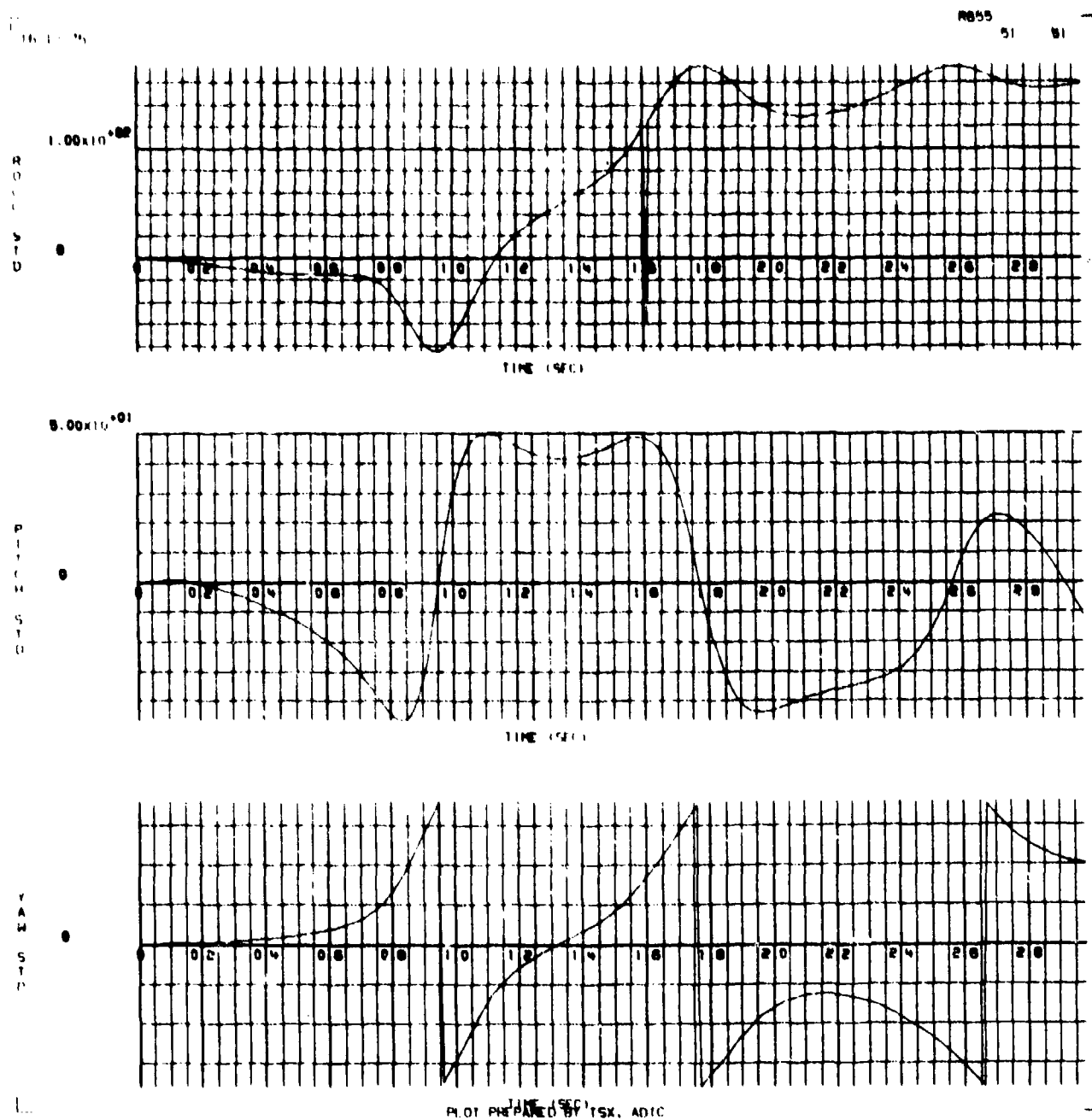
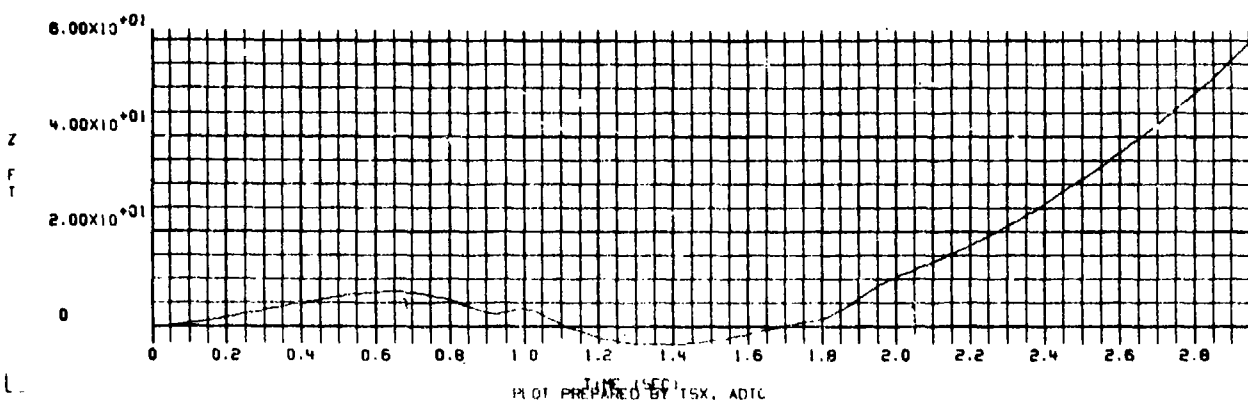
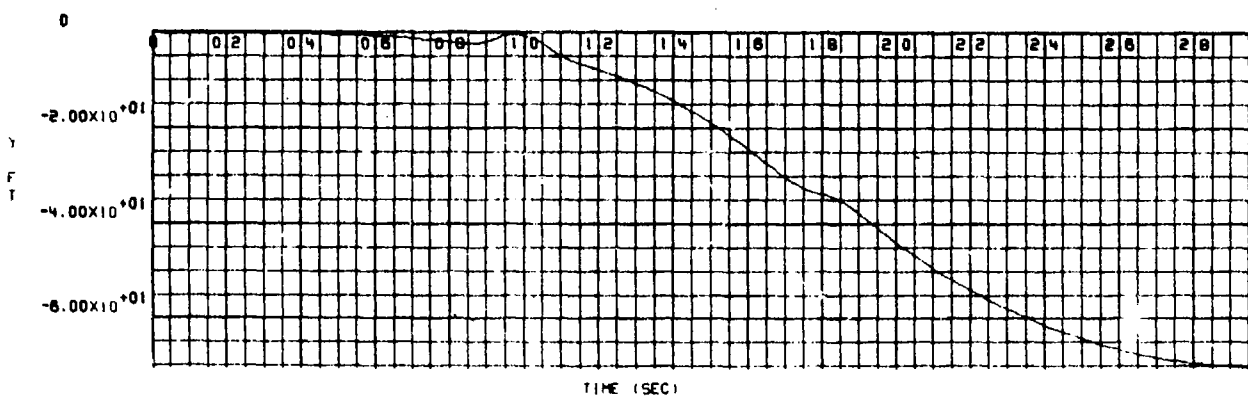
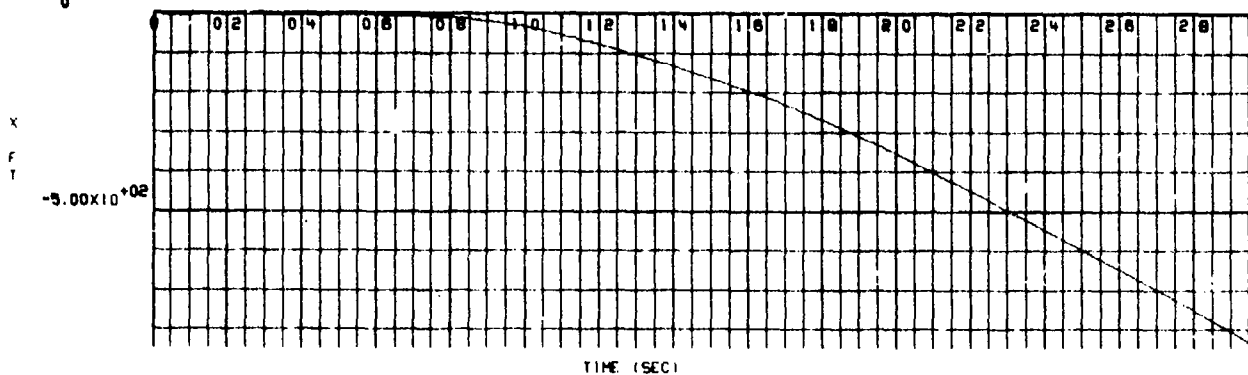


Figure W-6.  $\phi$ ,  $\theta$ , and  $\psi$  Rotation Versus Time for a Flow Field Intensity of 2

16/12/75  
0

R655 56 56



PIOT PREPARED BY TSX, ADIC

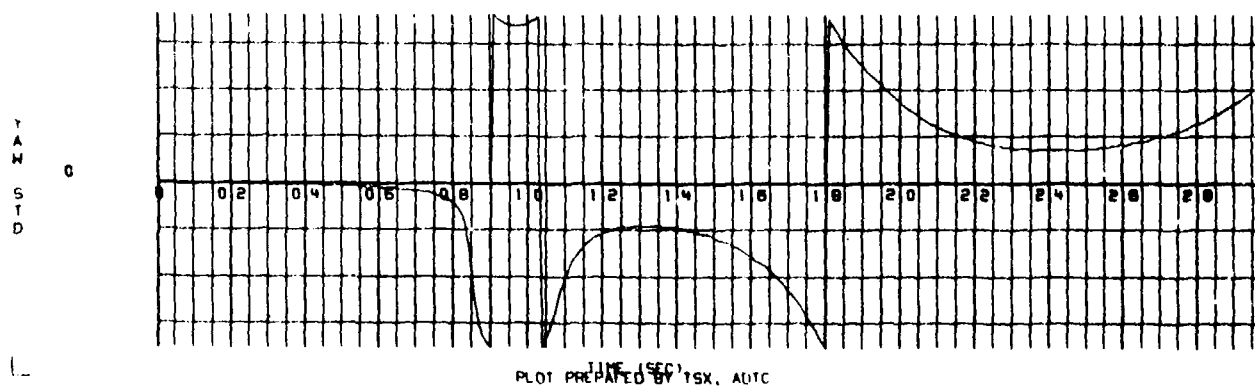
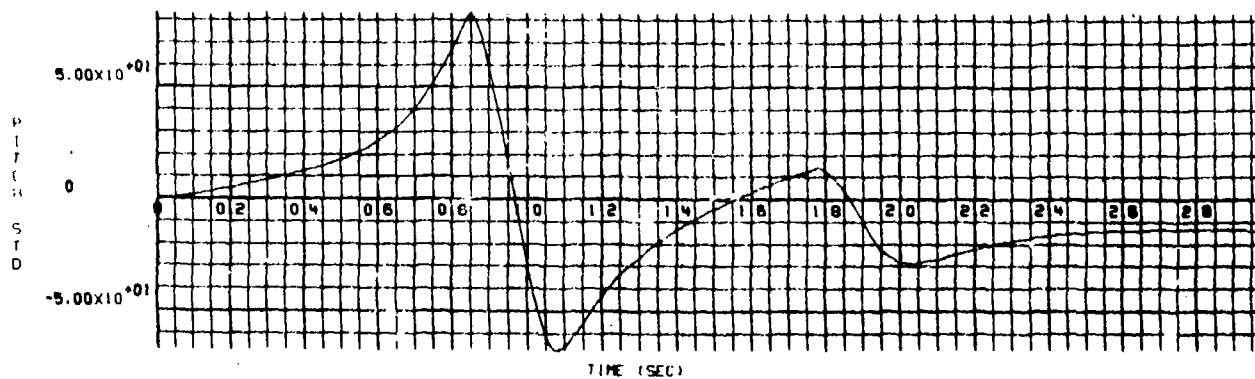
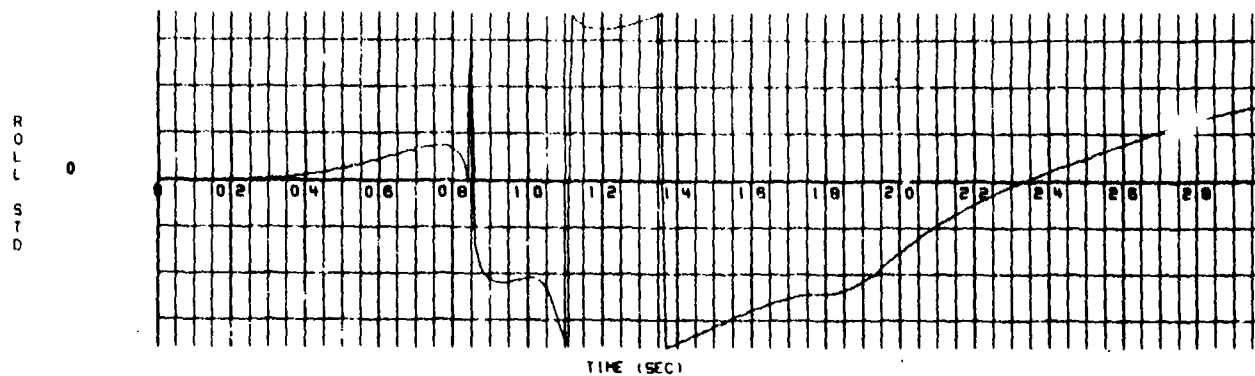
Figure W-7. X, Y, and Z Position Versus Time for a Flow Field Intensity of  $-1/2$

15/12/75

R055

55

55



TIME (SEC)  
PLOT PREPARED BY TSX, ADTC

Figure W-8.  $\phi$ ,  $\theta$ , and  $\psi$  Rotation Versus Time for a Flow Field Intensity of  $-1/2$



APPENDIX X

GBU-10 BOMB TRAJECTORIES RESULTING FROM A  
(-3/-5) ORIFICE COMBINATION AT MACH 1.2

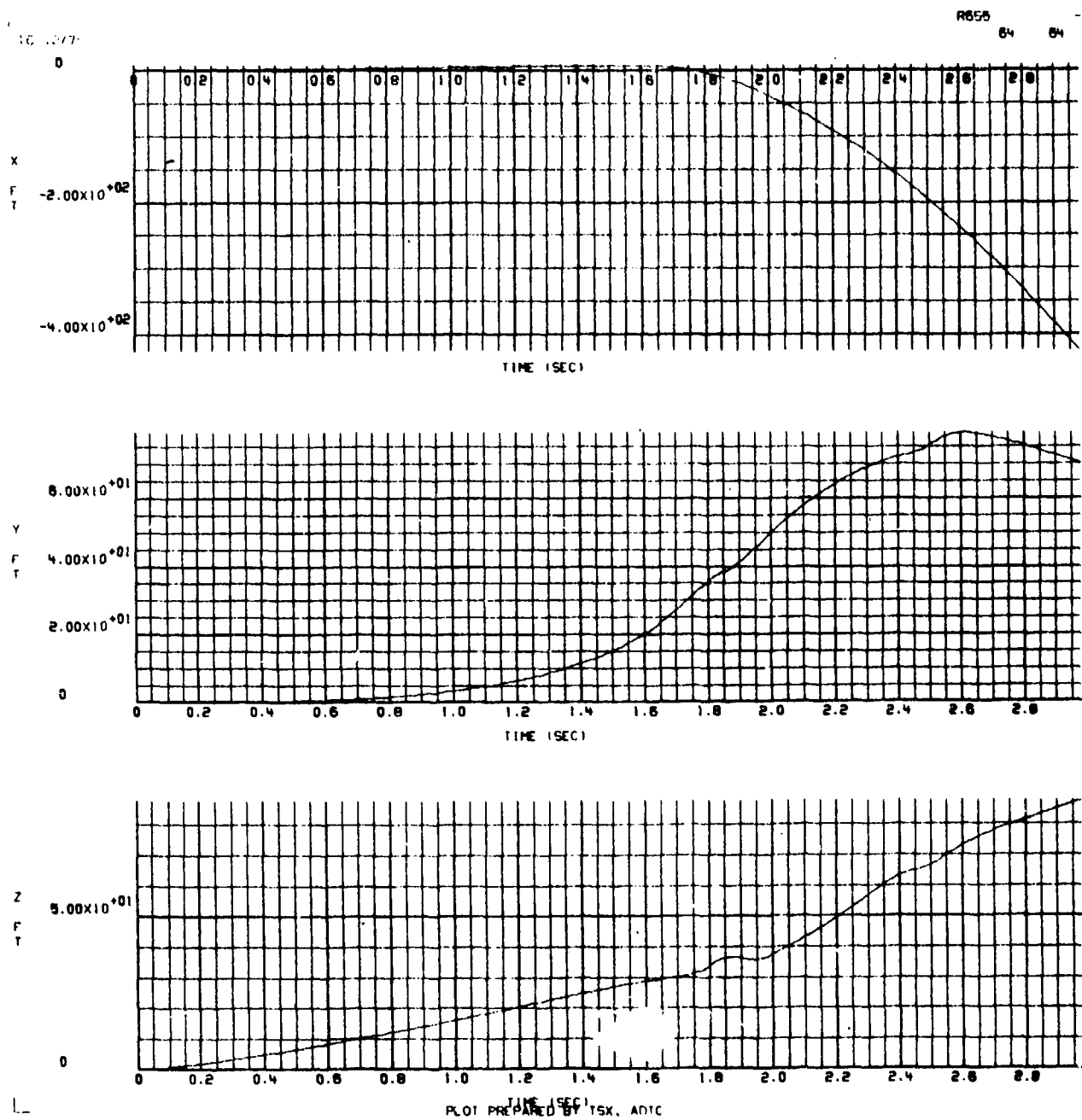


Figure X-1. X, Y, and Z Position Versus Time for a Flow Field Intensity of 1/2

10/12/79

R655

63 83

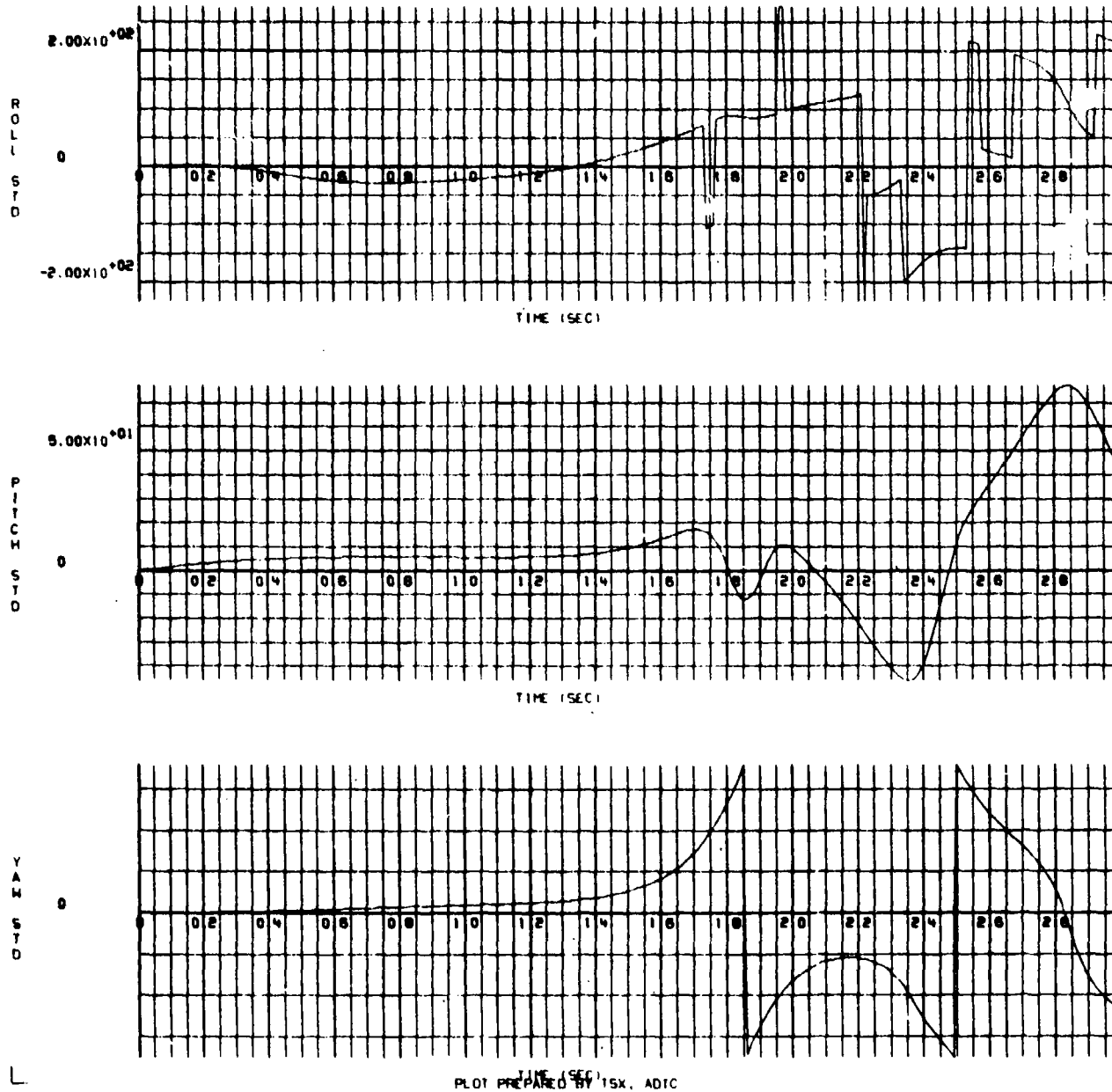


Figure X-2.  $\phi$ ,  $\theta$ , and  $\psi$  Rotation Versus Time for a Flow Field Intensity of 1/2

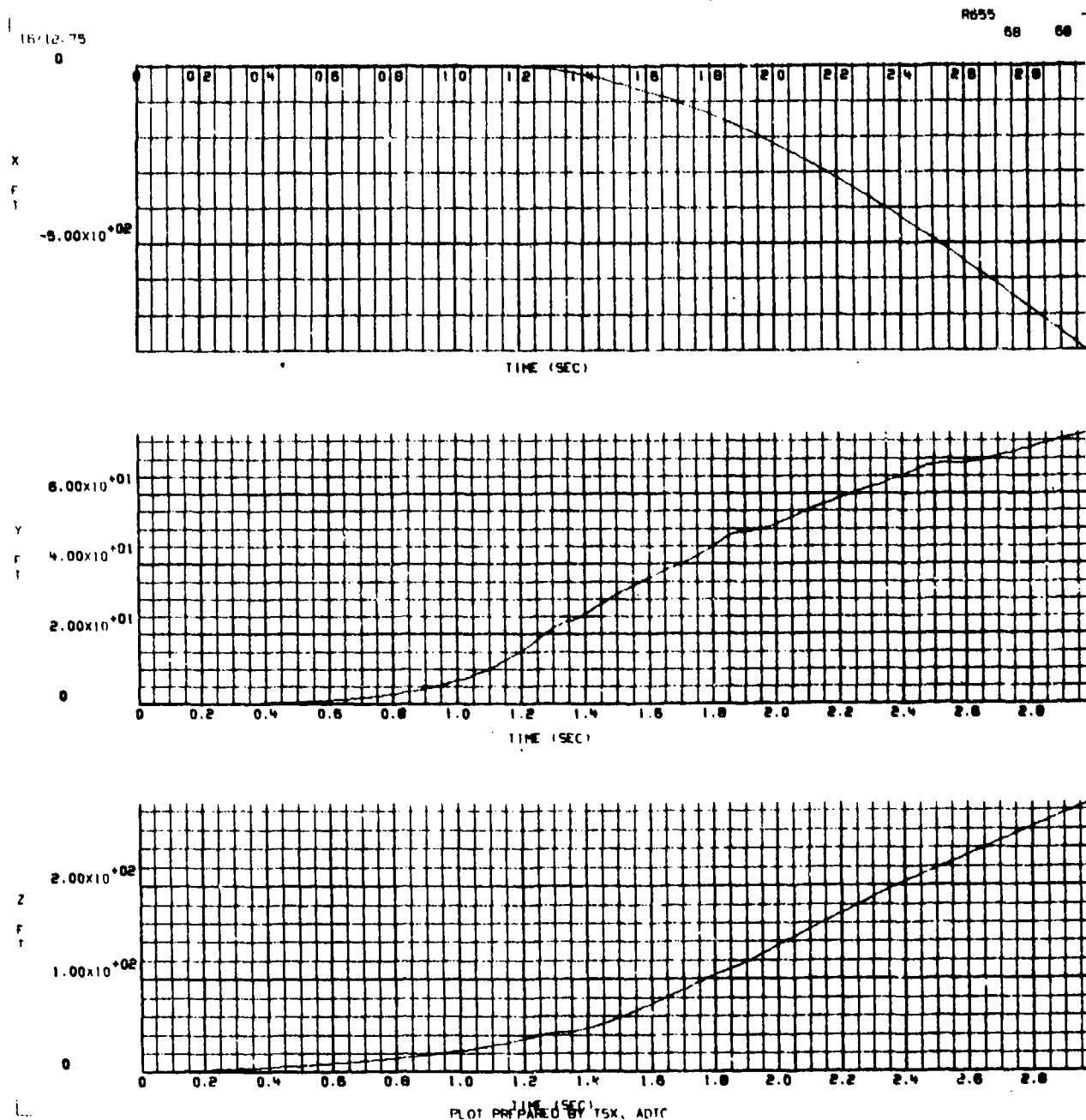


Figure X-3. X, Y, and Z Position Versus Time for a Flow Field Intensity of 1 (as measured in the wind tunnel)

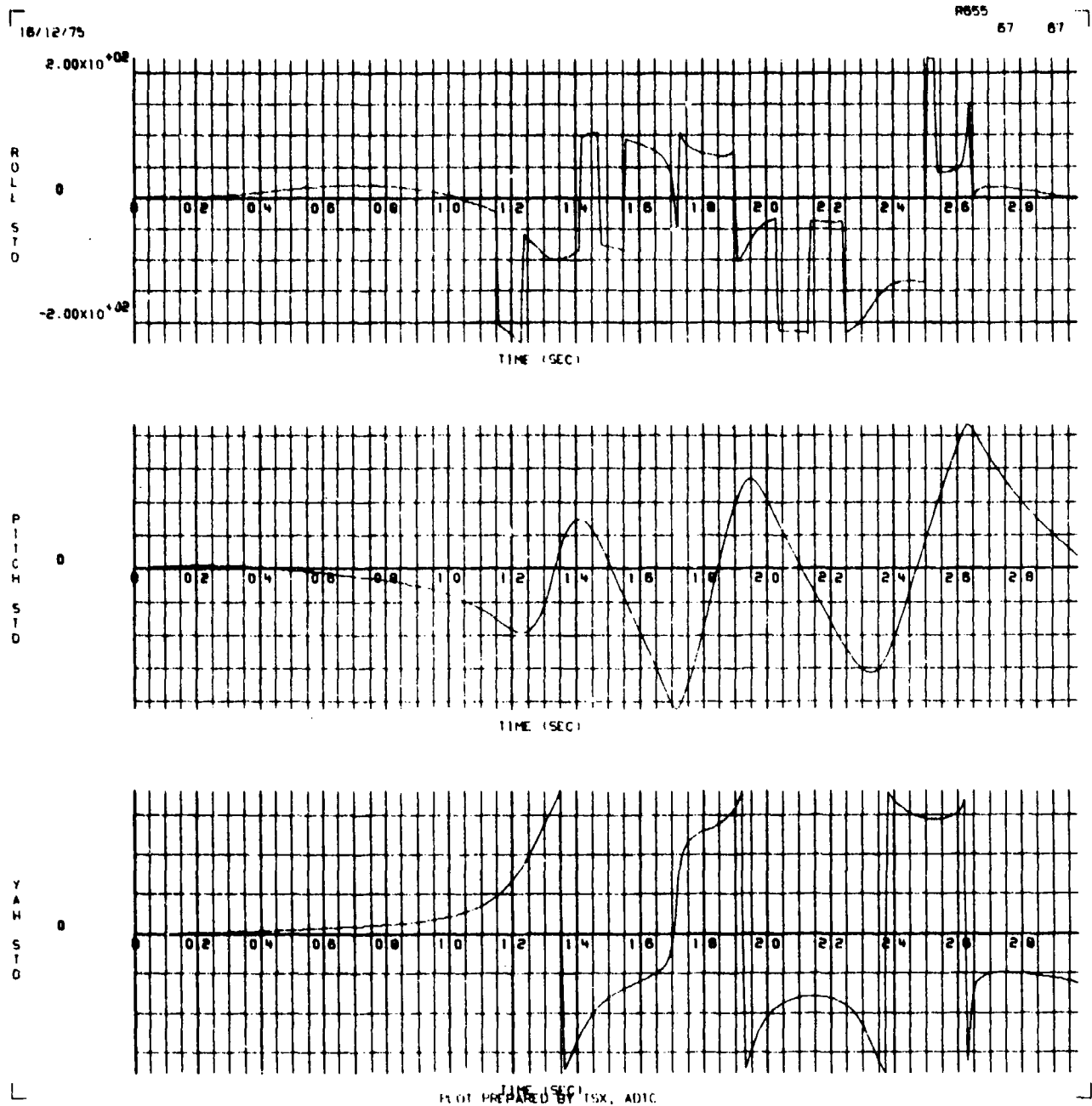


Figure X-4.  $\phi$ ,  $\theta$ , and  $\psi$  Rotation Versus Time for a Flow Field Intensity of 1 (unchanged from the wind tunnel measured values)

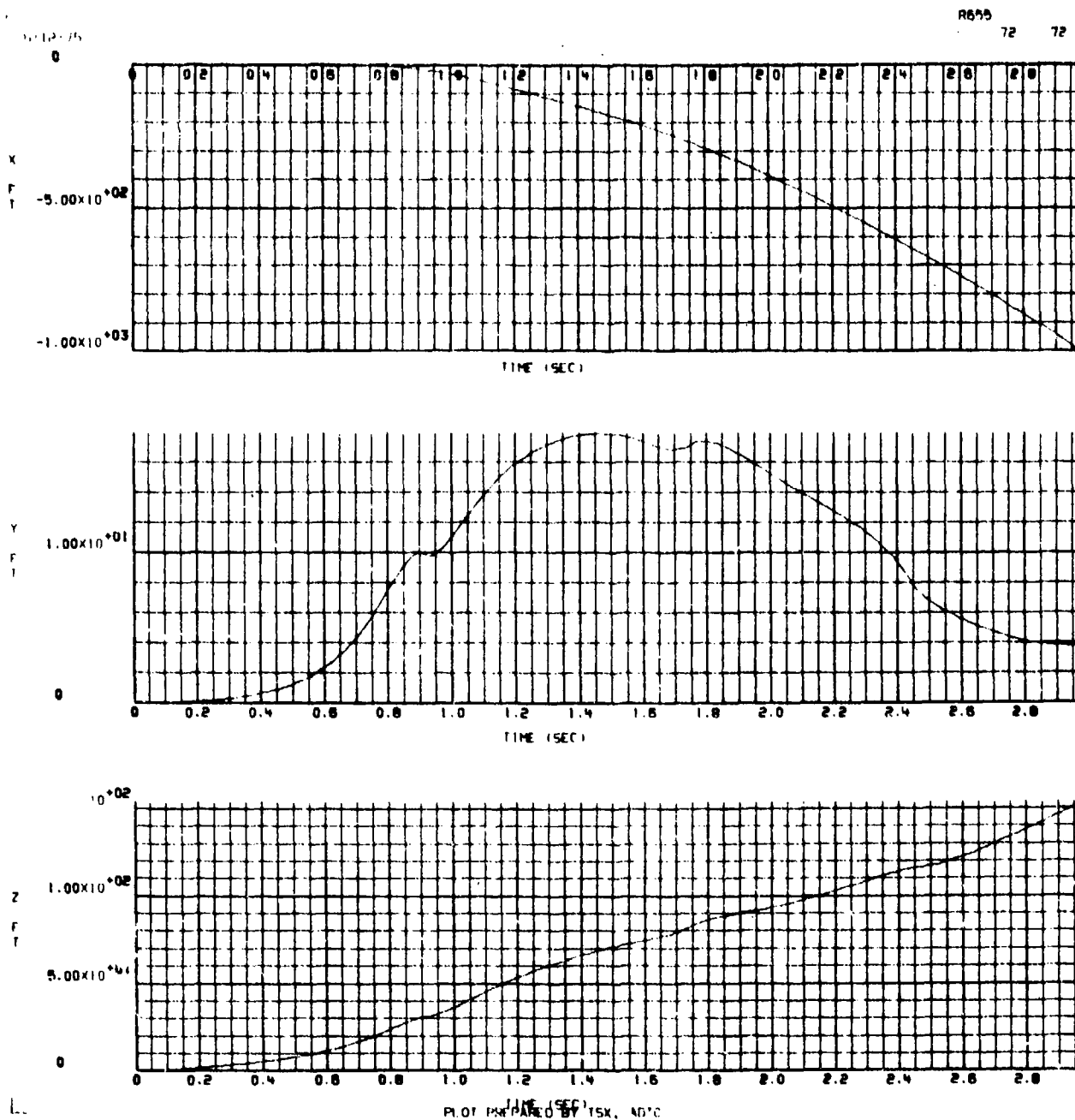
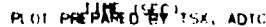


Figure X-5. X, Y, and Z Position Versus Time for a Flow Field Intensity of 2

KG55



220

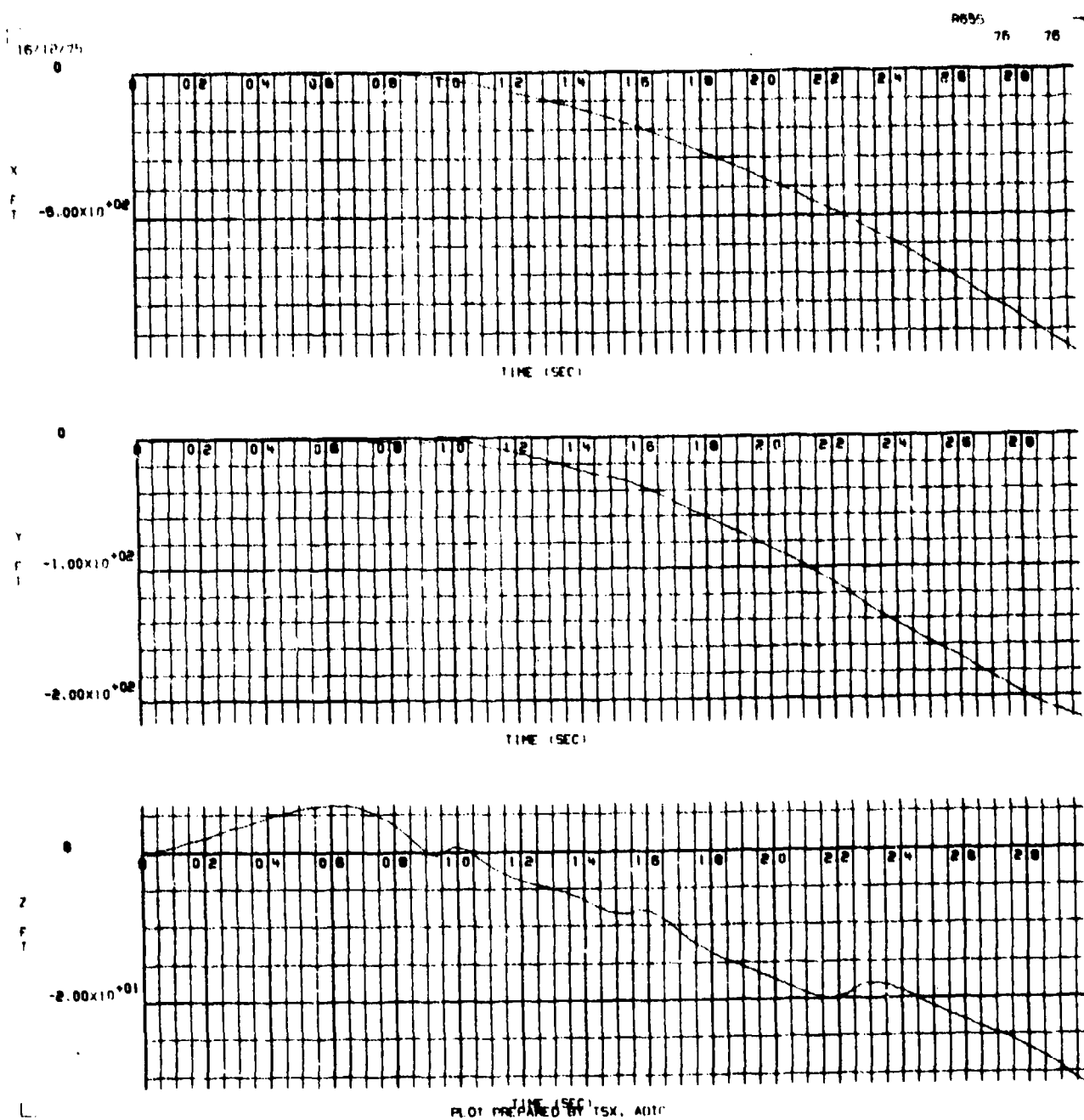


Figure X-7. X, Y, and Z Position Versus Time for a Flow Field Intensity of  $-1/2$



18/12/75

1855 75 75

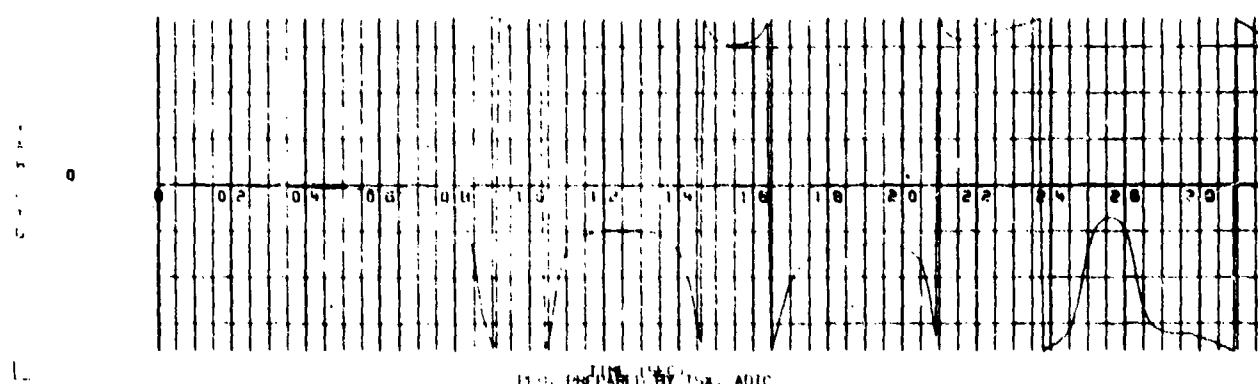
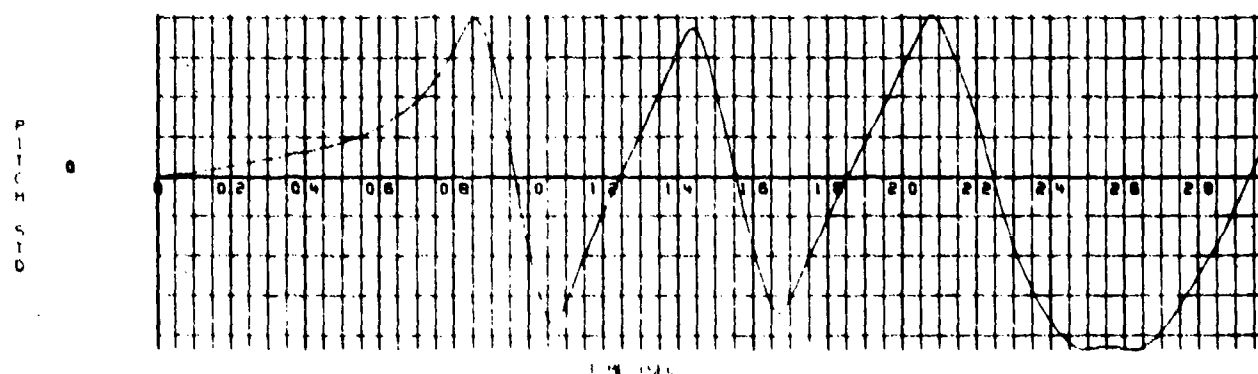
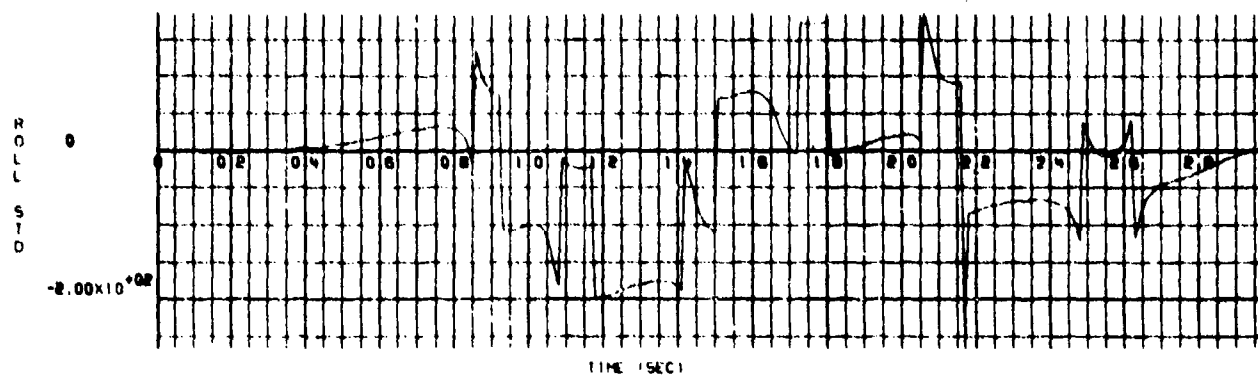


FIG. PREPARED BY TSK, ADIC

Figure X-8.  $\phi$ ,  $\theta$ , and  $\psi$  Rotation Versus Time for a Flow Field Intensity of  $-1/2$

APPENDIX AA

GBU-12 BOMB TRAJECTORIES RESULTING FROM A  
PARTIAL FIN OPENING AT MACH 0.7

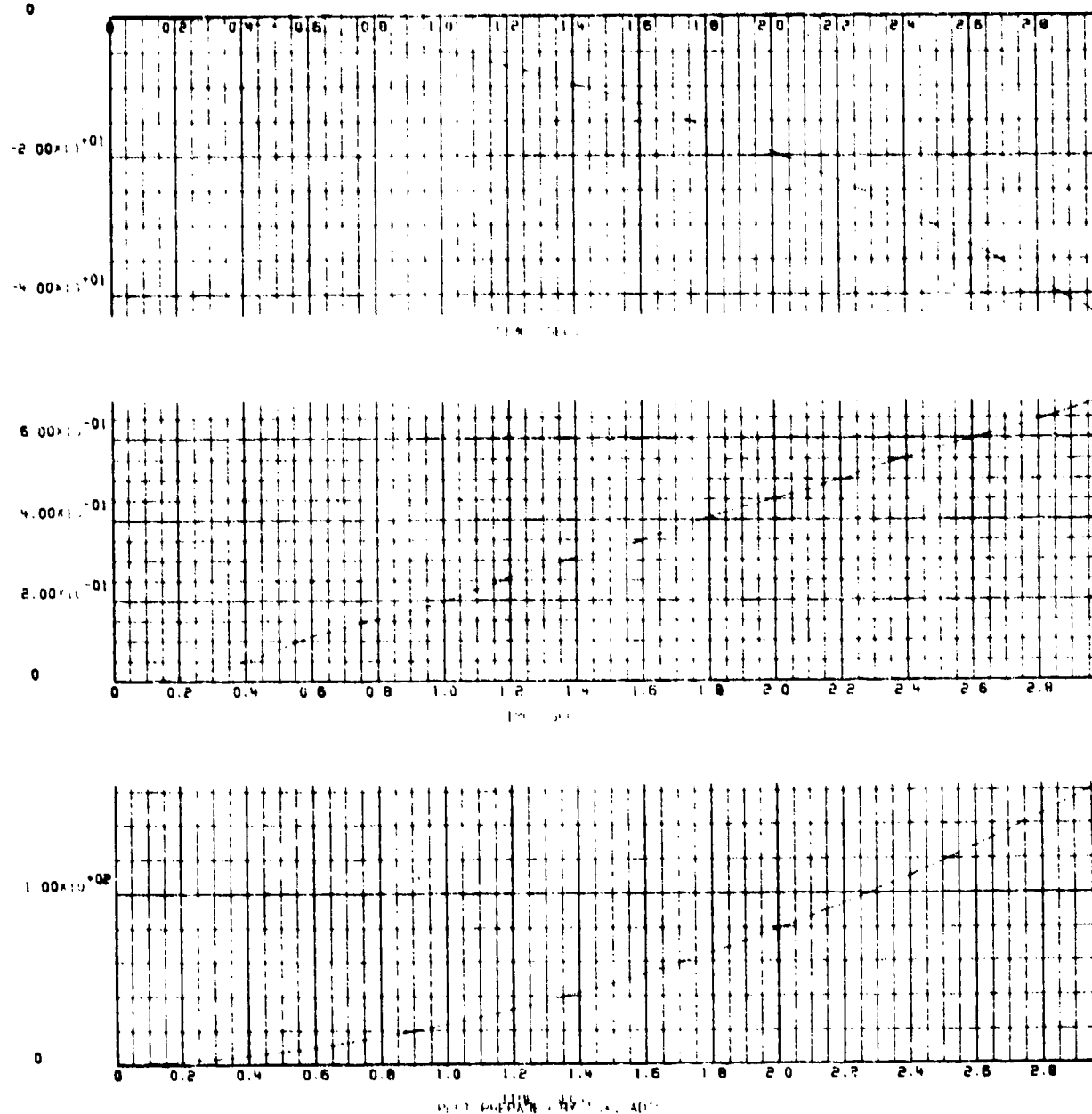


Figure AA-1. X, Y, and Z Position Versus Time for a Flow Field Intensity of 1/2

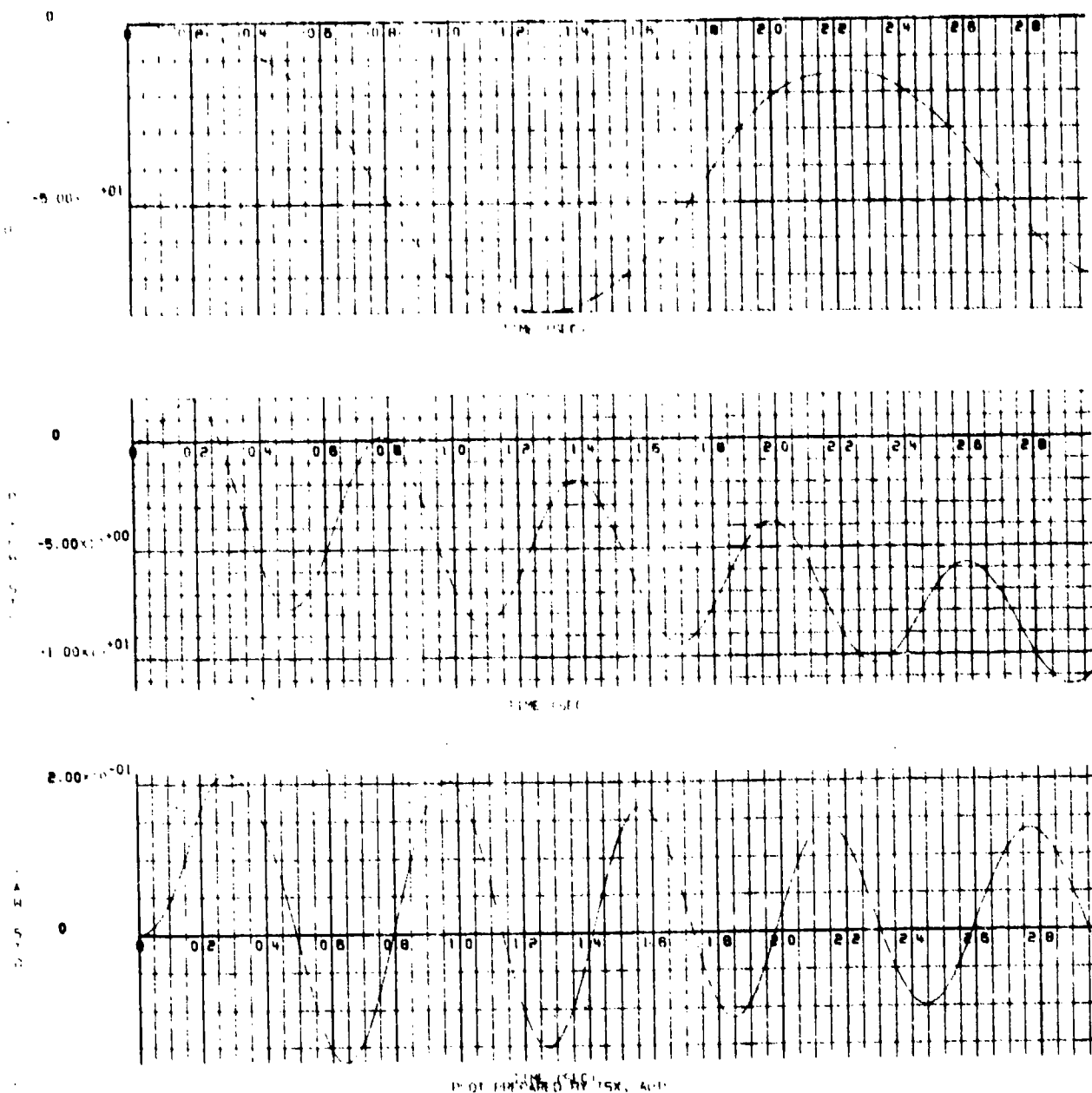


Figure AA-2.  $\phi$ ,  $\theta$ , and  $\psi$  Rotation Versus Time for a Flow Field Intensity of  $1/2$

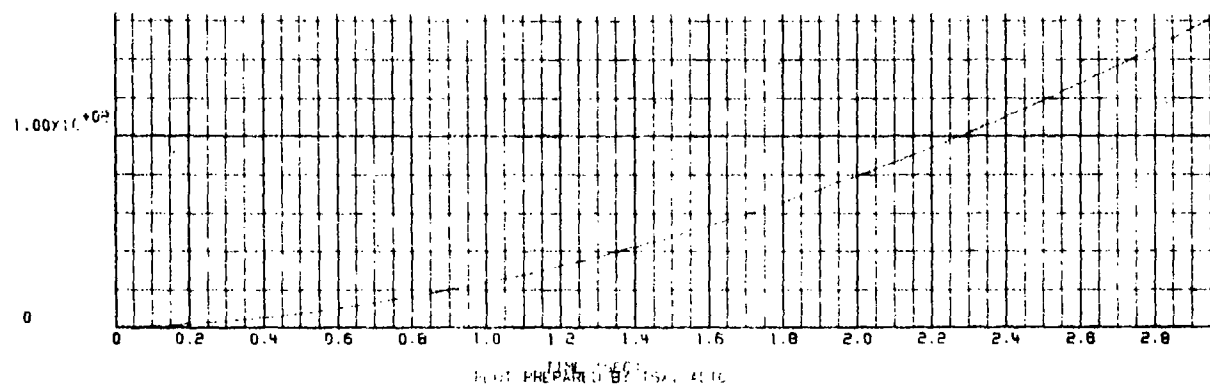
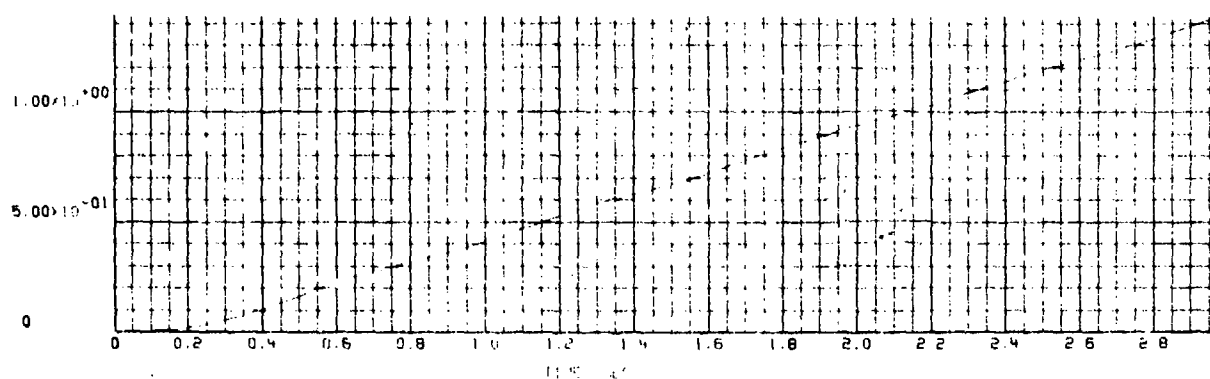
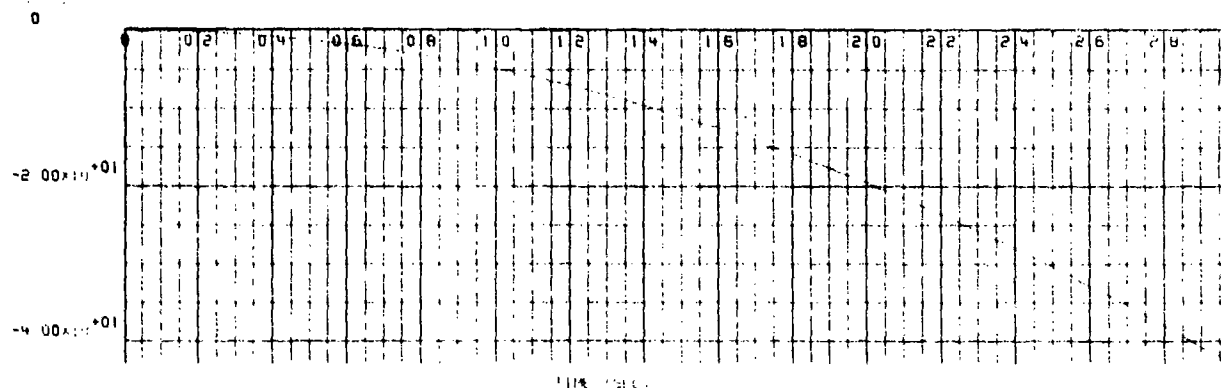


Figure AA-3. X, Y, and Z Position Versus Time for a Flow Field Intensity of 1 (as measured in the wind tunnel)

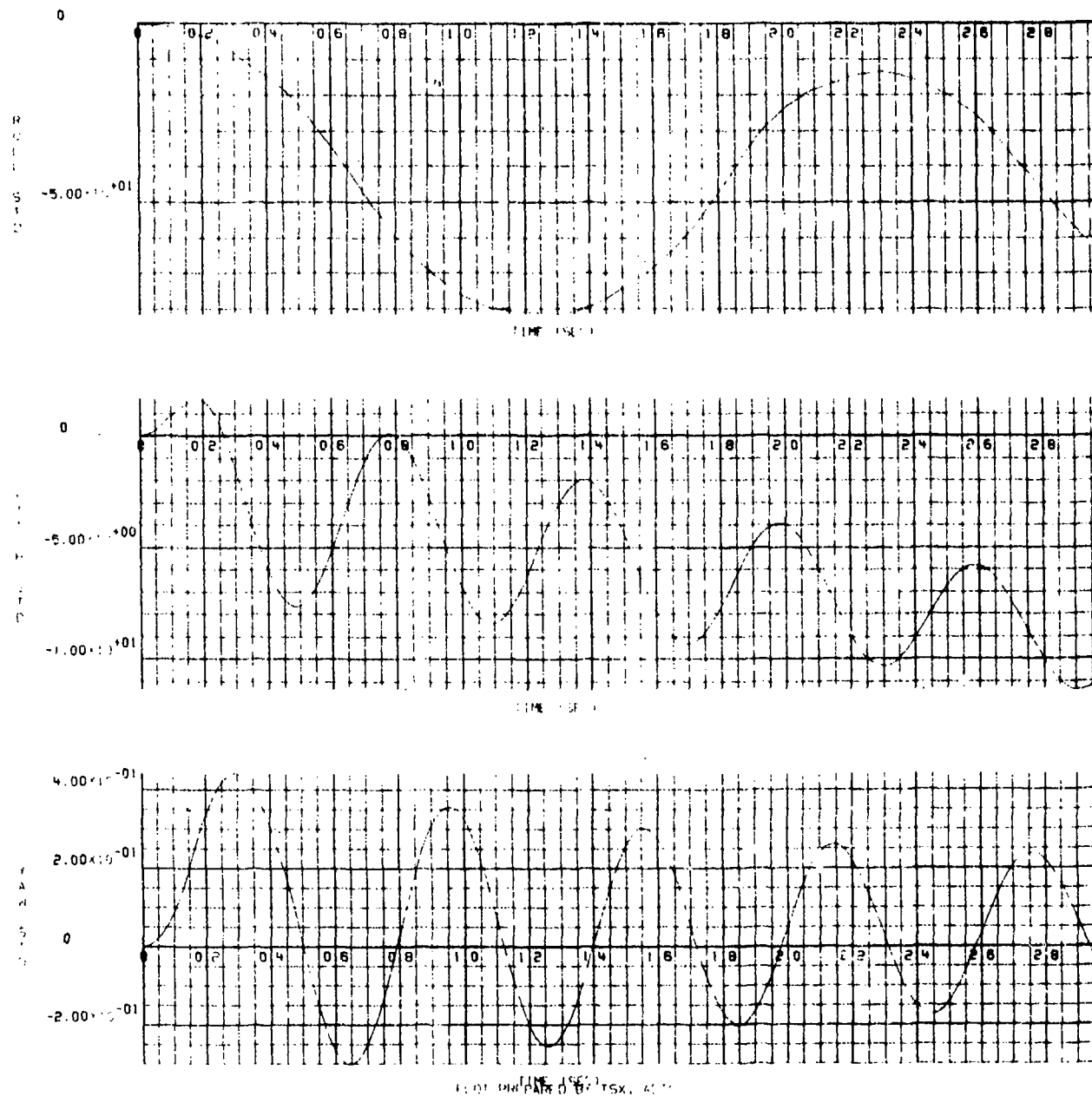


Figure AA-4.  $\phi$ ,  $\theta$ , and  $\psi$  Rotation Versus Time for a Flow Field Intensity of 1 (unchanged from the wind tunnel measured values)

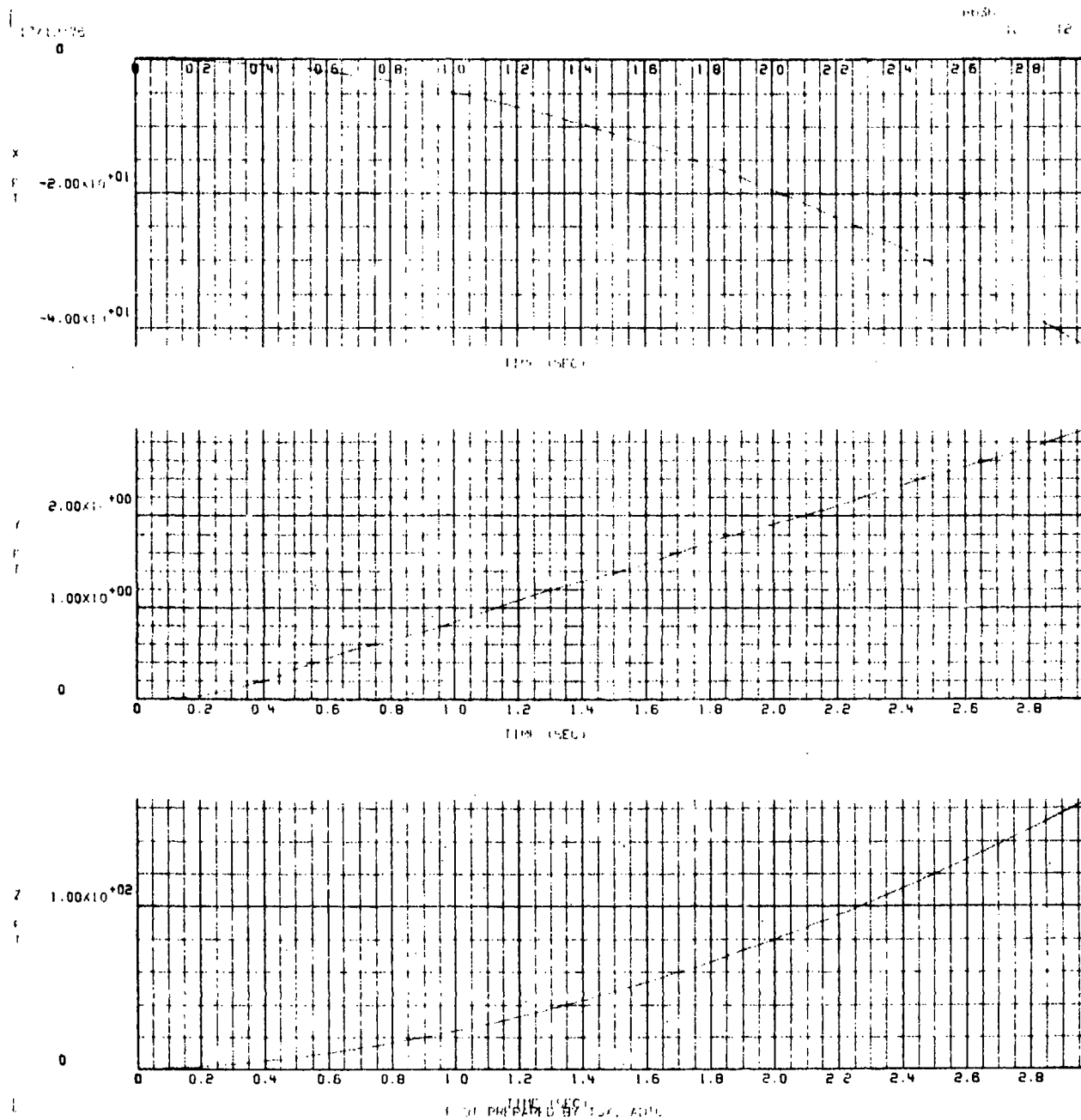


Figure AA-5. X, Y, and Z Position Versus Time for a Flow Field Intensity of 2

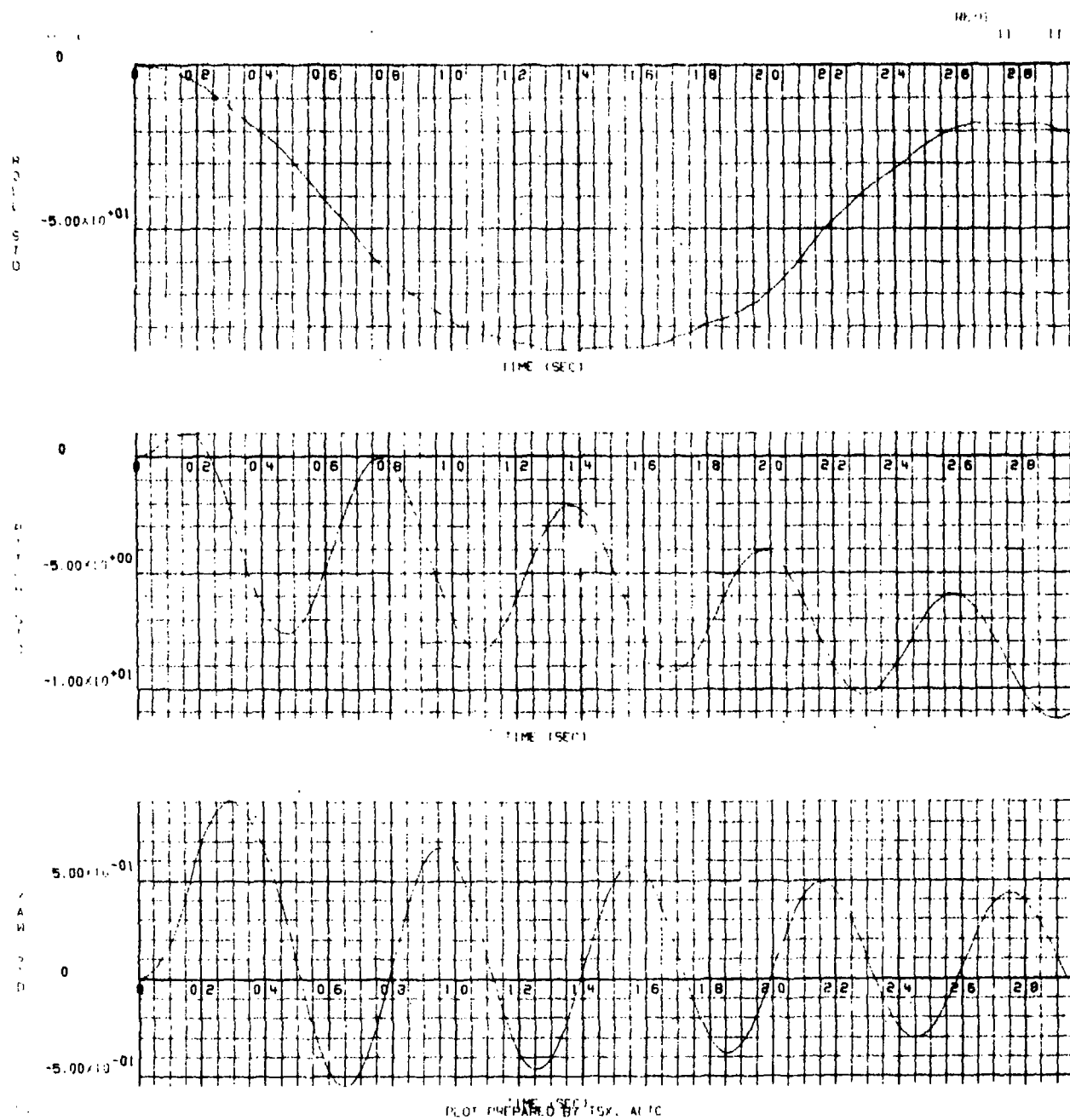


Figure AA-6.  $\phi$ ,  $\theta$ , and  $\psi$  Rotation Versus Time for a Flow Field Intensity of 2



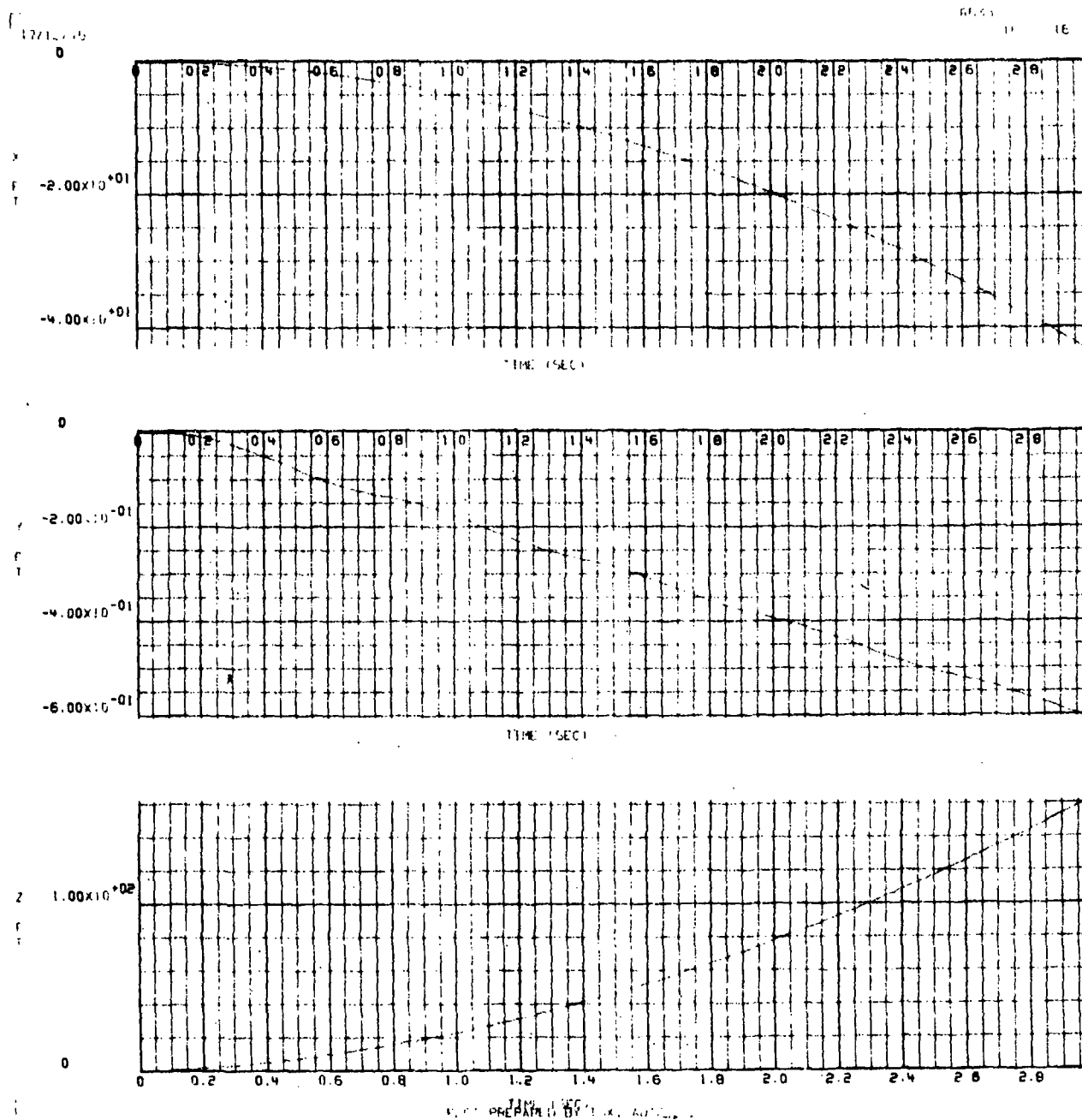


Figure AA-7. X, Y, and Z Position Versus Time for a Flow Field Intensity of  $-1/2$

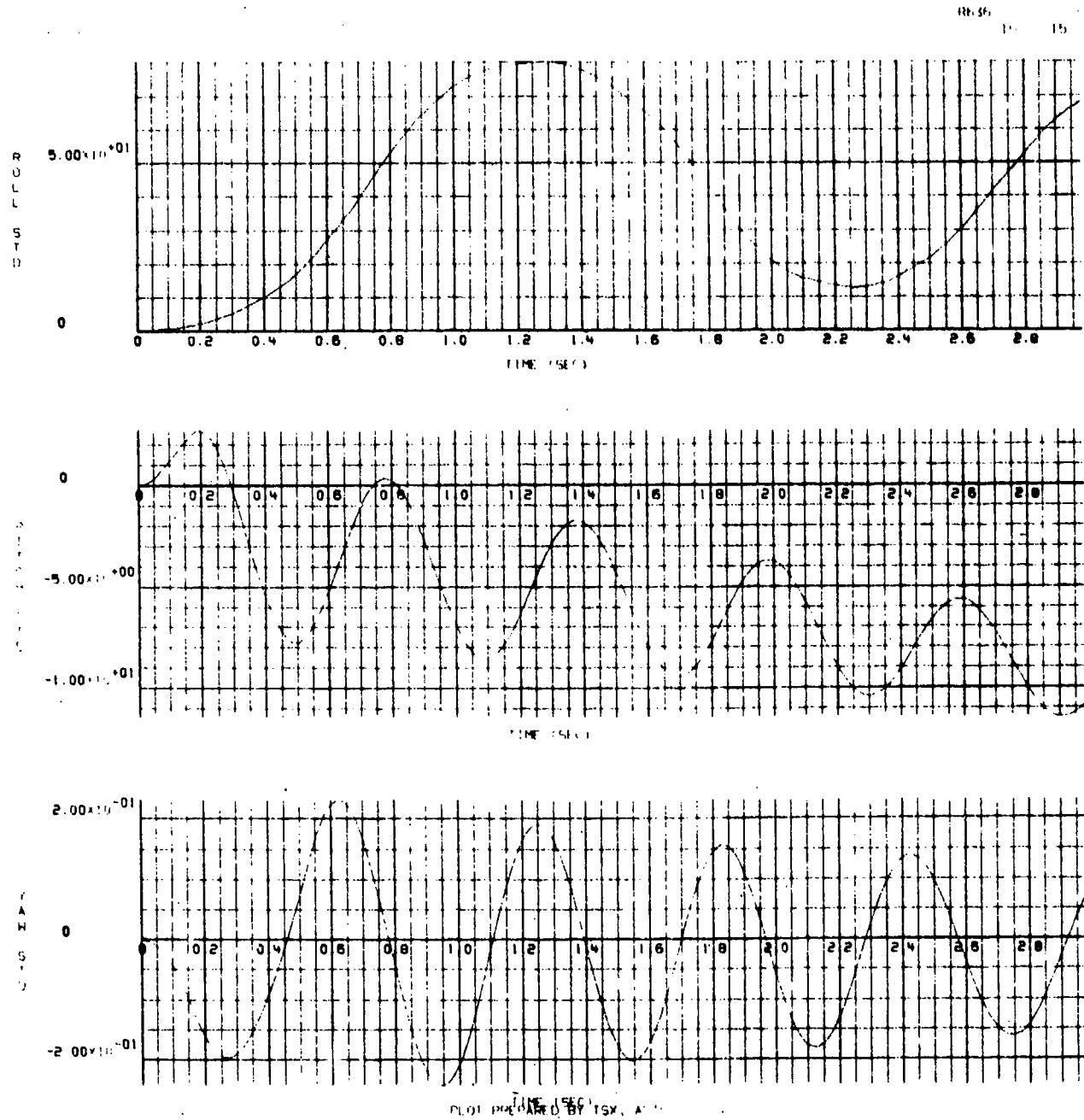


Figure AA-8.  $\phi$ ,  $\theta$ , and  $\psi$  Rotation Versus Time for a Flow Field Intensity of  $-1/2$

APPENDIX BB

GBU-12 BOMB TRAJECTORIES RESULTING FROM A  
PARTIAL FIN OPENING AT MACH 0.85



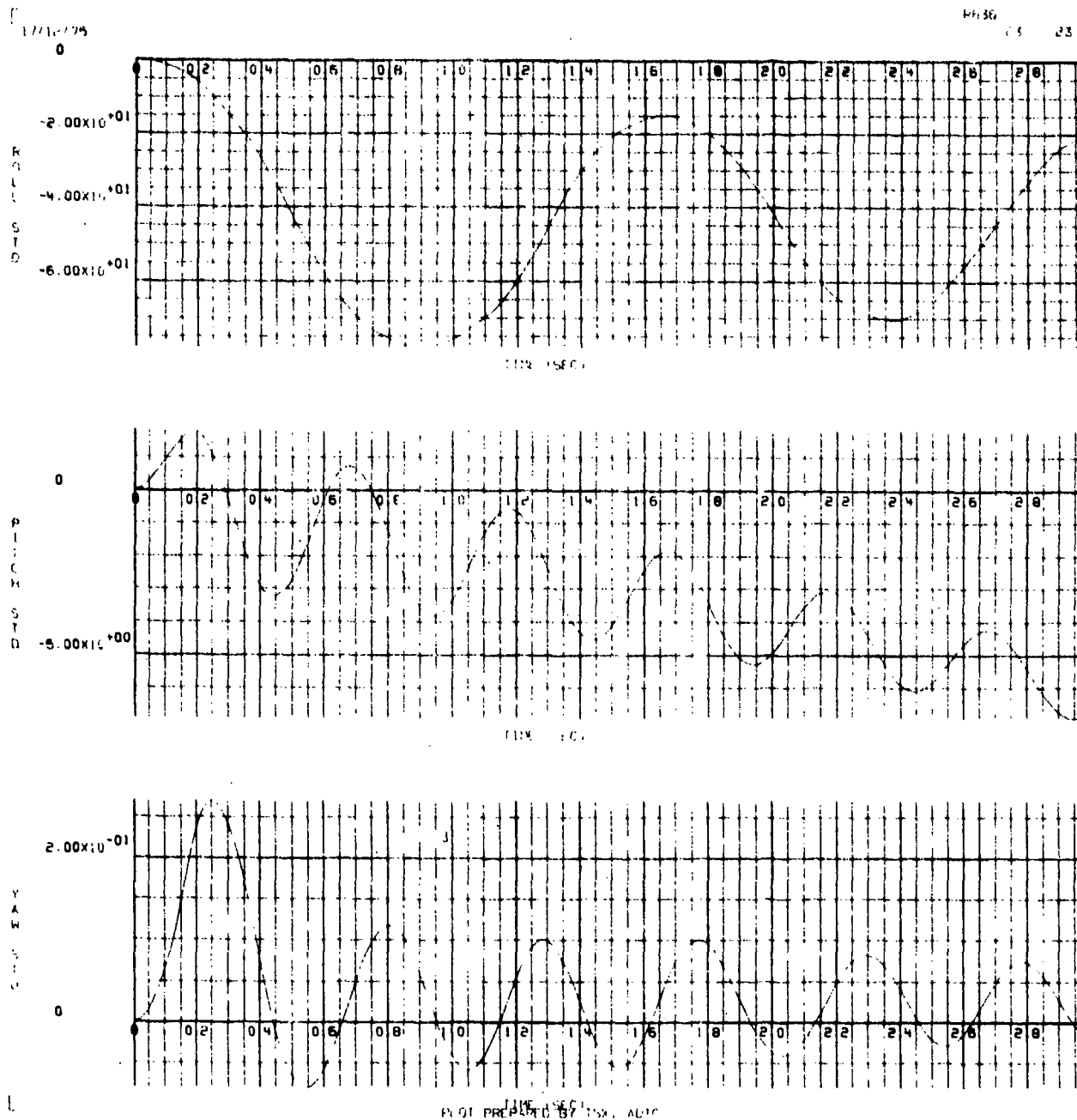


Figure BB-2.  $\phi$ ,  $\theta$ , and  $\psi$  Rotation Versus Time for a Flow Field Intensity of  $1/2$

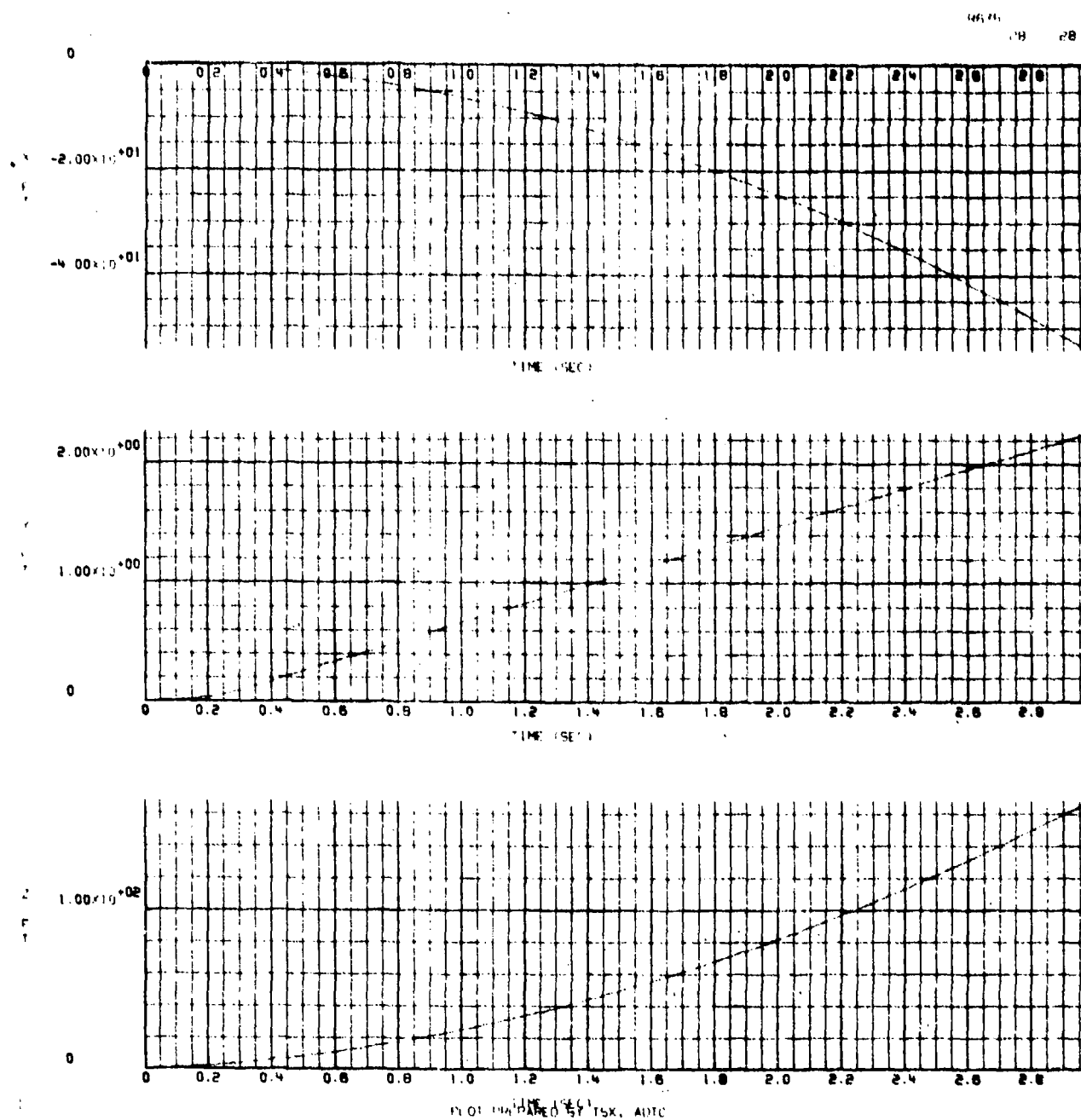


Figure BB-3. X, Y, and Z Position Versus Time for a Flow Field Intensity of 1 (as measured in the wind tunnel)

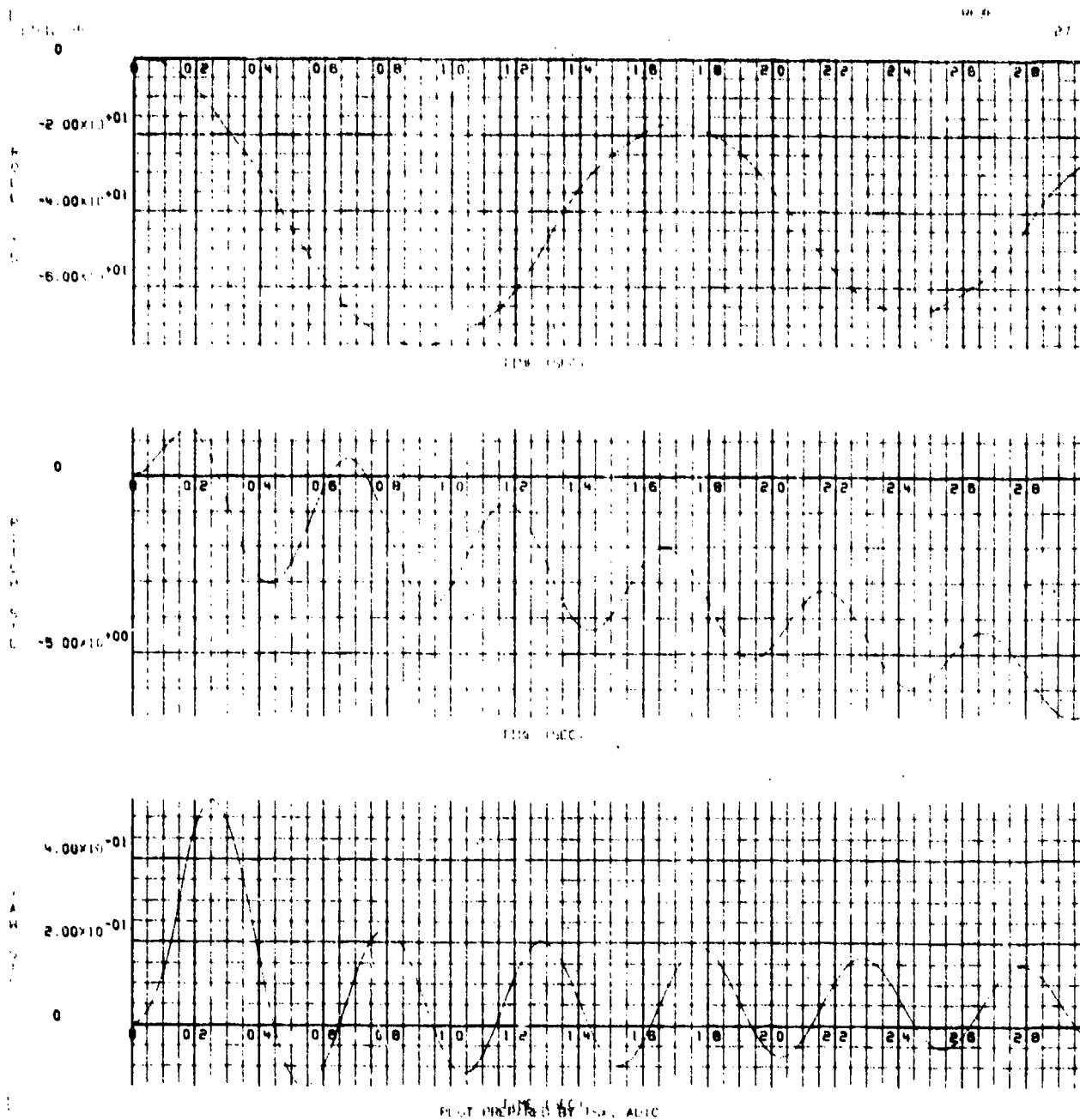


Figure BB-4.  $\phi$ ,  $\theta$ , and  $\psi$  Rotation Versus Time for a Flow Field Intensity of 1 (unchanged from the wind tunnel measured values)

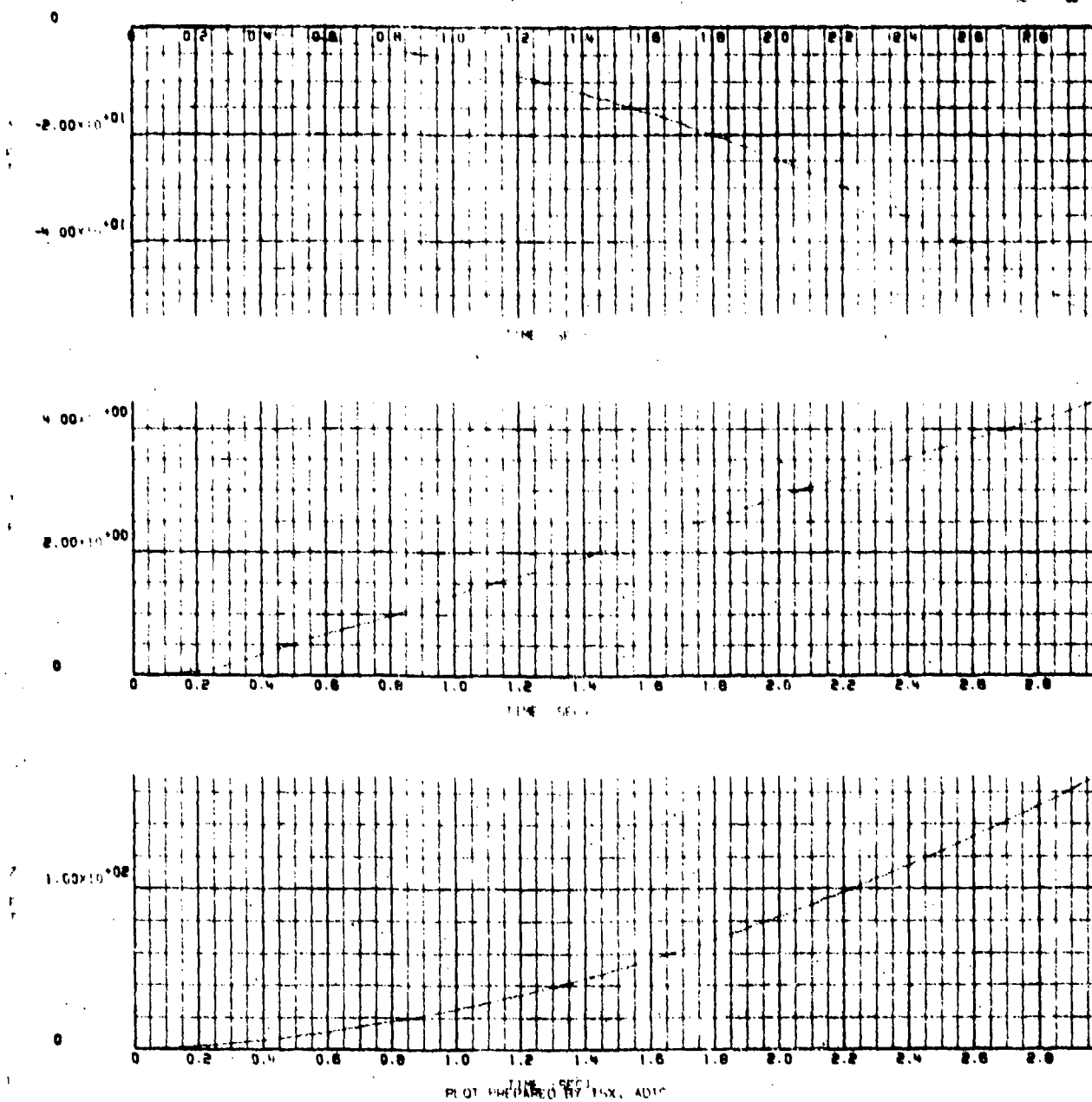
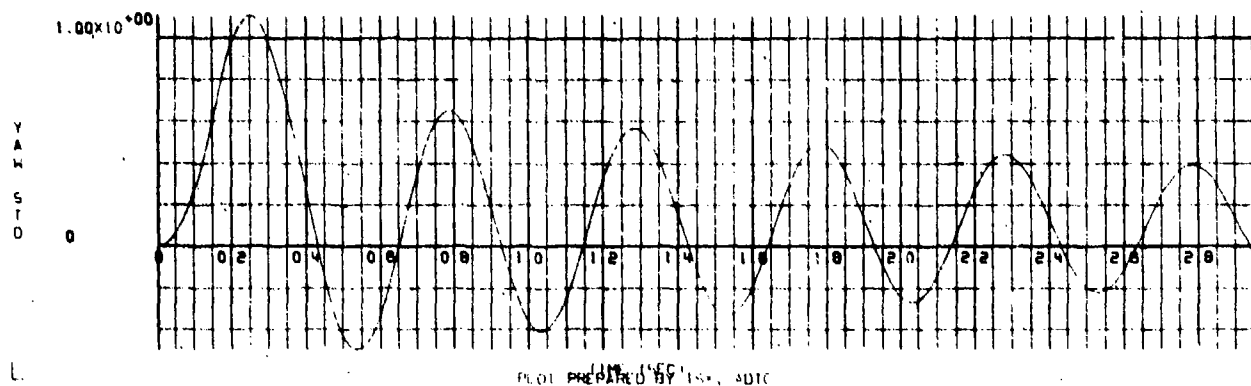
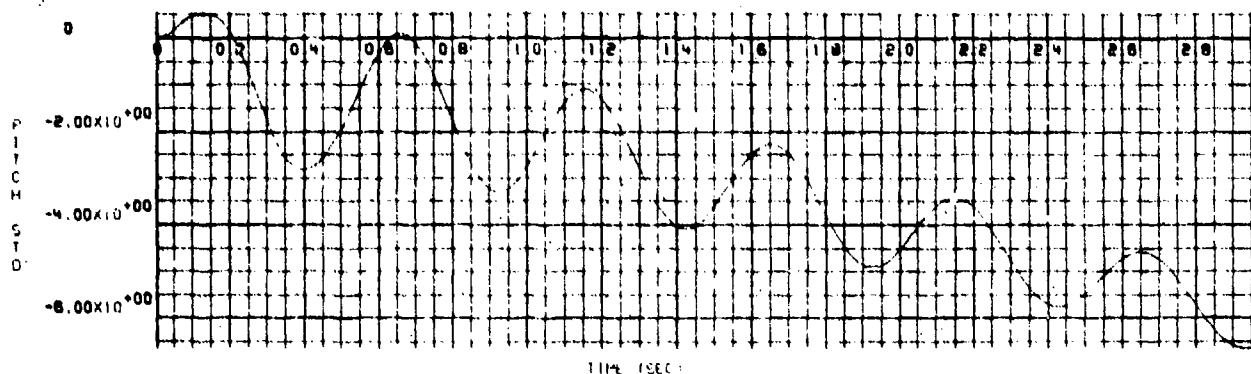
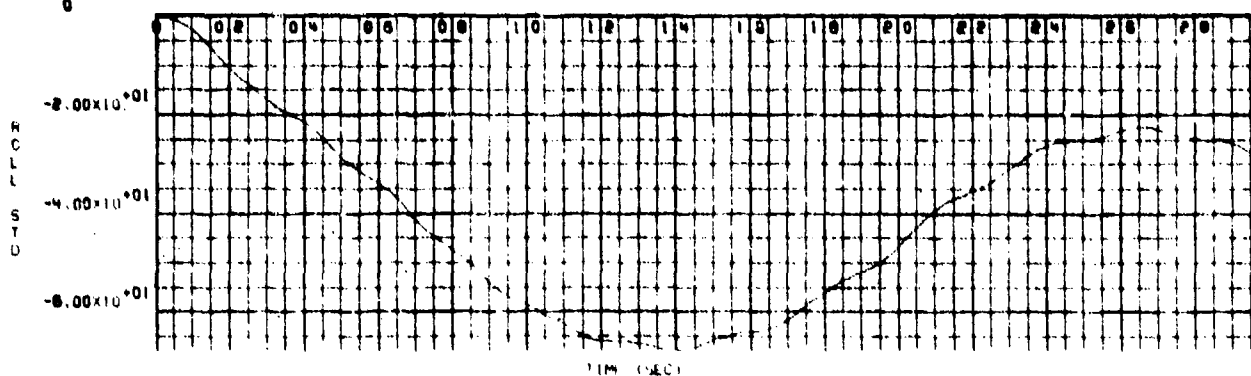


Figure BB-5. X, Y, and Z Position Versus Time for a Flow Field Intensity of 2



17-12-75  
0

RE 56



17-12-75  
PLOT PREPARED BY 154, ADIC

Figure BB-6.  $\phi$ ,  $\theta$ , and  $\gamma$  Rotation Versus Time for a Flow Field Intensity of 2

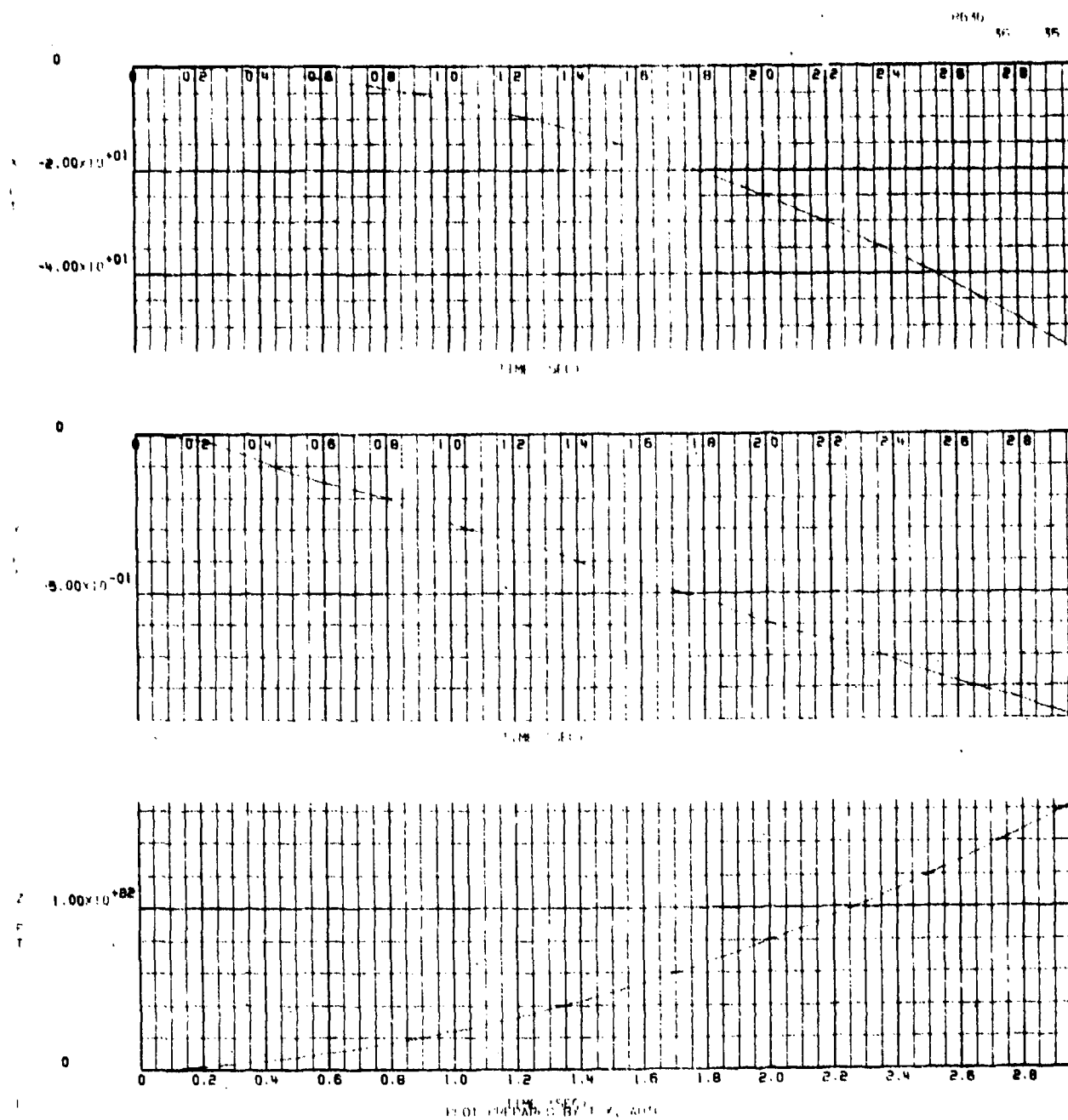


Figure BB-7. X, Y, and Z Position Versus Time for a Flow Field Intensity of  $-1/2$

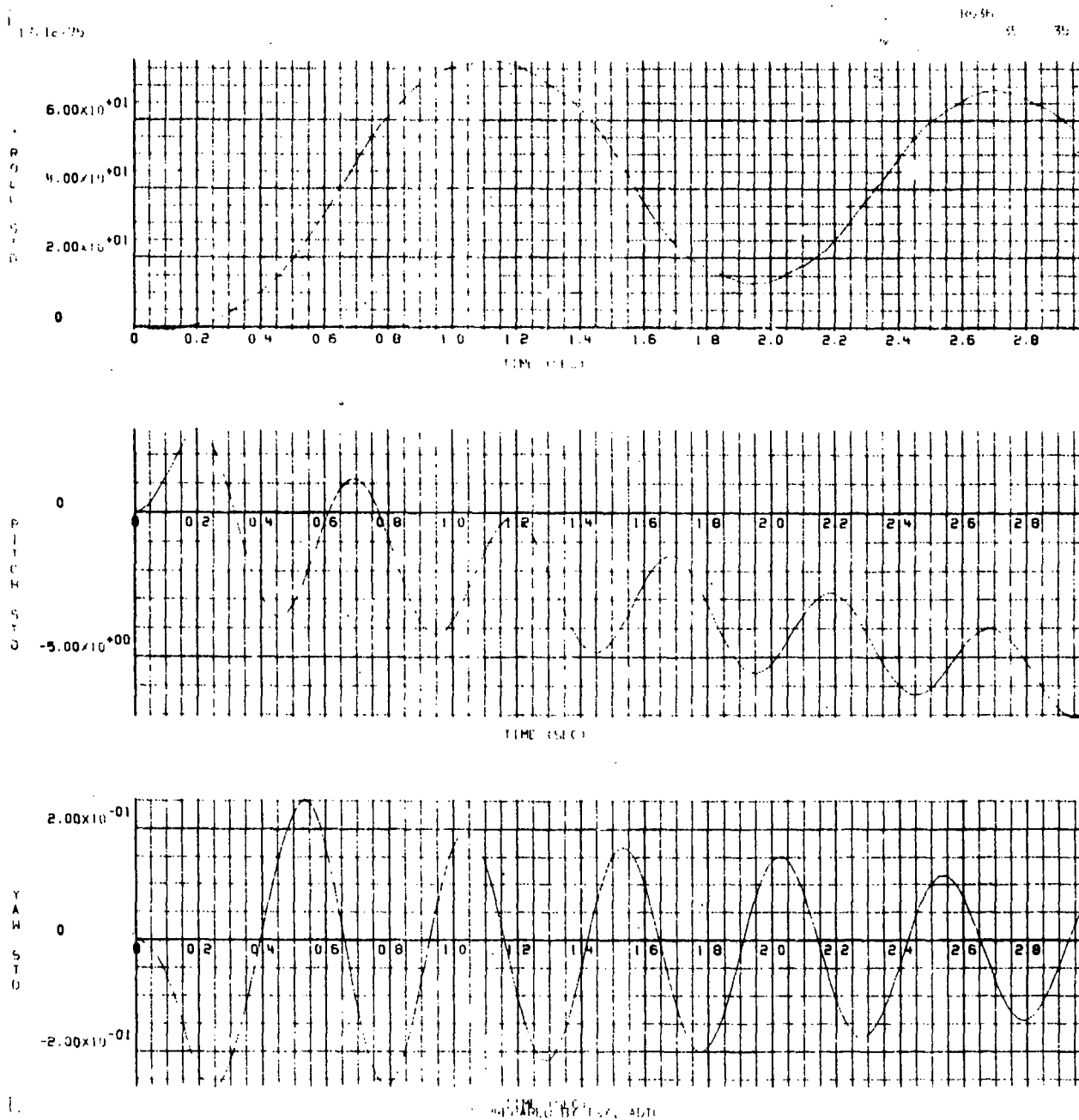


Figure BB-8.  $\phi$ ,  $\theta$ , and  $\psi$  Rotation Versus Time for a Flow Field Intensity of  $-1/2$

APPENDIX CC

GBU-12 BOMB TRAJECTORIES RESULTING FROM A  
PARTIAL FIN OPENING AT MACH 0.95

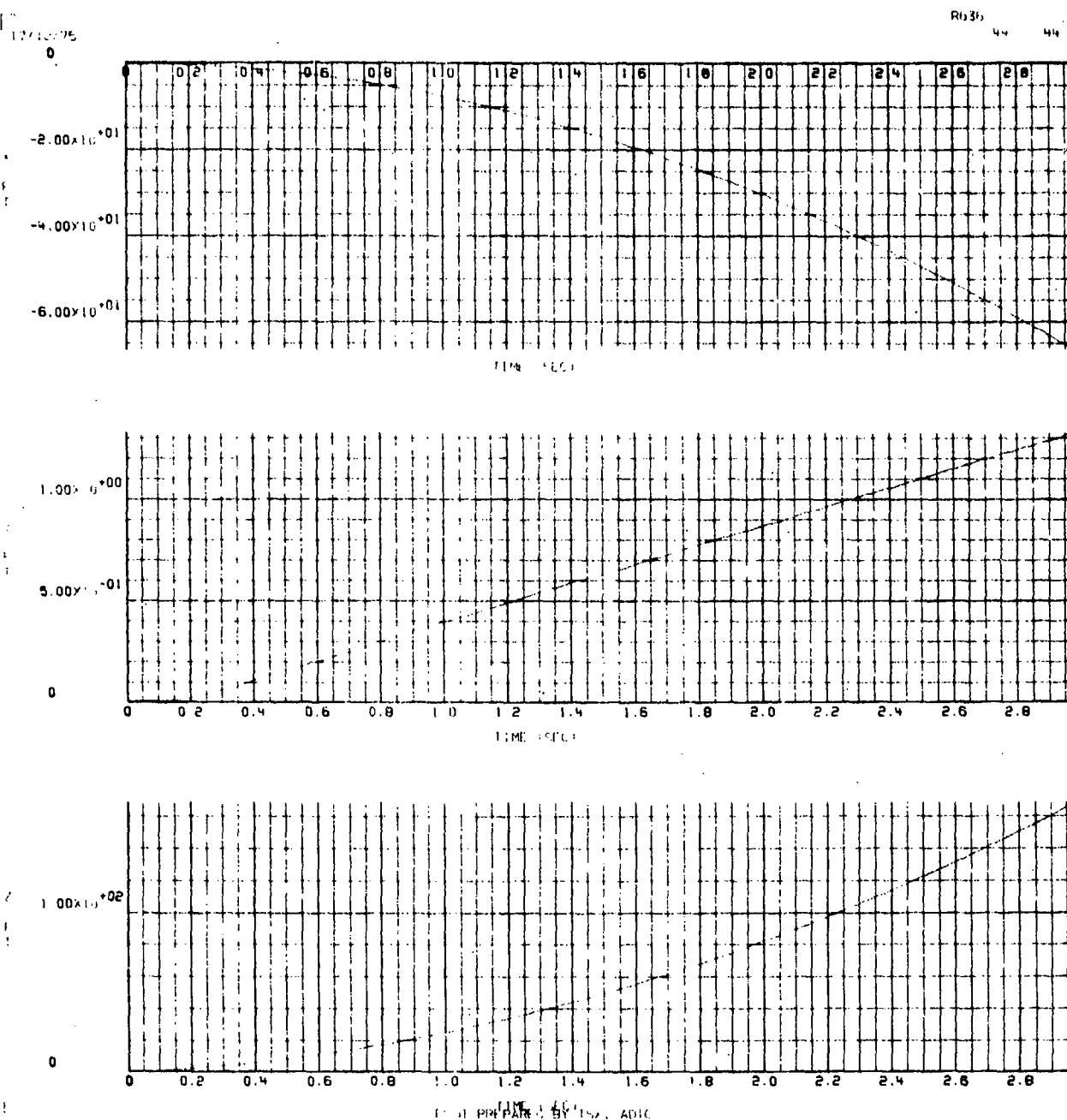


Figure CC-1. X, Y, and Z Position Versus Time for a Flow Field Intensity of  $1/2$

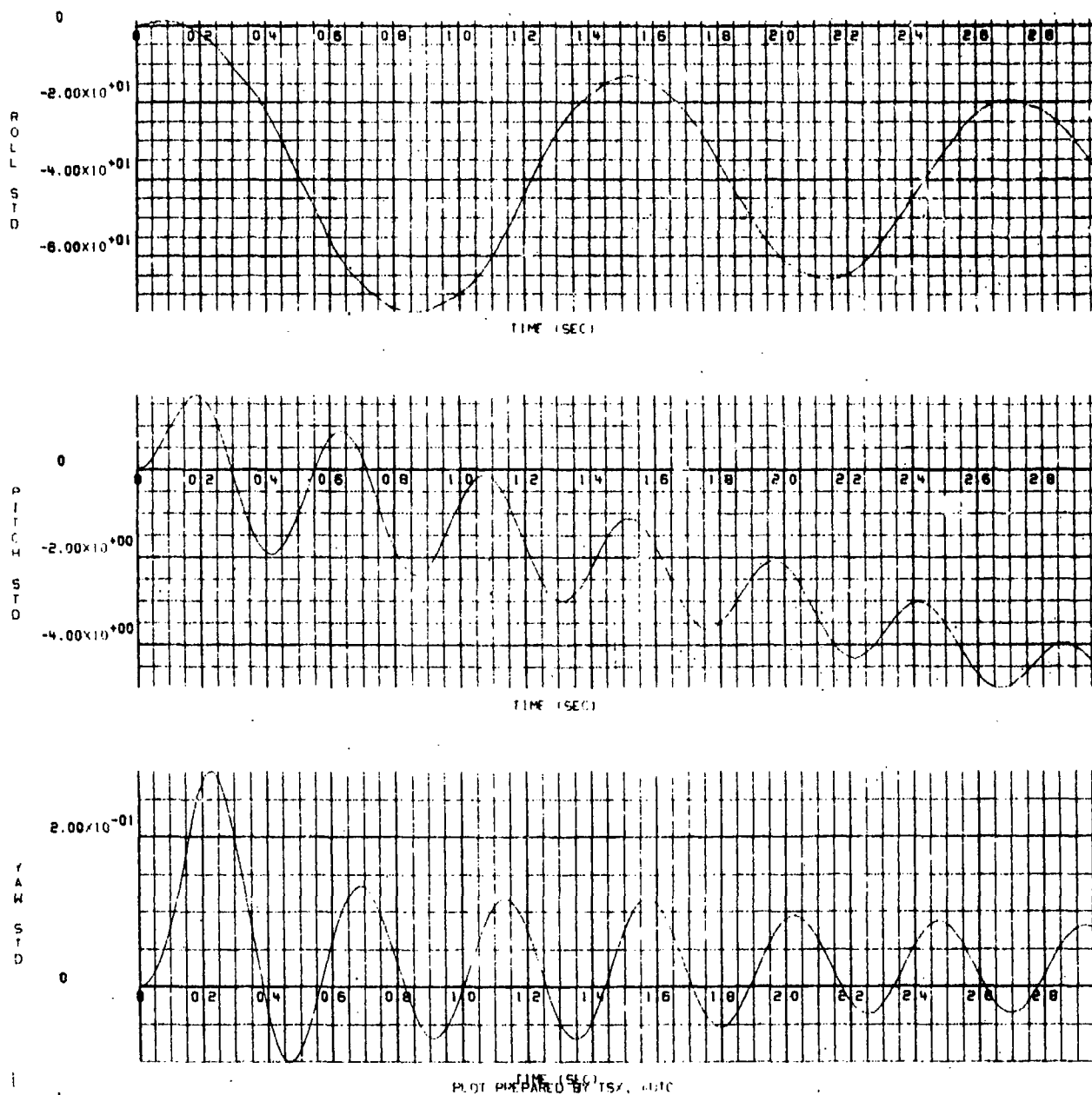


Figure CC-2.  $\phi$ ,  $\theta$ , and  $\psi$  Rotation Versus Time for a Flow Field Intensity of  $1/2$

17/12/75

R636

48 48

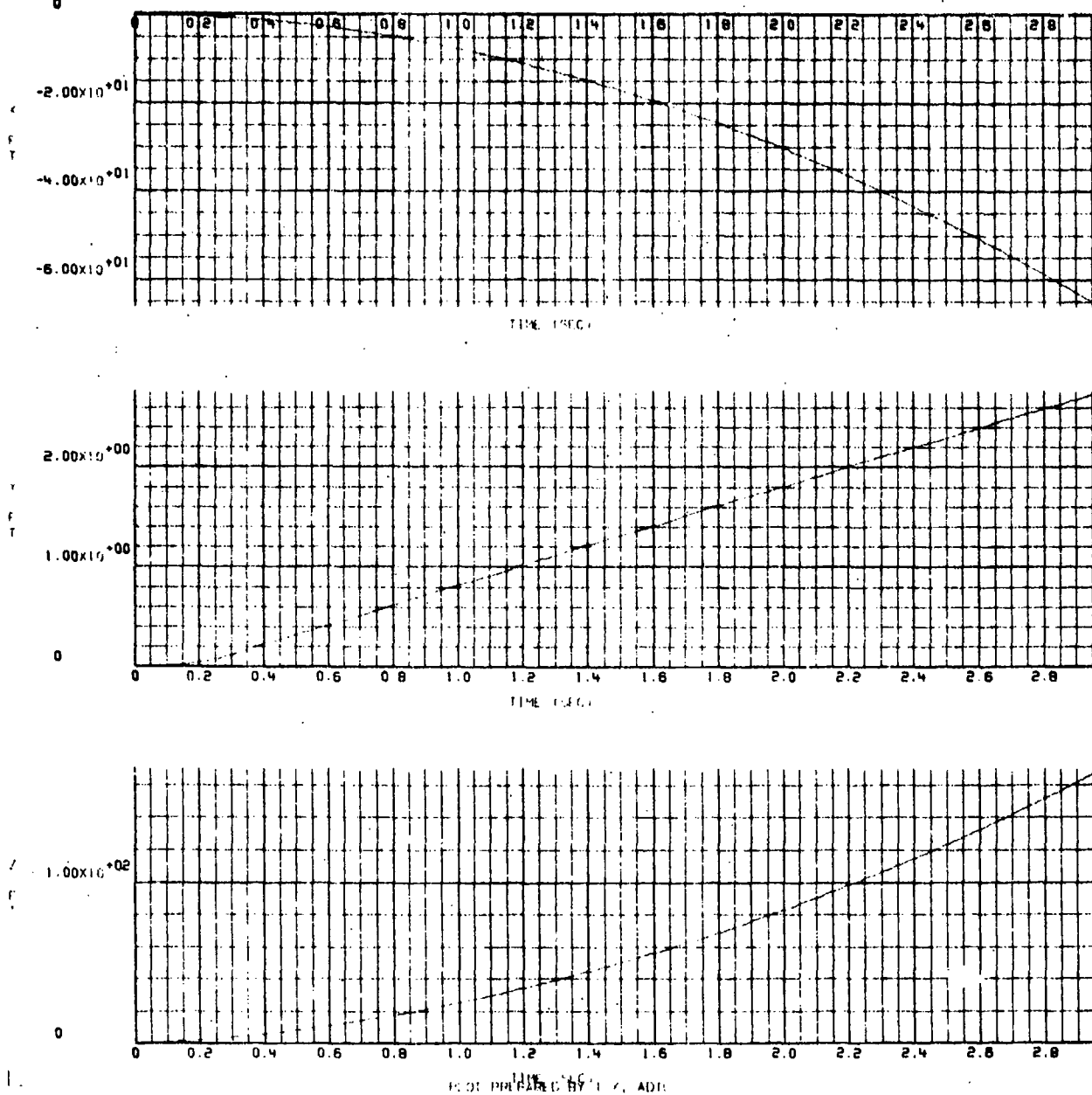


Figure CC-3.. X, Y, and Z Position Versus Time for a Flow Field Intensity of 1 (as measured in the wind tunnel)

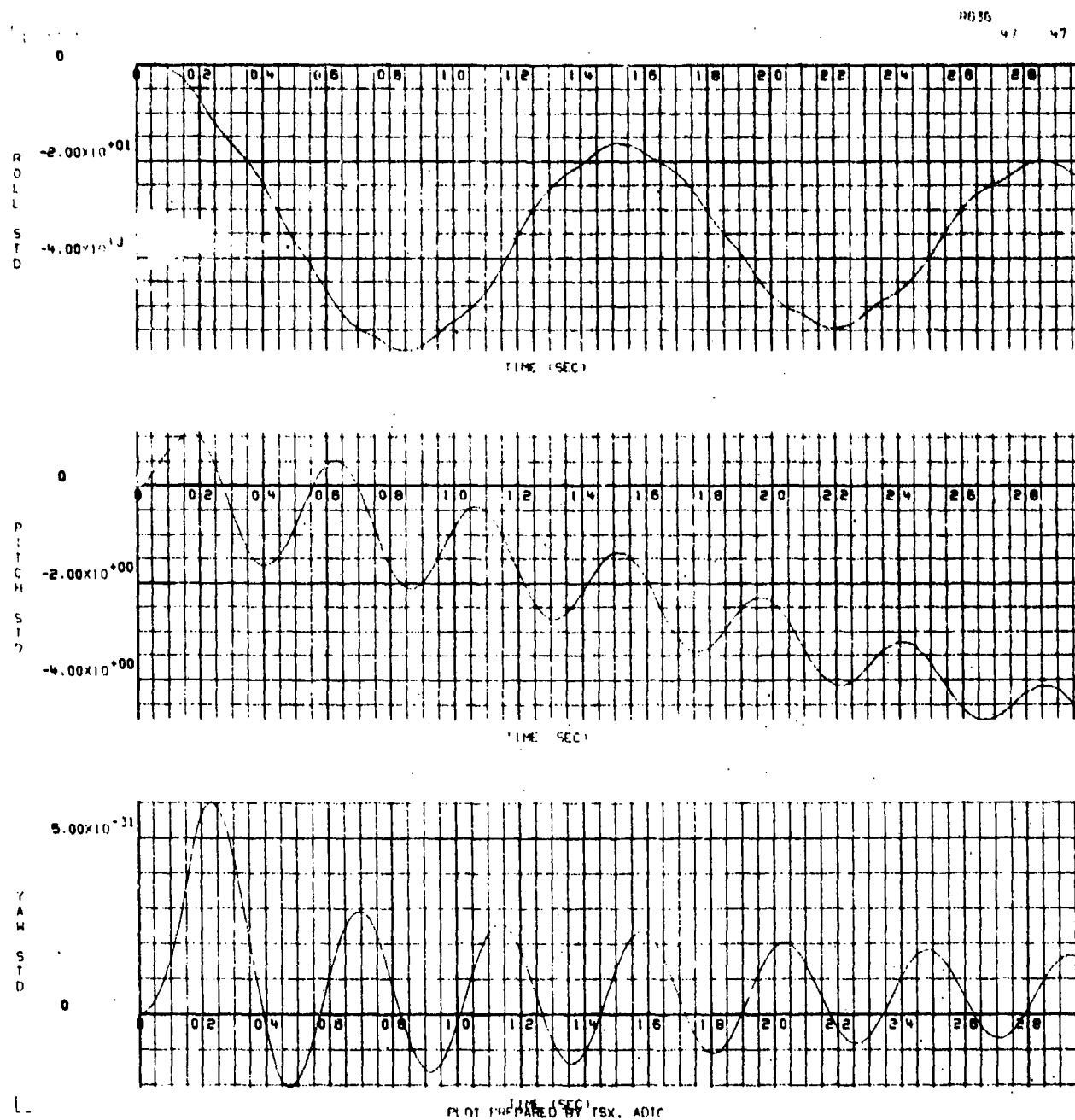
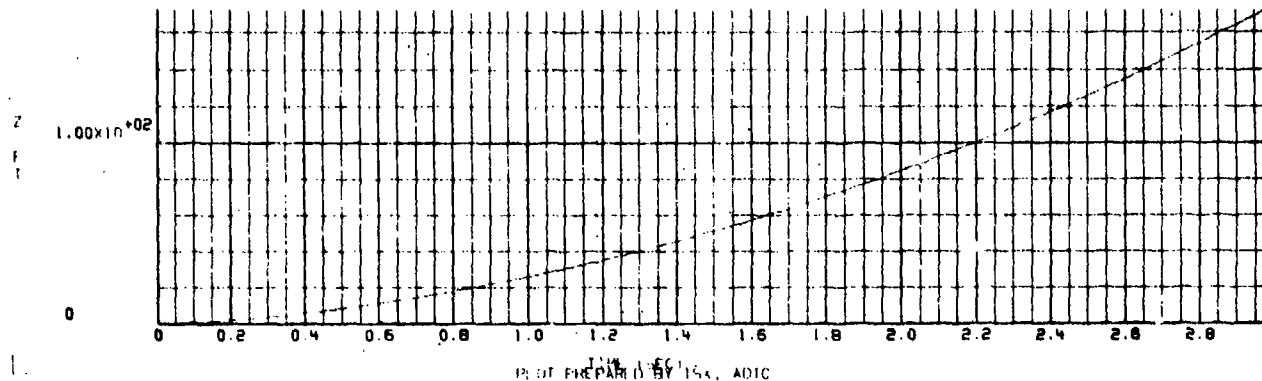
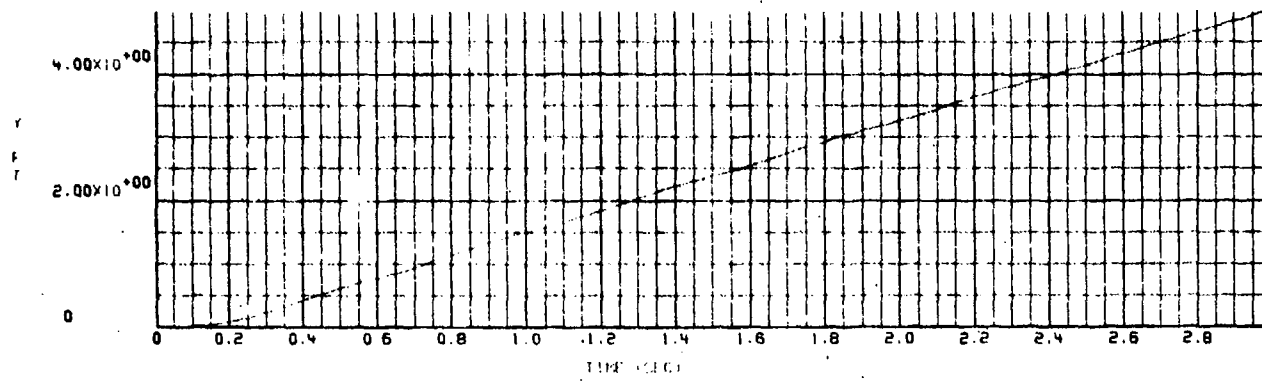
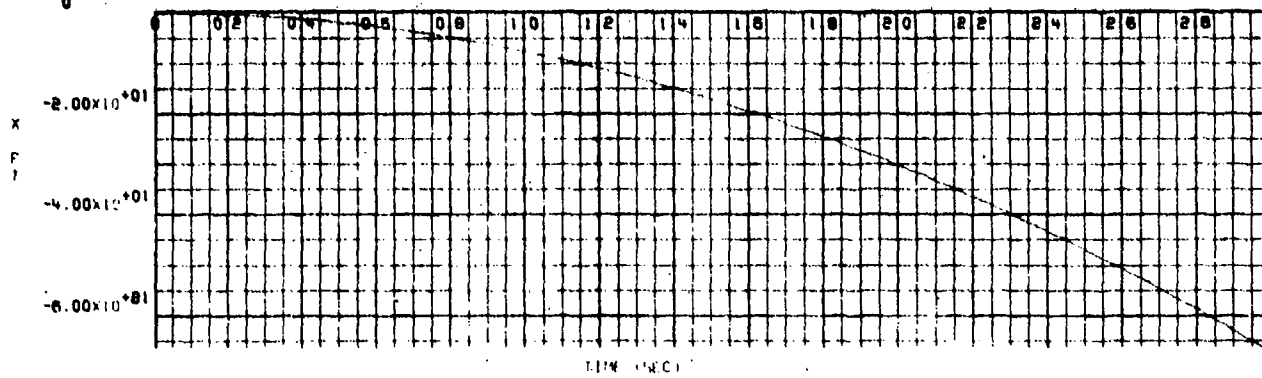


Figure CC-4.  $\phi$ ,  $\theta$ , and  $\psi$  Rotation Versus Time for a Flow Field Intensity of 1 (unchanged from the wind tunnel measured values)



17/12/75  
0

R636 52 52



PRINT PREPARED BY 154, ADIC

Figure CC-5. X, Y, and Z Position Versus Time for a Flow Field Intensity of 2

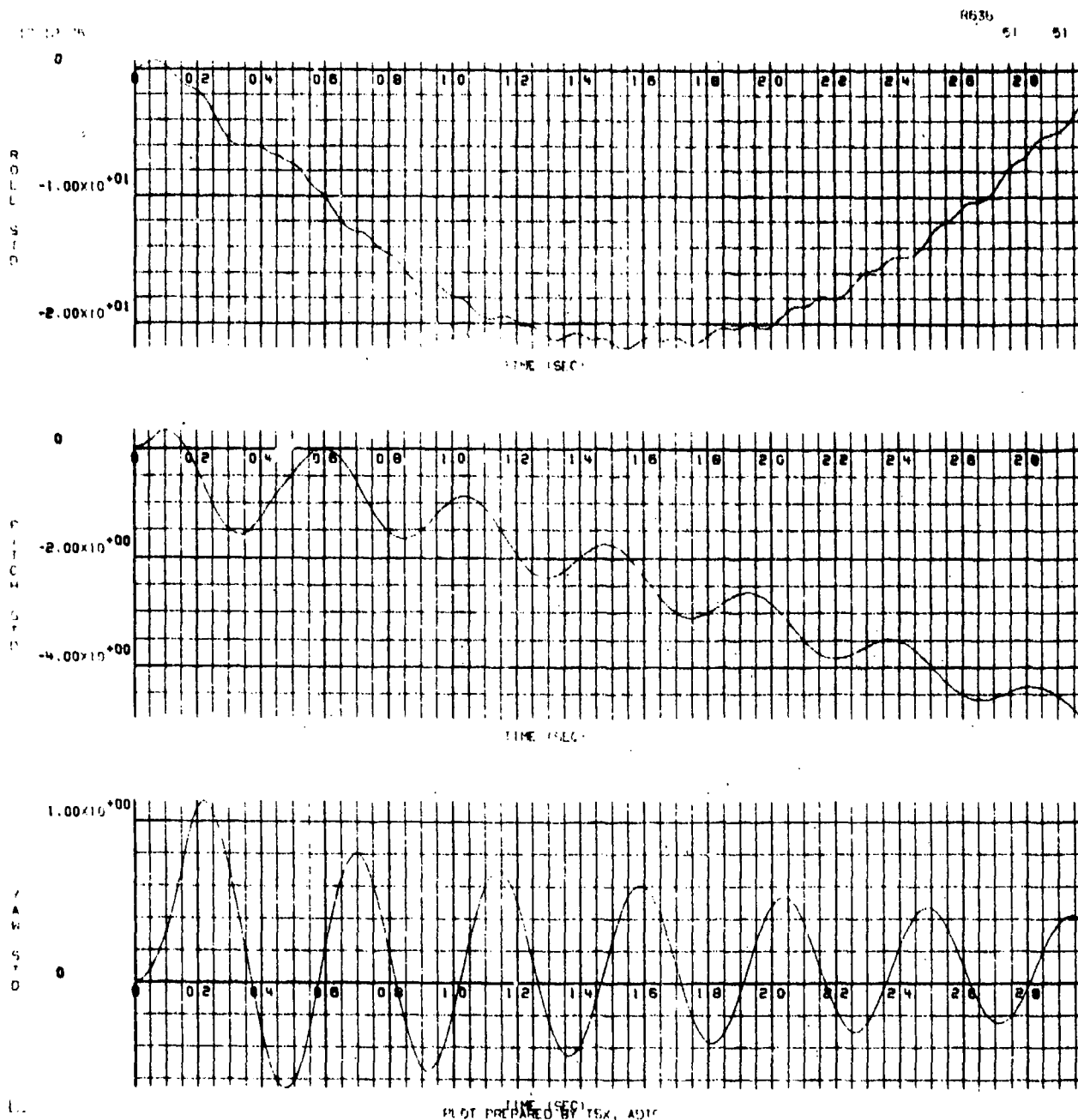
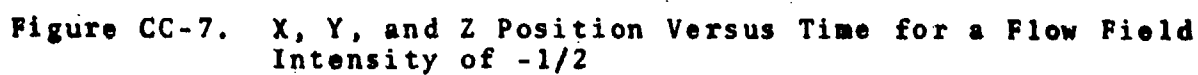


Figure CC-6.  $\phi$ ,  $\theta$ , and  $\psi$  Rotation Versus Time for a Flow Field Intensity of 2



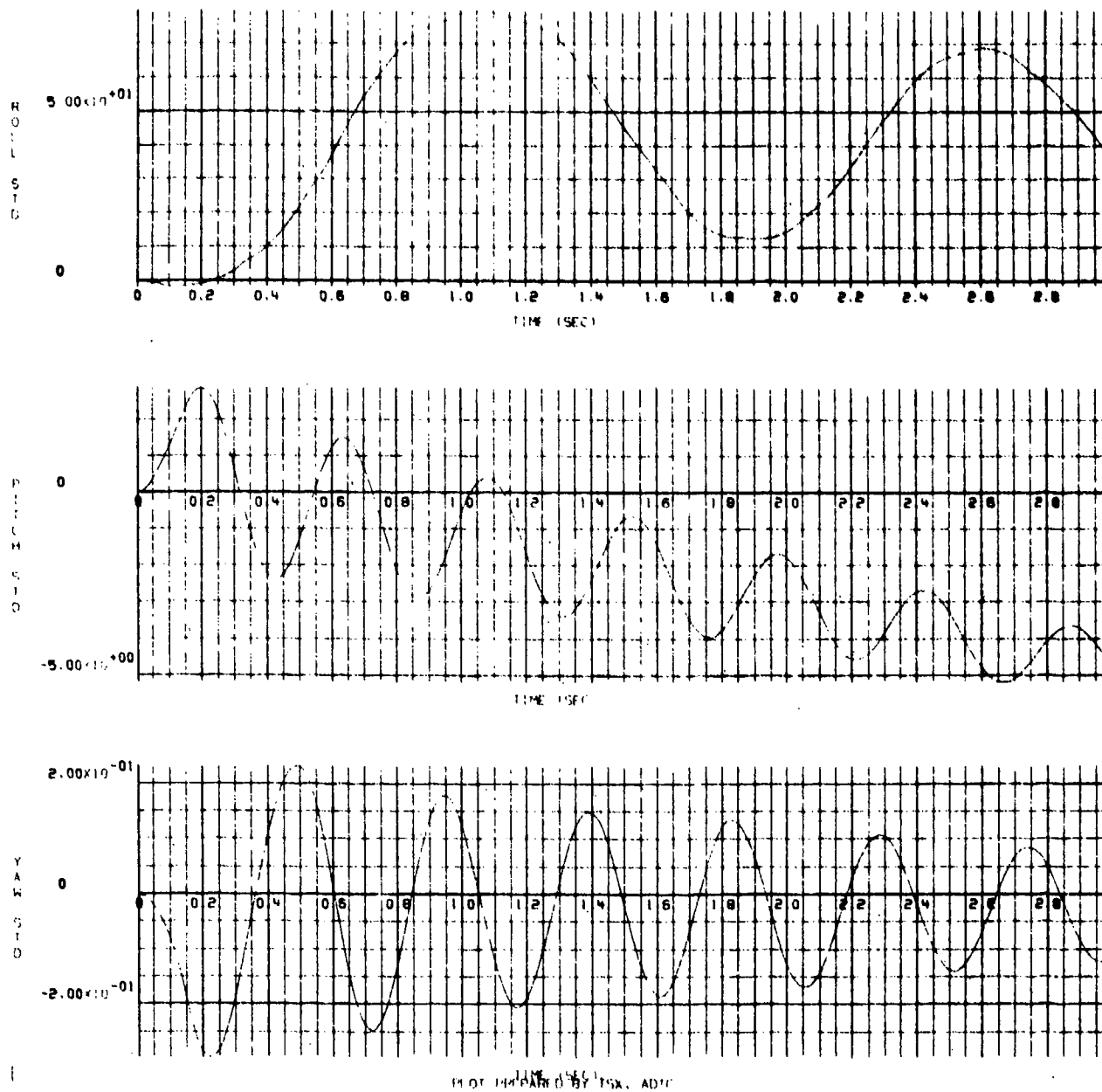


Figure CC-8.  $\phi$ ,  $\theta$ , and  $\psi$  Rotation Versus Time for a Flow Field Intensity of  $-1/2$

APPENDIX DD

GBU-12 BOMB TRAJECTORIES RESULTING FROM A  
PARTIAL FIN OPENING AT MACH 1.2

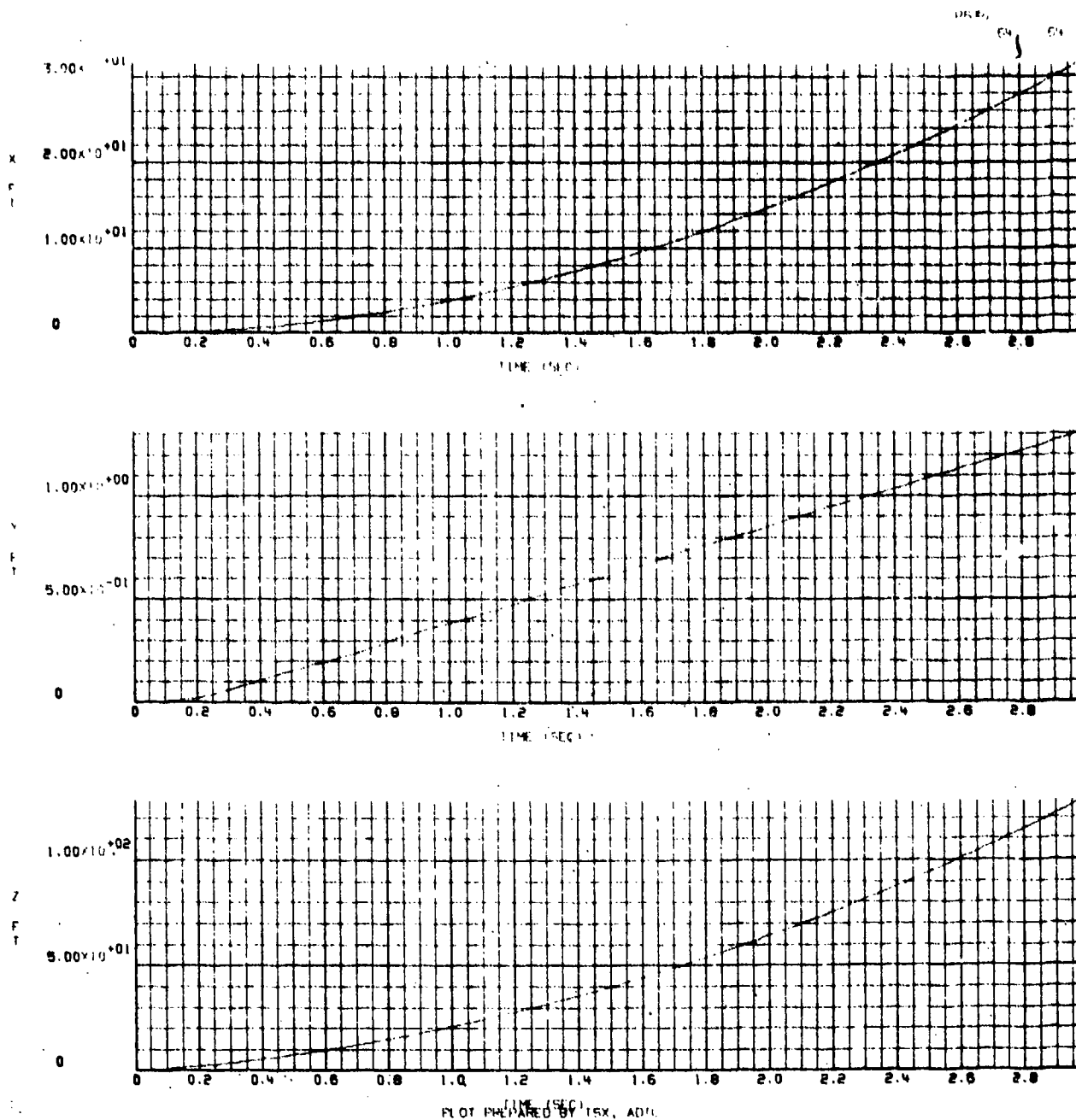
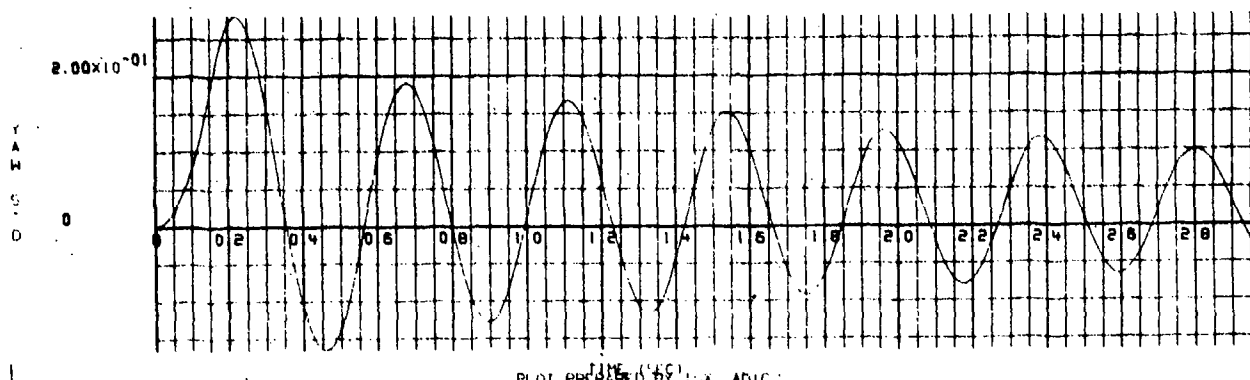
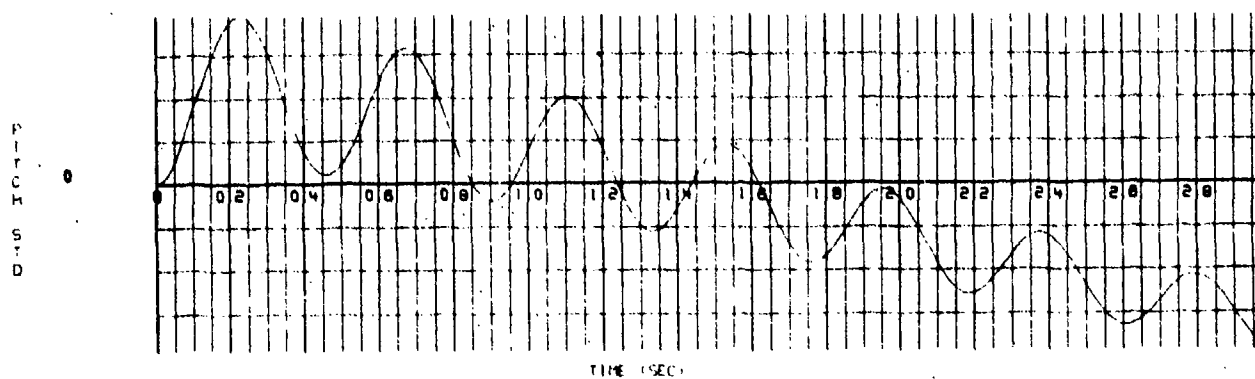
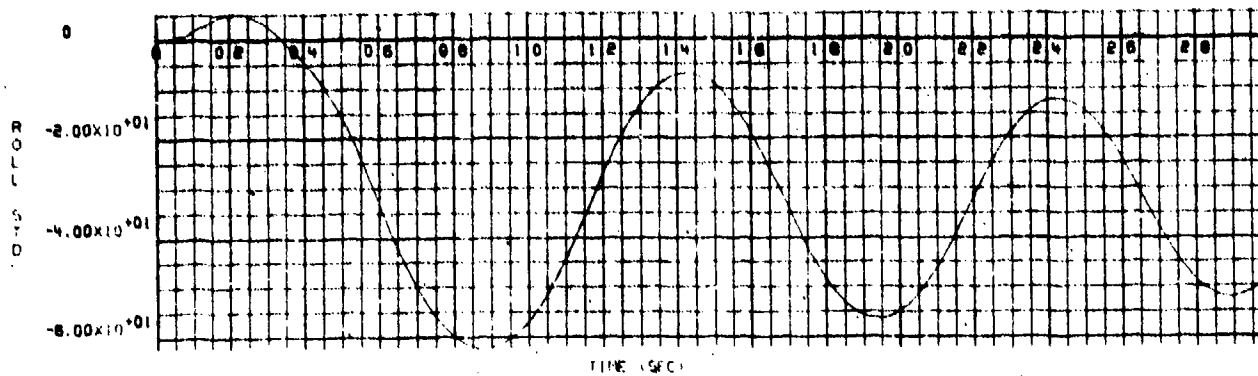


Figure DD-1. X, Y, and Z Position Versus Time for a Flow Field Intensity of  $1/2$

17/12/75

R631

E3 63



PILOT PREPARED BY: JAX, ADIC

Figure DD-2.  $\phi$ ,  $\theta$ , and  $\psi$  Rotation Versus Time for a Flow Field Intensity of  $1/2$

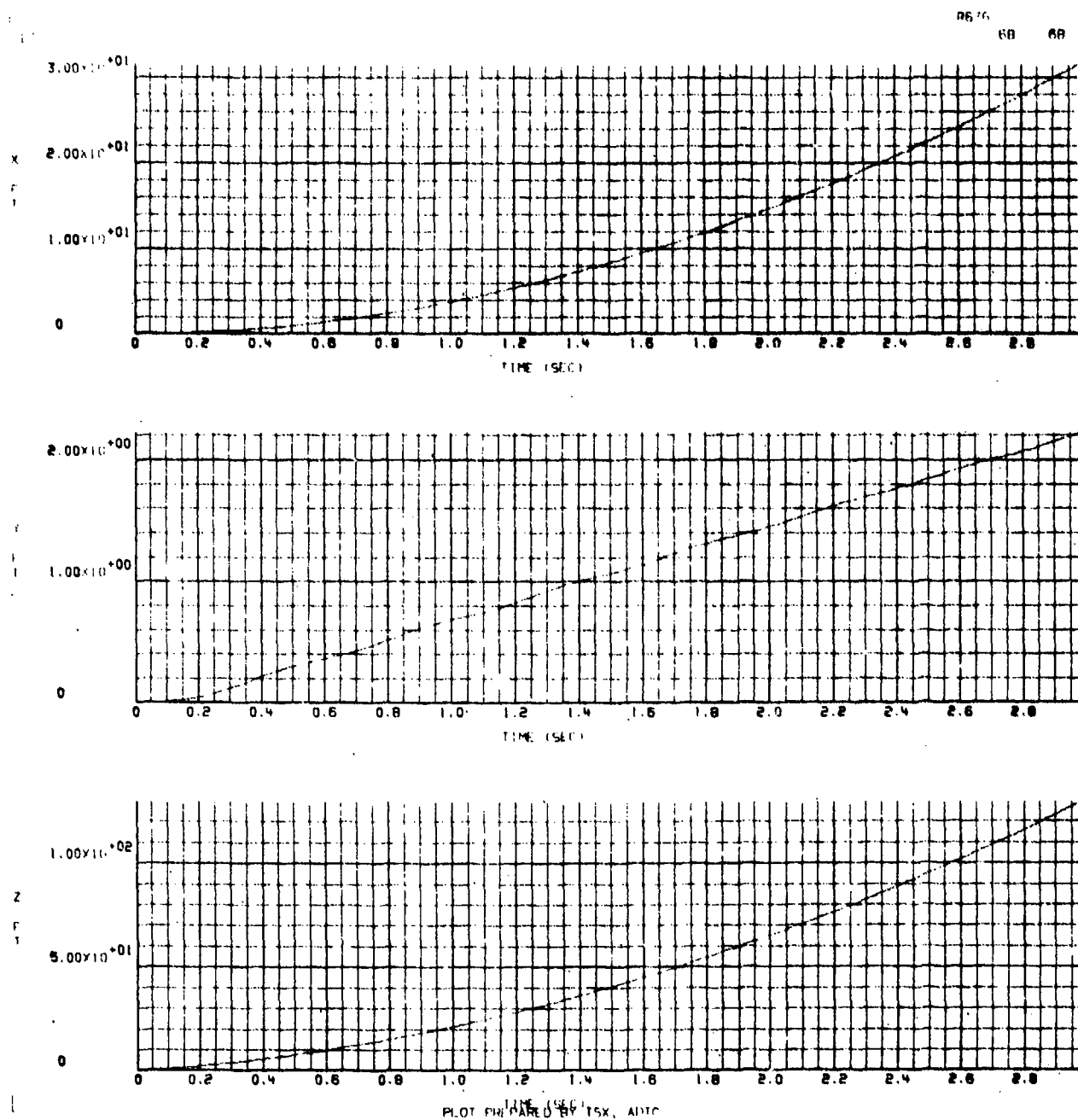


Figure DD-3. X, Y, and Z Position Versus Time for a Flow Field Intensity of 1 (as measured in the wind tunnel)



17/12-75

6536

67 67

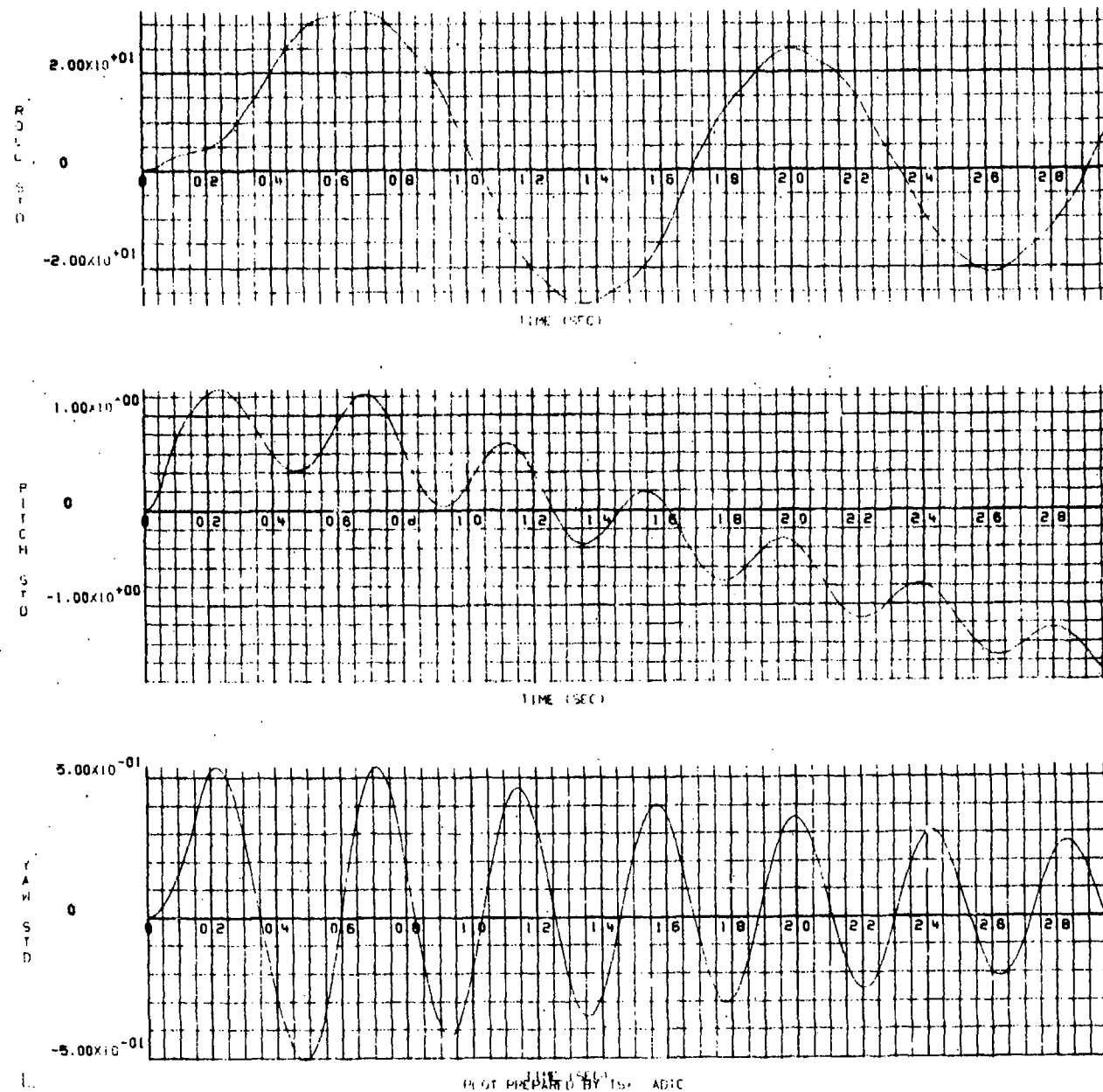


Figure DD-4.  $\phi$ ,  $\theta$ , and  $\psi$  Rotation Versus Time for a Flow Field Intensity of 1 (unchanged from the wind tunnel measured values)

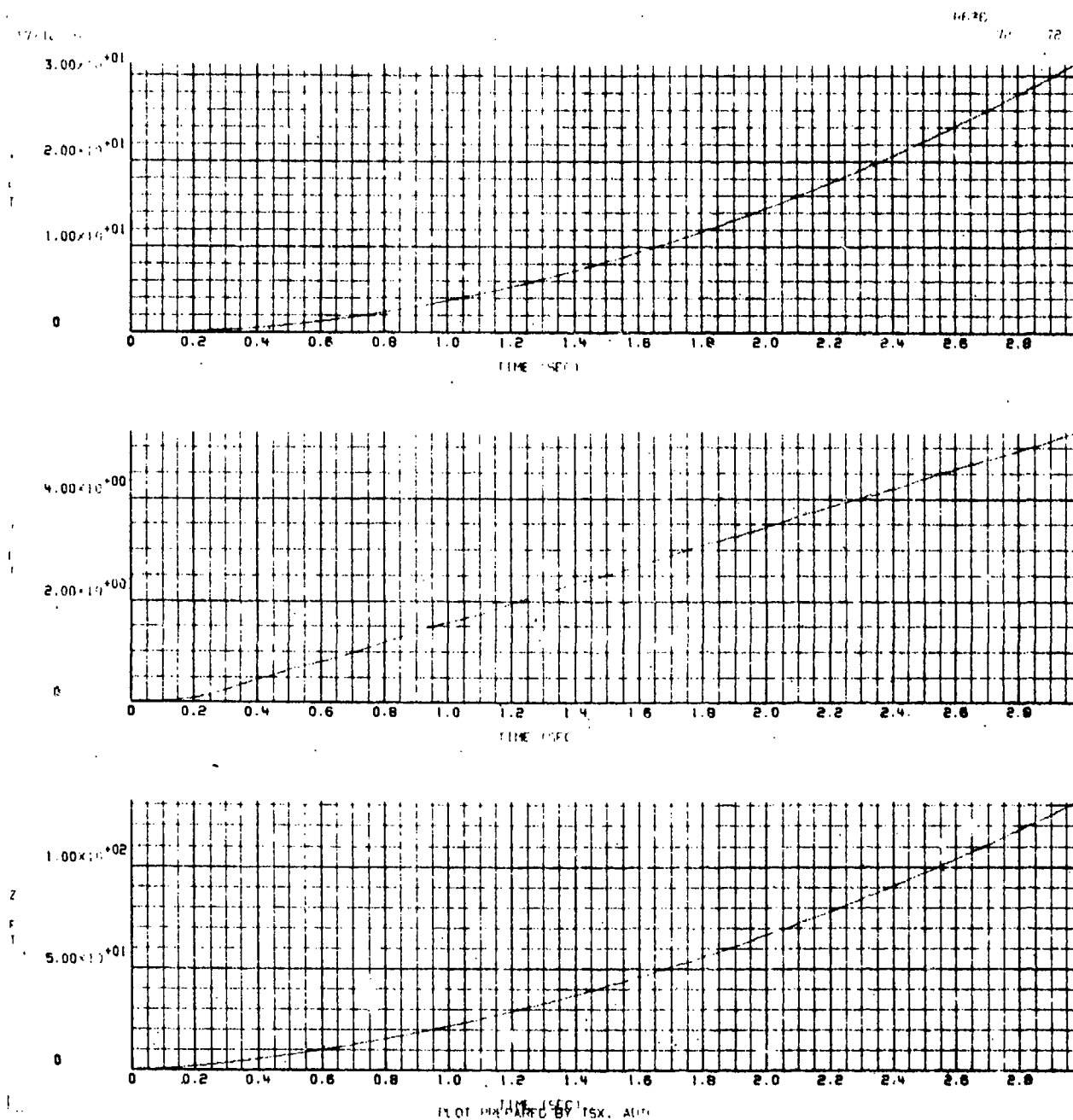


Figure DD-5. X, Y, and Z Position Versus Time for a Flow Field Intensity of 2



Figure DD-6.  $\phi$ ,  $\theta$ , and  $\psi$  Rotation Versus Time for a Flow Field Intensity of 2

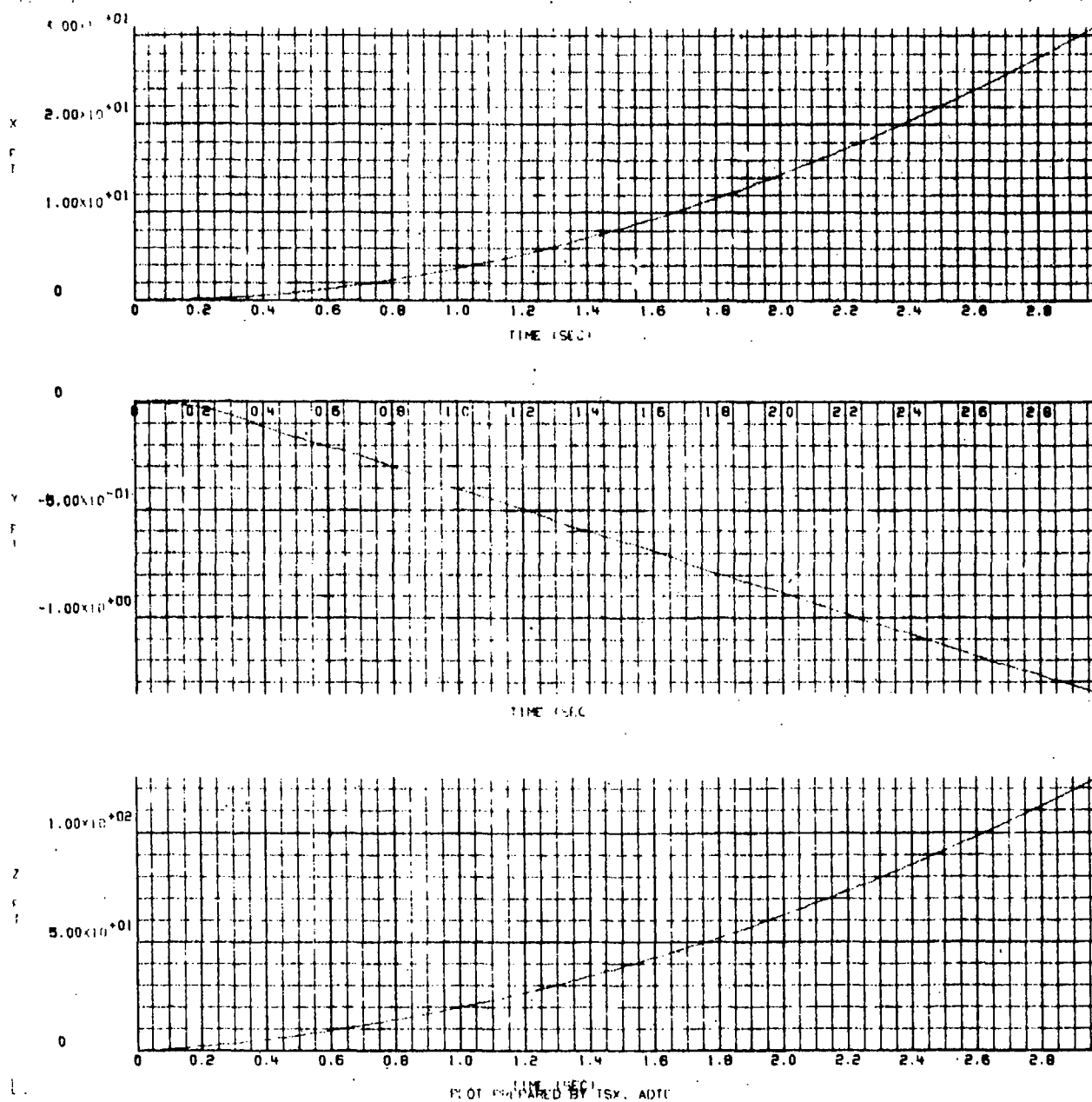
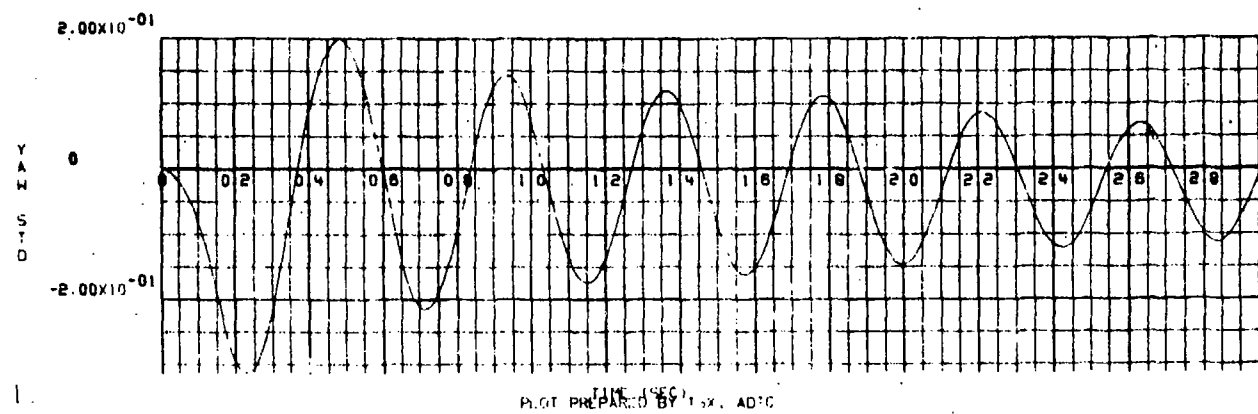
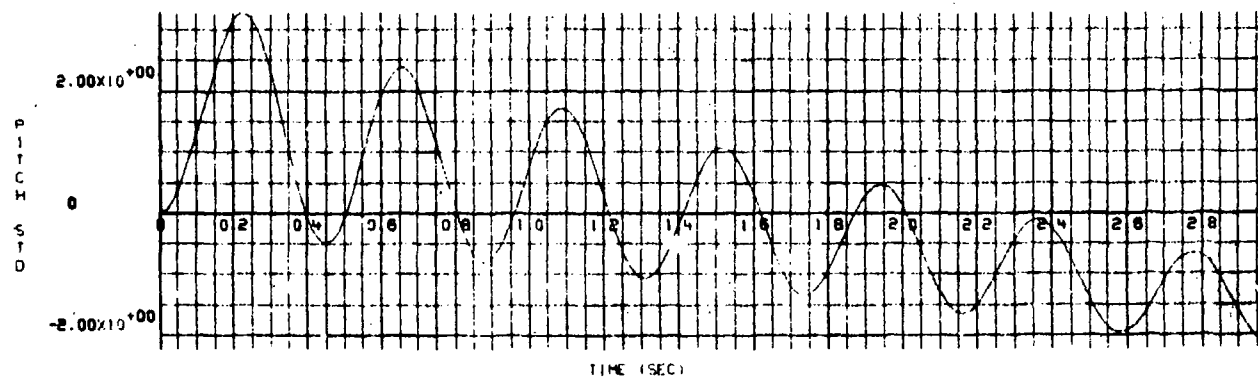
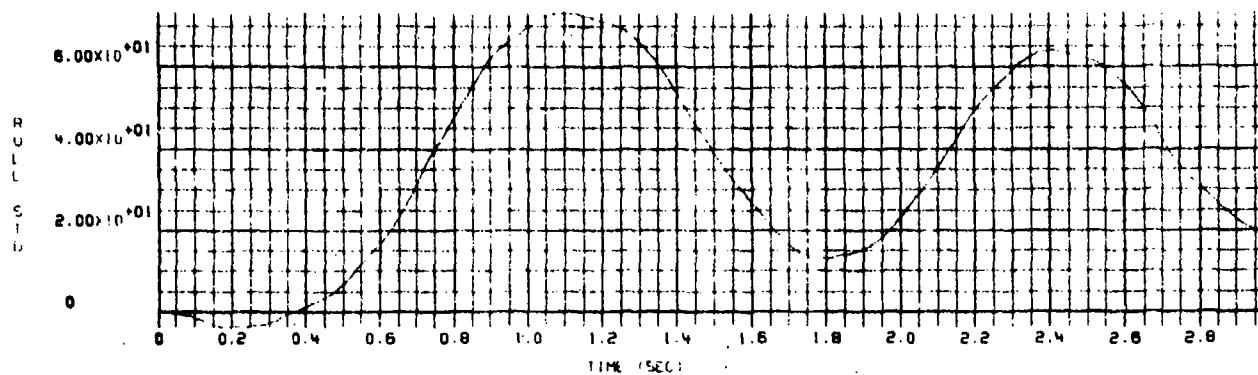


Figure DD-7. X, Y, and Z Position Versus Time for a Flow Field Intensity of  $-1/2$

17/12/75

75



PILOT PREPARED BY 1.5X. ADIC

Figure DD-8.  $\phi$ ,  $\theta$ , and  $\psi$  Rotation Versus Time for a Flow Field Intensity of  $-1/2$

APPENDIX EE

GBU-10 BOMB TRAJECTORIES RESULTING FROM A  
PARTIAL FIN OPENING AT MACH 0.7



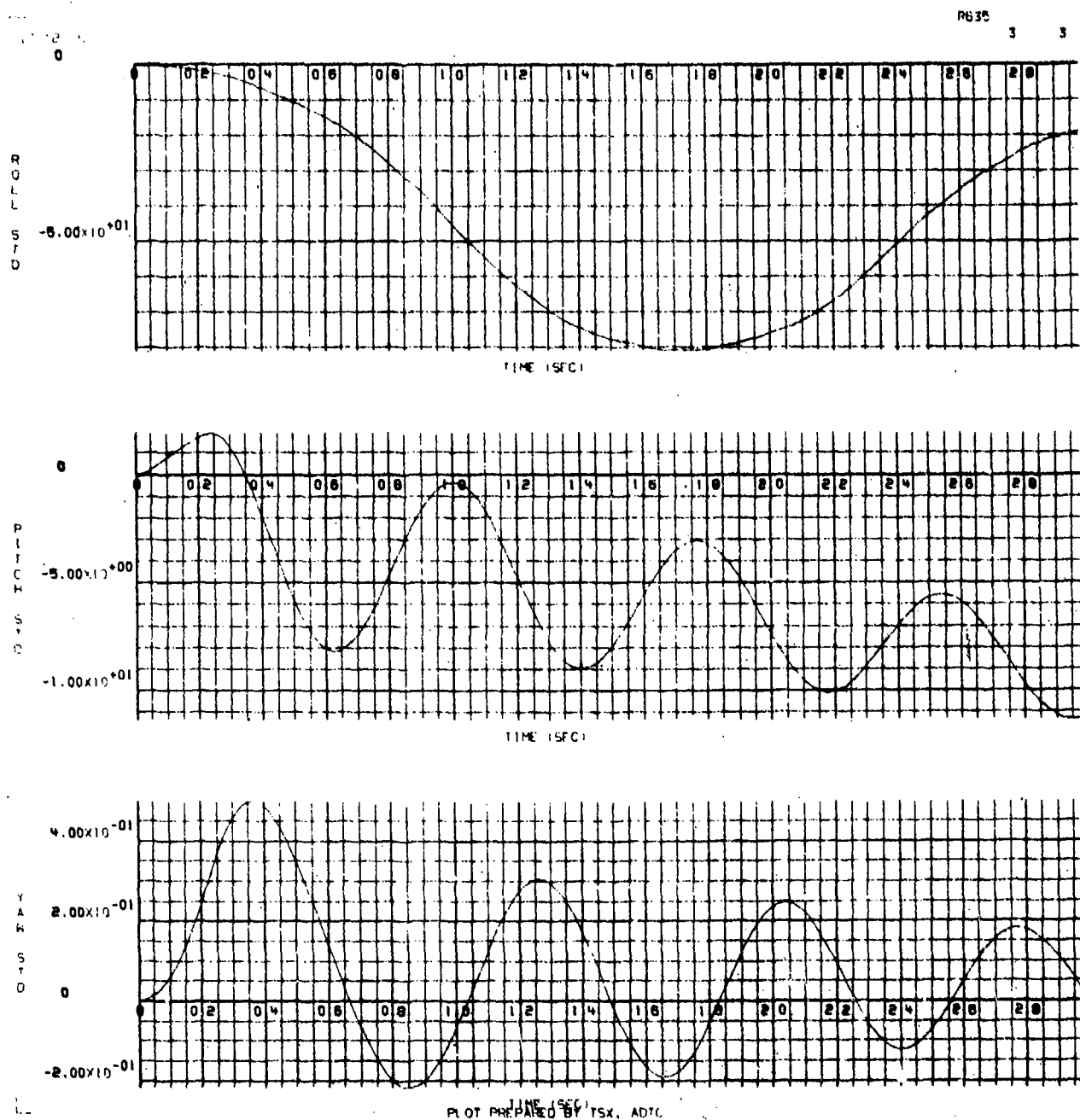


Figure EE-2.  $\phi$ ,  $\theta$ , and  $\psi$  Rotation Versus Time for a Flow Field Intensity of  $1/2$



17/12/75  
0

R635

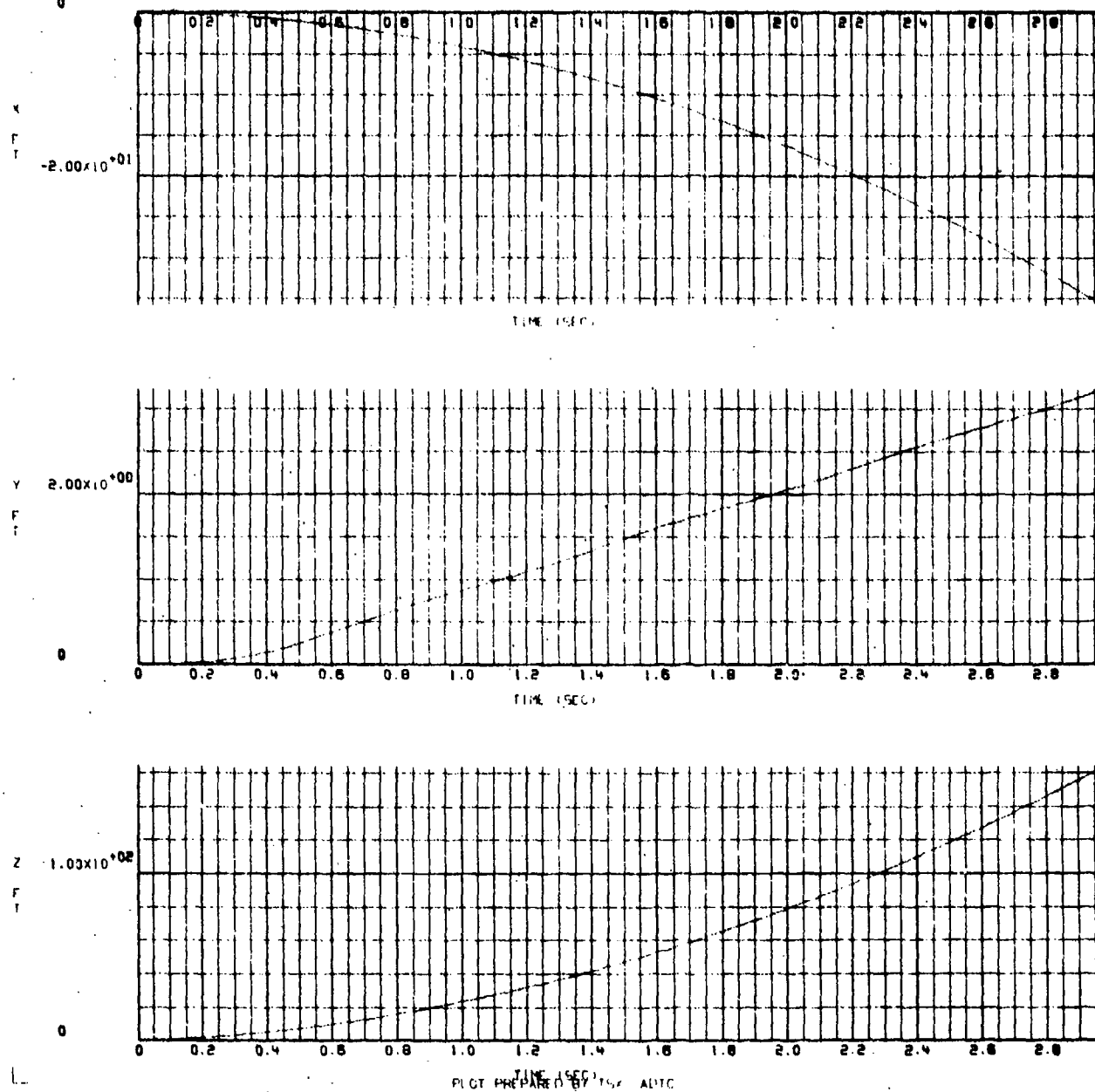


Figure EE-3. X, Y, and Z Position Versus Time for a Flow Field Intensity of 1 (as measured in the wind tunnel)

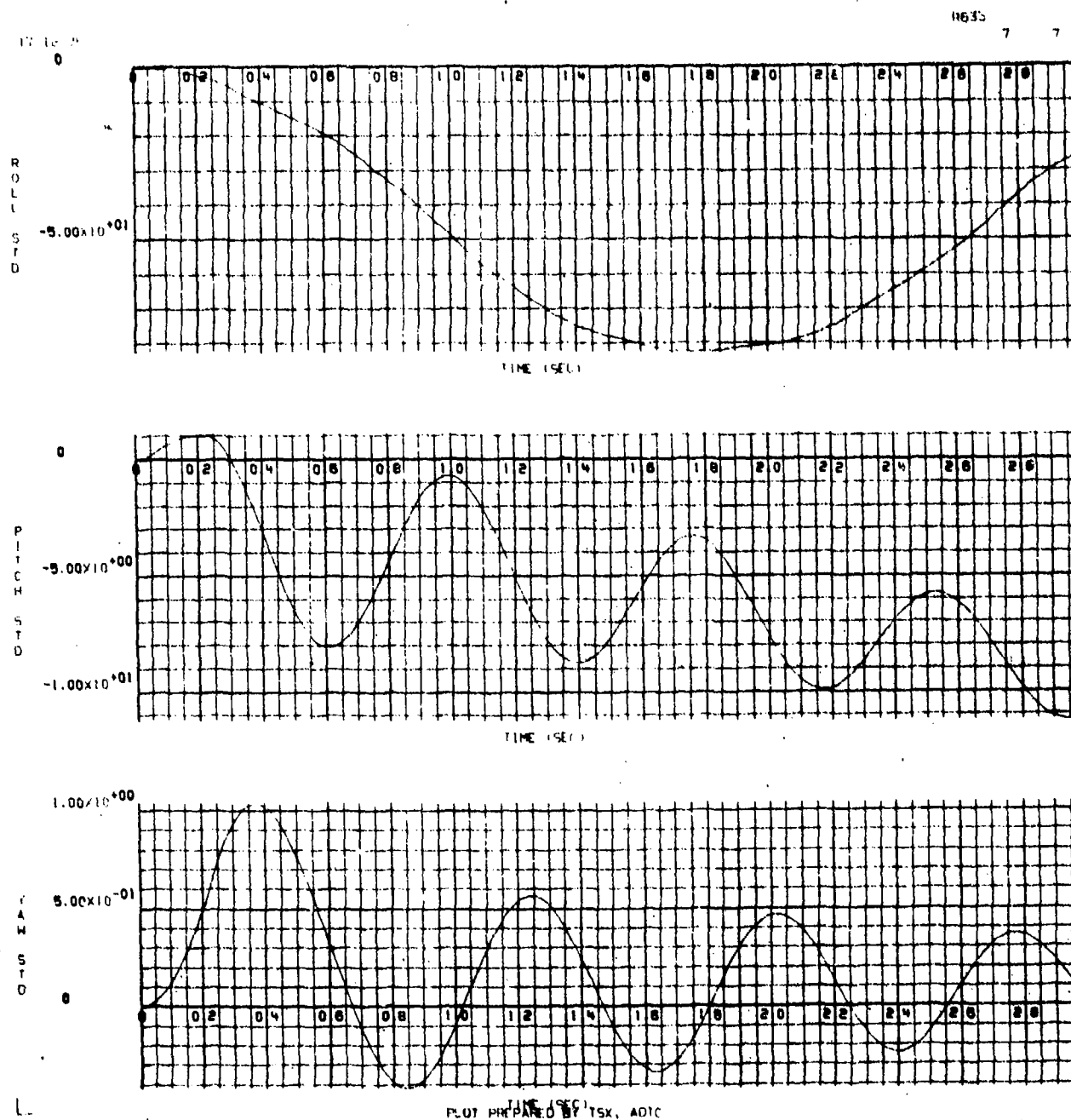
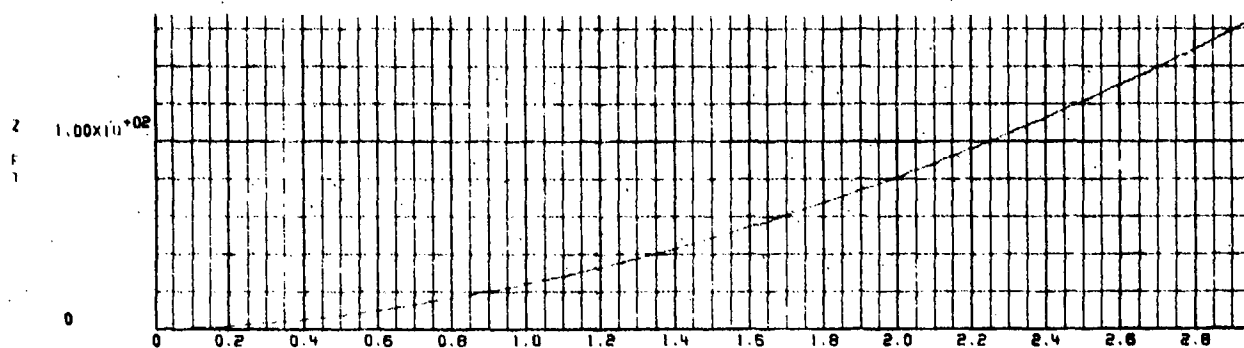
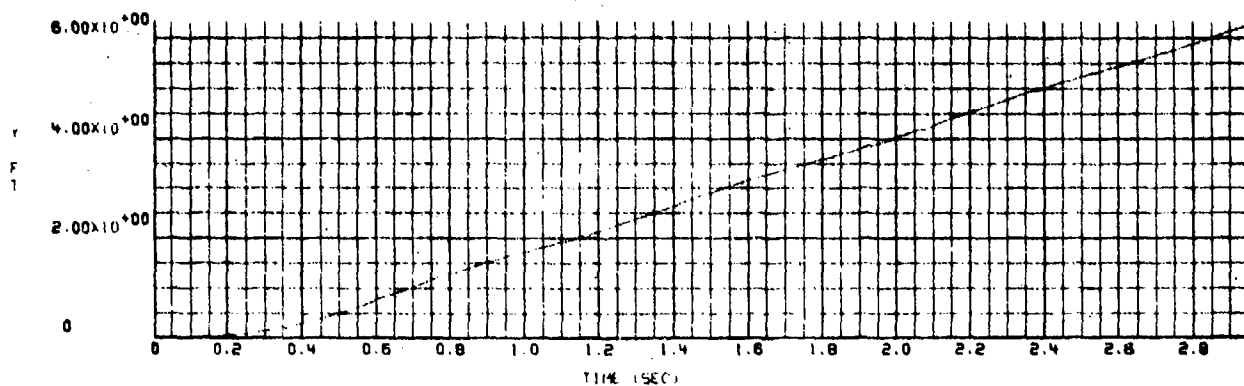
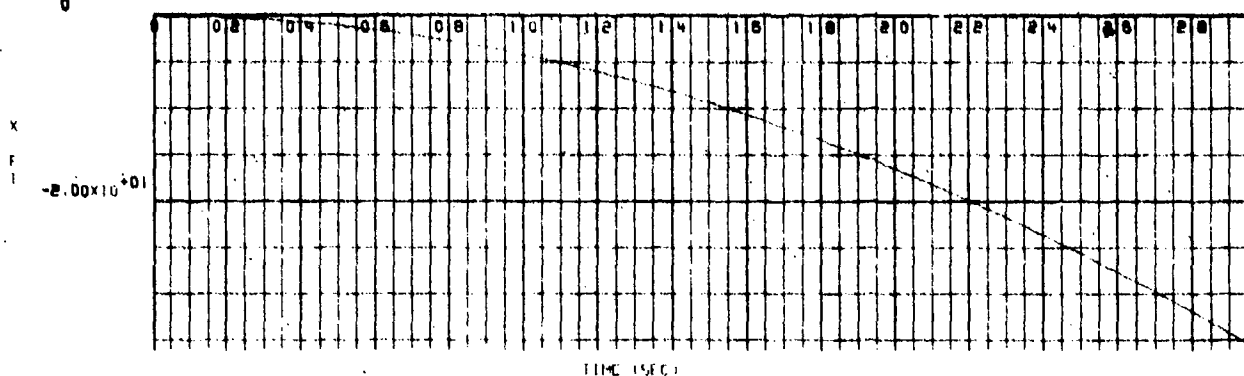


Figure EE-4.  $\phi$ ,  $\theta$ , and  $\gamma$  Rotation Versus Time for a Flow Field Intensity of 1 (unchanged from the wind tunnel measured values)

17/12/75  
0

RR 51 12 12



11/12/75  
PLOT PREPARED BY TSV, ADIC

Figure EE-5. X, Y, and Z Position Versus Time for a Flow Field Intensity of 2

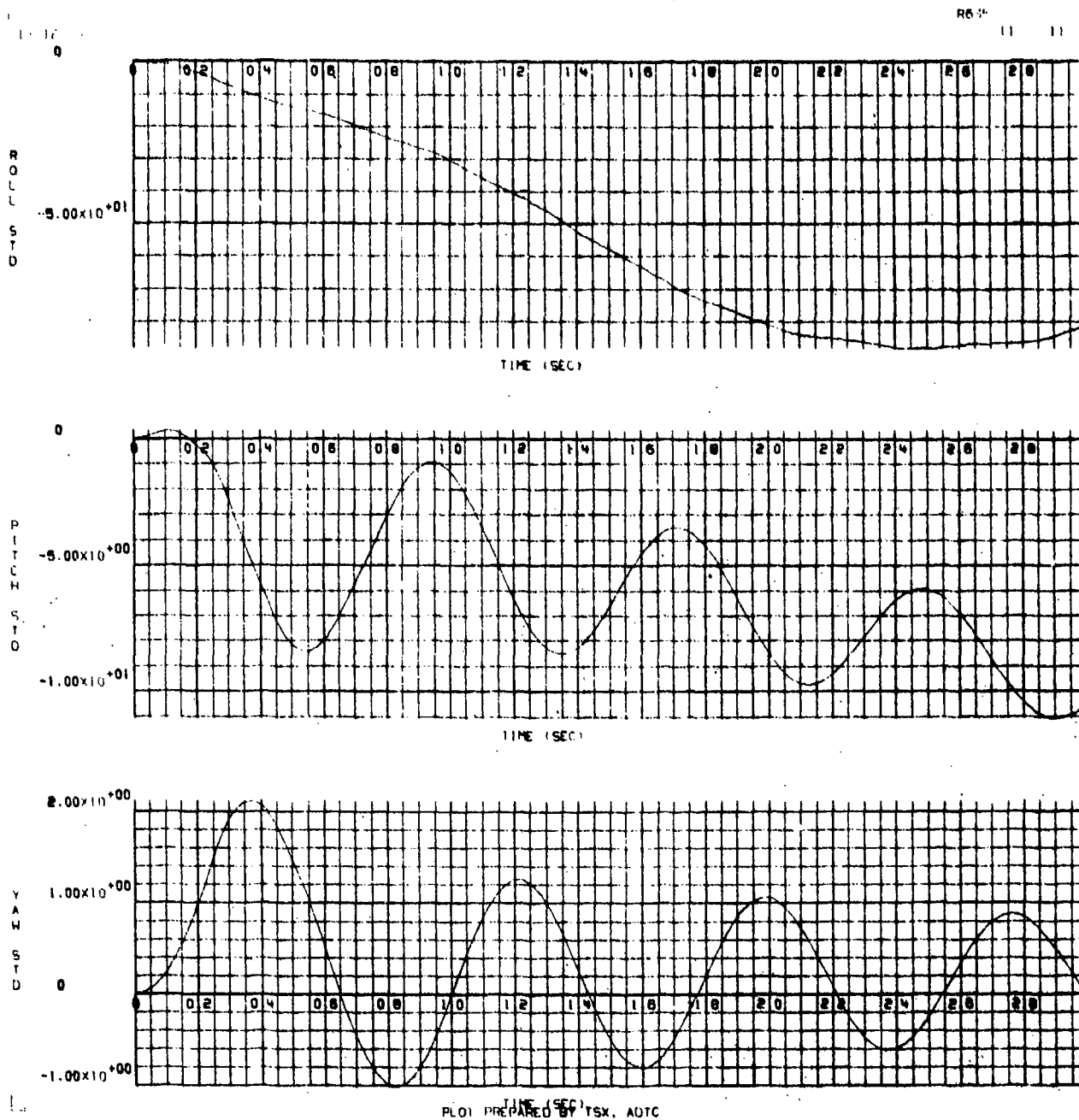


Figure EE-6.  $\phi$ ,  $\theta$ , and  $\psi$  Rotation Versus Time for a Flow Field Intensity of 2

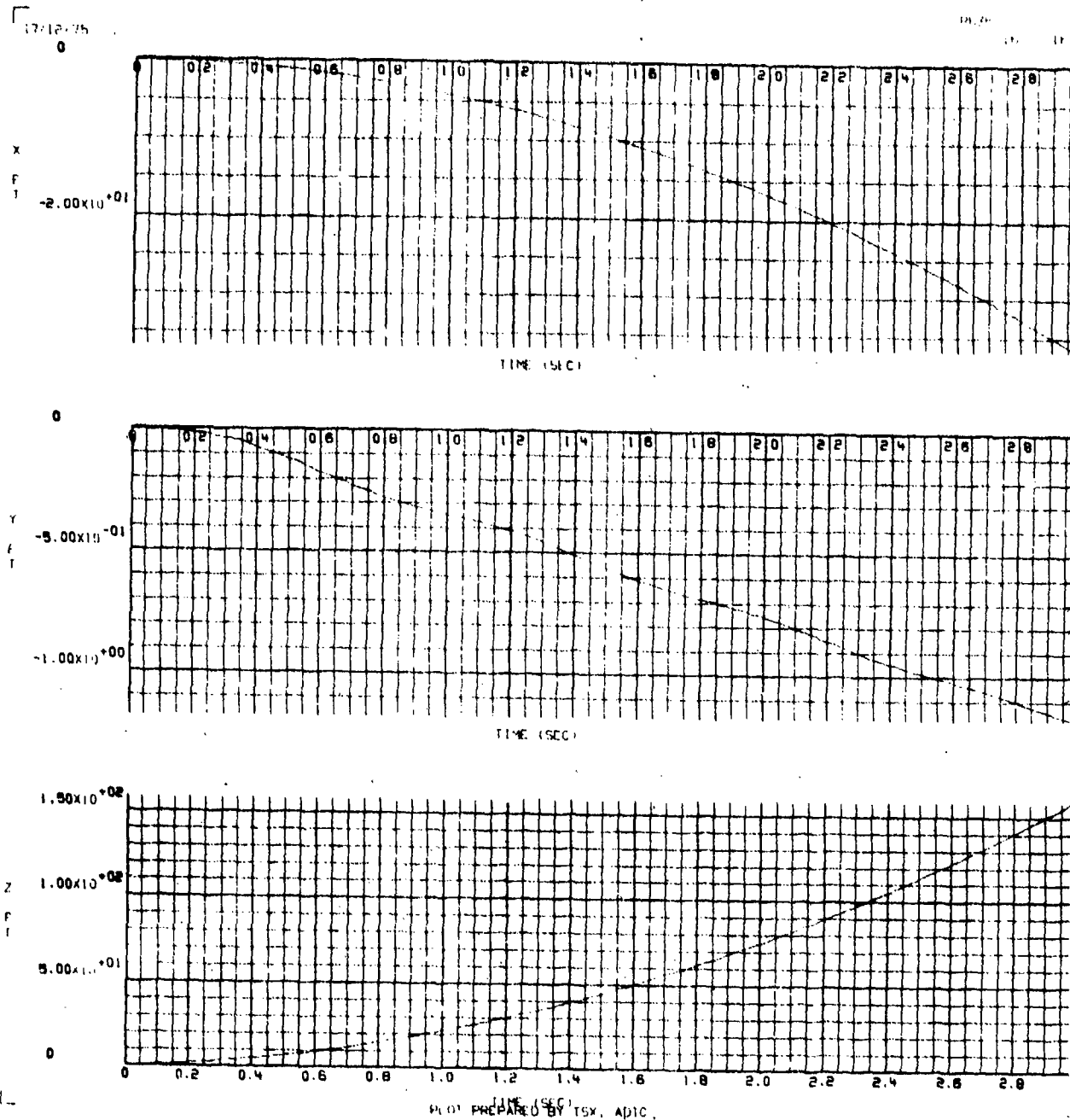


Figure EE-7. X, Y, and Z Position Versus Time for a Flow Field Intensity of  $-1/2$

17/12/77

4635 14 15

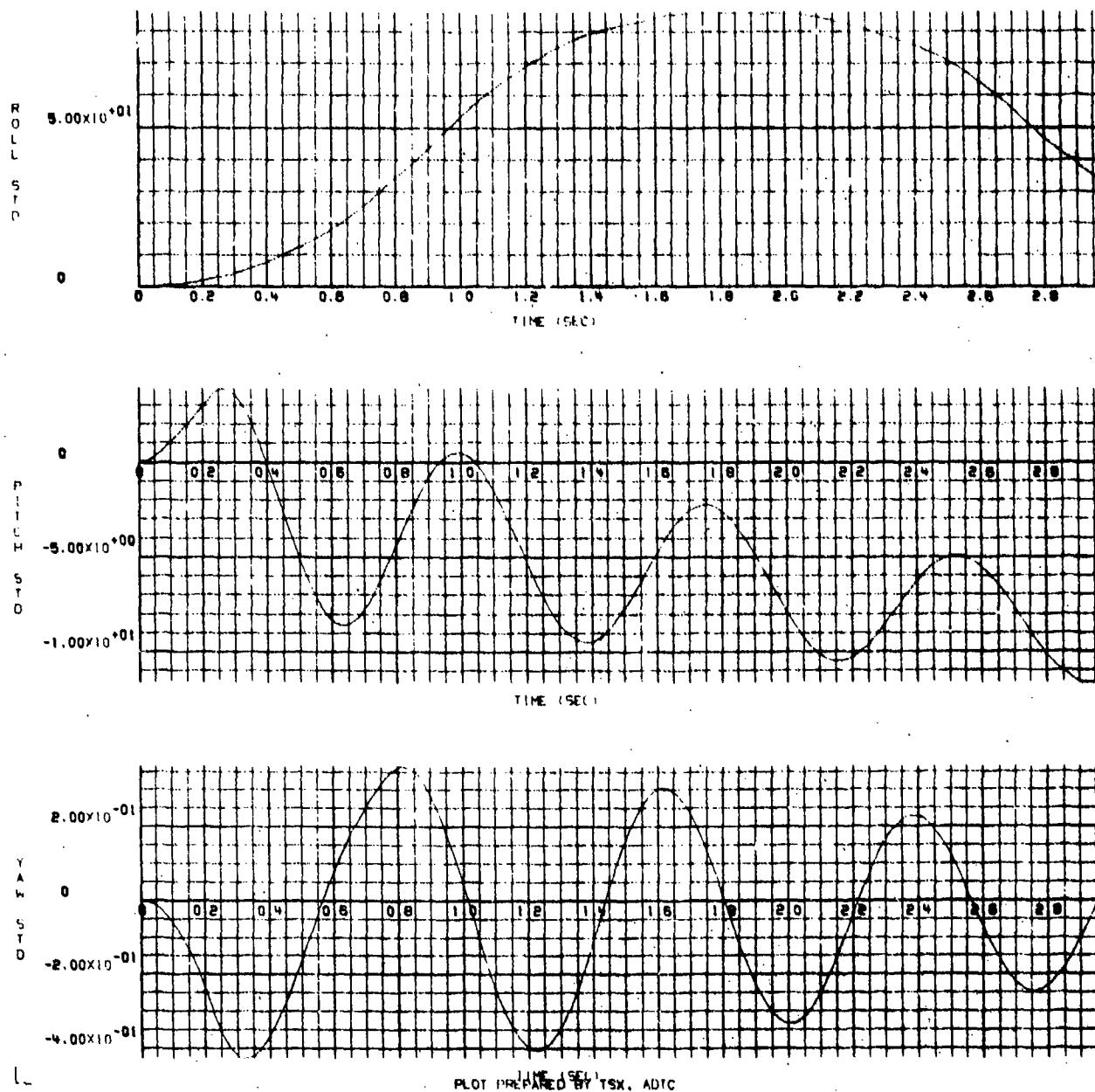


Figure EE-8.  $\phi$ ,  $\theta$ , and  $\psi$  Rotation Versus Time for a Flow Field Intensity of  $-1/2$

APPENDIX FF

GBU-10 BOMB TRAJECTORIES RESULTING FROM A  
PARTIAL FIN OPENING AT MACH 0.85

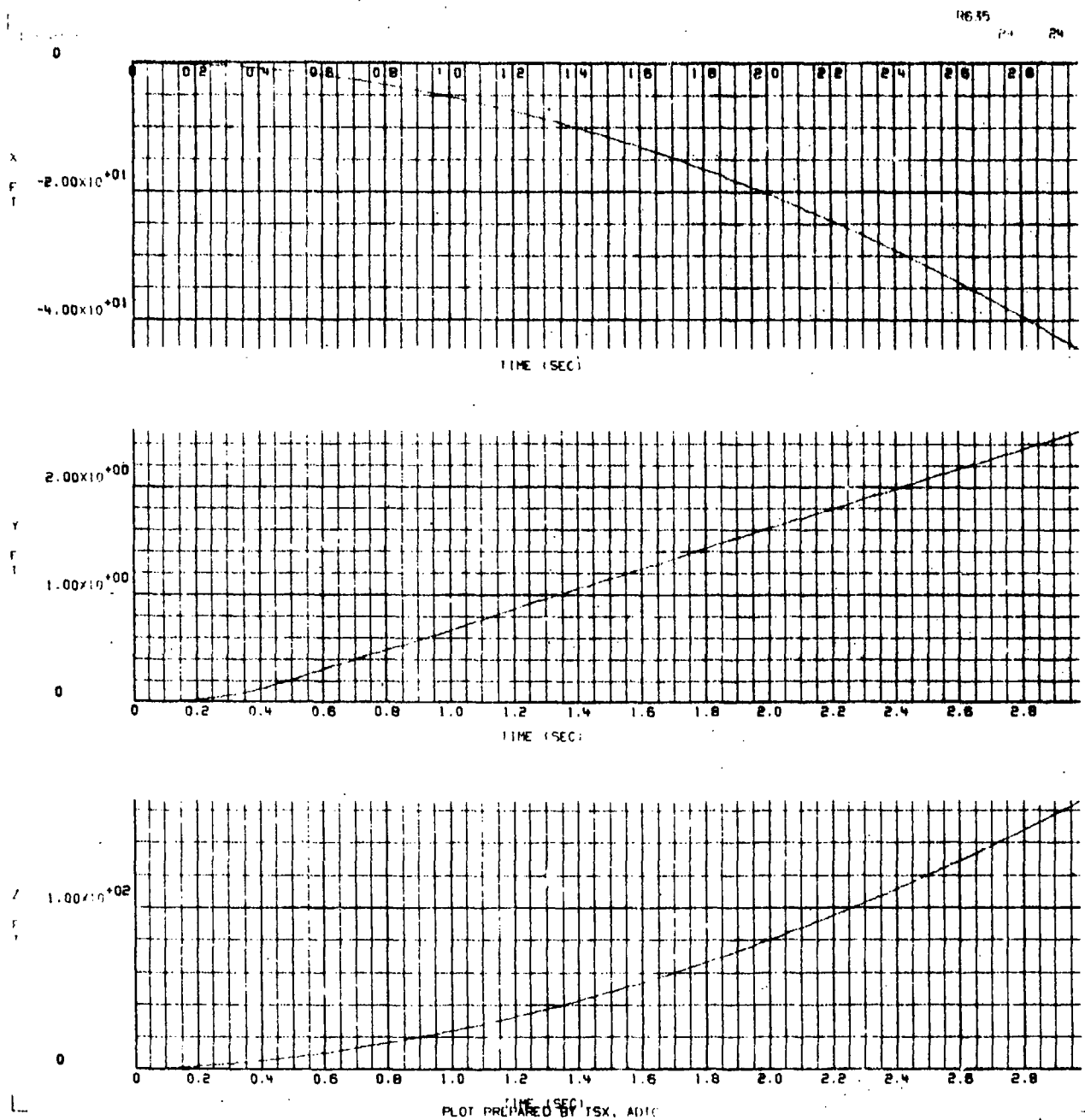
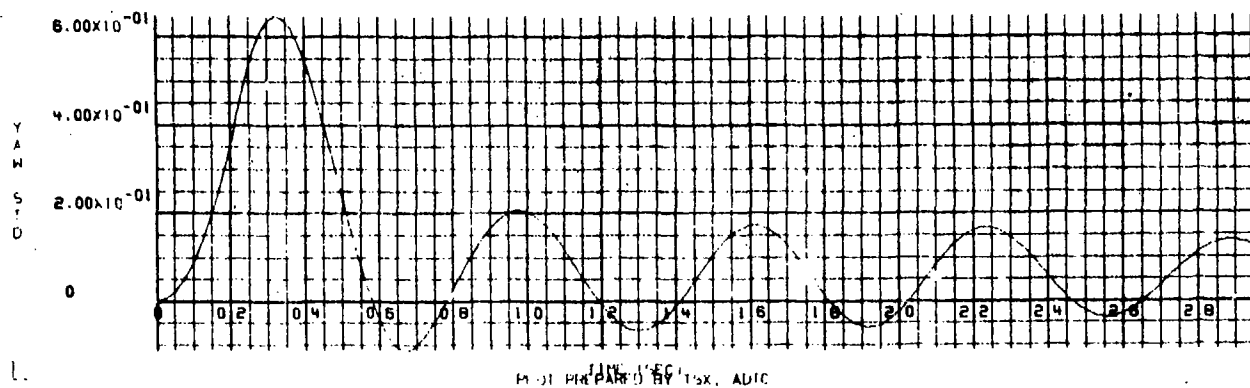
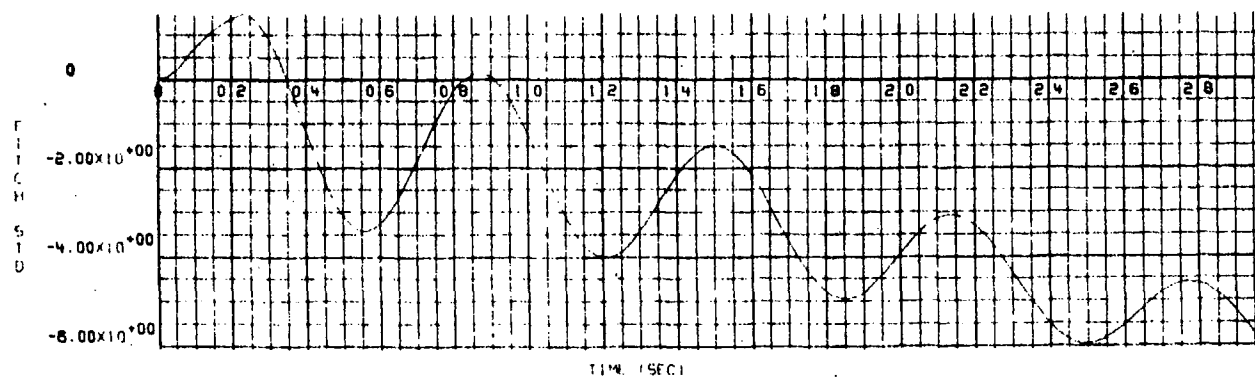
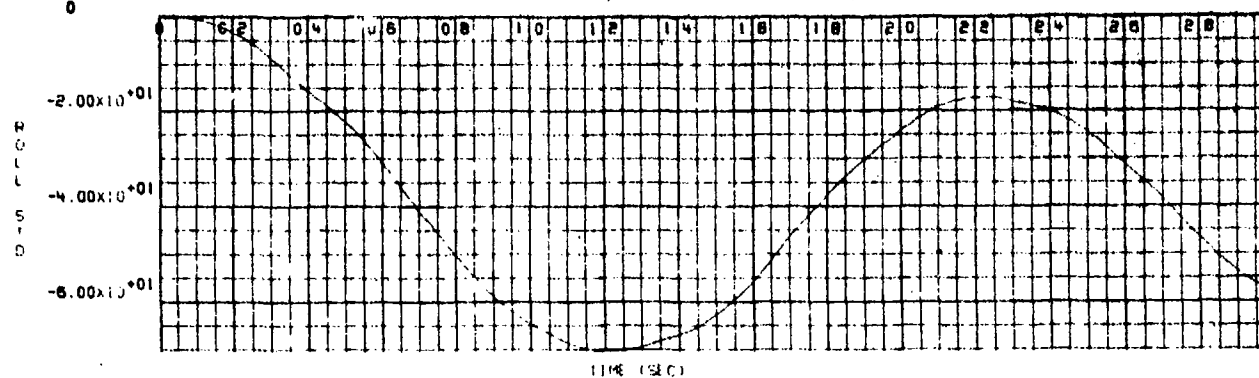


Figure FF-1. X, Y, and Z Position Versus Time for a Flow Field Intensity of 1/2



17/12/75  
0

P835 23 23



FILE 156  
M-01 PREPARED BY TSX, ADIC

Figure FF-2.  $\phi$ ,  $\theta$ , and  $\psi$  Rotation Versus Time for a Flow Field Intensity of  $1/2$

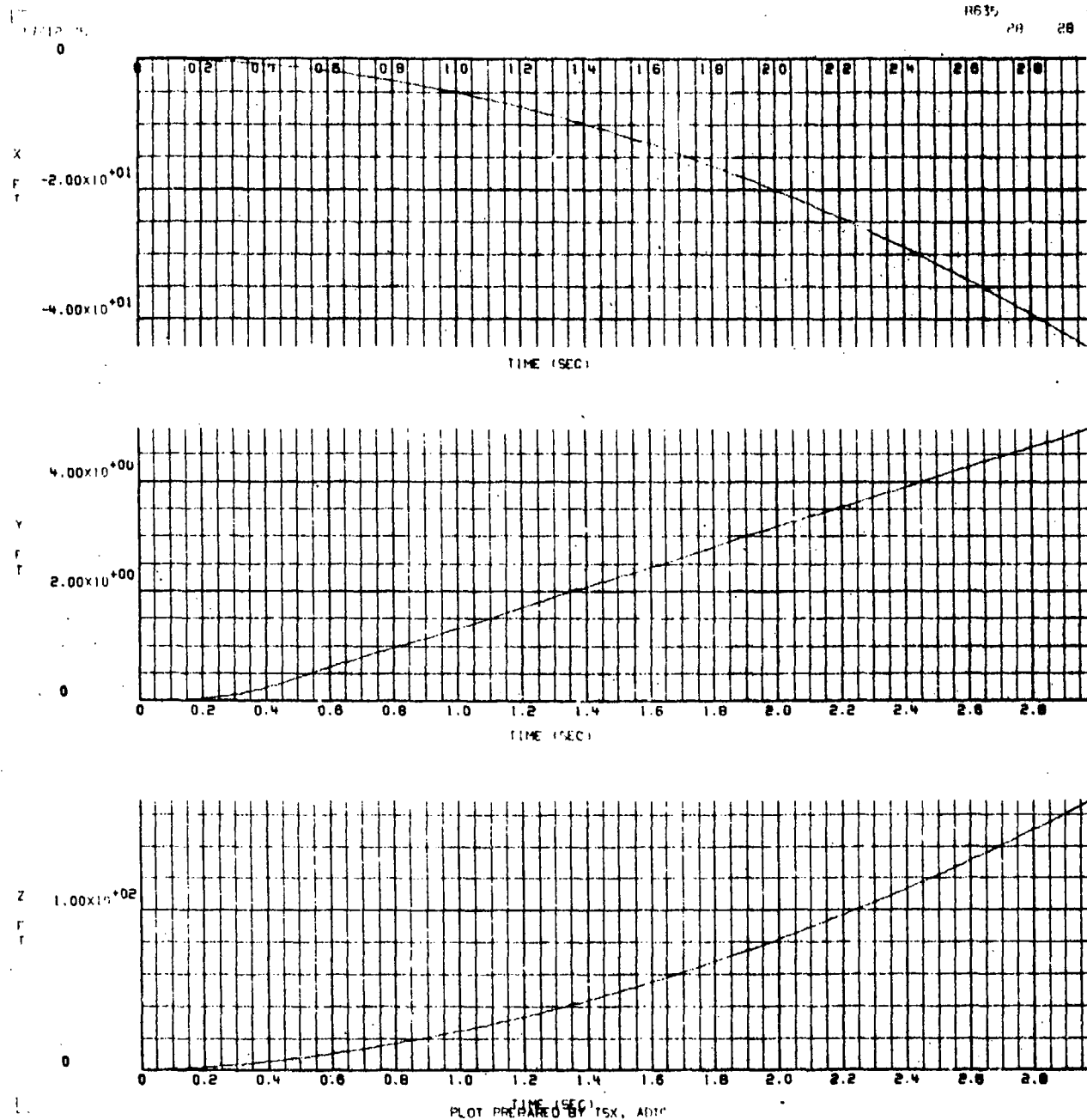


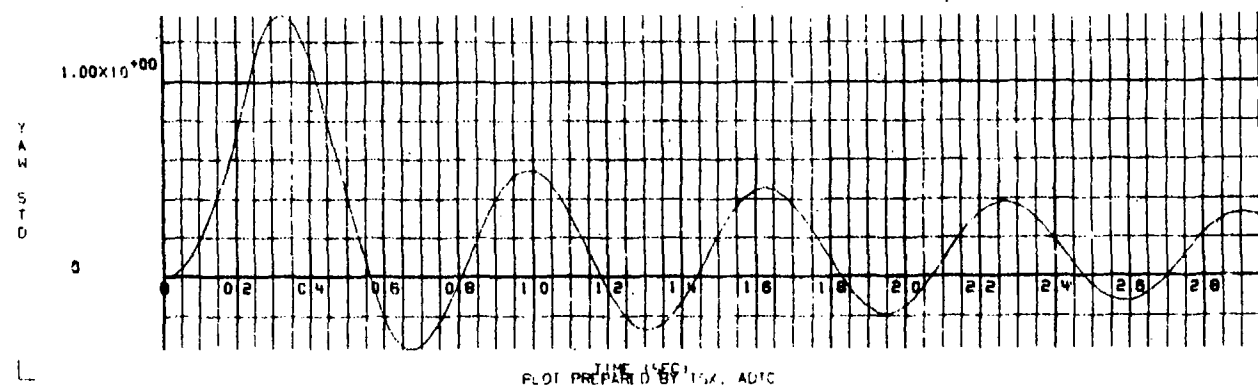
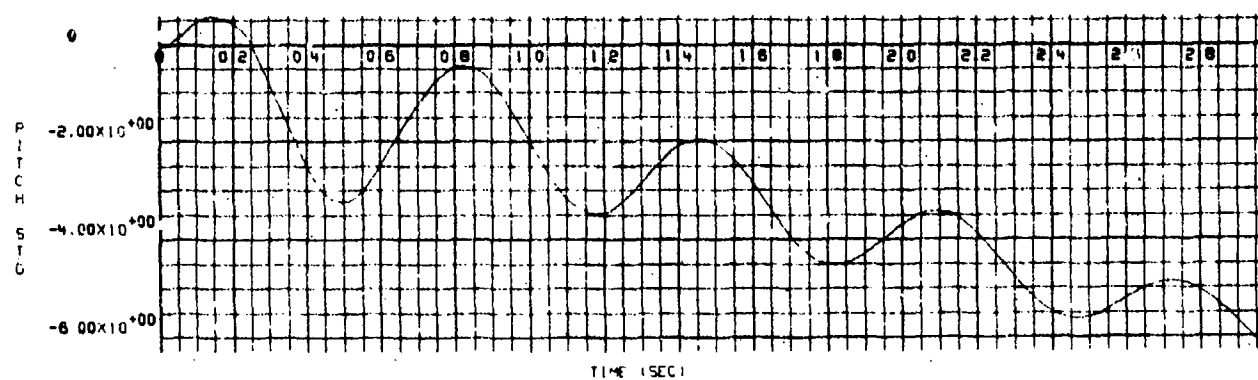
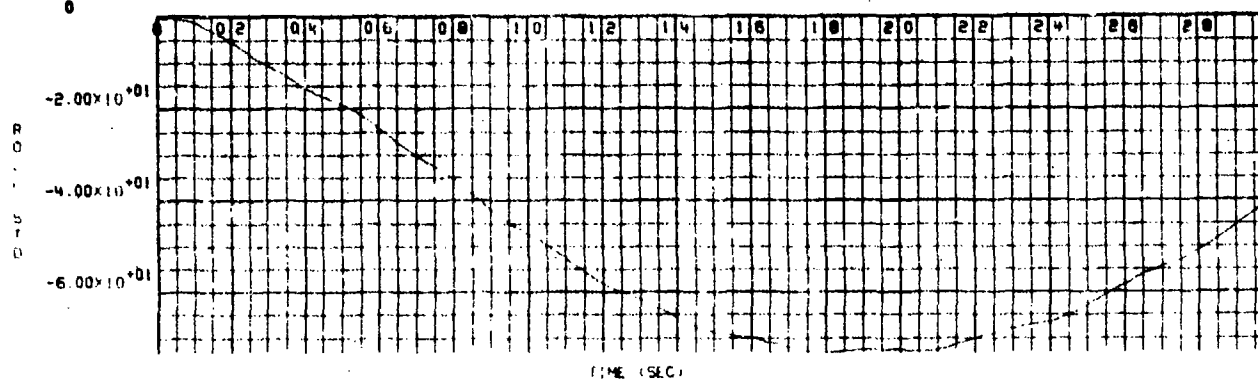
Figure FF-3. X, Y, and Z Position Versus Time for a Flow Field Intensity of 1 (as measured in the wind tunnel)

17-12-75  
0

R635

27

27



PLOT PREPARED BY TKA, ADIC

Figure FF-4.  $\phi$ ,  $\theta$ , and  $\psi$  Rotation Versus Time for a Flow Field Intensity of 1 (unchanged from the wind tunnel measured values)

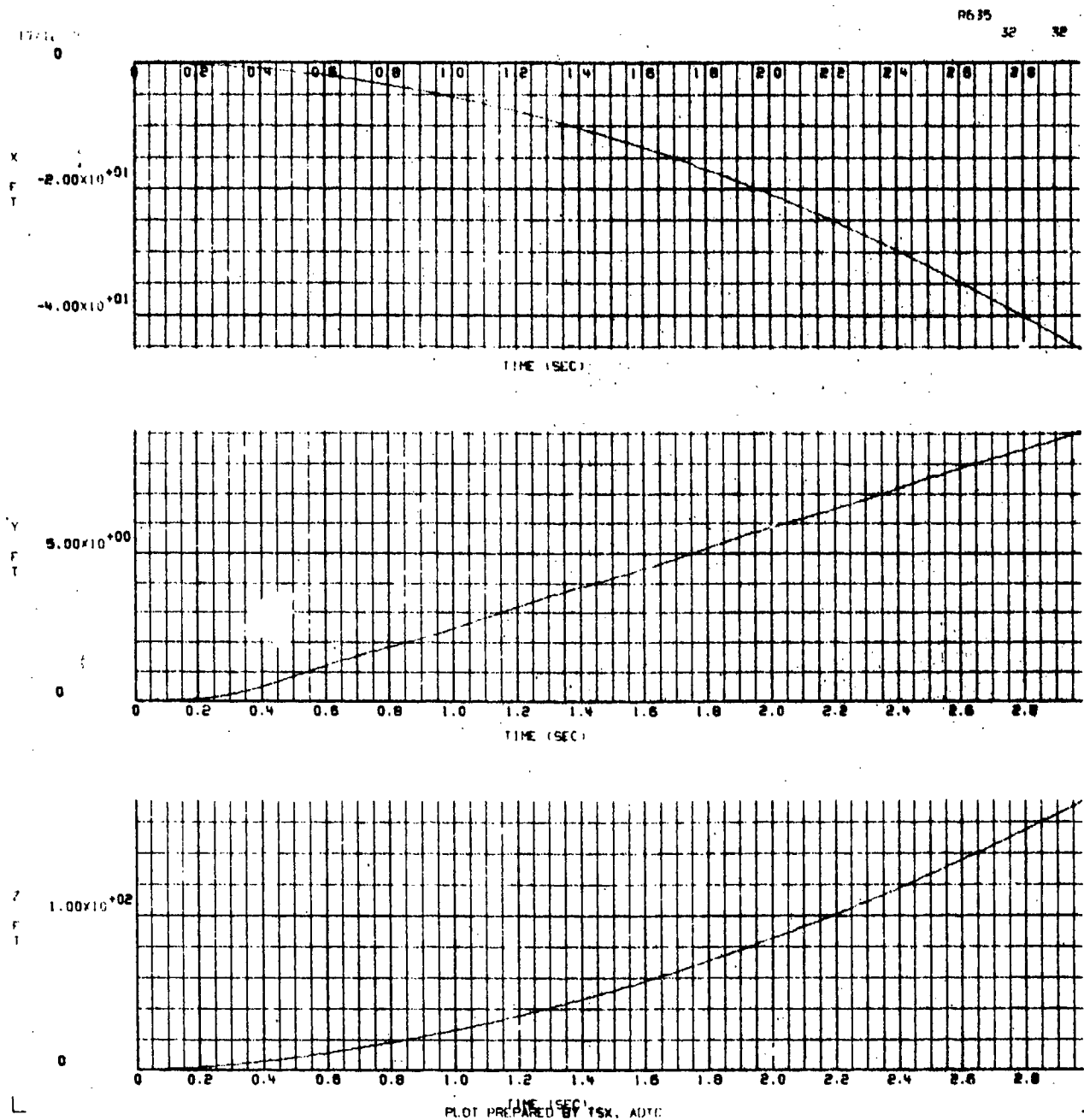


Figure FF-5. X, Y, and Z Position Versus Time for a Flow Field Intensity of 2

17/12/75

R6.35

31 31

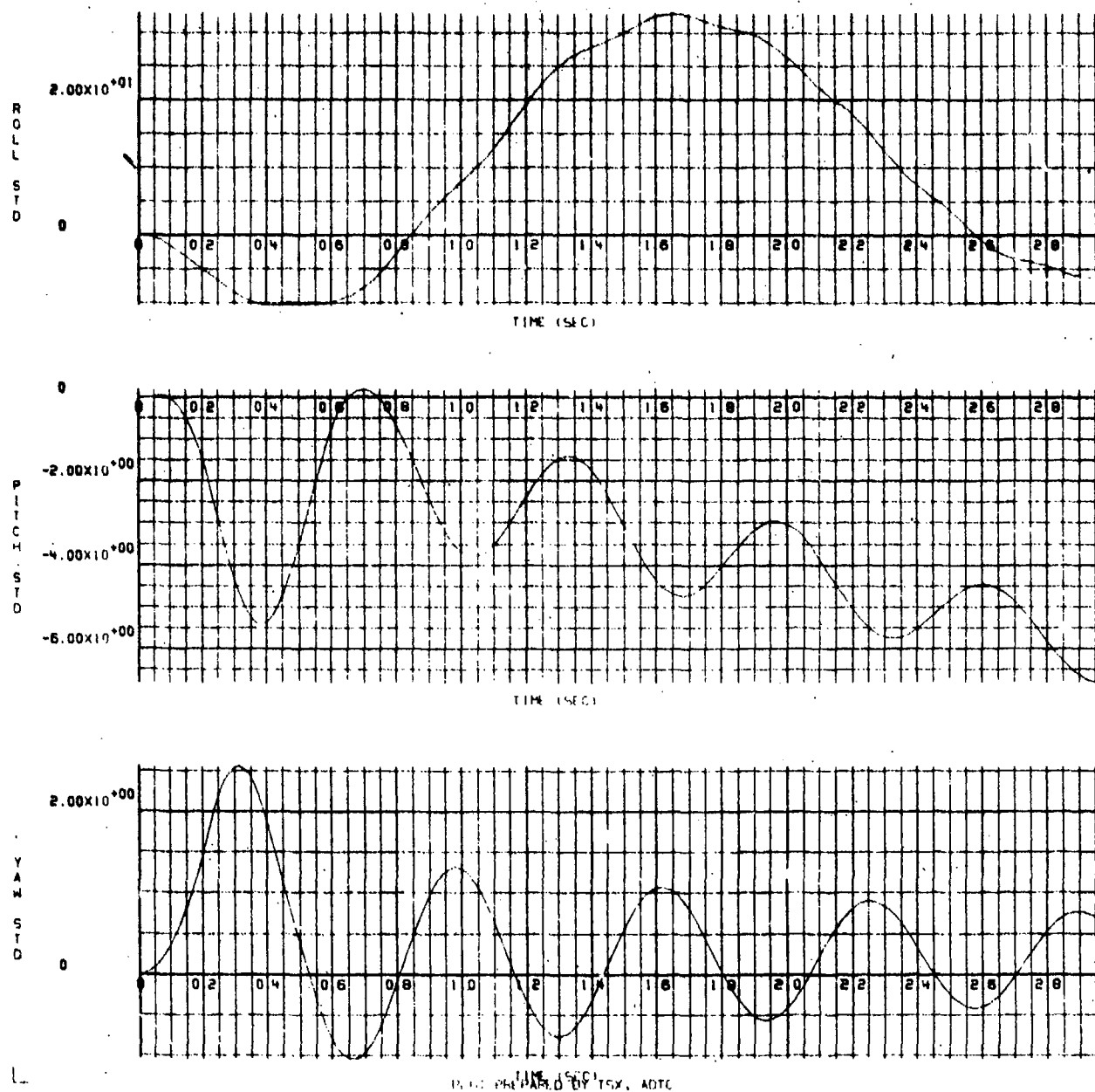


Figure FF-6.  $\phi$ ,  $\theta$ , and  $\psi$  Rotation Versus Time for a Flow Field Intensity of 2

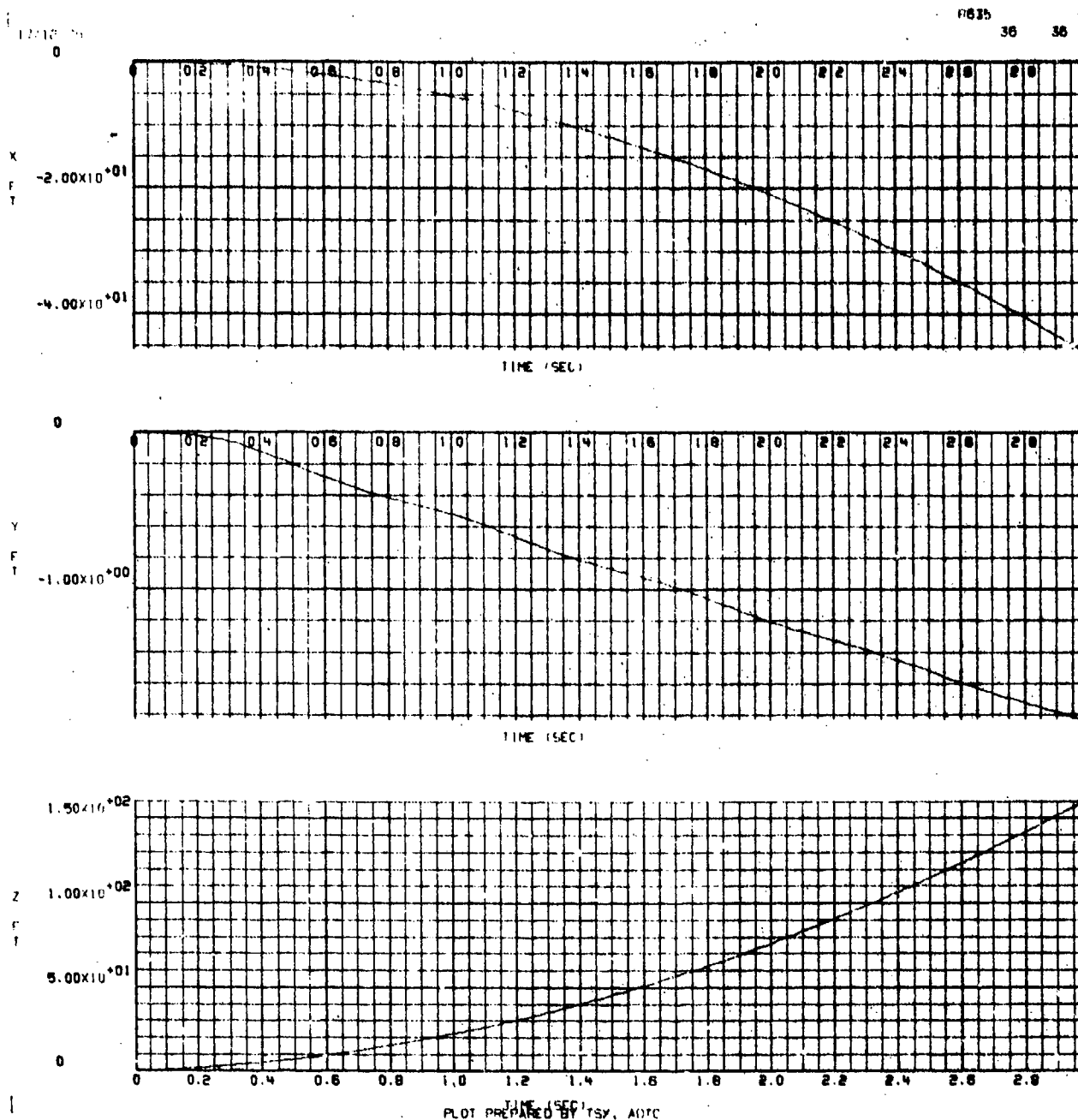


Figure FF-7. X, Y, and Z Position Versus Time for a Flow Field Intensity of  $-1/2$

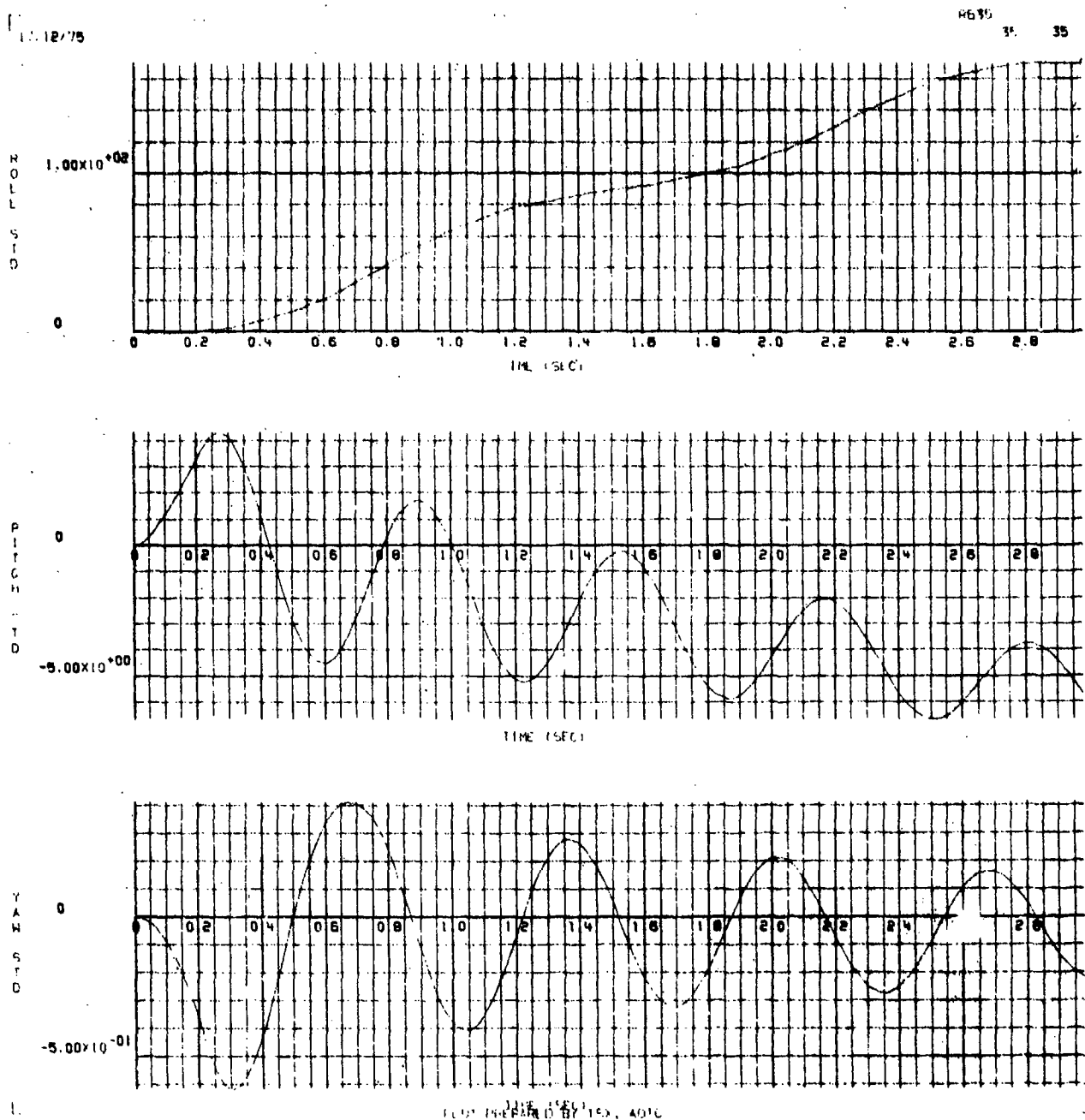


Figure FF-8.  $\phi$ ,  $\theta$ , and  $\psi$  Rotation Versus Time for a Flow Field Intensity of  $-1/2$

APPENDIX GG

GBU-10 BOMB TRAJECTORIES RESULTING FROM A  
PARTIAL FIN OPENING AT MACH 0.95



17/12/75  
0

R635

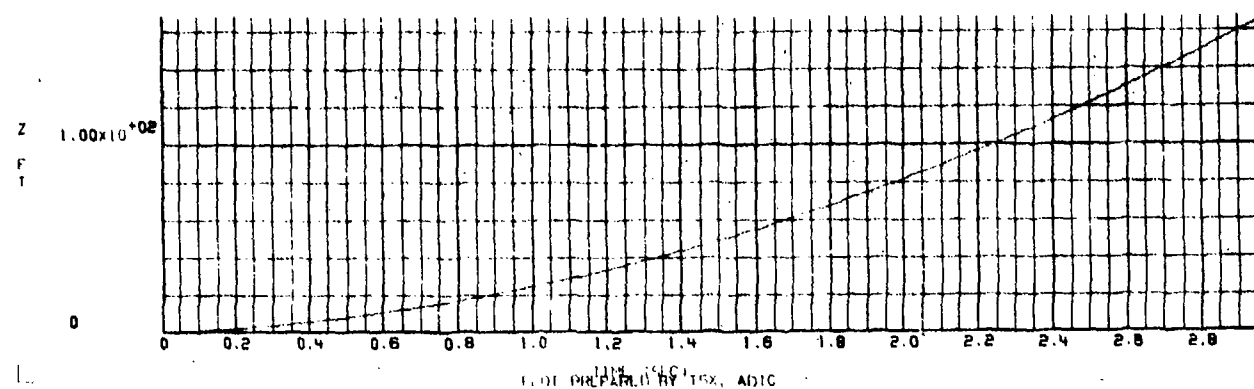
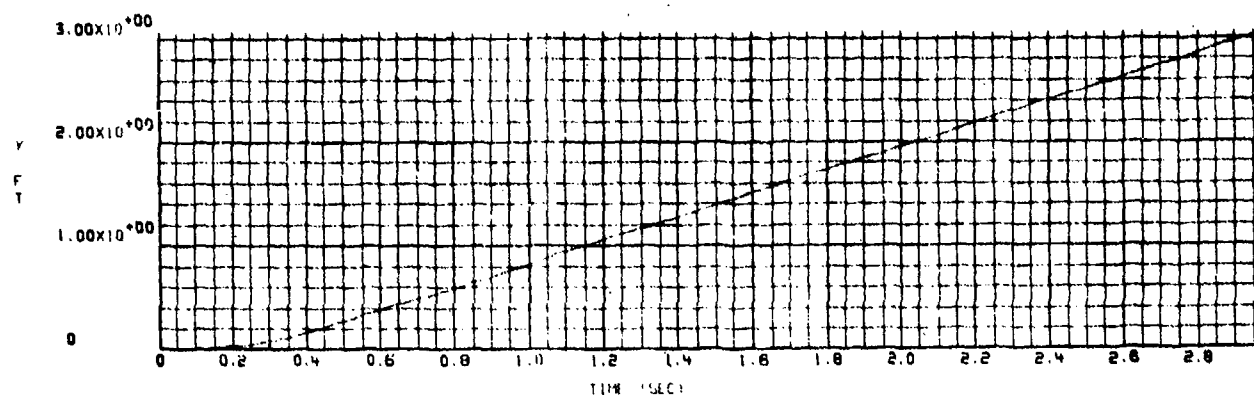
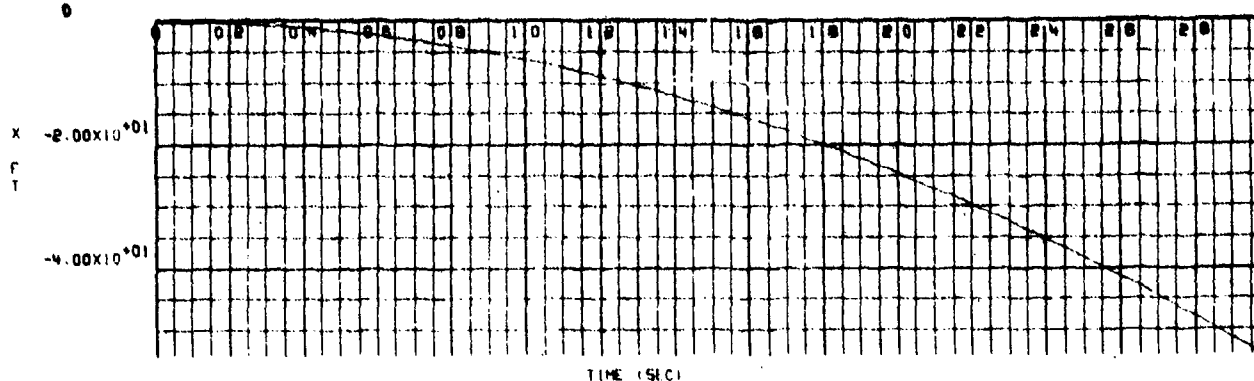


Figure GG-1. X, Y, and Z Position Versus Time for a Flow Field Intensity of 1/2

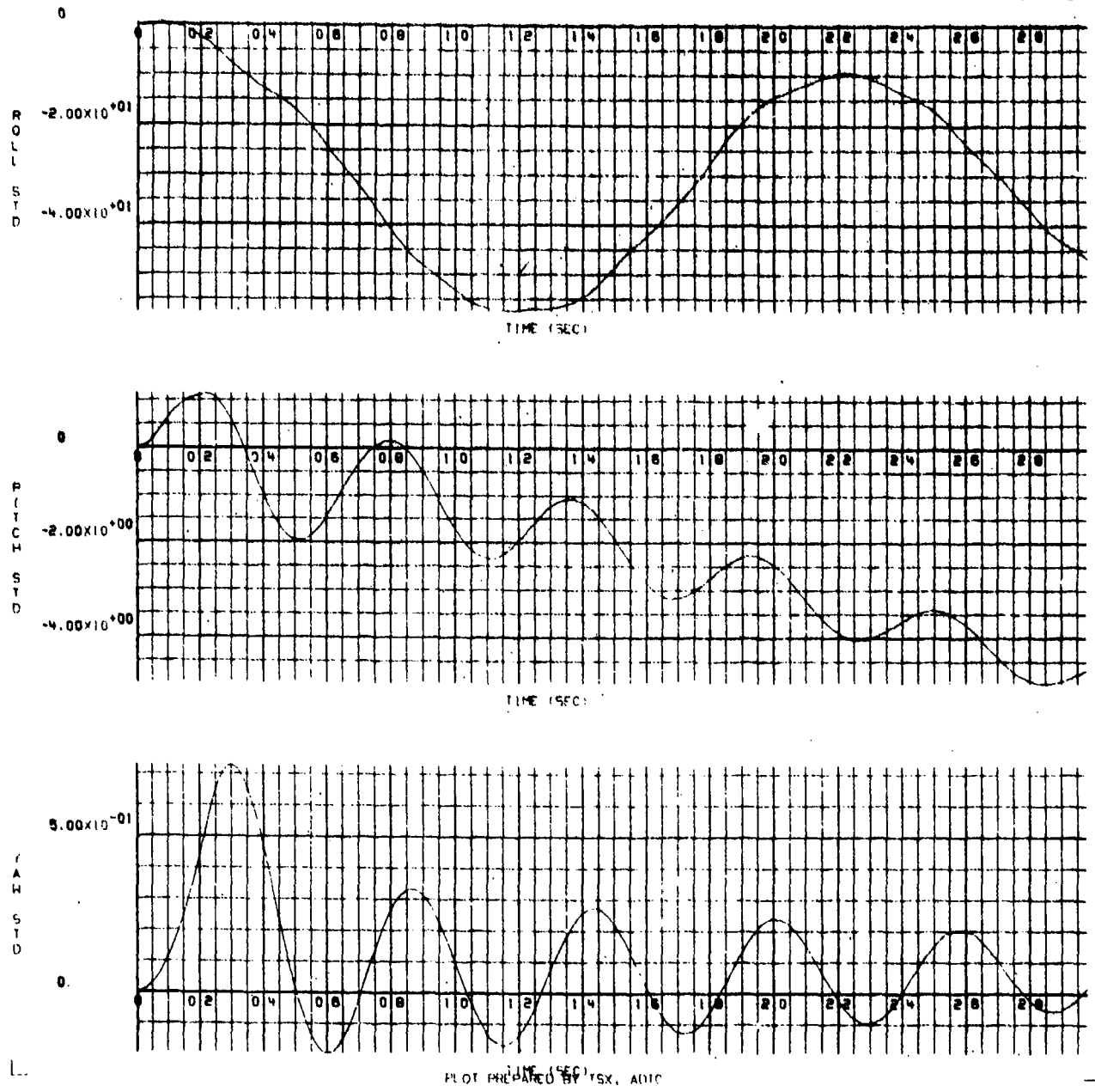
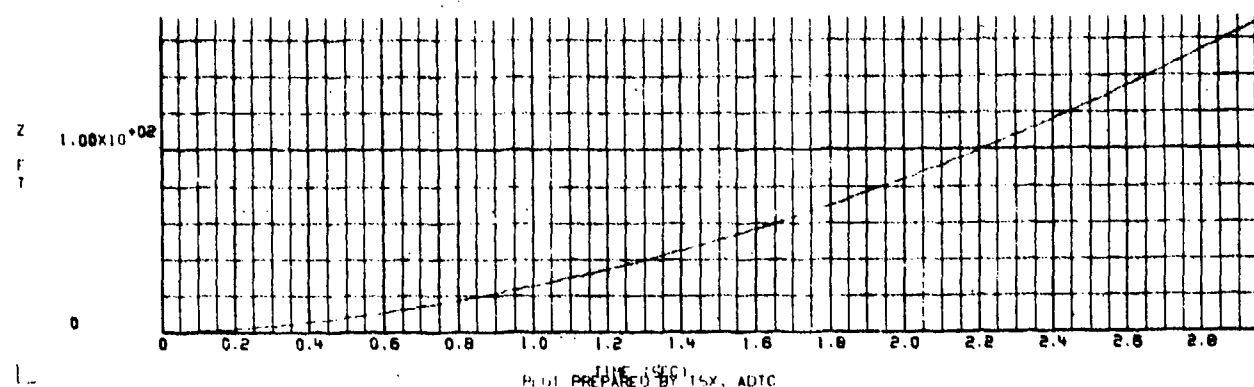
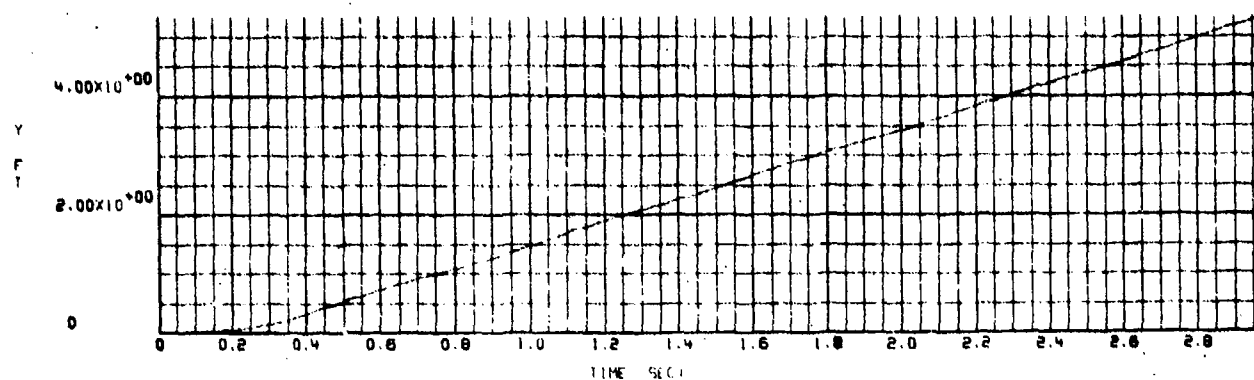
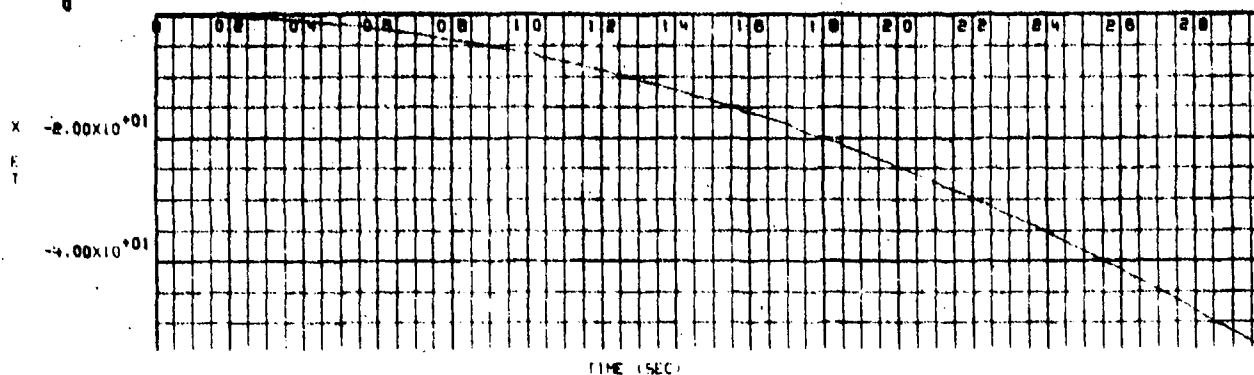


Figure GG-2.  $\phi$ ,  $\theta$ , and  $\psi$  Rotation Versus Time for a Flow Field Intensity of 1/2

17/12/75

R632



Plot prepared by TSX, ADTC

Figure GG-3. X, Y, and Z Position Versus Time for a Flow Field Intensity of 1 (as measured in the wind tunnel)

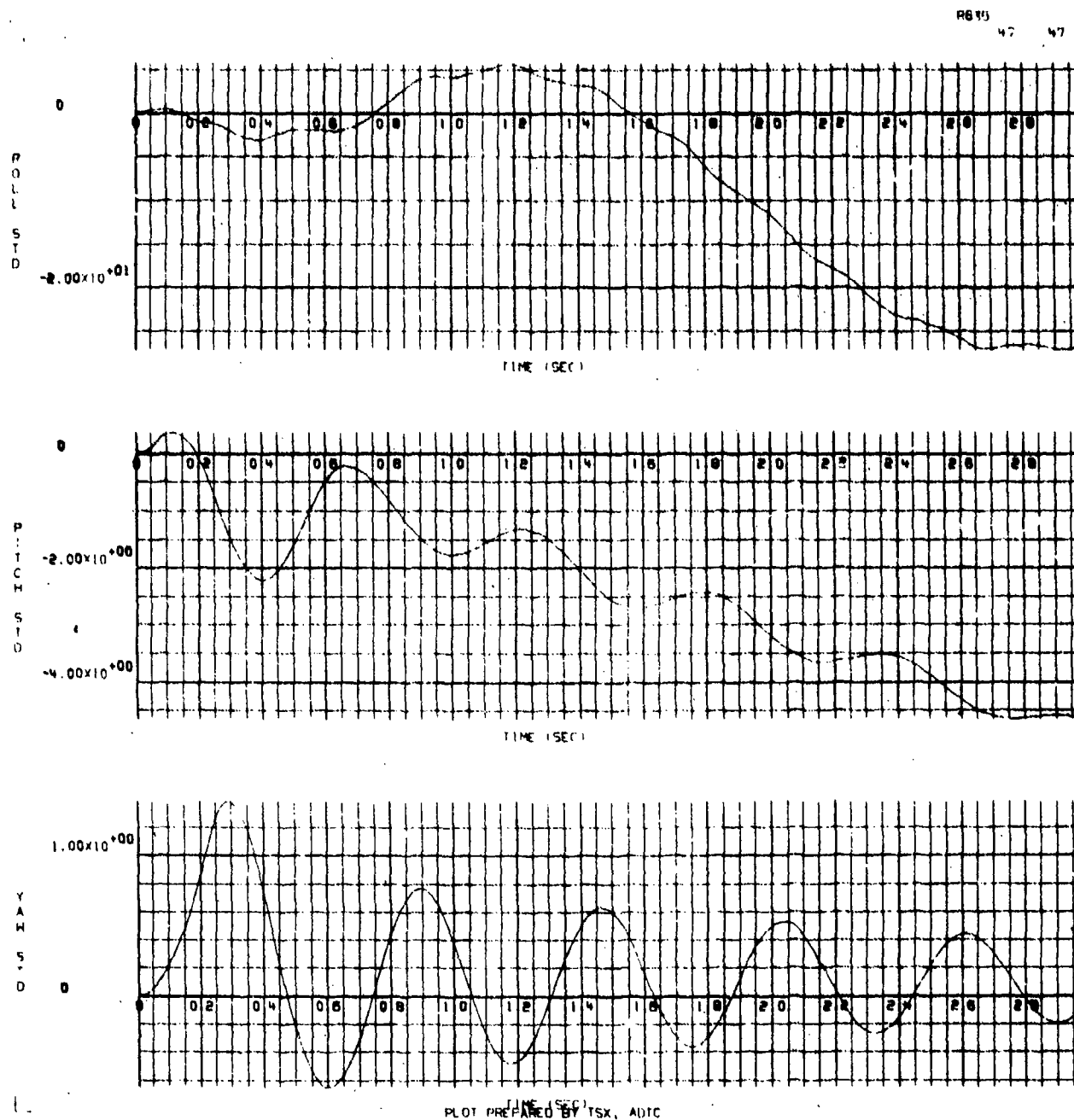
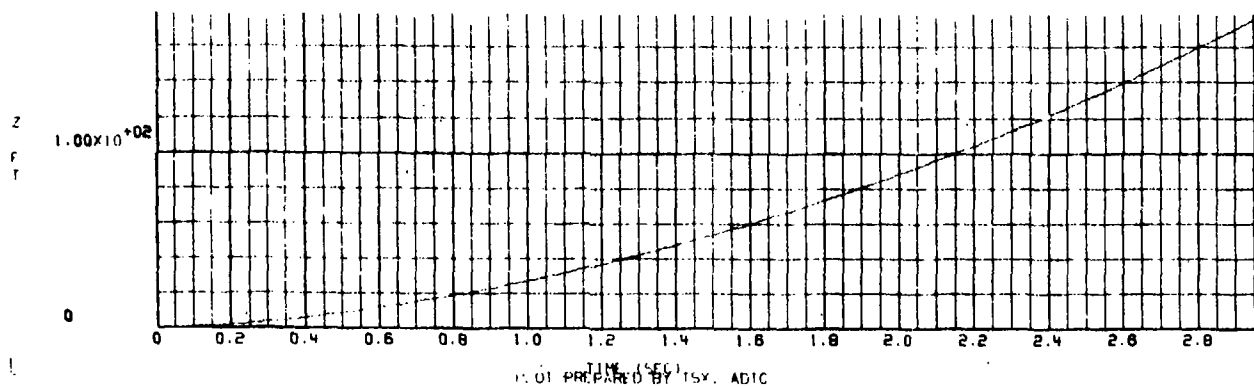
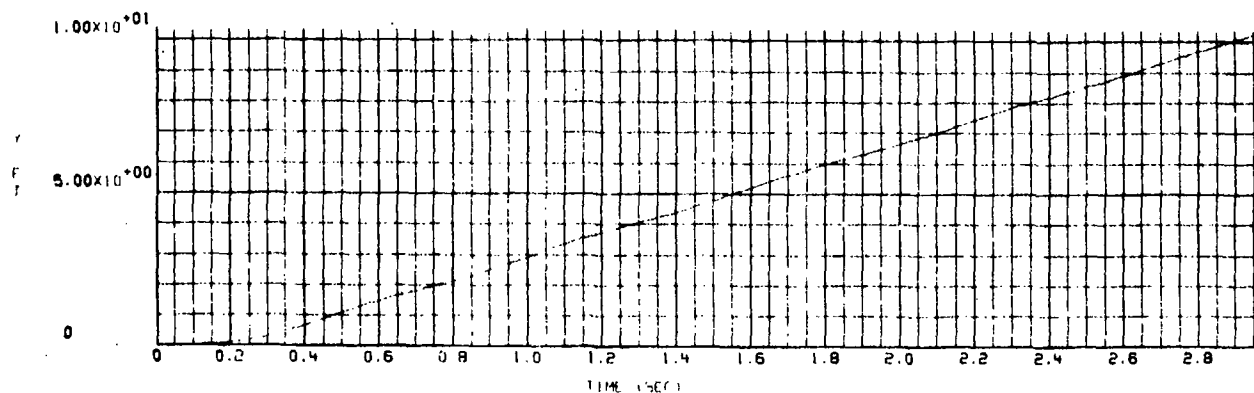
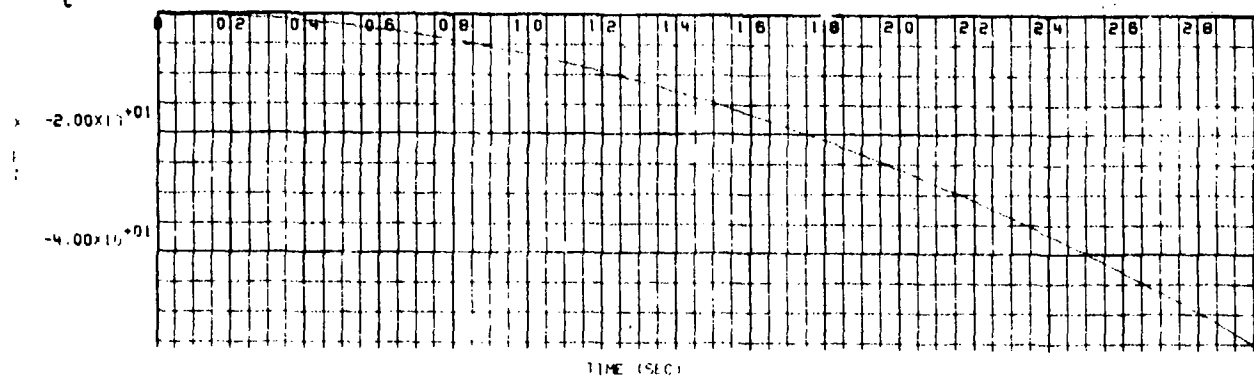


Figure GG-4.  $\phi$ ,  $\theta$ , and  $\psi$  Rotation Versus Time for a Flow Field Intensity of 1 (unchanged from the wind tunnel measured values)

17/12/75  
C

R635

52



1.01 PREPARED BY TSY. ADIC

Figure GG-5. X, Y, and Z Position Versus Time for a Flow Field Intensity of 2

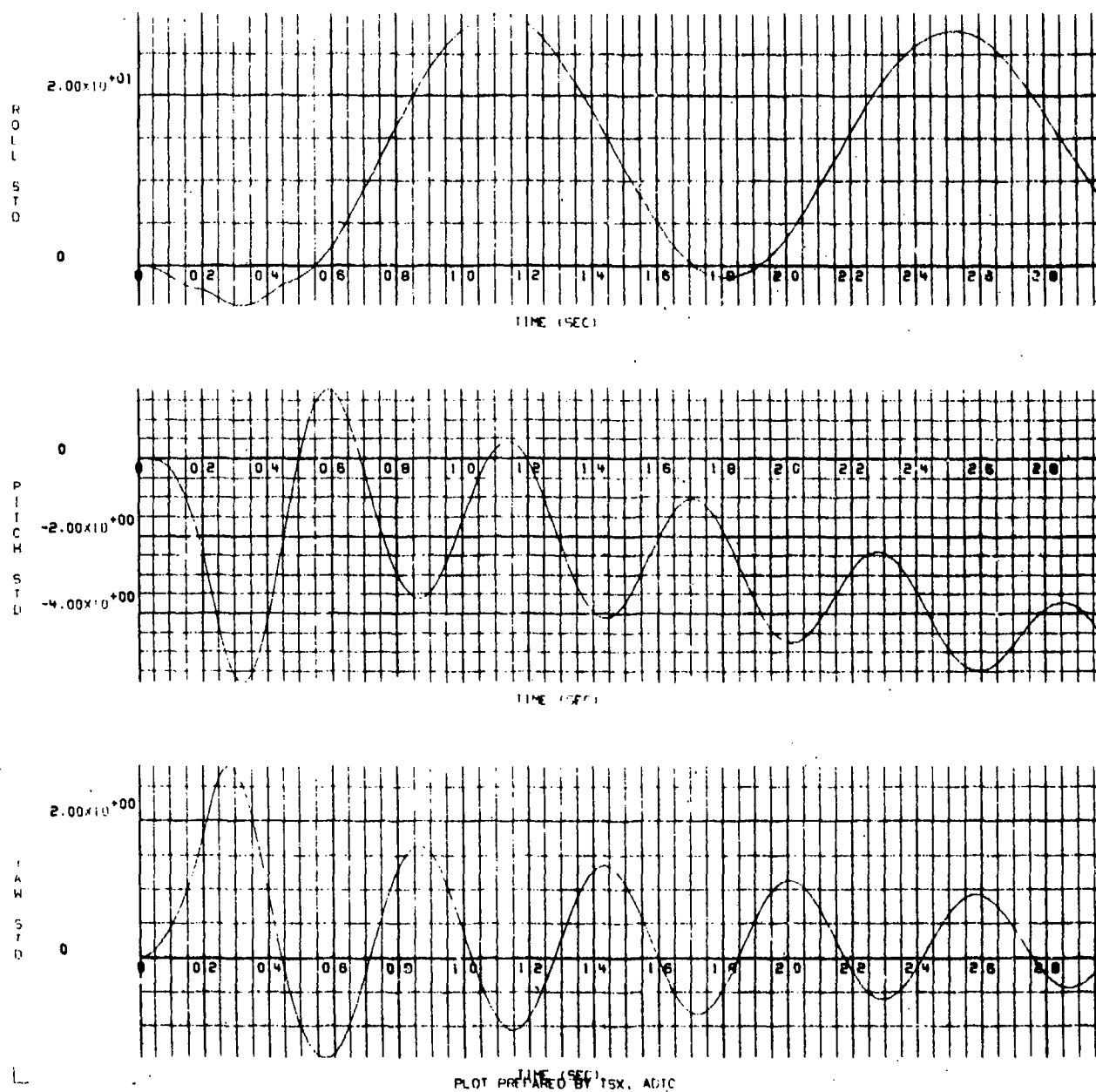
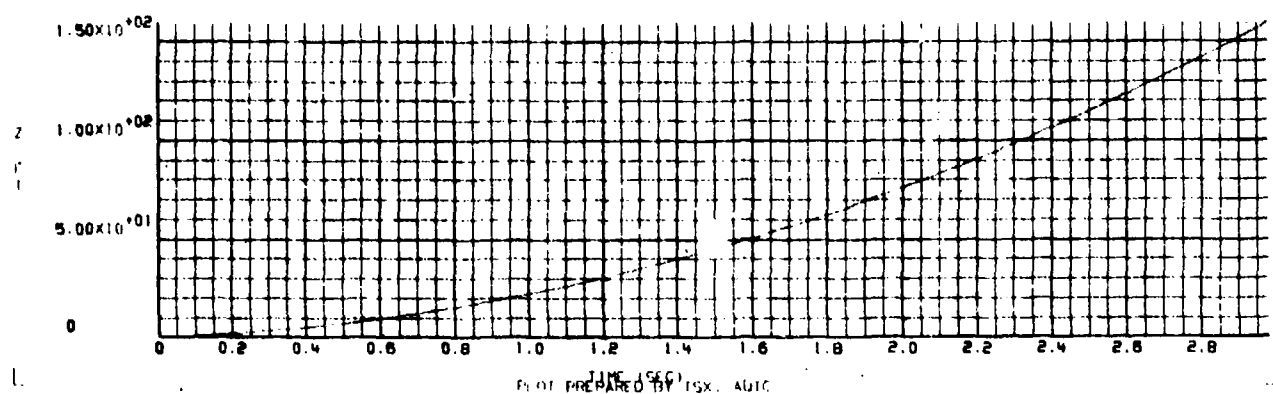
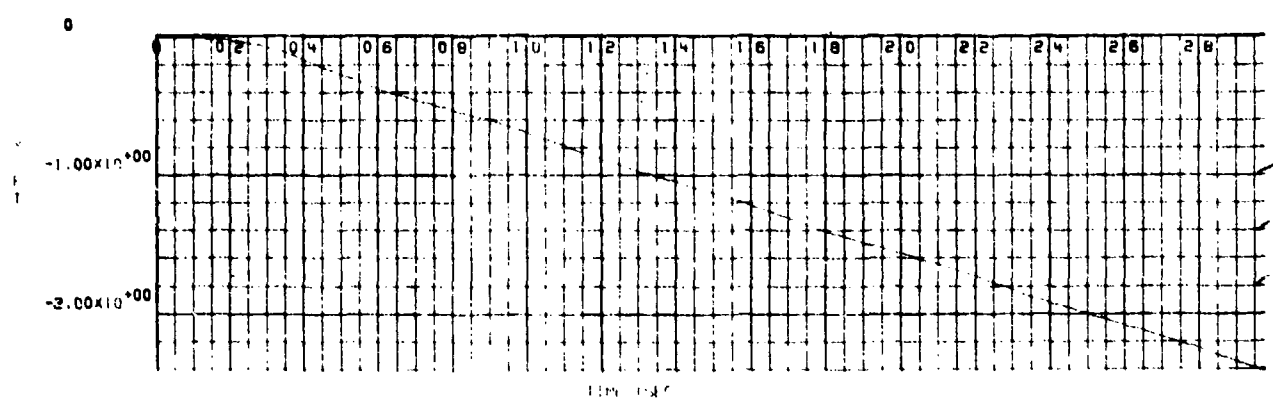
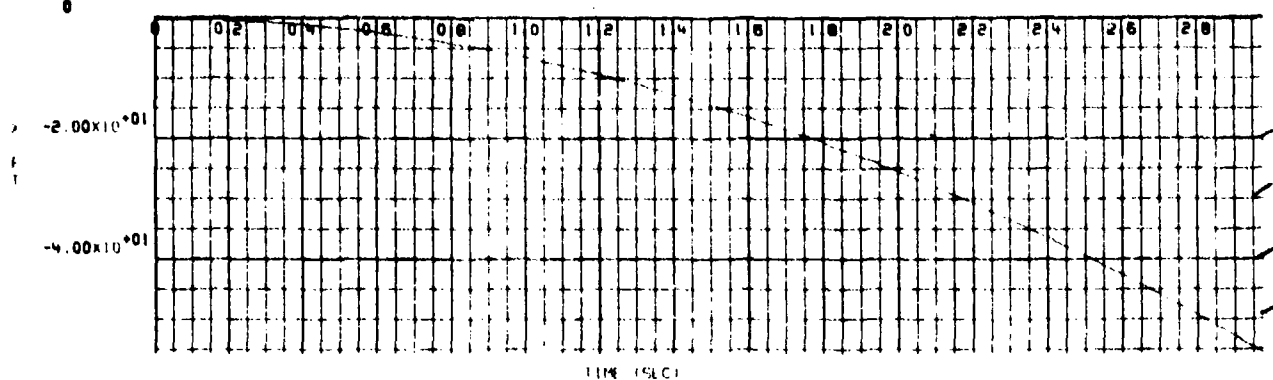


Figure GG-6.  $\phi$ ,  $\theta$ , and  $\psi$  Rotation Versus Time for a Flow Field Intensity of 2

17.12/75  
0

26.31  
56



17.12/75  
0  
PLOT PREPARED BY TSCX, AUTO

Figure GG-7. X, Y, and Z Position Versus Time for a Flow Field Intensity of  $-1/2$

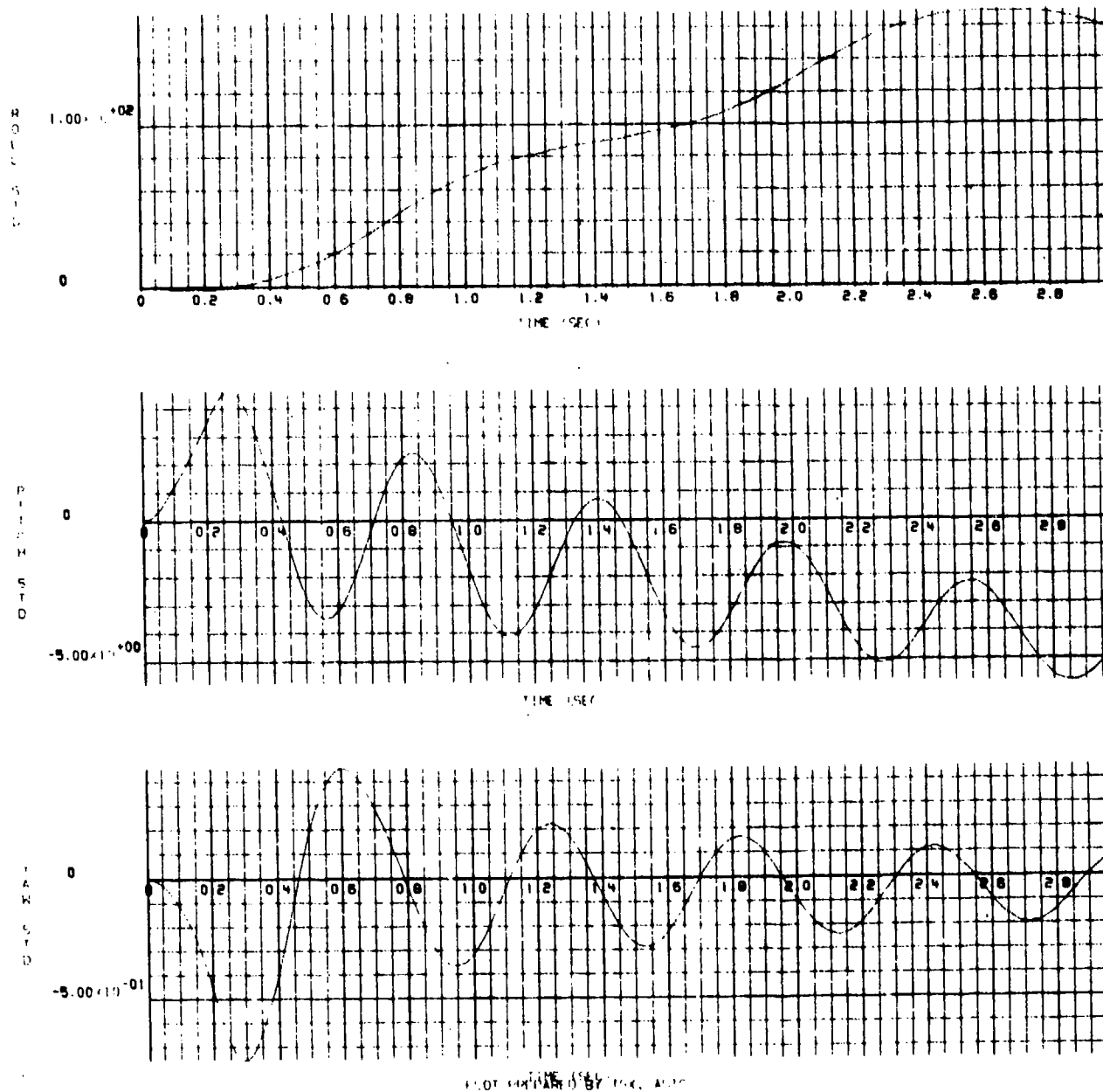


Figure GG-8.  $\phi$ ,  $\theta$ , and  $\psi$  Rotation Versus Time for a Flow Field Intensity of  $-1/2$



APPENDIX HH

GBU-10 BOMB TRAJECTORIES RESULTING FROM A  
PARTIAL FIN OPENING AT MACH 1.2

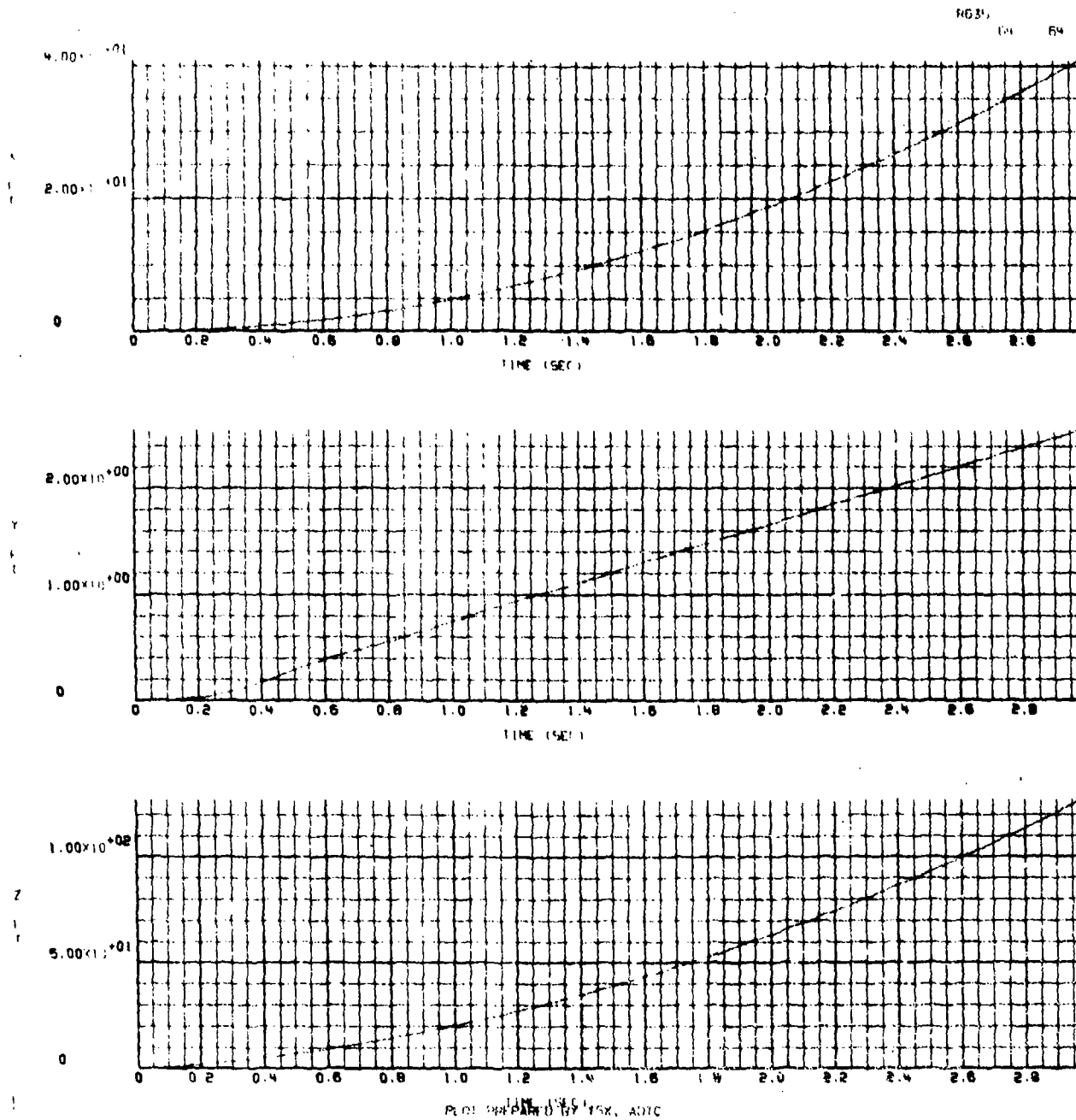


Figure HH-1. X, Y, and Z Position Versus Time for a Flow Field Intensity of 1/2

17-27-0

17-27-0

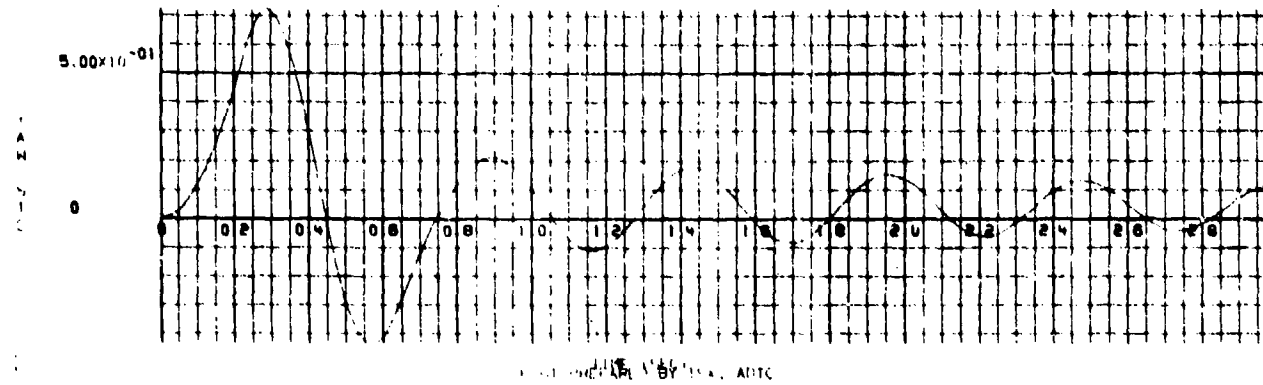
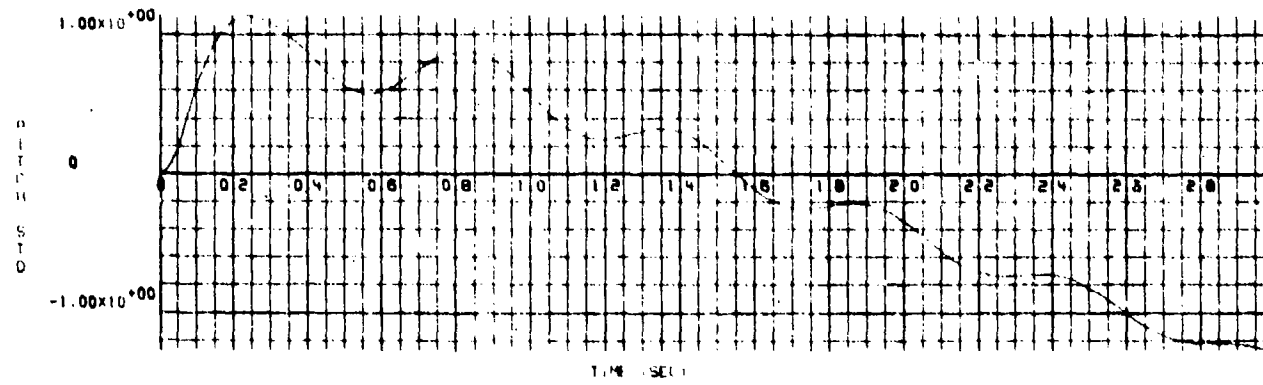
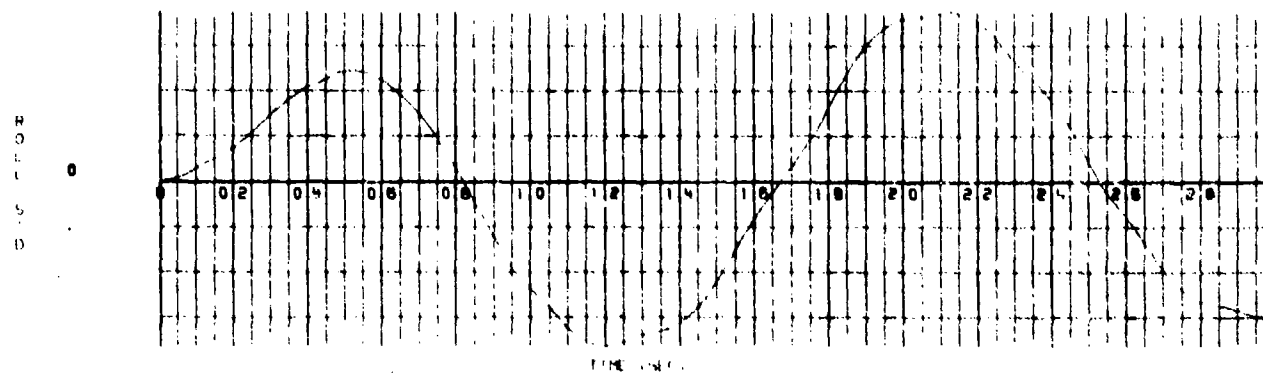


Figure HH-2.  $\phi$ ,  $\theta$ , and  $\psi$  Rotation Versus Time for a Flow Field Intensity of  $1/2$

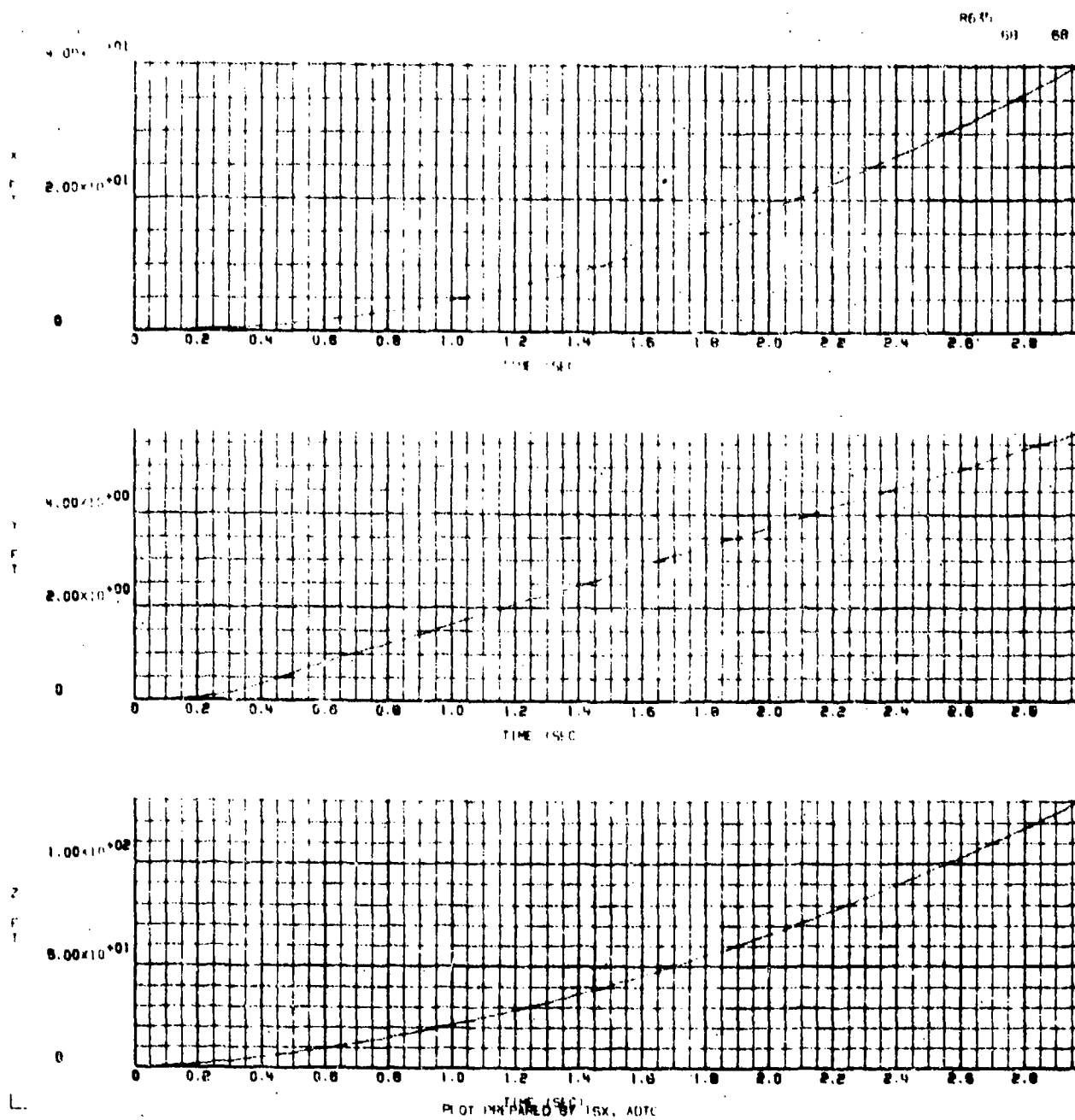


Figure HH-3. X, Y, and Z Position Versus Time for a Flow Field Intensity of 1 (as measured in the wind tunnel)

17-10-75

86.0

67

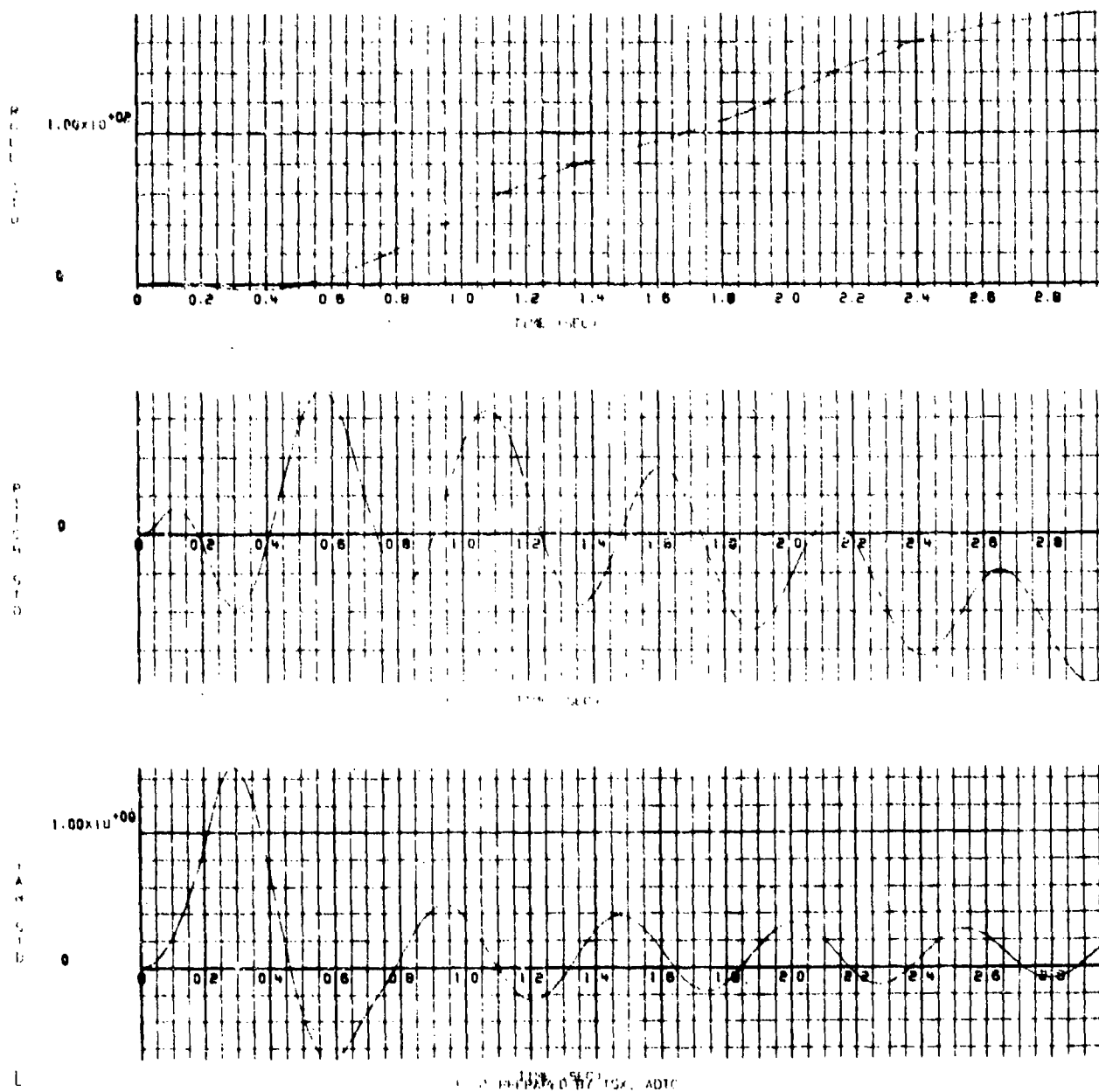


Figure HH-4.  $\phi$ ,  $\theta$ , and  $\gamma$  Rotation Versus Time for a Flow Field Intensity of 1 (unchanged from the wind tunnel measured values)

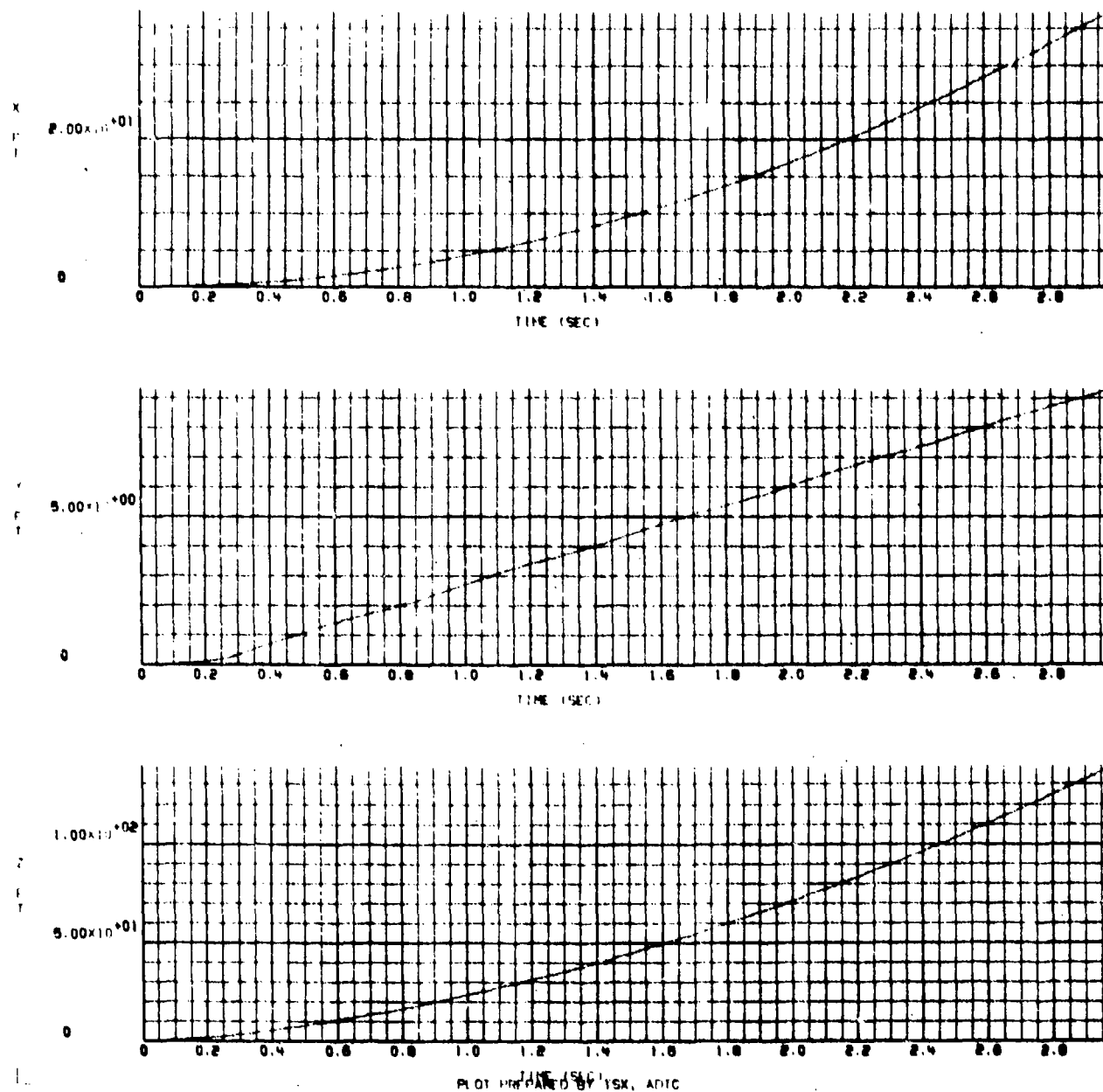


Figure HH-5. X, Y, and Z Position Versus Time for a Flow Field Intensity of 2

17/12/75

RE 81 71

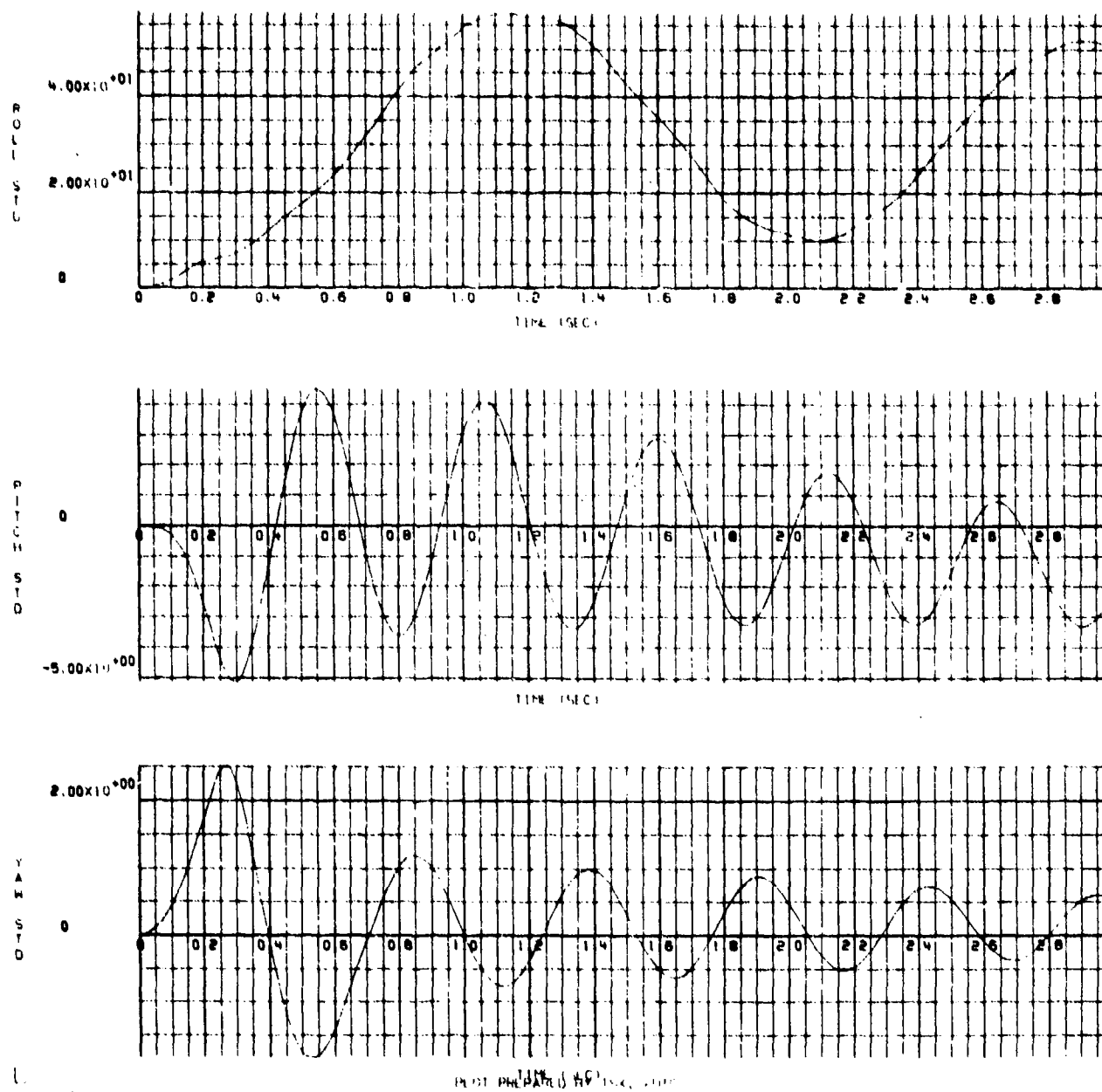


Figure HH-6.  $\phi$ ,  $\theta$ , and  $\psi$  Rotation Versus Time for a Flow Field Intensity of 2

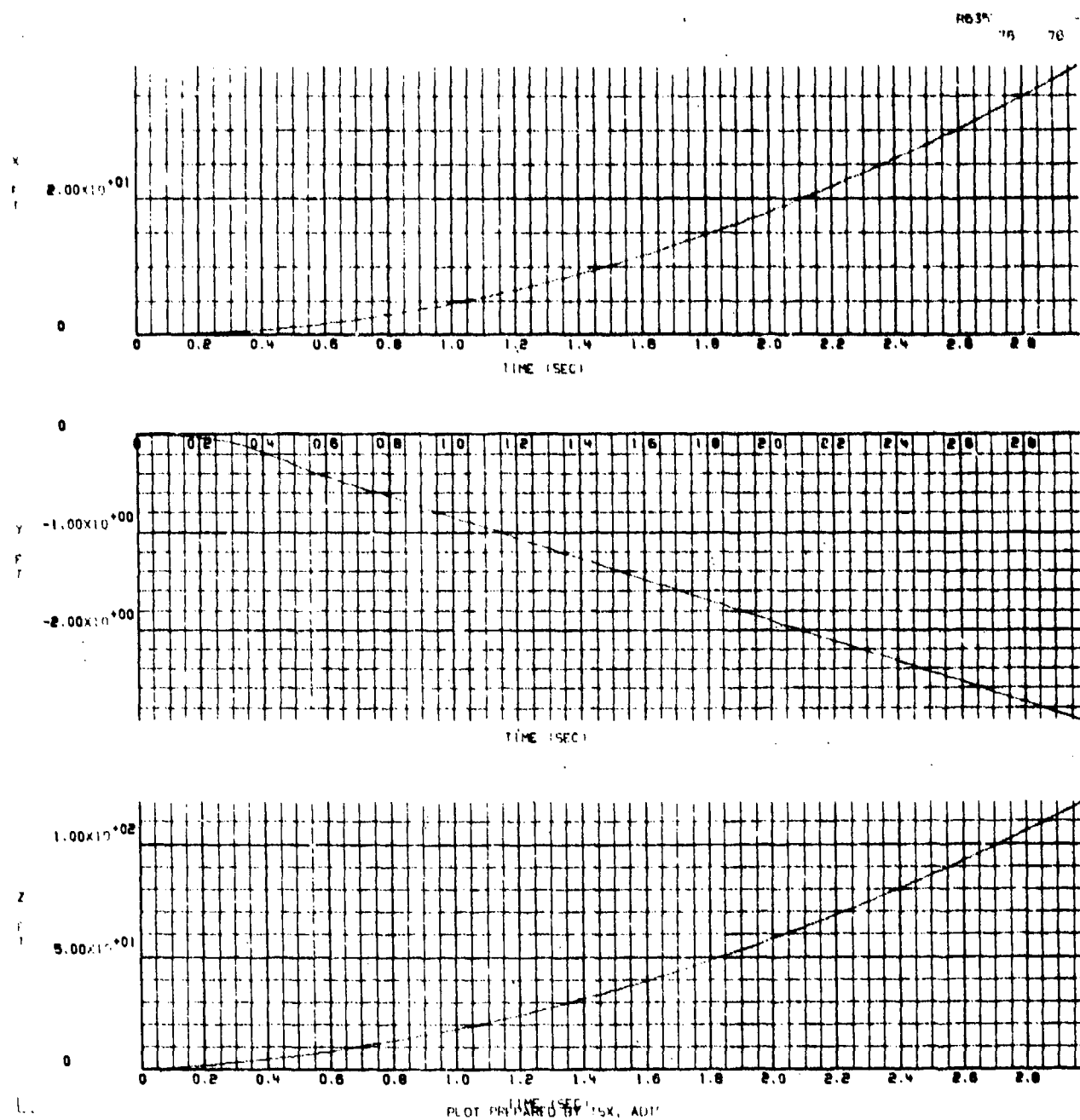


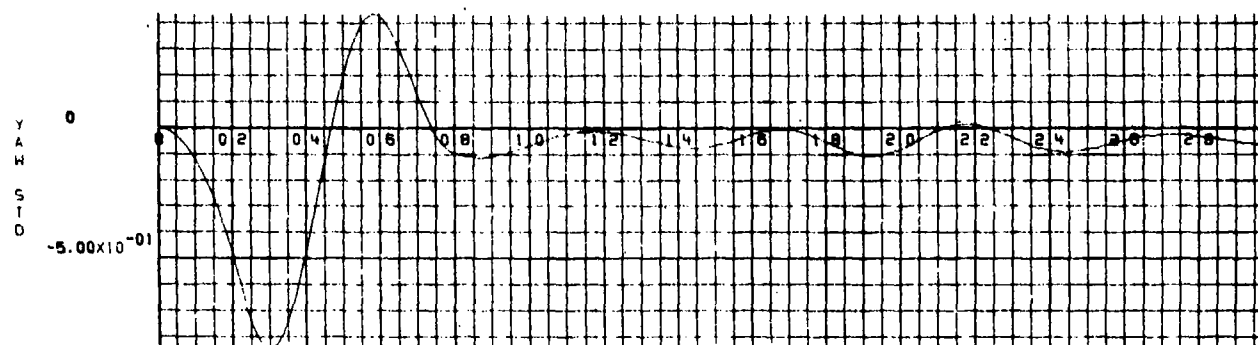
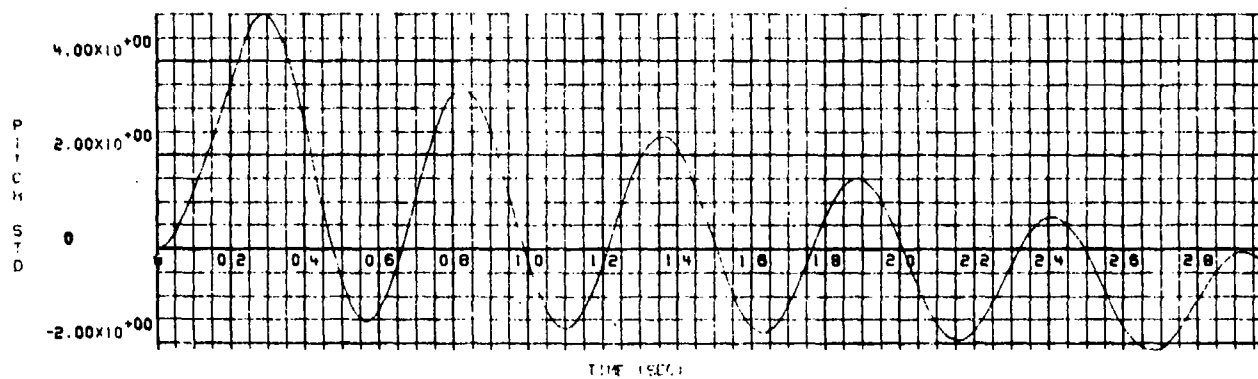
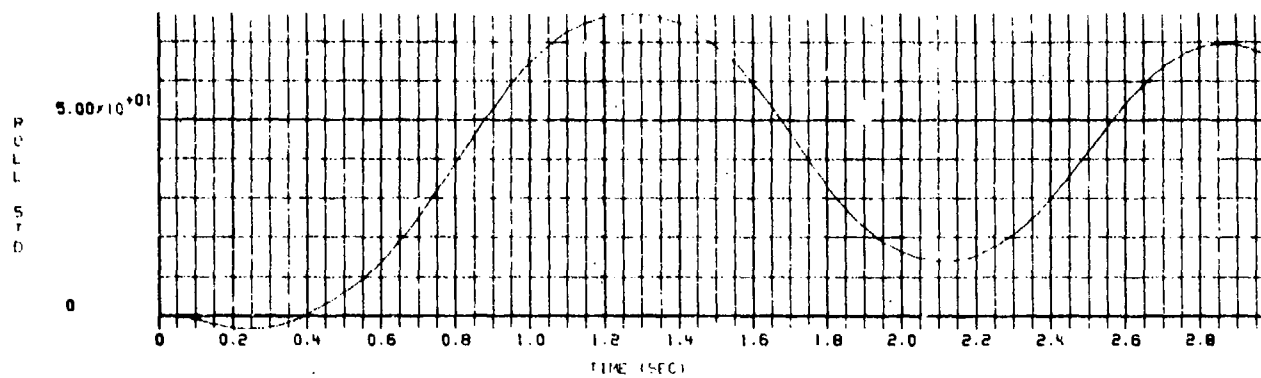
Figure HH-7. X, Y, and Z Position Versus Time for a Flow Field Intensity of  $-1/2$



17-12-75

H635

75 75



TIME 1566  
PLOT PREPARED BY TIA. ADIC

Figure HH-8.  $\phi$ ,  $\theta$ , and  $\psi$  Rotation Versus Time for a Flow Field Intensity of  $-1/2$

## REFERENCES

1. Korn, Stephen C., Use of the Flow Angularity Technique for Predicting Store Separation Trajectories, Air Force Armament Laboratory Technical Report AFATL-TR-71-140, October 1971 (AD 889 312).
2. Korn, Stephen C., Validation and Expansion of the Flow Angularity Technique for Predicting Store Separation Trajectories, Air Force Armament Laboratory Technical Report AFATL-TR-72-184, September 1972 (AD 905 447).
3. Hill D. W., Jr., Investigation of the Flow Field Beneath the Wing of the F-4C Aircraft with Various External Stores at Mach Number 0.85, Arnold Engineering Development Center Technical Report AEDC-TR-72-92/ Air Force Armament Laboratory Technical Report AFATL-TR-72-113, June 1972 (AD 900 393).
4. Pope, Y. C., VSD High Speed Wind Tunnel Force Tests of MK-82LGB and MK-82 LGB Models at Mach Numbers from .5 to 1.4, HSWT Test 464, Vought System Division (Prepared for Texas Instruments, Inc.), August 27, 1973.
5. Air Force Nonnuclear Stores Characteristics Data Bank, Aircraft Compatibility Branch, Munitions Division, Air Force Armament Laboratory, Eglin Air Force Base, Florida.

# INITIAL DISTRIBUTION

HQS USAF(RDQRM)	2	AFATL/DLY	1
HQ USAF(SAMI)	1	AFATL/DLJ	1
HQ USAF (XOXFM)	1	AFATL/DLJK	1
AFSC (IGFG)	1	AFATL/DLJF	1
AFSC (SDWM)	1	AFATL/DLJC	1
AFSC/DLCA	1	TAWC/TRADOCLO	1
AFSC/SDZA	1	ADTC/SES	1
ASD/ENFEA	1	USAF/XOOFa	1
AFAL/TEO	1	USAFE/LGWHM	1
FL2302, Tech Lib	1	AFFTC/FL 2806	1
AFAL/TEM	1	AFIT/LD	1
ASD/ENYW	1	AEDC (ARC, INC.)	1
FTD(PDXA-2)	1	USNWC (Code 4063)	1
TAC (DRA)	1	NAVAL SHIP R&D CEN (Code 166)	1
TAC (LGWM)	1	AFAL/DHO	1
SAC (LGW)	1	AFWAL/FL 2802	1
SAC (NRI)	1	AFML/LTM	1
NRSLC/MMEBL	1	AFWL/NSC	1
Ogden ALC/MMWM	2	AFWL/NSE	1
AFIS/INTA	1	NRSLC/MMIRBD	1
AFWL (SUL)	1	6510 ABG/SSD	1
AFWL/SECA	1	HQUSAFE/DOQ	1
AFEWC/SUR	4	HQPACAF/LGWSE	1
AUL (AU/LSE-70-239)	1	HQPACAF/DOO	1
NAV AIR TEST CEN/CT-17, TID	2	DRXSY-J	1
TACTEC/BATTELLE COLUMBUS LAB	1	USAE Waterways Exper Sta/WESFE	1
57 FWW/DOS	1	NAVAIR SYS COMD (Code 530-C)	1
USAFTFWC/TA	1	NAVAIR SYS COMD/AIR-954	1
REDSTONE SCJ INFO CEN/Doc Sec	2		
SARRI-LW	1		
DRXSY-A	3		
SARPA-TS-S#59	1		
NAV ORDNANCE STN/Tech Lib	1		
NAVAL SURFACE WPNS CENTER/Tech Lib	2		
USNWC (Code 533)	1		
NAV WPNS EVAL FAC/Weapons Dept	1		
NAVAL RESEARCH LAB (Code 2627)	1		
NAVAL RESEARCH LAB (Code 7785)	1		
SANDIA LAB/Tech Lib Div 3141	1		
THE RAND CORP/Lib-D	1		
DDC	12		
HQUSAFE (DOA)	1		
CINCPACAF (LGWLE)	1		
AFATL/DLOSL	9		
USAF TAWC (TEFA)	1		
AFATL/DL	1		